

Environmental Catalysis

Publication Date: February 23, 1994 | doi: 10.1021/bk-1994-0552.fw001

ACS SYMPOSIUM SERIES **552**

Environmental Catalysis

John N. Armor, EDITOR
Air Products and Chemicals, Inc.

Developed from a symposium sponsored
by the Catalysis and Surface Science Secretariat
at the 205th National Meeting
of the American Chemical Society,
Denver, Colorado,
March 28–April 2, 1993



**AIR
PRODUCTS & CHEMICALS**

AIR PRODUCTS AND CHEMICALS, INC.
ALLENTOWN, PA 18195
ATTN: INFO. SERVICES (R&D #1)

American Chemical Society, Washington, DC 1994



Library of Congress Cataloging-in-Publication Data

Environmental catalysis / John N. Armor, editor; developed from a symposium sponsored by the Catalysis and Surface Science Secretariat at the 205th National Meeting of the American Chemical Society, Denver, Colorado, March 28–April 2, 1993.

p. cm. — (ACS symposium series, ISSN 0097–6156; 552)

Includes bibliographical references and indexes.


ISBN 0–8412–2851–5

1. Pollution—Congresses. 2. Catalysis—Congresses.

I. Armor, John N., 1944– . II. American Chemical Society. Catalysis and Surface Science Secretariat. III. American Chemical Society. Meeting (205th: 1993: Denver, Colo.) IV. Series.

TD192.3.E58 1994
628.5'01541395—dc20

93–51098
CIP

The paper used in this publication meets the minimum requirements of American National Standard for Information Sciences—Permanence of Paper for Printed Library Materials, ANSI Z39.48–1984. 

Copyright © 1994

American Chemical Society

All Rights Reserved. The appearance of the code at the bottom of the first page of each chapter in this volume indicates the copyright owner's consent that reprographic copies of the chapter may be made for personal or internal use or for the personal or internal use of specific clients. This consent is given on the condition, however, that the copier pay the stated per-copy fee through the Copyright Clearance Center, Inc., 27 Congress Street, Salem, MA 01970, for copying beyond that permitted by Sections 107 or 108 of the U.S. Copyright Law. This consent does not extend to copying or transmission by any means—graphic or electronic—for any other purpose, such as for general distribution, for advertising or promotional purposes, for creating a new collective work, for resale, or for information storage and retrieval systems. The copying fee for each chapter is indicated in the code at the bottom of the first page of the chapter.

The citation of trade names and/or names of manufacturers in this publication is not to be construed as an endorsement or as approval by ACS of the commercial products or services referenced herein; nor should the mere reference herein to any drawing, specification, chemical process, or other data be regarded as a license or as a conveyance of any right or permission to the holder, reader, or any other person or corporation, to manufacture, reproduce, use, or sell any patented invention or copyrighted work that may in any way be related thereto. Registered names, trademarks, etc., used in this publication, even without specific indication thereof, are not to be considered unprotected by law.

PRINTED IN THE UNITED STATES OF AMERICA

1994 Advisory Board

ACS Symposium Series

M. Joan Comstock, *Series Editor*

- | | |
|---|---|
| Robert J. Alaimo
Procter & Gamble Pharmaceuticals | Douglas R. Lloyd
The University of Texas at Austin |
| Mark Arnold
University of Iowa | Cynthia A. Maryanoff
R. W. Johnson Pharmaceutical
Research Institute |
| David Baker
University of Tennessee | Julius J. Menn
Plant Sciences Institute,
U.S. Department of Agriculture |
| Arindam Bose
Pfizer Central Research | Roger A. Minear
University of Illinois
at Urbana–Champaign |
| Robert F. Brady, Jr.
Naval Research Laboratory | Vincent Pecoraro
University of Michigan |
| Margaret A. Cavanaugh
National Science Foundation | Marshall Phillips
Delmont Laboratories |
| Arthur B. Ellis
University of Wisconsin at Madison | George W. Roberts
North Carolina State University |
| Dennis W. Hess
Lehigh University | A. Truman Schwartz
Macalaster College |
| Hiroshi Ito
IBM Almaden Research Center | John R. Shapley
University of Illinois
at Urbana–Champaign |
| Madeleine M. Joullie
University of Pennsylvania | L. Somasundaram
DuPont |
| Lawrence P. Klemann
Nabisco Foods Group | Michael D. Taylor
Parke-Davis Pharmaceutical Research |
| Gretchen S. Kohl
Dow-Corning Corporation | Peter Willett
University of Sheffield (England) |
| Bonnie Lawlor
Institute for Scientific Information | |

Foreword

THE ACS SYMPOSIUM SERIES was first published in 1974 to provide a mechanism for publishing symposia quickly in book form. The purpose of this series is to publish comprehensive books developed from symposia, which are usually “snapshots in time” of the current research being done on a topic, plus some review material on the topic. For this reason, it is necessary that the papers be published as quickly as possible.

Before a symposium-based book is put under contract, the proposed table of contents is reviewed for appropriateness to the topic and for comprehensiveness of the collection. Some papers are excluded at this point, and others are added to round out the scope of the volume. In addition, a draft of each paper is peer-reviewed prior to final acceptance or rejection. This anonymous review process is supervised by the organizer(s) of the symposium, who become the editor(s) of the book. The authors then revise their papers according to the recommendations of both the reviewers and the editors, prepare camera-ready copy, and submit the final papers to the editors, who check that all necessary revisions have been made.

As a rule, only original research papers and original review papers are included in the volumes. Verbatim reproductions of previously published papers are not accepted.

M. Joan Comstock
Series Editor

Preface

CATALYSIS PLAYS A MAJOR ROLE IN CLEANING OUR AIR and reducing pollution. Since the late 1960s, when legislation restricting automobile emissions first passed, catalysis has provided a solution that allows automotive companies to meet the regulations. Today, catalytic, selective reduction of NO continues to offer the best solution for NO_x removal in power plants and utilities, and a variety of catalysts are widely employed as the method of choice for removing volatile organic compounds. For many of our current environmental problems, the obvious solutions have been attempted or the regulations have been made more strict; more elaborate or creative solutions are needed, and catalysis will continue to play an important role.

I considered several definitions of environmental catalysis and elected to use a broad definition. In the past two years, the term has been used in journal titles, symposia, proposals, and manuscripts. It refers to a collection of chemical processes that use catalysts to control the emission of environmentally unacceptable compounds. The term also encompasses the application of catalysts for the production of alternative, less polluting products, waste minimization, and new routes to valuable products without the production of undesirable pollutants.

The book focuses on catalytic solutions to improve our environment. Noncatalytic solutions, separation schemes, and unique absorbents can also be used to control or eliminate emissions, but these topics were not within the scope of this book. The book is organized somewhat differently than the symposium on which it is based. Specific sections are NO_x Removal, Mobile Engine Emission Control, Power Plant Emissions, Future Fuels, Control of Volatile Organic Compounds, and Other Opportunities. Fewer than half of the oral presentations appear as chapters. In addition, I have provided a short overview of each section. The subtopics developed along themes that are receiving the greatest attention in laboratories throughout the world. This emphasis does not mean that these are the only ideas deserving attention. Indeed, other topics have not received sufficient attention. One clear example is waste minimization: Many companies now practice this approach, but few are discussing their success. The field of environmental catalysis continues to evolve, so it is difficult to identify all the opportunities.

Acknowledgments

The symposium on which this book is based was scheduled within the Catalysis and Surface Science Secretariat with the sponsorship of the Divisions of Industrial and Engineering Chemistry, Inc.; Colloid and Surface Chemistry; and Petroleum Chemistry, Inc. My thanks go to the session chairs, who worked hard to produce a successful and meaningful symposium and book. A half-day session on catalysts related to the reformation of gasoline was assembled by Richard F. Wormsbecher and chaired by T. Roberie, both of W.R. Grace and Company. R. McCabe of Ford Motor Company put together three half-day sessions dealing with the mechanisms of NO_x removal. R. M. Heck and R. Farrauto of Engelhard Corporation assembled a day-long session on automotive and diesel emission control catalysts. Norman Kaplan of the U.S. Environmental Protection Agency generated a day-long session on NO_x technology for power plant emissions. Also, S. K. Agarwal and J. Spivey of the Research Triangle Institute coordinated a day-long session on volatile organic compound controls.

I gratefully acknowledge financial contributions to support the symposium provided by Air Products and Chemicals, Inc.; Allied Signal, Automotive Catalyst Company; Allied Signal, Inc.; Degussa Catalyst Ltd.; DuPont; Engelhard Corporation; Exxon Corporation; Ford Motor Company; Mobil Research & Development Corporation, Petroleum Chemistry Division; Prototech Company/United Catalysts, Inc.; Union Carbide Chemicals & Plastics Company; and W.R. Grace and Company.

JOHN N. ARMOR
Air Products and Chemicals, Inc.
7201 Hamilton Boulevard
Allentown, PA 18195-1501

September 29, 1993

Chapter 1

NO_x Removal: An Overview

John N. Armor

Air Products & Chemicals, Inc., 7201 Hamilton Boulevard,
Allentown, PA 18195

NO_x consists primarily of NO and NO₂ which are produced in all combustion processes by the oxidation of N₂ and fuel bound nitrogen. NO₂ is linked to causing bronchitis, pneumonia, susceptibility to viral infection, and alterations to the immune system. It also contributes to acid rain, urban smog, and ozone (1). Figure 1 illustrates the various chemical transformations of NO in our atmosphere that lead to air pollution problems (2). Note that NO is the key starting point for all of the other oxides of nitrogen. NO is not only produced by the burning of fossil fuels, but also by lightning, microbial decomposition of proteins in the soil, and volcanic activity. Once produced, NO is rapidly oxidized by ozone, OH, or HO₂ radicals (3) to form the higher oxides of nitrogen, such as NO₂, HNO₂, and HO₂NO₂. Thus, if NO is prevented from entering the atmosphere, most of the downstream effects of NO_x pollution can be eliminated. There are a number of commercial approaches to NO_x removal which include absorptive, thermal, and catalytic. Since the 1960's a great deal of work was accomplished to control NO_x emissions. For automotive exhausts, the current three-way catalyst uses an O₂ sensor to control the air/fuel ratio, which permits effective removal of NO_x, hydrocarbons and CO. For exhaust gases where excess O₂ is present, these same automotive catalysts are not effective for removing NO_x. These O₂ rich streams [such as in power plants and lean burn engines] represent major sources of NO_x which must be treated. The thorough review in 1988 by Bosch and Janssen is an excellent source for further details (4). Alternatively one can try to minimize NO_x formation with novel burner designs.

Among the catalytic approaches to NO_x emission from power plants, SCR (Selective Catalytic Reduction) is growing in application. SCR uses a catalyst to facilitate reactions between NO_x and NH₃ in the presence of oxygen. There are a number of variants of this technology depending on the supplier. First generation plants were built in Japan and newer facilities in Germany and Austria. The Clean Air Act Amendments of 1990 will likely prompt more widespread use of SCR in the USA. Standards for NO_x emission vary with the fuel and the type of utility.

0097-6156/94/0552-0002\$08.00/0
© 1994 American Chemical Society

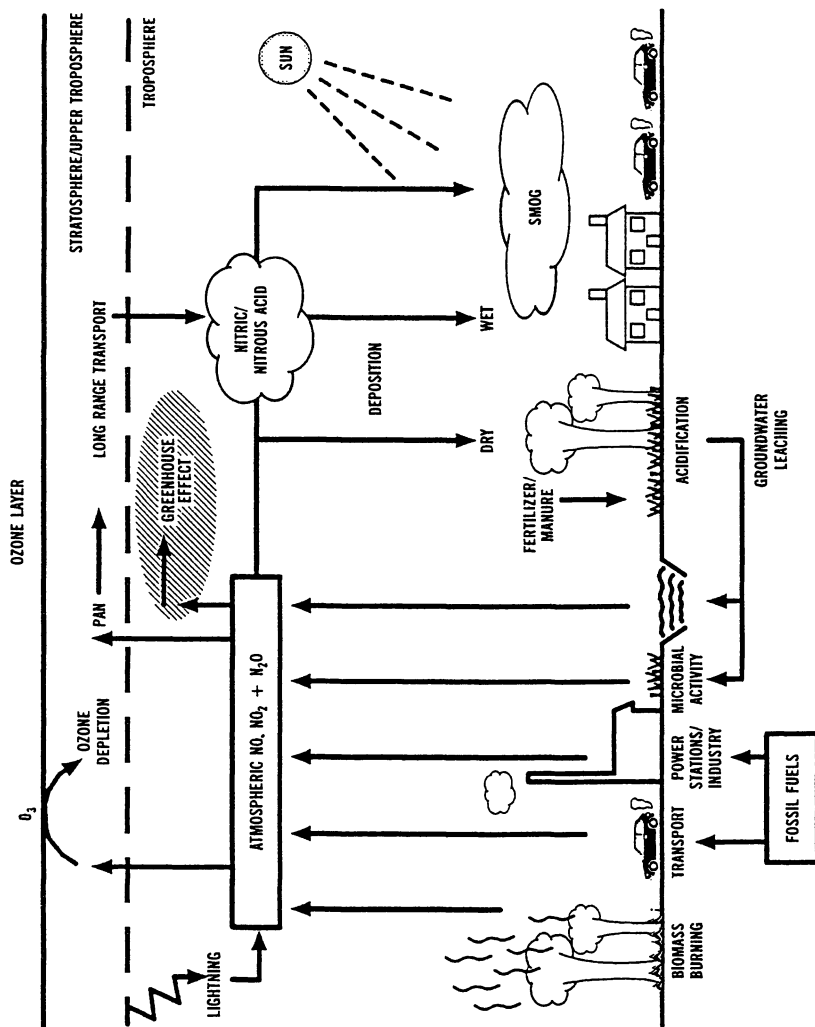


Figure 1. Cycling of nitrogen in the environment. (Reproduced with permission from reference 2. Copyright 1992 Noyes Data Corporation.)

Beyond current SCR technology, the catalytic decomposition of NO to N₂ and O₂ is an attractive way to remove NO from exhaust streams. Until recently, numerous metals and their oxides were tried (5), but none had sufficient activity to be practical. It is generally presumed that the strongly bound product oxygen on the catalytic sites inhibits further decomposition of NO. The direct decomposition of NO to its elements is thermodynamically favorable to ~1000°C, but it had not been demonstrated in any substantial yield until recently by Iwamoto and co-workers (6). They found that a copper ion exchanged zeolite molecular sieve, Cu-ZSM-5, was very active for the NO decomposition reaction. Over the Cu-ZSM-5, catalyst sustained activities were obtained. This catalyst was so much more active than previously tested materials, that it has provoked a great deal of interest and study. This work is the focus of several papers presented at this Symposium.

The reduction of NO_x with hydrocarbons, instead of ammonia, in an oxidizing atmosphere is also a subject of intense research for mobile engine applications. By using hydrocarbons, the problems [e.g., ammonia slip, transportation of ammonia through residential areas and equipment corrosion] associated with the SCR process can be avoided. Currently, propane, propylene and ethylene are the most intensely studied hydrocarbons for the NO_x reduction (7,8). In all these early reports, the presence of O₂ was essential for the NO_x reduction, demonstrating that hydrocarbons [present at low levels] readily found in most exhaust emissions can be effective for the selective reduction of NO_x. A number of the papers within this Symposium also deal with this approach to removing NO_x. Here the catalysts seem much more effective.

Already state and local regulations, such as those in California or New Jersey, effectively result in the application of SCR to new boilers and furnaces. Near-term needs include improving the performance of the catalysts at lower operating temperatures [e.g., 150-300°C] to allow NO_x control after other acid gas and particulate pollution controls, and improving the performance of the catalysts at higher operating temperatures [e.g., 1,450-2,000°C] to allow placement of the NO_x control system at the discharge of gas turbines.

The actual flow of papers within the Symposium covered all aspects of NO_x removal, but for organization, this broad topic will be segregated by catalysts that operate in O₂ rich or poor conditions. Robert McCabe was the chairperson of the topical area on "Mechanisms of NO_x Removal" and provided the following summary of the papers presented at this meeting: "The papers dealing with lean NO_x control by decomposition or selective hydrocarbon reduction, can best be described as a mechanistic free-for-all - as expected, given the relatively recent emergence of this area. Keynote lectures were delivered by W. K. Hall (Univ. of Pittsburgh) and M. Iwamoto (Hokkaido Univ.) Professor Hall, in addition to reviewing the general understanding of redox chemistry in metal-exchanged zeolites, also presented results of recent in-situ ESR experiments on Cu-ZSM-5 which showed that rates of selective NO reduction are highest when Cu is nominally in the +2 oxidation state. Hall also presented data suggesting the importance of NO₂ as a reaction intermediate. Professor Iwamoto reviewed his pioneering work in NO_x decomposition and selective reduction and presented recent IR spectroscopic and kinetic data suggesting that adsorbed isocyanate species are key intermediates in the selective reduction reaction. In contrast to the work of Hall and Iwamoto, A. P. Walker (Johnson Matthey Co.) used a temporal-

analysis-of-products (TAP) reactor to show that NO can react with adsorbed hydrocarbon residue ("coke") on Cu-ZSM-5 catalysts. Walker stressed the importance of zeolite acidity in forming the carbonaceous species and indicated that catalyst acidity is a key parameter being employed by Johnson Matthey in developing other zeolite and non-zeolite catalyst formulations. Additional studies dealing with mechanistic aspects of lean NO_x decomposition or selective reduction included presentations by G. Centi (Univ. of Bologna), showing reversible formation of mono- and dinitrosyl species on supported copper oxide catalysts, and presentations by H. W. Jen (Ford Motor) and J. P. McWilliams (Mobil Oil Co.), both stressing the importance of hydrocarbon oxidation in the overall NO_x reaction scheme. Other studies were directed at characterizing Cu-ZSM-5 and related catalysts by various techniques including TPD-TGA of isopropyl amine (D. Parillo - U. of Pennsylvania), XPS (M. Shelef - Ford) and XRD plus high-resolution TEM (K. Kharas - Allied Signal CO.). Another group of papers examined novel applications of lean NO_x catalysts and/or novel modifications of the catalyst formulation. The Editor reported on a new catalytic process that efficiently reduces NO_x with methane in the presence of excess O₂. This process, which is based on a cobalt-exchanged ZSM-5 catalyst, potentially provides an efficient low-temperature route to NO_x emission control in natural gas fired power plants. R. Gopalakrishnan (Brigham Young Univ.) described *Catalysts for Clean-Up of NO_x, NH₃ and CO from Nuclear Waste Processing*. They looked at a variety of catalysts for NO_x and CO removal and found that Cu-ZSM-5 was very good for ammonia SCR but not for CO oxidation. Pt/Al₂O₃ was very good for ammonia and CO oxidation but not for NO_x removal. They suggested using a two-stage catalyst: Cu-ZSM-5 followed by Pt/Al₂O₃ in order to remove pollutants from dilute waste streams containing NO_x, ammonia, and CO. M. Flytzani-Stephanopoulos (M.I.T.) reported on Cu-ZSM-5 catalysts prepared with a series of co-cations. Those prepared with rare-earth co-cations, in particular, showed improvements in low-temperature NO decomposition activity. It was clear from the wide range of papers presented, as well as the divergent mechanistic viewpoints, that NO_x removal in O₂ rich exhausts by selective hydrocarbon reduction is still in its infancy with respect to fundamental understanding and practical application. Clearly many materials are capable of promoting lean NO_x catalysis, and the many mechanisms offered strongly suggest that there is more than one pathway by which NO_x can be reacted with hydrocarbons in the presence of excess O₂. By way of juxtaposition, the invited lecture by A. T. Bell (Univ. of California - Berkeley), which dealt with conventional NH₃-based SCR over both Pt/Al₂O₃ and V₂O₃ and V₂O₃/TiO₂ catalysts, elegantly demonstrated the much greater extent of mechanistic understanding that has been garnered in the mature ammonia-based selective catalytic reduction process compared to the newer hydrocarbon-based processes." With the above as background to the problem of NO_x emissions and treatment, this section of the book will focus on these new approaches to controlling NO_x by catalytic decomposition or reduction. A majority of these presentations are presented as full papers within this book. Because of the current, intense interest in NO_x removal and Iwamoto's work many of the papers focused on Cu-ZSM-5 for NO decomposition or reduction by hydrocarbons. The following section of mobile engine exhausts will revisit this topic for exhaust streams which do not contain excess O₂.

References

1. Armor, J. N. *Appl. Catal. B*, **1992**, *1*, 221-256
2. Sloss, L.L.; Hjalmarsson, A-K.; Soud, H. N.; Campbell, L. M.; Stone, D. K.; Shareef, G. S.; Emmel, T.; Maibodi, M.; Livengood, D.; Markussen, J. *Nitrogen Oxides Control Technology Fact Book*, Noyes Data Corp.; Park Ridge, New Jersey, 1992; p. 5.
3. Seinfeld, J. H. *Science* **1989**, *243*, 745.
4. Bosch, H.; Janssen, F. *Catal. Today* **1988**, *2*, 369-532.
5. Hightower, J. W.; Van Leirsburg, D. A. In *The Catalytic Chemistry of Nitrogen Oxides*; Klimisch, R. L.; Larson, J. G., Eds.; Plenum Press: New York, 1975; p. 63.
6. Iwamoto, M. In *Future Opportunities in Catalytic and Separation Technology*; Misono, M.; Moro-oka, Y.; Kimura, S., Eds.; Elsevier: Amsterdam, 1990; p. 121
7. Hamada, H.; Kintaichi, Y.; Sasaki, M.; Ito, T. *Appl. Catal.*, **1990**, *64*, L1.
8. Sato, S. S.; Hirabay, H.; Yahiro, H.; Mizuno, N.; Iwamoto, M. *Catal. Lett.*, **1992**, *12*, 193.

RECEIVED November 16, 1993

Chapter 2

Catalytic Decomposition of Nitric Oxide over Promoted Copper-Ion-Exchanged ZSM-5 Zeolites

Yanping Zhang and Maria Flytzani-Stephanopoulos

Department of Chemical Engineering, Massachusetts Institute
of Technology, Cambridge, MA 02139

Alkaline earth and transition metal cocation effects are reported in this paper for Cu ion-exchanged ZSM-5 zeolites used for the catalytic decomposition of nitric oxide in oxygen-rich gases. The effect, manifested under a specific mode of ion exchange, enhances the catalytic activity at high temperatures (450-600°C) and appears to be due to stabilization of the active copper sites. The conversion of NO to N₂ is invariant to oxygen in the high temperature region for dilute NO gases. The coexistence of rare earth ions with Cu ions in ZSM-5 produced a markedly different effect promoting the activity of copper ions for the NO decomposition at low temperatures (300-400°C).

The direct catalytic decomposition of nitric oxide to nitrogen and oxygen in oxygen-rich post-combustion gas streams would greatly benefit the economics of post-combustion NO_x control in power plants, industrial boilers and engine systems. The initial report by Iwamoto (1) that Cu ion-exchanged ZSM-5 (Cu-Z) zeolite has stable steady-state activity for the direct decomposition of nitric oxide has been followed by many recent studies (2-9) of this catalyst system addressing pertinent issues potentially affecting its activity including copper exchange level, Si/Al ratio, oxygen effect, poisoning by SO₂, H₂O effect, etc.

The conversion of NO to N₂ over the Cu-Z materials is not a linear function of the copper ion-exchange level. Rather, very low activity exists for up to 40% exchange level, above which conversion increases rapidly with the exchange level (2). Over-exchanged (>100%) Cu-Z are active either

0097-6156/94/0552-0007\$08.00/0
© 1994 American Chemical Society

because copper ions adequately populate sites accessible to NO (i.e., in the 10-membered rings of the ZSM-5) or because catalytic activity only emerges if enough adjacent copper active sites exist (6). In recent work, Kagawa, et al (8) reported that the incorporation of cocations into Cu-Z promoted the catalytic activity of Cu ion for the direct NO decomposition in O₂-free gas streams at temperatures above 450°C. Transition metals or alkaline earths were equally effective cocations in Cu-Z at 550°C. The mode of ion exchange was important, i.e., the cocation had to be exchanged first followed by copper ion exchange, for the effect to show. The positive cocation effect was more pronounced for low Cu ion exchange levels. The effect of oxygen on the conversion of NO to N₂ was not examined in that work. Oxygen has been reported to inhibit the reaction over unpromoted Cu-Z catalysts, but the inhibition decreases with temperature (7). Iwamoto, et al (6) have reported that the conversion of NO to N₂ in the presence of oxygen is a function of both the Cu-exchange level and the ratio of P_{NO}/P_{O₂}.

In this paper we examine the cocation effect on the NO decomposition reaction in oxygen-containing gases over M/Cu-Z catalysts, where M is an alkaline earth or transition metal ion. The importance of the preparation method is discussed in terms of active (Cu ion) site stabilization. Rare earth metal-modified Cu-Z catalysts were also prepared and tested in this work both in oxygen-free and oxygen-containing gases.

Experimental

Catalyst Synthesis and Characterization. Catalysts were prepared by incorporating metal cations into ZSM-5 zeolite supports according to ion exchange procedures widely used in preparation of metal/zeolite catalysts. The starting materials were the Na⁺ form of ZSM-5 zeolites with Si/Al ratio of 21.5 synthesized by the Davison Chemical Division of W.R. Grace Co. In catalysts containing copper and a cocation, the ZSM-5 zeolites were first ion-exchanged with the cocation in nitrate form in dilute aqueous solution with concentration of 0.007M. The exchanges were made either at room temperature for 10 hours or at 85°C for 2 hours. After filtration, the metal ion-exchanged ZSM-5 zeolites were dried at 100°C for 10 hours, and some of them were further calcined in a muffle furnace in air at 500°C for 2 hours. The reason for calcining the catalysts was to stabilize cations in the zeolite. The catalysts were further ion-exchanged with Cu²⁺ in an aqueous solution of cupric acetate of concentration 0.007M at room temperature overnight. This was repeated several times, depending on the desired Cu exchange levels. Finally, the catalysts were washed with deionized water at room temperature and dried at 100°C overnight. For simplicity, a catalyst with intermittent air calcination of cocation exchanged ZSM-5 is designated as a precalcined M/Cu-Z catalyst in the text.

The mode of exchange described here was the evolution of several different preparation methods. A summary of observations made during this process when using Mg^{2+} as the cocation is as follows: a) exchanging copper ions first or co-exchanging copper and magnesium ions for Na^+ in the ZSM-5 did not succeed in high-exchange levels of Mg^{2+} in the zeolite; b) even when Mg^{2+} was exchanged first followed by copper ion exchange, we would observe loss of Mg^{2+} in the solution. Both a) and b) are the result of a more favorable exchange equilibrium for Cu^{2+}/Na^+ (10); c) when the Mg^{2+} ion solution was heated at 85°C for 2 hours, higher levels of exchange were obtained and better stability in subsequent room temperature copper ion exchanges; d) air calcination of Mg^{2+} -exchanged zeolites at 500°C for 2 hours was very effective in keeping the Mg^{2+} exchange high even after subsequent copper ion exchanges. This procedure was followed in preparing two of the Mg/Cu-Z catalysts as well as the Sr, Ni, Pd, Ce and La/Cu-Z catalysts shown in Table I.

The elemental analyses were performed by Inductively Coupled Plasma Emission Spectrometry (ICP, Perkin-Elmer Plasma 40) after catalyst samples were dissolved in HF(48%). It is noted that a small amount of Si and Al was extracted from the zeolite during the ion exchange procedures. A list of catalyst syntheses and properties is shown in Table I. In the text, the catalysts are identified in the following way: cocation type(percent exchange level)/Cu(percent exchange level)-Z, for example, Mg(34)/Cu(86)-Z, where 100% ion exchange level is defined as one Cu^{2+} (or Mg^{2+}) replacing two Na^+ (or neutralizing two Al^-) and the atomic ratio Cu (or Mg)/Al=0.5.

Conversion Measurements and Kinetic Studies. Conversion and kinetic studies were performed in laboratory-scale packed-bed reactors, consisting of a 60cm long quartz tube with I.D. equal to 1.1 cm (for conversion measurements) or 0.4 cm (for kinetic studies). A porous quartz fritted disk was placed in the middle of the tube to support the catalyst bed. The reactor was placed in a temperature-programmed furnace that was electrically heated and controlled by a temperature controller (Tetrahedron: Model Wizard). Three mass flow controllers were used to measure flow rates of $NO+He$, O_2+He and He. Certified standard helium and gas mixtures were used from Matheson and Airco. A gas chromatograph (Hewlett Packard: Model 5890) with a thermal conductivity detector, and a 5A molecular sieve column of 1/8 in. O.D. by 6 ft. long, was used to measure concentrations of nitrogen, oxygen and nitric oxide. A NO-NO_x analyzer (Thermo Electron: Model 14A) was also used to measure low NO/NO_x concentrations, ranging from 0.001ppm to 2,500 ppm. An amount of 0.5-1.0 g of catalyst was placed in reactor for conversion measurements, and 30-35 mg for kinetic studies. The catalyst packing density in the reactor was about 0.5 g/cc. Total flowrates of the feed gas were 30-90 cc/min. The contact time,

W/F, defined as the ratio of catalyst weight in the reactor to the total flowrate of the feed gas was 0.03- 1g s/cc(STP). The total gas pressure in the reactor was 1.5 atm during conversion measurements and about 2 atm in the kinetic studies. NO concentrations varied from 0.2%- 4% in the feed gas stream, O₂ from 0%-5%, balance He. The O₂+He stream was heated to 150°C before it was mixed with NO+He at the inlet of the reactor to avoid NO₂ formation (4). All measurements were made after steady state had been reached.

Results and Discussion

Nitric Oxide Decomposition in the Absence of Oxygen. The Cu-Z and Mg/Cu-Z catalysts shown in Table I were evaluated in a gas containing 2% NO-He, at contact time of 1g s/cc (STP) over the temperature range of 350 - 600°C. Control experiments with Mg-Z materials verified that the activity of Mg/Cu-Z was exclusively due to Cu ions. Figures 1 and 2 show the NO to N₂ conversion profiles obtained for the catalysts tested under these conditions.

For the same copper ion-exchange level (~70%), the Mg(52)/Cu(66)-Z catalyst shows a positive effect, i.e., higher NO to N₂ conversion than the Cu(72)-Z material, in the high temperature region (450 -600°C), as can be seen in Figure 1. These results are in agreement with the report by Kagawa, et al (8). While still present, this effect is not as pronounced for Mg/Cu-Z catalysts with Cu exchange level higher than about 110%.

Within the group of the Mg/Cu-Z catalysts, preparation conditions were important. As mentioned in the previous section, heating of the solution during Mg²⁺-exchange was necessary in order to preserve the Mg ions in the zeolite upon subsequent exchange with copper ion solutions. The effect of intermittent air calcination of Mg-Z material at 500°C for two hours on the catalytic activity has been evaluated. The precalcined catalyst, Mg(34)/Cu(86)-Z, gave higher NO to N₂ conversion over the whole temperature range (350-600°C) than the catalyst Mg(40.4)/Cu(91.2)-Z without intermittent air calcination, as shown in Figure 2.

At the present time, no consensus exists in the literature on the mechanism of NO decomposition over Cu-Z catalysts. This makes a mechanistic interpretation of the cocation effects reported here premature. However, the importance of ion exchange sequence and catalyst heat treatment on the NO decomposition activity is worth discussing in terms of active site modification on the basis of available information. In ESR studies, Kucherov, et al (11, 12) have identified two types of isolated Cu²⁺ ions: one in a five-coordinated square pyramidal configuration, the other in a four-coordinated square planar. At low Cu exchange level, the five-coordinated Cu²⁺ ions were preferably formed (12). Shelef (13) proposed the square planar copper ions as the active sites of Cu-Z for NO decomposition. This explains the negligible activity of Cu-Z catalysts with

Table I. Summary of Catalyst Syntheses and Properties

Catalysts	Si/Al	Cu/Al ^b	Cocation/Al ^b	Na/Al ^b	Cu exchange
Parent zeolite ^a	21.5			1.0	
Cu-Z	20.3	0.705 (141%)	-	~0	thrice, RT
Cu-Z	19.9	0.36 (72%)	-	0.25 (25%)	once, RT
Mg/Cu-Z ^c	18.0	0.456 (91%)	0.202 (40%)	~0	twice, RT
Mg/Cu-Z ^{d,e}	17.1	0.430 (86%)	0.170 (34%)	~0	twice, RT
Mg/Cu-Z ^{c,e}	19.5	0.33 (66%)	0.26 (52%)	~0	twice, RT
Ni/Cu-Z ^{c,e}	20.8	0.478 (96%)	-	~0	twice, RT
Sr/Cu-Z ^{c,e}	20.8	0.524 (105%)	0.194 (39%)	~0	twice, RT
Pd/Cu-Z ^{c,e}	20.7	0.45 (90%)	0.44 (88%)	~0	twice, RT
Ce/Cu-Z ^{c,e}	19.5	0.596 (119%)	0.036 (11%)	~0	twice, RT
La/Cu-Z ^{c,e}	19.4	0.627 (123%)	0.06 (18%)	~0	twice, RT

a. ZSM-5: SMR-2670-1191, as received from Davison Div., W.R. Grace. Co.

b. The values in parentheses are ion exchange levels, on the basis of Al content as measured by ICP.

c. Cocations exchanged once with Na/ZSM-5 at 85°C for 2 hours.

d. Cocation exchanged once with Na/ZSM-5 overnight at RT.

e. The cocation-exchanged ZSM-5 catalysts were dried in air at 100°C overnight, and calcined at 500°C for 2 hours.

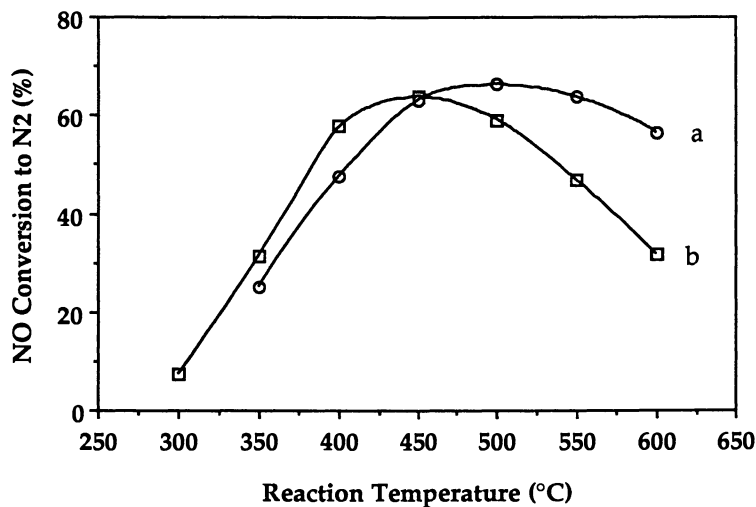


Fig. 1. Comparison of NO conversion to N₂ over (a) Mg(52)/Cu(66)-Z; (b) Cu(72)-Z at 2% NO and W/F=1 g s/cc (STP).

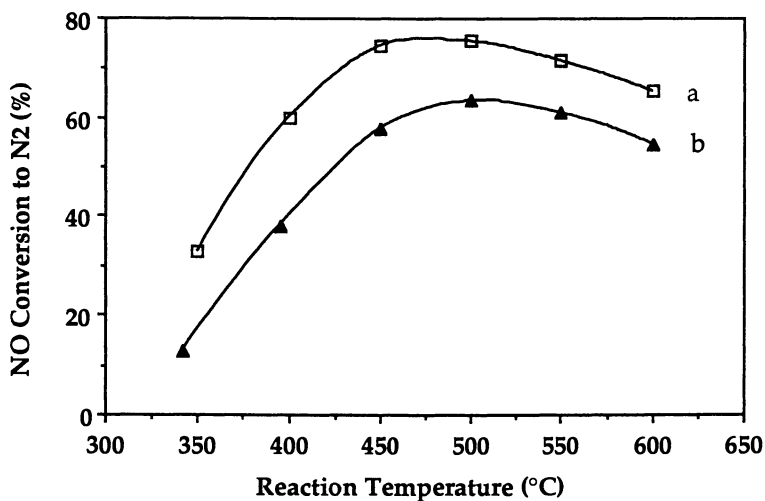


Fig. 2. Effect of intermittent Mg-Z calcination on Mg/Cu-Z catalyst activity for NO conversion to N₂ at 2% NO and W/F=1 g s/cc (STP); (a) calcined Mg(34)/Cu(86)-Z; (b) non-calcined Mg(40.4)/Cu(91.2)-Z.

low Cu ion-exchange level (<40%). To examine the validity of this assumption we have examined the NO conversion to N₂ over various Cu-Z catalysts as a function of the amount of square planar Cu²⁺ ions, calculated from the data given in Kucherov, et al (12) for Cu-Z catalysts prepared from a ZSM-5 zeolite which had a similar ratio of Si/Al=21 to the ZSM-5 zeolite used in this study. A linear relationship was found (14). The number of four-coordinated square planar Cu²⁺ in Cu-Z materials has been reported to decrease at high temperatures (12). Apparently then, the inert Mg ions stabilize the relative population of square planar Cu²⁺ ions resulting in higher NO conversion to N₂ at high temperatures, as shown in Figure 1.

The intermittent calcination effect may be explained by migration of Mg²⁺-bare ions, formed during calcination from their respective larger hydrated complex ions, to the 5- and 6-membered rings of ZMS-5. This would effectively keep the active Cu²⁺ in the 10-membered rings, where they are accessible to the reactant gas molecules. Hence, a higher NO conversion to N₂ is expected for the pre-calcined Mg(34)/Cu(86)-Z over the non-calcined Mg(52)/Cu(91)-Z catalyst as shown in Figure 2.

The observed cocation effect in Kagawa, et al (8) and the present work, therefore, may simply be one of stabilization of the copper active sites. To pursue this argument further, the performance shown in Figure 2 should not be sensitive to the type of cocation chosen. Figure 3 shows the NO conversion to N₂ over several precalcined M/Cu-Z catalysts with similar Cu²⁺ exchange level, where M is a transition metal or alkaline earth ion. Similar catalytic activity is indicated by the overlapping conversion profiles of Figure 3.

NO Decomposition in O₂-Containing Gases. Oxygen has been reported to inhibit the NO decomposition reaction, but the inhibition decreases with temperature (7). The oxygen effect was studied on Cu-Z catalysts using high NO concentrations (1-4%) in the feed gas. Iwamoto, et al (6) have reported that in oxygen-containing gas the NO conversion to N₂ does not decrease as much for over-exchanged Cu-Z catalysts. However, a large decrease was shown for low Cu ion-exchanged Cu-Z. A dependence on the ratio P_{O2}/P_{NO} was also suggested.

In the present work we examined the effect of oxygen both with over-exchanged Cu-Z as well as with the cocation-exchanged M/Cu-Z catalysts. Figure 4 shows typical conversion-temperature plots for the Cu (141)-Z catalyst with 0 and 5% O₂ containing gases with NO content fixed at either 2% or 0.2%, W/F=1g s/cc (STP). The data display the O₂-inhibition and the lower-sensitivity to O₂ at high temperature mentioned above. However, it is very interesting that a similar plot for low NO-content (0.2%) in the gas (Figure 4), shows much less inhibition by oxygen at low temperatures and no oxygen-effect in the high-temperature region.

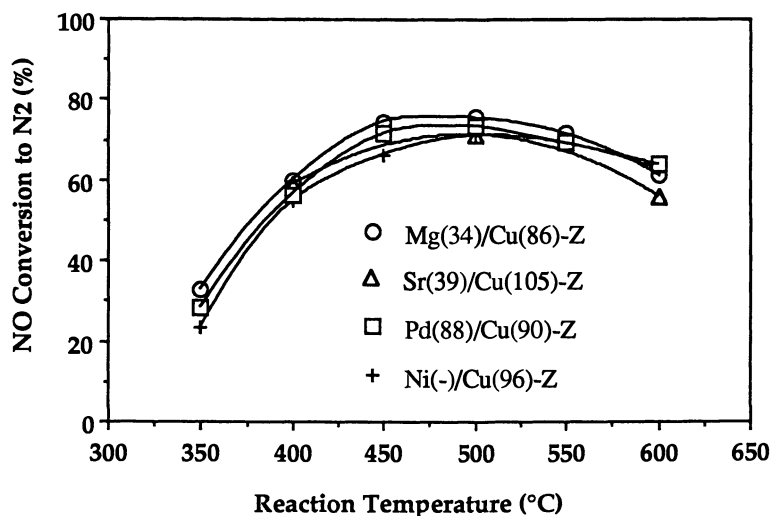


Fig. 3. NO decomposition over selected M/Cu-Z catalysts at 2%NO and W/F=1g s/cc (STP).

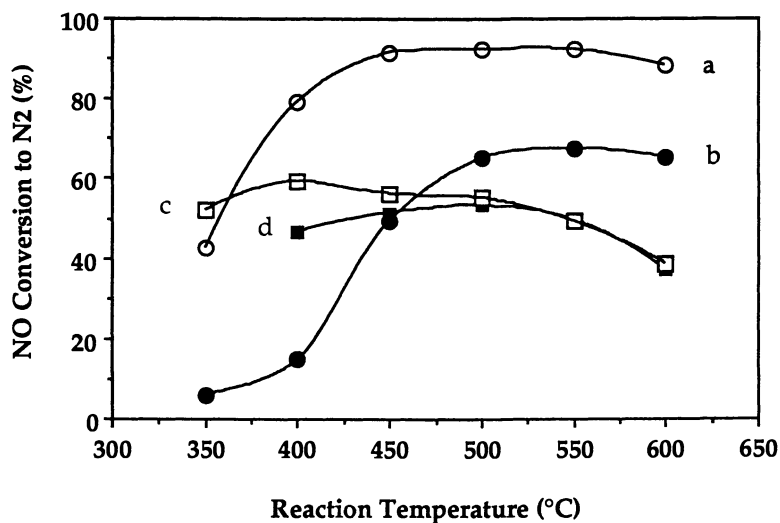


Fig. 4. Effect of O₂ and NO concentrations on the Cu(141)-Z activity for NO decomposition at W/F=1g s/cc (STP); (a) 2%NO-0%O₂; (b) 2%NO-5%O₂; (c) 0.2%NO-0%O₂; (d) 0.2%NO-5%O₂.

Similar experiments were run with the Mg/Cu-Z catalysts. Typical results are shown in Figure 5 for the Mg (34)/Cu (86)-Z material. Similar trends to those in Figure 4 for the Cu(141)-Z catalyst are seen for a feed gas with 2%NO, 0% or 5% O₂, and 1g s/cc contact time. When the inlet concentration of NO was 0.2%, however, the NO to N₂ conversion in the presence of 5% O₂ was higher than that in the absence of O₂ at temperatures above 450°C. Under these conditions, the catalytic activity is enhanced by the presence of O₂. The other Mg/Cu-Z catalysts gave conversions similar to those in Figure 5 for the catalyst Mg(34)/Cu(86)-Z. Overall then, we found that in low NO-containing gases the conversion of NO to N₂ is invariant to oxygen in the high temperature region (450-600°C). This finding is very significant for applications to dilute-NO, post-combustion gas streams.

Another feature of the conversion-temperature profiles becomes evident by comparing the data of Figures 4 and 5 for the 5% O₂-containing feed gas with low (0.2%)- or high (2%)-NO content. For both the Cu (141)-Z and Mg (34)/Cu (86)-Z catalysts, the conversion of NO to nitrogen increases as the NO-content decreases at temperatures below 450°C. Assuming that O₂ and NO compete for adsorption sites, oxygen would inhibit the reaction, especially at low temperatures. Under these conditions, NO₂ formation may be favored reducing the selectivity to N₂. It is not clear, however, why oxygen appears to inhibit the decomposition reaction more for the high NO concentration gas. More detailed studies of the product selectivity as a function of PO₂/PNO and temperature are warranted.

Kinetic Studies. The microcatalytic reactor described earlier was used with samples weighing 30-35mg for kinetic studies and measurements of turnover frequencies over the Cu (141)-Z and the Mg (34)/ Cu (86)-Z catalysts. Conversion-contact time plots, constructed for the NO decomposition reaction over each catalyst at 500°C with 4% NO-He gas, were linear for conversions up to 30% for the Mg(34)/Cu(86)-Z and 50% for Cu(141)-Z. In the kinetic studies the conversions were kept below 10% for Mg(34)/Cu(86)-Z and below 40% for Cu(141)-Z to ensure that reaction rates were not diffusion- limited.

Figure 6 shows Arrhenius-type plots for the turnover frequencies over the Cu (141)-Z and the Mg (34)/Cu(86)-Z catalysts. The turnover frequency (TOF), defined as the number of NO molecules converted to N₂ per second per Cu ion, is higher for the Cu (141)-Z than for the Mg (34)/Cu (86)-Z catalyst over the whole range of temperatures in agreement with the conversion-temperature plot of Figures 4 and 5. As has been reported before (7), the specific catalytic activity (turnover frequency) increases with the copper loading on the same parent ZSM-5. The difference is more pronounced at high temperatures. A maximum in the Arrhenius plots is seen, again in agreement with previous reports. In this work we have extended the measurements of activity to higher temperatures to measure

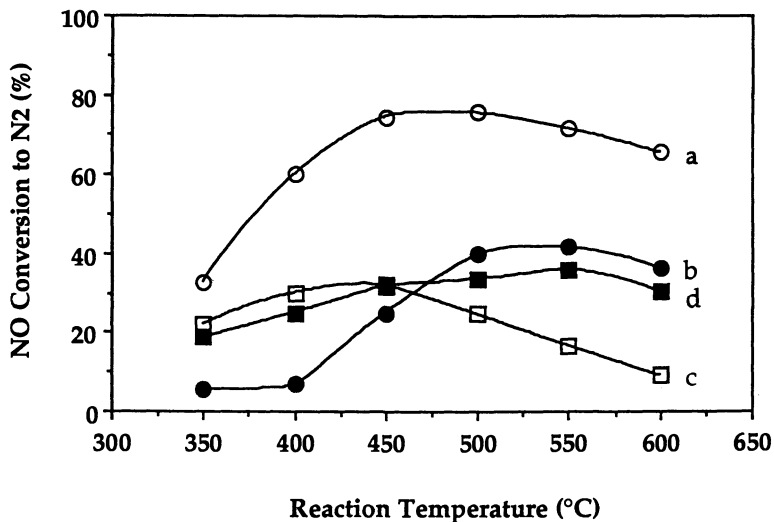


Fig. 5. Effect of O₂ and NO concentrations on the Mg(34)/Cu(86)-Z activity for NO decomposition at W/F=1g s/cc (STP); (a) 2%NO-0%O₂; (b) 2%NO-5%O₂; (c) 0.2%NO-0%O₂; (d) 0.2%NO-5%O₂.

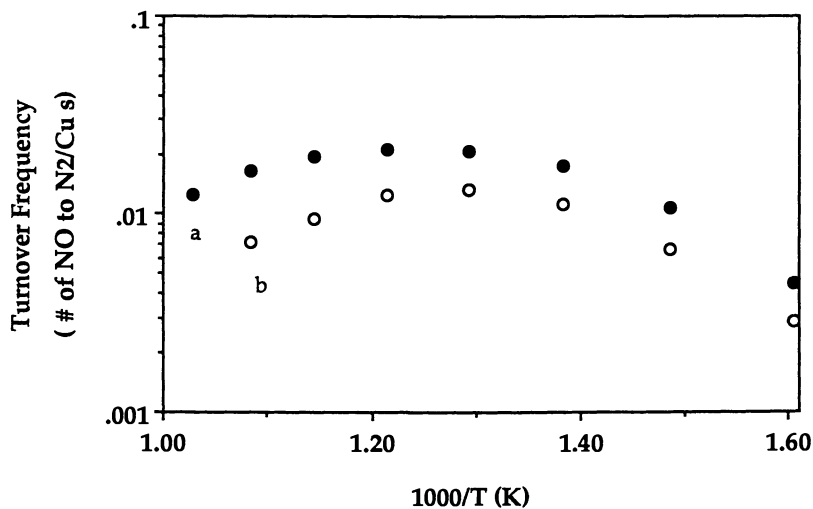


Fig. 6. Arrhenius plots for NO decomposition over (a) Cu(141)-Z; (b) Mg(34)/Cu(86)-Z at 4%NO and 1.7 atm of total gas pressure.

the corresponding activation energy. As can be seen in Figure 6, the apparent activation energy for NO decomposition over the Mg(34)/Cu(86)-Z catalyst is 12.3 Kcal/mole in the low temperature region, changing over to a negative value of -8.2 Kcal/mole in the high temperature region (>500°C). Over the Cu(141)-Z material, similar values of apparent activation energies, 12.6 Kcal/mole for the low temperature region and -7.6 Kcal/mole for the high temperature region, were obtained. A changing reaction mechanism or loss of copper active sites at high temperature may explain the observed reaction rate maximum. A similar study in the presence of oxygen is warranted, based on the conversion plots discussed in the previous section.

Detailed kinetic studies are presently underway in our laboratory with over-exchanged Cu-Z and Mg/Cu-Z catalysts. One interesting series of tests is reported here as it provides support to the data of Figure 5. A gas containing 0.2% NO in He and oxygen in the range of 0-5% was reacted over the Mg (34)/Cu (86)-Z catalyst at contact time of 0.03g s/cc (STP) and reaction temperature of 600°C. Conversion below 30% was used to measure TOF. The results, plotted in Figure 7, show the specific catalytic activity to be invariant to oxygen, i.e., a reaction order of zero in O₂ was obtained.

Rare Earth Metal Cation Modified Cu-ZSM-5. Two rare earth metal modified Cu-Z catalysts, namely Ce(11)/Cu(119)-Z and La(18)/Cu(123)-Z shown in Table I, were evaluated and compared to Cu(141)-Z and Mg(34)/Cu(86)-Z catalysts in a gas containing 2% NO-He at contact time of 1g s/cc (STP) over the temperature range of 300-600°C. Figure 8 shows the NO conversion to N₂ profiles obtained for these catalysts under the above conditions.

The coexistence of rare earth ions with copper in the ZSM-5 produced a markedly different effect promoting the activity of copper ions for the NO decomposition at low temperatures (300-400°C). The Ce(11)-Z material has very low (but measurable) activity, less than 10% conversion of NO to N₂, over the temperature region of 300-500°C. However, the Ce(11)/Cu(119)-Z catalyst showed higher conversion of NO to N₂ than the over exchanged Cu(141)-Z catalyst at temperatures in the range of 300-400°C, and higher than the Mg(34)/Cu(86)-Z catalyst at temperatures below 450°C, as seen in Figure 8. When a 50 - 50 mixture (by weight) of Ce(11)/Cu(119)-Z and Cu(141)-Z was tested, its catalytic activity was between those of Cu(141)-Z and Ce(11)/Cu(119)-Z (not shown in Figure 8).

Effect of Contact Time on Catalyst Activity. Contact time tests showed that the activity of Cu(141)-Z and Mg(34)/Cu(86)-Z catalysts did not decrease much at low NO concentration, oxygen-rich gas and low contact time. This is very important for practical application of the catalysts. Figure 9 shows profiles of NO conversion to N₂ over the Mg(34)/Cu(86)-Z and Cu(141)-Z

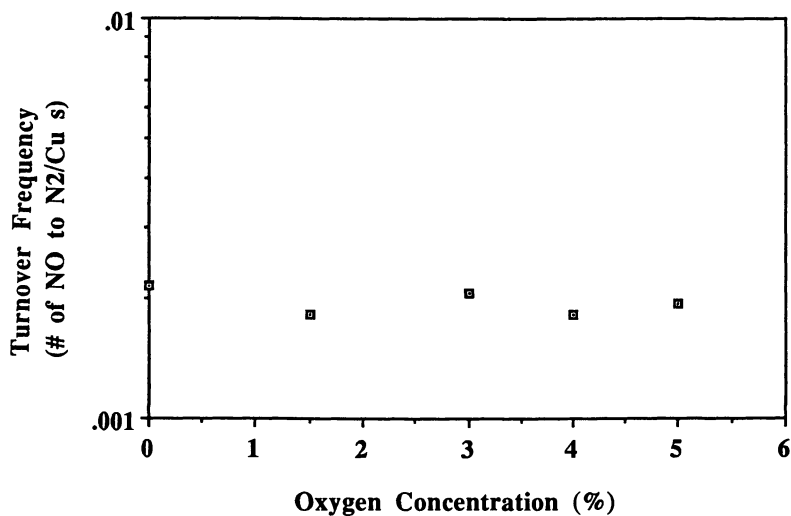


Fig. 7. Effect of oxygen on the NO decomposition rate(TOF) over Mg(34)/Cu(86)-Z at 0.2%NO, 600°C , and W/F=1g s/cc (STP).

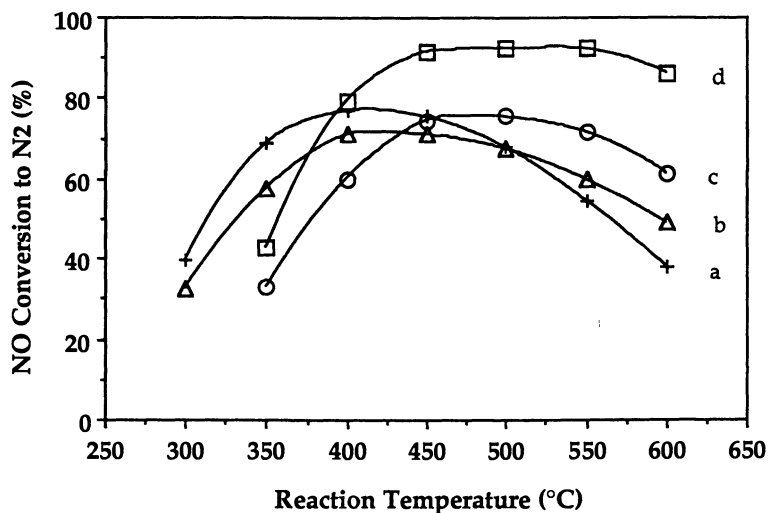


Fig. 8. Comparison of NO conversion to N₂ over (a) Ce(11)/Cu(119)-Z; (b) La(18)/Cu(123)-Z; (c) Mg(34)/Cu(86)-Z; (d) Cu(141)-Z at 2%NO and W/F=1g s/cc (STP).

catalysts at 2,000ppm NO and 2.5% O₂ in the feed gas and 0.05g s/cc of contact time(36,000 hr⁻¹ S.V.). Conversions are similar to those in Figures 4 and 5 obtained at higher contact time. Figure 9 also shows that the Ce(11)/Cu(119)-Z catalyst remained more active than Cu(141)-Z and Mg(34)/Cu(86)-Z below 400°C under these conditions.

The catalyst Ce(11)/Cu(119)-Z presented here gave higher NO conversion to N₂, compared with a Ce/Cu-Z material reported in the patent literature (15) (only 11% NO conversion to N₂ at 400°C under the conditions of Figure 9), which was prepared by exchanging Cu ions into the ZSM-5 first, followed by Ce ion exchange. Again, this shows that a proper mode of ion exchange is very important for a positive cocation effect.

Conclusion

Alkaline earth and transition metal ion-exchanged ZSM-5 zeolites further exchanged with copper ions are active catalysts for the NO decomposition reaction in the presence or absence of oxygen and over a wide range of temperatures (350 - 600°C). Proper mode of ion exchange is crucial for a positive cocation effect.

An extensive study of Mg/Cu-Z catalysts was performed in this work. The conversion and kinetic data indicate that the role of Mg ions is one of stabilizing the activity of copper ions, potentially by occupying the "hidden" sites of the zeolite. For the same total copper exchange level, the

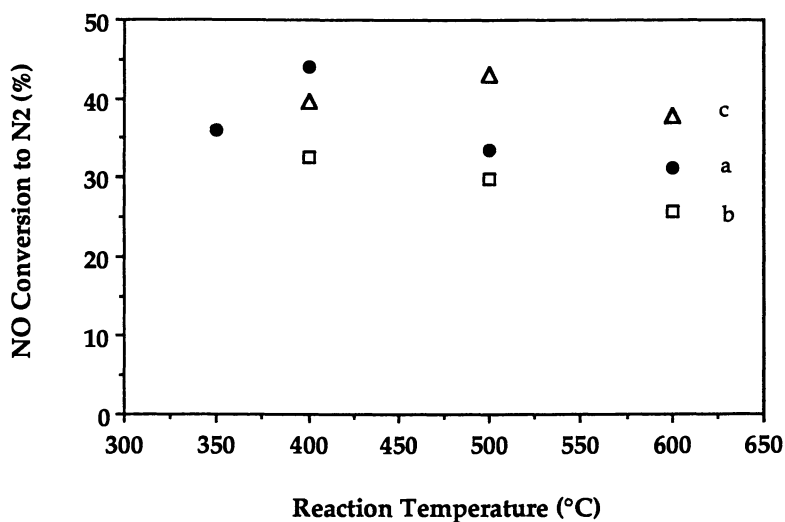


Fig. 9. NO decomposition over (a) Ce(11)/Cu(119)-Z; (b) Mg(34)/Cu(86)-Z; and (c) Cu(141)-Z at 0.2%NO, 2.5%O₂ and W/F=0.05g s/cc (STP).

Mg/Cu-Z catalysts show enhanced activity at high temperatures (450-600°C). Both the over-exchanged Cu-Z and the Mg/Cu-Z catalysts have low sensitivity to oxygen in dilute NO gases. At 600°C, a reaction order of zero in O₂ was found with the Mg(34)/Cu(86)-Z catalyst. Detailed kinetic studies with oxygen-containing gases are underway to further examine these effects.

The performance of (Ce, La)/Cu-Z catalysts is markedly different, the cocation effect being promotion of the Cu ion activity. This is displayed by the NO conversion to N₂ maximum shifting to lower temperatures ($\leq 400^\circ\text{C}$). The Ce(11)/Cu(119)-Z catalyst activity remained higher than that of the over-exchanged Cu(141)-Z in 2.5% oxygen, low NO content and high space velocity (36,000h⁻¹). Additional studies with rare earth modified Cu exchanged ZSM-5 are warranted.

Acknowledgments

Technical discussions with Dr. Zhicheng Hu of Engelhard Industries are greatly appreciated. Thanks are also due to Dr. Phil Thiel of the Davison Chemical Division of W.R. Grace Co. for the supply of ZSM-5 zeolites, and to the MIT Chemical Engineering undergraduate students Ernie Liang, Charles Armesto, Lizette Arce, and Katie Leo for assisting in catalyst preparation. Financial support for this project was provided by the U.S. Department of Energy/University Coal Research Program, under Grant No. DE-FG22-91PC923 with Dr. K. Das (DOE/METC) as Technical Project Officer.

Literature Cited

1. Iwamoto, M.; Furukawa, H.; Mine, Y.; Uemura, F.; Mikuriya, S.; Kagawa, S. *J. Chem. Soc. Chem. Commun.* **1986**, *15*, 1272-73.
2. Iwamoto, M.; Furukawa, H.; Kagawa, S. *Proceedings of the 7th International Zeolite Conference* (Ed. by Y. Murakami), Elsevier: Amsterdam, **1986**, pp17-21.
3. Iwamoto, M. *Future Opportunities in Catalytic and Separation Technology, Studies in Surface and Catalysis*, Elsevier: Amsterdam, **1990**, pp.121-143.
4. Li, Y.; Hall, W. J. *Phys. Chem.* **1990**, *94*, 6145-48.
5. Iwamoto, M.; Yahiro, H.; Shundo, Y.; Mizuno, N. *Appl. Catal.* **1991**, *69*, L15-19.
6. Iwamoto, M.; Yahiro, H.; Tanda, K.; Mizuno, N.; Mine, Y.; Kagawa, S. *J. Phys. Chem.* **1991**, *95*, 3727-30.
7. Li, Y.; Hall, W. J. *Catalysis*, **1991**, *129*, 202-215.
8. Kagawa, S.; Ogawa, H.; Furukawa, H.; Teraoka, Y. *Chem. Lett.* **1991**, 407-410.

9. Li, Y.; Armor, J. *Appl. Catal.* **1991**, *76*, L1-8.
10. Chu, P.; Dwyer, F. *Intrazeolite Chemistry, ACS Symposium Series 218*, **1983**, pp 59-77.
11. Kucherov, A. V.; Slinkin, A. A.; Kondrat'ev, D.A.; Bondarenko, T. N.; Rubinshtein, A. M.; Minachev, Kh. M. *Kinet. and Catal.* **1985**, *26*, 353-358.
12. Kucherov, A. V.; Slinkin, A. A.; Goryashenko, S. S.; Slovetskaja, K. I. *J. Catal.* **1989**, *118*, 459-465.
13. Shelef, M. *Catal. Lett.* **1992**, *15*, 305-310.
14. Zhang, Y, *Ph. D. Thesis* , Massachusetts Institute of Technology, Cambridge, (*work in progress*).
15. Li, Y.; Armor, J. N.; *U.S. Patent 5 149 512*, 1992.

RECEIVED September 29, 1993

Chapter 3

Reactivity of Cu-Based Zeolites and Oxides in the Conversion of NO in the Presence or Absence of O₂

G. Centi, C. Nigro, S. Perathoner, and G. Stella

Dipartimento di Chimica Industriale e dei Materiali, Via le
Risorgimento 4, 40136 Bologna, Italy

The reactivity of Cu-exchanged zeolites (ZSM-5 and Boralite) and Cu-loaded oxides (Al₂O₃, SiO₂, TiO₂ and ZrO₂) for the conversion of NO in the presence or absence of gaseous oxygen is compared. Cu-loaded oxides are active in NO conversion only when oxygen vacancies are created, whereas Cu-ZSM-5 shows a high stable activity, which, however, depends considerably on the NO concentration and formation of specific active sites. In the presence of O₂ a different reaction mechanism occurs and it is shown that O₂ can promote the conversion of NO to N₂, but at lower reaction temperatures and with a lower selectivity than those for the anaerobic decomposition. Furthermore, Cu-zeolites showing very different anaerobic activity in NO decomposition, have comparable behaviors in the aerobic conversion of NO. Cu-ZrO₂ and CuO-TiO₂ are different from CuO-Al₂O₃ and CuO-SiO₂, and the former show some analogies in the behavior with those of Cu-zeolites.

The direct conversion of NO to N₂ and O₂, even though thermodynamically feasible, occurs with rates too slow for practical applications and for several years no catalyst sufficiently active in this reaction could be found. The recent discovery of the high activity of Cu-ZSM-5 in this reaction (*1,2 and references therein*) has thus renewed interest in the decomposition of NO as an alternative possibility for the removal of NO in polluting emissions. An example is the reduction of NO in diesel-engine vehicle emissions for which noble-metal three-way catalysts do not operate efficiently. In the last two years, however, interest in the Cu-ZSM-5 system has shifted to its use in the reduction of NO in the presence of organic reducing agents (mainly hydrocarbons) (*3-7*), due to the

0097-6156/94/0552-0022\$08.00/0
© 1994 American Chemical Society

sensitivity of this system to poisoning (for example, by SO_2 (4)) and partial inhibition of the activity in the presence of O_2 . For the reduction of NO by organic compounds, on the contrary, oxygen promotes the reaction. However, it was soon found that several catalytic systems also are active in the conversion of NO by hydrocarbons and oxygen, including ZSM-5 exchanged with other transition metals, Cu-oxide supported on oxides such as alumina and the zeolite or oxide support itself (3-7), besides Cu-ZSM-5. On the contrary, Cu-ZSM-5 shows unique activity in the decomposition of NO even with respect to other Cu-zeolites. In addition, Cu-ZSM-5 also shows very high activity for the decomposition of N_2O (8), another reaction with interesting practical applications, but less demanding than decomposition of NO. On the other hand, $\text{CuO-Al}_2\text{O}_3$ is preferable over Cu-zeolites for the reduction of NO by NH_3/O_2 in the presence of a high concentration of SO_2 in order to realize the contemporaneous removal of SO_2 and NO from flue gas (9). CuO-SiO_2 samples are also active in this reaction (10). The presence of gaseous oxygen has a considerable influence on the activity of these samples in the reduction of NO by NH_3 . For example, the specific activity per copper ion in the presence of O_2 on Cu-SiO_2 decreases as copper loading increases and decreases in the absence of O_2 (11). The exact opposite effect is shown by the selectivity to N_2O in this reaction. In addition, an inverse correlation has been observed between activity in NO conversion by NH_3 in the presence and in the absence of gaseous oxygen of various copper-based samples (supported on different oxides or on zeolites (11)); the most active samples in the presence of O_2 were found to be the less active in the absence of O_2 .

Copper-based zeolites and oxides, therefore, show interesting catalytic properties in the conversion of nitrogen oxides to N_2 which can be usefully applied for the development of improved technologies for cleanup of polluting emissions, but there are two main open questions in the literature about i) the analogies or differences between the mechanisms of NO conversion and nature of active sites on copper-loaded oxides and zeolites and ii) the effect of O_2 in the modification of the surface reactivity of these two classes of samples. The aim of the research reported here was to contribute to the discussion of these questions reporting a comparison of the behavior of copper-based zeolites and oxides in NO conversion in the presence or not of gaseous oxygen.

Experimental

Copper-loaded oxides were prepared by an incipient wet impregnation method using copper-acetate solution and subsequent drying and calcination up to 450°C . If not otherwise indicated, the amount of copper in the various samples is 4.8% wt (as CuO). $\gamma\text{-Al}_2\text{O}_3$ (RP531 from Rhone-Poulenc, $115\text{ m}^2/\text{g}$), SiO_2 (RP540 from Rhone-Poulenc, $250\text{ m}^2/\text{g}$), ZrO_2 (prepared by the sol-gel method (11), $115\text{ m}^2/\text{g}$) and TiO_2 (prepared by the sol-gel method, $73\text{ m}^2/\text{g}$) were used as supports. The last one was obtained by controlled hydrolysis of titanium-isopropoxide in the presence of CH_3COOH . After calcination, the TiO_2 sample was in the anatase form, as confirmed by XRD analysis.

The Cu-exchanged zeolite samples were prepared following an ion-exchange procedure analogous to that reported by Iwamoto et al. (12) and Li and Hall (13). The

amount of copper exchanged was determined by a titrimetric method. Parent zeolites were commercial ZSM-5 (EKA-Nobel; $\text{SiO}_2/\text{Al}_2\text{O}_3 = 30$ or 49) and ZSM-5 synthesized according to the conventional procedure reported previously ($\text{SiO}_2/\text{Al}_2\text{O}_3 = 164$) (14). Boron pentasyl zeolite (hereinafter abbreviated as BOR; $\text{SiO}_2/\text{B}_2\text{O}_3=24$) was also synthesized using a similar procedure (14). The degree of ion-exchange was calculated as $2 \cdot (\text{amount of Cu})/(\text{amount of Al or B})$. Hereinafter the samples will be briefly indicated as Cu-ZSM-5(x,y) and Cu-BOR(x,y), where x indicates the $\text{SiO}_2/\text{Al}_2\text{O}_3$ or $\text{SiO}_2/\text{B}_2\text{O}_3$ ratio, respectively, and y the degree of ion exchange.

The catalytic tests of NO conversion were carried out in a quartz flow reactor at atmospheric pressure. The inlet and outlet flow of the reactor were continuously monitored by on-line mass quadrupole analysis with a suitable computer program to determine reagent and product compositions and to check the N, H and O balances. Details on the method of preparation of the various samples and on the methodology and apparatus for the catalytic tests have been reported previously (9,11).

Fourier-transform infrared (IR) measurements were made at room temperature in the transmission mode using the self-supported disk technique and a conventional IR vacuum cell and gas-manipulation ramp. Before adsorption of NO, the samples were evacuated (10^{-4} Torr) at 450°C , then cooled to room temperature in an oxygen atmosphere and finally gaseous oxygen was removed at room temperature following the method of Giamello et al. (15).

Results

Reactivity of NO on Copper-loaded Oxides. The pretreatment of the catalyst before the catalytic tests has a considerable influence on the transient activity of copper-loaded oxides in the conversion of NO to N_2 . This is shown in Table I which compares the anaerobic transient activity of CuO- Al_2O_3 in the NO conversion to N_2 of samples pretreated with O_2 , pure helium or H_2 . Helium induces a slight reduction of copper sites creating surface oxygen vacancies that are restored by the oxygen of NO which leads to the consequent formation of N_2 up to complete saturation of reduced sites. The transient activity in NO conversion of CuO- Al_2O_3 derives thus from the saturation of surface oxygen vacancies created during the pretreatment. More reducing pretreatments increase the number of sites created, but the activity declines to zero after enough time-on-stream in all cases. When O_2 is cofed with NO, a decrease in the transient activity is observed (Fig. 1a) due to the competition between O_2 and NO in the reoxidation of oxygen vacancies. It should be noted that the O_2 to NO inlet ratio is about 75. The transient activity in the conversion of NO, however, does not decrease proportionally (Fig. 1a), suggesting that NO has a higher reactivity than O_2 towards reoxidation of surface oxygen vacancies.

The presence of O_2 also modifies the selectivity to N_2 (Fig. 1b) which is 100% in the absence of O_2 and decreases to about 65-70% in the presence of O_2 due to the formation of N_2O . The selectivity, however, is nearly independent of the activity and thus of the number of oxygen vacancies, indicating the absence of cooperative effects between sites in the reaction mechanism. Changing the nature of the support for copper oxide in the

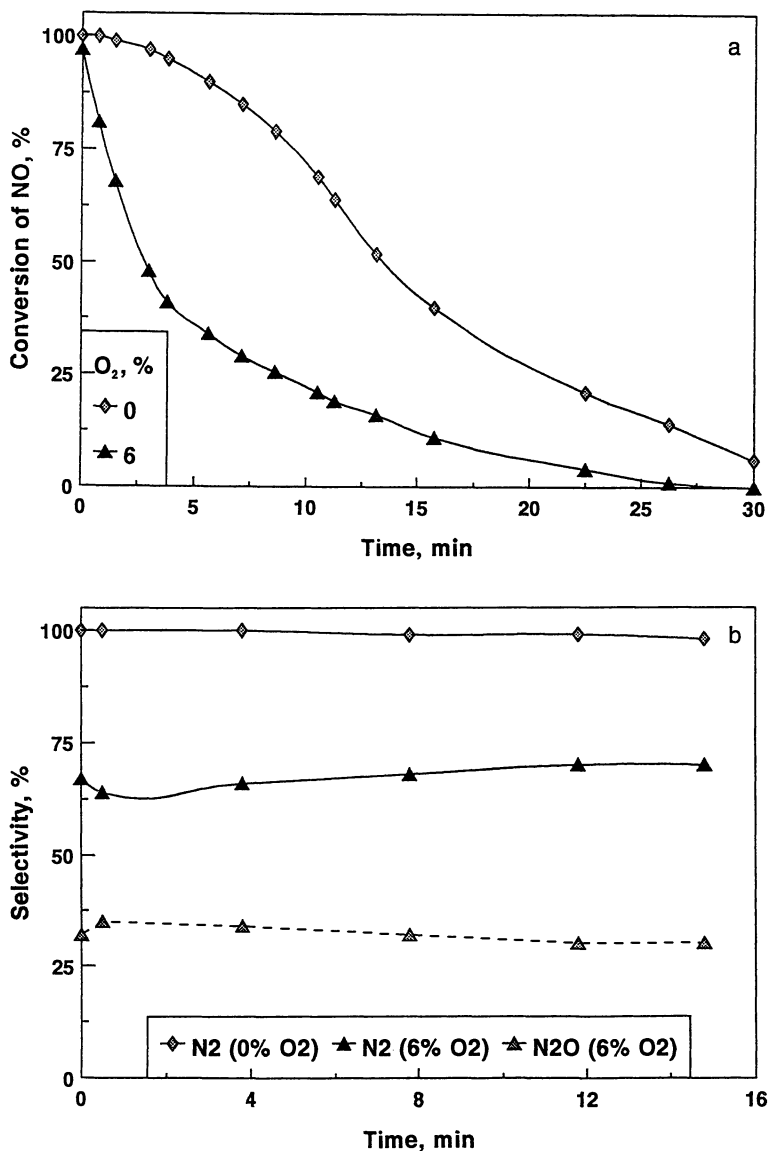


Fig. 1 Comparison of the transient conversion of NO at 300°C (a) and selectivity to by-products (b) of CuO-Al₂O₃ in the presence or absence of O₂ in the feed. Sample pretreatment: 450°C for 30 min in a flow of 2% H₂/helium followed by cooling to 300°C in helium. Experimental conditions: 800 ppm NO, 0% or 6% O₂, W/F_{Ao} = 2.5·10⁻² g·h/l.

Table I. Conversion of NO at 300°C on CuO-Al₂O₃ as a function of time-on-stream and of the type of pretreatment

Time-on-stream, min	NO conversion, %		
	Type of pretreatment		
	O ₂	He	H ₂
0	3	100	100
5	0.2	32	92
10	-	5	70
15	-	0.2	40
20	-	-	7
30	-	-	-

Pretreatment at 450°C for 30 min [O₂ (flow of 6% O₂ in helium), He (flow of pure helium) and H₂ (flow of 2% H₂ in helium)] followed by cooling to 300°C in a helium flow. Exp. conditions: 800 ppm NO, W/F_{A0} = 2.5 · 10⁻² g · h/l.

SiO₂, TiO₂, and ZrO₂ series qualitatively similar results were obtained. In all cases, only transient activity in NO conversion after a preliminary reduction is observed, without any significant activity in steady-state conditions up to about 500°C.

Effect of O₂. In the presence of O₂, on the contrary, the nature of the support influences considerably the type of by-products in NO conversion. On CuO-Al₂O₃ and CuO-SiO₂, when the pretreatment is made in an O₂/Helium flow, no reaction products are observed in the entire range of reaction temperatures up to 500°C using as reactants 1000 ppm NO and 6% O₂. For lower reaction temperatures (around 300°C) in the first 5 minutes of time-on-stream a small conversion of NO is noted (around 5-10%), but due only to the formation of adsorbed species (no reaction products). After approximately 5 min the conversion of NO is nearly zero. On the contrary, using TiO₂ and ZrO₂ as supports for CuO, a strong adsorption of NO is observed for over 3 hours of time-on-stream as well as the formation of NO₂ and N₂O as reaction products (Fig. 2 *a* and *b*, respectively). Very small amounts of N₂ were also noted (of the order of 20 ppm), but due to the highly probable error in such determinations deriving from the possible leakage of air, they are omitted from the Figures. The formation of NO₂ and N₂O takes account of about 20-30% of the fraction of converted NO. The lack of N balance is due to adsorbed species remaining on the catalyst. No other reaction products were, in fact, noted. Furthermore, when the temperature of the catalyst was raised after these catalytic tests, the clear desorption of nitrogen oxide species was observed (see below). It should also be noted that without O₂, NO does not adsorb on the catalyst. In fact, any product desorbs from the catalyst surface after the interaction with NO at 300°C when the reaction temperature is

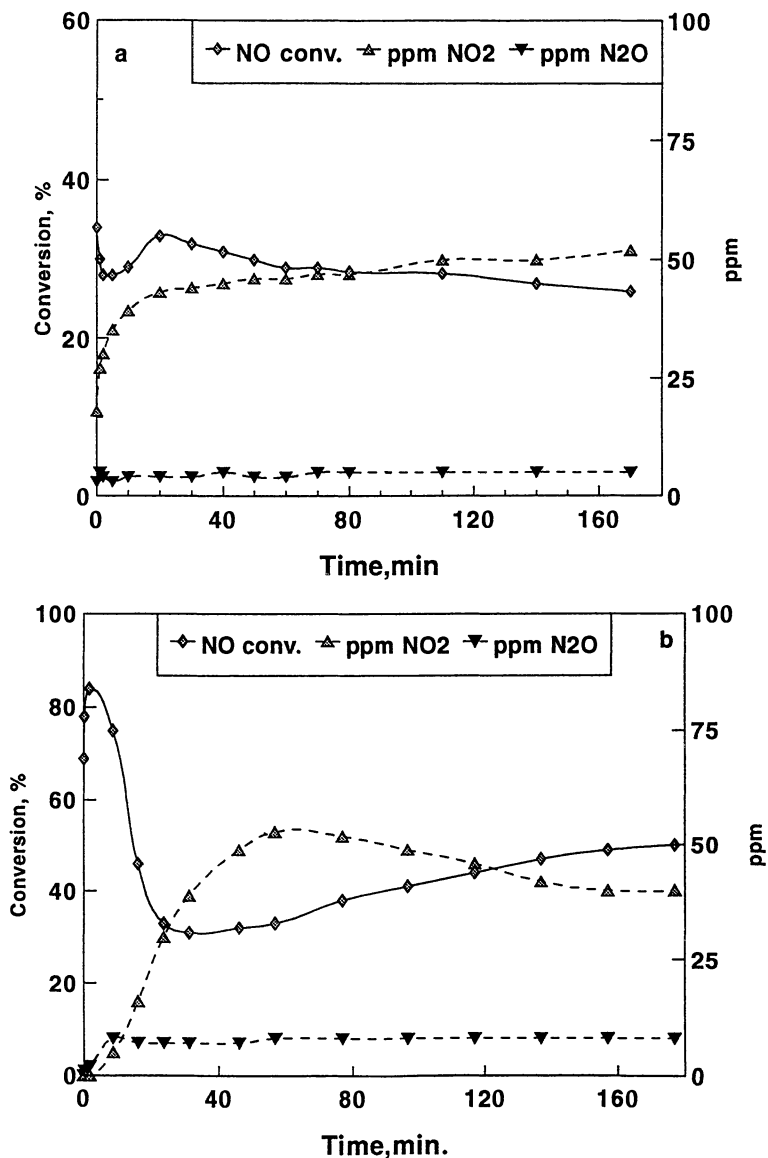


Fig. 2 Conversion of NO in the presence of O₂ and formation of by-products on CuO-TiO₂ (a) and CuO-ZrO₂ (b). Sample pretreatment: at the same reaction temperature (450°C for 30 min) in a flow of 6% O₂/helium. Exp. conditions: 0.5 g of sample, 6 L/h total flow rate, 1000 ppm NO, 6% O₂, reaction temperature 400°C (a) and 350°C (b).

increased up to 500°C. On the contrary, when NO interacts with the catalyst in the presence of O₂, relevant amounts of desorption products are observed. This clearly indicates that these adsorption phenomena are related to the products of transformation of NO in the presence of oxygen or to surface changes induced from the presence of O₂.

The analysis of the products of thermal desorption after these catalytic tests (Fig. 3) showed that a temperature increase of the samples leads to the desorption of O₂, NO and N₂O. These desorption products reasonably derive from the thermal decomposition of surface nitrite- or nitrate-like species formed by oxidation of NO by O₂ during the catalytic tests at 300°C. It is worthwhile to note that apparently two different species are present on the surface, one which decomposes at around 330°C and another which decomposes at higher temperatures (around 400°C). In fact, two distinct peaks for oxygen are noted (Fig. 3). The two adsorbed nitrogen oxide species, however, give rise to two different reaction products, the first one forming N₂O and the second one reforming NO. N₂O is also one of the reaction products observed, although in low amounts, indicating the apparently unexpected effect of a reduction of NO catalyzed from O₂. Both CuO-ZrO₂ and CuO-TiO₂, in fact, are inactive towards NO conversion in the absence of O₂, when prereducing treatments are avoided. It should also be pointed out that for the first desorption peak at around 330°C (Fig. 3) the formation of O₂ is higher than that of N₂O, the opposite of that observed for the higher temperature desorption peak. This suggests that the formation of N₂O does not derive from the disproportionation of a (NO)₂ dimer forming N₂O and 0.5O₂ or an exchange reaction between 3 NO to form N₂O and NO₂, but rather from a different mechanism. A tentative suggestion is that the reaction occurs between a (NO₂)^{δ+} and (NO₃)^{δ-} - like adsorbed species to form N₂O and 2O₂. More detailed studies are obviously necessary to clarify this mechanism and the differences in the behavior in comparison with copper-alumina and silica samples. The higher temperature desorption peak, on the contrary, derives from the simple decomposition of a nitrate-like species to reform NO and O₂. Results in line with these observations have been noted in a study of the products of thermal decomposition after adsorption of NO and NO₂ over Cu-ZSM-5 samples (16).

Activity of Cu-Zeolite Samples. In contrast to the behavior of copper-loaded oxide samples, Cu-ZSM-5 shows a high activity in the anaerobic decomposition of NO (conversion up to over 90%, depending on the reaction conditions and level of copper exchange) with a maximum in NO conversion at about 500°C, in agreement with literature results (1,12,13). N₂ is selectively formed in this reaction with minor amounts of NO₂ (selectivity of around 2-4%) deriving probably from the catalyzed oxidation of NO by the O₂ generated in the decomposition reaction. In fact, homogeneous, secondary reactions downstream from the reactor were minimized by heating all connection lines up to the head of the mass quadrupole detector used to monitor the composition in these experiments.

The activity of Cu-ZSM-5 depends considerably on the concentration of NO. Figure 4 shows that high conversions of NO are possible only for high concentrations of NO

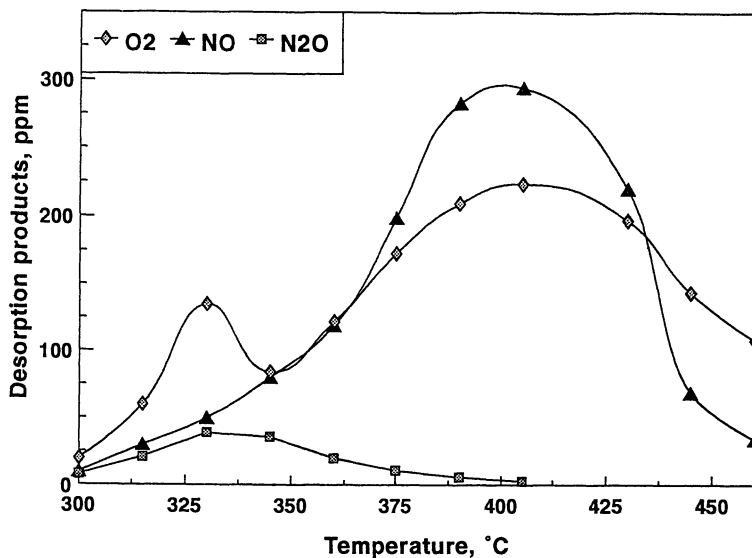


Fig. 3 Products of thermal desorption (reaction temperature increased at a rate of 20°C/min) in a helium flow (6 L/h) of CuO-ZrO₂ after 3 hours of time-on-stream at 300°C in the presence of 1000 ppm NO and 6% O₂. Before increasing the reaction temperature, gaseous species were removed in a helium flow for 5 min at 300°C.

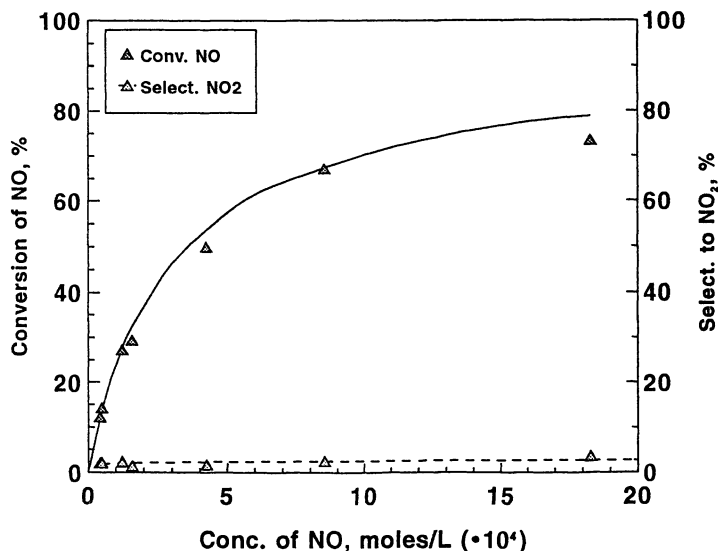


Fig. 4 Effect of NO concentration on the conversion of NO and selectivity to NO₂ (the remaining being N₂) at 500°C over Cu-ZSM-5(49,115). Experimental conditions: 1.5 g of catalyst, 6 L/h total flow rate.

(above around 10000 ppm), a negative aspect for what concerns the potential applicability of the catalyst. In fact, the fitting of the experimental results shows that the apparent reaction order for the dependence of the NO depletion rate from the concentration of NO is around 1.8. The fitting is based on the use of a monodimensional plug-flow reactor and an irreversible reaction of order n . In order to derive a reasonable kinetic reaction model which can explain this order of reaction, it is useful to utilize a Langmuir-Hinshelwood (LH) approach. It should be noted that various infrared evidences suggest as key step in the mechanism the formation of a dinitrosyl species on copper ions (15,17,18). It is possible thus to derive a LH kinetic reaction model based on the decomposition of a dinitrosyl species reversibly formed from a mononitrosyl species. The following reaction rate of NO depletion can be thus derived:

$$r = \frac{(k_1 \cdot l_{tot}) \cdot K_1 \cdot K_2 \cdot [NO]^2}{1 + K_1 \cdot [NO] + K_1 \cdot K_2 \cdot [NO]^2} \quad (1)$$

where l_{tot} indicates the total number of active sites, K_1 and K_2 the equilibrium constants for the reversible formation of mono- and di-nitrosyl species and k_1 the specific rate constant per active site. The values of conversion (solid line in Fig. 4) calculated using this rate expression [eq. (1)] and a monodimensional PFR reactor model correctly fit the experimental results at 500°C using the following kinetic parameters determined from non-linear regression analysis: $(k_1 \cdot l_{tot}) = 1.441 \cdot 10^{-2}$, $K_1 = 8.684 \cdot 10^2$ and $K_2 = 1.082 \cdot 10^{-1}$. This reaction model agrees with our IR evidences (see below) taking into account that IR data show only relatively stable surface species. Reaction intermediates may be thus evidenced only when their transformation is slowed down significantly making the IR studies at much lower temperatures than those of catalytic tests. At higher temperatures, however, the reaction mechanism may be different. The correct fitting of the experimental results (Fig. 4) using a kinetic model based on the reversible formation of dinitrosyl species, on the other hand, supports the correctness of the hypothesis of mechanism.

The nature of the copper species present in the zeolite considerably influences the catalytic behavior in the decomposition of NO. Compared in Fig. 5 are the activities in the anaerobic decomposition of NO of four Cu-zeolite samples. In the first two the SiO_2/Al_2O_3 ratio of the zeolite is 49, in the third the Al content is three times lower ($SiO_2/Al_2O_3 = 164$) and finally in the last sample Al was substituted with B ($SiO_2/B_2O_3 = 24$) in order to have a high number of Brønsted acid sites, together with a much lower acid strength (19). The preparation procedure for these four samples was exactly the same (ion-exchange with dilute aqueous Cu-acetate solution of the zeolite in the Na^+ form), except for the Cu-ZSM-5(49,115) sample for which the exchange procedure was repeated three times in order to increase the degree of copper exchange. Figure 5 also summarizes the amount of copper in these samples; in all cases neither crystalline CuO was observed by XRD analysis nor the presence of a separate phase of amorphous copper oxide was

Table II. Summary of the nitrogen oxide species detected by infrared analysis after 10 min in contact at room temperature with 55 torr of NO on Cu-ZSM-5(49,115) (a), Cu-ZSM-5(64,264) (b) and Cu-ZSM-5(49,60) (c)

<i>sample</i>	<i>IR band, cm⁻¹</i>	<i>attribution</i>
a,b,c	2131	(NO ₂) ^{δ+} - [Cu ²⁺]
a,c	1912	NO ^{δ+} - [Cu ²⁺]
b	1890	NO - [Cu ²⁺ or Na ⁺]
a,c	1823,1734	(NO) ₂ - [Cu ²⁺]
a,c	1811	NO ^{δ-} - [Cu ⁺]
a,b	1626,1613,1571	(NO ₂) ⁻ - [Cu ²⁺]

found by scanning electron microscopy. The results clearly show that notwithstanding the apparent analogy between these samples, very different activities can be obtained in the anaerobic decomposition of NO.

Infrared data, summarized in Table II, give some useful further data to clarify this different behavior, taking into account the above discussed limits of the information on the reaction mechanism which can be derived from IR studies. Various nitrogen oxide species form by interaction of NO at room temperature on the samples pretreated at 450°C under vacuum in order to clean the surface, but then cooled to room temperature in an O₂ atmosphere in order to have mainly Cu²⁺ ions; gaseous O₂ was then removed at room temperature. On the most active sample [Cu-ZSM-5(49,115)] mono- (both partially positively and negatively charged due to the interaction with Cu²⁺ or Cu⁺ ions) and dinitrosyl species were detected together with a partially positive NO₂ species and nitrite-like species. The dinitrosyl species, in particular, rapidly disappear for longer contact times. In the same sample with a lower Cu-exchange level [Cu-ZSM-5(49,60)] the same species are present, but the series of bands connected to the nitrite-like species are much less intense. On the contrary, in the sample with a very low activity [Cu-ZSM-5(164,264)] and similarly in the BOR(24,38) sample, the bands attributed to the dinitrosyl species and to negatively charged mononitrosyl species are absent, the band attributed to a positively charged mononitrosyl species shifts from 1912 to 1890 cm⁻¹ indicating the weakening of coordination with Cu²⁺ ions, and the series of bands near 1600 cm⁻¹ attributed to (NO₂)⁻-like species become the most intense. It should also be mentioned that IR characterization of NO adsorption on CuO-ZrO₂ and CuO-Al₂O₃ also shows the presence of a band centred near 1890 cm⁻¹ in both samples, indicating the very weak coordination to Cu²⁺ ions.

In conclusion, IR evidences, in agreement with literature data (15,17,18), indicate that only when copper ions interact with the strong Brønsted acid sites of the zeolite to form isolated Cu²⁺ species (made more ionic by the coordination to Al) may partially

positive mononitrosyl species and dinitrosyl species form which are intermediate to N_2 formation.

Conversion of NO in the Presence of O_2 . Compared in Figure 6 is the activity of Cu-ZSM-5(49,115), Cu-ZSM-5(164,264) and Cu-BOR(24,38) samples in the conversion of NO in the presence of 6% O_2 . On the contrary to the literature data (1,12,13), which indicate that O_2 deactivates the conversion of NO at 500°C on Cu-ZSM-5 due to the inhibition of the spontaneous reduction of copper ions, we found that the presence of oxygen promotes the conversion of NO at low temperatures (around 250°C). In fact, in the absence of O_2 , all these samples are inactive at these low temperatures. In the presence of O_2 , a maximum in activity at around 350°C is observed (Fig. 6). This temperature nearly corresponds to that for the maximum in the rate of the reversible formation of NO_2 from NO and O_2 . NO_2 , in agreement, is one of the main reaction products due to the catalyzed oxidation of NO. In fact, it was found that the conversion of NO depends on the amount of catalyst (Cu-ZSM-5), with a selectivity to NO_2 nearly independent of the conversion. However, together with a product of oxidation of NO, products of reduction of NO (N_2O , N_2) are also detected (see below). It should be also evidenced that the aerobic activity of Cu-zeolites significantly changes with time-on-stream (Fig. 7). The conversion of NO is initially nearly total, but rapidly declines after around 1 hour of time on stream up to nearly steady-state conditions. In addition, a significant lack of N balance is noted for the shorter times-on-stream. The formation of all products, in fact, is initially low and increases progressively. Furthermore, heating of the catalyst in a helium flow up to 500°C induces the desorption of significant amounts of NO, O_2 , N_2O and N_2 , similarly to what observed for CuO-ZrO₂ (Fig. 3) apart from a higher desorption of N_2O and N_2 . The formation of reduction products in the conversion of NO in the presence of O_2 is clearly the most interesting aspect. The conversion of NO is not selective to N_2 , but the results evidence that different surface pathways of NO conversion in the presence of O_2 may lead also to reduction products in conditions where the zeolite is not active without O_2 . It is interesting to observe that the formation of all products increases with time-on-stream up to arrive to a nearly steady-state condition after around 1 hour. Reasonably, this effect may be attributed to the formation and increase on the surface of the catalyst of adsorbed nitrogen oxide species. Further transformation of these surface species leads to the formation of reduction products of NO, tentatively with a mechanism similar to that previously discussed for the formation of N_2O on CuO-ZrO₂.

Figure 8 compares the catalytic behavior at 250°C after 1 hour of time-on-stream in the presence of O_2 of the same samples of Fig. 6. The different Cu-zeolites show similar behavior, apart from minor changes in the activity and selectivity to the various products, notwithstanding the considerable difference in activity shown in the anaerobic conversion of NO at higher temperature (compare Fig. 5 and Fig. 6). This suggests that at lower reaction temperatures and in the presence of O_2 the nature of the active sites and the reaction pathways for NO conversion markedly differ from those in the anaerobic decomposition, even if N_2 forms in both cases.

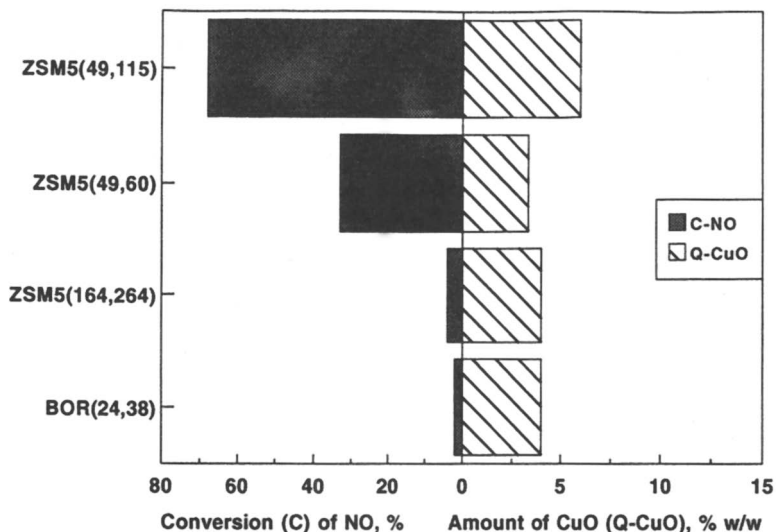


Fig. 5 Comparison of the conversion of NO at 500°C in the anaerobic decomposition of NO over Cu-ZSM-5(49,115), Cu-ZSM-5(49,60), Cu-ZSM-5(164,264) and BOR(24,38). For nomenclature of these samples see Experimental. The amount of copper in these samples, expressed as % w/w of CuO, is also given in the Figure. Experimental conditions: 4% NO, 1.5 g of catalyst, 6 L/h total flow rate.

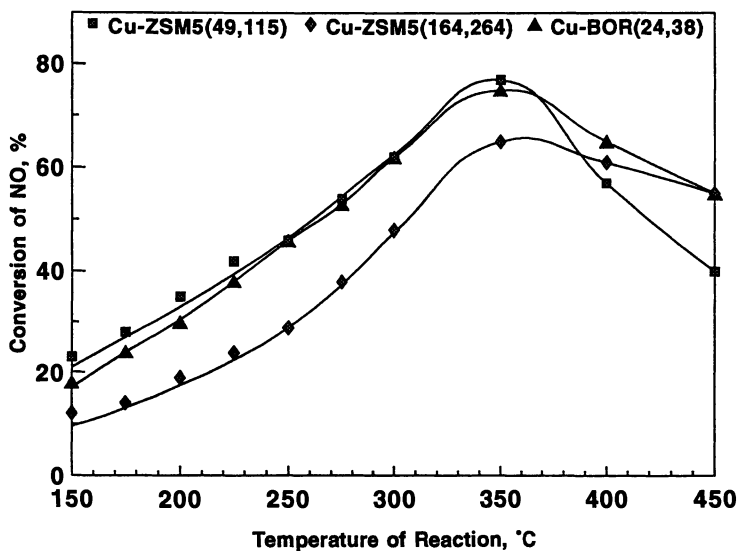


Fig. 6 Effect of the reaction temperature in the conversion of NO in the presence of O₂ over Cu-ZSM-5(49,115), Cu-ZSM-5(164,264) and Cu-BOR(24,38). Experimental conditions: 1000 ppm NO, 6% O₂, 0.5g of catalyst, 6 L/h total flow rate. Conversion data after 1 hour of time-on-stream.

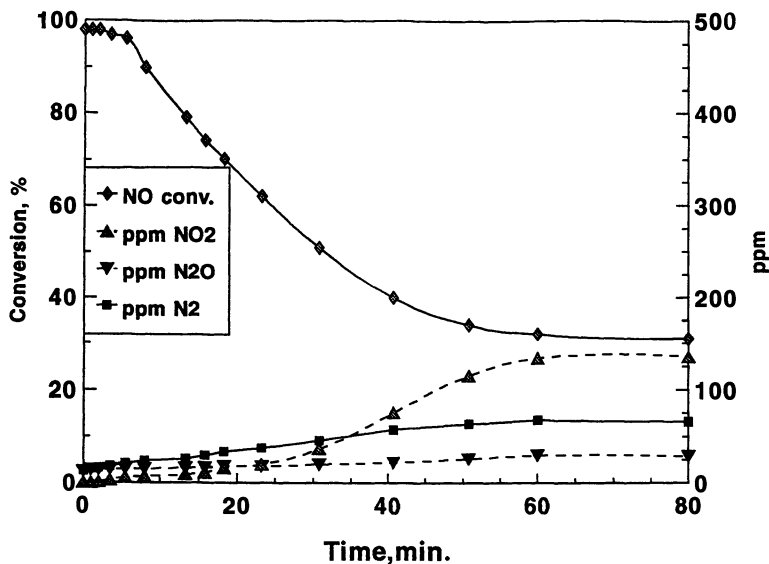


Fig. 7 Transient activity of Cu-ZSM-5(49,115) in the conversion of NO in the presence of O₂ at 250°C. Experimental conditions as in Fig. 6.

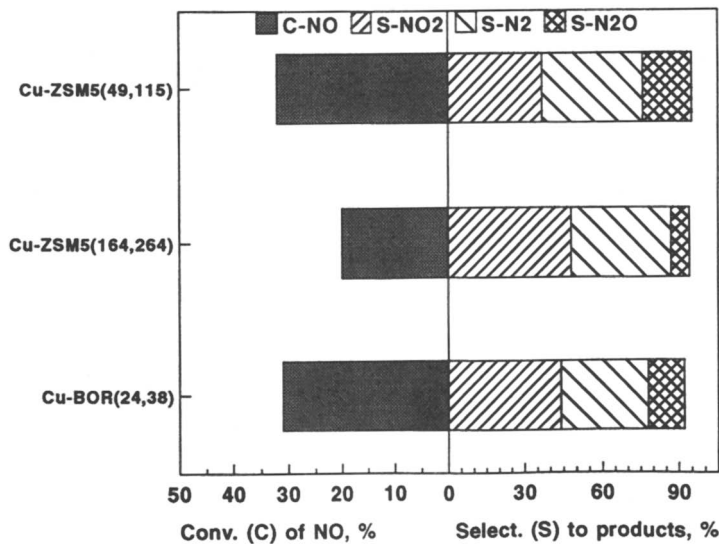


Fig. 8 Comparison of the conversion of NO and selectivity to NO₂, N₂O and N₂ at 250°C in the presence of O₂ on Cu-ZSM-5(49,115), Cu-ZSM-5(164,264) and Cu-BOR(24,38). Experimental conditions: 1000 ppm NO, 6% O₂, 0.5g of catalyst, 6 L/h total flow rate. Catalytic data after 1 hour of time-on-stream.

Table III. Comparison of the conversion of NO and selectivity to products at 250°C (after 2 hours of time-on-stream) over Cu-ZSM-5(49,115) and over the parent zeolite not exchanged with copper [H-ZSM-5(49)]

Sample	Conv. NO, %	Selectivity, %		
		NO ₂	N ₂	N ₂ O
Cu-ZSM-5(49,115)	32	37	39	19
H-ZSM-5(49)	59	78	-	20

Exp. conditions: 1000 ppm NO, 6% O₂, 0.5g of catalyst, 6 L/h total flow rate.

The anaerobic activity toward formation of N₂ from NO can be attributed to the presence of copper. Table III, in fact, compares the activity at 250°C of Cu-ZSM-5(49,115) with that of the corresponding parent zeolite (H⁺ form) not exchanged with copper [H-ZSM-5(49)]. The parent zeolite is more active toward NO conversion to NO₂, but does not form N₂. Only low selectivities to N₂O are observed.

Discussion

Influence of O₂ on the Reaction Mechanism of NO Conversion. Two main transformation mechanisms have been proposed to explain the activity of Cu-ZSM-5 in the decomposition of NO (1,13,15,17,18,20): *i*) a redox mechanism based on the spontaneous reduction of copper sites on the zeolite and reoxidation by NO (the first step is the rate determining) and *ii*) a mechanism involving the intermediate formation of a dinitrosyl copper species which then decomposes directly to N₂ + O₂ or via a more complex mechanism with the intermediate formation of an oxidized nitrogen oxide species (Cu-NO₂ like). The two mechanisms have obvious analogies and, in fact, it was observed that the oxidation state of copper (Cu²⁺ and Cu⁺) has a significant role on the nature of adsorbed nitrogen oxide species. Nevertheless, the presence of oxygen has a different effect in the two cases: in the first oxygen simply competes with NO for the reoxidation of reduced copper sites, whereas in the second case modifies the nature of the adsorbed species. According to the first mechanism thus only an inhibition may be expected, but in the second case more complex phenomena may occur and a promotion in some cases can be also expected. Literature data (1,13) clearly show that at high temperature (around 500°C) oxygen deactivates the conversion of NO on Cu-ZSM-5 and our result are in agreement with this indication. However, we found in addition that at low reaction temperatures (around 250°C) oxygen promotes the conversion of NO due to its catalyzed oxidation to NO₂, giving rise also to the formation of reduction products of NO (N₂O and N₂).

The reaction at low temperature in the presence of oxygen (LTO) is thus not selective to N₂ such as that at high temperature (HTA) which is deactivated by oxygen. However, LTO results indicate that a different reaction pathway on Cu-zeolites may be also possible

which leads also to the formation of N_2 , even though not selectively. Reasonably, thus, different mechanisms of NO conversion are predominant in the two reaction conditions.

It is also interesting to note that also different copper species may be responsible for the two reaction mechanisms. For the HTA mechanism isolated copper ions interacting with the strong Brønsted sites of ZSM-5 are required, whereas in the LTO mechanism different copper species are important, even though the comparison with the behavior of Cu-loaded oxides evidences a specific role of the zeolite structure also in this case.

Present data do not allow to discuss in deep the possible mechanism of promotion by O_2 of NO conversion at low temperature. It may be observed, however, that H-ZSM-5 is active in the oxidation of NO to NO_2 , but not in the formation of reduction products of NO (Table III), apart from small amounts of N_2O . In addition, the formation of these reduction products may be tentatively attributed to the further transformation of adsorbed nitrogen oxides species, reasonably oxidized, formed initially from the interaction of NO and O_2 with the catalyst surface (Fig. 7). Analysis of the products of thermal desorption after the catalytic tests in NO+ O_2 conversion on CuO-Zr O_2 (Fig. 3) suggests the possible mechanism of N_2O formation by reaction between $(NO_2)^{\delta+}$ and $(NO_3)^{\delta-}$ like adsorbed species. This hypothesis of mechanism is based only on the stoichiometry of N_2O and O_2 desorption products (Fig. 3), but is also in agreement with IR data on the nature of adsorbed nitrogen oxide species. Obviously these data do not proof this mechanism which requires much more detailed studies, but can be considered as a working tentative hypothesis for the analysis of the catalytic effects discussed above. It should be noted, however, that recent literature data (21) further support this hypothesis. A similar mechanism may also explain the formation of N_2O in the LTO mechanism on Cu-zeolites, whereas the formation of N_2 reasonably derives from the consecutive transformation of N_2O . Cu-zeolites in comparison with CuO-Zr O_2 and CuO-Ti O_2 sample have thus tentatively a higher rate of N_2O formation from adsorbed oxidized nitrogen oxide species and higher rate of the consecutive decomposition of this intermediate to N_2 . More studies, however, are necessary to demonstrate this tentative reaction mechanism.

Comparison between Cu-based Zeolites and Oxides. After a slight prereduction such as the simple treatment at 450°C with a helium flow, all CuO loaded oxides are initially very active in NO decomposition even at low temperature (300°C), but rapidly the activity declines to zero. This suggests that a main difference between Cu-based oxides and Cu-ZSM-5 is the much higher rate of spontaneous reduction of copper sites in the latter sample, which lead to the higher steady-state activity in NO decomposition. On the other hand, IR data evidence also the different nature of adsorbed nitrogen oxide species in the two series of samples (Table II and text). In particular, in Cu-ZSM-5 the stretching of the mononitrosyl species (positively charged) is found at higher frequency (1912 cm^{-1}) in comparison with the corresponding one in Cu- loaded oxides or inactive Cu-zeolites (1890 cm^{-1}). This indicates the stronger coordination of NO with Cu $^{2+}$ ions in active Cu-ZSM-5 with respect to other samples. The formation of dinitrosyl species in this sample can be also detected. These evidences point out the different electronic

characteristics of surface copper ions in the active or not active samples towards steady-state anaerobic decomposition of NO. The shift to higher frequencies of NO stretching implies a higher electron donation to copper ions with a consequent weakening of N-O bond and thus easier pathway towards decomposition. On the other hand, the higher electron acceptor characteristics of copper ions in the Cu-ZSM-5 zeolite and lower tendency towards back donation to NO, implies also the easier tendency in the spontaneous reduction of copper by loss of oxygen. It is thus evident that these two aspects are closely related. Results also indicate that these characteristics of copper ions derive from the type of interaction with the strong Brønsted sites of the zeolite. When this interaction does not occur, this specific copper species does not form and the zeolite is inactive in the high temperature anaerobic decomposition of NO.

In the presence of O₂ and at lower reaction temperatures, however, different types of surface properties becomes important. It is also worthnoting that H-ZSM-5 is very active in the oxidation of NO to NO₂. This suggests a possible specific role of acid site or more reasonably of defect sites of the zeolite induced by the interaction of oxygen with strong Brønsted sites in analogy with the interpretation of the enhanced low temperature aromatization rate of propane in the presence of O₂ on H-ZSM-5 (22). CuO-ZrO₂ and CuO-TiO₂ are also active in the oxidation of NO to NO₂, on the contrary of CuO-Al₂O₃ and CuO-SiO₂ samples. The oxidation of NO to NO₂ and the parallel formation of relevant amounts of adsorbed nitrogen oxide species are thus key factors which determine the possibility of further conversion to reduced nitrogen oxide species. These factors are apparently more related to the acid-base characteristics of the catalyst or to the surface changes induced by oxygen than to the presence of specific copper species. The latter, however, are important for the further transformation of these adsorbed oxidized nitrogen species, even though they seem to be not the only one active, because small amounts of N₂O using H-ZSM-5 are also observed (Table III). Present data do not allow to discuss more in deep the nature of the possible copper species responsible for the further transformation of adsorbed nitrogen oxides to N₂O and N₂, but Cu-zeolites show also in this case a higher activity with respect to CuO-ZrO₂ and CuO-TiO₂. Cu-oxide on alumina or silica, on the contrary, are inactive in the step of NO oxidation.

Conclusions

The analysis of the effect of O₂ on the reactivity of various copper-based samples supported on oxide or zeolites has shown that O₂ markedly modifies the surface reactivity of copper species toward NO conversion. Furthermore, the results suggest that different types of copper species are probably active in the presence of O₂ with respect to those responsible for the high activity of Cu-ZSM-5 in the anaerobic decomposition of NO. The reactivity of copper-based samples in the reduction of NO by organics in the presence of O₂ thus probably involves different active sites than those necessary for the decomposition of NO.

It should also be pointed out that the results obtained for the aerobic NO decomposition on Cu-zeolites indicate that conversion of NO is promoted at low temperatures by the

presence of O₂ with the non-selective formation of products of reduction (N₂, N₂O) together with products of oxidation (NO₂). On the contrary, N₂ is selectively formed at higher reaction temperatures, but O₂ deactivates this reaction. This suggests a difference in the reaction mechanism between low and high reaction temperatures. Even though the reaction mechanism may be only tentatively hypothesized, results suggest the possibility of disproportionation between (NO₂)^{δ+} and nitrite- nitrate-like species to give N₂ or N₂O and O₂.

Literature Cited

1. Iwamoto, M.; Hamada, H. *Catal. Today*, **1991**, *10*, 57.
2. Armor, J.N. *Appl. Catal.B: Environm.*, **1992**, *1*, 221.
3. Sato, S.; Yu-U, Y.; Yahiro, H.; Mizuno, N.; Iwamoto, M. *Appl. Catal.*, **1991**, *70*, L1.
4. Iwamoto, M.; Yahiro, H.; Shuido, S.; Yu-u, Y.; Mizuno, N. *Appl. Catal.*, **1991**, *69*, L15.
5. Li, Y.; Armor, J.N. *Appl. Catal. B: Environ.*, **1992**, *1*, 231.
6. d'Itri, J.L.; Sachtler, W.M.H. *Catal. Letters*, **1992**, *15*, 289.
7. Hamada, H.; Kintaichi, Y.; Sasaki, M.; Ito, T.; Tabata, M. *Appl. Catal.*, **1991**, *75*, L1.
8. Li, Y.; Armor, J.N. *Appl. Catal.B: Environm.*, **1992**, *1*, L21.
9. Centi, G.; Passarini, N.; Perathoner, S.; Riva, A. *Ind. Eng. Chem. Research*, **1992**, *31*, 1947.
10. Kiel, J.H.A.; Prins, W.; van Swaaij, W.P.M. *Appl. Catal.B:Environmental*, **1992**, *1*, 13.
11. Centi, G.; Nigro, C.; Perathoner, S.; Stella, G. *Catal. Today*, **1993**, *17*, 159.
12. Iwamoto, M.; Yahiro, H.; Tanda, K.; Mizuno, N.; Mine, Y.; Kagawa, S. *J. Phys. Chem.*, **1991**, *95*, 3727.
13. Li, Y.; Hall, W.K. *J. Phys. Chem.*, **1990**, *94*, 6145.
14. Zatorski, L.W.; Centi, G.; Lopez Nieto, J.; Trifirò, F.; Bellussi, G.; Fattore, V. In "Zeolites: Facts, Figures, Future", P.A. Jacobs, R.A. van Santen Eds., Elsevier Science Pub.: Amsterdam 1989, Vol. 2, p. 1243.
15. Giamello, E.; Murphy, D.; Magnacca, G.; Morterra, C.; Shioya, Y.; Nomura, T.; Ampo, M. *J. Catal.*, **1992**, *136*, 510.
16. Li, Y.; Armor, J.N. *Appl. Catal.*, **1991**, *76*, L1.
17. Spoto, G.; Bordiga, S.; Scarano, D.; Zecchina, A. *Catal. Letters*, **1992**, *13*, 39.
18. Valyon, J.; Hall, W.K. in "New Frontiers in Catalysis", Proceedings 10th International Congress on Catalysis, Budapest 1992, L. Guzzi, F. Solymosi, P. Tetenyi Eds., Elsevier Science pub. 1993, p. 1339.
19. Courdurier, G.; Vadrine, J.C., in "New Developments in Zeolite Science and and Technology", Y. Murakami, A. Iijima, J.W. Ward Eds., Elsevier Science Pub.: Amsterdam 1986, p. 643.
20. Li, Y.; Hall, W.K. *J. Catal.*, **1991**, *129*, 202.
21. Hierl, R.; Urbach, H.-P.; Knozinger, H. *J. Chem. Soc. Faraday Trans.*, **1992**, *88*, (1992).
22. Centi, G.; Golinelli, G. *J. Catal.*, **1989**, *119*, 113.

RECEIVED September 29, 1993

Chapter 4

Deactivation of Cu-ZSM-5

Probable Irrelevance of Modest Zeolite Degradation Compared to Cupric Sintering to CuO

Karl C. C. Kharas¹, Heinz J. Robota¹, and Abhaya Datye²

¹AlliedSignal Research & Technology, Des Plaines, IL 60017–5016

²The University of New Mexico, Albuquerque, NM 87131–1341

Cu-zeolite catalysts enable NO_x reduction in gas streams that model oxidizing emissions from advanced lean-burn engines but are not durable and deactivate after catalysis at 800 °C. Precisely determined variation of micropore volumes correlate well with catalyst deactivation. CuO can be observed in catalytically or hydrothermally deactivated catalysts but not in fresh catalysts by XRD. High resolution TEM reveals a loss of crystallinity of the zeolite in thin regions of the exterior surfaces of zeolite crystal grains. Two phenomena accompany, and probably cause, catalyst deactivation: 1. superficial amorphization of the crystalline zeolite and 2. sintering of CuO and resultant local destruction of zeolite crystallinity in the vicinity of sintering oxides of Cu.

Cu-ZSM-5 can reduce NO under net oxidizing conditions (1-14) but the performance is not durable (15). Catalytic deactivation of Cu-ZSM-5-387 caused more substantial declines in pore volume than simple hydrothermal aging in air at comparable temperatures (15). Catalysis induced sintering of the initially present copper species to CuO, as shown by EXAFS and XRD(15). We suggested that deactivation is caused primarily by this sintering process and that degradation of the crystalline zeolite was subsidiary in cause and secondary in effect (15).

Here we report more extensive laboratory characterization of Cu-ZSM-5-207 deactivation. As was the case with Cu-ZSM-5-387, we observe sintering of copper species to CuO as deactivation proceeds. High resolution TEM reveals additional phenomena that appear consistent with our overall model of catalyst deactivation.

0097–6156/94/0552–0039\$08.00/0

© 1994 American Chemical Society

Experimental

The ZSM-5 was purchased from PQ Corporation (H-ZSM-5, CBV 8020, lot ZN 10, Si/Al = 30.5). Samples were suspended in deionized water and treated with sufficient cupric acetate solution to provide an overall Cu/Al atom ratio of about 1.0. The resulting material, Cu-ZSM-5-207, the primary catalyst studied here, has a nominal cupric ion exchange content is 207% and a Cu/Al mol ratio of 1.035. After stirring overnight, the addition of small amounts of concentrated ammonia raised the pH of the solution to 7.5. After holding the pH constant for 2 hr, the suspension was filtered and dried. Subsequently, the Cu-ZSM-5 was calcined typically at 400 °C, but sometimes at 500 °C, 600 °C, 700 °C, or 800 °C.

Powder X-ray diffraction data were collected by standard methods with a Rigaku diffractometer equipped with a rotating anode X-ray source. Micropore volume determinations were obtained from Ar sorption data using Micromeritics Instrument Corporation ASAP 2000M porosimeter. TEM analysis was performed using a JEOL 2000 FX microscope.

Catalytic treatments use simulated lean-burn gas mixtures found in the patent literature (6,7). Specifically, the model A/F 18 gas mix contained 3000 ppm CO, 1000 ppm H₂, 1600 ppm C₃H₆, 1200 ppm NO, 3.2% O₂, 10% CO₂, 10% H₂O, balance N₂. The chemical equivalence ratio (oxidants/reductants) for this mixture is 3.54. Generally, 1 gram of 20-40 mesh granules is used in catalytic evaluations where the volumetric flow rate is 5 liters/minute. A space velocity of about 120,000 hr⁻¹ results. Hydrocarbon conversion was monitored with a FID (Rosemount Analytical Model 400A), NO_x reduction with a NO_x chemiluminescent analyzer (Rosemount Analytical 951A set to determine NO_x), O₂ with an Horiba Magnetopneumatic analyzer (MPA-21), CO and N₂O with nondispersive IR analyzers (Rosemount Analytical 880). The N₂O analyzer is equipped with filters to compensate for CO₂ and, in particular, CO present in the gas stream. At high CO conversion and low N₂O concentrations, the analyzer registers "negative" amounts of N₂O.

Results

Figure 1 shows performance of fresh Cu-ZSM-5-207. As reported previously (1-5), Cu-ZSM-5 can reduce NO under net oxidizing conditions. If NO reduction under these conditions were durable, emissions could be controlled from lean-burn engines that offer increased fuel economy and correspondingly decreased CO₂ emissions. Catalysts offering NO reduction under oxidizing conditions should not produce much N₂O since N₂O is itself believed to be a potent greenhouse gas. Reassuringly, this catalyst produces little N₂O in this fully formulated synthetic exhaust. This confirms the relevance of previous studies performed under more idealized conditions that reported high selectivity of NO reduction to N₂ (1-5).

Figure 2 shows performance of Cu-ZSM-5-207 both when fresh and after one hour of catalytic treatment at A/F 18 at various temperatures. Noticeable deactivation follows one hour of catalysis at 600 °C. However, a 4 hour calcination in static air at 600 °C results in fresh performance essentially indistinguishable from the fresh catalyst shown in Figure 2 which had been calcined to only 400 °C.

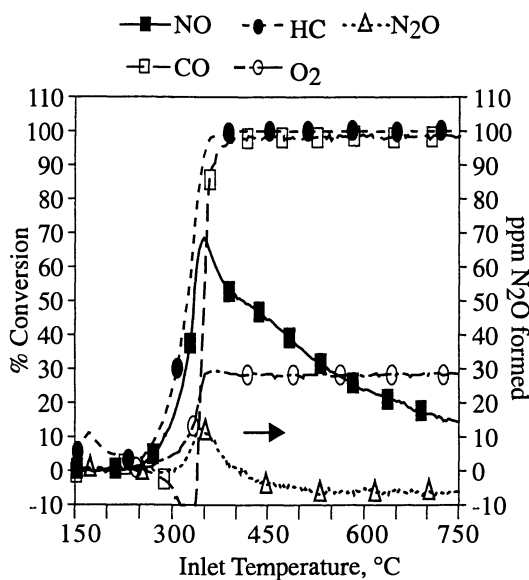


Figure 1. Conversion of NO, HC (propene), CO, O₂ (in %) and N₂O formation (in ppmv) as a function of temperature. NO reduction over fresh Cu-ZSM-5-207 bends over as temperature increases; little N₂O is formed.

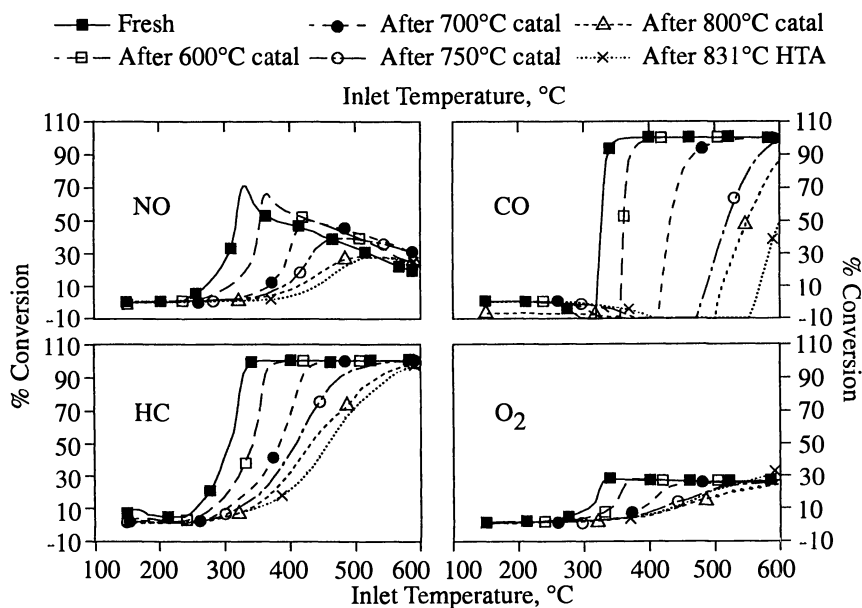


Figure 2. Conversion vs. temperature of fresh Cu-ZSM-5-207 and of Cu-ZSM-5-207 after one hour of catalysis at A/F 18 at stipulated temperatures or after hydrothermal aging. Stepwise deactivation is observed after one hour catalytic treatment at increasingly high temperatures; hydrothermal treatment at 831 °C is worst of all.

Subjecting the material calcined at 600 °C to one hour of catalysis at 600 °C causes deactivation comparable to that shown in Figure 2 (15). Sequentially greater deactivation follows sequentially hotter catalytic treatments. Deactivation after one hour of hydrothermal treatment at 831 °C is a little more severe than one hour of catalysis at 800 °C. The exotherm across the catalyst bed during catalysis at 800 °C is about 50 °C, so the temperatures of the two treatments are similar. The time spent at high temperature may be a little longer for the hydrothermal aging since the cooling rate was slower. As detailed below, other differences are observable between the 800 °C catalytically aged and the hydrothermally aged catalysts.

Figure 3 shows the evolution of micropore volume as a function of catalyst treatment. Micropore volumes shown here were calculated from the Ar sorption data using the Horváth-Kawazoe method (16). Pore volume corresponding to pore diameters less than 9 Å is considered zeolitic micropore volume in these measurements. Both the Horváth-Kawazoe and the T-plot methods provide similar pore volume loss results. Since this is true, the higher precision Horváth-Kawazoe method was used. Analysis of differential pore volume vs. pore diameter reveals the fresh material to possess a step function pore size distribution centered at 5.4 - 5.5 Å, which conforms well with known crystallographic properties of ZSM-5 (17-19). The slit-pore assumption inherent in the Horváth-Kawazoe method does not result in incorrect estimates of the diameter of the cylindrical pores of ZSM-5.

The pore size distribution after catalysis or aging is no longer a simple step function. Several maxima in the differential pore volume appear between 5 - 6 Å and another small local maximum occurs at about 8.0 Å. Interestingly, less micropore volume is lost after hydrothermal aging than after catalysis at comparable temperatures (Fig. 3). Both atmospheres contained the same amount of steam, and, if anything, the hydrothermal aging may have been a little more severe since the catalyst was exposed to high temperatures for a longer time. Although increasingly hot catalysis results both in uniformly decreasing micropore volumes and uniformly declining performance, aged performance doesn't correlate precisely with micropore volume. The hydrothermally aged catalyst is more severely deactivated but has lost a smaller fraction of its original micropore volume.

Figure 4 reveals formation of CuO, as detected by X-ray diffraction, in the aged but not in the fresh catalyst. Two reflections of CuO, centered at 35.5° and 38.7° 2θ, grow in as severity of catalyst treatment increases. Features at 35.75°, 36.05°, and 37.20° 2θ appear to arise from (080); (800) and (035); and (-562), (-713), (354), (534) reflections of H-ZSM-5, respectively (19). Crystallite sizes of CuO cannot be extracted from these data since both observed reflections have contributions from two crystallographic planes: (002) and (-111) for 35.5° 2θ and (111) and (200) for 38.7° 2θ, but the CuO crystallites must be at least 4 nm to be seen by XRD. The increasing magnitude of these two reflections relative to the zeolitic reflections suggests that as the severity of aging increases a larger fraction of total copper occurs as crystalline CuO. Unlike what was observed in Cu-ZSM-57-387, no crystalline Cu₂O is observed (15).

Figure 5 shows the formation of a halo due to amorphous material as the severity of catalytic treatment increases. A broad halo, centered at about 23° 2θ but observable from 11° to 39.9° 2θ, is essentially absent in the fresh catalyst but is pronounced in materials aged catalytically at 800 °C or hydrothermally at about

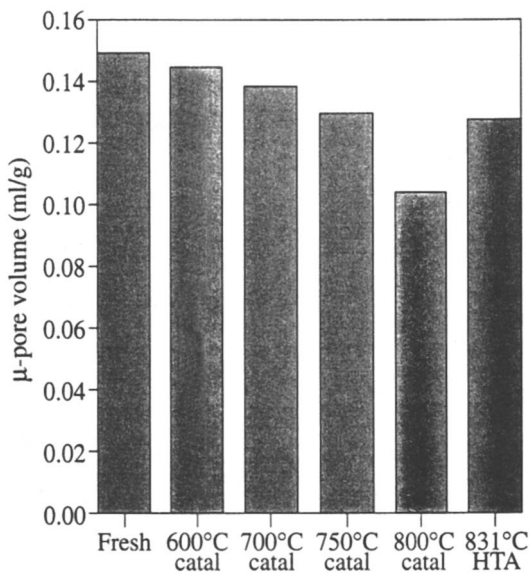


Figure 3. Micropore volume, determined by Ar sorption, as a function of deactivation severity: micropore volume decreases after catalytic or hydrothermal treatments do not correlate precisely with catalytic deactivation.

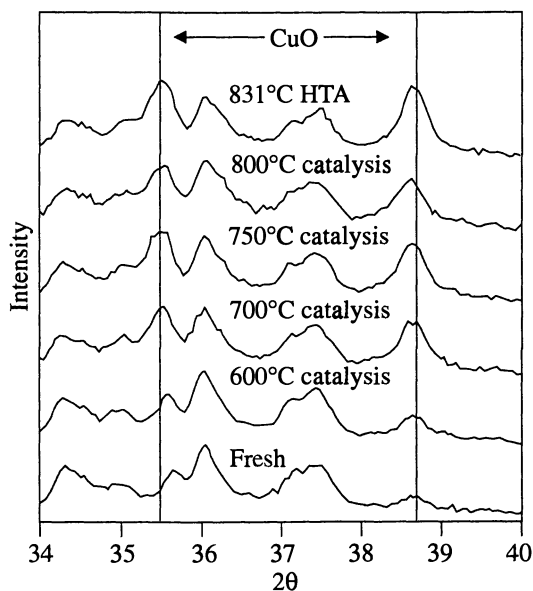


Figure 4. X-ray diffraction patterns of the various Cu-ZSM-5-207 samples reveal sintering of copper species to CuO correlates with deactivation.

831 °C. The halo is observed due to the presence of crystallographically amorphous silica-alumina. Copper does not contribute to the halo. Initially, it is not detectable crystallographically and appears highly dispersed. The copper crystallizes to CuO after severe treatments. Zeolite crystallinity degrades somewhat with increasingly severe treatments.

Of six reflections attributable to the zeolite examined in detail, three show substantial decreases in relative intensity as aging severity increases, two show moderate intensity declines, while one appears not to be affected. These data are gathered in Table I. Maximum intensities of the various reflections are tabulated relative to the intensities (defined as 100) of the corresponding fresh material. Relative zeolite crystallinity of a series of similar samples is generally measured by scaling the maximum intensity of a strong reflection to the maximum intensity of an arbitrarily chosen reference (20). We choose the fresh material as the reference. One could measure relative crystallinity using integrated intensities rather than maximum intensities; both methods provided equivalent trends for Cu-ZSM-5-387 (15). Since CuO is absent in the fresh material, the background intensities at angles where CuO reflections grow in are defined as 100. With the exception of data for the material treated catalytically at 800 °C, CuO relative intensities increase monotonically with severity of the aging. Intensities of the material that had been exposed to 800 °C catalysis appear systematically low for unknown reasons. For example, the zeolite reflection at 29.90° 2θ is about constant for this series except for the 800 °C sample. If the 29.90° 2θ reflection for this sample is scaled to 100, the CuO intensity at 35.55° 2θ is 143 and at 38.65° 2θ is 146, which is similar to the 750 °C sample.

Table I. Relative intensities of selected reflections of ZSM-5 and CuO

	ZSM-5						CuO	
	23.05°	23.90°	24.35°	29.90°	36.05°	37.20°	35.55°	38.65°
Fresh	100	100	100	100	100	100	100 ^a	100 ^a
600°C	108	110	96	111	101	100	123	108
700°C	97	101	87	107	96	95	138	137
750°C	93	100	87	107	97	94	143	145
800°C	72	77	75	84	87	88	120	123
831°C AHTA	88	93	85	100	94	95	151	165

^aBackground intensity defined as 100

If one scales the intensity of the major ZSM-5 reflections (23.05° through 24.35° 2θ) to the 29.90° 2θ zeolite reflection, the loss of crystallinity of ZSM-5 after catalysis at 800 °C appears comparable to the material that underwent hydrothermal aging. Zeolite crystallinity, as assessed by maximum diffraction intensities of several reflections, degrades modestly. However, the amount of amorphous material, as indicated by the intensity of the amorphous halo, increases with aging severity.

An impervious shell of amorphous material forms on the exterior of crystals

of TPZ-3 after steaming at 676 °C (21). Although the abstract indicates the surface area of the steamed TPZ-3 (as determined by N₂ BET measurements) was reduced to essentially that of the exterior of the crystallites (21), which is not what we observe for Cu-ZSM-5, we wanted to examine this possible mode of catalyst deactivation. Our efforts have concentrated on the fresh material, material exposed to catalytic conditions at 800 °C, and the hydrothermally aged material.

The fresh zeolite appears crystalline right up to the edge of the crystal. "Postage stamp" perforations due to 1-dimensional pores along the 010 direction can be observed in Fig 6. Not all regions of the fresh catalyst exhibit such extremely high crystallinity out to the exterior surface. The lattice fringes of the fresh material shown in Fig. 7 appear to stop about 7 Å from the exterior surface. This smearing out of the fringes may be an artifact due to imaging through a portion of material insufficiently thick to have the periodicity required to produce lattice fringes. No evidence of sintered copper-containing materials is evident in the fresh material. The copper (presumably cupric) species appear to occur as small, highly dispersed species, unresolvable at the resolution (3 Å) of the microscope used.

The catalytically "aged" material shows evidence of an amorphous film at the surface, sintering of copper to relatively large, dark (dense) objects (which XRD indicates should be CuO), and a pitted, "karst" topography suggestive of voids. (A referee suggests that the amorphous film might be carbon since the catalyst is expected to be black after reaction. Our catalysts, which are tested in the presence of steam, are not black but rather blue-gray and contain only 200-300 ppm C. Through discussion with other researchers in the area, we find that catalysts tested in the absence of steam are, indeed, black. Since both the catalytically used and hydrothermally aged catalysts show the film, film formation is not uniquely due to catalysis. The fresh materials were subjected to the same treatment in the microscope, but do not reveal films. The films in the aged, deactivated materials probably are not artifacts due to microscopy.) Fresnel contrast from the sample as one goes through focus is akin to that expected for voids. When they are apparent, fringes due to crystalline zeolite are mottled. This could be due to either amorphous material on the "top" and "bottom" of the materials or, more likely, due to beam damage. The used catalyst appears more susceptible to beam damage than the fresh material. Figure 8 exhibits all of these features. Numerous 30-40 Å copper particles appear in this image; three are pointed out. We have observed Cu particles as large as 400 Å in other photos. We have yet to observe any Cu particles on the exterior surface of a zeolite sample aged catalytically. The copper particles in catalytically aged materials tend to occur in regions that apparently contain voids. Two probable voids are pointed out. However, not all regions apparently containing voids are associated with copper particles. As copper sinters to CuO particles larger than the micropore diameter of ZSM-5 (about 5.5 Å) on the interior of Cu-ZSM-5 particles, local destruction of the initially crystalline zeolite should occur(22).

However, when we hydrothermally aged H-ZSM-5 to dealuminate it and then made Cu-ZSM-5 in an otherwise normal fashion, agglomerates of CuO are clearly observable by TEM on the exterior surface of the zeolite. Catalytic properties of the pre-dealuminated Cu-ZSM-5 are consistent with CuO, as expected, and very little NO is reduced. We believe the sintered CuO tends to occur on the interior of the ZSM-5 particles that were aged catalytically.

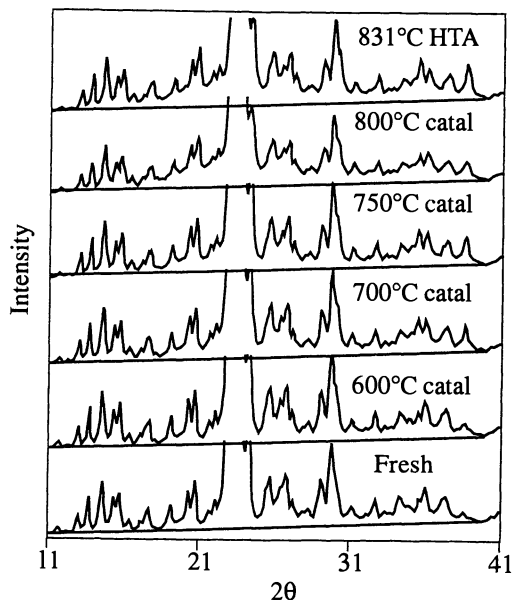


Figure 5. X-ray diffraction patterns of the various Cu-ZSM-5-207 samples reveal a halo due to amorphous material that grows in as the catalyst deactivates.

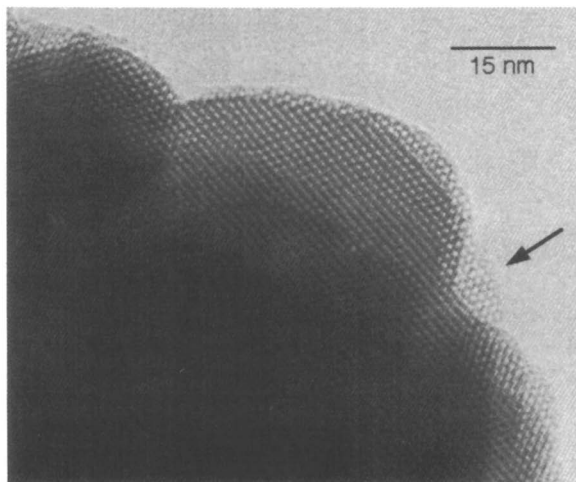


Figure 6. This TEM image of fresh Cu-ZSM-5-207 reveals "Postage stamp" perforations at the edge of the zeolite particle due to 010 channels showing the fresh catalyst to be crystalline out to exterior edges.

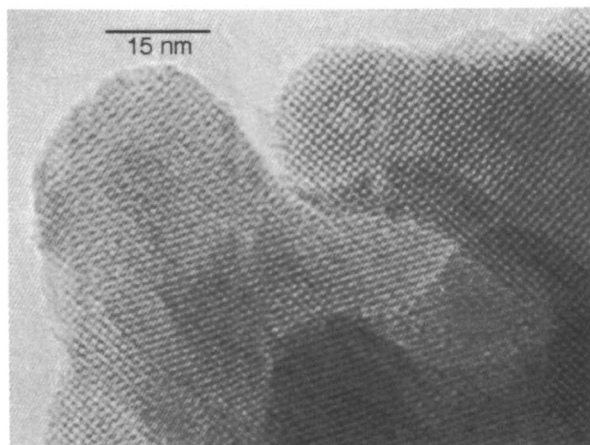


Figure 7. This TEM image, together with others not shown, fail to reveal copper-containing particles observable by TEM in the fresh catalyst while the zeolite appears crystalline to the exterior surface.

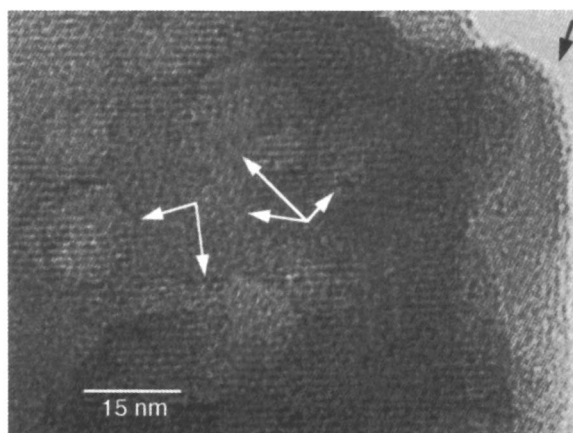


Figure 8. This TEM image of a material subjected to catalysis at 800 °C exhibits sintered copper, an amorphous film, and features that may be due to void regions inside the zeolite.

The lattice fringes appear to stop about 15-40 Å short of the exterior surface of the zeolite in the catalytically aged sample. Apparently, exposure to catalytic gases can cause some amorphization of the zeolite. Figure 9 shows: (a) two dark particles attributable to CuO, one of which is pointed out; (b) the zeolite to display a pitted morphology, as pointed out; and (c) lattice fringes that run to within 8-25 Å of the exterior edge. Other photos reveal regions where lattice fringes appear to stop as far as 80 Å from the nearest visible exterior edge. The amorphized surface layer is thin.

The hydrothermally aged material is similar to the material treated catalytically at 800°C. Amorphous films, typically 40 Å thick and dark particles attributable to CuO are both observed. Figure 10 shows lattice fringes that stop about 25-35 Å from exterior edges while Figure 11 shows lattice fringes that stop as far as 80 Å from exterior edges. Figure 10 also shows regions apparently devoid of lattice fringes (and are therefore probably amorphous) and dark spots attributable to CuO about 30-35 Å across.

Discussion

Catalysis at 600 - 800 °C causes subsequent loss of performance and changes of several catalyst features generally associated with deactivation. Specifically, losses of microporosity, sintering of cupric species to cupric oxide, formation of an halo in the X-ray diffraction pattern due to amorphous material and a thin film on zeolite exteriors, and a pitted "karst" topography of the zeolite, consistent with voids and often associated with putative CuO particles, are all observed. It is interesting to assess which phenomena correlate best with catalyst deactivation.

The thin amorphous films observed by TEM are apparently porous since micropore volumes remain considerable. The films forming in Cu-ZSM-5 after hydrothermal treatments or catalytic treatments (that are also hydrothermal since steam contents are comparable) apparently do not form an "impervious shell" as occurred in TPZ-3 (21). Films of comparable thickness occur in materials deactivated to different degrees. It would be instructive to show that this film does not contribute substantially to deactivation. Experiments concerning this point continue.

Catalyst deactivation does not correlate exactly with pore volume loss. Catalysts subjected to catalytic treatments do show monotonically decreasing activity and pore volumes as treatment severity increases. However, the hydrothermally aged catalyst is least active but does not have the lowest pore volume. Pore volume measurements provide insight regarding zeolitic degradation. The degree of zeolitic degradation following hydrothermal aging is not greater than less highly deactivated, catalytically used materials.

Hydrothermal aging does appear to result in somewhat more sintering of cupric species to CuO. Bulk CuO is relatively inactive for selective reduction of NO. Catalyst deactivation correlates most strongly overall with the degree of sintering to CuO.

Sintering of copper species to CuO appears to be the dominant pathway toward deactivation of Cu-ZSM-5 as a catalyst for selective NO reduction. Degradation of ZSM-5, an unusually stable zeolite, appears to have subsidiary

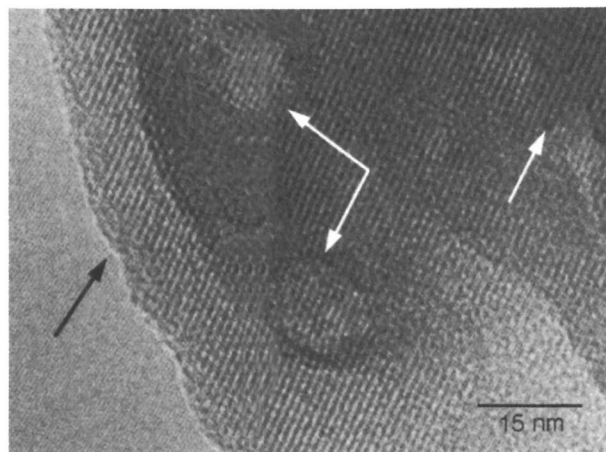


Figure 9. This TEM image of a material subjected to catalysis at 800 °C reveals 30-50 Å films formed after 800 °C catalysis, copper-containing particles, and "karst" regions consistent with voids.

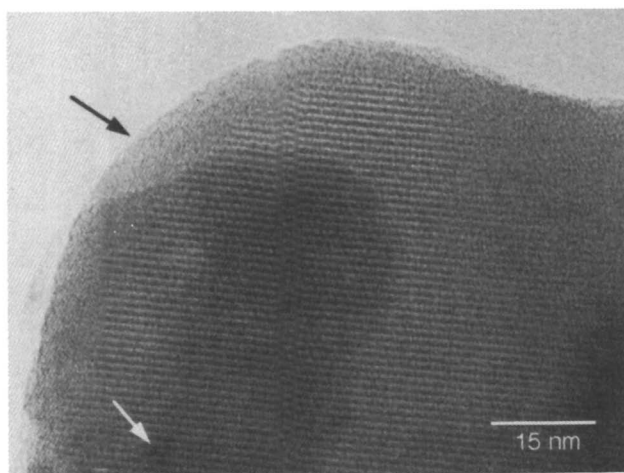


Figure 10. This TEM image of the hydrothermally aged material reveals films of similar thicknesses to those formed during high temperature catalysis.

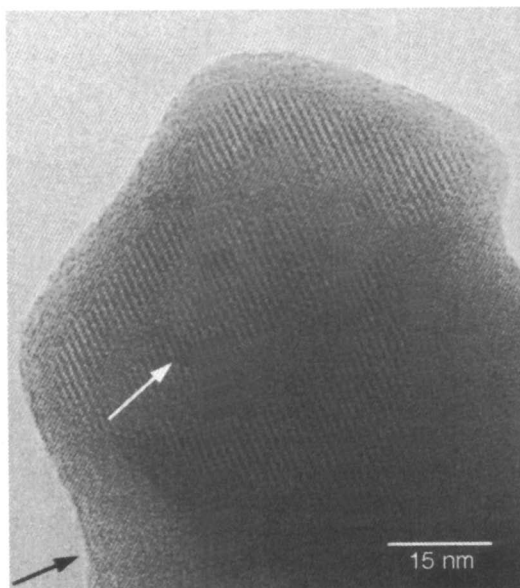


Figure 11. This TEM image of the hydrothermally aged material reveals copper particles and an amorphous (presumably silica-alumina) film.

importance. One can envision the sintering process to consist of two important elementary processes. Ligand substitution at cupric ions in the zeolitic environment results in cupric ion migration. Exchange of water ligands in aqueous cupric solutions occurs near the diffusion control limit, and is 10 orders of magnitude faster than, for example, substitution of water ligands around $[Al]^{3+}$ (23). It is plausible that migration of extraframework cupric species may be faster than migration of framework Al. Previous nmr work (15) suggests that dealumination of Zn-ZSM-5 is largely suppressed during hydrothermal aging at 800 °C. Formation of larger copper-containing clusters from smaller ones should be thermodynamically favored (24). Dehydration of growing cupric clusters should be favorable at high temperatures, in spite of the hydrothermal environment. Slowing this process is a daunting task.

Conclusion

Cu-ZSM-5 is confirmed to reduce NO under oxidizing conditions. The catalyst appears selective toward production of N_2 since only small amounts of N_2O are formed. The catalyst is unstable and deactivates considerably after brief periods of catalysis at elevated temperatures. Not much zeolitic degradation occurs. Increasingly severe catalyst treatments result in increasing degrees of sintering of copper species to CuO. The sintering of the catalytically active components, rather than degradation of the metastable support, probably dominates deactivation.

Acknowledgments

Transmission electron microscopy was performed at the Microbeam Analysis Laboratory within the Department of Geology at the University of New Mexico. We thank AlliedSignal Research & Technology colleagues Al van Til, Franz Reidinger, Anthony Eck, and Mark West for their contributions involving micropore analysis, X-ray diffraction analysis, catalyst preparation, and catalyst testing, respectively.

References

1. For a review with leading references, see Iwamoto, M.; Hamada, H. *Catal. Today*. **1991**, *10*, 57-71.
2. Teraoka, Y.; Ogawa, H.; Furukawa, H.; Kagawa, S. *Catal. Lett.* **1992**, *12*, 361-6.
3. Inui, T.; Iwamoto, S.; Kojo, S.; Yoshida, T. *Catal. Lett.* **1992**, *13*, 87-94.
4. Inui, T.; Kojo, S.; Shibata, M.; Yoshida, T.; Iwamoto, S. In *Zeolite Chemistry and Catalysis*, Jacobs, P.A.; Jaeger, N.I.; Kubelková, L.; Wichterlová, B., Eds.; Studies in Surface Science and Catalysis, Elsevier: Amsterdam, 1991, Vol. 69, 355-364.
5. Iwamoto, M.; Mizuno, N.; Yahiro, H. *Seikiyu Gakkaishi*. **1991**, *34*, 375-90.
6. Muraki, H.; Kondo, S. Japanese Kokai Patent 127 044, 1989.
7. Ishibashi, K.; Matsumoto, N. Japanese Kokai Patent 310 742, 1989.
8. Kawaki, C.; Muraki, H.; Kondo, S.; Ishitani, A. Japanese Kokai Patent 265 249, 1990.

9. Takeshima, S. U.S. Patent 5 017 538, 1991.
10. Yoshihide, W.; Mareo, K.; Shinichi, M. European Patent Application 90108236.2, 1990.
11. Held, W.; König, A.; Richter, T.; Puppe, L. Society of Automotive Engineers paper 900496, 1990.
12. Montrueil, C.N.; Shelef, M. *Appl Catal B. Environmental*. **1992**, *1*, L1-L8
13. Bennett, C.J.; Bennett, P.S.; Golunski, S.E.; Hayes, J.W.; Walker, A.P. *Appl. Catal. A. General*. **1992**, *86*, L1-L6.
14. K.C.C. Kharas, *Appl. Catal. B. Environmental*. **1993**, *2*, 207-24.
15. K.C.C. Kharas, D.J. Liu, H.J. Robota, *Appl. Catal. B. Environmental*. **1993**, *2*, 225-37.
16. Horváth, G.; Kawazoe, K. *J. Chem. Eng. Japan*. **1983**, *16*, 470-5.
17. Wu, E.L.; Lawton, S.L.; Olson, D.H.; Rohrman, A.C. Jr.; Kokotailo, G.T. *J. Phys. Chem.* **1979**, *83*, 2777-81.
18. Olson, D.H.; Kokotailo, G.T.; Lawton, S.L.; Meier, W.M. *J. Phys. Chem.* **1981**, *85*, 2238-43.
19. van Koningsveld, H.; Jansen, J.C.; van Bekkum, H. *Zeolites*. **1990**, *10*, 235-42.
20. van Hooff, J.H.C.; Roelofsen, J.W. In *Introduction to zeolite science and practice*, van Bekkum, H.; Flanigen, E.M.; Hansen, J.C., Eds.; Studies in Surface Science and Catalysis; Elsevier: Amsterdam, 1991, Vol. 58, 241-283, in particular 246.
21. von Ballmoos, R.; Koermer, G.S.; Sung, S.; Allen, F.M. "Deactivation of Catalyst TPZ-3 by formation of impervious shell", Twelfth North American Meeting of the Catalysis Society, Talk D21, Lexington, Kentucky, May 5-9, 1991.
22. Schulz-Ekloff, G.; Jaeger, N. *Catal. Today*. **1988**, *3*, 459-66.
23. Purcell, K.F.; Kotz, J.C. *Inorganic Chemistry*; W.B. Saunders: Philadelphia, PA, 1977; pg. 717-718.
24. Kelvin, W.T. *Phil. Mag.* **1871**, *42*, 448-452.

RECEIVED September 29, 1993

Chapter 5

Catalytic Reduction of NO by Hydrocarbon in Oxidizing Atmosphere

Importance of Hydrocarbon Oxidation

H. W. Jen and H. S. Gandhi

Chemical Engineering Department, Ford Research Laboratories, Ford
Motor Company, Mail Drop 3179, 20000 Rotunda Drive,
Dearborn, MI 48121-2503

The reduction of NO by C₃H₆ in excess O₂ was studied over Cu/ZSM5, Cu/ γ -Al₂O₃, Pd/ZSM5, and Au/ γ -Al₂O₃. The catalyst with higher activity of C₃H₆-oxidation incurred the reduction of NO at lower temperature. The effects of various reaction parameters were also examined in detail, especially for Cu/ γ -Al₂O₃. Under the integral reaction conditions studied, the effects of P(C₃H₆) and P(O₂) on the conversion of NO varied with temperature. There is little effect of P(NO) on the conversions of C₃H₆ and NO. The activity profiles against temperature also varied with space velocity for Cu/ZSM5 catalyst. The interrelated effects of the reaction parameters suggests that the evaluation of lean-NO_x catalysts cover a broad range of reaction conditions. These observed results can be explained by relating the reactivity pattern of NO-reduction to the activity of hydrocarbon oxidation.

Automobiles equipped with three-way-catalysts (TWC's) operate at an air/fuel ratio (A/F) around the stoichiometric value. Catalytic reduction of NO to N₂ decreases precipitously as A/F increases to an excess of O₂ in the exhaust (lean condition). There have been commercial efforts to apply lean-burn engine technology for enhancing fuel economy and lowering pollutants (1-2). Even with lean-burn engines most cars may still need catalysts to further lower the emissions in order to meet the coming regulation standards. However, no manufacturer has yet utilized a catalyst specifically developed to decrease NO_x emission under lean conditions. Thus, a catalyst, other than the current TWC's, is a requisite for the application of lean-burn engine technology to production vehicles.

Direct decomposition of NO is too slow to be a viable method for removing NO_x from automobile exhaust (3), even over recently developed Cu-based zeolite catalysts (4-8). The selective reduction of NO by NH₃ has been used for stationary exhaust, but the method is not practical for automobiles. Recently, the reduction of NO by hydrocarbons under lean conditions has been reported for Cu-based zeolites (9-11). This reaction has also been examined on non-Cu/zeolite catalysts (12-20).

0097-6156/94/0552-0053\$08.00/0
© 1994 American Chemical Society

Cu/ZSM5 is among the most active catalysts studied (21-22). These results prompt our interest in developing catalysts that under lean conditions catalyze the reduction of NO by residual hydrocarbons in the exhaust.

In contrast to these recent reports, a previous study (23) showed that the activities of Cu/ZSM5 catalysts under slightly lean conditions were not high enough for practical application on automobiles. This contrast is understood now because the activity is dependent on the concentration of O₂ (11). In the process of evaluating potential catalysts, we also found that the activities were strongly dependent on reaction conditions. Similar work by others has shown that the relative order of the activities for two catalysts can be reversed by changing the temperature or space velocity (10,16-17). These results suggest that the activity measurement or comparison should cover a broad range of reaction conditions. An applicable explanation for the interrelated effects can serve as a guideline for the evaluation process and for establishing reaction mechanism. At present there is no reported study exploring in detail the interdependence of the reaction parameters.

In this report, the effects of temperature, space velocity, and the concentration of each reactant on the catalytic reduction of NO by C₃H₆ were examined. The NO-conversion for various catalysts with different activities of hydrocarbon oxidation were compared. The oxidation of hydrocarbon is proposed as a key step to explain the experimental results.

Experimental

All the catalysts used in this study were powders. Cu/ZSM5 (Si/Al = 15, 2.47 wt% Cu) was obtained from UOP. Cu/ γ -Al₂O₃ (2 wt%) was prepared by wet-impregnation of γ -Al₂O₃ (Degussa, 60-80 mesh) with Cu(NO₃)₂ solution, drying at 70°C, and calcination at 450°C for 4 hours. Pd/ZSM5 (5.4 wt%) was prepared by ion-exchange of H-ZSM5 (UOP, Si/Al = 15) with Pd(NH₃)₄Cl₂ in a solution of 3 x 10⁻² M, washing the powder after the exchange, and drying at 100°C. Au/ γ -Al₂O₃ (2 wt%) was prepared by wet-impregnation of γ -Al₂O₃ with HAuCl₄ solution, drying at 100°C, and calcination at 500°C. Prior to activity measurements, the catalysts were generally pretreated in situ at 550°C in a flow of 20% O₂/N₂.

The activity under steady state reaction conditions was measured. For the activity measurement, a mixture of reaction gases was passed through the catalyst powder which was sandwiched between two layers of quartz wool in a 0.75 inch I.D. quartz reactor tube. Two buttons of ceramic monolith were used to hold the catalyst bed in place. The downstream button was drilled through to fit a thermocouple tube (O.D. = 1/16 inch) with the tip of the tube touching the bottom of the catalyst bed. The standard reaction mixture flowing at 3 l/min contained 500 ppm NO, 500 ppm C₃H₆, 3% O₂, and N₂ as balance to achieve atmospheric pressure. The concentrations of NO, C₃H₆, and occasionally O₂ were monitored continuously. The change in the concentration was used to calculate the conversion of each reactant. The detectors were Beckman Model 951 for NO, Model 400A for C₃H₆, and Model OM11EA for O₂. Because of the presence of excess O₂, the NO-detector was set to measure the sum of NO and NO₂.

For the Al₂O₃-based catalyst about 1 gram sample was used to obtain reasonable conversion of NO. For the ZSM5 based catalyst about 0.5 g sample was used and the conversion of NO was generally substantial. The back pressure from using a larger load of ZSM5 based catalyst would be too high for the reactor system used in this study. It was realized that packing a uniform and continuous layer of catalyst bed from the 0.5g sample was sometimes not successful. Some reactions were

repeated over different loads of Cu/ZSM5 catalysts and different activities were measured, but the reactivity patterns were generally found to be the same. Therefore, this report is mainly focused on the effect of reaction parameters on the reactivity patterns over catalysts. The data in each table or figure were obtained from the same load of catalyst.

The experimental data were obtained mostly under integral reaction conditions since a substantial conversion of NO can only be achieved with a high conversion of C₃H₆. The values in Table I were obtained by simply plotting the logarithm of the integral reaction rate against the logarithm of the initial concentration of a reactant. Thus, the calculated dependence on the initial reactant concentration, P_O, in Table I are empirical. Table I is used only to show the broad features of the reactions, e.g. the effects of temperature and the initial reactant concentration, because many reports in the literature show the effect of a parameter on the activity only at one set of reaction conditions. No attempts are made to use the apparent kinetic parameters to develop a quantitative reaction model.

Results

Cu/ZSM5. Under the standard reaction condition, the NO and C₃H₆ conversions increased with the temperature up to 530°C (Figure 1). The conversions were low at temperatures below 400°C. Thus, a reasonable Arrhenius plot was made from a separate experiment in the 300 - 400 °C range (Figure 2) resulting in the apparent activation energies (E_a) of 11 ± 3 kcal/mol for NO conversion and 10 ± 2 kcal/mol for C₃H₆. The result indicates a possibly common rate determining step. One of the reasons why the rate is used in Figure 2 is that the correct rate equation is not known and the simple relationship, $R = k[\text{NO}]^a[\text{C}_3\text{H}_6]^b[\text{O}_2]^c$, is unlikely the right rate law based on the result of NO conversion vs. temperature. Bennett and coworkers (25) report a similar E_a for C₃H₆ conversion but their E_a for NO conversion is about twice of our result. They obtained E_a from the rate constants of a simple rate equation derived from a spinning basket reactor system. This can be the reason of difference. In addition, the catalysts used may be different since their catalyst would yield only 6% NO-conversion at 400 °C with 5% O₂, 800ppm C₃H₆ and 500ppm NO (the flow is equivalent to 3.1 l/min over one gram catalyst).

In the range from 1.5% to 4.5% O₂, there was virtually no effect of O₂ concentration on the NO conversion in agreement with other reports (11, 24). At 3% O₂, the conversion of NO increased monotonously with the partial pressure of C₃H₆. The empirical relationship, $\text{Rate}(\text{NO}) \propto P_{\text{O}}(\text{C}_3\text{H}_6)^{0.66}$, was obtained at 475 °C in the range from 100 to 500 ppm C₃H₆. The similar effect of P(C₃H₆) has been reported by others (14, 25).

The effect of space velocity in Figure 3 was obtained in a different flow reactor equipped with G. C. to analyze the effluents. The profile of NO-conversion was shifted to higher temperature by applying higher space velocity, but the activity converged around 500 °C. In contrast to many reports (10-11,26), the NO-conversion profiles against temperature are not convex up to 600 °C. Neither is the result in Figure 1. This is due to the difference in the catalysts or the reaction conditions used. The lower activity in Figure 1 is probably due to the inappropriate packing of catalyst bed.

Cu/γ-Al₂O₃. In contrast to Cu/ZSM5, a maximum at 420 °C was observed in the NO conversion over the Cu/γ-Al₂O₃ catalyst, while the conversion of C₃H₆ rose to 100% with increasing temperature (Figure 4). As in the case of Cu/ZSM5, the

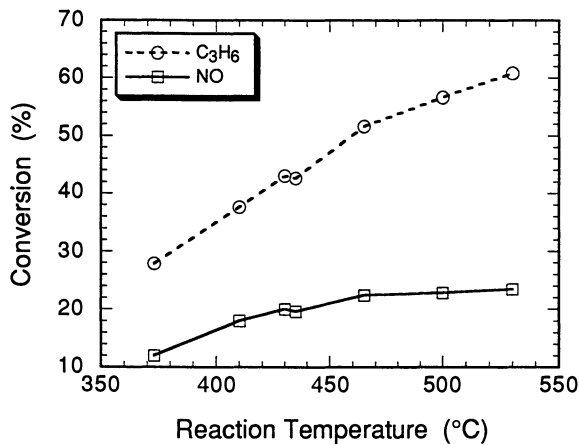


Figure 1. Effect of Temperature on NO- and C₃H₆-Conversion over 0.5 g Cu/ZSM5 in Standard Reaction Mixture

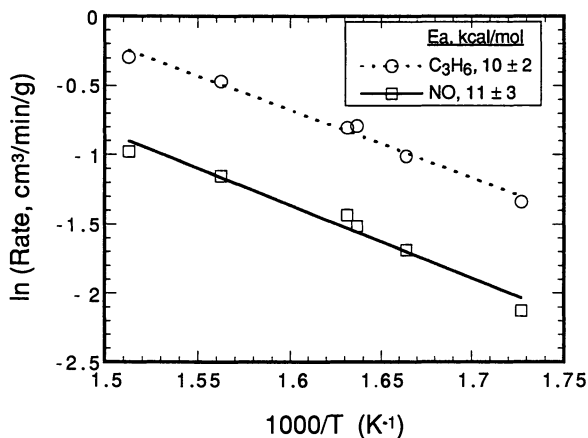


Figure 2. Arrhenius Plot for Cu/ZSM5 in Standard Reaction Mixture

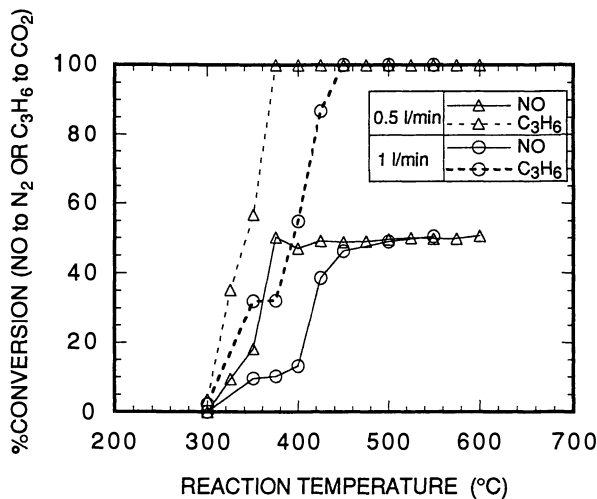


Figure 3. Effect of Flow Rate on The Activity over Cu/ZSM5 (0.15g, 1000 ppm NO, 500 ppm C₃H₆, 3% O₂)

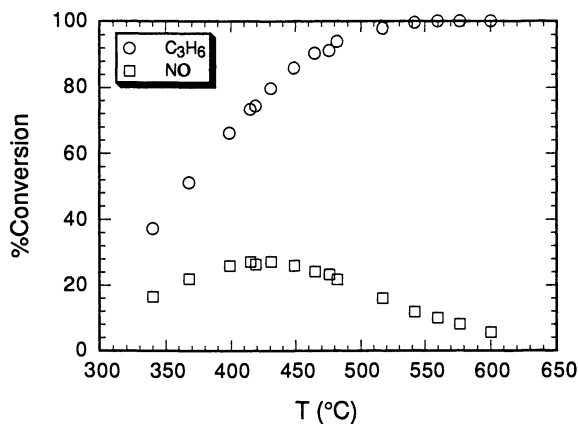


Figure 4. Effect of Temperature on NO- and C₃H₆-Conversion over 1g Cu/Al₂O₃ in Standard Reaction Mixture

Arrhenius plot was made at low temperatures resulting in $E_a = 15 \pm 3$ kcal/mol for NO conversion and 13 ± 2 kcal/mol for C₃H₆.

The effect of O₂ concentration is shown in Figure 5 for three temperatures selected below and above the temperature for maximum NO conversion (T_{max}) in Figure 4. At 300°C, the conversion of NO increased monotonously with increasing O₂ concentration. At 350°C or 482 °C, the NO-conversion increased sharply by the increase of O₂ concentration from 0% to 0.2% and decreased by the additional increase of O₂ from 0.2% to 3%. The decrease in the profile is steeper at 482 °C than at 350 °C. It is noted that there was substantial conversion of NO at 0% O₂ and 482°C indicating the direct reaction of NO and C₃H₆ at high temperature. At all temperatures, the conversion of C₃H₆ increased following the increase in O₂ concentration. The dependence of the NO-conversion on the initial concentration of O₂ is shown in Table I. The empirical dependence on $P_o(O_2)$ for the conversion rate of NO or C₃H₆ varies with temperature.

Table I. Rate Dependence on Initial Reactant Concentration over Cu/ γ -Al₂O₃
(Rate(RE) \propto {P_o(NO)}^a, Rate(RE) \propto {P_o(C₃H₆)}^b, Rate(RE) \propto {P_o(O₂)}^c)

T (°C)	RE	a	b	c
300	NO	1.0	0.25	0.21
	C ₃ H ₆	0.0	0.61	0.39
350	NO	N. M.	0.44	-0.09
	C ₃ H ₆	N. M.	0.74	0.18
482	NO	1.0	0.74	-0.36
	C ₃ H ₆	0.0	0.93	0.05

N. M. : not measured.

The conversion of NO increased with C₃H₆-concentration (Figure 6), like the results for Cu/ZSM5. It is noted that the NO conversion at 350°C in 3% O₂ was larger than that at 482°C for $P(C_3H_6) \leq 250$ ppm. Neither the NO nor the C₃H₆ conversion was affected by a change in P(NO) over the range of 500 - 2500 ppm (Figure 7). When expressed in terms of reaction rate, the rate dependence on P(NO) is 1 for the NO reaction and 0 for the C₃H₆ reaction at 300°C or 482°C (Table I). Apparently, the rate of C₃H₆ converted was invariant with the rate of NO reaction at constant temperature, O₂ concentration, and C₃H₆ concentration.

The experimentally determined dependencies on the reactant concentrations are summarized in Table I. As stated previously, these values are not necessarily the true reaction orders. They are used only to show the empirical relationship between the reaction rates and the reaction parameters under the conditions studied here.

Pd/ZSM5. This catalyst is comparatively active for hydrocarbon oxidation with 100% C₃H₆ conversion above 350°C in 3% O₂, while 15% is the maximum conversion for NO at 270°C (Figure 8) which is much lower than 420 °C for Cu/ γ -Al₂O₃. The effect of P(O₂) on the conversion of NO varies with temperature (Figure 9). The conversion of NO increased at 208 °C but decreased at 372 °C as the O₂ concentration was increased from 1.5% to 6%.

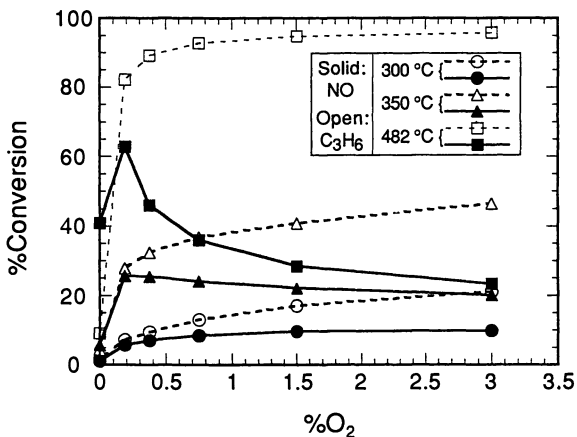


Figure 5. Effect of O₂-Content on NO- and C₃H₆-Conversion over 1g Cu/Al₂O₃ (500 ppm NO, 500 ppm C₃H₆, 3 l/min)

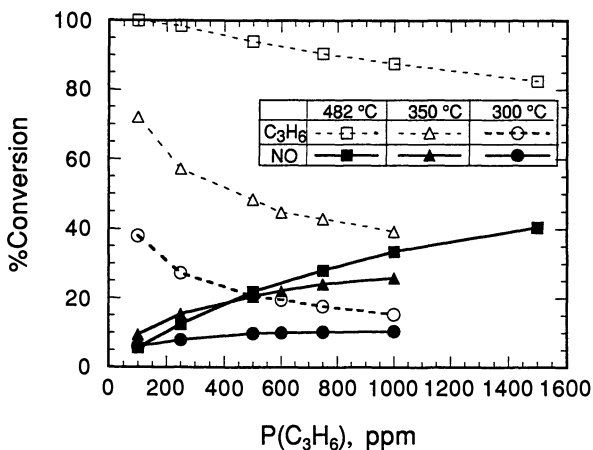


Figure 6. Effect of C₃H₆-Concentration on NO- and C₃H₆-Conversion over 1g Cu/Al₂O₃ (500 ppm NO, 3% O₂, 3 l/min)

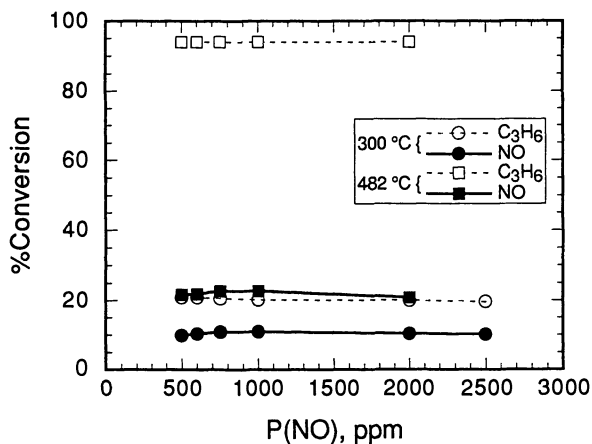


Figure 7. Effect of NO-Concentration on NO- and C₃H₆-Conversion over 1g Cu/Al₂O₃ (500 ppm C₃H₆, 3% O₂, 3 l/min)

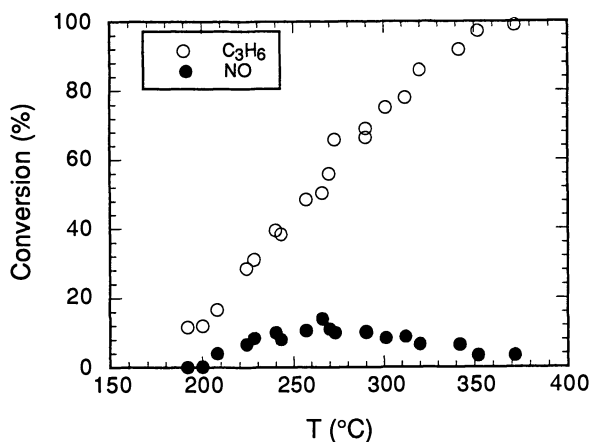


Figure 8. Effect of Temperature on NO- and C₃H₆-Conversion over 0.6 g Pd/ZSM5 in Standard Reaction Mixture

Au/ γ -Al₂O₃. The catalyst is much less active for the oxidation of C₃H₆ (Figure 10) in comparison to the other catalysts described above. The conversion of NO was significant only at or above 450 °C with a maximum value of 5%.

Discussions

The experimental results have shown that the catalytic conversion for NO under lean conditions is not only dependent on the type of catalyst but is also very sensitive to reaction conditions. This implies that the relative activities of different catalysts are dependent on the experimental conditions. For example, the activity for Pd/ZSM5 at 270 °C is 15% which is larger than that for Cu/ZSM5, but above 400 °C Cu/ZSM5 is much more active. Sato et al. (10) reported that Al₂O₃ was more active than Cu/ZSM5 at a space velocity below 10,000 hr⁻¹, but the relative activity was reversed at space velocities above 10,000 hr⁻¹. The interrelated effects of reaction parameters are clearly illustrated by the variation of the empirical rate dependencies with temperature for Cu/ γ -Al₂O₃ (Table I). Thus, we propose that the evaluation of potential catalysts needs to incorporate a wide range of reaction parameters and encompass conditions close to those in actual engine exhaust.

Scheme A is proposed to help explain the observed results. This simple scheme lists the feasible reactions between the reactants without involving any detailed surface interactions. Our results can not be used to either confirm or refute any of the possible mechanistic features that others have suggested, e.g. NO adsorption (27-29), NO₂ formation (13, 14), NO decomposition (30), or reduction-oxidation of the catalyst (31-32). The scheme is similar to that suggested by Hamada et al. (13, 14). However, the importance of hydrocarbon oxidation is stressed here and only NO is involved without the need to invoke any other NO_x intermediate species.

The complete oxidation of one C₃H₆ molecule requires nine oxygen atoms. The amount of NO converted is not sufficient to supply the oxygen for the C₃H₆ conversion in our results that substantial conversion of NO was detected under lean conditions. The majority of C₃H₆ was converted by reacting with O₂. C₃H₆ can react directly with NO at 482 °C over Cu/ γ -Al₂O₃ (Figure 5) or at 372 °C over Pd/ZSM5 (Figure 9) as evidenced by the NO conversion in the absence of O₂. The direct reduction of NO by C₃H₇OH was reported (24) over Cu/ZSM5 at 482 °C. At 500 °C, little conversion of NO was observed over Cu/ZSM5 (11,24). Thus, the occurrence of the direct reduction is related to the reaction temperature, the catalyst, and the reductant used.

However, the direct reduction can not be used to explain why, by increasing the O₂ concentration from 0% to 0.2%, the NO conversion at 482 °C increased from 40% to 62 % as the C₃H₆ conversion increased from 10% to 82% (Figure 5). Nor can it explain why at lower temperatures (e.g. 300 °C or 350 °C in Figure 5) the NO conversion reached significant values only in the presence of O₂. Also, there was no effect of P(NO) on the conversion of C₃H₆ (Figure 7). Thus, O₂ has to be involved in the selective reduction of NO under lean conditions and NO is not directly involved in the determining step of C₃H₆ oxidation. These observations lead to a simple explanation that NO is reduced by reacting with an intermediate generated from the incomplete oxidation of C₃H₆ as shown in Scheme A. The empirical relationship of $\text{Rate}(\text{NO}) \propto \text{P}_o(\text{NO})^1$ agrees with this simple explanation, too.

The intermediate can be further oxidized by O₂ with no chance of reacting with NO. The complete oxidation of C₃H₆ by O₂ is then a side reaction competing with NO reduction. The effect of P(O₂) on the conversion of NO in Figure 5 implies that

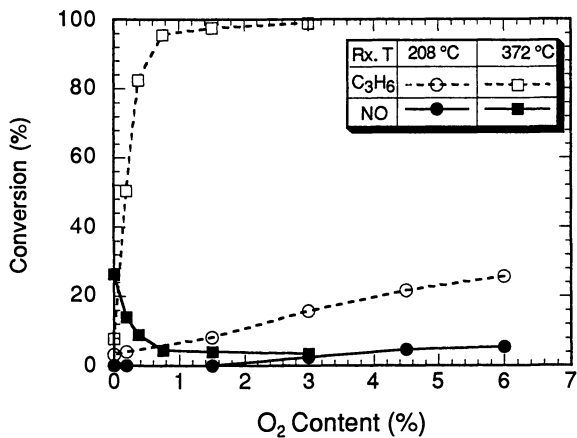


Figure 9. Effect of O₂-Content on NO- and C₃H₆-Conversion over 0.6 g Pd/ZSM5 (500 ppm NO, 500 ppm C₃H₆, 3 l/min)

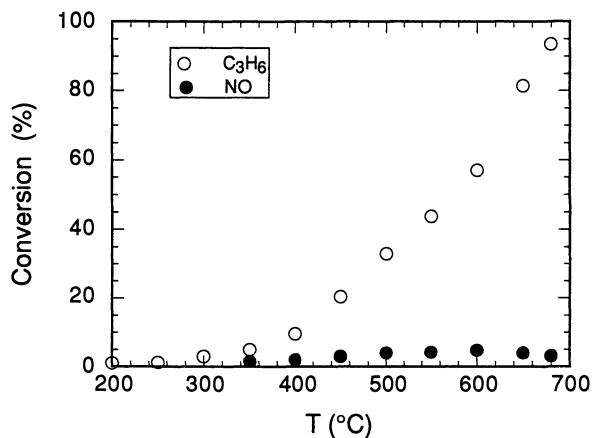


Figure 10. Effect of Temperature on NO- and C₃H₆-Conversion over 0.75g Au/Al₂O₃ in Standard Reaction Mixture

the conversion of NO may be increased by decreasing P(O₂) at high temperature and vice versa. The detrimental effect of increasing P(O₂) at high temperature indicates that the competition of the side reaction increases with temperature. This increasing competition explains the observation of a convex profile in the plot of NO-conversion against temperature (Figure 4). The temperature of the maximum activity, T_{max}, for the selective reduction of NO by hydrocarbon is related to the oxidation of hydrocarbon. Over a catalyst, the value of T_{max} would decrease as the combustibility of the hydrocarbon used increases, as shown by Hamada et al. (14) for the order of T_{max}: CH₃OH ≈ C₂H₅OH ≈ C₃H₇OH < C₃H₆ < C₃H₈.

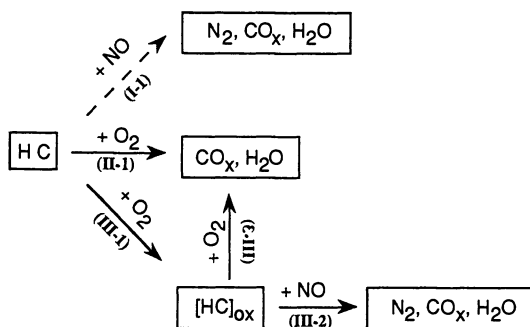
For the catalysts with various activities of hydrocarbon oxidation, the order of T_{max} values should be the reverse order of the oxidation activity. Our results agrees with the expectation: T_{max} = 270 °C for Pd/ZSM5 (figure 8), 420 °C for Cu/γ-Al₂O₃ (Figure 4), or ~600°C for Au/γ-Al₂O₃ (Figure 10). Thus, one important feature of the catalyst for the selective reduction of NO under lean conditions is to promote the incomplete oxidation of the reductant used. The catalyst with high activity for the complete oxidation of hydrocarbon would result in low concentration of intermediate(s) and low NO conversion. The catalyst with low activity for the oxidation would need high temperature to generate substantial concentration of intermediate(s) for NO reduction, which may poses a problem for practical application.

Scheme A basically agrees with that proposed by Hamada et al. (13, 14) and that suggested by Bennett et al. (25). However, we present more data to support the scheme and stress the importance of hydrocarbon oxidation. In a recent paper (33), Sasaki et al. propose that the reduction of NO by C₃H₈ over H-ZSM5 involves the direct reaction of NO₂ with C₃H₈ under lean conditions. By the estimation from their report the direct interaction alone can not explain why the amount of oxygen provided by the NO₂ conversion is less than the demand for C₃H₈ oxidation. Thus, O₂ has to be involved in the overall reaction scheme. In addition, the direct interaction of hydrocarbon with NO₂ can not explain our result that the conversion of C₃H₆ was unchanged as the NO conversion increased linearly with P(NO) (Figure 10).

It has been shown that CO or H₂ is unlikely the reactive intermediate under lean conditions (22,34). There have been reports about the reactive intermediates for the reduction of NO: carbon species (25), oxygenates (24), isocyanate (-CNO) (35), and C(O) species on carbon surface (36). Our current results can not confirm any one of them. However, it is proposed that the stable oxygenates (such as aldehydes, alcohols, and ketones) may not be the reactive intermediates because these oxygenates resulted in lower reduction temperature for NO than the corresponding hydrocarbons (14) or the effect of P(O₂) on the NO conversion was different between the two types of reductants (24).

Under our reaction conditions, it was found that the there was little NO conversion over H-ZSM5 which turned black after the reaction up to 600 °C. Black color was not observed for Cu/Al₂O₃, while the color was seen on the Cu/ZSM5 powders after the reaction. Therefore, the presence of carbon deposit does not warrant a good activity for NO conversion. The reactive intermediates is produced in the process of incomplete oxidation of the hydrocarbon before being further oxidized. We can only speculate that the carbon deposit generated over Cu/ZSM5 catalyst during the reaction may act as another source of reductant for NO. The requirement of high temperature to generate reactive intermediates from the oxidation of the deposit may be one reason why the NO conversion over the Cu/ZSM5 catalyst was flat over a wide range of high temperatures (Figure 1 and 3), in contrast to the result over Cu/Al₂O₃. If the reaction profile was extended to higher temperature in Figure 1 or 3, the convex curve might be observed. The above speculation is consistent with our results that the

SCHEME A



[HC]_{ox} : intermediates from partial oxidation of hydrocarbon

reactivity pattern for the reaction is closely related to the oxidation of reductant. Further work is needed to isolate and identify the intermediate(s). Also, the explanation linked the intermediate(s) to the experimental observations has to be rationalized.

Conclusion

1. Empirical rate dependencies on the reactants were obtained for Cu/ γ -Al₂O₃ and the numbers varied with temperature. The catalytic activity for the reduction of NO under lean conditions is dependent on not only the type of catalyst but also the reaction conditions. The evaluation of potential catalysts should be done for a broad range of conditions encompassing the operating range of lean-burn engines.

2. A simple scheme is proposed for the selective reduction of NO under lean conditions. One key factor in the reaction is the oxidation of the hydrocarbon. The experimental results can be explained by the balance between the complete oxidation and the partial oxidation of the hydrocarbon to produce reactive intermediates.

Acknowledgment

It is greatly appreciated that J. S. Hepburn provided a reactor system for the activity measurements and gave many suggestions. Discussions with M. Shelef, R. W. McCabe, K. Otto, and A. D. Logan are also appreciated.

Literature Cited

1. *Automotive Fuel Economy: How Far Should We Go?*; National Research Council; National Academy Press: Washington, D.C., 1992, pp 217-226.
2. Kummer, J. T., In *Fuel Economy*; Hillard, J. C.; Springer, G. S., Eds.; Plenum: New York, NY, 1984; pp 35-90.
3. Shelef, M.; Otto, K.; Gandhi, H. *Atm. Environ.* **1969**, *3*, 107.
4. Iwamoto, M.; Hamada, H. *Catal. Today.* **1991**, *10*, 57.

5. Iwamoto, M.; Furukawa, H.; Mine, Y.; Uemura, F.; Mikuriya, S.; Kagawa, S. *J. Chem. Soc., Chem. Commun.* **1991**, 272.
6. Li, Y.; Hall, W. K. *J. Phys. Chem.* **1990**, *94*, 6145.
7. Truex, T. J.; Searles, R. A.; Sun, D. C. *Platinum Metal Rev.* **1992**, *36*, 2.
8. Kagawa, S.; Ogawa, H.; Furukawa, H.; Teraoka, Y. *Chem. Lett.* **1991**, 407.
9. Held, W.; König, A.; Richter, T.; Puppe, L. *SAE; Paper #900496*.
10. Sato, S.; Yu-u, Y.; Yahiro, H.; Mizuno, N.; Iwamoto, M. *Appl. Catal.* **1991**, *70*, L1.
11. Iwamoto, M.; Yahiro, H.; Shundo, S.; Yu-u, Y.; Mizuno, N. *Appl. Catal.* **1991**, *69*, L15.
12. Hamada, H.; Kintaichi, Y.; Sasaki, M.; Ito, T.; Tabata, M. *Appl. Catal.* **1991**, *64*, L1.
13. Hamada, H.; Kintaichi, Y.; Sasaki, M.; Ito, T.; Tabata, M. *Appl. Catal.* **1991**, *70*, L15.
14. Hamada, H.; Kintaichi, Y.; Sasaki, M.; Ito, T.; Tabata, M. *Appl. Catal.* **1991**, *75*, L1.
15. Hamada, H.; Kintaichi, Y.; Tabata, M.; Sasaki, M.; Ito, T. *Chem. Lett.* **1991**, 2179.
16. Torikai, Y.; Yahiro, H.; Mizuno, N.; Iwamoto, M. *Catal. Lett.* **1991**, *9*, 91.
17. Torikai, Y.; Yahiro, H.; Mizuno, N.; Iwamoto, M. *Chem. Lett.* **1991**, 1859.
18. Misono, M.; Kondo, K. *Chem. Lett.* **1991**, 1001.
19. Kikuchi, E.; Yogo, K.; Tanaka, S.; Abe, M. *Chem. Lett.* **1991**, 1063.
20. Li, Y.; Armor, J. N. *Appl. Catal. B: Environmental.* **1992**, *1*, L31.
21. Konno, M.; Chikakisa, T.; Murayama, T.; Iwamoto, M. *SAE; Paper #920091*.
22. Iwamoto, M.; Mizuno, N. *J. Automobile Eng. Part D: Proc. Inst. Mech. Eng.* **1993**, *207*, 23.
23. Rirscher, J. S.; Sandner, M. R. U. S. Patent 4 297 328, 1981.
24. Montreuil, C. N.; Shelef, M. *Appl. Catal. B: Environmental.* **1992**, *1*, L1.
25. Bennett, C. J.; Bennett, P. S.; Golunski, S. E.; Hayes, J. W.; Walker, A. P. *Appl. Catal. A: General.* **1992**, *86*, L1.
26. Sato, S.; Hirabayashi, H.; Yahiro, H.; Mizuno, N.; Iwamoto, M. *Catal. Lett.* **1992**, *12*, 193.
27. Shelef, M. *Catal. Lett.* **1992**, *15*, 305.
28. Giamello, E.; Murphy, D.; Magnacca, G.; Morterra, C.; Shioya, Y.; Nomura, T.; Anpo, M. *J. Catal.* **1992**, *136*, 510.
29. Iwamoto, M.; Yahiro, H.; Mizuno, N.; Zhang, W. X.; Mine, Y.; Furukawa, H.; Kagawa, S. *J. Phys. Chem.* **1992**, *96*, 9360.
30. Li, Y.; Hall, W. K. *J. Phys. Chem.* **1990**, *94 (16)*, 6145.
31. Hall, W. K.; Valyon, J. *Catal. Lett.* **1992**, *15*, 311.
32. d'Itri, J. L.; Sachtler, W.M.H. *Catal. Lett.* **1992**, *15*, 289.
33. Sasaki, M.; Hamada, H.; Kintaichi, Y.; Ito, T. *Catal. Lett.* **1992**, *15*, 297.
35. Ukisu, Y.; Sato, S.; Muramatsu, G.; Yoshida, K. *Catal. Lett.* **1992**, *16*, 11.
36. Tomita, A.; Yamada, H.; Kyotani, T.; Radovic, L. *Energy Fuels.* **1993**, *7(1)*, 85.

RECEIVED September 29, 1993

Chapter 6

X-ray Photoelectron Spectroscopy of Cu-ZSM-5 Zeolite

L. P. Haack and M. Shelef

Scientific Research Laboratory, Ford Motor Company, Mail Stop 3061,
P.O. Box 2053, Dearborn, MI 48121-2053

The determination of the oxidation state of copper in Cu-exchanged ZSM-5 is important for understanding its role in the mechanism of decomposition and selective reduction of NO. The task is difficult using any of the common methods. Here we evaluate the use of XPS. This work confirms that prolonged exposure of the material to the X-ray or neutralizing electron beam, needed for signal acquisition, partially reduces the Cu-ions in situ. Contrary to some prior reports such reduction by dehydration during heating up to 500°C was not observed. Heat treatment under oxidizing conditions induces changes in the populations of Cu²⁺ ions in different spatial coordinations. At the same time, the severe oxy-reduction treatments do not appear to cause any Cu migration out of the zeolite framework.

Copper-exchanged ZSM-5 zeolite is currently the subject of intense study because of its activity in NO decomposition and selective reduction in excess oxygen (1). While the recent literature indicates that there may be more active or selective catalysts for these reactions (2), Cu-ZSM-5 will likely be used in any case as the template for unraveling the mechanism, and to gain a deeper understanding of the operation of zeolite catalysts in general.

An important part in deciphering the mechanism is the identification of the active site, which in the case of the reduction or decomposition of NO, must allow for the formation of dinitrogen; i.e. the pairing of nitrogens in NO. In the original scheme of Iwamoto (1) and in other schemes (3) this site was assigned to the cuprous ion. Considering the very strong oxidizing conditions of the reaction, the plausibility of this assignment has been called into question (4). To be able to identify different oxidation states, preferably under conditions similar to those of actual use, unambiguous experimental measurements are required.

0097-6156/94/0552-0066\$08.00/0
© 1994 American Chemical Society

To follow the changes in the oxidation state of copper in Cu-ZSM-5 electron paramagnetic resonance (EPR) (3,5,6) is the method of choice. There are several difficulties with its use under any conditions apart from vacuum at low temperatures because even the adsorption of inert gases alters the signal from the paramagnetic Cu^{2+} ions located at specific sites in the zeolite (6).

Here we attempt to explore whether X-ray photoelectron spectroscopy (XPS), a technique thought to be less sensitive to interferences in the identification of oxidation states, can be of use. XPS has been used previously to investigate X- and Y-type Cu-exchanged zeolites (7-10) which have a relatively high Al content and concomitant high Cu-loadings, as well as to determine copper speciation in a copper-containing intercalation phase (11) and to identify the oxidation state of copper in spent catalysts on different supports (12). Recently there was one XPS study of the Cu-ZSM-5 zeolite (13). In the present work the oxidation state of copper in copper-exchanged ZSM-5 zeolite was determined following various *in situ* oxidizing and reducing treatments at atmospheric pressure, and the results were compared with those of a previous study (13) where heat treatments were conducted *in vacuo*.

Experimental

Explicit details describing the XPS analytical system and attached catalytic reactor have been reported in an earlier paper (14). A summary of the experimental conditions pertaining to this study is given below.

Copper-exchanged ZSM-5. The H-ZSM-5 zeolite, exhibiting a $\text{SiO}_2/\text{Al}_2\text{O}_3$ molecular ratio of 30, was purchased from the PQ Corporation, Zeolites & Catalysts Division. The zeolite was 40 at. % exchanged with copper (1.31 wt. % or 0.41 at. % overall Cu, as determined by ICP-MS). The sample is close in composition to the one used in ref. 13 where the Si/Al atomic ratio was 13.4 and the exchange was 46 at. %. The zeolite powder was pressed into a 6-mm diameter pellet to allow for reactor treatment and analysis by XPS.

XPS Analytical System. Spectra were acquired on an M-Probe XPS spectrometer manufactured by Surface Science Instruments, VG Fisons, using monochromatic $\text{AlK}\alpha$ X-rays (1486.7 eV, 80W) focused to a 1200- μm diameter beam. Unless stated otherwise, total time for acquisition of the Cu core level spectrum was 10 min. The relatively low X-ray power, large spot diameter, and short acquisition time were chosen to insure that minimal reduction of the cupric ion by the X-ray flux occurred during analysis, which has been observed by others (9,10,13) for the sensitive zeolite structure. A low energy (1-3 eV) electron flood gun and a Ni charge neutralization screen placed 1-2 mm above the sample were employed to minimize surface charging effects (15). The analyzer was operated at a 150-eV pass energy. Binding energies reported for the Cu $2p_{3/2}$ core level spectra were referenced to the Si 2p line at 102.9 eV, i.e. adventitious aliphatic C 1s line at 284.6 eV. All binding energy positions quoted in this work were measured to an accuracy of ± 0.2 eV. The raw data from the Cu $2p_{3/2}$ core level spectra were smoothed using the Savitsky-Golay method. Photoionization yields of the Cu

2p_{3/2} and Si 2p lines were normalized to give Cu/Si atomic ratios by means of routines based on Scofield's photoionization cross-section values (16).

The samples were treated in a PHI Model 04-800 Reactor System mounted directly onto the preparation chamber of the spectrometer (14). The treatments were carried out at 500°C and atmospheric pressure for 6 h, after which the samples were cooled in the flowing reactor gases to below 100°C (about 30 min). At this point gas flow was ceased, and the reactor door was opened to vacuum. Samples were transferred between the reactor and spectrometer *in vacuo* to eliminate contamination and reoxidation by air. The reactor gases used were Ar (99.9995%), O₂ (99.98%), H₂ (99.9995%) and CO (99.99%), purchased from Matheson.

Results and Discussion

Cu-exchanged ZSM-5 sample A was subjected to the sequence of treatments given in Table I. Each reactor treatment, at 500°C for 6 h, was followed immediately by XPS analysis. After analysis, the sample was transferred back into the reactor for the next successive treatment, and so forth. A second sample, B, was subjected to O₂ and CO treatments only, to discern how CO treatment directly after oxidation compares to CO treatment after the cyclic oxidative and reductive treatments subjected to sample A. Table I also includes 9 measurements of the Cu/Si atomic ratio attained after the different treatments, plus the mean and standard deviation of these measurements. The mean Cu/Si atomic ratio of 1.58×10^{-2} was close (within a standard deviation of ± 0.27) to 1.33×10^{-2} , the value derived for the sample bulk from ICP-MS. The lowest Cu/Si ratios measured by XPS for sample A, 1.34×10^{-2} , 1.22×10^{-2} and 1.31×10^{-2} , appeared after reductive Treatment Nos. 2, 5 and 7, respectively. (Treatment No. 2, a 400-min XPS acquisition, was in essence equivalent to a reductive treatment, as will be explained later under the "Discussion" section.) However this trend was not observed in sample B, since the Cu/Si ratio measured after reductive CO treatment was 1.70, consistent with the higher ratios measured for sample A, after oxidative treatments. Nonetheless, it should be noted that even after the harsh reduction in Treatment No. 5 no substantial surface migration of Cu out of the zeolite structure was evidenced by XPS, which, assuming surface Cu at these low levels remains mostly dispersed, would have been observed as an enhanced Cu/Si atomic ratio.

Figure 1 shows the Cu 2p_{3/2} core level spectra acquired for sample A initially, and after reactor treatments at 500°C in O₂, Ar, and again in O₂ immediately following reduction in H₂. The sequence of these spectral acquisitions corresponds to Treatment Nos. 1, 3, 4 and 6, respectively, in Table I. For all spectra, the Cu core level consisted of two main peaks at 933.5 and 936.5 eV, referred to as peaks I and II, respectively, and a corresponding broad satellite peak centered at 944.5 eV (943.5 eV in the initial spectrum). The presence of Cu²⁺ is confirmed by the appearance of the satellite peak (7), which is absent in Cu⁰ and Cu¹⁺ states. The binding energy for peak I, 933.5 eV, is similar to that observed for CuO (17). However, the binding energy noticed for peak II is considerably higher, indicating that 1) the copper oxidation state is

Table I. XPS Cu/Si atomic ratio of Cu-exchanged ZSM-5 as a function of treatment

Sample	Treatment No. (Description)	Cu/Si Ratio $\times 10^2$
A	1 (initial, 10-min XPS acquisition)	1.33 ^a
	2 (initial, 400-min XPS acquisition)	1.42
	3 (500°C O ₂)	1.73
	4 (500°C Ar)	1.68
	5 (500°C H ₂)	1.22
	6 (500°C O ₂)	2.04
	7 (500°C CO)	1.31
B	1 (500°C O ₂)	1.79
	2 (500°C CO)	1.70
		1.58 (0.27) ^b

^aIn the bulk of the Cu-ZSM-5 sample, as determined by ICP-MS.

^bMean (standard deviation), both samples.

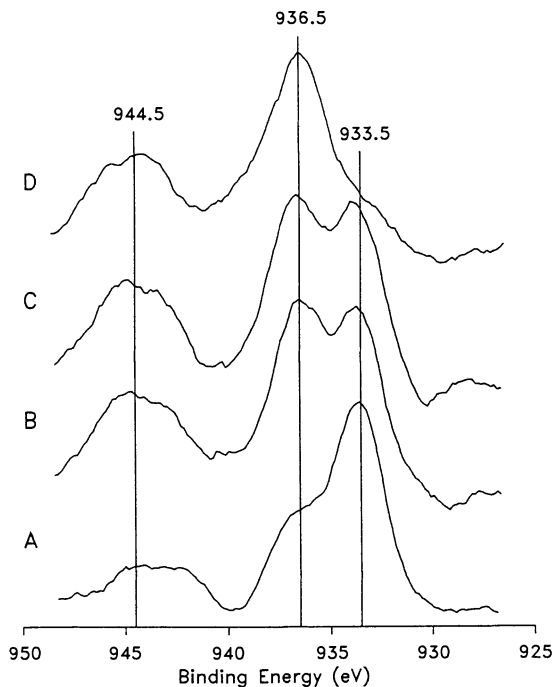


Figure 1. XPS Cu $2p_{3/2}$ core level spectra of Cu-exchanged ZSM-5 zeolite A) initially, B) after oxidation at 500°C for 6 h, C) after heating in Ar at 500°C for 6 h and D) after reduction in H₂ at 500°C followed by oxidation at 500°C for 6 h.

probably +2, and 2) that this state is highly ionic in nature; i.e. a binding energy of $\sim 936\text{eV}$ is observed for CuF_2 (18). Within the zeolite framework, this species may be more properly viewed as being coordinatively unsaturated. While the binding energy positions of both peaks I and II are consistent with divalent copper, the satellite envelope represents a combination of peaks, each corresponding to one of the Cu^{2+} core lines (9). However, since the peak definition under the satellite envelope is quite subtle, no attempt is made to deconvolute this region. The satellite peak is uniquely associated with the Cu^{2+} state because in this case two channels for core level screening, a local and non-local one, are possible during the photoemission process. For Cu^{2+} the photoelectron emitted is screened either by the $3d^9$ electrons, or by the $3d^9$ electrons plus one electron from the ligand. The former gives rise to the satellite peak, while the later, being equivalent to a full $3d^{10}$ configuration as is present in Cu^0 and Cu^{1+} , contributes to the main core line.

The core level peaks I and II, previously observed in Cu-ZSM-5 (13) as well as in copper-exchanged X- and Y-type sodium zeolites (9), have been assigned by Contarini and Kevan to tetrahedrally and octahedrally coordinated Cu^{2+} , respectively. This assignment of both peaks to the cupric ion was supported by ESR measurements where both states were shown to be associated with the paramagnetic response. It was suggested that the octahedrally coordinated Cu^{2+} in the zeolite was hydrated, with the cupric ions coordinated by three framework oxygens and three water molecules. In an XPS study of Cu-ZSM-5 and Cu-Y zeolite by Jirka and Bosacek (13), two peaks with similar binding energies were present. Peak II has been observed to disappear after prolonged *in vacuo* heat treatment and then reappear after exposure to ambient air, i.e. water vapor. For the Cu-exchanged ZSM-5 in this work, the initial Cu $2p_{3/2}$ spectrum (Figure 1A) showed a more prominent peak at 933.5 eV (peak I). After heating in O_2 at 500°C the peak at 936.5 eV (peak II) was enhanced (Figure 1B), while an additional heating in Ar (Figure 1C), essentially an inert heat treatment, did not change this spectrum. In addition, after a subsequent reduction in H_2 and reoxidation in O_2 (Figure 1D), peak II virtually displaced peak I. Thus, treatment under oxidizing conditions gradually shifts the coordination of the cupric ions towards a configuration associated with the peak having the higher binding energy. Once the copper has been reduced to the metallic state (*vide infra*) and reoxidized, most copper ions, at the examined exchange level, end up in the higher binding energy state.

These results differ somewhat from those of Jirka and Bosacek. However, reactor treatments in this study were done at atmospheric pressure, whereas in both refs. 9 and 13 the heat treating was accomplished *in vacuo*. It is postulated, based on the extensive work of Kucherov *et al.* (5,6) and at variance with Jirka and Bosacek, that the coordination of the cupric ions in Cu-ZSM-5 and Cu-Y zeolite differs. According to Kucherov a CuH-ZSM-5 sample exchanged to 20% by copper and dehydroxylated at 500°C , i.e. very close to that used in this work, contains two differently coordinated isolated Cu^{2+} ions. Both kinds of Cu^{2+} ions are coordinatively unsaturated; one in a square-planar configuration and the other in a square pyramidal configuration. These unsaturated cupric ions do coordinate a wide variety of ligands upon adsorption, oxygen molecules included

(5), so it is probable that not only hydration may induce changes in coordination leading to the observed changes in binding energy. Also, consider that coordination changes can be induced in Cu-ZSM-5 by mere adsorption of non-polar adsorbents (6).

Figure 2 compares the Cu $2p_{3/2}$ spectrum obtained initially to those obtained after reductive treatments. Spectra A, B, C and D correspond to Treatment Nos. 1, 2, 5 and 7 in Table I, respectively. In contrast to the initial spectrum of the copper-exchanged zeolite observed after a 10-min spectral acquisition (Figure 2A), after a 400-min spectral acquisition (Figure 2B) the satellite peak and peak II (936.5 eV) of the Cu $2p_{3/2}$ core line disappeared, while the peak at 933.5 eV persisted. The disappearance of the satellite peak implies a reduction of the Cu below the +2 state. The remaining peak at 933.5 eV did not shift, but the binding energy is also consistent with what has been observed previously for Cu¹⁺ by Jirka and Bosacek after X-ray induced reduction in Cu-ZSM-5.

The Cu $2p_{3/2}$ spectrum obtained after H₂ reduction is shown in Figure 2c. The satellite peak was absent, and the core level peak was shifted to 932.0 eV. One may conclude that after these severe reduction conditions the copper was reduced to metallic Cu⁰. The binding energy observed is consistent with that reported previously for Cu metal (9). Reduction by CO (Figure 2d) also caused the satellite peak to disappear, implying a reduction of the copper below the +2 state. However, a broad core level peak appeared, centered between 933.5 and 932.0 eV. It is reasonable to assume that the less severe reduction in CO may have reduced the copper to a mixture of Cu¹⁺ and Cu⁰ states. This agrees completely with the previous observation that the cupric ions in Cu-ZSM-5 are more easily reduced by H₂ than by CO (5). A second reduction with CO was performed on sample B, after the sample was subjected to an initial oxidation only (Table I). The Cu $2p_{3/2}$ core level spectrum obtained from that sample was identical to that of sample A shown in Figure 2d.

In principle, a more precise definition of the chemical state of copper could have been obtained by measurement of the Auger parameter (19). Such information would have been helpful to differentiate the reduced states of copper found in Figure 2. As it happens, the most intense copper Auger line, Cu L₃M₄₅M₄₅, is considerably broader, and only about half as intense as the Cu $2p_{3/2}$ core line. This means that at the low levels of copper present in the ZSM-5 zeolite, a large acquisition time would have been necessary to obtain an accurate measurement of the kinetic energy of the Cu L₃M₄₅M₄₅ line. During this time, any further X-ray induced reduction of copper would have been inevitable, and the measurement would no longer reflect the original state of copper associated with the Cu $2p_{3/2}$ core level obtained after a short acquisition time of 10 min. Thus, for this system, measurement of the Cu Auger parameter is impractical.

Conclusions

The results of this study indicate that Cu-ZSM-5 is stable with respect to the migration of the Cu-ions out of the zeolitic framework up to 500°C under severe non-hydrothermal oxy-reductive treatments. Although explicit assignments of

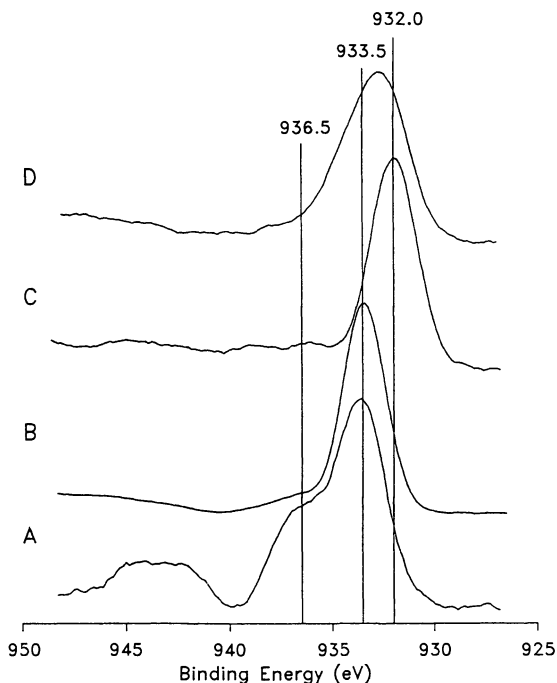


Figure 2. XPS Cu $2p_{3/2}$ core level spectra of Cu-exchanged ZSM-5 zeolite A) after a 10-min acquisition, B) after a 400-min acquisition, C) after reduction in H_2 at $500^\circ C$ for 6 h and D) after reduction in CO at $500^\circ C$ for 6 h.

configurations of Cu in the zeolite structure to the specifically observed Cu $2p_{3/2}$ lines could not be made, it was nevertheless shown that heat treatment under oxidizing conditions induces changes in the populations of Cu^{2+} ions in different spatial coordinations. One state is similar in binding energy to CuO, while the other state appears to be highly ionic in nature, i.e. coordinatively unsaturated. The Auger parameters necessary for the unambiguous assignment of the reduced copper states can only be obtained in the low-Cu specimens (i.e. Cu exchanged into high Si/Al ratio zeolites) when simultaneous *in situ* instrumentally induced reduction is made possible during the long acquisition times. This will be still more difficult to avoid in the interpretation of data obtained under less definable conditions such as those encountered in real catalytic practice.

Acknowledgment

We thank George Graham for going over the manuscript and his incisive comments.

Literature Cited

1. Iwamoto, M.; Hamada, H. *Catal. Today*. **1991**, *10*, 57-71.
2. Misono, M.; Kondo, K. *Chem. Lett.* **1991**, *6*, 1001-2.
3. Giamello, E.; Murphy, D.; Magnacca, G.; Morterra, C.; Shioya, Y.; Nomura, T.; Anpo, M. *J. Catal.* **1992**, *136*, 510-20.
4. Shelef, M. *Catal. Lett.* **1992**, *15*, 305-10.
5. Kucherov, A. V.; Slinkin, A. A.; Kondrat'ev, D. A.; Bondarenko, T. N.; Rubinshtein, A. M.; Minachev, Kh. M. *Zeolites*. **1985**, *5*, 320-4.
6. Kucherov, A. V.; Slinkin, A. A. *J. Phys. Chem.* **1989**, *93*, 864-7.
7. Jirka, I.; Wichterlova, B.; Maryska, M. *Stud. Surf. Sci. Catal.* **1991**, *69*, 269-76.
8. Narayana, M.; Contarini, S.; Kevan, L. *J. Catal.* **1985**, *94*, 370-5.
9. Contarini, S.; Kevan, L. *J. Phys. Chem.* **1986**, *90*, 1630-2.
10. Kaushik, V. K.; Ravindranathan, M. *Zeolites*. **1992**, *12*, 415.
11. Guerrero-Ruiz, A.; Rodriguez-Ramos, I.; Siri, G. J.; Fierro, J. L. G. *Surf. Interface Anal.* **1992**, *19*, 548-52.
12. Malitesta, C.; Sabbatini, L.; Torsi, L.; Zambonin, P. G.; Ballivet-Tkatchenko, D.; Galy, J., Parize, J. L.; Savariault, J. M. *Surf. Interface Anal.* **1992**, *19*, 513-18.
13. Jirka, I.; Bosacek, V. *Zeolites*. **1991**, *11*, 77-80.
14. Shelef, M.; Haack, L. P.; Soltis, R. E.; deVries, J. E.; Logothetis, E. M. *J. Catal.* **1992**, *137*, 114-26.
15. Bryson III, C. E. *Surf. Sci.* **1987**, *189-190*, 50-8.
16. Scofield, J. H. *J. Electron Spectrosc. Relat. Phenom.* **1976**, *8*, 129-37.
17. Wolberg, A.; Ogilvie, J. L.; Roth, J. F. *J. Catal.* **1970**, *19*, 86-9.
18. Wagner, C. D.; Riggs, W. M.; Davis, L. E.; Moulder, J. F. In *Handbook of X-ray Photoelectron Spectroscopy*; Muilenbery, G. E., Ed.; 1st Edition; Perkin-Elmer Corporation, Physical Electronics Division: Eden Prairie, Minnesota, 1979, p 82.
19. Wagner, C. D.; Gale, L. H.; Raymond, R. H. *Anal. Chem.* **1979**, *51*, 466-82.

RECEIVED September 29, 1993

Chapter 7

Catalysts for Cleanup of NH_3 , NO_x , and CO from a Nuclear Waste Processing Facility

R. Gopalakrishnan, J. Davidson, P. Stafford, W. C. Hecker, and
C. H. Bartholomew¹

Catalysis Laboratory, Department of Chemical Engineering, Brigham
Young University, Provo, UT 84602

Performance of Cu-ZSM-5, Pt/ Al_2O_3 and Cu-ZSM-5 + Pt/ Al_2O_3 for NH_3 (425-750 ppm) and CO (~1%) oxidation in the presence of NO (250 ppm), O_2 (14-15%) and H_2O (~20%) was studied as a function of temperature. Pt/ Al_2O_3 is more active for NH_3 and CO oxidation, while Cu-ZSM-5 is more selective for conversion of NO and NH_3 to N_2 . NH_3 and CO are completely oxidized above 300°C on Pt/ Al_2O_3 , while on Cu-ZSM-5 about 99% of NH_3 and NO are converted to N_2 at 450-500°C, although only about 50% of CO is converted to CO_2 . The selectivity of Cu-ZSM-5 for conversion of NH_3 and NO to N_2 is about 100%, while selectivities of Pt/ Al_2O_3 for N_2 and N_2O are 35-40% and 20-40% respectively. However, the activity and selectivity of a Cu-ZSM-5 + Pt/ Al_2O_3 dual catalytic system are very high, converting 99% of NH_3 , 94% of NO, and 100% of CO simultaneously at 485°C with a 100% selectivity to N_2 .

An interesting application of emissions control catalysts occurs in management and immobilization of spent radioactive fuels and wastes in the nuclear industry. During nuclear waste processing (NWP) NO_x (NO and NO_2) and CO pollutants are typically discharged at levels of 1-3% to a waste gas stream. It is necessary to control both NO_x and CO emissions in order to comply with current and anticipated regulatory requirements.

In earlier work, Thomas and coworkers (1-3) found that NO_x in a NWP offgas (also containing 2% CO, 3% CO_2 , 14% O_2 , 20% H_2O and the remainder of N_2) could be removed from levels of 10,000 - 30,000 ppm to 300-1,000 ppm by selective catalytic reduction with ammonia over a commercial H-mordenite catalyst at 300-500°C. Based on this work it was anticipated that at high conversion rates of NO_x , ammonia slippage of 100-500 ppm might occur. However, acceptable levels of ammonia slippage for SCR facilities are generally 5-10 ppm to prevent ammonium nitrate and sulfate formation downstream of the reactor. Moreover, the extent to which CO is converted during SCR on mordenite catalysts under these conditions is apparently low. Accordingly, the need for an additional catalytic reactor designed for clean-up of ammonia, NO_x and CO to low ppm levels is anticipated; ideally, the catalyst used in this reactor should be capable of catalyzing simultaneously the oxidations of CO and NH_3 and the selective catalytic reduction (SCR) of NO_x with ammonia.

¹Corresponding author

0097-6156/94/0552-0074\$08.00/0

© 1994 American Chemical Society

The principal objective of this study was to investigate the activity/selectivity behavior of Cu-ZSM-5, Pt/Al₂O₃, and a combined Cu-ZSM-5 + Pt/Al₂O₃ system for simultaneously oxidizing ammonia and CO and reducing NO_x under conditions applicable to NWP. Pt/Al₂O₃ was selected as a candidate catalyst because of its known high activity for CO oxidation and SCR of NO_x with NH₃ (4,5). Cu-ZSM-5 was chosen as a test catalyst for NH₃ and NO_x removal because of its promising performance as an SCR catalyst using hydrocarbon (6-8) and NH₃ (9,10) reducing agents. Although H and metal ion exchanged mordenite have been studied widely for NO_x reduction by NH₃ (3,11-17) it appears that only two preliminary studies have reported on ZSM-5 catalysts (9,10). For example, NC-300 (Zeolon 900H), a mordenite based catalyst from Norton company, is a well known commercial SCR catalyst for NO_x reduction by NH₃ (Norton Company. "NC-300 Catalysts for NO_x Removal"; commercial report, 1992). In general, it is observed that NO_x conversion increases on H-mordenite with increasing temperature at a given space velocity, then passes through a maximum and decreases above a certain temperature at which direct oxidation of NH₃ becomes a significant competing reaction (11,14). Catalytic activity decreases with increasing space velocity and presence of water vapor, SO₂ etc. (11,12,17). A dual catalyst system, H-mordenite/2.2% Cu-mordenite, decreases the temperature window of maximum NO conversion (~100%) from 500-550°C to 350-400°C at a space velocity of 241,000 h⁻¹ (13).

Co and Cu ion exchanged Y-zeolites (18,19) and SiO₂ supported CuO (20) have also been tested for SCR activity using NH₃ as the reducing agent; while relevant to the performance of zeolite catalysts for NO reduction with NH₃ the previous work has not adequately defined the performance of such catalysts for NWP applications. This paper reports the results of comprehensive tests on Cu-ZSM-5, Pt/Al₂O₃, and Cu-ZSM-5 + Pt/Al₂O₃ dual catalysts over wide ranges of conversion, temperature and species concentration representative of NWP applications.

Experimental

Materials. The Cu-ZSM-5 used in this study was previously investigated for the SCR of NO by propane (5); it consisted of 1% Cu ion-exchanged into a ZSM-5 (Si/Al = 21) supplied by the PQ corporation. The promoted Pt/Al₂O₃ catalyst was supplied by the Engelhard Corporation.

Nitric oxide (>99% pure, 3000 ppm in He), NH₃ (>99.5% pure, 2000 ppm in He), and 10% CO in He were obtained from the Matheson gas company. Helium and oxygen tanks were purchased from Whitmore Oxygen Co., Salt Lake City, UT. Gases other than NO and NH₃ were dried with zeolite traps.

Procedure and Equipment. Oxidation of CO and NH₃ and reduction of NO on Cu-ZSM-5 and Pt/Al₂O₃ catalysts were investigated at near atmospheric pressure over a temperature range of 150-550°C in a quartz flow microreactor. In a typical experiment, about 0.3 g of Cu-ZSM-5 or 0.5 g of Pt catalyst was used to obtain a space velocity of 63,000-65,000 h⁻¹. The reactor system was equipped with an on-line Gas Chromatograph (Hewlett Packard 5890), a NO/NO_x analyzer (Rosemount Analytical, Model 951A), an NH₃ gas analyzer (Rosemount Analytical, Model 880) and an Allen CO/HC infrared analyzer. The analyzers and GC were calibrated every other day using appropriate calibration gases (NO, NH₃, CO, CO₂, N₂O, and N₂) obtained from the Matheson gas company. Concentrations of NO, NH₃, and CO were measured before and after reaction and conversions were plotted as a function of temperature. Concentrations of NH₃, NO, NO₂, and CO were measured by continuous analyzers to within ± 2-3%, while concentrations of N₂O and CO₂ could be analyzed by GC to within ±5%. However, measurement of the N₂ concentration was less reproducible and hence, it was calculated based on a N-material balance by assuming NO, NO₂ and N₂O as the only other N-containing products.

The flow reactor used in a previous study (6) was modified to incorporate water vapor and NH_3 in the feed stream to the reactor cell and a condenser to trap the water vapor in the effluent. The reactant gas mixture was bubbled through a water reservoir heated at a fixed temperature to maintain an appropriate concentration of water vapor. NH_3 was introduced just before the reactor cell. It was found that NH_3 was completely soluble in water, and hence none was detected in the gas phase. In this case, the dissolved NH_3 was estimated using an aqueous NH_3 analyzer (Orion model 720A) by collecting water every 30 minutes.

Results and Discussion

CO Oxidation. The results of CO oxidation tests carried out on Cu-ZSM-5 at different space velocities are presented in Figure 1. At a space velocity of $10,000 \text{ h}^{-1}$, CO conversion apparently reaches 100% at 400°C . However, at a higher space velocity ($65,000 \text{ h}^{-1}$), CO conversion does not exceed 90% even at 500°C . Moreover, the presence of 28% water vapor considerably reduces CO conversion levels; for example, a maximum of only 55% conversion is obtained at 500°C . Thus, Cu-ZSM-5 is limited to CO clean-up applications involving dry conditions, high reaction temperatures or lower space velocities.

CO conversion versus temperature data for $\text{Pt}/\text{Al}_2\text{O}_3$ are likewise shown in Figure 1. CO oxidation in the absence of water is extremely rapid, as indicated by 100% conversion at 280°C . Unlike Cu-ZSM-5, the presence of water vapor enhances CO conversion on $\text{Pt}/\text{Al}_2\text{O}_3$; indeed 100% conversion is obtained at 258°C . The increase in CO conversion could be due to promotion of the water-gas shift reaction by the Pt catalyst.

Ammonia Oxidation/SCR of NO. A range of NH_3 slippages (50-500 ppm) is anticipated for NWP clean-up (1-3) depending upon the fluctuations in NH_3 feed concentration and in temperature of the SCR beds. Hence, NH_3 oxidation activity tests were conducted starting with an excess of NH_3 ; for example, $[\text{NH}_3] = 500 \text{ ppm}$, $[\text{NO}] = 0$ or 250 ppm, $[\text{CO}] = 1\%$, and $[\text{O}_2] = 14\%$.

Cu-ZSM-5. Results of NH_3 oxidation activity (in the absence of NO) obtained under dry and wet conditions on Cu-ZSM-5 are presented in Figure 2. Conversion of NH_3 is relatively low below 400°C , while 99% conversion to all products is obtained only at greater than 500°C . Nevertheless, the selectivity towards N_2 formation is better than 95% at all temperatures; no N_2O is formed. NH_3 oxidation to NO and NO_2 is the competing reaction with less than 5% selectivity. Although the presence of 22% water decreases the NH_3 conversion at temperatures lower than 500°C , it increases the N_2 selectivity to about 100% at 500°C . Addition of 250 ppm of NO and 1% CO improves the conversion efficiency of the catalyst for NH_3 and NO to N_2 at lower temperatures, reaching 96% at 450°C (Figure 2). It should be remembered that reduction of NO by NH_3 is a highly favorable reaction at these temperatures. Hence, NH_3 is probably oxidized by at least two routes; with dioxygen and with NO. A maximum of 100% is apparently reached at 337°C . Nevertheless, the conversion significantly decreases above 337°C , suggesting that NH_3 oxidation by dioxygen to NO_x is a competing reaction with SCR of NO by NH_3 at high temperatures. It appears, however, that NH_3 oxidation by dioxygen does not occur up to temperatures around 500°C in the presence of water. With addition of water the conversion of NH_3+NO to N_2 is decreased at lower reaction temperatures.

The role of water in the NH_3 oxidation/SCR reaction is not clear. However, it is possible that water vapor could affect the concentration and strength of Bronsted acid sites on the zeolite surface, which in turn could act as sites in the SCR reaction. Water vapor might also affect the surface concentration of hydrogen through the water-gas-shift (WGS) reaction. Under these conditions, however, CO conversion is only about 46% at 483°C indicating that SCR and NH_3 oxidation are the dominant reactions on Cu-ZSM-5 compared to CO oxidation and CO WGS. Moreover, the results for Cu-

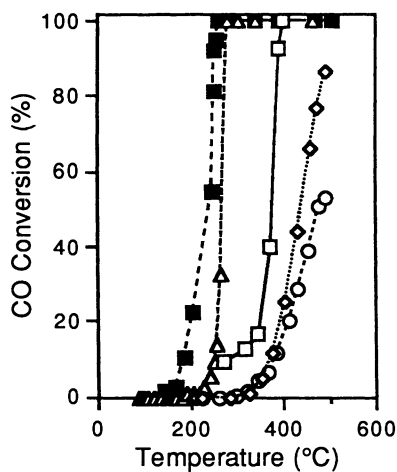


Figure 1. Conversion vs. temperature behavior of Cu-ZSM-5 and Pt/Al₂O₃ catalysts for CO oxidation with 14% O₂. (i) Cu-ZSM-5; \square : GHSV = 10,000 h⁻¹ and no water, \diamond : GHSV = 65,000 h⁻¹ and no water, \circ : GHSV = 65,000 h⁻¹ and 28% water. (ii) Pt/Al₂O₃, GHSV = 63,000 h⁻¹, Δ : no water and \blacksquare : 16% water.

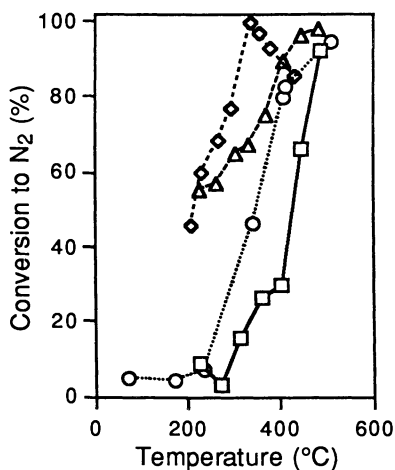


Figure 2. Ammonia oxidation with 14% O₂ on Cu-ZSM-5 at various conditions. (i) GHSV = 64,000 h⁻¹, [NH₃] = 425 ppm; \circ : no water, \square : 22% water, (ii) GHSV = 64,000 h⁻¹, [NH₃] = 425 ppm, [NO] = 250 ppm, [CO] = 1%; \diamond : no water, Δ : 22% water.

ZSM-5 in Figure 1 suggest that CO conversion by the WGS reaction is probably less important than by reaction with dioxygen.

Effects of NH_3/NO ratio on NH_3 , NO, and CO conversions in the presence of water on Cu-ZSM-5 are summarized in Figures 3-8. NH_3 conversion is higher at lower NH_3/NO ratios at reaction temperatures below 400°C but nearly independent of NH_3/NO ratio at 500°C as all approach 100% conversion (Fig. 3). NO_x conversion is 90-100% over a wide range of conversion at NH_3/NO ratios of unity or greater (Figure 4). Apparently, the maximum conversions of NO and NH_3 to N_2 (~100%) are observed for an NH_3/NO ratio of unity (Figure 5). Again, the only nitrogen-containing products other than N_2 are NO and NO_2 ; no N_2O formation is observed up to 500°C. Even in the case of $\text{NH}_3/\text{NO} > 1$, Cu-ZSM-5 appears to oxidize the excess NH_3 with a high selectivity to N_2 (see Fig. 5). On the other hand, CO conversion is generally only 10-40% in the temperature range of 350-500°C with little dependence on NH_3/NO ratio (maximum CO conversion of 60% occurs at 500°C and $\text{NH}_3/\text{NO} = 0.5$; see Figure 6). This indicates that since the mordenite catalyst in the front end of the NWP clean-up process is relatively inactive for CO oxidation, a backup to the Cu-ZSM-5 catalyst (possibly a layer of $\text{Pt}/\text{Al}_2\text{O}_3$) will probably be necessary for complete CO oxidation.

Figures 7 and 8 summarize the conversion behavior for Cu-ZSM-5 as a function of NH_3/NO ratio at the optimum operating temperature of 450°C. The data in Figure 7 indicate that greater than 90% conversion of ammonia and NO to N_2 occurs mainly at NH_3/NO ratios of 1-2. Moreover, the data in Figure 8 show that ammonia slip is also quite low under these conditions. For example, for NH_3/NO ratios of 1-2 NH_3 slip at 450°C is only 5-25 ppm. Ammonia slip may be lowered by (1) operating at an NH_3/NO ratio of 1 or less, (2) increasing reaction temperature, and (3) decreasing space velocity (adding more catalyst). Thus, for simultaneous removal of NH_3 and NO the optimum NH_3/NO ratio is one.

Pt/ Al_2O_3 catalyst. Ammonia conversion on $\text{Pt}/\text{Al}_2\text{O}_3$ reaches 100% above 250°C in the presence of 14% O_2 at a GHSV = 63000 h^{-1} (Figure 9). However, the Pt catalyst suffers from low selectivity to N_2 . That is, large quantities of N_2O (32% at 330°C) and NO_x (62% at 500°C) are produced above 250°C. This observation agrees well with the data of Katona et al. (21) that above 250°C the N_2 selectivity decreases and N_2O and NO formation increase. It appears that addition of water does not substantially affect the NH_3 oxidation behavior (compare Fig. 10 with Fig. 9).

Ammonia oxidation/SCR activity of the $\text{Pt}/\text{Al}_2\text{O}_3$ catalyst was studied as a function of temperature in the presence of a mixture of NH_3 , NO, O_2 , and H_2O (see Figure 11). NH_3 is completely oxidized above 300°C. Apparently a large quantity of N_2O (~84%) is produced at 226°C due to NH_3 oxidation/NO reduction. At temperatures above 270°C NO conversion and N_2O production decrease very significantly to 53 and 47% at 385°C, 37 and 36% at 414°C, and 2 and 14% at 482°C; however, NO_2 production increases to about 14% and N_2 production increases to about 31% at 482°C. Thus, at 311°C the 750 ppm of total nitrogen equivalents (originally present in the feed as 500 ppm NH_3 and 250 ppm NO) leaves the reactor as 2% NH_3 , 1% NO_2 , 78% N_2O , 17% N_2 , and 7% NO (10 ppm NH_3 , 8 ppm NO_2 , 292 ppm N_2O , 64 ppm N_2 , and 21 ppm NO).

It appears that NH_3 is consumed on the $\text{Pt}/\text{Al}_2\text{O}_3$ catalyst in at least two reactions: (1) direct oxidation by O_2 and (2) oxidation by NO. Since the formation of N_2 and N_2O at lower reaction temperatures (250-330°C) correlates with higher conversions of NO, it is probably due to SCR of NO by NH_3 and N_2O could be an intermediate of NO reduction at high temperature. The substantial decrease in NO conversion and in the formation of NO_2 above 300°C suggests that oxidation of NH_3 to NO_x is favored at higher reaction temperatures.

Figure 12 summarizes the ammonia conversion activity of the $\text{Pt}/\text{Al}_2\text{O}_3$ catalyst as a function of temperature in a mixture of NO, O_2 , CO, and H_2O . The conversion trends are similar to those of Figure 11 for which no CO was present. However, NO

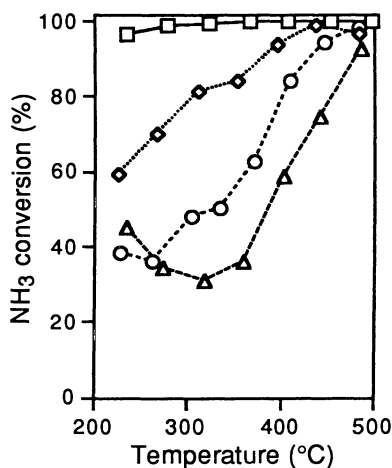


Figure 3. Ammonia conversion vs. temperature during its oxidation with 14% O₂ over Cu-ZSM-5 in the presence of NO, CO and H₂O as a function of NH₃/NO ratio. GHSV = 64,000 h⁻¹, [NO] = 250 ppm, [CO] = 1%, [H₂O] = 20%; □: NH₃/NO = 0.5, ◇: NH₃/NO = 1.0, ○: NH₃/NO = 2.0, △: NH₃/NO = 3.0.

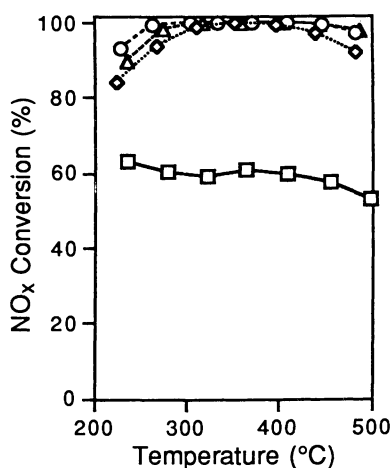


Figure 4. NO conversion vs. temperature during ammonia oxidation with 14% O₂ over Cu-ZSM-5 in the presence of NO, CO and H₂O as a function of NH₃/NO ratio. GHSV = 64,000 h⁻¹, [NO] = 250 ppm, [CO] = 1%, [H₂O] = 20%; □: NH₃/NO = 0.5, ◇: NH₃/NO = 1.0, ○: NH₃/NO = 2.0, △: NH₃/NO = 3.0.

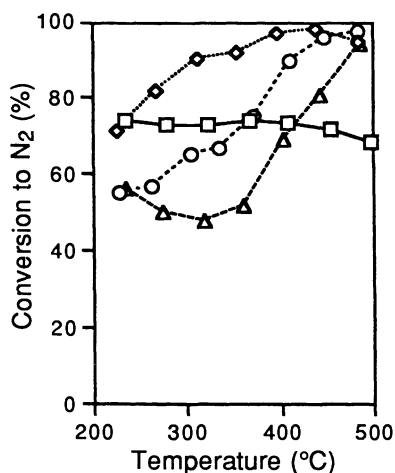


Figure 5. Selectivity of NH₃ and NO to N₂ over Cu-ZSM-5 in the presence of NO, CO and H₂O as a function of NH₃/NO ratio. GHSV = 64,000 h⁻¹, [NO] = 250 ppm, [O₂] = 14%, [CO] = 1%, [H₂O] = 20%; □: NH₃/NO = 0.5, ◇: NH₃/NO = 1.0, ○: NH₃/NO = 2.0, △: NH₃/NO = 3.0.

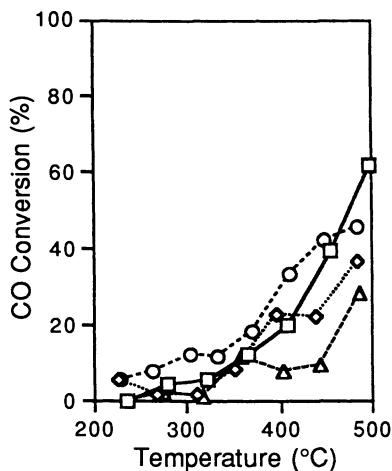


Figure 6. CO conversion vs. temperature during ammonia oxidation with 14% O₂ over Cu-ZSM-5 in the presence of NO, CO and H₂O as a function of NH₃/NO ratio. GHSV = 64,000 h⁻¹, [NO] = 250 ppm, [CO] = 1%, [H₂O] = 20%; □: NH₃/NO = 0.5, ◇: NH₃/NO = 1.0, ○: NH₃/NO = 2.0, △: NH₃/NO = 3.0.

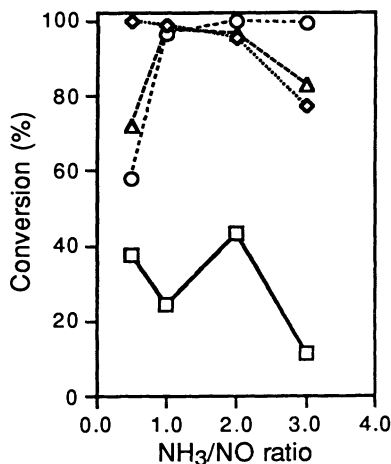


Figure 7. Effects of NH₃/NO ratio on the conversions of NH₃, NO, and CO and selectivity to N₂ at 450°C on Cu-ZSM-5. □: CO conversion, ○: NO conversion, ◇: NH₃ conversion, and Δ: conversion to N₂. Data from Figures 3-6.

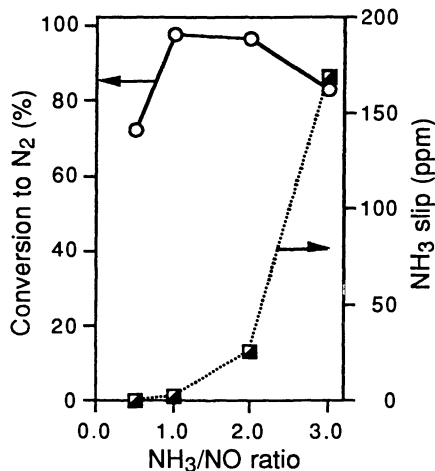


Figure 8. Comparison of selectivity to N₂ and NH₃ slippage at 450°C on Cu-ZSM-5 as a function of NH₃/NO ratio. Data from Figures 3-6.

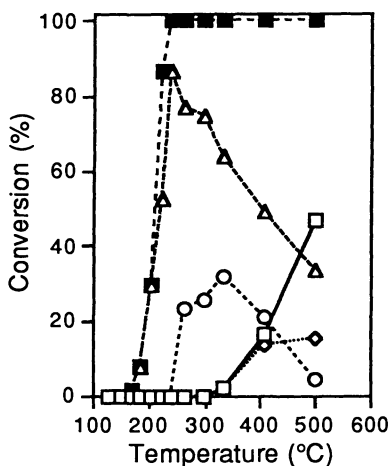


Figure 9. Ammonia oxidation with 14% O₂ on Pt/Al₂O₃. GHSV = 63,000 h⁻¹, [NH₃] = 500 ppm. ■: NH₃ conversion, □: conversion to NO, ◇: conversion to NO₂, ○: conversion to N₂O, and Δ: conversion to N₂.

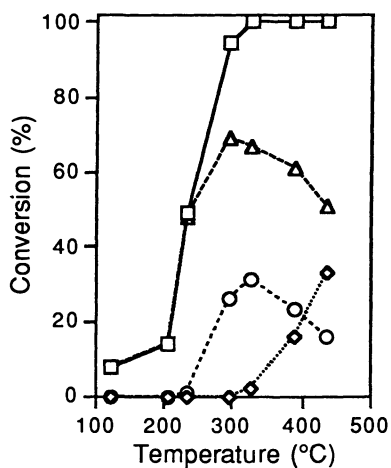


Figure 10. Ammonia oxidation with 14% O₂ on Pt/Al₂O₃ under wet condition. GHSV = 63,000 h⁻¹, [NH₃] = 500 ppm. □: NH₃ conversion, ◇: conversion to NO_x, ○: conversion to N₂O, and Δ: conversion to N₂.

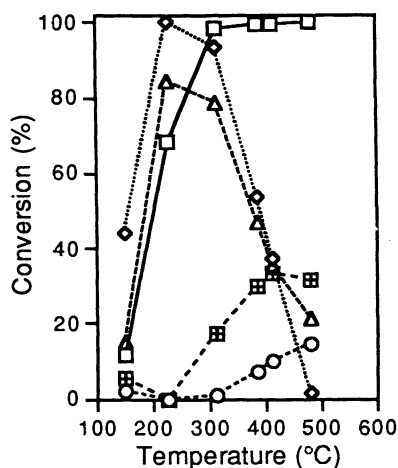


Figure 11. Ammonia oxidation with 14% O₂ in the presence of NO and H₂O on Pt/Al₂O₃. GHSV = 65,000 h⁻¹, [NH₃] = 500 ppm, [NO] = 250 ppm, and [H₂O] = 18%. □: NH₃ conversion, ◇: NO conversion, ○: conversion to NO₂, Δ: conversion to N₂O, and ▣: conversion to N₂.

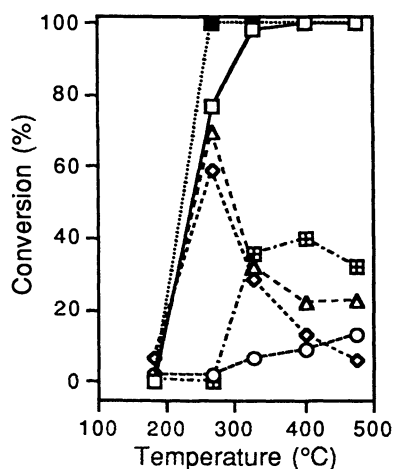


Figure 12. Ammonia oxidation with 14% O₂ in the presence of NO, CO and H₂O on Pt/Al₂O₃. GHSV = 65,000 h⁻¹, [NH₃] = 500 ppm, [NO] = 250 ppm, [CO] = 1%, and [H₂O] = 18%. □: NH₃ conversion, ◇: NO conversion, ■: CO conversion, ○: conversion to NO₂, Δ: conversion to N₂O, and ▣: conversion to N₂.

conversion is significantly reduced by the presence of CO below 250°C. A maximum of only about 60% NO conversion is obtained at 260°C (Fig. 12), while about 100% conversion is observed in the absence of CO (Fig. 11). Both NH₃ and CO are completely oxidized above 300°C. About 70% N₂O is produced at 268°C which is 14% lower than in Figure 11 suggesting that CO reduces N₂O formation. At temperatures above 300°C NO and N₂O conversions decrease, NO₂ formation increases to about 9%, and conversion of nitrogen to N₂ increases to about 20% (Figure 12). For example, at 328°C the 750 ppm of total nitrogen equivalents (originally present in the feed as 500 ppm NH₃ and 250 NO) leaves the reactor as 2% NH₃, 8% NO₂, 38% N₂O, 23% N₂, and 29% NO (10 ppm NH₃, 64 ppm NO₂, 144 ppm N₂O, 85 ppm N₂, and 218 ppm NO). The results of Figure 12 further support the hypothesis that NH₃ is oxidized in at least two reactions; in direct oxidation with O₂ and in SCR of NO. Also, NO₂ appears to be formed at high temperatures due to NH₃ oxidation with O₂, while NO is mostly consumed via the SCR mechanism. In general, the results of NH₃ oxidation and SCR of NO by NH₃ reactions are consistent with the earlier reports on Pt catalysts (22-25). Although Pt is a good oxidation catalyst, it suffers selectivity limitations for N₂, N₂O, and NO formation. To our knowledge no study has been reported on a Pt system for the NH₃-NO SCR reaction in the presence of CO. Moreover, there are some significant differences compared with the SCR reaction without CO.

The Combined Cu-ZSM-5 + Pt/Al₂O₃ System. The catalytic activity of the combined Cu-ZSM-5 + Pt/Al₂O₃ catalyst system was determined with equal amounts of the two catalysts (0.46 cc) each packed in series (Cu-ZSM-5 followed by Pt/Al₂O₃) and separated by about a 3 to 5 mm thickness of quartz wool. The reaction conditions and the results are presented in Figure 13.

The data indicate that the dual catalyst system is very active for the simultaneous removal of NH₃, NO, and CO from a NWP offgas with high selectivity to N₂ and desirably low selectivity to N₂O. For example, at 485°C the conversions of NH₃, NO, and CO are 99%, 94%, and 100% respectively while selectivities for N₂ and N₂O are 94 and 0% respectively. The incomplete NO conversion suggests that about 6% NH₃ slips through Cu-ZSM-5 even at 485°C, which is subsequently oxidized to NO on Pt/Al₂O₃. N₂O is formed at low temperatures, its formation reaching a maximum of about 28% at 285°C, but dropping to 0% at 425°C. It is reasonable to assume that N₂O formation occurs at low temperatures on Pt/Al₂O₃ because (1) selectivity to N₂O formation on Cu-ZSM-5 is negligible (Figs. 2 and 5) and (2) a significant amount of NH₃ slips through Cu-ZSM-5 due to its low SCR/NH₃ oxidation activity at low temperatures (Figs. 2 and 9 and Table I). At temperatures above 285°C the N₂O formation decreases, since NH₃ slippage through Cu-ZSM-5 decreases. In other words, NH₃ conversion via SCR/NH₃ oxidation reactions increases with temperature on Cu-ZSM-5. However, about 60-70% CO slippage through Cu-ZSM-5 is expected even at 485°C (Fig. 6). The 100% CO conversion on the dual catalytic system (Fig. 13) indicates that the CO not converted in the Cu-ZSM-5 bed is completely oxidized by Pt/Al₂O₃.

Based on the results of this study, it appears that both Cu-ZSM-5 and Pt/Al₂O₃ have promise as clean-up catalysts for NWP applications. However, the two catalysts differ significantly in their activity/selectivity behavior. They have, for example, different optimum operating temperature windows for NH₃, NO_x and CO clean-up applications as summarized in Table I. Cu-ZSM-5, for example, effectively converts NH₃ and NO_x to N₂ with a selectivity of about 100% in the temperature range of 450-500°C at NH₃/NO ratios of 0.5 to 1.5 in the presence of CO and water vapor (Figures 3 and 4). However, the application of Cu-ZSM-5 has two potential disadvantages: (1) its temperature window is narrow and high enough (450-500°C) that thermal stability of the catalyst could be a problem, and (2) its CO removal efficiency is considerably low (only 40-50% conversion even at 500°C). Sintering of zeolites in steam at

temperatures above 500°C is a recognized problem (26-28). The Pt catalyst, on the other hand, has a very wide temperature window for CO and NH₃ oxidation. CO, for example, is completely oxidized to CO₂ above 250°C (Figure 1) and NH₃ is completely oxidized above 300°C (Figures 9-12). However, the Pt catalyst suffers from a serious selectivity limitation. A maximum selectivity to N₂ of only 40% is obtained in the presence of NO, CO and H₂O (Figure 12) at 400°C and it decreases to 32% at 475°C. Also, a large quantity of N₂O is produced (70-85%) at low temperatures (250-300°C). This is a serious problem since N₂O is a green house gas and ozone destroyer. Nevertheless, N₂O formation is reduced to 20-25% as the temperature is raised to 500°C.

TABLE I. Summary of catalytic performance of Cu-ZSM-5, Pt/alumina, and Cu-ZSM-5 + Pt/alumina catalysts for the removal of NH₃, NO_x and CO. Data from Figures 3-6, 12, and 13

<i>Properties</i>	<i>Cu-ZSM-5</i>	<i>Pt/alumina</i>	<i>Cu-ZSM-5 + Pt/alumina</i>
Optimum temperature window (°C)	450-480	330-500	425-500
<i>Conversion^a</i>			
NH ₃ (%)	94-99	98-100	99
CO (%)	43-47	100	100
NO (%)	98-100	6-29	88-94
<i>Selectivity^{a,b}</i>			
NO ₂ (%)	0	7-13	1-2
N ₂ O (%)	0	22-32	0
N ₂ (%)	96-98	32-40	95-97

^a Conversions and selectivities are estimated at the optimum temperature window.

^b 100 x conc. of product formed/Total conc. of N-containing gases in the feed.

Hence, the Pt catalyst might be operated at higher reaction temperatures (450-500°C) to lower N₂O production. Interestingly, the dual catalyst system, Cu-ZSM-5 + Pt/Al₂O₃, combines the best features of these two catalysts, i.e., it is very active for NH₃, NO, and CO clean-up with high selectivity to N₂ and negligible production of N₂O at temperatures of 425-500°C. Indeed, the conversions of NH₃, NO and CO in this optimum temperature window are 99, 88-94, and 100% respectively, while selectivities to N₂ and N₂O are 88-94 and 0% respectively.

Comparison of NO_x reduction by NH₃ on metal ion-exchanged ZSM-5 with previous work. Table II summarizes the previously reported research on NO_x reduction by NH₃ on metal ion exchanged ZSM-5 studied under different conditions. It appears that there were only two studies reported previously on metal ion (Cu and Pt) exchanged ZSM-5 (20,21) and the data are very preliminary. Teraoka et al. (21) tested Cu-ZSM-5 and Pt-ZSM-5 for simultaneous removal of NO and SO₂ at GHSV = 12,000 h⁻¹. Only NO and SO₂ conversions were measured; NH₃ conversion and the SCR activity were not measured. Also, effects due to CO were not studied. However, the combined Cu-ZSM-5 + Pt-ZSM-5 system was found to convert all NO and SO₂ at 300°C (21). Centi et al. (22) studied the role of copper sites in NO reduction on Cu-ZSM-5, Cu-SiO₂, Cu-Vycor, and V₂O₅-TiO₂ catalysts at 3,000-5,000 h⁻¹. NH₃ conversion and the effects due to CO and SO₂ were not investigated. This paper reports new results on Cu-ZSM-5 and the Cu-ZSM-5 + Pt/Al₂O₃ dual system using NH₃ as a reducing agent in the presence of CO and at high space velocity (65,000 h⁻¹) applicable to NWP. This is probably the first paper to report a detailed study on the

TABLE II. Studies of SCR of NO_x with NH₃ on metal ion exchanged ZSM-5 catalysts
Summary of results and inference

Catalyst system	Reactants and Concentrations	Space velocity (h ⁻¹)	Temp. range (°C)	Gas analyzed (Yes/No)				Ref.
				NO	NH ₃	CO	SO ₂	
Cu-ZSM-5	[NH ₃]=1000-1250 ppm, [NO]=250 ppm, [O ₂]=5%, [H ₂ O]=11%, [SO ₂]=500 ppm	12,000	300-350	N	N	-	Y	9
								Initial 80% SO ₂ conv. decreased to ~5% in 10 min. at 350°C. SCR activity and effects of CO were not studied.
Pt-ZSM-5	"	"	"	Y	N	-	Y	9
								100% NO conv. at 200°C decreased to ~70% at 350°C. 55% SO ₂ conv. at 200°C increased to 100% at 350°C. NH ₃ conv. and effect of CO were not studied.
Cu-ZSM-5 + Pt-ZSM-5	"	"	"	Y	N	-	Y	9
								NO and SO ₂ were completely removed at 300°C. Effects of CO were not studied.
Cu-ZSM-5	[NH ₃]=649 ppm, [NO]=612 ppm, [O ₂]=3%, no water	3,000-5,000	200-350	Y	N	-	-	10
								100% NO conv. at 200-350°C. NH ₃ conv. and effects of CO and SO ₂ were not studied.
Cu-ZSM-5	[NH ₃]=125-750 ppm, [NO]=250 ppm, [O ₂]=14%, [H ₂ O]=18-20%, [CO]=1%	64,000	200-500	Y	Y	Y	-	this work
								100% N ₂ selectivity. Effect of NH ₃ /NO ratio and CO were studied and the N material balance was closed. Only 30-40% CO conv. observed at 300-500°C.
Cu-ZSM-5 + Pt/Al ₂ O ₃	[NH ₃]=500 ppm, [NO]=250 ppm, [O ₂]=14%, [H ₂ O]=20%, [CO]=1%	"	"	Y	Y	Y	-	this work
								100% N ₂ selectivity. Closed the N material balance and the conversions of NH ₃ , NO, and CO were 99%, 94%, and 100% respectively at 485°C. Selectivities for N ₂ and N ₂ O were 94% and 0%.

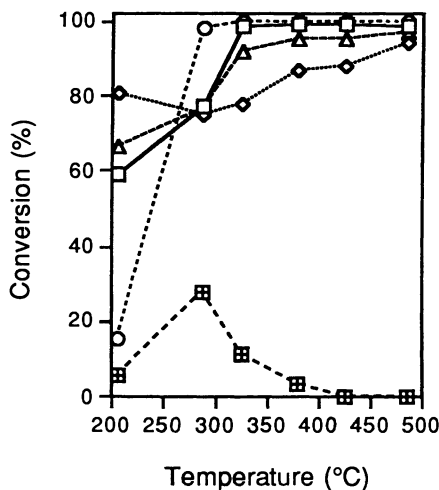


Figure 13. Conversion vs. temperature behavior of Cu-ZSM-5 + Pt/Al₂O₃ dual catalytic system for simultaneous removal of NH₃, NO, and CO from NWP offgas in the presence of O₂ and water vapor. GHSV = 65,000 h⁻¹, [NH₃] = 500 ppm, [NO] = 250 ppm, [CO] = 1%, [O₂] = 14%, and [H₂O] = 20%. □: NH₃ conversion, ◇: NO conversion, ○: CO conversion, △: conversion to N₂, and ⊠: conversion to N₂O.

SCR of NO by NH₃ with a complete nitrogen material balance and analysis of all the important species including NH₃, NO, CO, and N₂O gases.

Summary and Conclusion

Pt/alumina and Cu-ZSM-5 catalysts were studied on a laboratory scale for clean-up of NO_x, NH₃, and CO in nuclear waste processing (NWP). The results indicate that both catalysts have useful temperature windows in which simple oxidation of CO and ammonia and reduction of NO_x with NH₃ occur readily. Although significantly more active for these oxidation and reduction reactions, the Pt/alumina catalyst suffers from selectivity limitations in complex reactant mixtures, i.e., conversion to N₂ is only 35-40%; moreover in the temperature range of 200-300°C a large fraction of an NO, NH₃, O₂ mixture is converted to N₂O (60-85%) while in a mixture of NO, NH₃, CO and O₂ much of the nitrogen is oxidized to NO_x at higher reaction temperatures. Cu/ZSM-5, on the other hand, reduces the reactant NO with NH₃ to N₂ with 100% selectivity over the temperature range of 260-450°C (in a reactant mixture of NO, NH₃, CO, O₂, and H₂O); stoichiometric amounts of ammonia are completely converted above about 350°C, while in a mixture of NH₃/NO = 2, complete conversion of ammonia occurs at 475°C. The drawbacks of the Cu/ZSM-5 catalyst are (i) that only 20-40% of the CO in this reactant mix is oxidized in the temperature range of 300-500°C and (ii) >95% NH₃ conversion can be achieved only at high temperatures (above 450°C) under which conditions Cu-ZSM-5 may suffer from thermal deactivation. In general, the Pt catalyst performs better for oxidation reactions, and Cu-ZSM-5 performs better for the selective catalytic reduction of NO by NH₃. A combination of the two catalysts (Cu/ZSM-5 and Pt/alumina-- in that order) cleans-up NO_x, NH₃, and CO to low ppm levels; at 485°C the conversions of NH₃, NO, and CO are 99%, 94%, and 100% respectively; selectivities to N₂ and N₂O are 94% and 0%.

Acknowledgments

This work was supported by Westinghouse Idaho Nuclear Company, a DOE subcontractor of EG&G at the Idaho National Engineering Laboratory and also by the Advanced Combustion Engineering Research Center, Brigham Young University, Provo, Utah. Funds for this Center are received from the National Science Foundation, the State of Utah, 26 industrial participants, and the U.S. Department of Energy.

References

1. Pence, D.T.; Thomas, T.R. *Proc. AEC Pollution Control Conf., Conf-721030*, October **25, 1972**, p 115.
2. Thomas, T.R.; Pence, D.T. *Proc. 67th Annual Meeting, Air Pollution Control Association*, June **1974**, pp 75-258.
3. Thomas, T.R. "An Evaluation of NO_x Abatement by NH₃ over Hydrogen Mordenite for Nuclear Fuel Reprocessing Plant"; report to DOE by Allied Chemical, Idaho National Engineering Laboratory. Contract #EY-76-C07-1540, January, **1978**.
4. Dwyer, F.G. *Catal. Rev. Sci. Eng.* **1972**, *6*, 261.
5. Heck, R.M.; Bonacci, J.C.; Chen, J.M. *Proc. APCA 8th Annu. Meet.*, **1987**, *3*, 36.
6. Gopalakrishnan, R.; Stafford, P.; Davidson, J.; Hecker, W.C.; Bartholomew, C.H. *Applied Catal. B.* **1993**, *2*, 183.
7. Sato, S.; Yu-u, Y.; Yahiro, H.; Mizuno, N.; Iwamoto, I. *Appl. Catal.* **1991**, *70*, L1.
8. Iwamoto, M.; Yahiro, H.; Yu-u, Y.; Shundo, S.; Mizuno, N. *Shokubai* . **1990**, *32*, 430.
9. Teraoka, Y.; Shimanoe, K.; Yamazoe, N. *Chem. Lett.* **1987**, p 2047.
10. Centi, G.; Peranthoner, S.; Shioya, Y.; Anpo, M. *Research on Chem. Intermediates* **1992**, *17*, 125.
11. Kiovsky, J.R.; Koradia, P.B.; Lim, C.T. *Ind. Eng. Chem. Res.* **1980**, *19*, 218.
12. Nam, I.S.; Eldridge, J.W.; Kittrell, J.R. *Stud. Surf. Sci. Catal.* **1988**, *38*, 589.
13. Medros, F.G.; Eldridge, J.W.; Kittrell, J.R. *Ind. Eng. Chem. Res.* **1989**, *28*, 1171.
14. Andersson, L.A.H.; Brandin, J.G.M.; Odenbrand, C.U.I. *Catal. Today* **1989**, *4*, 173.
15. Brandin, J.G.M.; Andersson, L.A.H.; Odenbrand, C.U.I. *Catal. Today* **1989**, *4*, 187.
16. Choi, E.Y.; Nam, I.S.; Kim, Y.G.; Chung, J.S.; Lee, J.S. *J. Mol. Catal.* **1991**, *69*, 247.
17. Ham, S.W.; Choi, E.Y.; Nam, I.S.; Kim, Y.G. *Catal. Today* **1992**, *11*, 611.
18. Williamson, W.B.; Lunsford, J.H. *J. Phys. Chem.* **1976**, *24*, 2664.
19. Iizuka, T.I.; Lunsford, J.H. *J. Am. Chem. Soc.* **1978**, *100*, 6106.
20. Kiel, J.H.A.; Edelaar, A.C.S.; Prins, W.; van Swaaij, W.P.M. *Appl. Catal. B.* **1992**, *1*, 41.
21. Katona, T.; Guzzi, L.; Somorjai, G.A. *J. Catal.* **1992**, *135*, 434.
22. Markvart, M.; Pour, V. *J. Catal.* **1967**, *7*, 279.
23. Markvart, M.; Pour, V. **1975**, 546.
24. Meier, H.; Gut, G. *Chem. Eng. Sci.* **1978**, *33*, 123.
25. Youn, K.C. *Hydrocarbon Processing*, February **1979**, p 117.
26. Heinemann, H. *Catal. Rev.-Sci. Eng.* **1981**, *23*, 315.
27. Ward, J.W. *In Applied Industrial Catalysis*; Leach, B.E., Ed.; Academic: New York, NY, **1984**; *3*, pp 274-392.
28. Vaughan, D. E. W. *Chem. Eng. Prog.*, **1988**, *84*, 25.

RECEIVED September 29, 1993

Chapter 8

Mobile Engine Emission Control: An Overview

John N. Armor

Air Products & Chemicals, Inc., 7201 Hamilton Boulevard,
Allentown, PA 18195

Recalling the origin and importance of control of NO_x emissions from the preceding section in this book, the other half of the NO_x problem emerges. Here the story is more developed because automotive emission control catalysts have been commercialized for over 20 years. Current catalysts allow automobile companies to meet the mandated standards for removal of hydrocarbons [HCs], CO, and NO_x (1). Recent Clean Air Act Amendments will require significantly greater reductions in the future. Stringent local standards in California and Vermont will require up to a tenfold reduction in emissions by the late 1990's. Here new opportunities will emerge for catalytic solutions providing higher activity, lower temperatures, less rhodium, and lean engine operation.

NO_x control is linked with HC and CO control as well. In addition fuel economy and maximum power vary considerably with the air:fuel ratio. Typical three way catalysts contain Rh, Pt and often Pd with base metal additives on monolith supports (300-400 channels per square inch) and operate at 300-900°C. Rh is present to promote reduction of NO to N₂. Pd and/or Pt is used for CO and HC oxidation, especially during cold starts. CeO₂ (~20 wt% of wash coat Al₂O₃) is added to promote the water gas shift reaction, store O₂ under lean (fuel deficient) conditions, stabilize noble metal dispersion against thermal damage, and alter CO oxidation kinetics (2).

There has been a great deal of effort to search for less costly alternatives to Noble metals without much success (3). Other opportunities for research include catalysts effective for the normal fluctuations in emissions, especially during cold start and catalysts useful for alternate fuels. Short term needs include raising catalyst performance guarantees from 50,000 to 100,000 mi and reducing the effects of such poisons as lead, phosphorous, and sulfur (4).

For greater fuel efficiency, an alternative is the lean burn engine. Unfortunately, this engine fails to provide sufficient NO_x control with the current 3-way catalyst unless one goes to unacceptable HC emission levels (5). Until NO_x emissions can be handled, the development of lean burn engines will be delayed.

0097-6156/94/0552-0090\$08.00/0
© 1994 American Chemical Society

In Environmental Catalysis; Armor, J.;
ACS Symposium Series; American Chemical Society: Washington, DC, 1994.

In addition there is a need for catalytic converters to handle diesel engine exhaust. Diesel engines run in excess O₂, at lower temperatures (150-500°C) and their emissions are complicated by the presence of particulates and higher SO₂/SO₃ levels. Under these oxidizing conditions, three way catalysts are inappropriate for NO_x control. Various traps, off-line regeneration, and flow through catalysts are being considered (6). In 1994, the Clean Air Act requires a >50% reduction in particulates and by 1998 a drop in NO_x levels by 20% in the U.S. There is a tradeoff between particulates and NO_x, because engine designs can prolong combustion and reduce particulates- but NO_x emissions increase! Relatively high levels of sulfur compounds in diesel fuel adds a further complication. Diesel exhaust treatment has to handle solid, liquid, particulate, and gaseous components. Diesel oxidation catalysts (7) can oxidize the liquid portion of the particulates, gaseous HCs and CO but do not address NO_x emissions. These latter catalysts have been used on >60,000 fork lift trucks and mining vehicles since 1967. Similar to gasoline engines, they use honeycomb monolith supports with a Pt and/or Pd on high surface area carriers. One future focus for diesel emissions will be on NO_x removal and treatment via NO_x decomposition or reduction with hydrocarbons.

From the Symposium's session on Mechanisms of NO_x Removal, Robert McCabe summarized presentations related to mobile engine emissions as follows: "The sub-session on stoichiometric NO_x removal dealt mostly with rhodium-containing catalysts. The keynote address, *Why Rhodium in Three-way Automotive Catalysts*, (M. Shelef, Ford Motor Company) surveyed the attributes of Rh which have resulted in its current status as the noble metal of choice for NO_x conversion in automotive exhaust. Shelef noted the ability of highly dispersed Rh to adsorb NO in a dinitrosyl configuration, and suggested the Rh may be distinguished from other noble metals in its ability to promote N-pairing in adsorbed NO molecules prior to N-O bond rupture. Theoretical support for Shelef's arguments was offered by T. R. Ward (work carried out at Cornell University) who presented results of molecular orbital calculations which indicated that Rh is more likely than either Pt or Pd to form paired interactions between gem-dinitrosyl NO molecules. In contrast to the dinitrosyl mechanism, studies by G. B. Fisher (General Motors), B. E. Nieuwenhuys (Univ. of Leiden) and D. N. Belton (General Motors) all dealt with dissociative mechanisms of NO_x reaction on extended metal surfaces. Fisher compared rates of NO reduction on Pt-Rh alloy single crystals with those on Pt (111) and Rh (111), respectively, and found that the alloys were generally intermediate in their activity between Pt and Rh. Nieuwenhuys examined N₂ vs. NH₃ product selectivity in the reaction steps such as N-atom recombination. Belton used isotope experiments and electron-beam dissociation of adsorbed NO(a) + N(a) → N₂(g) + O(a) (not important) and NO(a) + N(a) → N₂O(g) (important). R. Gorte (U. of Pennsylvania) examined NO reduction by CO on model Pt/ceria and Rh/ceria catalysts. Interactions between the metal and ceria were weak in the case of Pt but strong in the case of Rh as evidenced by the generation of CO₂ with the simultaneous reduction of near-surface ceria during temperature-programmed desorption of CO."

Ron Heck of Engelhard led the session on automotive emission control catalysts and summarized the papers in his section as follows: "*The Evolution of Automobile Exhaust Emission Control* - K. Taylor: Her keynote address involved the evolution of the automotive catalyst from the oxidation catalyst in the mid 1970's to the current

three way catalysts for nitrogen oxides, carbon monoxide and hydrocarbons. A new generation of catalysts will be required to meet the recently adopted Federal and California regulations for the 1990's. The immediate challenges are lower hydrocarbon emissions and 100,000 mile durability. *La³⁺ Modified Al₂O₃ as a Support for CeO₂* - G. W. Graham, P. J. Schmitz, R. K. Usmen, R. W. McCabe and W. L. Watkins: Studies were conducted to show the effect of lanthanum on the ceria used in the automotive catalyst. The ceria is considered the key component for maintaining oxygen storage during rich perturbation of the automobile engine. If lanthanum is incorporated in the gamma alumina before the ceria is added, a higher ceria dispersion and a greater range of reversibility of the ceria was obtained. This is beneficial for activity and durability of a three way catalyst. *NOx Control in Lean Burn Engine Exhaust* - B. Bykowski and M. Heimrich: For lean burn engines, the three way catalyst is ineffective for NOx reduction. Studies were conducted with engine exhaust on different types of zeolite catalysts for selective reduction of NOx using exhaust hydrocarbons as the reactant. Short term conversions of NOx up to 95% were obtained, however the durability of the zeolites remains a serious challenge. *Distinguishing Between Chemical and Physical Promotion Mechanisms by CeO₂ in Pt, Rh Three-way Automotive Catalysts Under Practical Industrial Conditions* - J. G. Nunan and H. J. Robota: In order to better understand the function of ceria in the three way catalyst, engine aging studies were conducted on catalysts with and without ceria. Adding ceria enhanced the carbon monoxide conversion but not the water gas shift reaction. Aging without ceria reduced both the carbon monoxide and nitrogen oxides conversion. Also it was noted in the aging studies that a platinum/rhodium alloy was formed, and the ceria appeared to prevent alpha alumina formation at the higher temperature (850°C). Adding ceria to the aged catalyst restored fresh activity. *Interaction of NO and CO on Rh/SiO₂ and Ce-Rh/SiO₂ Catalysts: A transient In-Situ IR Spectroscopic Study* - G. Srinivas, C. Chuang and S. Debnath: Infrared studies were conducted for a better understanding of the carbon monoxide and nitrogen oxides reaction over rhodium/ceria and ceria/rhodium/silica catalysts. Studies indicated that cyanide and isocyanate are intermediates in the reduction reaction."

Robert Farrauto led the later session on diesel emission control catalysts and summarized the papers in this session as follows: *"Palladium Only Catalysts For Closed Loop Control: A Review* by J. Summers and W. B. Williamson: The development of a Pd only catalyst for three way control of CO, HC and NOx in gasoline fueled vehicles was announced. It contains proprietary oxides to promote the Pd and is now commercially in practice in at least three automobile applications. This development represents a cost savings to the automotive industry in that the more expensive Pt and Rh, currently present in most automobile converters, is not necessary. *Treatment of Diesel Exhaust Using A Novel Oxidation Catalyst* by K. E. Voss, J. K. Lampert, R. J. Farrauto, R. M. Heck and G. Rice: A base metal oxide catalyst deposited on a flow through honeycomb for oxidation of diesel particulates was described. Traces of Pt can be added to enhance the oxidation of CO, and HC with minimal production of sulfates. This new catalyst will be commercialized in the US for trucks in May 1994. *The Effects of Support Material and Noble Metal On The Catalytic Oxidation of Diesel Exhaust Gases* by T. I. Maunula, M. A. Harkonen, M. I. Kivioja, T. O. B. Slotte and K. Oy: This paper described a comparison of Pt, Pd and

Rh on various supports for the oxidation of CO, HC and SO₂ emitted from the exhaust of a diesel engine. Pt was shown to be the most active catalyst and the Al₂O₃ carrier the most likely to store sulfates. *Catalytic Diesel Engine Emission Control: Oxidation of NO to NO₂ In The Presence of SO₂ Over Pt/ZrO₂/SO₄* by E. Xue, K. Seshan, P. L. D. Mercera, and J. R. H. Ross: Their premise was that NO₂ can oxidize the soot generated in diesel exhaust. The importance of support acidity for the oxidation of NO to NO₂ and SO₂ to SO₃ was investigated using a Pt based catalyst. *Platinum impregnated ZrO₂/SO₄ superacid enhanced the oxidation of both gaseous species. Catalytic Decomposition of Nitrous Oxide On Metal Exchanged Zeolites* by John N. Armor, P. J. Cook, T. S. Farris, P. J. Battavio, T. A. Braymer and Yuejin Li: A family of zeolite exchanged catalysts were reported to be effective for the decomposition of N₂O in O₂ and H₂O containing environments (8). The authors reported that Cu and Co exchanged onto ZSM-5 and 11, mordenite, beta, and ferrierite are effective." Several of these presentations are included in this section on Mobile Engine Emissions Control.

References

1. Farrauto, R. J.; Heck, R. M.; Spononello, B. K. *Chem. Eng. News*, September 7, 1992, pp. 34-44.
2. Taylor, K. C. *CHEMTECH*, September 1990, pp. 551-555.
3. Taylor, K. C. *Automobile Catalytic Convertors*; Springer-Verlag: New York, 1984.
4. Armor, J. N. *Appl. Catal. B*, **1992**, *1*, 221-256.
5. Acres, G. J. K. In *Perspectives in Catalysis*; Thomas, J. M.; Zamaraev, K. I., Eds.; Blackwell: Oxford, 1991; pp. 359-369.
6. Truex, T. J.; Searles, R. A.; Sun, D. C. *Platinum Met. Rev.*, **1992**, *36*, 2-11.
7. Farrauto, R.; Adomaitis, J.; Tiethof, J.; Mooney, *Automotive Eng.*, February, 1992, pp. 19-22.
8. Li, Y.; Armor, J.N. *Appl. Catal. B*, **1992**, *1*, L21-L29.

RECEIVED November 8, 1993

Chapter 9

Palladium-Only Catalysts for Closed-Loop Control

J. C. Summers and W. B. Williamson

AlliedSignal Environmental Catalysts, P.O. Box 580970,
Tulsa, OK 74158

The commercialization of palladium-only closed-loop control automotive catalysts represents a significant technology breakthrough. The use of a single noble metal catalyst to simultaneously control hydrocarbon, CO and NO_x emissions has been developed, extensively evaluated by automobile manufacturers and demonstrated opportunities in meeting the more stringent emission standards. Palladium-only three-way catalysts not only can have the durability performance of commercial platinum/rhodium catalysts, but also have performance advantages and offer cost reduction opportunities. Palladium improves HC emission control for gasoline, methanol or methanol/gasoline blends, and natural gas applications. Palladium technologies have superior thermal stability to conventional rhodium-containing technologies for higher exhaust temperature applications, which may be necessary for achieving low emission vehicle (LEV) and ultra low emission vehicle (ULEV) HC standards.

The roles of the various noble metals (platinum, palladium and rhodium) used in automotive emission control catalysts to simultaneously convert hydrocarbon (HC), CO and NO_x emissions from closed-loop control vehicles were defined from research in the 1970s(1,2). In brief summary, platinum and palladium were necessary to control HC and CO emissions both during lightoff and warmed-up operation(3) while rhodium was considered essential in controlling NO_x emissions(4), although it was well known that both platinum and palladium could convert some NO_x about the stoichiometric point (1,5,6) (Figure 1)(6). Furthermore, platinum was preferred over palladium because it was more poison resistant to gasoline and motor oil contaminants (i.e., lead, phosphorus and sulfur compounds)(7,8), although palladium was more resistant to thermal sintering than platinum(9,10,11).

It has been recognized for some time that there were problems connected with palladium usage. These included alloy formation with rhodium(12,13), platinum(14),

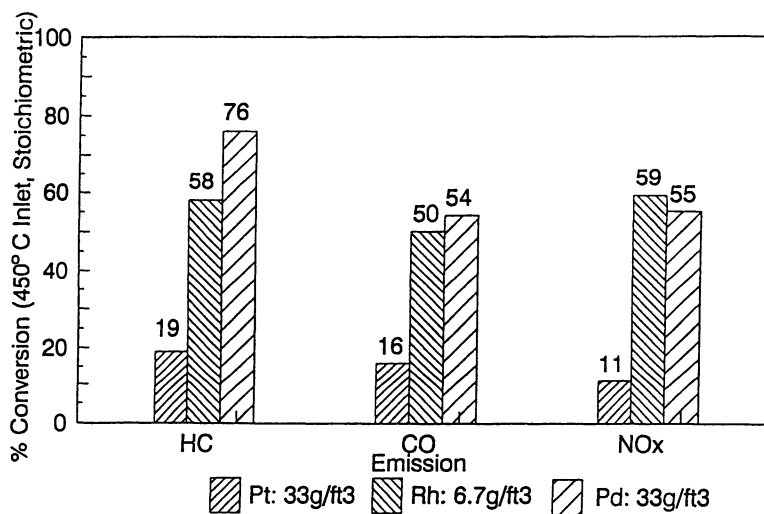


Figure 1. Durability of single noble metal catalysts at stoichiometry after severe engine aging for 100h at 850°C inlet temperatures. (Reproduced with permission from ref. 6. Copyright 1991 Society of Automotive Engineers, Inc.)

and lead (15), as well as poisoning by sulfur compounds and lower activity for oxidizing C₃ or higher molecular weight paraffins(16).

The idea of using a single noble metal to simultaneously control HC, CO and NO_x emissions about the stoichiometric point was first proposed in 1968 by Esso workers(17). However, the first serious attempt to develop an automotive emission control catalyst technology employing only a single noble metal to simultaneously control HC, CO and NO_x did not occur until the early 1980s.

H. S. Gandhi and co-workers at Ford Motor Company demonstrated that palladium, in the presence of base metal promoters, could convert significant quantities of NO_x (in addition to HC and CO) about the stoichiometric point(18-21). In the presence of MoO₃, palladium's activity and selectivity for converting NO to N₂ was significantly improved, exhibiting performance characteristics analogous to rhodium(18,19). This work was followed by the development of WO₃ containing palladium catalysts(20a). These palladium formulations were characterized as having good saturated hydrocarbon activity performance coupled with an enhanced capability of selectively reducing NO to N₂.

The importance of these studies exceeded the technology developed, as the technology was never commercialized. However, for the first time, the potential of using a single noble metal to control automotive emissions in a practical closed-loop environment was demonstrated.

H. Muraki and researchers at Toyota Motor Company published a series of papers in the mid-to-late 1980s describing their attempts to modify the three-way catalytic performance of palladium by the addition of lanthanum oxide. The Toyota researchers reported that lanthanum weakens the strength of adsorption of hydrocarbons on palladium(22,23), promotes the CO and NO reaction in the presence of hydrocarbons(22), increases the activity and selectivity of NO reduction by H₂ to N₂(24), and hinders the reduction of palladium oxide(23). It should be noted that these studies were conducted with fresh catalysts and in the absence of SO₂ in the reactor feedstream.

During the late 1980s, J. C. Summers and co-workers at AlliedSignal applied palladium-only three-way technology to a variety of vehicle applications. The technology used a proprietary base metal promoter package that increased the effectiveness and durability of palladium. The initial objective in the early stages of their development effort was noble metal cost reduction achieved by the substitution of palladium for the more expensive platinum and rhodium(25-27,6). The performance target of the early generation of technology was to achieve approximate equivalency to commercially loaded platinum/rhodium catalysts. For example, in one comprehensive durability study the goal was to achieve equivalence in durability performance of a 2.0g/L palladium (56g/ft³) catalyst with a relatively low-loaded 0.7g/L platinum/rhodium (5/1 @ 20g/cf) catalyst(26). (Note: Noble metal concentrations are expressed as grams of noble metal per volume of ceramic monolith substrate with nominal cell geometry of 62 square cells/cm²).

Significantly lower platinum/rhodium usage can be achieved by using a combination of palladium technology with improved platinum/rhodium technology in a two-catalyst system to replace current production platinum/rhodium three-way catalysts. A catalyst system using a platinum/rhodium technology followed by a

palladium catalyst (Figure 2) improved stoichiometric CO and NO_x conversions and significantly lowered the light-off temperature for 50% conversions over a current production technology (Table I).

Table I - Use of Pd-Only Technology
for 50% Pt/Rh Reduction
Dyno Aged: 150h 760-850°C Inlet
Fuel-Cut Cycle

Stoichiometric A/F = 14.56	Conversion (450°C, 30K/h)	
	<u>Pt/Rh</u>	<u>Pt/Rh + Pd</u>
HC	94	96
CO	80	88
NO _x	76	88
50% Conversion		
HC	389°C	361°C
CO	386	360
NO _x	367	356
Catalyst Vol (L)	1.52	1.52

With further improvements in palladium-only technology, the development emphasis changed as the superior HC activity and durability performance of palladium was demonstrated in applications for gasoline (28,29), methanol(30) and compressed natural gas(31,32). With the enactment of the 1990 Clean Air Act and the more stringent California emission standards, the use of palladium technology showed considerable promise in controlling HC emissions.

Palladium Performance Characteristics

An acceptable palladium-only closed-loop catalyst technology for modern vehicle application needs to exhibit

- Comparable thermal durability to conventional platinum/rhodium catalysts.
- Acceptable NO_x performance.
- Acceptable tolerance to poisoning by exhaust stream lead and sulfur compounds.

Current state-of-the-art palladium-only technology performance will be examined with respect to these issues.

Thermal Durability Performance. The thermal durability performance of platinum/rhodium and palladium/rhodium catalysts is strongly dependent on noble metal loading(33) and platinum or palladium/rhodium ratio(34). However, for a series of platinum/rhodium catalysts having a 5/1 ratio, durability performance is generally known to be essentially constant at total noble metal loadings above 1.4-1.8g/L (40-50g/cf).

This is not the case for palladium-only catalysts. Even at much higher noble metal loadings, palladium-only catalyst show increasing performance with increasing

palladium loadings(12,29). Table II(29) shows the effect of palladium loading on the conversions of HC, CO and NO_x at the stoichiometric point, and Figure 3(29) gives the temperature-conversion performance of the catalysts. These data suggest that increasing relatively low cost palladium loadings is an inexpensive way of improving the durability performance of three-way catalysts.

Table II - Pd Loading Effects on
Durability Performance
Aging Cycle: 100h, 760°C Inlet Temperature
+ 50h, 850°C Inlet Temperature
Aging Fuel: Commercial Unleaded

Pd Loading (g/L)	Integral Conversion (%)		
	HC	CO	NO _x
0.68	91	83	76
1.71	91	82	76
3.4	93	90	78
17.0	97	90	82

(Reproduced with permission from Ref. 29.
Copyright 1993 Society of Automotive Engineers,
Inc.)

To test the effectiveness of the first generation AlliedSignal technology, the durability performance of a 2.0g/L palladium catalyst was extensively compared with a platinum/rhodium catalyst (0.71g/L, 5/1)(26). The catalysts were aged on dynamometer cycles of increasing thermal severity, and then evaluated under a variety of dynamometer and vehicle conditions. A vehicle aging durability study of 40,000 km (25K miles) duration was also conducted. The HC and CO conversion performance of the palladium catalyst was equivalent or superior to the commercial platinum/rhodium catalyst (Figures 4 and 5)(26). Increasing the thermal severity of the aging resulted in an increasing performance advantage for the palladium-only catalyst.

About the stoichiometric point, the NO_x conversion across the palladium catalyst was equivalent or superior to the commercial platinum/rhodium catalyst (Figure 5). Rich of the stoichiometric point, the platinum/rhodium catalyst was clearly superior to the palladium catalyst. With increasing thermal severity of the aging, the palladium catalyst improved relative to the platinum/rhodium catalyst at the stoichiometric point, but its disadvantage increased rich of the stoichiometric point.

At the highest aging temperatures (maximum inlet temperature = 850°C), the palladium was significantly more effective than the platinum/rhodium catalyst in converting HC and CO from a stoichiometric exhaust. This is important during the warm-up portion of the FTP-75 vehicle evaluation cycle. The relative FTP-75 performance of the two pairs of aged catalysts was a function of vehicle configuration (Table III)(26). A tight air/fuel control system and/or with slightly lean calibration could largely compensate for the rich side NO_x disadvantage of the palladium catalyst. Solving the weakness in NO_x control was a major research objective.

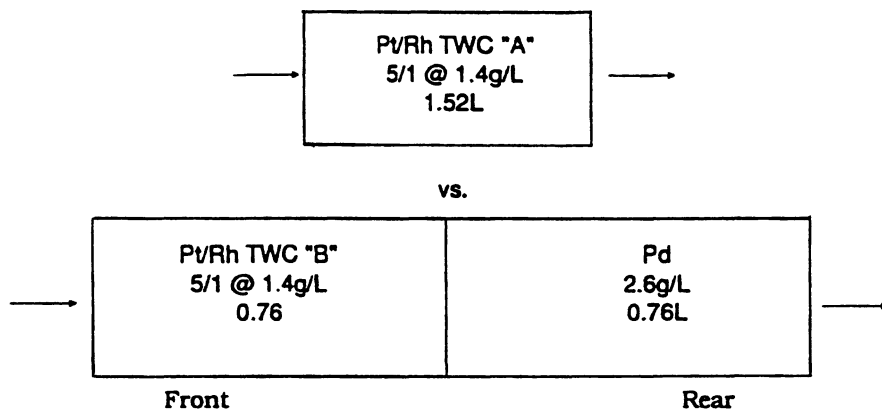


Figure 2. System comparison of 50% Pt-Rh reduction by using Pd catalysts.

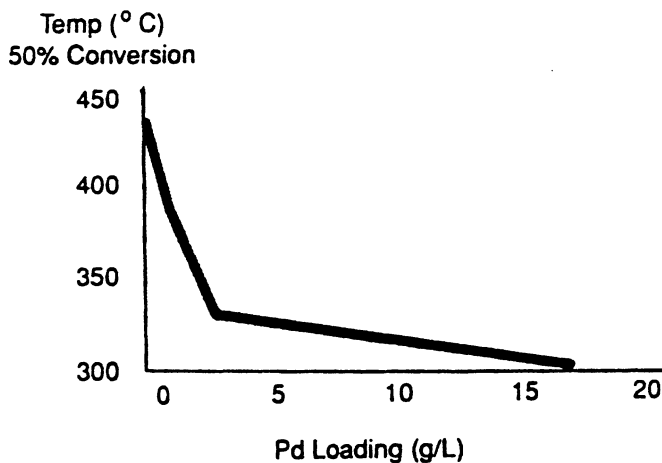


Figure 3. Beneficial effects of increased Pd loadings on HC light-off performance. (Reproduced with permission from ref. 29. Copyright 1993 Society of Automotive Engineers, Inc.)

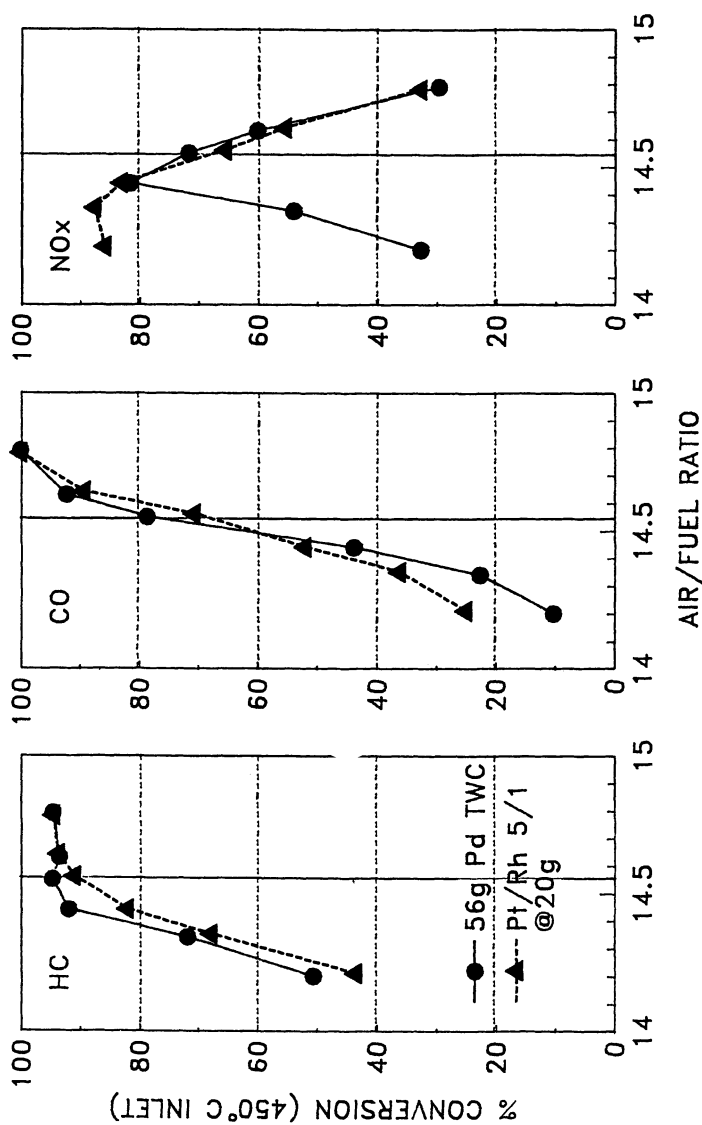


Figure 4. Conversions of Pd vs Pt/Rh TWCs at 450°C after 100h engine aging using a 760°C inlet fuel-cut cycle with fuel containing 15mg Pb + 2mg P/gal. (Reproduced with permission from ref. 26. Copyright 1989 Society of Automotive Engineers, Inc.)

Publication Date: February 23, 1994 | doi: 10.1021/bk-1994-0552.ch009

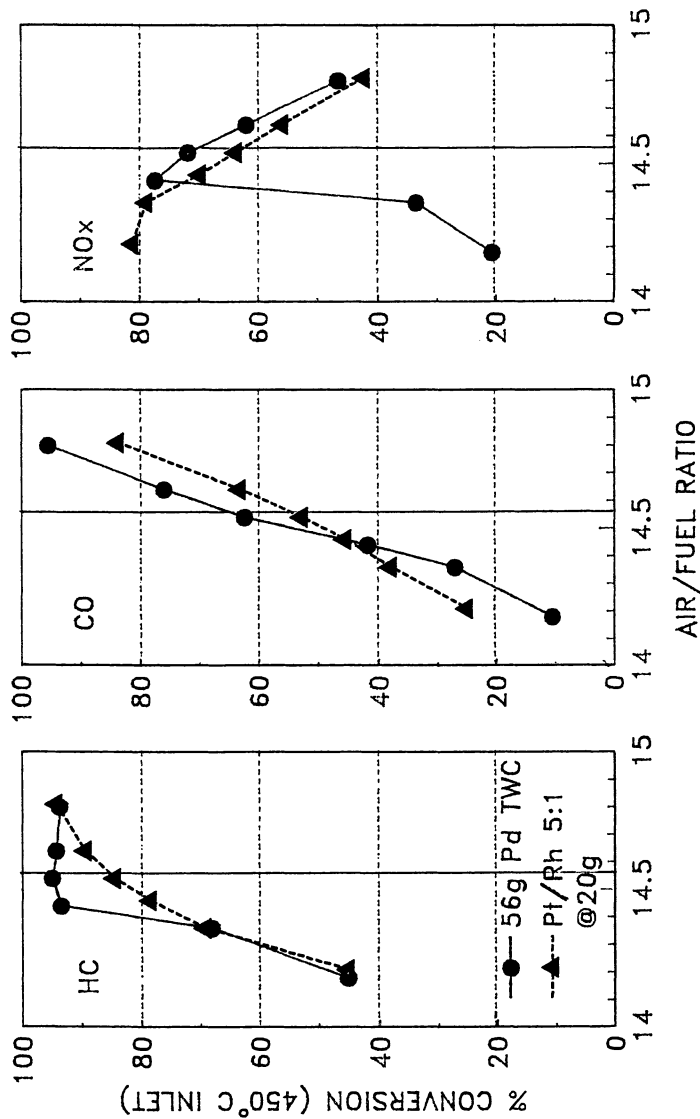


Figure 5. Conversions of Pd vs Pt/Rh TWCs at 450°C after 100h engine aging using an 850°C inlet fuel-cut cycle with fuel containing 15mg Pb + 2mg P/gal. (Reproduced with permission from ref. 26. Copyright 1989 Society of Automotive Engineers, Inc.)

By 1992 the level of palladium-only technology had advanced to the point that it exhibited considerably better durability performance than a highly loaded platinum/rhodium (5/1, 1.4g/L) catalyst (Table IV)(28). Furthermore, this platinum/rhodium technology is considerably more thermally durable than the platinum/rhodium catalyst from the earlier studies. With this accomplishment, palladium-only closed-loop control technology became a reality.

Table III - Vehicle Evaluation of Pd-Only
TWC Catalysts

FTP Performance: 1982 Chevrolet Citation

Modal Summary	Pd TWC Type	Pt/Rh TWC Type
<u>Total FTP-75</u>	<u>Washcoat</u>	<u>Washcoat</u>
HC	89	84
CO	76	60
NOx	72	64

(Reproduced with permission from Ref. 26. Copyright
1989 Society of Automotive Engineers, Inc.)

Table IV - Comparison of the Durability Performance
of a Sulfur Tolerant Pd Catalyst and a
Commercial Pt/Rh Catalyst

Aged: 100h, 850°C Fuel-Cut Cycle

Evaluation Gasoline: Commercial Unleaded (90ppmS)

Conv. (%)	450°C, 30K/h	
Stoich Point	Pd	Pt/Rh
<u>(A/F = 14.56)</u>		
HC	95	93
CO	96	73
NOx	92	78
Conv. (%), A/F = 14.25		
HC	65	57
CO	33	33
NOx	94	96
Temp (°C, 50% Conv.)		
HC	351	408
CO	351	410
NOx	354	391

(Reproduced with permission from Ref. 28. Copyright
1992 Society of Automotive Engineers, Inc.)

Rich NO_x Performance. A fundamental issue associated with palladium-only three-way catalyst technology is lower rich A/F NO_x durability(20). In earlier studies conducted during the 1980s, no acceptable solution was found to this problem. The importance of rich A/F NO_x conversion performance has decreased over the last few years with improvements in fuel management systems. With tighter A/F control, the catalysts are less exposed to rich exhaust.

The earlier generation of AlliedSignal catalysts had excellent NO_x conversion performance about the stoichiometric point, but poor rich NO_x conversions(26). However, across vehicles with tight air/fuel ratio control, they gave a similar performance to the platinum/rhodium catalyst. The latest generation of palladium technology has essentially solved the rich side NO_x conversion problem in addition to its superior stoichiometric conversion performance(28) coupled with tighter A/F ratio control.

Lead Poisoning. Palladium is well-known to be much more susceptible to poisoning by lead and phosphorus than platinum(8,21). Rhodium is also particularly susceptible to poisoning by lead and phosphorus(12). Hence, the issue is not deactivation of palladium versus platinum, but rather deactivation of palladium versus rhodium. Since it is not apparent that a palladium-only catalyst would be less poison-resistant than a platinum/rhodium catalyst, the durability performance was compared for a palladium-only (2.0g/L) and a platinum/rhodium (0.71g/L, 5/1). The lead fuel content was 13mg Pb/L (the maximum allowable level for European gasolines) and the maximum catalyst inlet temperature was only 625°C, a condition that favors lead poisoning.

The HC, CO and NO_x conversion performance of the catalysts are shown in Figure 6(26). These data indicate that these palladium catalysts have comparable poison resistance to platinum/rhodium catalysts. The conversions at the stoichiometric point are essentially equivalent and slightly greater than those in Figure 5 due to the lower aging temperature. The rich-side HC conversion of the palladium catalyst is greater than that of the platinum/rhodium catalyst, and the rich-side NO_x conversions are similar.

SO₂ Poisoning. Sulfur dioxide is known to inhibit the catalytic performance of noble metals(35). Recent vehicle studies(36) have confirmed earlier laboratory studies. Conventional wisdom teaches that palladium is poisoned to a greater extent than platinum catalysts. This is certainly true when the metals are supported on alumina.

The impact of variable levels of SO₂ on the performance of palladium, platinum/rhodium and palladium/rhodium catalysts was evaluated in a recent study(28). For one early level of palladium-only technology, both rhodium-containing catalysts were significantly more resistant to SO₂ poisoning than the palladium-only catalyst. The platinum/rhodium catalyst was more resistant than the palladium/rhodium catalyst. However, all three noble metal formulations were poisoned to some degree.

The performance measures of the palladium-only catalyst most seriously poisoned by SO₂ were rich side NO_x conversions and the temperature-performance obtained at the stoichiometric point. Increasing the gasoline sulfur level from 14ppm to 6000ppm resulted in a systematic loss of performance.

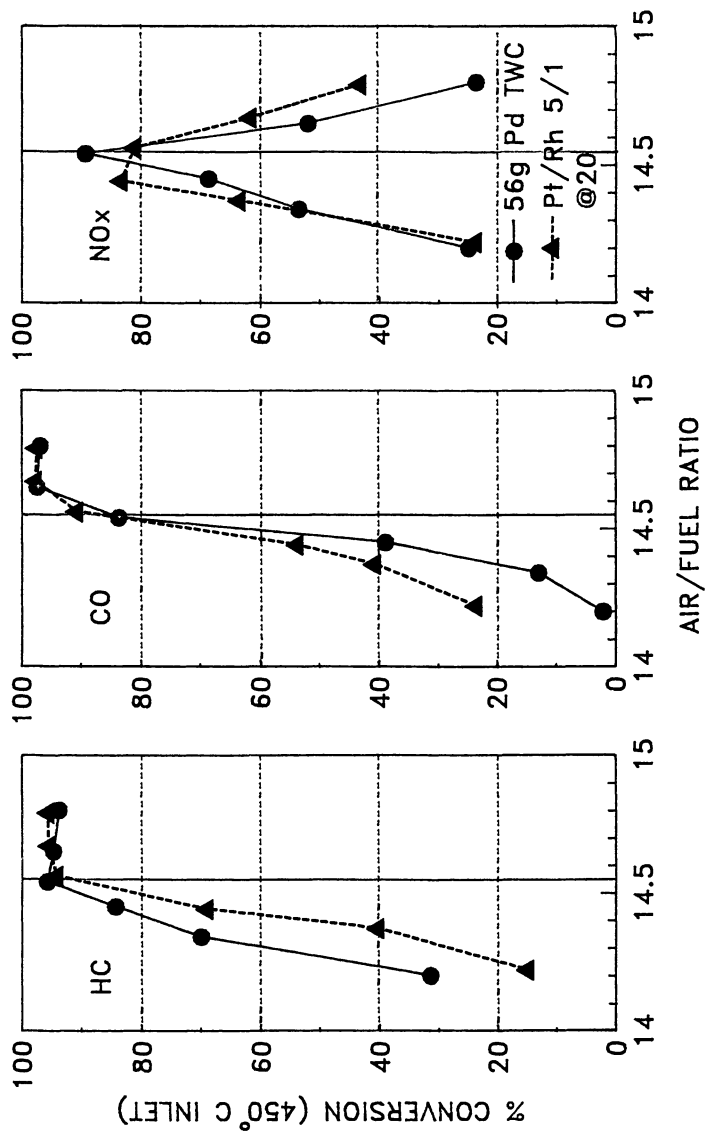


Figure 6. Conversions of Pd vs Pt/Rh TWCs at 450°C after 100h engine aging using a 625°C inlet 3-mode cycle with fuel containing 50mg Pb/gal. (Reproduced with permission from ref. 26. Copyright 1989 Society of Automotive Engineers, Inc.)

An advanced sulfur tolerant palladium-only technology was also compared to the same platinum/rhodium technology while the sulfur gasoline content was varied from 14ppm to 500ppm (Table V)(28). The CO and NO_x FTP-75 performance of the two catalysts were similar and poisoned to about the same extent, but the palladium-only catalyst had superior HC performance. The advanced palladium-only catalyst was significantly less poisoned by SO₂ than the platinum/rhodium catalyst. Unlike the earlier generation of palladium-only technology, the sulfur tolerant technology exhibited NO_x performance and low temperature (Bag 1) performance at least equivalent to that of the platinum/rhodium technology.

Effect of Exhaust A/F on Aging. The various noble metals sinter at varying rates depending on air/fuel ratio(37,38). For example, platinum supported on alumina sinters more readily in oxygen than in hydrogen, whereas palladium supported on alumina sinters more readily in hydrogen than in oxygen.

Table V - FTP-75 Performance

Catalyst	Sulfur	HC	CO	NO _x
	Level	(g/mi)	(g/mi)	(g/mi)
	ppm	Total	Total	Total
Pd	14	0.07	1.72	0.18
	90	0.09	2.2	0.23
	500	0.1	2.42	0.24
Pt/Rh	14	0.1	1.78	0.17
	90	0.14	2.15	0.26
	500	0.19	2.86	0.25

(Reproduced with permission from Ref. 28. Copyright 1992 Society of Automotive Engineers, Inc.)

The impact of high temperature exposure of rhodium supported on alumina as a function of aging environment is much more complicated. Not only does sintering occur, but in an oxidizing environment at sufficiently high temperature, rhodium appears to enter the alumina lattice and be irreversibly lost for catalyzing the three-way reactions(39,40).

Exposing platinum/rhodium automotive catalysts to a net oxidizing exhaust at sufficiently high temperatures ($\geq 700^{\circ}\text{C}$) is very deleterious to their durability performance(41). Under such conditions platinum sinters and rhodium interacts irreversibly with the alumina support. Much of the research and development activity of the 1980s was aimed at identifying catalyst formulations that would be resistant to such exhaust operating conditions(42). Palladium-containing catalysts, on the other hand, were thought to be particularly susceptible to performance loss upon rich air/fuel high temperature exposure. Recent work with advanced formulations suggest that this may not be the case(43).

The impact of aging environment on the durability performance of palladium-only and platinum/rhodium catalysts has been systematically evaluated(29). Pairs of these catalysts were aged for 100 hours on aging cycles employing a stoichiometric exhaust or a stoichiometric exhaust with superimposed lean fuel cuts ($A/F \approx 22$) for about 8% of the total aging time. The aging catalyst inlet temperature was varied from 760 to 900°C. The data obtained from these experiments are contained in Figures 7 through 9(29). For aging in a continuous stoichiometric exhaust there was a slightly larger loss of performance for the palladium catalyst than the platinum/rhodium catalyst (Figure 8). When lean spikes were introduced into a stoichiometric exhaust, there is almost no effect on the performance of the palladium-only catalyst. The platinum/rhodium catalyst, however, suffered a significant loss of three-way and light-off performance (Figure 7).

These results indicate that Pd catalysts are competitive with Pt/Rh catalysts for stoichiometric operation, and will be most effective for the leaner calibrations in pursuit of improved fuel economy. The preferred mode of operation for lowest emissions is at the stoichiometric point and rich excursions are inevitable. Palladium performance for these conditions can be maintained by also incorporating slightly lean excursions periodically(21). Of course, tighter fuel control systems will also benefit platinum/rhodium systems in minimizing lean excursions at high temperature conditions.

Palladium Manifold-Mounted Converter Advantages. The key to excellent catalytic control of HC emissions is to place an active highly durable catalyst as close to the engine manifold as feasible(e.g.,44). This is especially true for controlling Bag 1 emissions, where the great majority of HC emissions occur.

Palladium-only three-way technology can have excellent thermal stability(28,29). The latest generation of technology is superior to the more conventional rhodium-containing technologies. This fact suggests its potential applicability for use in high temperature locations, e.g., near the engine manifold.

A palladium manifold converter by itself is particularly effective in controlling total hydrocarbon emissions. On the other hand, the significantly larger (but cooler operating) underfloor converter reduces the total FTP-75 hydrocarbon emission by a much smaller fraction as illustrated in Figure 10(29). For hydrocarbon control, the manifold catalyst had a conversion of 92% which accounted for the far majority of the total hydrocarbon performance. The underfloor catalyst only contributed to 5% of the total catalyst performance. The manifold reactor also does a majority of the total CO and NO_x conversion. Note that the greatest contribution of the underfloor converter is for NO_x performance under high speed and high space velocity operation.

The California low emission (LEV) and even ultra low emission (ULEV) vehicle standards were achieved using a 1987 2.5L TBI Buick Somerset retrofitted with a small engine-mounted converter containing a palladium-only catalyst using a non-optimized converter system(29). An important element to that accomplishment was the strong relationship that exists between durability performance and loading associated with palladium catalysts.

A useful method of assessing relative tailpipe emissions can be obtained by plotting cumulative emissions (weighted) throughout the FTP-75 test cycle. Weighting factors are applied to the emissions in the same manner as bag weighting occurs: 0.43

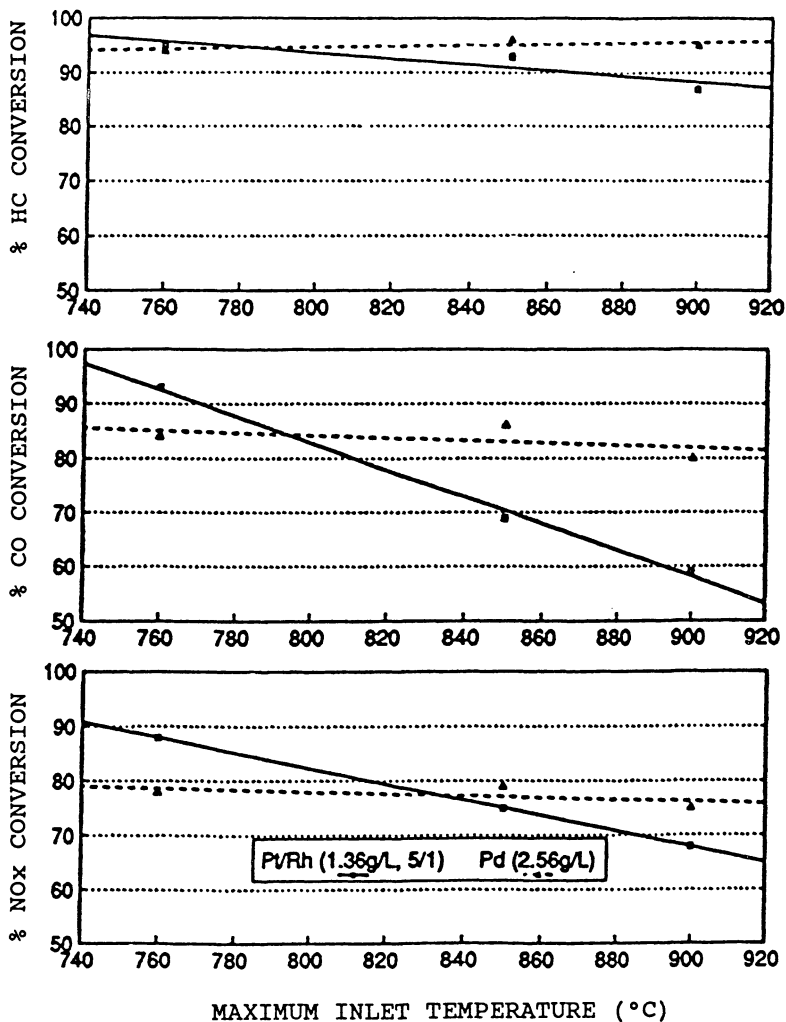


Figure 7. Effect of high-temperature fuel-cut aging (8% of 100h) on Pd-only and Pt/Rh catalyst activity. (Reproduced with permission from ref. 29. Copyright 1993 Society of Automotive Engineers, Inc.)

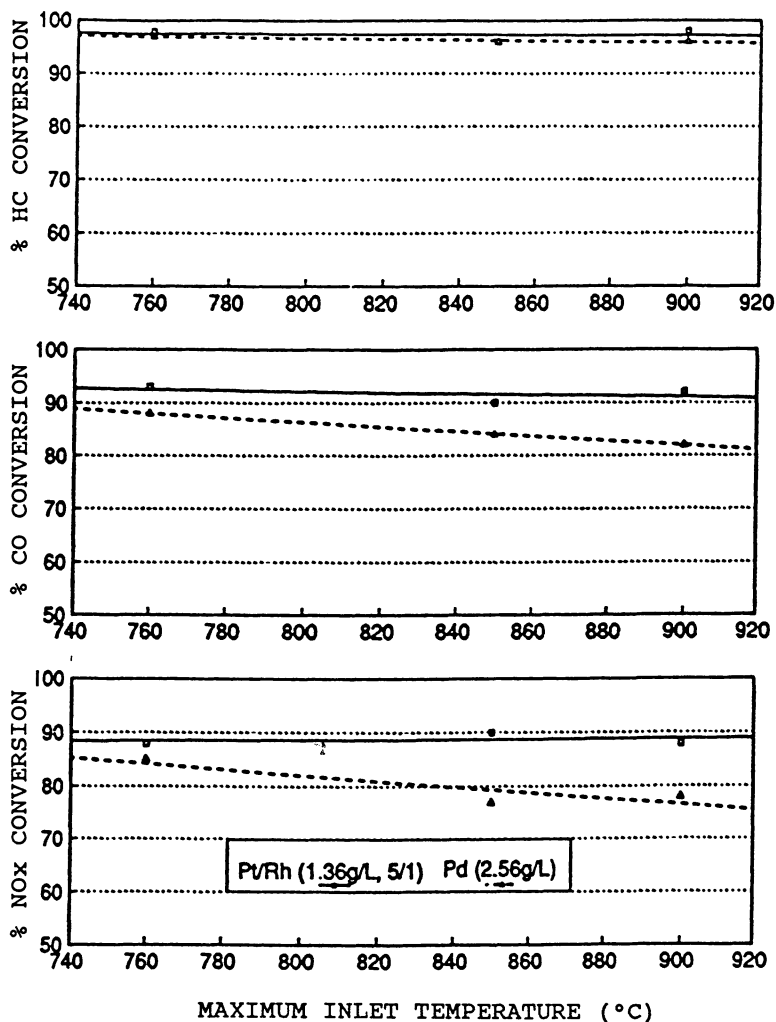


Figure 8. Effect of stoichiometric aging temperature for 100h on Pd-only and Pt/Rh catalyst activity. (Reproduced with permission from ref. 29. Copyright 1993 Society of Automotive Engineers, Inc.)

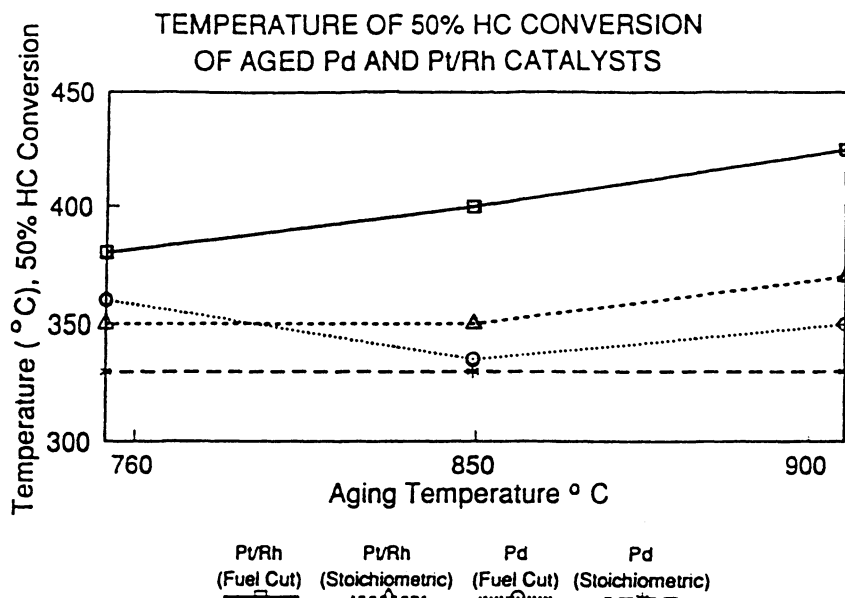


Figure 9. HC light-off durability of Pd-only and Pt/Rh catalysts as a function of aging and peak temperatures for 100h. (Reproduced with permission from ref. 29. Copyright 1993 Society of Automotive Engineers, Inc.)

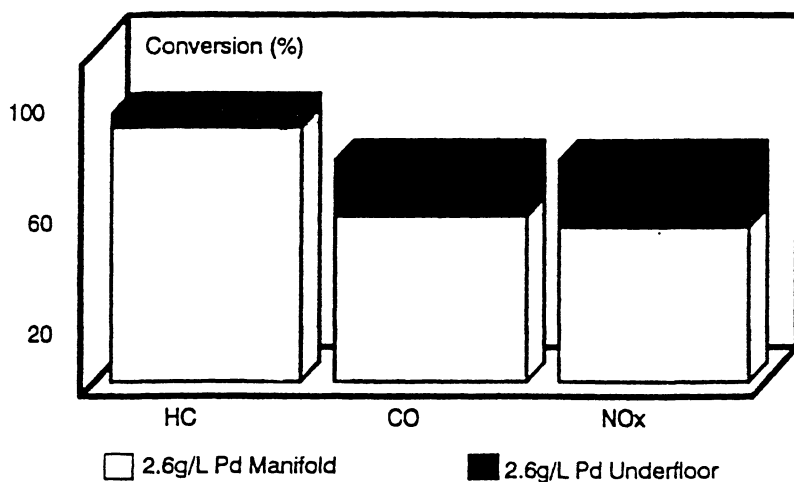


Figure 10. Relative performance contributions of aged manifold and underfloor Pd catalysts in a two converter system. (Reproduced with permission from ref. 29. Copyright 1993 Society of Automotive Engineers, Inc.)

for Bag 1, 1.0 for Bag 2 and 0.57 for Bag 3. Three aged converter system results were plotted in this manner: (1) 2.6g/L palladium underfloor only; (2) 2.6g/L palladium manifold and underfloor; and (3) 10.6g/L palladium for both the manifold and underfloor locations (Figure 11)(29).

When the 2.6g/L palladium underfloor catalyst was evaluated without a manifold catalyst, it was found that nearly 60% of the weighted total hydrocarbons were emitted during the first 320 seconds of the test. It failed to meet the LEV standard after only 300 seconds into the test. The majority of the hydrocarbon emissions were due to the relative ineffectiveness of the catalyst during the cold start portion of Bag 1. A significant amount of hydrocarbons are emitted during the high speed acceleration.

When the 2.6g/L palladium manifold catalyst was added to the system, the weighted total hydrocarbon emissions were decreased significantly during the cold start portion of Bag 1. Not only did this converter system meet the hydrocarbon LEV emission standards, but the CO and NO_x LEV standards as well. The 10.6g/L palladium manifold and underfloor catalyst system met the extremely demanding ULEV standards.

When using the dual catalyst system, there are two additional factors to consider when determining the amount of noble metal used: catalyst location and catalyst volume. Figure 12(29) summarizes the results of using two noble metal loadings in two catalyst locations. The line graph shows the weighted tailpipe hydrocarbon emissions for each catalyst set, and the bar graph indicates the total noble metal loading for the catalyst set.

As expected, Set 1 which uses the least noble metal had the poorest hydrocarbon catalyst performance, and Set 4 which uses the most noble metal had the best hydrocarbon catalyst performance. Set 2 has a high noble metal loading in the larger underfloor catalyst, and the noble metal usage is much higher. Set 3, which has the high noble metal loading in the manifold catalyst has a relatively low noble metal usage because of the small manifold catalyst volume. In this case, the hydrocarbon catalyst performance does not correspond with noble metal usage, but rather with the placement of the noble metal. The application of the higher loading in the manifold catalyst resulted in more effective use of the metals.

Conclusions

AlliedSignal's program to develop palladium-only three-way automotive catalyst technology has yielded a new emission technology breakthrough demonstrating the following advantages and opportunities:

- (1) Palladium-only three-way catalyst technologies are effective alone or in conjunction with rhodium-containing technologies to lower both platinum and rhodium usage and noble metal costs.
- (2) Palladium-only catalysts have superior HC conversion performance relative to conventional platinum/rhodium catalysts for a variety of fuels including gasoline, methanol or methanol/gasoline blends, and compressed natural gas.
- (3) The use of high loadings of the relatively inexpensive palladium in small manifold catalysts offer superior thermal durability and light-off performance relative to platinum/rhodium catalysts.

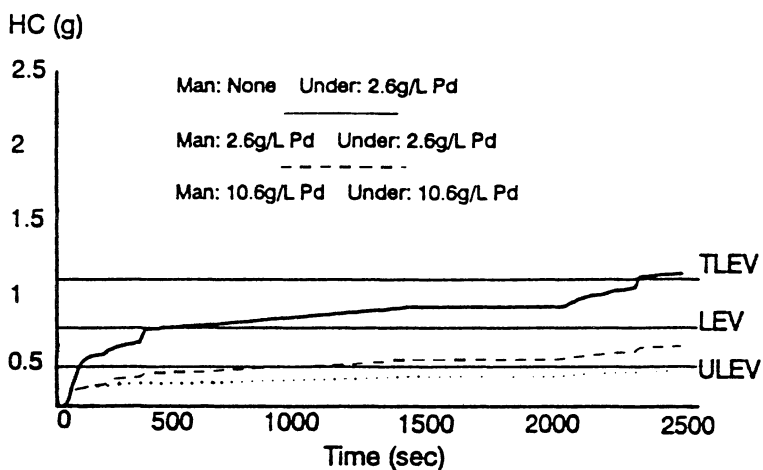


Figure 11. FTP-75 accumulative weighted emissions of three system configurations relative to various low emission vehicle standards. (Reproduced with permission from ref. 29. Copyright 1993 Society of Automotive Engineers, Inc.)

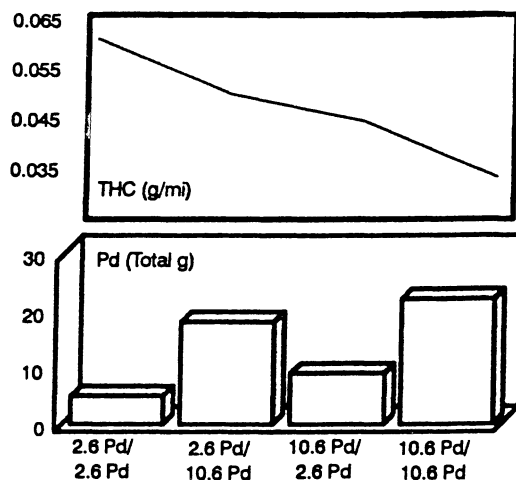


Figure 12. Effect of manifold/underfloor Pd loadings (g/L) on total FTP-75 hydrocarbon emissions relative to total system metal loading. (Reproduced with permission from ref. 29. Copyright 1993 Society of Automotive Engineers, Inc.)

Publication Date: February 23, 1994 | doi: 10.1021/bk-1994-0552.ch009

- (4) Manifold and close-coupled palladium-only three-way catalysts are effective for lowering hydrocarbon emissions to help meet California's LEV and ULEV standards. For cooler underfloor locations, palladium-only catalysts are also effective for CO and NO_x emission control performance.
- (5) State-of-the-art palladium-only catalysts exhibit particularly good CO and NO_x performance about the stoichiometric point after severe high temperature aging.

Acknowledgments

L. A. Butler, J. R. Cantley, J. R. Coopmans, K. J. Foley, M. G. Henk, D. G. Linden, M. J. Miller, K. I. Mitchell, P. C. Nawodylo, R. J. Shaw, R. G. Silver, J. F. Skowron, D. M. Thomason, J. H. White.

Literature Cited

1. Schlatter, J.C.; Taylor, K.C. *J. Catal.* **1977**, *49*, 42.
2. Gandhi, H.S.; Piken, A.G.; Stepien, H.K.; Shelef, M.; Delosh, R.G.; Heyde, M.E. SAE (Society of Automotive Engineers), **1977**, Paper 770196.
3. Jones, J.H.; Kummer, J.T.; Otto, K.; Shelef, M.; Weaver, E.E. *Environ. Sci. Technol.* **1971**, *5*, 790.
4. Bauerle, G.L.; Service, G.R.; Nobe, K. *Ind. Eng. Chem. Prod. Res. Dev.* **1972**, *11*, 54.
5. Gandhi, H.S.; Yao, H.C.; Stepien, H.K. ACS Symposium Series, **1982**, *178*, 143.
6. Summers, J.C.; Hiera, J.P.; Williamson, W.B. SAE, **1991**, Paper 911732.
7. Koenig, A.; Gellback, H.; Doering, G. SAE, **1974**, Paper 741059.
8. Gallopoulos, N.E.; Summers, J.C.; Klimisch, R.L. SAE, **1973**, Paper 730598.
9. Schlatter, J.C. In *Sintering of Supported Metals*, (Materials Science Research), G.C. Kuczynski, Ed., Plenum Press, N.Y., **1975**, p141.
10. Klimisch, R. L.; Summers, J. C.; Schlatter, J. C. In *Catalysts for the Control of Automotive Pollutants*; McEvoy, J. E., Ed.; Adv. Chem. Ser. No. 143; ACS: Washington, DC, **1975**, p. 103.
11. Summers, J.C.; Monroe, D.R. *Ind. Eng. Chem. Prod. Res. Dev.* **1981**, *20*, 23.
12. Hegedus, L.L.; Summers, J.C.; Schlatter, J.C.; Baron, K. *J. Catal.* **1979**, *56*, 321.
13. Graham, G.W.; Potter, T.; Baird, R.J.; Gandhi, H.S.; Shelef, M. *J. Vac. Sci. Technol.* **1986**, *4*, 1613.
14. Summers, J.C.; Hegedus, L.L. *J. Catal.* **1978**, *51*, 185.
15. Gandhi, H.S.; Williamson, W.B.; Logothetis, E.M.; Tabock, J.; Peters, C.; Hurley, M.D.; Shelef, M. *Surf. Interface Anal.* **1984**, *6*, 149.
16. Yao, Y.F. *Ind. Eng. Chem. Prod. Res. Dev.* **1980**, *19*, 293.
17. Gross, G.P.; Biller, W.F.; Green, D.F.; Kearby, K.K. U.S. Patent 3 370 914, Feb. 1968.
18. Gandhi, H.S.; Watkins, W.L.; Stepien, H.K. U.S. Patent 4 192 779, 1980.
19. Gandhi, H.S.; Yao, H.C.; Stepien, H.K. ACS Symp. Ser. **1982**, *178*, 143.
20. (a) Adams, K.M.; Gandhi, H.S. *Ind. Eng. Chem. Prod. Res. Dev.* **1983**, *22*, 207.
(b) Shelef, M.; Gandhi, H.S. loc cit **1972**, *11*, 393.

21. Williamson, W.B.; Lewis, D.; Perry, J.; Gandhi, H.S. *Ind. Eng. Chem. Prod. Res. Dev.* **1984**, *23*, 531.
22. Muraki, H.; Fujitani, Y.; Shinjoh, H. *Appl. Catal.* **1986**, *22*, 325.
23. Muraki, H.; Fujitani, Y.; Yokota, K. *Appl. Catal.* **1989**, *48*, 93.
24. Muraki, H.; Fujitani, Y.; Sohukawa, H.; Yokota, K.; Shinjoh, H. *Ind. Eng. Chem. Prod. Res. Dev.* **1986**, *25*, 202.
25. Summers, J.C.; Williamson, W.B.; Henk, M.G. SAE, **1988**, Paper 880281.
26. Summers, J.C.; White, J.J.; Williamson, W.B. SAE, **1989**, Paper 890794.
27. Summers, J.C.; Hiera, J.P. SAE, **1989**, Paper 891245.
28. (a) Summers, J.C.; Skowron, J.F.; Williamson, W.B.; Mitchell, K.I. SAE, **1992**, Paper 920558, (b) Summers, J. C.; Williamson, W. B.; Silver, R. G. patent pending.
29. Summers, J.C.; Skowron, J.F.; Miller, M. SAE, **1993**, Paper 930386.
30. Williamson, W.B.; Summers, J.C.; Scaparo, J.A. In *Catalytic Control Of Air Pollution Mobile and Stationary Sources*; Silver, R.G., Sawyer, J.E., Summers, J. C., Eds.; ACS Symp. Ser. 495; ACS: Washington, DC, **1992**, p26.
31. Summers, J.C.; Frost, A.C.; Williamson, W.B.; Friedel, I.M. *Air & Waste Mgt Assoc. 84th Annual Meeting, Vancouver, B.C., 1991*, Paper 95.4.
32. Summers, J.C.; Silver, R.G. to be published.
33. Monroe, D.R.; Krueger, M.H. SAE, **1987**, Paper 872130.
34. Williamson, W.B.; Summers, J.C.; Skowron, J.F. SAE, **1988**, Paper 880103.
35. Summers, J.C.; Baron, K. *J. Catal.* **1979**, *57*, 380.
36. Benson, J.D.; Burns, V.; Gorse, R.A.; Hochhauser, A.M.; Koehl, W.J.; Painter, L.J. SAE, **1991**, Paper 912323.
37. Fiedorow, R.M.J.; Chahar, B.S.; Wanke, S.E. *J. Catal.* **1978**, *51*, 193.
38. Flynn, P.C.; Wanke, S.E. *J. Catal.* **1974**, *34*, 390.
39. Yao, H.C.; Japar, S.; Shelef, M. *J. Catal.* **1977**, *50*, 407.
40. Yao, H.C.; Stepien, H.K.; Gandhi, H.S. *J. Catal.* **1980**, *61*, 547.
41. Summers, J.C.; Hegedus, L.L. *Ind. Eng. Chem. Prod. Res. Dev.* **1979**, *18*, 318.
42. Summers, J.C. *Air & Waste Mgt. Assoc.*, **1989**, Paper 89-96A.1.
43. Summers, J.C.; Williamson, W.B.; Scaparo, J.A. SAE, **1990**, Paper 900495.
44. Skowron, J.F.; Williamson, W.B.; Summers, J.C. SAE, **1989**, Paper 892093.

RECEIVED September 29, 1993

Chapter 10

Differences in Behavior of Pt, Rh, and Pt–Rh Alloy Surfaces toward NO Reduction

Bernard E. Nieuwenhuys¹, Jacobus Siera¹, Ken-ichi Tanaka², and Hideki Hirano²

¹Gorlaues Laboratories, Leiden University, P.O. Box 9502, 2300 RA Leiden, Netherlands

²The Institute for Solid State Physics, University of Tokyo, 7–22–1 Roppongi, Minato-ku, Tokyo 106, Japan

Rh is the key component of the automotive three-way catalyst for the conversion of NO_x to nitrogen. In the present paper we focus on the mechanisms of NO reduction reactions, the factors determining the activity and the selectivity of metal catalysts toward NO reduction and our understanding of the different behavior of Pt, Rh and Pt-Rh alloy catalysts. Major emphasis will be on NO-hydrogen reactions. The routes leading to N₂, NH₃ and N₂O formation will be addressed. The excellent performance of Rh will be discussed in relation to the behavior of this metal in NO adsorption, dissociation, interaction with N, O, CO and H. It will be shown that the surface structure and alloy formation can affect the behavior of the precious metals toward NO reduction.

The automotive three-way catalyst is an excellent catalyst for purification of automotive exhaust gas. Its high activity and selectivity combined with its outstanding thermal stability and resistance to poisoning make it a very effective catalyst. The active components include the precious metals platinum or palladium and rhodium.

In 1992 the automotive catalyst already accounted for 34% of the total demand for Pt and for 87% of the Rh demand.⁽¹⁾ Pt is an effective catalyst for the oxidation of CO and hydrocarbons. Rh is superior to Pt for the NO reduction to N₂ (2):



NO can also react to the undesired N₂O and NH₃ with overall reactions



It has been found that the reduction of NO by CO is much slower than by H₂. (3-5) Hecker and Bell (6) showed that in H₂/CO mixtures most of the NO reduction over supported Rh occurs through the consumption of H₂ even when the CO partial pressure exceeds the H₂ partial pressure. The selectivity of Pt to promote NO reduction to N₂ rather than to NH₃ is poor especially at low temperatures. (4) Rh is the essential ingredient of the automotive catalyst for the selective conversion of NO to N₂. (2) It has been found that Pt and Rh form alloy particles in the three-way catalyst. (7,8) Alloy particles often exhibit catalytic properties (e.g. selectivity, activity, stability and poison resistance) different from those of the constituent metals. Despite of the wildspread use of the bimetallic Pt-Rh catalysts, only a few studies have been published concerning the performance of Pt-Rh alloy catalysts in the relevant reactions. (5,9-17) This contrasts with the monometallic Pt and Rh catalysts about which several investigations have been reported.

In view of the enormous importance of bimetallic Pt-Rh catalysts we have investigated in our laboratories the properties of various Pt-Rh alloy single crystal surfaces and supported Pt-Rh alloy catalysts. (5,9-16) In this paper we describe comparative studies of NO reduction with hydrogen over several Pt-Rh alloy, pure Pt and pure Rh catalysts, in the form of both well defined single crystal surfaces and silica supported catalysts. The main purpose of this paper is to review our current knowledge concerning (1) the mechanisms of the various NO reduction reactions, and their relative contributions (2) our understanding of the different behavior of Pt and Rh in NO reduction and (3) the effects of Pt-Rh alloy formation and of surface structure.

Experimental

For details concerning the experimental equipment and procedure used, the reader is referred to our previous papers. (5,9-16) The experiments with single crystals were carried out in UHV systems with base pressures better than 2×10^{-10} mbar. The sample was cleaned by cycles of Ar-ion bombardment, oxidation and reduction cycli and flashing to high temperature in vacuum. The activity and the selectivity measurements over the supported catalysts were performed in a single-pass fixed-bed flow reactor operating at atmospheric pressure. The gases used contained a mixture of 5% of the reactive gases in helium. The gas flow in the system was 20 cm³/min. Analysis of the gas stream containing the products was accomplished using a computer controlled quadrupole mass spectrometer, which was differentially pumped by a turbomolecular pump group. During the measurements the catalyst temperature was increased with a linear heating rate of 4.5 K.min⁻¹. This heating rate was sufficiently slow to maintain steady-state reaction rate conditions at each temperature.

In order to avoid possible support effects, SiO₂ was used as the support for the noble metal particles. Pt and Rh catalysts were prepared by homogeneous precipitation of Aerosil 200 (200 m²/g) with aqueous solutions of either Rh(NO₃)₂

or $\text{H}_2\text{Pt}(\text{OH})_6$. The alloy catalysts were also prepared by homogeneous precipitation of Aerosil 200, but with both precursors in aqueous solution. The metal loading of all catalysts was 5 wt%. Each catalyst was calcined overnight at 383 K and, subsequently, reduced in flowing H_2 at 673 K for 16 h. All catalysts were examined using X-ray diffraction to determine the average particle size, and, in the case of the alloy catalysts, to ensure that alloy particles had been formed. Metal surface areas were determined by CO adsorption assuming a 1:1 stoichiometry between noble metal atoms on the surface and adsorbed CO molecules. These measurements showed that the difference in specific surface areas of the catalysts was less than 25%

Results and Discussion

NO reduction over silica-supported catalysts. The experiments were performed in a single-pass fixed bed flow reactor operating at atmospheric pressure. The gas stream contained 5% of the reactive gases. For the NO + CO reaction argon was used as carrier gas with a flow of $30 \text{ cm}^3 \text{ min}^{-1}$. For the NO + H_2 reaction helium was used as carrier gas with a flow of $20 \text{ cm}^3 \text{ min}^{-1}$. The catalyst temperature was increased according to a standard temperature-time program starting at room temperature. The linear heating rate of 4.5 K min^{-1} was sufficiently slow to maintain steady-state reaction rate conditions at each temperature. To assess the effect of catalyst aging, each catalyst was measured three times for each gas composition. First, the freshly reduced catalyst was measured. After exposing the catalyst to the reaction mixture at the maximum reaction temperature of 673K the series of experiments using the same catalyst was repeated twice. The results of the last series of measurements were similar to those of the 2nd series within experimental accuracy. Generally, the freshly reduced catalyst was somewhat more active than the aged catalyst. However, this effect was small and completely reversible after reduction. X-ray diffraction showed that the mean particle size of the aged catalyst was equal to that of the fresh catalyst. The results presented here concern the results obtained for the aged catalysts.

Five different catalysts have been selected viz. pure Pt, 25 at % Rh, 50 at % Rh, 75 at % Rh and pure Rh. For illustration the figures 1 and 2 show examples of the performance of some of these catalysts under our standard experimental conditions using about 200 mg of catalyst and a constant number of surface atoms of precious metal. The results for the NO reduction reactions are summarized in the figures 3 and 4, which show the temperature required to achieve a constant turnover frequency versus the catalyst composition. The turnover frequency is defined as the number of NO molecules reacting per second per metal (Pt and Rh) atom on the catalyst surface. The number of metal atoms on the surface per gram catalyst was estimated on the basis of CO adsorption.

Since a mass spectrometer was used for gas phase analysis the selectivity of the NO + CO reaction towards N_2O and N_2 could not be determined. In earlier work it was found that N_2O is a major product for the NO + CO reaction over supported Rh. (6) For the NO + H_2 reaction large concentrations of N_2O and NH_3

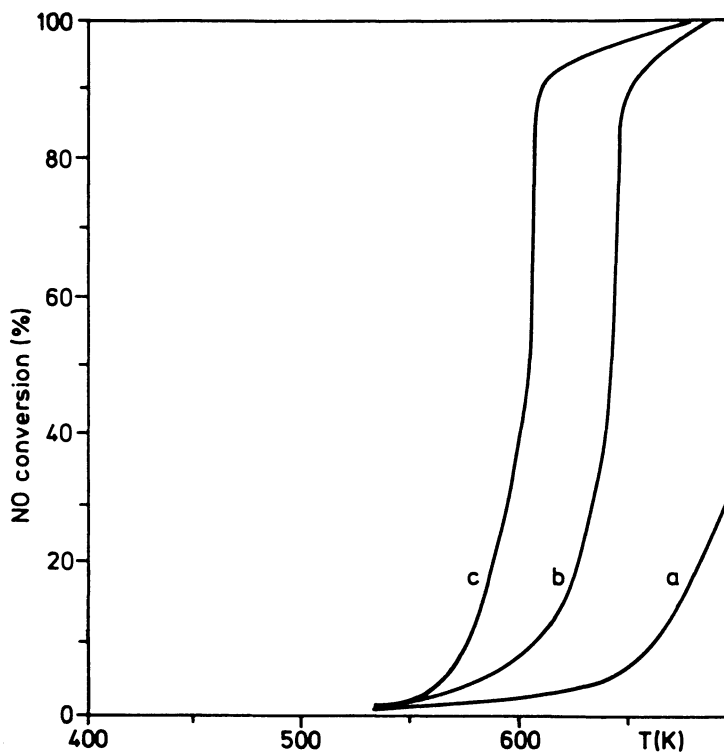


Fig.1a NO conversion, reaction of NO + CO (1/1) over
a) Pt; b) Pt_{0.75}-Rh_{0.25}; c) Rh on silica catalysts

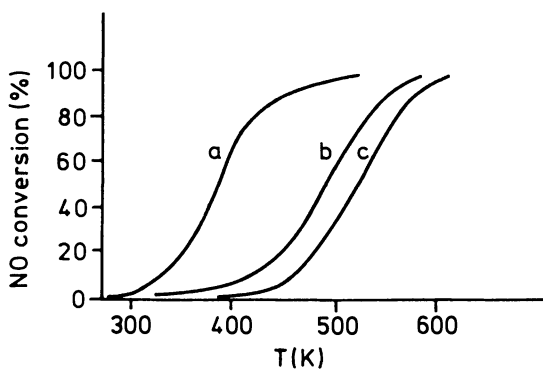


Fig.1b NO conversion, reaction of NO + H₂ (1/1) over
a) Pt; b) Pt_{0.75}-Rh_{0.25}; c) Rh on silica catalysts

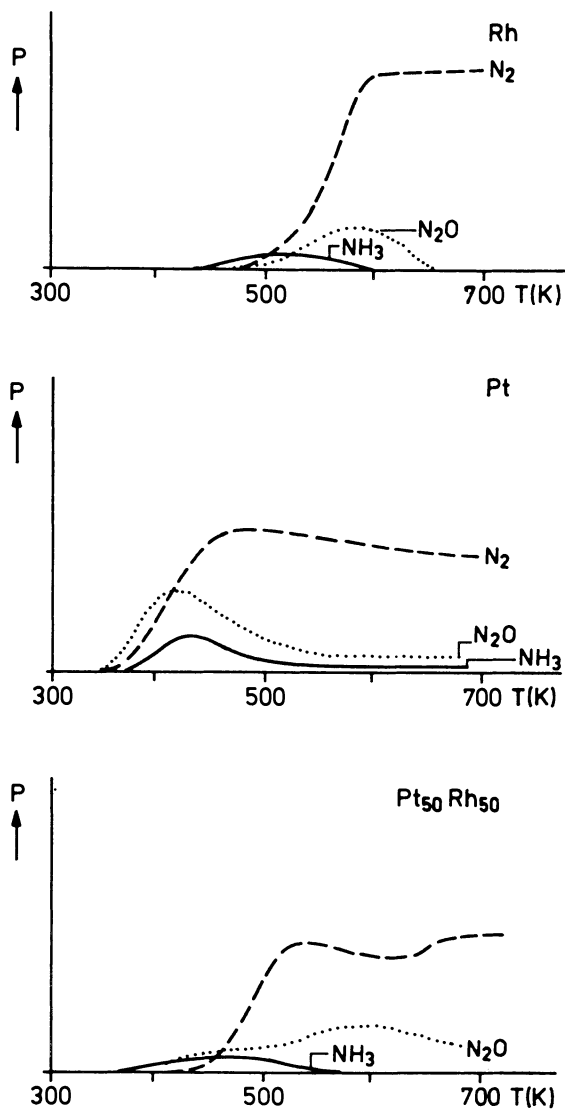


Fig.2 Variation of the product distribution with temperature for pure Pt, Pt_{0.5}Rh_{0.5} and pure Rh. NO/H₂ = 1

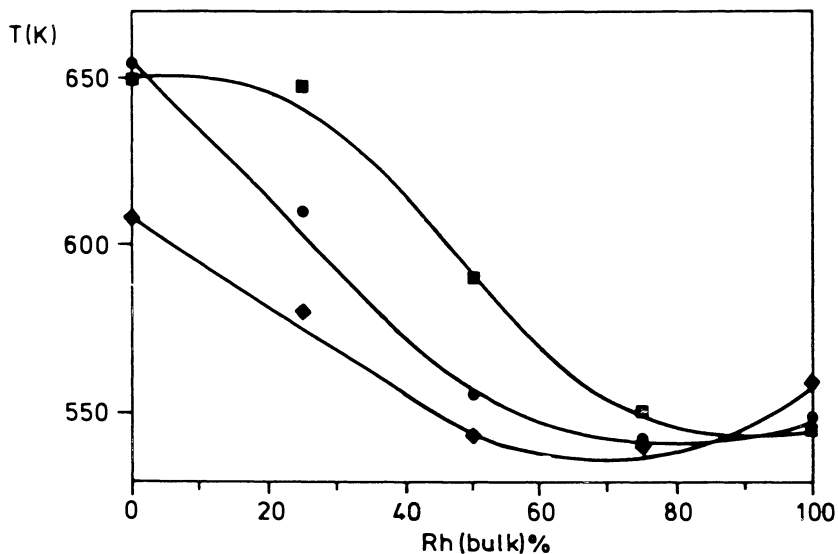


Fig.3 Temperature required for a constant turnover frequency of 0.05 s^{-1} for the $\text{NO} + \text{CO}$ reaction over Pt-Rh alloys as a function of the bulk composition for three NO/CO ratios. ■: $\text{NO}/\text{CO} = 1/4$, ●: $\text{NO}/\text{CO} = 1$, ◆: $\text{NO}/\text{CO} = 4$

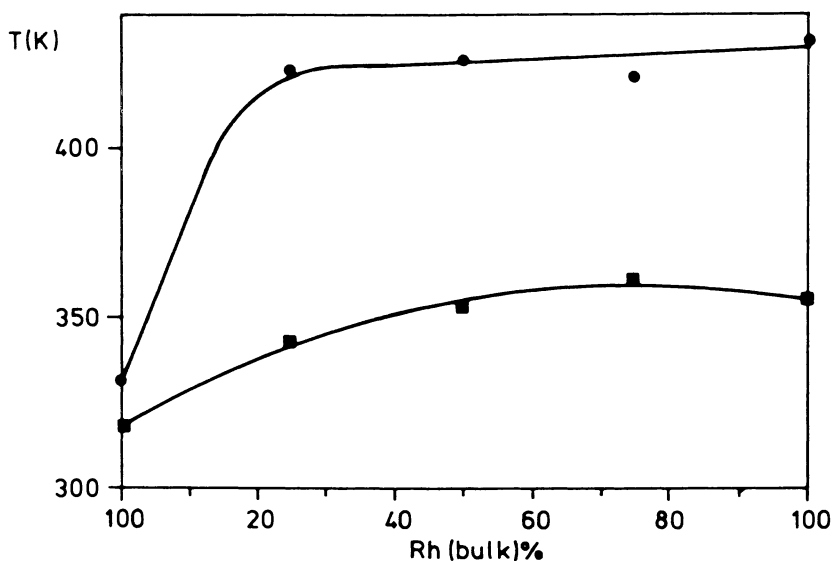


Fig.4 Temperature required for a constant turnover frequency of 0.005 s^{-1} for the $\text{NO} + \text{H}_2$ reaction over Pt-Rh alloys as a function of the bulk composition for two NO/H_2 ratios. ●: $\text{NO}/\text{H}_2 = 1$, ■: $\text{NO}/\text{H}_2 = 1/3$.

were found in addition to N_2 . For a NO/H_2 ratio of $1/3$, all the catalysts produce large amounts of NH_3 at T below 525K. The differences in selectivity are smaller than for the NO/H_2 ratio of 1/1, shown in figure 2.

The relevant observations can be summarized as follows.

- Much higher temperatures are required for achieving a high NO conversion using CO as reducing agent than with hydrogen. This observation is in agreement with that reported by Kobylinski and Taylor (3) and by Hecker and Bell. (6)
- Synergetic effects like enhancement of the reaction rate for the Pt-Rh alloy catalysts, compared with the pure component catalyst are absent. In all cases, the activity of the alloy catalyst is between those of the pure Pt and pure Rh catalysts.
- For the CO + NO reaction, the activities of Rh and the Rh rich alloy vary only slightly with the flow composition whereas for Pt and the Pt rich alloy the influence of the flow composition is large.
- For the NO + H_2 reaction, the activity of the Pt catalyst varies only slightly with changing flow composition whereas for the Rh containing catalysts the influence of the flow composition is large.
- Rh and Rh rich alloys are much better catalysts for the NO + CO reaction than Pt and Pt rich alloys both under CO rich as under CO lean conditions.
- Pt is a much more active catalyst in the low temperature reaction between NO and H_2 than Rh or Rh containing catalysts.
- For the NO + CO reaction the activity of the $Pt_{0.25}-Rh_{0.75}$ catalyst is almost equal to that of the pure Rh catalyst. For stoichiometric and CO lean mixtures, the $Pt_{0.5}-Rh_{0.5}$ alloy has an activity for the NO + CO reactions almost equal to that of Rh. Under reducing conditions, however, its activity is between those of Pt and Rh. The $Pt_{0.75}-Rh_{0.25}$ catalysts show an activity, equal to that of pure Pt under net-reducing conditions. Under stoichiometric and net-oxidizing conditions, its activity is between those of Pt and Rh.
- For the NO + H_2 reaction all Rh containing catalysts have the same activity as Rh at stoichiometry. In excess hydrogen $Pt_{0.75}-Rh_{0.25}$ has an activity intermediate to those of Pt and Rh. $Pt_{0.5}-Rh_{0.5}$ and $Pt_{0.25}-Rh_{0.75}$ have the same activities as that of pure Rh.
- Rh has a better selectivity toward N_2 formation, while Pt produces relatively large amounts of N_2O and NH_3 at temperatures below 525K.

Mechanistic studies using a $Pt_{0.25}-Rh_{0.75}$ (100) single crystal surface as a model catalyst. It has been suggested that N_2 is formed via dissociation of NO (18,19)



followed by either a reaction of N_{ads} with NO_{ads} or with N_{ads} :



The relative contribution of (4) and (5) to the formation of N_2 is not known. The mechanism of ammonia formation is unclear. The most likely mechanisms are

hydrogenation of N_{ads} formed by (3):



or hydrogenation of molecularly adsorbed NO:



The O_{ads} of reactions (3), (4) and (7) reacts with H_{ads} to water or with CO to CO_2 . The mechanism of N_2O formation has not been investigated in detail. Most likely, it is formed via



or via reaction between two molecularly adsorbed NO molecules:



In principle, also the following path should be considered:



In an attempt to shed more light on the mechanisms of the various reactions and their relative contributions, a detailed study has been carried out concerning NO adsorption, decomposition and reduction under widely different experimental conditions on the $\text{Pt}_{0.25}\text{-Rh}_{0.75}$ (100) surface. (15) This alloy surface was selected as a well defined model catalyst for the automotive catalyst. The composition of the Pt-Rh (100) surface is about 42% Pt and 58% Rh following annealing at 1100K. However, the actual surface composition may vary during the experiments. Thermal desorption spectroscopy (TDS), reactivity and selectivity studies were performed including the use of isotopically labelled NO and NH_3 molecules and, in addition, the surface sensitive techniques electron energy loss spectroscopy (EELS), Auger Electron Spectroscopy (AES) and Low Energy Electron Diffraction (LEED). Some of the results are summarized now.

Spectroscopic data. At 520K the surface was exposed to a reaction mixture consisting of 1×10^{-7} mbar NO and 5×10^{-8} mbar H_2 . Under reaction conditions the (1x1) structure, representative of the clean surface, changes into the c(2x2) surface structure. Analysis of the c(2x2) surface by means of TDS, AES and EELS, indicated that atomic nitrogen was the main surface species present. For comparative purposes similar experiments were carried out on the Rh(100), Pd (100) and Pt (100) surfaces. (20) Figure 5 illustrates some of the results. Accumulated N atoms ordered in the c(2x2) surface structure were found both on Pt-Rh(100) and Rh(100), but not on Pt(100). In the presence of H_2 or D_2 at a crystal temperature of 400K a nitrogen-hydrogen vibration was found. Its intensity depends strongly on the partial pressure of hydrogen. Evacuation of H_2 and D_2 results in a quick loss of the signal. Based on these results it is concluded that hydrogenation of N

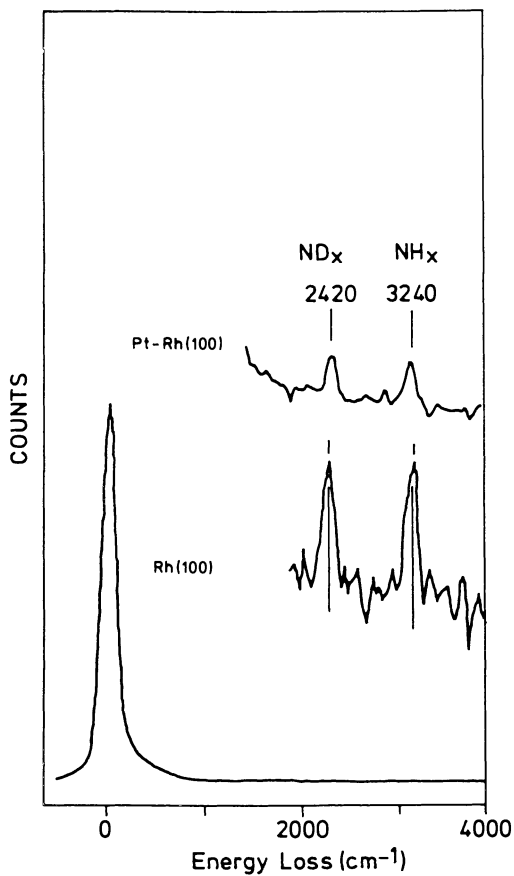


Fig.5 In situ EELS spectra of $c(2 \times 2)$ -N on the Rh(100) and Pt-Rh(100) surface in equilibrium with a hydrogen deuterium mixture at 10^{-7} Torr and a temperature of 400K. The intensity of the N-H signal is 1.6 larger on Rh(100) than on Pt-Rh(100).

can occur via:



The hydrogenation of atomic nitrogen is largely reversible. By means of AES it was established that the N/Rh signal ratio was decreased only a little during the hydrogen treatment. This indicates that complete hydrogenation of the atomic nitrogen to NH_3 can occur but with a very low rate only under these experimental conditions. It appears that the intensity of the N-H EELS signal varies with the square root of the hydrogen pressure:

$$I_{\text{N-H}} = A P_{\text{H}_2}^{1/2} \quad (12)$$

Furthermore, N-H scissor vibrations were absent in the EELS spectra. Both observations indicate that the dominant NH_x adsorption complex is NH_{ads} and not $NH_{2,\text{ads}}$ or $NH_{3,\text{ads}}$. Hence, eq.(11) can be rewritten to



Attempts to form a N-layer on the Pt(100) surface by means of the NO- H_2 reaction were unsuccessful. The NO and H_2 partial pressures were varied from 10^{-8} to 10 mbar and the temperature was varied from 400 to 600K. Formation of a nitrogen overlayer was not observed under these conditions.

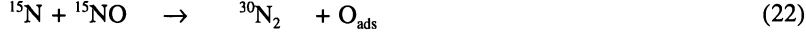
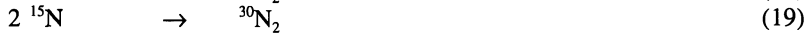
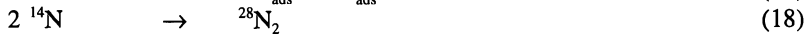
In one series of experiments temperature programmed reaction spectroscopy experiments were performed. In the presence of a NO + hydrogen (H_2 or D_2) flow ($\sim 2 \times 10^{-7}$ mbar) the largest ammonia formation is observed around 500K (heating rate used $\sim 3 \text{ K s}^{-1}$). However, if the surface was precovered with ^{15}N prior to exposure to the ^{14}NO + hydrogen flow, ammonia resulting from ^{15}N was already found at 435K. These results which have been described in more detail elsewhere (15), show that N atoms on the surface can react with hydrogen to ammonia at a temperature of 435K. On the basis of these observations and the EELS results we can conclude that hydrogenation of atomic nitrogen via NH_{ads} is most likely the reaction route to ammonia formation (process 6).

NO + H_2 and NO + NH_3 reactions under steady-state conditions in the 10^{-6} - 10^{-8} mbar range. The formation rates of N_2 , NH_3 and N_2O as a function of crystal temperature are shown in figure 6 for a mixture of 1.2×10^{-7} mbar NO and 3.6×10^{-7} mbar H_2 under steady-state conditions. The N_2 and NH_3 formation rates increase rapidly from 400K until the maximum rates are obtained at approximately 600K for N_2 and at the significantly lower temperature of about 525K for NH_3 . Nitrous oxide (N_2O) is only a minor product in the whole temperature range under these experimental conditions. N_2 production remains high and almost constant until a temperature of about 1000K is reached indicating that the reaction rate in this temperature range may be controlled by the collision frequency of NO on the surface. Above this temperature the formation rate drops. For reaction mixtures with excess of hydrogen the N_2 formation rate is almost independent on the hydrogen pressure (0th order) at temperatures from 600 to 800K. The ammonia

production is about 1st order in hydrogen in the whole temperature range of 400 to 800K. N_2O formation is only observed at relatively high NO pressures and it is only slightly affected by changing the hydrogen pressure. Under the conditions of these experiments ($p_{NO} < 5 \times 10^{-6}$ mbar) the N_2 formation remains at least a factor of 100 larger than the N_2O production rate.

In another series of experiments the H_2 in the gas flow was replaced by NH_3 and the ^{14}NO by ^{15}NO in order to examine the distribution of the two types of N atoms over the N containing products. Figure 7 shows the variation of dinitrogen formation rates with increasing temperature in the presence of a flow of 1.2×10^{-7} mbar of ^{15}NO and 3.0×10^{-7} mbar of $^{14}NH_3$. In the low temperature range ($T < 800K$) the rate of $^{14}N^{15}N$ formation is larger than the rate of $^{15}N^{15}N$ formation which in turn is much larger than the $^{14}N^{14}N$ formation. It should be noted in this context that the ^{14}N ($^{14}NH_3$) concentration in the gas phase is a factor of 2.5 larger than the ^{15}N (NO) concentration. The relatively low production of $^{14}N^{14}N$ is in qualitative agreement with earlier results reported by Otto et al (21) for the NO + NH_3 reaction over supported Pt. Using N isotopes these authors showed that N_2 formed over Pt exclusively from NH_3 is only a minor path. Under our conditions N_2 is formed over Pt-Rh(100) exclusively from NH_3 albeit with a much lower rate than from NO + NH_3 and from NO_3 only. Above 700K the rate of $^{14}N^{15}N$ formation drops rapidly with increasing temperature and the $^{15}N^{15}N$ production becomes larger. The $^{14}N^{14}N$ production shows the same temperature dependence as that of the $^{14}N^{15}N$ production.

Let us now turn to the mechanisms of dinitrogen formation. Does the major step of N_2 formation involve NO decomposition followed by combination of two N adatoms (process 5) or is it a reaction between adsorbed N and adsorbed NO (process 4)? A comparison of the $^{14}NH_3 + ^{15}NO$ and $NO + H_2$ reactions can provide valuable information concerning this question. The relevant processes that can take place are:



The temperature dependence of the N_2 formation is the same for the $NH_3 + ^{15}NO$ and the $H_2 + NO$ reactions suggesting that the same processes are involved. The N combination reactions can occur in the whole temperature range as demonstrated by the rate of $^{28}N_2$ formation. The production of $^{28}N_2$ is much smaller than the production of $^{29}N_2$ and $^{30}N_2$, while the $^{14}NH_3$ concentration in the gas phase is a factor of 2.5 greater than that of ^{15}NO . This may indicate that NH_3 is a slower producer of N_{ads} than NO is. However, this argument is in contradiction with the large rate of $^{29}N_2$ formation. In our opinion these results point to the importance

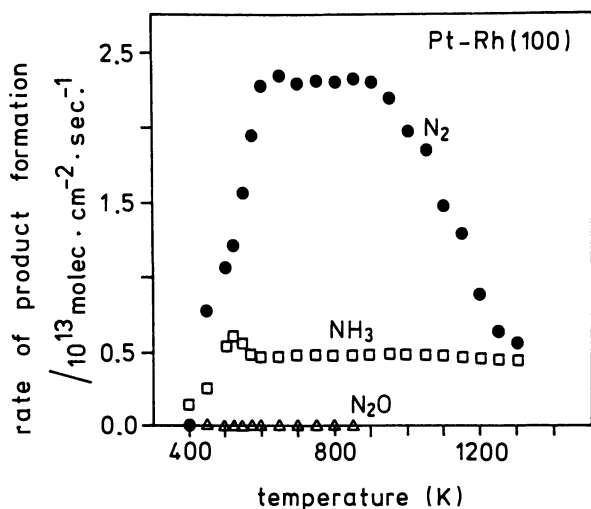


Fig.6 Steady state formation of N₂(●), NH₃(□) and N₂O(Δ) on the Pt-Rh(100) surface in the presence of 1.2×10^{-7} mbar NO and 3.6×10^{-7} mbar H₂. (Reproduced with permission from reference 15. Copyright 1992 Elsevier Science Publishers BV.)

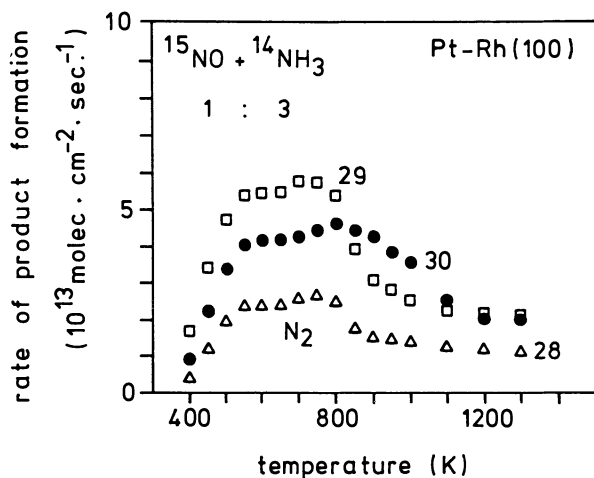


Fig.7 Steady state formation rates of N₂ over Pt-Rh(100) with amu 28(Δ), 29(□) and 30(●) in the presence of 1.2×10^{-7} mbar ¹⁵NO and 3.0×10^{-7} mbar ¹⁴NH₃. (Reproduced with permission from reference 15. Copyright 1992 Elsevier Science Publishers BV.)

of the reactions of N_{ads} with NO_{ads} (processes 21 and 22) for N_2 formation in the lower temperature regime ($T < 700\text{K}$). In the temperature range between 700 and 900K the rate of $^{29}N_2$ production decreases with a factor of two. The rate of $^{30}N_2$ formation, on the other hand, becomes only marginally smaller. This suggests that the reactions involving NO_{ads} and N_{ads} become less important than the combination reactions of two N adatoms. However, the $^{28}N_2$ formation rate decreases also strongly in this temperature range showing that NH_3 becomes a less effective N_{ads} producer than NO in this temperature range. At a temperature of 1100K the rate of $^{28}N_2$ formation is a factor of 1.5 smaller than at 600K, the rate of $^{29}N_2$ formation a factor of 2.5 and the rate of $^{30}N_2$ formation is only slightly lower. Hence, it can be concluded that in a high T range (1100K) the importance of the N combination reaction is much larger than in the low temperature range and that ammonia becomes a less effective N producer than NO.

NO + H₂ and NO + NH₃ reactions in the 10 mbar pressure range. The reactions were studied at different temperatures and for various reactant ratios. As examples figure 8 shows the reduction of NO with hydrogen at 550K for NO/H₂ ratios of 1/5 and 1. At $T < 500\text{K}$ and a NO/H₂ ratio of 1/5 most of the NO reacts at low conversion to N_2 and the formation of NH_3 is larger than that of N_2O . However, as the temperature increases above 500K the NH_3 production exceeds the N_2 production and N_2O formation essentially ceases. The rate of NO conversion is much slower for the NO/H₂ ratio of unity than for the ratio of 1/5. N_2 production is only slightly affected by the lowering of H₂ pressure. However, NH_3 decreases drastically by lowering the hydrogen pressure. As a result the selectivity toward dinitrogen is much improved by lowering of the H₂/NO ratio. The hydrogen pressure was varied from 1.2 mbar to 24 mbar using a constant NO pressure of 1.2 mbar. It appeared that the reaction order in hydrogen is essentially zero for N_2 and N_2O formation and about unity for NH_3 formation under these conditions. This pressure dependence is almost similar to that observed for the low pressure experiments.

In order to gather additional information concerning the contributions of the possible mechanisms leading to the various reaction products, the $^{15}NO + ^{14}NH_3$ reaction was also studied in the pressure range of 10 mbar. Some results are shown in figure 9 for a $^{15}NO/^{14}NH_3$ ratio of 1 at 600K.

The relevant observations are:

- 1) The N_2 formation rates decrease in the order rate $^{14}N^{15}N > \text{rate } ^{15}N^{15}N > \text{rate } ^{14}N^{14}N$.
- 2) $^{14}N^{14}NO$ is not formed under these experimental conditions.
- 3) $^{14}N^{15}NO$ is formed with a higher rate than $^{15}N^{15}NO$.
- 4) at 600K the N_2O concentration reaches a maximum concentration after three minutes and decreases subsequently.

The results will be discussed now. It should be emphasized that NO decomposition, NH_3 decomposition, N_2O decomposition, NO + H₂ reaction and $NH_3 + NO$ reaction can occur simultaneously. Hence, useful information concerning one specific reaction is only obtained in the beginning of the reaction when the conversion is still low. The results obtained in the higher pressure regime are in line with those obtained in the low pressure regime and the discussion can,

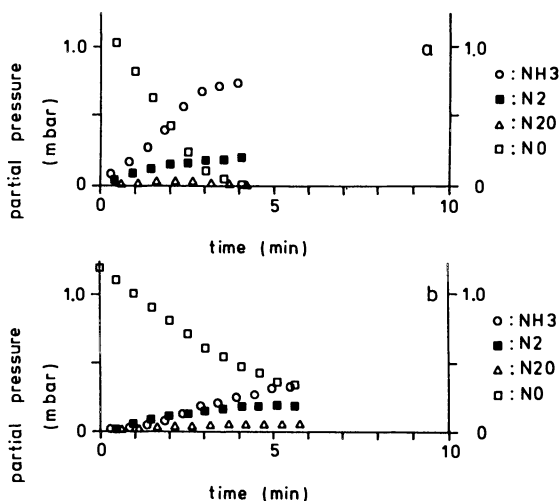


Fig.8 Formation of N_2 , NH_3 and N_2O over Pt-Rh(100) at 550K using a NO/H_2 ratio of 1/5 (a) and 1/1 (b), total pressure is 3 mbar. (Reproduced with permission from reference 15. Copyright 1992 Elsevier Science Publishers BV.)

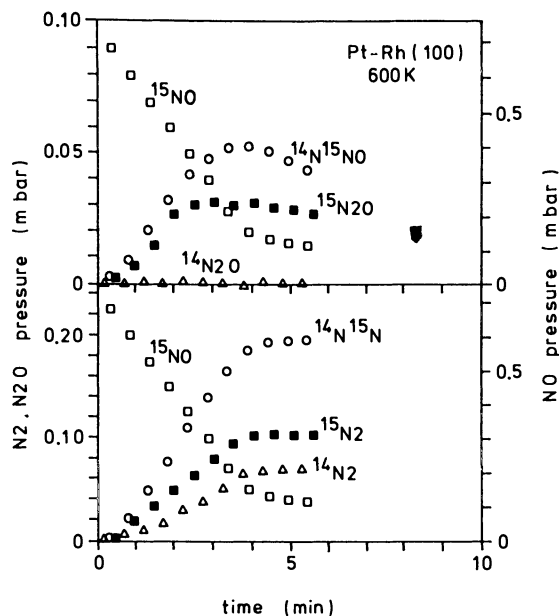


Fig.9 The observed reaction products for the $^{15}NO + ^{14}NH_3$ reaction over Pt-Rh(100) as a function of reaction time at 600K at a $^{15}NO/^{14}NH_3$ ratio of 1 and a total pressure of 3 mbar. (Reproduced with permission from reference 15. Copyright 1992 Elsevier Science Publishers BV.)

therefore, be brief and focus on the differences. The most striking differences are (1) the relatively high selectivity to N_2O in the higher pressure regime, and (2) the relatively high selectivity to ammonia. The observation (1) is completely in line with the expectations based on the mechanism for N_2O formation via process (8) requiring a high concentration of molecularly adsorbed NO. The dissociation of NO is inhibited by a high concentration of adsorbed NO as discussed before. It has also been described in the literature that for the NO reduction reaction a silica supported Rh catalyst is largely covered with NO. (6) On the other hand in the low pressure regime Rh surfaces are covered with N_{ads} . (22) As the temperature increases the concentration of NO_{ads} will decrease due to desorption and the selectivity to N_2O should decrease. This expectation is indeed consistent with the observations.

The same argument can be used for the interpretation of the relatively high selectivity to NH_3 . A high concentration of N_{ads} favors a high selectivity to N_2 via process (5). A low concentration of N_{ads} favours the formation of NH_3 (process (6)). Obviously, the N_{ads} concentration at 600K in the 10 mbar pressure regime is lower than in the 10^{-7} mbar regime. It has been described that the selectivity to NH_3 on supported metals like Pt and Rh increases with increasing temperature up to a maximum T_m after which it decreases (4), for Pd and Pt T_m is about 600K. The maximum temperature used in this study was 600K and, hence, the increasing selectivity to NH_3 observed when the temperature increases is in agreement with these literature data.

The results obtained for the $^{15}NO + ^{14}NH_3$ reaction in the 10 mbar range are also completely in agreement with the models described in previous sections. $^{14}N_2O$ is not formed, while $^{14}N^{15}NO$ and $^{15}N_2O$ are both formed, showing that N_2O is only formed via process (8). At 600K the formation rate of $^{14}N^{15}NO$ is faster than that of $^{15}N_2O$ suggesting that NH_3 is a better producer of N than NO at this temperature. $^{14}N_2$ formation is not detected at 550K while at 600K the rate of $^{14}N_2$ formation is much smaller than that of $^{14}N^{15}N$ and $^{15}N_2$. This observation again suggests that process (4) is the dominant path for N_2 production in this low temperature range.

The molecular picture that emerges from this work is the following one. At low temperatures ($T \sim 450K$) the majority of the adsorbed species is NO while N is only a minor species. Adsorbed hydrogen is very mobile and can easily react with either O or N provided that it can find a vacant site in the neighborhood of an adsorbed O or N atom. The concentration of vacant sites is rather low in this temperature range. As the temperature increases the concentration of NO becomes lower and the concentration of N_{ads} increases. When the NO_{ads} concentration becomes much lower than the N_{ads} concentration the rate of process (8) and, hence, the selectivity to N_2O becomes low. For N_2 formation via process (4) high concentrations of both N_{ads} and NO_{ads} are required, for N_2 formation via process (5) a high concentration of N_{ads} is required. Consequently, process (4) has a large contribution to the N_2 formation in the lower temperature range and process (5) dominates in the higher temperature range. The selectivity to NH_3 increases with increasing temperature in the temperature range 300-600K. This again suggests that the dominant mechanism of NH_3 formation is via process (6) and not via hydrogenation of NO_{ads} . The selectivity to NH_3 will be the largest at a temperature

where both the N_{ads} and H_{ads} concentrations are sufficiently high. The strong positive reaction order in hydrogen pressure shows that the concentration of H_{ads} is the limiting factor under the experimental conditions used. At very high temperature the reaction rates of both NH_3 and N_2 formation will decrease because of the decrease of N_{ads} and H_{ads} concentrations. Obviously, this temperature depends strongly on the absolute NO and H_2 pressures and on the surface used. Rh with its much stronger metal-N bond strength will exhibit a much better selectivity toward N_2 than Pt with its weaker metal-N bond strength in the high temperature range. The observed decrease in selectivity toward NH_3 at very high temperatures can be attributed to a combination of limited availability of H at high temperature and the high rate of NH_3 decomposition.

The final point to be discussed is the factor determining the selectivity toward N_2O and N_2 at low temperatures.



The availability of a vacant site \square near to NO_{ads} and N_{ads} may play a central role. A situation like the one sketched under b may possibly result in N_2 formation, whereas situation a will result in N_2O formation.

The picture described above certainly needs several refinements. For example, the distribution of NO_{ads} , N_{ads} , O_{ads} and H_{ads} over the surface is not known. It was found that N_{ads} forms a $c(2 \times 2)$ surface structure on the Pt-Rh(100) surface in a large range of coverages. Hence, it is likely that N islands are formed on the surface. N_2 via process (4) and N_2O via process (6) are then formed at the boundaries of N and NO islands. Most probably, NH_3 is also formed at the boundaries of the N islands.

Comparative studies of NO reduction by hydrogen over Pt, Rh and Pt-Rh alloy single crystal surfaces. This section describes the reduction of NO by hydrogen over the (111), (100) and (410) surfaces of a $\text{Pt}_{0.25}\text{-Rh}_{0.75}$ single crystal and the pure Pt(100) and Rh(100) single crystal surfaces. The purpose of this section is to establish the effects of the surface structure and alloying on the kinetics and selectivity of the NO-H_2 reaction.

For illustration figure 10 shows the conversion of NO and the formation of NH_3 , N_2 and N_2O over the five surfaces at a temperature of 575K. The reaction was studied in the batch reactor at a total pressure of 6 mbar and a NO/H_2 ratio of 1 to 5. The conversion of NO over Rh(100) proceeds much slower than over Pt(100). However, the selectivity to dinitrogen is much better for the Rh(100) surface. The conversion of NO over Pt-Rh(111) is slower than over Pt-Rh(100). The only reaction product formed over Pt-Rh(111) is ammonia. The NO conversion over Pt-Rh(410) is slower than over the Pt(100) and Pt-Rh(100) surfaces but higher than over the Pt-Rh(111) surface. The selectivity toward N_2 is relatively high. Figure 11 and 12 summarize the results for the activity expressed as conversion after 3 minutes of reaction time at 520K and the selectivity toward N_2 formation at a NO conversion of 10% for 520 and 575K.

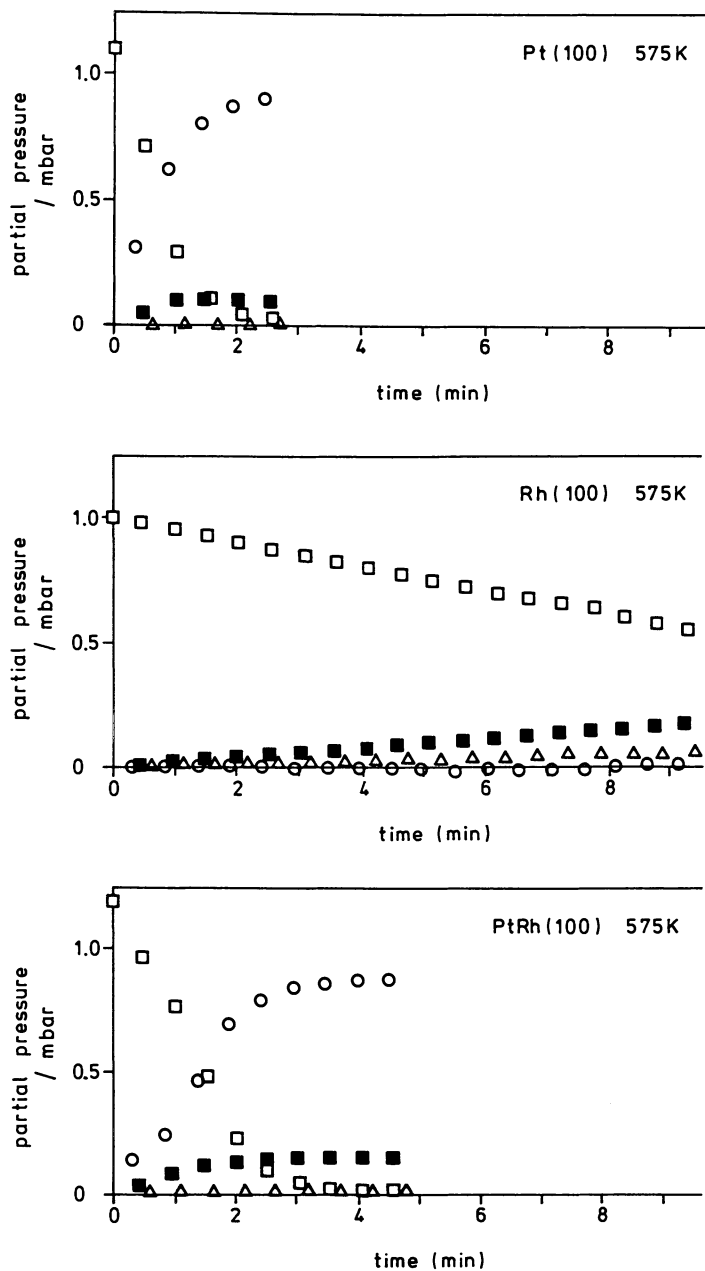


Fig.10 Formation of N_2 , NH_3 and N_2O at 575K for $NO/H_2 = 1/5$ and a total pressure of 6 mbar.

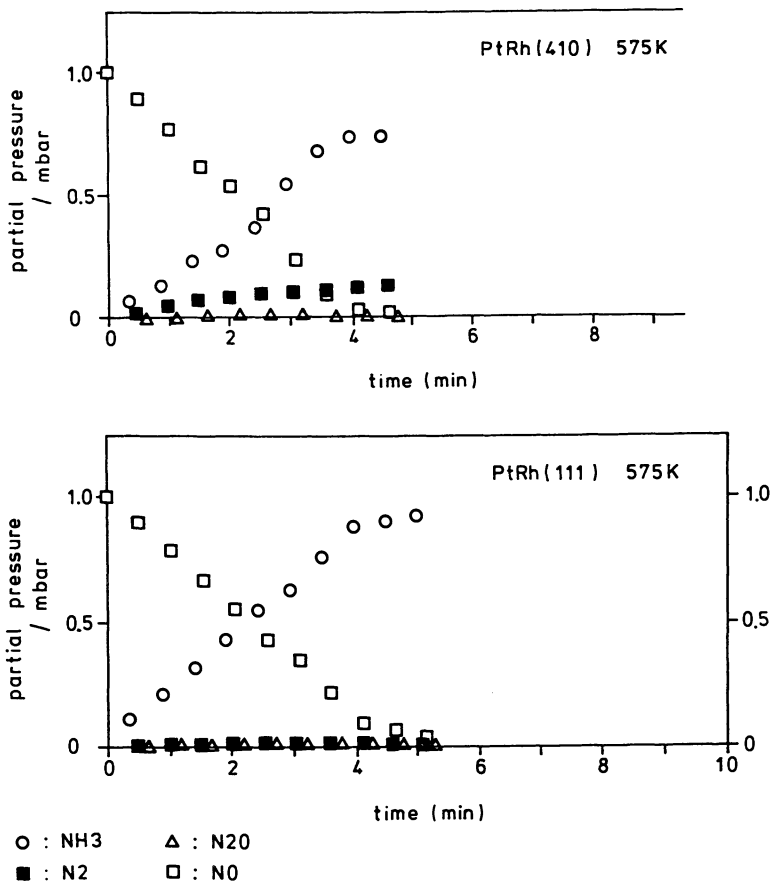


Figure 10. *Continued.*

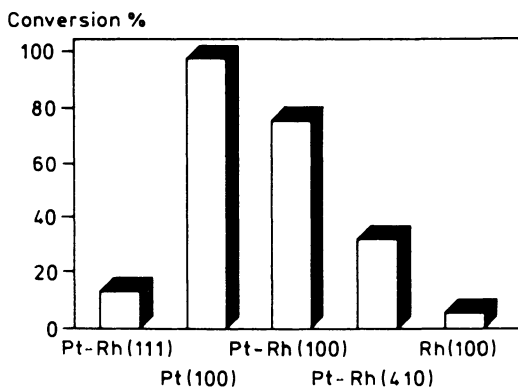


Fig.11 NO conversion after 3 minutes of reaction time at 520K.
(Adapted from reference 16.)

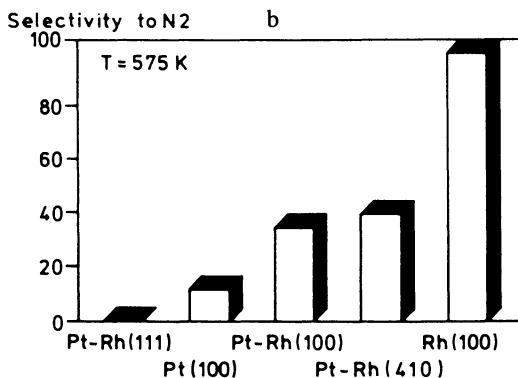
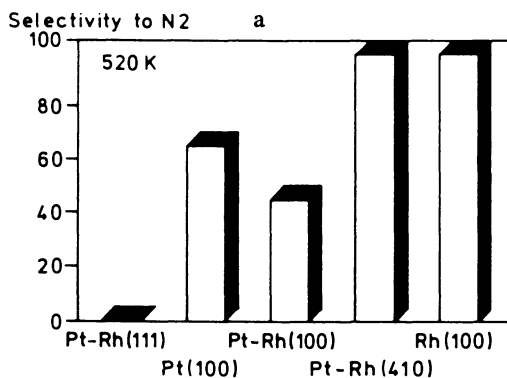


Fig.12 Selectivity (0-100%) of the NO-H₂ reaction toward N₂ determined at a total conversion of 10% at a) 520K and b) 575K.(Adapted from reference 16.)

After the reaction was stopped, the reactor was evacuated and the sample was analyzed by AES, EELS and LEED. The results are summarized in table I. It should be noted that the information concerning the physical and chemical state of the surfaces is obtained after the reaction was stopped and the surface composition and structure may not be the same as under the reaction conditions. However, as will be shown further on, the results provide useful additional information which may lead to a better understanding of the processes taking place on the various surfaces. Dissociation of the NO molecule (step 3) is very sensitive to the surface structure and composition. This is illustrated by the very low activity for bond scission of the Pt(111) surface and a high dissociation rate on the Pt(410) surface. (23) The high activity for NO bond scission of the Pt(410) surface may be due to an enhanced interaction of the oxygen atom at the step sites. Masel (23) suggested that the Pt(410) surface structure exhibits an electron orbital symmetry at these sites which matches the symmetry of the antibonding orbitals of the NO molecule. This causes a strong weakening of the N-O bond strength and dissociation may occur. It is known that NO dissociation occurs more efficiently on Rh than on Pt surfaces. (9,24) The order in intrinsic activity for N-O bond breaking is Pt-Rh(410) > Rh(100) > Pt-Rh(100) > Pt(100) > Pt-Rh(111). It is also well established that a number of free metal sites is needed for NO dissociation. (24)

Table I. LEED, EELS observations and Auger signal intensity ratios after the reduction of nitric oxide by hydrogen over Pt, Rh and Pt-Rh single crystal surfaces at a total pressure of 6 mbar, a NO/H₂ ratio of 1/5 and a temperature of 520K, divided by the (a) Rh₃₀₂ and (b) Pt₆₄ AES signal intensity

Surface	N ₃₈₀	O ₅₁₀	LEED	EELS
Pt-Rh(111)	0.057 ^a	0.006 ^a	diffuse(1x1)	NO
Pt-Rh(100)	0.038 ^a	0.055 ^a	c(2x2)	N
Pt-Rh(410)	0.065 ^a	0.035 ^a	(2x1)	N
Pt(100)	0.013 ^b	0.006 ^b	diffuse(1x1)	N+NO
Rh(100)	0.045 ^a	0.012 ^a	c(2x2)	N

The adsorption of the H₂ molecule proceeds with a relatively low sticking probability on Pt and Rh surfaces at 400-500K. The sticking probability of hydrogen depends on the surface structure. On the Pt(100) surface a higher sticking probability is measured than on the Pt(111) surface. The dissociation of the H₂ molecule proceeds very fast on group VIII metals at 400-500K. (19)

On the Pt-Rh(100) and Rh(100) surfaces it was found that hydrogenation of N_{ads} (step 6) occurs at 400-450K. NH_{ads} was found as a major surface intermediate when N_{ads} was exposed to hydrogen. The formation of NH₃ via N_{ads} + 3H_{ads} was found at a temperature of 450K. The decomposition of NH₃ over Pt surfaces increases in the order (111)<(100)<(210). (25) The NH surface intermediate may decompose before total hydrogenation has occurred. The formation of H₂O is a very fast process. (19)

The combination of two N_{ads} adatoms (step 5) occurs in a wide temperature range. This step also strongly depends on the surface structure and the metal being used. On Rh surfaces the metal-N bond is stronger than on the corresponding Pt surfaces. The metal-N bond strength increases in the order (111) < (100). In contrast to the Pt(100) surface where desorption of nitrogen occurs almost instantaneously at the reaction temperatures considered, build-up of N_{ads} takes place on the Rh(100), Pt-Rh(100) and Pt-Rh(410) surfaces.

The $\text{NO}_{\text{ads}} + N_{\text{ads}}$ reaction can give $\text{N}_{2(\text{g})} + \text{O}_{\text{ads}}$ or $\text{N}_2\text{O}_{(\text{g})}$ via steps 4 and 8, respectively. On Pt-Rh(100) it was found that step 4 is a main route through which $\text{N}_{2(\text{g})}$ is formed in the temperature range below 600K. At higher temperatures step 5 is the dominant mechanism for N_2 formation. Little is known about the specific contributions of steps 4 and 5 over Pt and Rh surfaces.

A slow conversion over Pt-Rh(111) is observed in combination with a high selectivity towards NH_3 ($\approx 100\%$). It is known that dissociation of NO is slow over the Pt-(111) surface, and that the behaviour of Pt-Rh alloy surfaces towards NO dissociation displays a Pt-like behaviour at high NO coverages. (26) Under reaction conditions the Pt-Rh(111) surface is largely covered by NO and the coverages of N_{ads} and O_{ads} are small. The only reaction product is NH_3 . NH_3 may be formed through process (6) as over Pt-Rh(100) or via an [NOH] intermediate (process (7)). Gorodetskii et al (27) reported the formation of [NOH] on Pt. However, the [NOH] intermediate was found to be unstable at temperatures higher than 400K. The formation of NH_3 is favored over the formation of N_2O or N_2 . No ordered LEED structures were observed on Pt-Rh(111), indicating that the NO molecules do not form large ordered islands. Thus, for the Pt-Rh(111) surface it is assumed that step (3) occurs relatively slow, and N_{ads} reacts to NH_3 through step (6). N-N combination is unlikely due to the low concentration of N_{ads} . The formation of N_2 and N_2O is below the limit of detection, indicating that steps (4) and (8) do not take place at a detectable rate.

The conversion of NO over the Pt-Rh(100) surface after 3 min. reaction time at 520K is almost 70% and the selectivity towards N_2 is 32%. The normalised $\text{N}_{380\text{eV}}$ AES signal intensity is 0.038 and for the $\text{O}_{510\text{eV}}$ normalised signal intensity a value of 0.055 has been found. By EELS it was found that the $\text{N}_{380\text{eV}}$ signal intensity is caused by nitrogen atoms. This surface is covered by a small amount of NO_{ads} , and a larger amount of N_{ads} . A $\text{N c}(2\times 2)$ surface structure was observed. Islands of N adatoms may facilitate the formation of N_2 via step 5. The large $\text{O}_{510\text{eV}}$ signal is partly due to the formation of subsurface oxygen. Thus, for this surface NO dissociation occurs easily and the formation of N_2 through step (5) will be fast. The high activity indicates that free sites remain available during the reaction. These sites probably consist of Pt atoms since the Rh atoms will be covered by N_{ads} .

Over Pt(100) the highest NO conversion rate was observed at low temperatures and the selectivity towards N_2 is 60% at 520K. The dissociation of NO over Pt(100) proceeds easily provided that vacancies are available. The Pt(100) surface exhibits a higher selectivity toward N_2 than the Pt-Rh(100) alloy surface at 520K. Pure Rh, however, has a higher selectivity toward N_2 than pure Pt. This may be explained by an effect of strongly bound nitrogen atoms on the rhodium atoms surrounding the platinum atoms. At 520K, the nitrogen atoms adsorbed on Rh sites are strongly bound to the surface and the formation of N_2 is slow. If an NO

molecule dissociates on Pt sites, the nitrogen atoms may be surrounded by a matrix of strongly bound nitrogen atoms on Rh sites. The formation of N_2 will be slow at this temperature and the subsequent hydrogenation of this N-atom on the Pt-site can occur. On Pt(100), the nitrogen atom may recombine with NO, or N on other neighboring Pt-sites forming N_2 or N_2O and N_2 respectively. The formation of NH_3 through $N_{ads} + H_{ads}$, over "isolated" Pt-sites is reduced. This may explain the enhanced NH_3 production over the Pt-Rh(100) alloy surface at 520K in comparison with pure Pt(100). The high conversion of NO over the Pt-Rh(100) and Pt(100) surfaces is explained by the intrinsic high NO dissociation activity combined with the relatively low M-N bond strength on platinum which prevents that the reaction is inhibited by blocking of active sites by N_{ads} . At 575K, the selectivity towards N_2 over the Pt-Rh(100) surface is higher than over the Pt(100) surface. At this temperature the enhancement of the N_2 production over Pt-Rh(100) may be ascribed to N-N combination from sites containing few or more Rh atoms. N_2 production over the Rh(100) surface is observed at 575K.

The dissociation of NO proceeds relatively easily on Pt-Rh(410). The nitrogen atoms adsorbed at the steps of the single crystal surface have an enhanced adsorption energy. The activity will decrease due to the higher number of metal sites which are occupied by strongly bound nitrogen. At the step sites an enhanced decomposition may also take place before total hydrogenation to NH_3 has occurred. The oxygen concentrations near the surface layer is also large. The LEED pattern after the reaction points to a (2x1) surface structure. The single crystal surface may facet under the reaction conditions. However, if this would be the case, desorption of the adsorbates restores the structure characteristic of the fcc(410) surface.

The selectivity toward N_2 has the highest value over the Rh(100) surface. However, the conversion of NO is low at temperatures below 600K, due to the high concentration of strongly bound nitrogen atoms. The high selectivity toward N_2 can be explained by the high concentration of nitrogen atoms on the surface. A c(2x2) surface structure was found by means of LEED. The relatively low O_{510eV} AES signal indicates that this structure consists mainly of N_{ads} . Therefore, it is believed that large islands of N_{ads} are formed during the reaction. This facilitates the formation of N_2 via step (5). By EELS it was found that NH_{ads} can actually be formed on the Rh(100) surface. However, NH_3 is not formed under the described reaction conditions. The low rate of NH_3 formation may be caused by a low H_{ads} concentration in the N_{ads} islands and the formation of NH species at the boundaries of these islands only. Also, an enhanced decomposition of NH could take place on Rh. The low activity for the NO/ H_2 reaction at 520K is ascribed to the low concentration of free active sites available for reaction. Most of the metal atoms are blocked by nitrogen atoms, or NO molecules. At 575K, N_2O formation is observed, this indicates that even at this temperature the number of free sites must be relatively small. The N_2O intermediate will decompose into N_2 and O_{ads} if a sufficient number of vacancies is available. If these vacancies are absent, N_2O will desorb from the surface.

Comparison of NO reduction over silica supported catalysts and single crystal surfaces. The differences in activity and selectivity found between silica support-

ted Pt and Rh catalysts are in line with those found between Pt and Rh single crystal surfaces and, hence, most likely the same mechanisms are operative.

Rh is a much better catalyst for the NO reduction by CO than Pt, an observation that is consistent with literature data. For this reaction the effect of changing feed composition was small for Rh under our experimental conditions. Hecker and Bell (6) reported that for NO conversions below 50% a Rh catalyst is almost saturated with adsorbed NO. Variation of the NO and CO partial pressures at low NO conversion (< 50%), however, showed competitive adsorption of the two reactants. This observation has been made before and, indeed, in a number of UHV studies the reaction rate is shown to be very slow functions of the chosen NO/CO ratio. (21,28-30) For Pt, our results point to a significant CO inhibition. This result may indicate that CO does inhibit the dissociative adsorption of NO on the Pt surface. NO dissociation requires an ensemble of more than one vacant Pt atom. In a survey on the catalytic properties of Pt, Ru and Pd toward NO reduction with CO or H₂, Kobylinski and Taylor (3) noticed that especially on Pt the NO reduction is strongly inhibited by CO. Since then CO inhibition on Pt has been observed in many other studies. Using IR, Alikina et al (31) showed that CO prohibits NO adsorption on the surface and is also able to displace preadsorbed NO at room temperature. Under low pressure conditions, CO poisoning was observed by Schwarz and Schmidt. (32) Only in large excess of NO, their CO precovered Pt(100) surface could be saturated with NO.

In the reduction of NO with H₂, Pt is more active than Rh. This is in agreement with a study by Kobylinski and Taylor (3) who found, that Pt is more active than Rh in the NO + H₂ reaction, but that Rh is more active than Pt in the NO + CO reaction. Furthermore, they showed that both on Pt and Rh catalysts, the reaction temperature for 50% NO conversion is considerably lower when H₂ is used as the reductor instead of CO.

The better activity of Rh for the NO + CO reaction, may be attributed to the better activity of Rh in the NO dissociation which is often assumed to be the rate determining step. However, this model fails to explain the better activity of Pt for the NO + H₂ reaction, because NO dissociation proceeds more rapidly on Rh than on Pt. Therefore, a different rate determining step should be considered. On Rh the reaction takes place at temperatures that are much higher than the NO dissociation temperature. Apparently, the reaction rate is limited by the presence of N and NO on the Rh surface.

Since the light-off temperatures on the Pt catalyst for the NO + H₂ reaction are not far above the temperatures at which NO dissociates under UHV conditions, it is not certain whether NO dissociation or NO desorption initiates the reaction on Pt.

The selectivity for the reduction of NO with hydrogen toward N₂ rather than NH₃ or N₂O is the second factor determining the overall performance of the catalysts. Pure platinum catalysts produce much NH₃, while pure rhodium catalysts produce mainly N₂. This difference can again be understood on the basis of the relative concentrations of atomic hydrogen and atomic nitrogen on the surface of the catalyst. When the concentration of atomic nitrogen is relatively low as on a platinum catalyst, the NH₃ production will be high. On rhodium the NO dissociation proceeds more easily, the Rh-N bond strength is higher than the

Pt-N bond strength and thus the atomic nitrogen concentration will be higher, resulting in higher N_2 production.

Both the activity and the selectivity of the Pt-Rh alloy catalysts are between those of the constituent metal catalysts.

A factor that could influence the behavior of the alloy catalysts is the effect of the particle size on both selectivity and activity. There are however, no indications that the contribution of this possible effect might have a larger contribution to the catalyst performance than that of alloying alone. Moreover, the difference in particle sizes was not more than 10% (around 170 Å).

The catalytic performance of Pt-Rh alloy catalysts has been correlated with the surface composition expected on the basis of our single crystal work. (9,10) The surface composition of the Pt-Rh alloys varies strongly with the experimental conditions such as the gas phase composition. (9,10,12) Clean Pt-Rh alloy surfaces are enriched with Pt. Adsorbates can easily induce segregation of Pt or Rh to the surface. Oxygen in the gas phase induces a Rh surface segregation because of the high Rh-O bond strength relative to that of Pt-O. For the NO + CO and NO + H_2 reactions the activity of the $Pt_{0.5}-Rh_{0.5}$ alloy catalysts is like pure Rh under net-oxidizing conditions, whereas under net-reducing conditions its activity is between those of Pt and Rh. This may suggest that the surface composition varies with the experimental conditions from almost pure Rh under net-oxidizing conditions to, perhaps, a bulk-like surface composition under net-oxidizing conditions. However, the selectivity of this catalyst for the NO + H_2 reactions is different from both Pt and Rh. This indicates that this catalyst contains Pt atoms in the surface that influence the selectivity. The activity of the $Pt_{0.75}-Rh_{0.25}$ alloy catalyst is almost equal to that of pure Pt under net-reducing conditions whereas its activity is between those of Pt and Rh under stoichiometric and net-oxidizing conditions. Again, this suggests that the surface composition changes with the feed composition.

The properties of the $Pt_{0.25}-Rh_{0.75}$ alloy catalysts are noticeable. Both for the NO + CO and NO + H_2 reactions its activity is like that of pure Rh under net-oxidizing, stoichiometric and net-reducing conditions. Under net-oxidizing conditions a behavior like that of pure Rh may indeed be expected. However, under net-reducing conditions the presence of both Pt and Rh atoms should be expected on the surface. The relatively high activity of this catalyst for the NO + CO reaction might be caused by a beneficial effect of the presence of both Rh and Pt: the low CO inhibition on Rh sites and a beneficial effect of Pt on, for example, the amount of N or NO on the surface. For the NO + H_2 , however, the presence of Pt atoms does not seem to diminish the inhibition effect of NO, probably because of the lower reaction temperatures.

In conclusion, it was shown that the catalytic properties of silica supported Pt-Rh alloy catalysts are strongly dependent on the gas phase composition, the bulk composition of the alloy particles and the reaction temperature. A complex of factors determine the activity of the different catalysts. Under oxidizing conditions at sufficiently high temperatures Rh segregation to the surface takes place. This is reflected in the catalytic activity of the Pt-Rh alloys which can vary between that of pure Pt and pure Rh. No synergism, caused by alloying of Pt with Rh was observed. The differences in activity and selectivity observed for the different

catalysts, can be explained in terms of specific properties of the pure metals toward the adsorbates. Although our results show that the behavior of the alloy catalysts vary between those of Pt and Rh, care must be taken when interpreting the results in terms of absolute surface concentrations of Pt and Rh. The activity of an alloy catalyst depends on the surface composition of the metal particles. However, the relationship between activity, selectivity and surface composition may be complicated for a number of reasons. The catalytic behavior will vary with the concentration and the size of the various ensembles of atoms on the surface. All the reaction steps (molecular adsorption, dissociation, reaction between the species on the surface) may depend in a different way on the distribution of atoms over the surface. Also the small effect of alloying on the binding energies of adsorbed atoms and molecules may play a subtle, additional role on the catalytic performance of the alloy catalysts.

Concluding remarks

It was shown that the catalytic properties of silica supported Pt-Rh alloy catalysts are strongly dependent on the gas phase composition, the bulk composition of the alloy particles and the reaction temperature. A complex of factors determine the activity of the different catalysts. Under oxidizing conditions and at temperatures higher than 600K, Rh segregation to the surface takes place. This is reflected in the catalytic activity of the Pt-Rh alloys which can vary between that of pure Pt and pure Rh. No synergism because of the alloying of Pt with Rh was observed. The differences in activity, observed for the different catalysts can be explained in terms of the specific properties of the pure metals toward the adsorbates. The activity and the selectivity of the NO-H₂ reaction over Pt, Rh and Pt-Rh surfaces depend strongly on the metal and surface structure. The selectivity is determined by the relative concentrations of NO, N and N adsorbed on the various surfaces.

In fresh automotive exhaust catalysts the precious metals are well distributed in the form of small crystallites with sizes between 0.5 and 5 nm. During ageing a severe loss of Pt surface area occurs due to sintering. Rh, however, remains in a highly dispersed state probably because it is partly in an oxidized state whereas the Pt particles remain metallic. The morphology and composition of the catalyst particles change continuously during operation. Pt-Rh alloy particles are formed under reducing conditions. Under oxidizing conditions dealloying takes place resulting in Rh oxide particles separated from metallic Pt and Pt-Rh alloy particles. Cerium changes continuously its valency, noble metal-Al₂O₃ (especially Rh) interactions, Ce-noble metal and Ce-support interactions can occur. Hence, a continuous restructuring and modification of catalytic behavior can occur. All these effects make the automotive three-way catalyst to one of the most dynamic catalysts in use.

Literature Cited

1. Platinum 1993; Johnson Matthey: London.
2. Taylor, K.C. *Automotive Catalytic Converters*; Springer Verlag: Berlin, 1984.

3. Kobylinski, T.P.; Taylor, B.W. *J.Catal.*, **1974**, *33*, 376.
4. Shelef, M.; Ghandi, H.S. *Ind.Eng.Chem.Proc.Res.Develop.*, **1972**, *8*, 393.
5. Heezen, L.; Kilian, V.N.; van Slooten, R.F.; Wolf, R.M.; Nieuwenhuys, B.E. *Stud.in Surf.Sci.& Catal.*, **1991**, *71*, 381.
6. Hecker, W.C.; Bell, A.T. *J.Catal.*, **1983**, *84*, 200 and **1984**, *88*, 289.
7. Powell, B.R.; Yen-Lung, C. *Appl.Catal.*, **1989**, *53*, 233.
8. Kim, S.; d'Aniello, M.J. *Appl.Catal.*, **1989**, *56*, 23.
9. Wolf, R.M.; Siera, J.; van Delft, F.C.M.J.M.; Nieuwenhuys, B.E. *Faraday Disc.Chem.Soc.*, **1989**, *87*, 275.
10. van Delft, F.C.M.J.M.; Nieuwenhuys, B.E.; Siera, J.; Wolf, R.M. *Iron & Steel Inst.Japan (ISIJ)*, Int., **1989**, *29*, 550.
11. Siera, J.; Rutten, F.; Nieuwenhuys, B.E. *Catal.Today*, **1991**, *10*, 353.
12. Siera, J.; van Langeveld, A.D.; van Delft, F.C.M.J.M.; Nieuwenhuys, B.E. *Surf.Sci.*, **1992**, *264*, 435.
13. Yamada, T.; Hirano, H.; Tanaka, K.I.; Siera, J.; Nieuwenhuys, B.E. *Surf.Sci.*, **1990**, *226*, 1.
14. van Slooten, R.F.; Nieuwenhuys, B.E. *J.Catal.*, **1990**, *122*, 429.
15. Hirano, H.; Yamada, T.; Tanaka, K.I.; Siera, J.; Cobden, P.; Nieuwenhuys, B.E. *Surf.Sci.*, **1992**, *262*, 97.
16. Hirano, H.; Yamada, T.; Tanaka, K.I.; Siera, J.; Nieuwenhuys, B.E. *proceedings 10th ICC, Budapest/1992 (1993)* 38.
17. Oh, S.H.; Carpenter, J.E. *J.Catal.*, **1986**, *98*, 178.
18. Campbell, C.T.; White, J.M. *Appl.Surf.Sci.*, **1978**, *1*, 347.
19. Nieuwenhuys, B.E. *Surf.Sci.*, **1983**, *126*, 307.
20. Tanaka, K.I.; Yamada, Y.; Nieuwenhuys, B.E. *Surf.Sci.*, **1991**, *242*, 503.
21. Otto, K.; Shelef, M.; Kummer, J.T., *J.Phys.Chem.*, (**1970**) *74*, 2690.
22. Schwartz, S.B.; Fisher, G.B.; Schmidt, L.D. *J.Phys.Chem.*, **1988**, *92*, 389.
23. Masel, R.I. *Catal.Rev.*, **1986**, *28*, 335.
24. Wolf, R.M.; Bakker, J.W.; Nieuwenhuys, B.E. *Surf.Sci.*, **1991**, *246*, 135.
25. Löffler, P.G.; Schmidt, L.D. *Surf.Sci.*, **1976**, *59*, 195.
26. Siera, J.; Koster van Groos, M.; Nieuwenhuys, B.E. *Recl.Trav.Chim.Pays-Bas* **1990**, *109*, 127.
27. Gorodetskii, V.V.; Smirnov, M.Y.; Cholach, A.R. *Proceedings 10th ICC, Budapest/1992 (1993)* 1587.
28. Caballo, L.M.; Hahn, T.; Lintz, H.G. *Surf.Sci.*, **1989**, *40*, 53.
29. Oh, S.H.; Fisher, G.B.; Carpenter, J.E.; Goodman, D.W. *J.Catal.*, **1986**, *100*, 360.
30. Peden, C.H.F.; Goodman, D.W.; Blair, D.S.; Berlowitz, P.J.; Fisher, G.B.; Oh, S.H. *J.Phys.Chem.*, **1988**, *92*, 1563.
31. Alikina, G.M.; Davydov, A.A.; Sazanova, I.S.; Popovkii, V.V. *React.Kinet.Catal.Lett.*, **1985**, *27*, 279.
32. Schwartz, S.B.; Schmidt, L.D. *Surf.Sci.*, **1988**, *206*, 169.

RECEIVED September 29, 1993

Chapter 11

Adhesion of Rh, Pd, and Pt to Alumina and NO Reactions on Resulting Surfaces Model Calculations

Thomas R. Ward¹, Pere Alemany², and Roald Hoffmann³

Department of Chemistry and Materials Science Center, Cornell
University, Ithaca, NY 14853-1301

We report here approximate molecular orbital computations of adhesion and NO reduction in the Three Way Catalyst, modeled by a monolayer of either Rh, Pd or Pt on the (0001)O and (0001)Al faces of α -Al₂O₃. Platinum and palladium form stable interfaces with both oxygen and aluminum faces. Only the aluminum interface is stable with rhodium. Depending on the nature of the interface, the Fermi level of the composite systems varies dramatically. This, in turn, affects the adsorption mode, molecular or dissociative, of nitric oxide. From our study, it appears that an oxygen-platinum interface is best suited for both dissociative adsorption of NO as well as the coupling of two adsorbed nitrosyls to form a reduced dinitrosyl species with significant N-N double bond character.

Although nitric oxide was recently named molecule of the year for some of its physiological properties, it remains a major pollutant. In this respect, the 1990 amendments to the Clean Air Act set some stringent standards for the automotive industry (1). To meet some of these by the end of the millennium will take much work, one in which chemistry must participate. We believe that quantum mechanical modeling may aid in this effort.

Since 1981, rhodium has been a major component in automotive catalysts in order to meet the standards for NO_x emissions (2). Although the nitrosyl reduction mechanism has not been fully elucidated, it is generally accepted that nitrosyls adsorbed on group 9 metal surfaces (3-6) dissociate more readily than on group 10 ones (7-13). This is often believed to be a key factor in determining the greater efficiency of Rh vs. Pd or Pt in the nitrosyl reduction process in the Three Way Catalyst (TWC).

There is strong experimental evidence for the dissociative adsorption of NO on Ir, Mo, Al, Pt, Rh, Ru, Ni, Ti, and Zn (8,14). In addition to linear M(NO)⁺, bent M(NO)⁻ (15-

¹Current address: ICMA, Université de Lausanne, Place du Château 3, CH-1005 Lausanne, Switzerland

²Current address: Departamento de Química Física, Universidad de Barcelona, Barcelona, Catalunya, Spain

³Corresponding author

19), and atomic N and O adsorption, surface dinitrosyl species, $M(\text{NO})_2$, have been reported on Pd(100)(20), Pd(111) (21) and Pt(111) surfaces (22,23).

What if these dinitrosyl species were reaction intermediates in the nitric oxide reduction mechanism? In such a case, the formation of an N-N bond would precede the N-O bond cleavage. This appears to be the case for many gas phase reactions involving NO. As early as 1918, Bodenstein postulated the presence of a nitrosyl-dinitrogen dioxide pre-equilibrium to account for the third order rate law of many gas phase reactions involving NO (24,25).

The actual TWC systems consist of metals supported on oxides. Much experimental work has been done on Cr-SiO₂ (26,29) as well as Ni-SiO₂(30,31). In both cases dinitrosyl species, $M(\text{NO})_2$, have been detected. Such dinitrosyl entities are also present with transition metals supported on alumina, e.g. Rh (32,33), Cr, Mo, W (34) and Co (35,36). More recently, aluminosilicates (zeolites) have received increasing attention as supports. Again, dinitrosyl species recur in this field, i.e., Cr (37), Co (38), Fe (40) and Rh (41,42) exchanged into X or Y zeolites, as well as Cu^I exchanged into ZSM-5 zeolites (43).

Adsorbed dinitrosyl entities have received little attention as possible intermediates in the transition metal mediated reduction of nitric oxide. Their frequent occurrence, especially with supported catalysts, triggered our curiosity.

Therefore, we set out to analyze the possible role of dinitrosyl entities as possible intermediates in the nitric oxide reduction mechanism, by means of the extended Hückel methodology. To do this we shall study the adsorption of nitric oxide and a dinitrosyl moiety on bare metals, rhodium, palladium and platinum, as well as on metals supported on alumina.

Geometry

Since our main purpose here is the comparison of NO and N₂O₂ adsorption on bare and supported metal catalysts, the transition metals were modeled by a slightly modified three layer slab with the same geometry for all three metals. Rh, Pd and Pt crystallize in the fcc structure with cell parameters 3.804, 3.891 and 3.924 Å respectively (50). In this study, we used the value of 3.803 Å for all three metal model slabs. This value leads to a triangular (hexagonal close-packed) mesh with an M-M distance of 2.70 Å for each layer. The inter-layer separation is 2.20 Å for the (111) face. The results obtained using this geometry are in close agreement with a previous study where the correct cell parameters were chosen (51).

The extended Hückel method does not allow reliable optimization of interatomic distances, so we must fix these. It is necessary to keep distances constant, so as to obtain a relative ordering of bond strengths for the systems considered. With this in mind, we set the N-O distance to 1.17 Å and the M-N distance to 1.8 Å for all calculations.

Since the coupling of two adsorbed nitrosyls will be considered, yielding a dinitrogen dioxide, we include two NOs per unit cell. This simplifies the analysis, since both reactant **1** and coupled product **2** have the same number of FMO's. We shall focus on the interaction of the frontier orbitals of the adsorbate with the surface. For the adsorbate's FMO's, we introduce labels which hint at their origin, derived from 5σ and 2π .

In the starting geometry, both nitrosyls lie parallel to each other, 2.70 Å apart. At this separation, the in- and out-of-phase linear combinations of the FMOs show practically no splitting. Bringing the two nitrosyls together in the yz plane, as depicted above, lifts the degeneracy of the π_x and π_y orbitals. As the nitrogens approach, the FMO's with N-N bonding character are stabilized, and the splitting between the in- and out-of-phase combinations becomes substantial. In **2**, the N-N distance was set to 1.44 Å (51). A Walsh diagram for the coupling of two NO molecules with the formation of an N-N bond is presented in Figure 1.

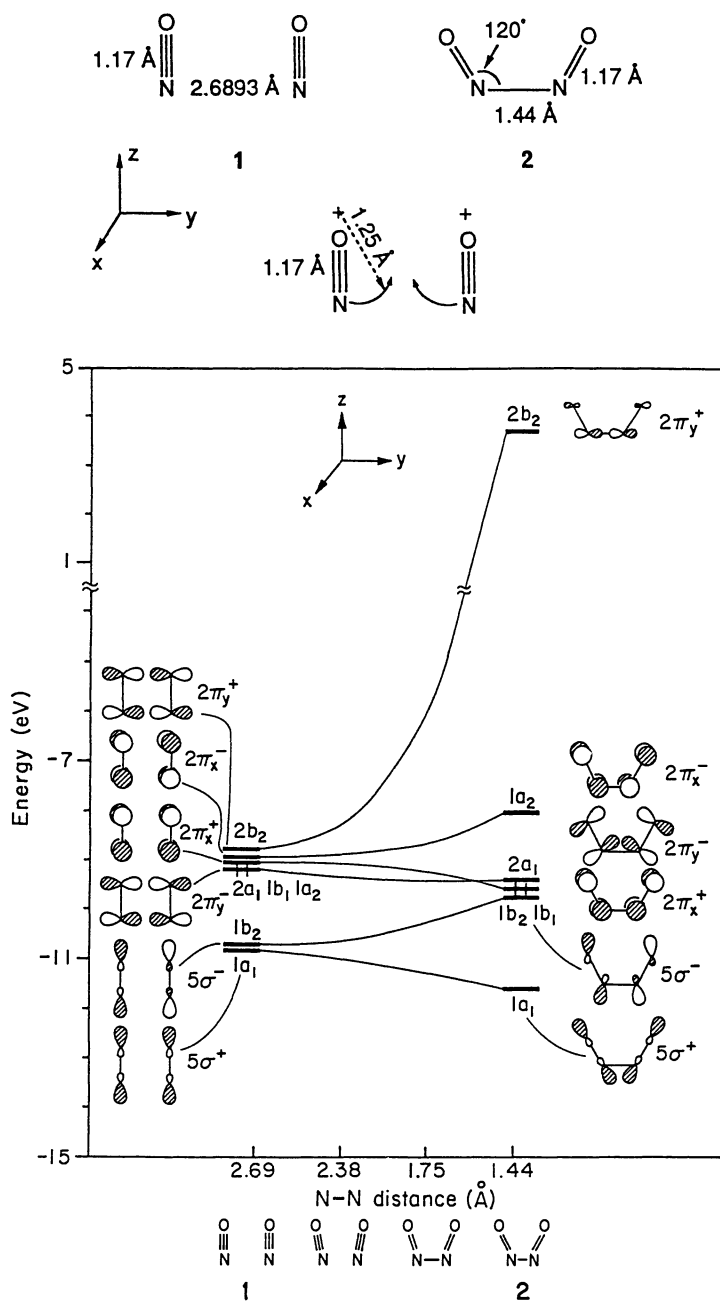


Figure 1. Walsh diagram for the coupling of a pair of nitrosyls **1** forming an N-N bond.

Before considering specific adsorption geometries for both **1** and **2**, let us compare the molecular orbital energies of the adsorbates to the DOS of the metal slabs. Figure 2 depicts the DOS of the three three-layer slabs Rh₃, Pd₃ and Pt₃, as well as the MO levels for a nitrosyl and those of a dinitrogen dioxide **2**. Clearly, the band widths differ significantly from slab to slab, rhodium having the widest d-band.

In our previous contribution, we showed that for nitrosyl chemisorption, the energy term $E_i^\circ - E_j^\circ$ in the second order perturbation expression (1) dominates (51). Independent of adsorption geometry, we found that the energy match controls the stabilization energy.

$$\Delta E = \frac{|H_{ij}|^2}{E_i^\circ - E_j^\circ}. \quad (1)$$

For a nitrosyl molecule, the $2\pi^*$ level is occupied by one electron. The computed N-O overlap population for a pair of nitrosyls **1** is 1.13. Upon interaction with a surface, if this level is located above the Fermi level, electrons will be dumped from the $2\pi^*$ level into the slab, resulting in a strengthening of the N-O bond, Figure 3a. If the $2\pi^*$ level is located below the Fermi level, the electron flow is reversed, weakening the N-O bond, Figure 3b. This latter situation corresponds to backbonding in the Blyholder model, the bonding being provided to a great extent by the $5\sigma \rightarrow$ Metal interaction (52). Therefore, by inspecting the electron occupation in the $2\pi^*$ level once the interaction with the slab is turned on, it is possible to predict whether the N-O bond is strengthened or weakened upon interaction.

On the M(111) face of the metals there are three common adsorption geometries of a linear nitrosyl adsorbate to consider: *on-top* M(NO) **3a**, *bridging*-M(NO) **3b** and *capping* M(NO) **3c**. However, we must bear in mind that we need two nitrosyls in close proximity in order to couple them. The various adsorption geometries of linear M(NO) are depicted below:

From these starting geometries, we may consider a number of coupling paths to afford adsorbed N₂O₂ **2**. Three of these are depicted below:

We shall discuss in detail the *on-top*M(NO) **3a** geometry and the corresponding coupled product *bridging* M(N₂O₂) **4a**. Keeping in mind that the energy term in (1), which is independent of adsorption geometry, dominates, similar results are expected for these geometries. The reader should refer to a the complete account of this work for details on other geometries (53).

We may now turn on the interaction between the adsorbate and the slab. From Figure 2a, we predict a good interaction for all 5σ and 2π levels of NO **2** adsorbed on Rh(111). As all these levels are all located "in the d band", a good interaction is expected. The palladium situation is quite different, Figure 2b. Since the d band is significantly narrower for palladium than for rhodium, the 2π levels are expected to interact only weakly with the d band. The 5σ levels lie at the top of the d band, and their interaction with the palladium slab is expected to be good. The platinum situation is intermediate between rhodium and palladium, Figure 2c. Again, the width of the d band allows prediction of the strength of interaction: the 5σ levels interact very strongly, whereas the 2π levels, lying slightly above the d band, should interact moderately with the platinum slab.

From our computations, it appears the interaction between 5σ levels and the slab is more or less independent of the nature of this latter. By comparing both 5σ electron occupations after interaction for all metal situations, these numbers vary little. Of the two electrons present before interaction, ~0.25 electrons are donated to the slab. On the other hand, the 2π electron occupation varies dramatically. For this FMO, the resulting electron occupation is 0.90, 0.09 and 0.28 for *on-top* Rh(NO), *on-top* Pd(NO) and *on-top* Pt(NO) respectively. Upon interaction with either Pd or Pt, the electron present in the 2π FMO has been dumped into the metal slab (Figure 3): the computed N-O overlap populations are 0.91, 1.32 and 1.23 for *on-top* Rh(NO), *on-top* Pd(NO) and *on-top* Pt(NO) respectively.

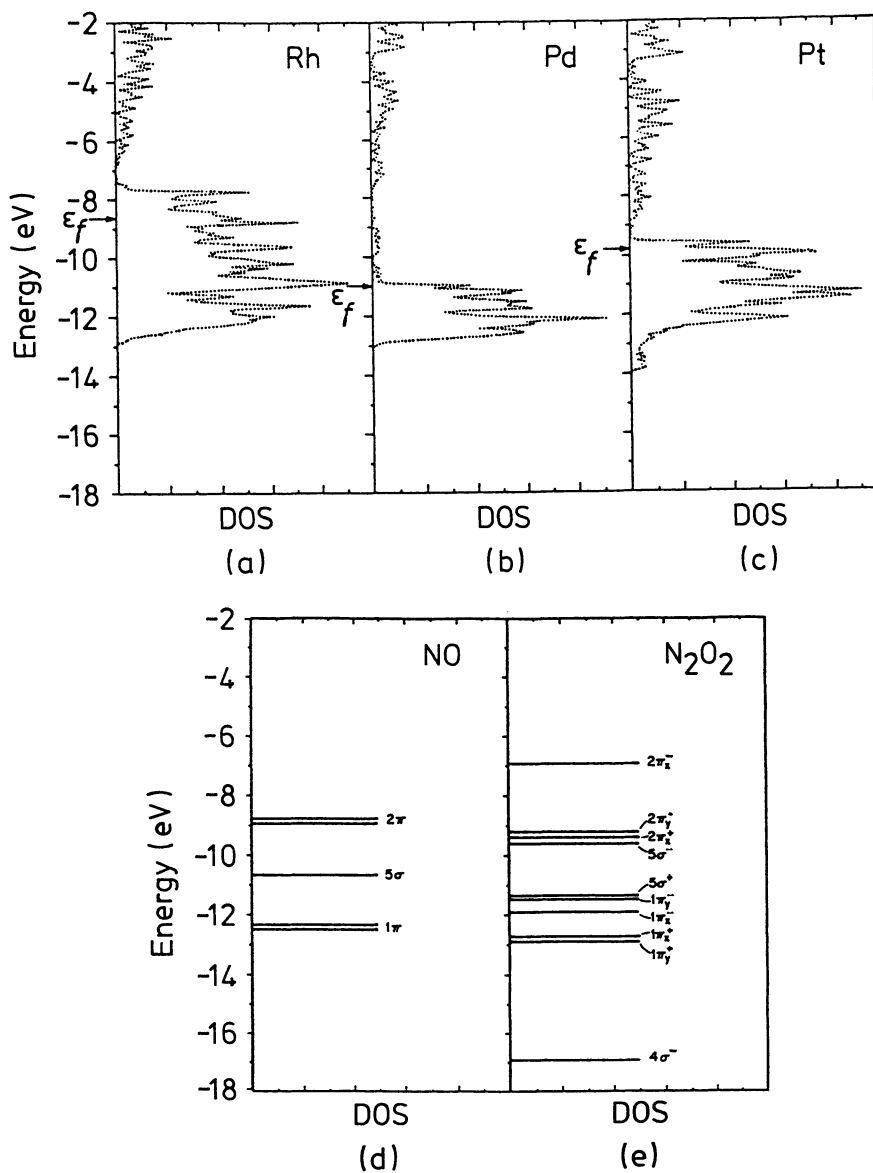


Figure 2 a-c). Total DOS of a three layer metal slab M_3 where a) $M = \text{Rh}$; b) $M = \text{Pd}$; c) $M = \text{Pt}$ d) MO levels of NO ; e) MO levels of N_2O_2 .

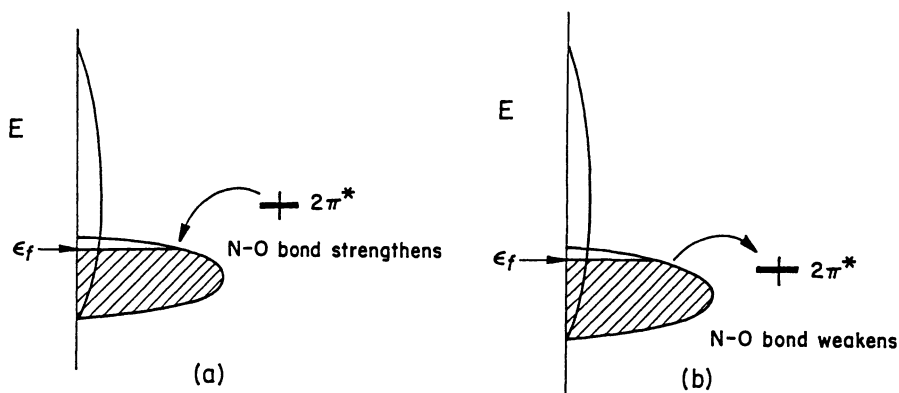
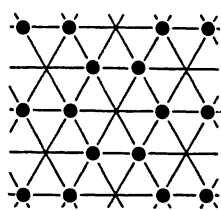
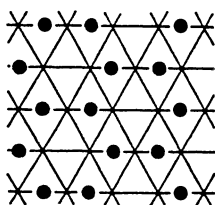


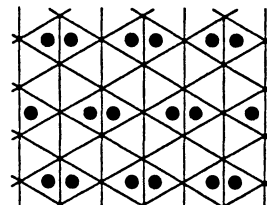
Figure 3. The Effect of Fermi level on the N-O bond strength.

*on-top* M(NO)

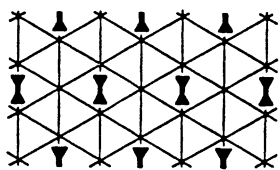
3a

*bridging* M(NO)

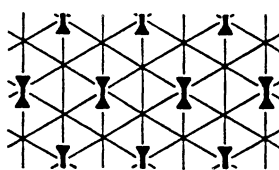
3b

*capping* M(NO)

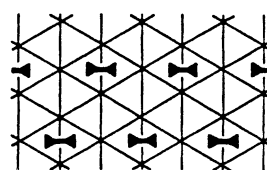
3c

*bridging* M(N₂O₂)

4a

*on-top* M(N₂O₂)

4b

*perp* M(N₂O₂)

4c

Since the N-O Overlap Population of free nitric oxide is 1.13, it appears that the strength of interaction between the 2π FMO and the slab determines the electron flow and therefore the adsorption mode: dissociative for Rh and molecular for Pd and Pt.

The same analysis can be carried out for the coupled product adsorbed on the various metal slabs, Figure 2e. The $2\pi\gamma^+$ level is shifted up in energy to 3.68 eV upon coupling. Its interaction with either metal slab will be insignificant. For the rhodium slab, all other levels are expected to interact strongly with the metal surface. Since for the palladium case only the $5\sigma^+$ level lies within the d band, no other level will interact very significantly with the slab. Finally, for N_2O_2 **2** adsorbed on platinum, except for the $2\pi\gamma^+$ and $2\pi\kappa^-$, all other levels lie in the d band, and, therefore, their interactions with the metal slab are expected to be good. In the case of adsorbed N_2O_2 **2**, we should focus both on the N-O and N-N overlap population. Indeed, we wish to have a coupled product with a strong N-N bond and an N-O bond as weak as possible. For comparison, we may consider two limiting structures, dinitrosyl **2** and hyponitrite **5**, and their respective N-O and N-N overlap populations. The hyponitrite **5** corresponds to a reduced dinitrosyl with a 6π electron system.

The computed N-N and N-O overlap populations, as well as the Fermi levels for *bridging* $M(N_2O_2)$ **4a** are summarized in Table I. Again in this case, rhodium stands out. The N-O overlap population points towards that of a single bond as in **5** whereas the N-N overlap population is intermediate.

Table I. Overlap Populations and Fermi Level for *bridging* $M(N_2O_2)$

	<i>bridging</i> Rh(N_2O_2)	<i>bridging</i> Pd(N_2O_2)	<i>bridging</i> Pt(N_2O_2)
E_f (Ev)	-8.57	-9.54	-9.57
N-O OP	0.84	1.11	1.03
N-N OP	0.70	0.61	0.62

Next we shall study the adhesion of these metals on alumina, and its consequences on the nitric oxide reduction.

Models

Computational constraints prevents us from using the γ - Al_2O_3 modification as the support. Instead, we used α - Al_2O_3 , which has a considerably smaller unit cell, and has been shown to be usable as the support in the TWC (54,55).

α - Al_2O_3 has a corundum structure with all aluminum atoms in an octahedral coordination geometry, while γ - Al_2O_3 has a vacant spinel structure with aluminum atoms both in octahedral and tetrahedral holes of the structure (56). From our previous experience, adhesion properties are not strongly affected by the coordination geometry of the surface aluminum atoms (57,58). The most important factor is the surface Al/O ratio for each face. Thus, it seems reasonable to assume that adhesion strength on the (0001)O and the (0001)Al faces of α - Al_2O_3 will give lower and upper bounds for the adhesive properties of transition metals on different forms of alumina. The main features of the DOS for γ - Al_2O_3 will closely resemble those of α - Al_2O_3 ; only the magnitude of the interaction of surface states with the metal bands may differ.

The choice of γ - Al_2O_3 as a support is due to a great extent to its high surface area. This allows a high dispersion of the precious metal. In our models, we must assume coverages of 1ML (*MonO* and *MonAl*) or 2/3ML (*M₂Al*), while in industrial catalysts the metal coverage used is never higher than 0.1ML. The particle size of the noble metal rafts in a fresh TWC is less than 50 Å. This can increase to 1000 Å, or more, at the high temperatures of vehicle operation. Since most of the catalytic activity is preserved (59), we

may consider our metal coverage of 1.0ML as approximating such large rafts. However, we cannot simulate interactions between the adsorbates and the support. The formation of rafts or islands thicker than one layer is also not incorporated in our models. This phenomenon can lead to adsorption of NO on a different face of the metal or to simultaneous interactions of the adsorbate with metal and support.

Other effects that have been omitted in our models are modifications of metal-support interactions due to dopants in the oxide phase (NiO, CeO₂). Nickel oxide is added to the system to inhibit the diffusion of the precious metal in the spinel (59). Cerium oxide is added to prevent sintering of the catalyst and to increase the dispersion of the noble metal. Finally, physical characteristics of the support (polycrystalline, rough surfaces, diffusion of metal into oxide and of Al or O into the metal) were not included in our simulations either.

Our model of the interface consists of the superposition at a fixed distance (2.0 Å) of two two-dimensionally infinite slabs of oxide and metal, respectively. Keeping this interface distant constant allows us to compare trends in adhesion energies. Comparable results were obtained with a 2.5 Å separation. In our previous study (57,58), the metal geometry was adjusted to fit the rigid α -Al₂O₃ slab. Since our main purpose here is the comparison of NO and N₂O₂ adsorption on bare and supported metal catalysts, a different approach was followed. The transition metals were modeled by a slightly modified three layer slab with the same geometry for all three metals (*vide infra*).

The oxide slab has been modified to provide epitaxy with the rigid metal slab. Our model consists of four layers of close-packed oxygen atoms with interlayer O-O distance of 2.70 Å. Three layers of aluminum cations, occupying two-thirds of the octahedral holes between oxygen layers, and a passivating hydrogen layer on the back surface of the slab, complete our model for the (0001)O face. In our model slab all aluminum atoms between two oxygen layers are located in a single plane, centering octahedral holes. All Al-O distances have the value 1.903 Å.

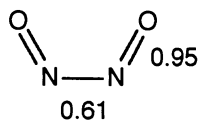
The (0001)Al face is modeled by a slab obtained by removal of both the topmost oxygen layer and one of the aluminum atoms on the first aluminum layer. Figure 4 shows a schematic representation of two views of the (0001)O surface model slab.

Adhesion

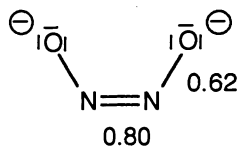
Let us review briefly the results of our earlier study of the interfaces formed between first row transition metals and different faces of α -Al₂O₃ (57,58). Two main interactions were found to dictate the adhesive properties:

- Net destabilizing O-M interactions (See schematic diagram 6) are responsible for the weak (or even repulsive) adhesion energies found for oxide surfaces with high oxygen concentration. Filling of an interface M-O* band leads to a highly unfavorable situation in the case of high d-electron counts (late transition metals).
- Aluminum cations on the oxide surface are capable of forming strong charge transfer bonds with the metal. These bonds result from interaction of empty aluminum dangling bond states with the d band of the metal 7.

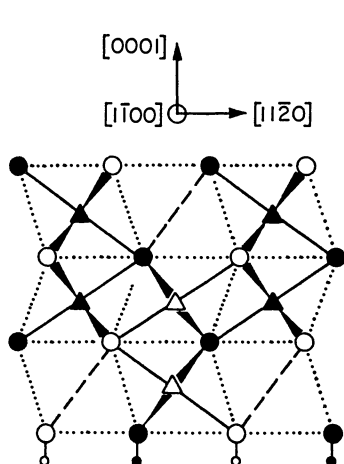
A balance of both interactions determines the adhesion of a particular transition metal to α -Al₂O₃. The most important factor is the ratio of Al/O atoms directly exposed to the metal surface. Aluminum-rich surfaces are predicted to form strong interfaces with almost all first transition row metals, while oxygen-rich surfaces do not result in strong interfaces, especially with late transition metals. The coordination geometry of atoms at the surface does not seem to be a major factor in determining adhesion properties for different faces. For instance, calculations of the adhesion energy for first row transition metals on different faces of α -Al₂O₃ surfaces indicates that the (0001)O and the (0001)Al surfaces give upper and lower bounds for the adhesion energies. Surfaces with intermediate Al/O ratios yield interfaces with intermediate energies.



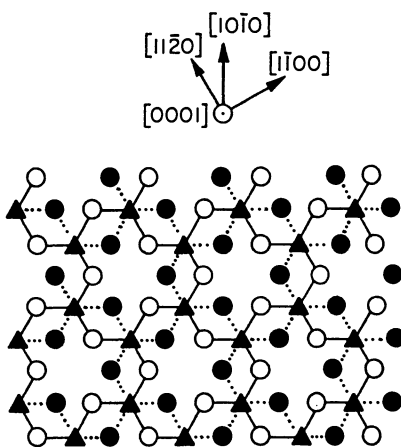
2



5

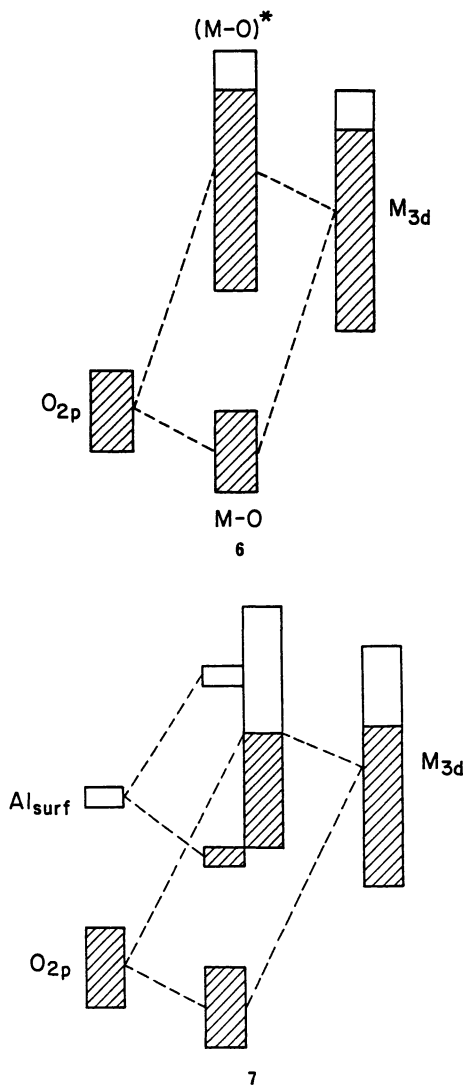


- Oxygen (1st layer)
- Oxygen (2nd layer)
- △ Aluminum (1st layer)
- ▲ Aluminum (2nd layer)
- Hydrogen
- Octahedral holes



- Oxygen (1st layer)
- ▲ Aluminum
- Oxygen (2nd layer)

Figure 4. Top and side views of the (0001)O surface model slab of $\alpha\text{-Al}_2\text{O}_3$.



These findings agree with recent experimental results by Ealet and Gillet for the alumina (-1012) surface (60) as well as Gorte *et al.* work on alumina (0001) (61,62).

Results

Table II shows the adhesion energy values obtained for both the (0001)O- and the (0001)Al-Metal interfaces. For simplicity, we abbreviate these as $M_{3on}O$ and $M_{3on}Al$, respectively. M_3 symbolizes a three layer metal slab. Surprisingly, we obtain stable interfaces for both Pd and Pt with the (0001)O surface, $Pd_{3on}O$ and $Pt_{3on}O$. Such stabilization was not observed for Ni in our previous work (57,58). The charge transfer, $\Delta q_M(e^-)$, (Table II) also indicates the magnitude of the charge transferred to the metal (positive values) or to the ceramic (negative values).

Table II. Adhesion energies and charge transfer for the (0001)O and the (0001)Al metal interfaces, $M_{3on}O$ and $M_{3on}Al$ respectively

	$M_{3on}O$			$M_{3on}Al$			ionic contribution	
	eV/uc	J/m ²	$\Delta q_M(e^-)$	eV/uc	J/m ²	$\Delta q_M(e^-)$	eV/uc	J/m ²
Rh	0.483	0.409	+0.11	-3.616	-3.059	-0.32	-0.874	-0.739
Pd	-0.921	-0.779	+0.16	-1.999	-1.691	+0.11	-0.135	-0.114
Pt	-0.324	-0.274	+0.16	-2.508	-2.122	-0.24	0.000	0.000

uc refers to unit cell

$\Delta q_M(e^-)$ refers to the charge transfer

For the interaction with the aluminum surface a different factor, ionic charge transfer, has to be included in our discussion. This term arises from the electrons being transferred from the slab with the highest Fermi level to the other slab. It gives an additional stabilizing factor for the interface. In a one-electron calculation, such as the extended Hückel one we use, this ionic component is overestimated. In order to assess the relative magnitude of ionic charge transfer and covalent interactions we performed two separate calculations with interfacial separations of 2.0 and 10.0 Å, respectively. At an interfacial distance of 10.0 Å all overlap terms between orbitals of both slabs, metal and ceramic, are zero, and the entire stabilization energy comes from the ionic term. The last entry of Table II shows that the magnitude of ionic charge transfer is important for Rh, moderate for Pd, and non-existent for Pt. Analysis of the changes in average charge on the metal atoms leads to the qualitative diagram shown in Figure 5. From this figure we can see that the interface with Rh is unstable for the (0001)O surface, $Rh_{3on}O$, but strongly stabilized when interacting with the (0001)Al surface, $Rh_{3on}Al$. Important ionic charge transfer to the empty aluminum dangling states and the good energy match of these with the d band of the metal provide a substantial adhesion energy in this case.

The case of palladium, with stable interfaces for both $Pd_{3on}O$ and $Pd_{3on}Al$, is more complicated. Interaction of the d-band with the O2p band gives a destabilizing contribution that is overcome by the attractive interaction of the empty metal s band with the O2p band of the oxide. The s-band lies much lower for palladium than for rhodium, and is able to interact much more (better energy match) with the oxide band. This mechanism of interface stabilization is corroborated by the electron transfer to the metal: almost all charge has been transferred to the s levels of palladium. The low lying bands of palladium also give rise to an ionic charge transfer term, in an opposite direction in this case, electrons flowing from the oxide to the metal.

The interaction with platinum is intermediate between those of rhodium and palladium. The position of the Fermi level of the metal slab in this case does not permit any ionic charge transfer in either direction. For the (0001)O surface, $Pt_{3on}O$, a weak,

attractive adhesion energy is found. The repulsive (O2p-Md) and attractive (O2p-Ms) interactions do not balance, and the latter slightly dominates. For the interface formed with the (0001)Al surface, Pt_{3onAl}, a good energy match of the metal d band with the dangling aluminum states provides better stabilization compared to palladium, Pd_{3onAl}. Compared to rhodium, however, the absence of ionic charge transfer and poorer energy match results in a weaker interface.

Our models of supported catalysts will consist of a single layer of metal atoms on both oxide surfaces, MonO, and aluminum surfaces, MonAl, respectively. It is thus important that all the trends, especially the change in the position of the Fermi level upon interaction, found for the three layer slab models, be reproduced for these simpler cases. A comparison of both models (3 layer vs. 1 layer) shows good agreement in the basic features of the interaction. The changes observed for the Fermi levels agree in direction in all cases, although there is some variation in magnitude. The Fermi levels for all three metals, M = Rh, Pd, Pt, and interfaces are presented in Table III.

Table III. Summary of Fermi level variation (eV) as a function of interface and metal

	$E_f(M_3)$	$E_f(M_{3onO})$	$E_f(M_{3onAl})$	$E_f(MonO)$	$E_f(MonAl)$	$E_f(M_2Al)$
Rh	-8.62	-8.38	-8.68	-8.28	-9.56	-8.38
Pd	-10.97	-10.20	-10.73	-10.26	-10.71	-9.48
Pt	-9.76	-9.35	-9.77	-9.48	-10.39	-8.61

A model with metal coverage of 0.667ML, where the transition metal atoms sit in the empty aluminum positions of the surface, has also been considered. In this case, a mixed Al/M layer, abbreviated M₂Al **8** (M = Rh, Pd, Pt), is exposed to the adsorbate. The Fermi level for all three metals rises in this situation, compared to the bare metal slabs (Table III).

Supported Catalysts

As shown above, the support affects dramatically the Fermi level of the metal ceramic-composite system. Let us now study the consequence of this on the adsorption of both NO and N₂O₂. This is best accomplished graphically by comparing the Fermi level variation to the resulting N-O Overlap Population.

on-top M(NO) 3a. In Figure 6a, we plot the Fermi levels for the *on-top* M(NO) **3a** geometry with M = Rh, Pd and Pt. Along the abscissa we report the various metal-support interactions for M₃, the bare metal three-layer slab, a one-layer slab over an oxygen layer, MonO, a one-layer slab over an aluminum surface, MonAl, and the mixed layer slab, M₂Al. The dotted line marks the energy level of the 2π* orbital of a pair of nitrosyls **1**. From this figure alone, we conclude that the ceramic support significantly affects the Fermi level of the composite system, and consequently the electron flow between adsorbate and slab. Clearly, the rhodium slab stands out, with its Fermi level consistently above the 2π* level. For all slabs, the metal on the mixed layer M₂Al gives rise to the highest Fermi levels. In fact, the *on-top* Pt₂Al(NO) situation ($E_f = -8.25$ eV) has a higher Fermi level than both the bare rhodium slab, *on-top* Rh₃(NO), ($E_f = -8.45$ eV) and *on-top* RhonAl(NO) ($E_f = -8.59$ eV).

In Figure 6b, we report the N-O Overlap Population as a function of metal slab and all four adhesion situations. The horizontal line corresponds to the N-O overlap population for a pair of nitrosyls **1** (1.13). From our computations, it appears the interaction between both 5σ⁺ and 5σ⁻ levels and the slab is more or less independent of the nature of this latter (*vide infra*). Therefore, we can expect the N-O overlap population to correlate closely with the Fermi level. This is nicely reflected in the comparison the Fermi level for various slabs

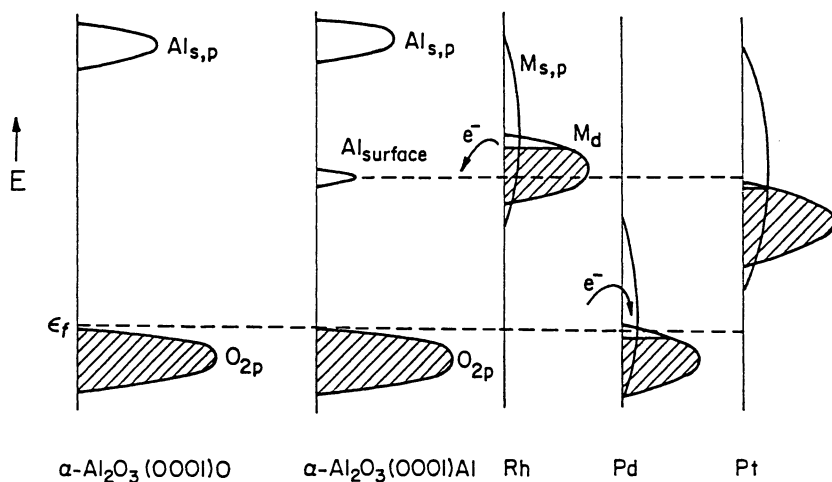
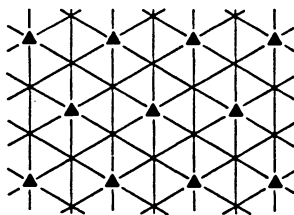


Figure 5. Qualitative illustration of charge transfer between metal and ceramic.



- ▲ Aluminum
- * M (Rh, Pd, Pt)
- M_2Al

and adhesion situations in Figure 6a with the corresponding N-O overlap population (Figure 6b). As the Fermi level rises above the $2\pi^*$ level, the N-O overlap population drops below that of free N-O (1.13), indicative of bond weakening in the adsorbate. For all three slabs, this effect is most dramatic for the M_2Al situation.

bridging $M(N_2O_2)$ 4a. We turn to the coupled product dinitrogen dioxide **2**. At this stage, we shall not only focus our attention on the N-O overlap population, but also on the N-N overlap population. We wish to form an intermediate N_2O_2 **2**, with a strong N-N bond and a weak N-O bond — product-like, $N_2 + O_2$, in the sense of the Hammond postulate.

From *on-top* $M(NO)$ **3a**, a nitrosyl-nitrosyl coupling most naturally leads to *bridging* $M(N_2O_2)$ **4a**. The Fermi level, as well as N-O and N-N Overlap Populations, are presented in Figure 7 a, b and c, respectively.

Here again, the rhodium Fermi levels are consistently highest and the corresponding N-O overlap population smallest. As the Fermi level rises, e.g. *bridging* $RhON(N_2O_2)$ and *bridging* $Rh_2Al(N_2O_2)$, the $2\pi_y^-$ FMO gets populated. This is reflected by a decrease in the N-N Overlap Population, since this orbital has both N-N and N-O antibonding character (Figure 7c). It is therefore no surprise to see the N-N Overlap Population of both *bridging* $Rh_2ON(N_2O_2)$ (0.73) and *bridging* $Rh_2Al(N_2O_2)$ (0.67) smaller than those of either palladium or platinum analogs, where this same FMO is hardly populated.

We also examined the computed reaction enthalpy of *on-top* $M(NO)$ **3a** \rightarrow *bridging* $M(N_2O_2)$ **4a** as a function of metal and interface. The detailed results are not presented here, but reaction intermediate **2** seems energetically accessible in most cases. Consistently, the smallest reaction enthalpies are encountered with platinum as a catalyst, and/or metal oxide interfaces. The extended Hückel calculations predict the reaction *on-top* $PtON(NO)$ \rightarrow *bridging* $PtON(N_2O_2)$ to be thermoneutral. However, we do not trust these calculations in their quantitative detail. In this particular case, the N-O overlap population varies from 0.88 to 0.82 and, correspondingly, a strong N-N bond is formed (0.74). This overlap population is intermediate between that of dinitrogen dioxide **2** (0.61) and that of hyponitrite **5** (0.80).

Clearly, there are other situations, especially with rhodium-based catalysts, where the coupled product has significant N-N double bond character, but the energetics of the reaction leading to their formation are somewhat unfavorable.

Conclusion

The present study has focused on adhesive as well as catalytic properties of rhodium, palladium and platinum on $\alpha-Al_2O_3$. Despite our simplified model of a supported catalyst, we think that interesting conclusions can be extracted. Our hope is that these results will aid in the development of more elaborate models, that will, in turn be able to give results of direct applied interest.

The trends noted for the variation of the Fermi level as a function of metal-ceramic interface indicate that the ceramic may be more than an inert support. Aluminum-metal and oxygen-metal interfaces are predicted to be stable for both palladium or platinum. The oxygen-metal interface, unstable for rhodium, is predicted to be particularly favorable both for dissociative adsorption of NO, as well as for a coupling reaction, yielding a reduced form of N_2O_2 . Therefore, a catalyst with a platinum oxygen interface seems competitive with one containing a rhodium aluminum interface.

Eventually, other ceramics with less electronegative elements could be tested, as a higher Fermi level for the ceramic should be reflected in the Fermi level of the resulting catalysts.

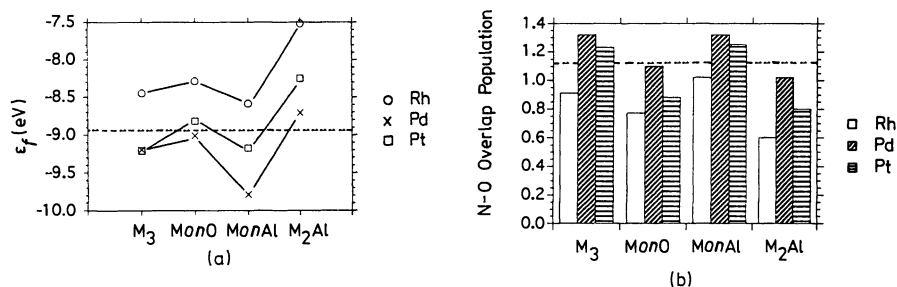


Figure 6. a) Fermi level variation for *on-top* M(NO) and b) resulting N-O overlap population. The horizontal line in a) corresponds to the $2\pi^*$ energy of nitrosyl and b) corresponds to the N-O overlap population of a pair of nitrosyls 1.

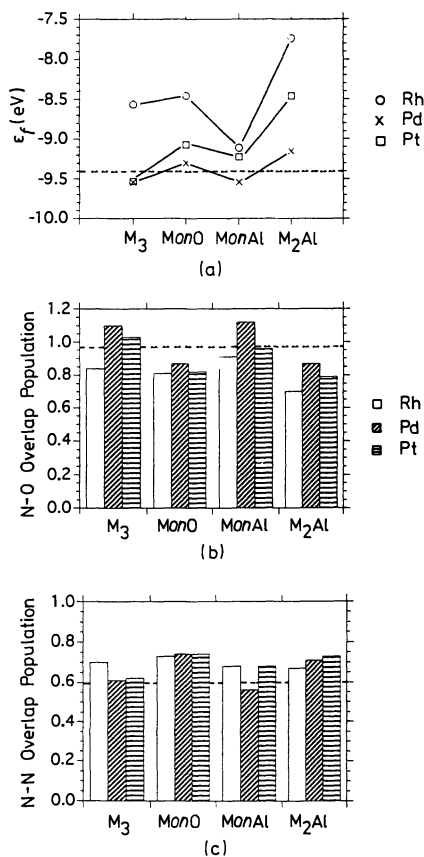


Figure 7. a) Fermi level variation for *bridging* M(N_2O_2) 4a; b) resulting N-O Overlap Population and c) resulting N-N Overlap Population. The horizontal line corresponds to a) the $2\pi_y^-$ level of N_2O_2 2; b) the N-O Overlap Population of N_2O_2 2 and c) the N-N Overlap Population of N_2O_2 2.

Acknowledgments

All figures are reproduced from our reference 53. Our research was supported by a grant from the Ford Motor Corporation. TRW is thankful to the Swiss National Science Foundation for the award of a postdoctoral fellowship. The stay of P. A. at Cornell University has been made possible through a post-doctoral grant of the *Ministerio de Educación y Ciencia* of Spain. We thank Dr. Mordecai Shelef and Dr. Ken Hass for many discussions and are grateful to Jane Jorgenson for her expert drawings.

Appendix

Tight-binding extended Hückel calculations, with a weighted H_{ij} approximation, have been applied throughout this paper. All computational details, including extended Hückel parameters for all atoms can be found in the full account of this study (53).

Literature Cited

1. Farrauto, R. J.; Heck, R. M.; Speronello, B. K. *C & E News*. **1992**, Sept. 7, 34.
2. Taylor, K. C. *Chemtech* **1990**, 20, 551.
3. Pirug, G.; Bonzel, H. P.; Hopster, H.; Ibach, H. *J. Chem. Phys.* **1979**, 71, 593.
4. Carley, A. F.; Rassias, S.; Roberts, M. W.; Wang, T.-H. *Surf. Sci.* **1979**, 84, L227.
5. Schwartz, S. C.; Fisher, G. B.; Schmidt, L. D. *J. Phys. Chem.* **1988**, 92, 389.
6. Bowler, M.; Guo, Q.; Joyner, R. W. *Surf. Sci.* **1991**, 257, 33.
7. Brodén, G.; Rhodin, T. N.; Bruckner, C.; Benbow, R.; Hurych, Z. *Surf. Sci.* **1976**, 59, 593.
8. Bonzel, H. P.; Pirug, G. *Surf. Sci.* **1977**, 62, 45.
9. Klein, R. L.; Schwarz, S. C.; Schmidt, L. D. *J. Phys. Chem.* **1985**, 89, 4908.
10. Gorte, R. J.; Schmidt, L. D. *Surf. Sci.* **1981**, 111, 260.
11. Obuchi, A.; Naito, S.; Onishi, T.; Tamaru, K. *Surf. Sci.* **1982**, 122, 235.
12. Jorgenson, S. W.; Canning, N. D. S.; Madix, R. J. *Surf. Sci.* **1987**, 179, 322.
13. Conrad, H.; Ertl, G.; Küppers, J.; Latta, E. E. *Surf. Sci.* **1977**, 65, 235.
14. Richter-Addo, G. B.; Legzdins, P. *Metal Nitrosyls*, Oxford University Press: New York, Oxford, 1992, 205.
15. deLouise, L. A.; Winograd, N. *Surf. Sci.* **1985**, 154, 79.
16. Hoffmann, R.; Chen, M. M.-L.; Elian, M.; Rossi, A. R.; Mingos, D. M. P. *Inorg. Chem.* **1974**, 13, 2666-2675.
17. Eisenberg, R.; Meyer, C. D. *Acc. Chem. Res.* **1975**, 8, 26.
18. Enemark, J. H.; Feltham, R. D. *Coord. Chem. Rev.* **1974**, 13, 339.
19. Hoffmann, R.; Chen, M. M.-L.; Thorn, D. L. *Inorg. Chem.* **1977**, 16, 503.
20. Nyberg, C.; Uvdal, P. *Surf. Sci.* **1988**, 204, 517.
21. Schick, H.-D.; Wassmuth, H.-W. *Surf. Sci.* **1982**, 123, 471.
22. Bertolo, M.; Jacobi, K. *Surf. Sci.* **1990**, 236, 143.
23. Ibach, H.; Lehwald, S. *Surf. Sci.* **1978**, 76, 1.
24. Bodenstein, M. *Helv. Chim. Acta* **1935**, 18, 745.
25. Greenwood, N. N.; Earnshaw, A. *Chemistry of the Elements*, Pergamon Press: Oxford, 1984, 513.
26. Ghiotti, G.; Garrone, E.; Gatta, G. D.; Fubini, B.; Giamello, E. *J. Catal.* **1983**, 80, 249.
27. Garrone, E.; Ghiotti, G.; Giamello, E.; Fubini, B. *J. Chem. Soc., Faraday Trans. 1* **1981**, 77, 2613.
28. Zecchina, A.; Garrone, E.; Monterra, C.; Coluccia, S. *J. Phys. Chem.* **1975**, 79, 978.
29. Garrone, E.; Ghiotti, G.; Coluccia, S.; Zecchina, A. *J. Phys. Chem.* **1975**, 79, 984.

30. Morrow, B. A.; Sont, W. N.; Onge, A. S. *J. Catal.* **1980**, *62*, 304.
31. Morrow, B. A.; Moran, L. E. *J. Catal.* **1980**, *62*, 294.
32. Anderson, J. A.; Millar, G. J.; Rochester, C. H. *J. Chem. Soc., Faraday Trans.* **1990**, *86*, 571.
33. Liang, J.; Wand, H. P.; Spicer, L. D. *J. Phys. Chem.* **1985**, *89*, 5840.
34. Kazusaka, A.; Howe, R. F. *J. Catal.* **1980**, *63*, 447.
35. Mauge, F.; Valet, A.; Bachelier, J.; Duchet, J. C.; Lavalley, J. C. *Catal. Lett* **1989**, *2*, 57.
36. Roustan, J. L.; Lijour, Y.; Morrow, B. A. *Inorg. Chem.* **1987**, *26*, 2509.
37. Pearce, J. R.; Sherwood, D. E.; Hall, M. B.; Lunsford, J. H. *J. Phys. Chem.* **1980**, *84*, 3215.
38. Newcomb, T. J.; Gopal, P. G.; Watters, K. L. *Inorg. Chem.* **1987**, *26*, 809.
39. Morrow, B. A.; Baraton, M. I.; Lijour, Y.; Roustan, J. L. *Spectrochim. Acta.* **1987**, *43A*, 1583.
40. Morrow, B. A.; Baraton, M. I.; Roustan, J. L. *J. Am. Chem. Soc.* **1987**, *109*, 7541.
41. Iizuka, T.; Lunsford, J. H. *J. Mol. Cat.* **1980**, *8*, 391.
42. Praliaud, H.; Coudurier, G. F.; Taarit, Y. B. *J. Chem. Soc., Faraday Trans. 1* **1978**, *74*, 3000.
43. Spoto, G.; Bordiga, S.; Scarano, D.; Zecchina, A. *Catal. Lett.* **1992**, *13*, 39.
44. Hoffmann, R.; Lipscomb, W. N. *J. Chem. Phys.* **1962**, *37*, 2872.
45. Hoffmann, R.; Lipscomb, W. N. *J. Chem. Phys.* **1962**, *36*, 2179.
46. Hoffmann, R. *J. Chem Phys.* **1963**, *39*, 1397.
47. Whangbo, M.-H.; Hoffmann, R. *J. Am. Chem. Soc.* **1978**, *100*, 6093.
48. Whangbo, M.-H.; Hoffmann, R.; Woodward, R. B. *Proc. Roy. Soc.* **1979**, *A366*, 23.
49. Hoffmann, R. *Solids and Surfaces: A Chemist's View of Bonding in Extended Structures*, VCH Publisher, Inc.: New York, Weinheim, 1988, 1.
50. Donohue, J. *The Structure of the Elements*; Kreiger, R. E., Publ. Comp., Inc: Malabar FL, 1982.
51. Ward, T. R.; Hoffmann, R.; Shelef, M. *Surf. Sci.* **1993**, *289*, 85.
52. Blyholder, G. *J. Phys. Chem.* **1964**, *68*, 2772.
53. Ward, T. R.; Alemany, P.; Hoffmann, R. *J. Phys. Chem.* **1993**, in press.
54. Yao, Y. F.; Kummer, J. T. *J. Catal.* **1977**, *46*, 388.
55. Yao, H.; Stephen, H.; Gandhi, H. *J. Catal.* **1980**, *61*, 547.
56. Wells, A. F. *Structural Inorganic Chemistry*; Clarendon Press: Oxford, 1990, 457.
57. Alemany, P.; Boorse, R. S.; Burlich, J. M.; Hoffmann, R. *J. Phys. Chem.* **1992**, *submitted*.
58. Alemany, P.; Boorse, R. S.; Burlich, J. M.; Hoffmann, R. *Chem. Mat.* **1992**, *submitted*.
59. Kummer, J. T. *Prog. Energy Combust. Sci.* **1980**, *6*, 177.
60. Ealet, B.; Gillet, E. *Surf. Sci.* **1993**, *281*, 91.
61. Altman, E. I.; Gorte, R. J. *J. Phys. Chem.* **1989**, *93*, 1993.
62. Roberts, S.; Gorte, R. J. *J. Chem. Phys.* **1990**, *93*, 5337.

RECEIVED September 29, 1993

Chapter 12

Interaction of NO and CO on Rh-SiO₂ and Ce-Rh-SiO₂ Catalysts

A Transient In Situ IR Spectroscopic Study

Girish Srinivas, Steven S. C. Chuang, and Santanu Debnath

Department of Chemical Engineering, The University of Akron,
Akron, OH 44325-3906

In situ infrared spectroscopic studies of NO-CO reaction on Rh/SiO₂ and Ce-Rh/SiO₂ reveal that Si-NCO and Rh-NCO are the dominant species during the reaction at 723 K. The growth rate of Rh-NCO is greater than that of Si-NCO on the Ce-Rh/SiO₂ catalyst at the beginning of the reaction. In contrast, the concentration of Rh-NCO and Si-NCO increases at about the same rate on the prerduced and preoxidized Rh/SiO₂. Steady-state isotopic transient study at 573 K shows that Si-NCO is a spectator species under reaction conditions; the addition of Ce increases the reactivity and decreases the average residence time of intermediates leading to CO₂ over Rh/SiO₂.

Rh has been successfully used in three-way catalysts to control the emission of NO_x from automobile exhaust (1-4). Due to the shortage of Rh and the increasingly stringent standards for NO_x emission, continuing improvement of the catalyst performance and development of substituents remain to be major challenges in the area of environmental catalysis. Investigation of adsorbed species on the Rh catalyst during NO-CO reaction could lead to a better understanding of how Rh catalyzes the reaction and help to improve catalyst performance.

Infrared (IR) studies have shown that CO may chemisorb on Rh in the forms of linear CO and bridged CO on the reduced Rh site as well as linear CO and gem-dicarbonyl on the Rh⁺ site (5-10). The mode of adsorption and stability of the adsorbed CO depend on the surface state and the chemical environment of the catalyst. Adsorption of NO on metals displays three modes of adsorbed NO: a cationic Rh-NO⁺ species, a neutral Rh-NO species, and an anionic Rh-NO⁻ species (10-13). *In situ* infrared studies reveal that adsorbed NO is the dominant species on the Rh surface with a small coverage of NCO and adsorbed CO during NO-CO reaction over Rh/SiO₂ at 463-523 K and NO conversion below 50% (14,15). Increasing NO conversion increases the coverage of adsorbed CO and NCO.

Cerium has been an important promoter in three-way catalysts (16-20). The major role of Ce has been identified to be (a) storage of oxygen, (b) stabilization of Al₂O₃ and metals, (c) promotion of the water-gas shift reaction, (d) suppression of N₂O formation and (e) modification of the kinetics (rate law) of the reaction. It remains

0097-6156/94/0552-0157\$08.00/0
© 1994 American Chemical Society

unclear how Ce modifies the intrinsic kinetics, i.e., the intrinsic rate constant k , and the surface coverage of intermediates Θ , resulting in an increase in the overall reaction rate of the NO-CO reaction. k (the reactivity of intermediates) is the reciprocal of τ (the residence time of intermediates) if the reaction of intermediates leading to gaseous product is a first-order irreversible reaction (21). Determination of k and Θ requires the use of steady-state isotopic transient technique. Steady-state isotopic pulse technique incorporated with *in situ* IR has been developed to investigate the effect of Ce on the dynamic behavior of adsorbed species and the residence time of intermediates leading to CO₂ during the CO-NO reaction. This study provides an insight into the catalysis of NO-CO reaction under reaction conditions.

Experimental

The Rh/SiO₂ catalyst (5 wt% Rh) was prepared by incipient wetness impregnation of RhCl₃·3H₂O (Alfa) onto a silica support (Strem); the Rh-Ce/SiO₂ catalyst (atomic ratio of Rh:Ce = 1:1 containing 5 wt% Rh) was prepared by co-impregnating a solution of RhCl₃·3H₂O (Alfa) and Ce(NO₃)₃·6H₂O (Alfa) onto the silica support (Strem). The catalysts were dried in air overnight followed by reduction in flowing H₂ at 673 K for 8 hours. During pulse CO chemisorption at 303 K, the Rh/SiO₂ catalyst chemisorbed 17.4 μ mol CO/gm catalyst; and the Ce-Rh/SiO₂ catalyst chemisorbed 28.5 μ mol CO/gm catalyst. An *in situ* infrared reactor cell capable of operating upto 873 K and 6 MPa was used for the NO-CO reaction. The catalysts were pressed into disks and placed in the reactor cell. The catalysts were further prereduced or preoxidized at 573 K before the reaction study. The reaction mixture consisted of CO/Ar (Commercial grade), NO (UHP) and He (UHP) controlled by mass flow meters.

An inlet system was designed to introduce an abrupt change in the concentration of CO in the form of a ¹³CO pulse or step change from ¹²CO to ¹³CO (21). Since the ¹³CO has the same chemical properties as ¹²CO, a change in the concentration from ¹²CO to ¹³CO would not affect the environment of the catalyst surface and the total concentration of all CO species. The ¹²CO contained 2% Ar, an inert gas, which was used to determine the effect of flow pattern through the reactor and transportation lines on the transient response. The change in concentration of adsorbed species was monitored by an FT-IR spectrometer with a resolution of 4 cm⁻¹. The effluent from the reactor was monitored continuously using a Balzers QMG 112 quadrupole mass spectrometer. Steady-state IR spectra were recorded using 32 co-added scans and transient spectra, using 3 co-added scans.

Results and Discussion

Steady-State NO-CO Reaction on Prereduced and Preoxidized Rh/SiO₂.

Figure 1 shows the IR spectra of the prereduced and preoxidized Rh/SiO₂ catalysts during NO-CO reaction at 723 K with a CO:NO = 5:1 ratio (CO: 12.5 cm³/min, NO: 2.5 cm³/min and He: 28 cm³/min). The prereduced catalyst was reduced in flowing hydrogen at 573 K for 1 hour and the preoxidized catalyst was oxidized in flowing air at 573 K for 1 hour. Both the prereduced and preoxidized catalysts achieved nearly total conversion of NO at 723 K. No NO₂ was detected and the amount of CO₂, N₂ and N₂O could not be quantified due to overlapping of signals in the mass spectrometer. The spectra for the prereduced Rh show a strong band at 2288 cm⁻¹, attributed to an isocyanate species (NCO) adsorbed on the SiO₂ support (11-15). A shoulder band at 2173 cm⁻¹ is assigned to an isocyanate species (NCO) on the Rh metal (14,15,22) and a shoulder band at 2358 cm⁻¹ is due to CO₂. A weak band appearing at 2003 cm⁻¹ is due

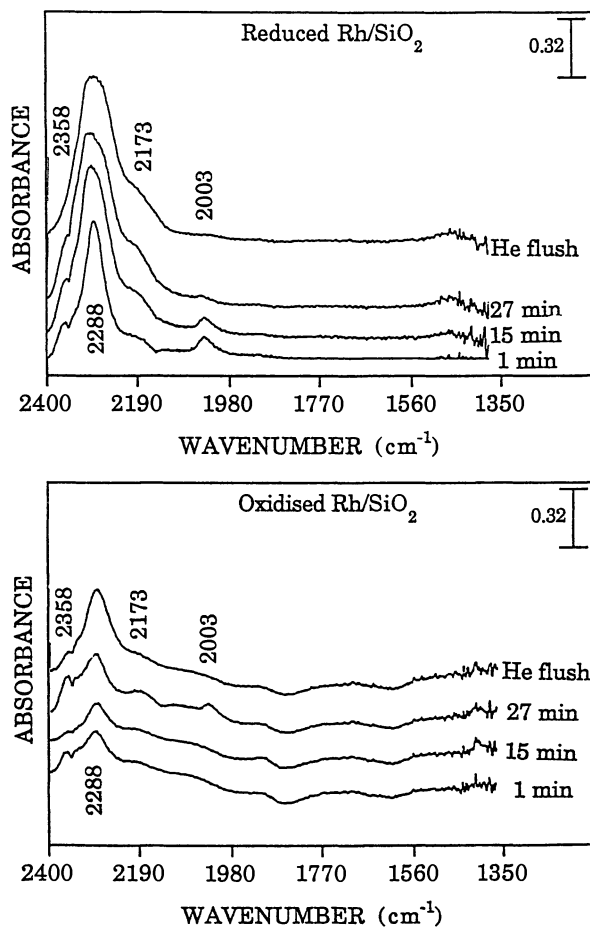


Figure 1. IR spectra of steady-state NO-CO reaction on pre-reduced Rh/SiO₂ and pre-oxidised Rh/SiO₂ catalysts.

to linear CO on the reduced Rh surface. The intensity of linear CO decreased with reaction time. In contrast, the intensity of NCO species on Rh and SiO₂ grew with reaction time, regardless of the reaction temperature. The NCO species remained on the catalyst surface following a long period of flowing He. The behavior of NCO observed here at 723 K is consistent with previous studies at 463-523 K (14,15) showing that Si-NCO is very stable in the presence and absence of reactants.

The preoxidized catalyst exhibited similar IR spectral features with a low intensity of the isocyanate species. No chemisorbed NO species were observed in the case of either prereduced or preoxidized Rh. Linear CO is the only adsorbed CO present on the surface of both prereduced and preoxidized catalysts at 723 K. The presence of linear CO could be due to the use of a high ratio of CO to NO. The excess CO chemisorbs as linear CO while most of the NO was rapidly converted to products. Hecker and Bell reported that preoxidized Rh is more active for the NO-CO reaction than prereduced Rh catalyst and both catalysts exhibit similar IR spectra after a long break-in period (14). The slow growth of NCO on the preoxidized Rh as compared to that on the prereduced Rh could be due to the high activity of the preoxidized Rh which is more effective than prereduced Rh in removing adsorbed NO and CO before they could be converted to NCO.

Steady-State NO-CO Reaction on Ce-Rh/SiO₂. Figure 2(A) shows the IR spectra of the steady-state reaction on Ce-Rh/SiO₂ catalyst carried out under the same condition as that of prereduced and preoxidized Rh/SiO₂ catalysts. Nearly complete conversion of NO was observed. The spectra show prominent bands due to isocyanate species at 2288 and 2178 cm⁻¹, attributed to those chemisorbed on SiO₂ and on the Rh metal, respectively. The development of these bands is slower and the Rh-NCO band observed at 27 min is more prominent than that observed on prereduced or preoxidized Rh/SiO₂. The intensity of Rh-NCO, which grows at a higher rate than that of NCO on the support, reached steady-state after 15 min of reaction. The intensity of Si-NCO continued to increase during the reaction.

In order to investigate the effect of CO lean and NO lean atmospheres on the Ce-Rh/SiO₂ catalyst performance, the catalyst was subjected to an abrupt stoppage of CO or NO flow. Figure 2(B) shows the IR spectral features observed following abruptly stopping either CO or NO flow to the reactor at 723 K. Following 11 min of steady-state reaction where Rh-NCO and linear CO slowly approach steady-state, the NO flow was terminated abruptly. Figures 3 (A) and (B) show the mass spectroscopic (MS) analysis of the effluents during the transient experiments. Shutting NO flow to the reactor resulted in the decrease in the CO₂ IR band while the remaining bands showed no variation except the slight increase in the linear CO band. The effluents from the reactor indicated a decrease in the CO₂ concentration following the stoppage. The IR spectra, following stopping CO flow to the reactor, showed the following: (i) an almost total disappearance of the Rh-NCO band at 2178 cm⁻¹ (ii) a decrease in the Si-NCO band at 2288 cm⁻¹, and (iii) the disappearance of the linear CO band at 2009 cm⁻¹. The disappearance of the chemisorbed CO band is accompanied by an enhancement of the Rh(NO)⁺ band at 1900 cm⁻¹ while the CO₂ band at 2358 cm⁻¹ remained present. Stopping CO flow also resulted in a momentary and abrupt enhancement followed by a decrease of the gaseous CO₂ concentration in the effluent. This suggests that gaseous CO is an inhibitor for the formation of CO₂. Similar observations on the negative order dependence of the reaction rate with respect to the partial pressure of CO on Ce-Rh/Al₂O₃ have been reported (18).

Steady-State Isotopic Transient Study. Transient isotopic studies were performed on Rh/SiO₂ and Ce-Rh/SiO₂ catalysts at 573 K under near complete conversion of NO. The studies were undertaken by pulsing 10 cm³ of ¹³CO into a

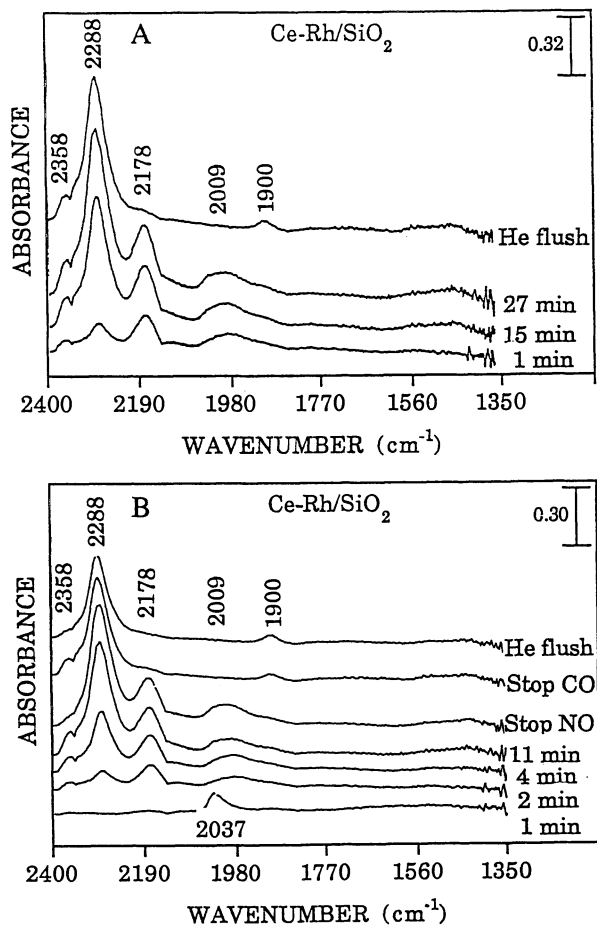


Figure 2. (A) IR spectra of steady-state NO-CO reaction on Ce-Rh/SiO₂ (B) IR spectra following transient stopping of stopping NO flow and CO flow on Ce-Rh/SiO₂.

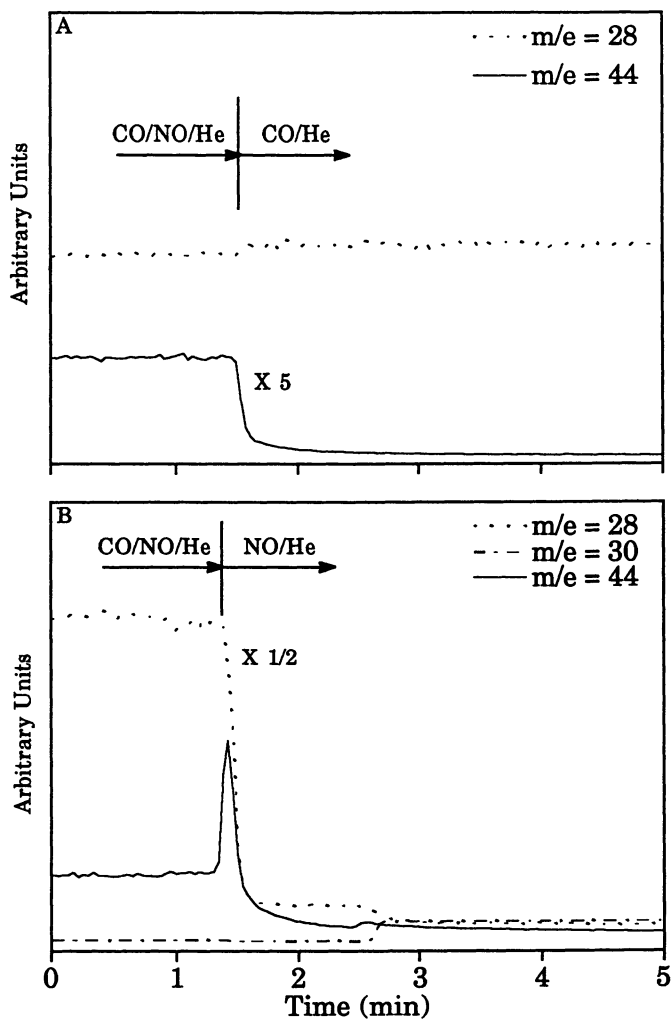


Figure 3. M.S. analysis of the transient on Ce-Rh/SiO₂
 (A) during stopping of NO flow (B) during stopping of CO flow

steady-state flow of CO/Ar-NO-He. The ratio of CO:NO was maintained at 1:1 during the transient study. Figure 4 shows the normalized MS analysis of the transient pulse on Rh/SiO₂. Figures 5 (A) and (B) show the IR spectra and difference spectra during the transient isotopic study on Rh/SiO₂. Steady-state IR spectra before the pulse shows the following bands: (i) a prominent Si-NCO band at 2295 cm⁻¹, and a weak Rh-NCO band at 2160 cm⁻¹ and, (ii) a prominent CO₂ band at 2358 cm⁻¹ and a weak Rh-NO band at 1683 cm⁻¹. Pulsing ¹³CO into a ¹²CO/Ar flow did not shift the intensity and wavenumber of the Si-NCO band indicating that this species is a spectator species during the formation of CO₂. A downward shift of CO₂ and Rh-NCO bands immediately, followed by an upward shift back to the original wavenumber can be clearly observed in the difference spectra obtained by subtracting the spectrum taken before the pulse from each transient spectra.

The turnover frequency for CO₂ formation (TOF) can be expressed in terms of intrinsic rate constant (k) and coverage of intermediate species (Θ);

$$\text{TOF} = k \cdot \Theta = (1/\tau) \cdot \Theta,$$

where τ is the residence time of the intermediate (21,23). Since there was almost total conversion of NO, the TOF determined does not represent the intrinsic activity of the catalyst and the coverage, Θ, was not determined. Preliminary study shows that the coverage can be determined at lower temperatures where the conversion is lower; however, the lower temperature may result in a different surface chemistry of the catalysts. The residence times of the carbon-containing species leading to CO₂ formation for Rh/SiO₂ has been calculated from the normalized curves shown in Figure 4, taking into account the residence time of the inert Ar representing the inherent delay due to the reactor and transportation lines (21).

Figure 6 shows the MS analysis during the isotopic transient experiment on Ce-Rh/SiO₂. Symmetry in ¹²CO and ¹³CO responses indicated that there was no perturbation to the total concentration of gas phase CO (including both ¹²CO and ¹³CO). The response of the ¹³CO and ¹³CO₂ curves indicate that the formation of ¹³CO₂ is faster than the desorption of ¹³CO. The residence times for ¹³CO desorption and intermediates leading to ¹³CO₂ formation are smaller than those obtained for Rh/SiO₂. Figures 7 (A) and (B) show the IR spectra and difference spectra during the isotopic pulse on Ce-Rh/SiO₂. Steady-state spectra before the pulse show the CO₂ band at 2358 cm⁻¹, Si-NCO band at 2309 cm⁻¹, Rh-NO⁺ band at 1913 cm⁻¹ Rh-NO band at 1691 cm⁻¹ and N₂O bands at 2241 and 2205 cm⁻¹. Introducing a ¹³CO pulse into ¹²CO/Ar flow resulted in a downward shift of CO₂ bands, immediately followed by an upward shift to their original wavenumbers. There was, however, no change in the intensity and wavenumber of the Si-NCO band, indicating that it was a spectator species. Rh-NCO did not exhibit a distinct IR band at 573 K. Preliminary study at 523 K shows that the rate of displacement of Rh-N¹³CO is slower than that of formation of ¹³CO₂. This result suggests that Rh-NCO is also a spectator species, consistent with Hecker and Bell's suggestion (15).

Oh has reported (18) that on Ce-Rh/Al₂O₃ catalysts containing 0.5 wt% Ce exhibit essentially the same activity as Rh/Al₂O₃, but catalysts containing 2 wt% or more of Ce show a significantly higher activity than Rh/Al₂O₃. The catalyst used in this study has a Ce loading of 6.8 wt% and exhibits a significant increase in the intrinsic rate constant as compared to Rh/SiO₂, agreeing well with reported high activity of Ce-Rh/Al₂O₃ from the study undertaken by Oh (18).

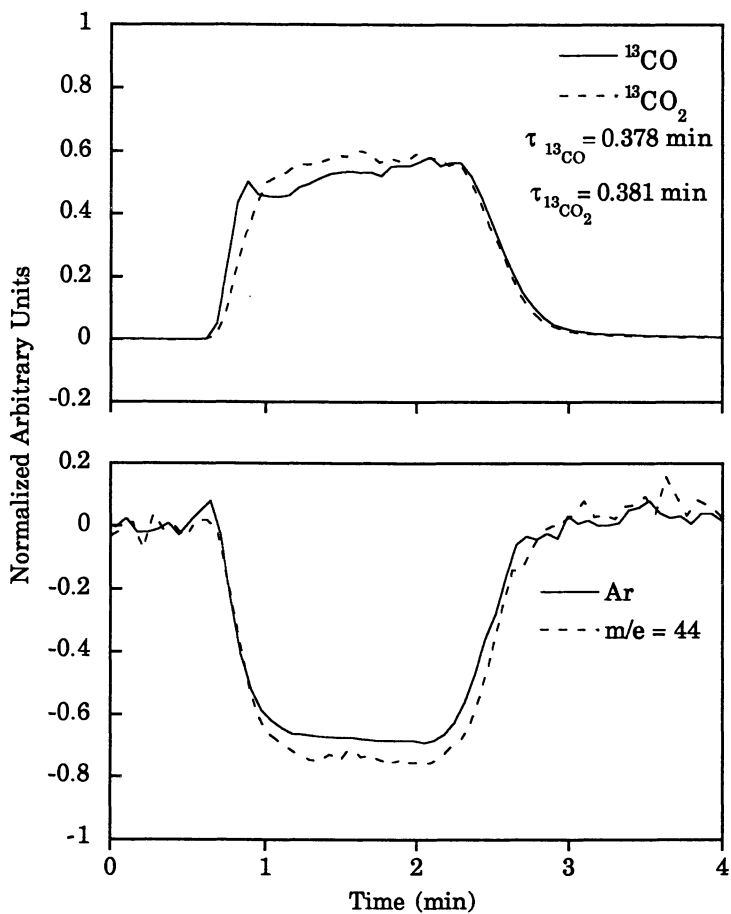


Figure 4. MS analysis of the transient during isotopic pulse over prereduced Rh/SiO₂.

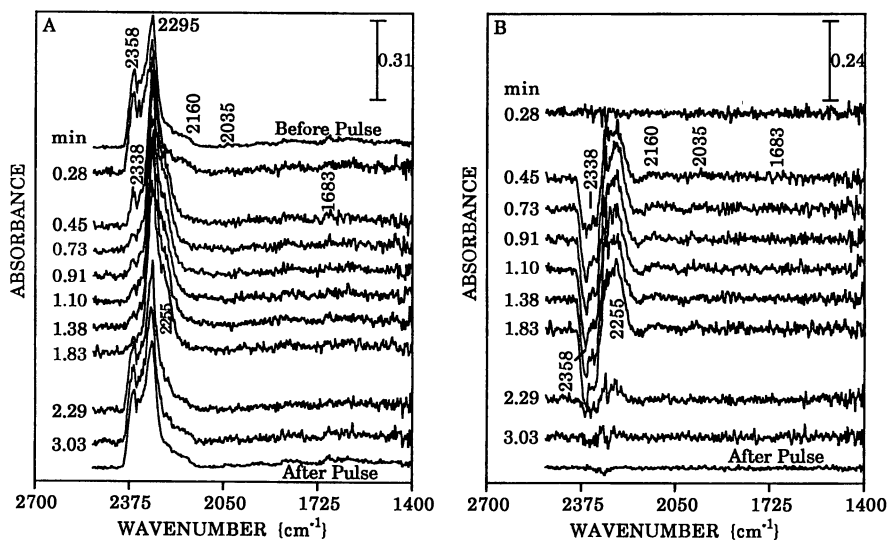


Figure 5. (A) IR spectra during isotopic pulse over pre-reduced Rh/SiO₂. (B) Difference spectra of Figure 5 (A).

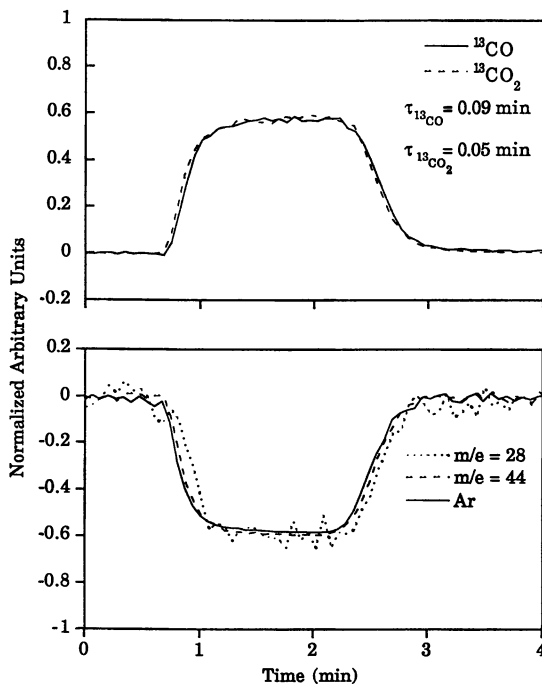


Figure 6. MS analysis of the transient during isotopic pulse over Ce-Rh/SiO₂.

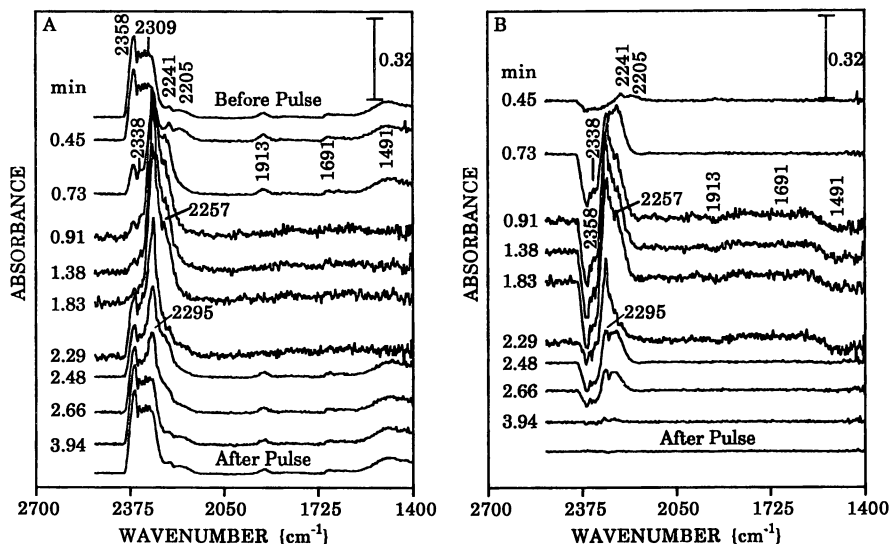


Figure 7. (A) IR spectra during isotopic pulse over prerduced Rh/SiO₂.
(B) Difference spectra of Figure 7 (A).

Conclusions

Steady-state isotopic pulse technique has been developed to investigate the kinetics of the NO-CO reaction under reaction conditions. The major chemisorbed species observed during the NO-CO reaction at 723 K on Rh/SiO₂ and Ce-Rh/SiO₂ is an NCO species on SiO₂. The Ce-Rh/SiO₂ catalyst also showed a higher intrinsic rate constant for CO₂ formation and a lower residence time of intermediates leading to CO₂ than those for Rh/SiO₂. Combined *in situ* IR and transient isotopic studies on Rh/SiO₂ and Ce-Rh/SiO₂ have shown that the NCO is a spectator species during the NO-CO reaction.

Literature Cited

1. Taylor, K. C. In *Catalysis Science and Technology*; Boudart, M.; Anderson, J. R., Eds.; Springer Verlag: New York, NY, 1984, Vol. 5; p 119.
2. Cooper, B. J.; Evans, W. D. J.; Harrison, B. In *Catalysis and Automotive Pollution Control*; Crucq, A.; Frennet, A., Eds.; Elsevier: New York, NY, 1987, Vol. 30; p 117.
3. Funabiki, M.; Yamada, T.; Kayano, K. *Catalysis Today*. **1981**, *10*, 33.
4. Farrauto, R. J.; Heck, R. M.; Spononello, B. K. *Chem. and Eng. News*. **1992**, Sept. 7, 34.
5. Yates, Y. T.; Duncan, T. M.; Vaughn, R. W. *J. Chem. Phys.* **1979**, *71*, 3908.
6. Worley, S. D.; Rice, C. A.; Mattson, G. A.; Curtis, C.W.; Guinn, J. A.; Tarrer, A. A. *J. Phys. Chem.* **1982**, *86*, 2714.
7. Solymosi, F.; Pasztor, M. *J. Phys. Chem.* **1985**, *89*, 4789.
8. Dictor, R. *J. Catal.* **1988**, *109*, 89.
9. Chuang, S. S. C.; Pien, S.I. *J. Catal.* **1992**, *135*, 618.

10. Chuang, S. S. C.; Pien, S.I. *J. Catal.* **1992**, *138*, 536.
11. Arai, H.; Tominaga, H. *J. Catal.* **1976**, *43*, 131.
12. Solymosi, F.; Bansagi, T.; Novak, E. *J. Catal.* **1983**, *112*, 83.
13. Solymosi, F.; Novak, E. *J. Catal.* **1990**, *125*, 112.
14. Hecker, W. C.; Bell, A. T. *J. Catal.* **1983**, *84*, 200.
15. Hecker, W. C.; Bell, A. T. *J. Catal.* **1984**, *85*, 389.
16. Gandhi, H. S.; Piken, A. G.; Shelef, M.; Delosh, R. G. *SAE* . **1976** Paper No. 760201.
17. Hindin, S. G. U.S. Patent 3, 870, 455 **1973**.
18. Oh, S. *J. Catal.* **1990**, *124*, 477.
19. Nakamura, R.; Nakai, S.; Sugiyama, K.; Echigoya, E. *Bull. Chem. Soc. Japan.* **1981**, *54*, 1950.
20. Fisher, G. B.; Theis, J. R.; Casarella, M. V.; Mahan, S. T. *SAE*. **1993** Paper No. 931034.
21. Srinivas, G.; Chuang, S. S. C.; Balakos, M. W. *AIChE Journal.* **1993**, *39*, 530.
22. Rasko, J.; Solymosi, F. *J. Catal.* **1981**, *71*, 219.
23. Biloen, P. *J. Mol. Catal.* **1983**, *21*, 17.

RECEIVED September 29, 1993

Chapter 13

Power Plant Emissions: An Overview

John N. Armor

Air Products & Chemicals, Inc., 7201 Hamilton Boulevard,
Allentown, PA 18195

Most people probably do not appreciate the magnitude of the problem with regard to stack gas emissions from power plants. The combustion of fossil fuels is conducted in the presence of excess air and results in huge volumes of emissions of low levels of NO_x, SO_x, CO, and particulates. Although emitted at low concentrations [ppm levels], the number of sources and the total volume of the emissions are large and thus contribute significantly to atmospheric pollution.

The primary gaseous pollutants generated from power plants are NO_x and SO_x. The combustion of coal generally converts about 95% of the sulfur content to SO₂, about 1 or 2 % to SO₃, and the remainder to solid sulfur compounds in the ash; US coals contain ~0.5 to 5. % sulfur. Current commercial technologies used to control SO₂ emissions from coal-fired boilers include wet scrubbing of the flue gas with a lime or a limestone slurry, spray drying of the lime slurry in the flue gas, and several less prevalent processes that produce elemental sulfur or a concentrated stream of SO₂ which may be further processed to sulfuric acid. Some of the wet scrubbing processes produce a commercial grade of gypsum. Commercial methods of controlling NO_x emissions from coal-fired boilers include combustion modifications, natural gas reburning, selective catalytic reduction [SCR], and selective non-catalytic reduction [SNCR] (1,2). The method of choice is usually determined by regulatory requirements and process economics. NO_x control at power plants by SCR is discussed in the overview chapter on "NO_x Removal" The thermal methods of NO_x removal are not discussed in this book.

Norman Kaplan of the US Environmental Protection Agency led the sessions on catalytic approaches to power plant emissions. He summarized the papers in this area as follows: "Speakers in the session cited experience with selective catalytic reduction (SCR) for control of NO_x emissions in Japan and Germany. Systems were categorized as high dust, low dust, and tail end. Applications of the high dust configuration predominate in foreign applications. The advantages and disadvantages of catalyst types (e.g., plate, honeycomb, various compositions) were contrasted based on some German experience with power plant applications. Some data indicated acceptable

catalyst activity (80-100% of initial level) for periods of >18,000 hours of operation. Systems are usually designed to emit less than 1 ppm of unreacted ammonia when installed, and about 5 ppm at the end of the useful catalyst life. The SNOX process, of Danish origin, for simultaneous catalytic NO_x reduction and SO₂ control by catalytic conversion to sulfuric acid was described as having the capability for >95% control of both pollutants, with fewer problems caused by unreacted ammonia. The advantages of a family of catalysts for various applications including coal-fired boilers, nitric acid plants, and refinery heaters were cited with indication of commercial experience. Most of the catalytic processes described above employ vanadium pentoxide/titanium dioxide catalysts with various modifiers. Another process being developed in Germany for reducing NO_x at low temperature using an activated carbon pseudo catalyst was also described and compared to the more prevalent V₂O₅/TiO₂ processes. R. A. Dalla Betta, et al (Catalytica, Inc.) reported on *New Catalytic Combustion Technology for Very Low Emissions Gas Turbines*. They described their new process for catalytic methane combustion in gas turbines by burning methane at about 1300°C with a 20 milli-second residence time at 10 atmosphere pressure. Here the levels of NO_x will be less than 10 ppm. The metal monolith support provides rapid transfer of heat and thus the catalyst avoids over-heating beyond 1300°C. Apparently the equilibrium between Pd and PdO helps limit the catalyst temperature to 1300°C. They obtain less than 1 ppm of NO_x and less than 2 ppm of CO at 11 atmospheres with 10,000 liter/minute of air using a 2" diameter catalyst. They are working with several turbine companies to evaluate the technology." Several of these presentations are included in this section on Power Plant Emissions.

References

1. Armor, J. N. *Appl. Catal. B*, **1992**, *1*, 221-256.
2. Bosch, H.; Janssen, F. *Catal. Today* **1988**, *2*, 369-532.

RECEIVED November 8, 1993

Chapter 14

NO_x Abatement by Selective Catalytic Reduction

G. W. Spitznagel, K. Hüttenhofer, and J. K. Beer

**Power Generation Group KWU, Siemens AG, Freyeslebenstrasse 1, 91058
Erlangen, Germany**

Since 1986 more than 50 coal fired boilers in the FRG have been equipped with Siemens SCR catalytic converters for NO_x-control. Especially in high dust applications plate type catalytic converters have proven to achieve optimum performance even under the worst flue gas conditions. In this connection, the proper design of catalytic converters concerning geometry and chemical composition is essential for reliable operation. This resulted in the development of a new poisoning resistant catalytically active material. Experience from more than five years of operation downstream of coal-fired boilers with various catalysts is presented. New application areas for catalysts, e. g. DeNO_x air preheaters or combined dioxin and NO_x control for waste incineration plants, and initial operating results with this new technology are presented.

The Federal Republic of Germany has an installed power plant capacity of 109.7 GW_{el}. 23.6 GW or 22% of this total capacity is provided by nuclear power, 6.9 GW or 6% by hydroelectric power and 1.2 GW or 1% by renewable sources of energy. The lion's share, 78 GW or 71%, of the energy supply is based on fossil fuels (see table I), mainly coal (1).

If one considers the emissions from a typical hard coal-fired 750 MW plant (see Figure 1), it soon becomes apparent that in a densely-populated country such as the Federal Republic of Germany and especially at times when the environmental awareness of the citizens is clearly on the increase, legislators are forced to introduce strict environmental standards.

Table I: Generating capacity in FRG (status 1990) without new federal countries according to (1)

Type of Power Source	Generating Capacity [GW]	Percentage
Nuclear	23.6	21.5
Water	6.9	6.3
Hardcoal	39.5	36.0
Lignite	12.3	11.2
Oil	9.7	8.9
Gas	16.5	15.0
Others	1.2	1.1
Total	109.7	100.0

Dust emissions from power plants (see Figure 2) were restricted as early as 1964 and as of 1975 the SO₂ limits were reduced even further in North Rhine Westphalia. However, a definite step toward emission control was made when the Ordinance on Large Combustion Facilities came into force 1983 which prescribed a reduction in SO₂ emissions to 400 mg/m³ (140 ppm) by 1988 (by installing flue gas desulfurization plants) and by the Conference of Environmental Ministers 1984 which limited NO_x emissions from power plants to 200 mg/m³ (97 ppm) as of 1988 to 1990 (2). In the meantime, licensing practice in urban areas in the FRG for new power plants demands levels of 50 mg SO₂/m³ (17.5 ppm) and 100 mg NO_x/m³ (49 ppm).

Up to now, approximately 150 power plants in the FRG with a combined electrical rating of 33,000 MW have been backfitted with SCR DeNO_x equipment (see Figure 3). While primary measures are usually sufficient to meet NO_x limits in lignite-fired plants, technology SCR DeNO_x has established itself and been proven on an industrial scale in over 95% of hard coal-fired power plants (3), while other processes proved unsuitable for technical reasons (e.g. achievable abatement efficiency) or owing to problematic secondary emissions (e.g. N₂O in SCNR (4)).

Catalytic Material and Shapes of Catalysts

The heart of an SCR DeNO_x plant is the catalytic converter (see Figure 4). It is usually a ceramic mass based on titanium dioxide, to which the active components, oxides of vanadium and tungsten or molybdenum, are added. Despite this significant similarity between all SCR DeNO_x catalytic converters there are great variations in their activity and geometry.

When the SCR DeNO_x technology came to Germany in 1984, catalytic converters were well-suited to Japanese power plant requirements

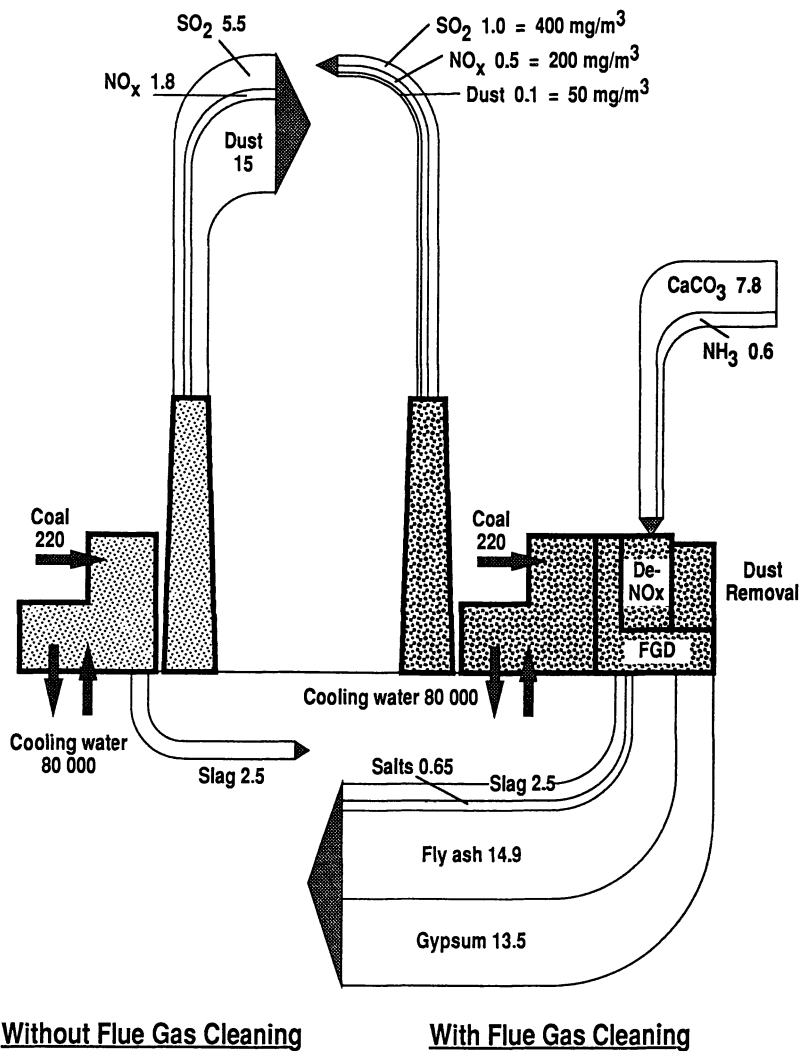


Figure 1: Media and end products of a 750 MW hard coal fired power plant with and without flue gas cleaning

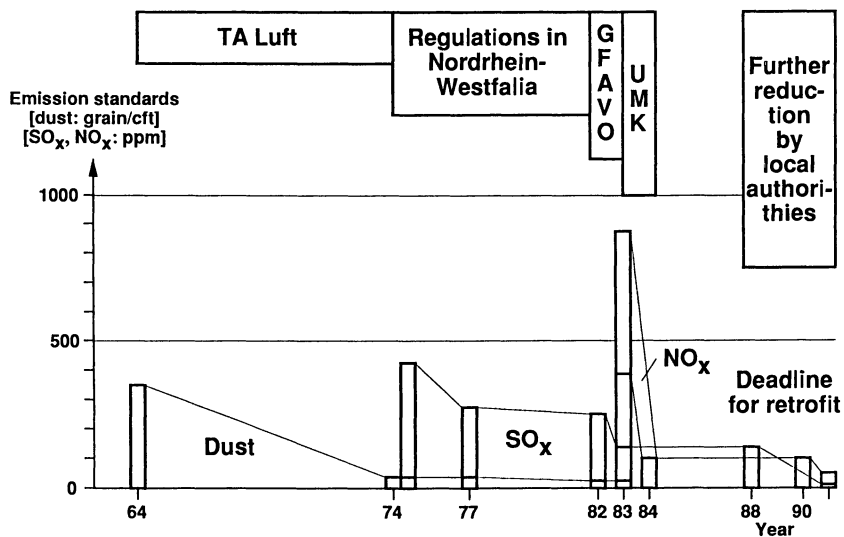


Figure 2: Development of emission standards in the FRG

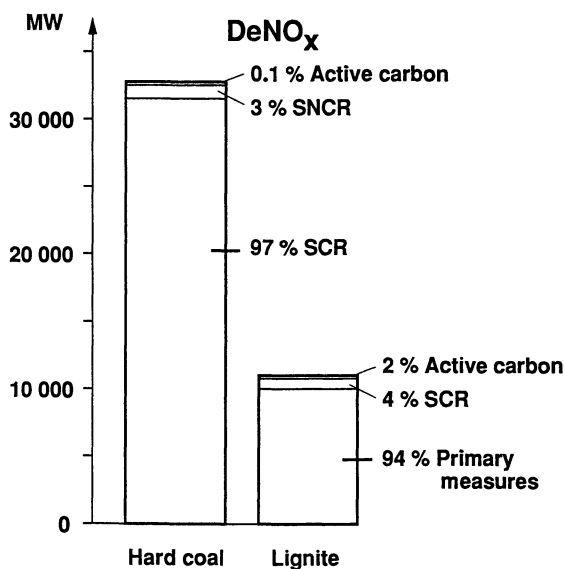


Figure 3: DeNO_x measures in German coal fired power plants

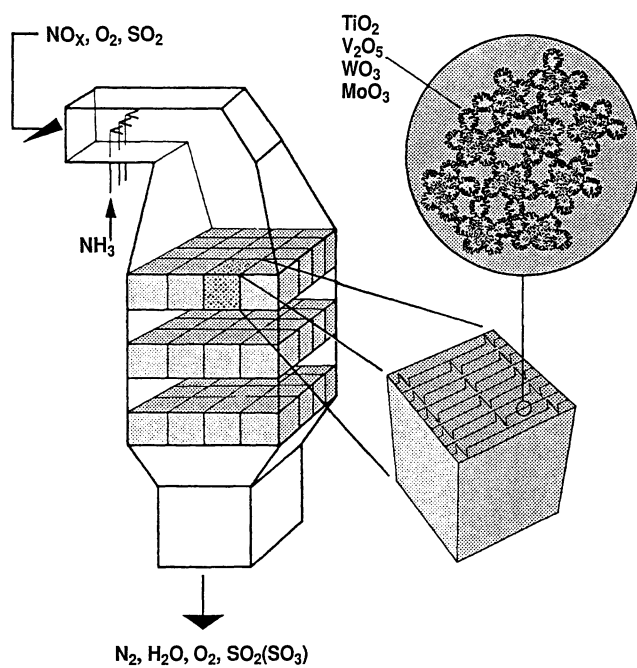


Figure 4: Schematic view of a SCR DeNO_x reactor

(high-grade coals, base load operation, boiler with dry ash extraction) but these special conditions meant the manufacturers had only developed a few models (5). The special requirements of German power plants, such as frequent load changes in intermediate load power plants, slag tap furnaces with ash recirculation and the use of coal from all over the world (USA, Poland, Australia, etc.) or German high inerts coal, forced Siemens to develop the plate-type catalytic converter (6) in addition to licensing the honeycomb-type catalytic converter. This development made it possible to gain extensive know-how on the selection and fabrication of the correct type and design of catalytic converter, active surface and material activity to suit the application (7).

Plate-type catalytic converters are typically used in high-dust configurations, i.e. immediately downstream of the boiler at a point where the flue gases have already reached the optimal temperature for the DeNO_x reaction of about 350°C (660°F). The distance between the catalyst plates is 4-6 mm which results in a specific surface area of 280-380 m²/m³. Honeycomb-type catalytic converters, on the other hand, perform better in low-dust areas, i.e. downstream of dust collection and desulfurization of flue gases. In this configuration, they form very compact DeNO_x reactors with channel openings of 3-4 mm and specific surface areas of 650-900 m²/m³. Honeycomb-type catalytic converters are used less often in very high-dust applications (however in moderate dust laden flue gases both systems are comparable). Typical channel openings are 6 mm, which result in surface areas of 480 m²/m³ (see table II).

Table II: Selection of catalytic converter according to operating conditions

Fuel	Arrangement	Dust concentration gr/scf	Temperature range °F	Type	Spec. surface area m ² /m ³	Remarks
High inerts coal	Before APH (high dust)	> 6.5	610 - 810	Plate	285 - 350	
	Other arrangements see hard coal					
Hard coal	Before APH (high dust)	< 6.5	610 - 810 610 - 810	Honeycomb Plate	427/486 330 - 380	Depending on operation conditions
	After FGD (low dust)	< 0.02	540 - 630	Honeycomb	751/881	
	After charcoal FGD (low dust)	< 0.002	390 - 480	Honeycomb	881	
Oil LS/HS	Before APH (high dust)	< 0.05	660 - 840	Honeycomb	550/654	
	After FGD (low dust)	< 0.02	570 - 660	Honeycomb	751	
Gas		< 0.002	540 - 720	Honeycomb	881	

Catalytic Converter Arrangement

For new power plants, a high-dust configuration (see Figure 5) is preferable. On the one hand, this configuration involves less capital investment since neither complicated flue gas piping routes nor a reheat system have to be installed and on the other hand, no additional energy costs are caused by the reheat system in normal operation. For the above-mentioned reasons, the high-dust configuration is also preferable for backfitting operations provided this configuration is practicable, which it usually is.

Apart from oil or gas-fired power plant units, plate-type catalytic converters are preferable in high dust and high sulfur applications in coal-fired power plants. There are four reasons for this:

1. Plate-type catalytic converters are less prone to blockage owing to their structure which permits slight vibration of the individual plates (adhering dust is continually dislodged). As it can be seen from Figure 6 in addition to this effect dust deposition on the plate-type catalytic converter is lower than on the honeycomb type due to its geometric properties.
2. Plate-type catalytic converters have a higher resistance to erosion than their ceramic-base counterparts. As soon as the metal mesh is exposed on the end face of the catalyst plate, erosion does not progress further into the element in contrast to the all-ceramic honeycomb material (see Figure 7).
3. Plate-type catalytic converters have very thin plates and therefore only a small area of the cross-section is obstructed. This results in low pressure drop across the catalytic converter.
4. As SO₂-conversion is a bulk reaction the lower installed catalytic mass in a plate-type catalytic converter leads to lower SO₂/SO₃ conversion rates.

Plate-type catalytic converters are fault tolerant systems concerning poor flue gas distribution, highly erosive fly ashes, blockage of the system, frequent coal and load changes.

Selection Criteria for a Catalytic Converter

Figure 8 shows the basic types of SCR DeNO_x catalytic converters.

First and foremost, the dust content of the flue gas is the critical factor in selection of the catalyst geometry, which the honeycomb-type catalytic converter has an advantage in dust-free or low-dust flue gases the plate-type catalytic converter is advantageous in dust-laden flue gases.

With plate-type catalytic converters, geometry can be tailored to the dust content of the flue gases to be treated. In extremely high-dust applications (40-50 g/m³ \approx 17 - 22 gr/scf), 6 mm gaps are preferable be-

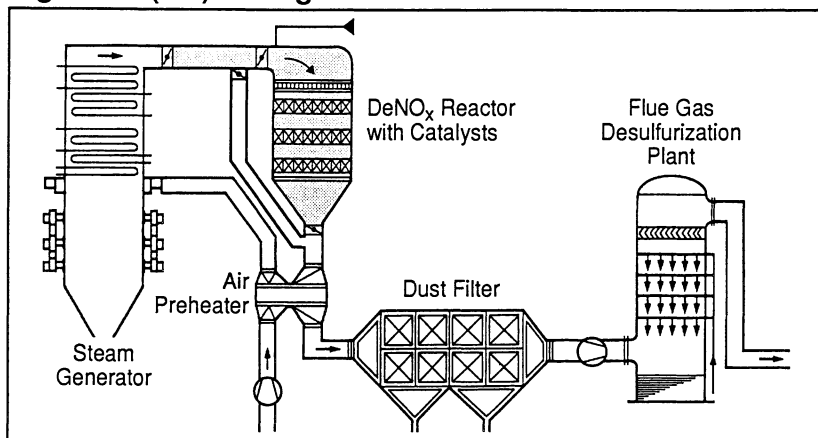
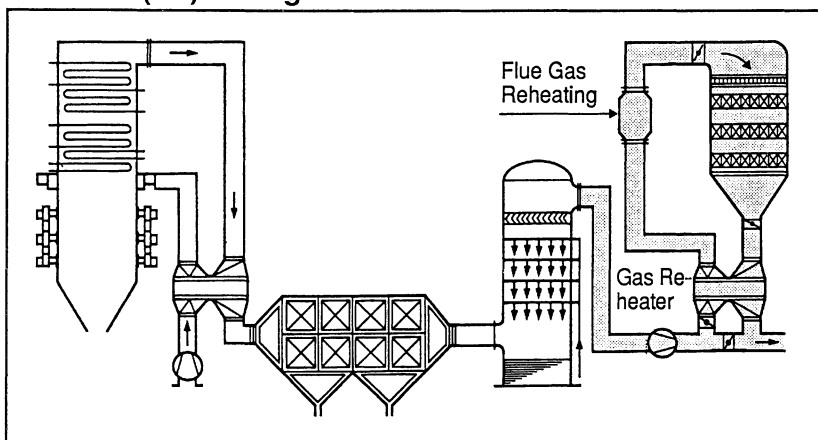
High-dust (HD) Arrangement**Low-dust (LD) Arrangement**

Figure 5: Catalytic converter arrangements (the low dust arrangement is often also referred to as tail gas arrangement)

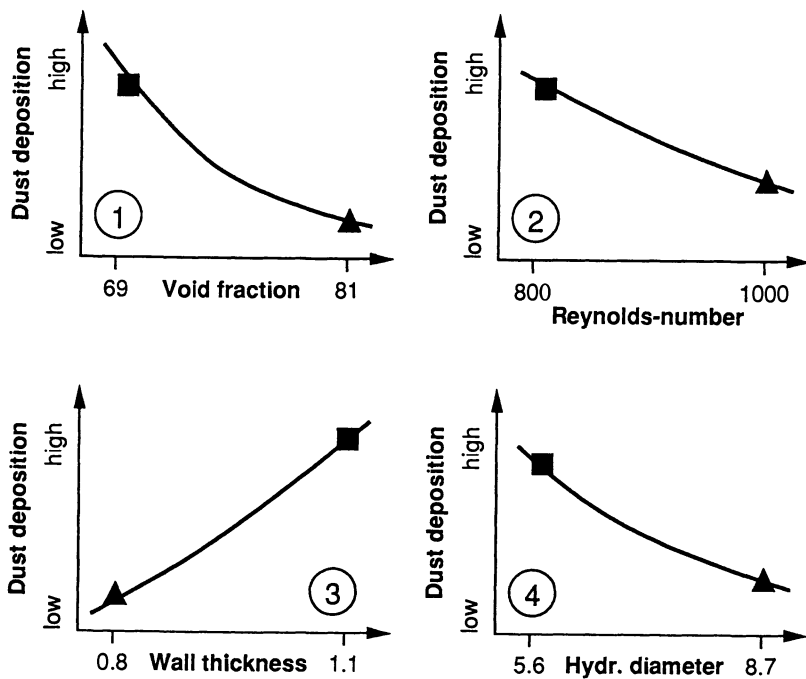


Figure 6: Dust deposition on catalytic converters as a function of geometric and fluid dynamic parameters

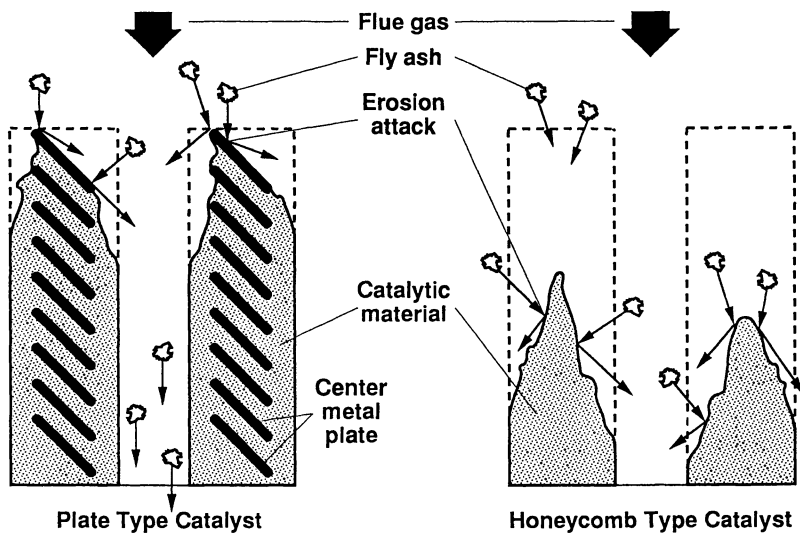


Figure 7: Principle of erosion resistance of catalytic converters

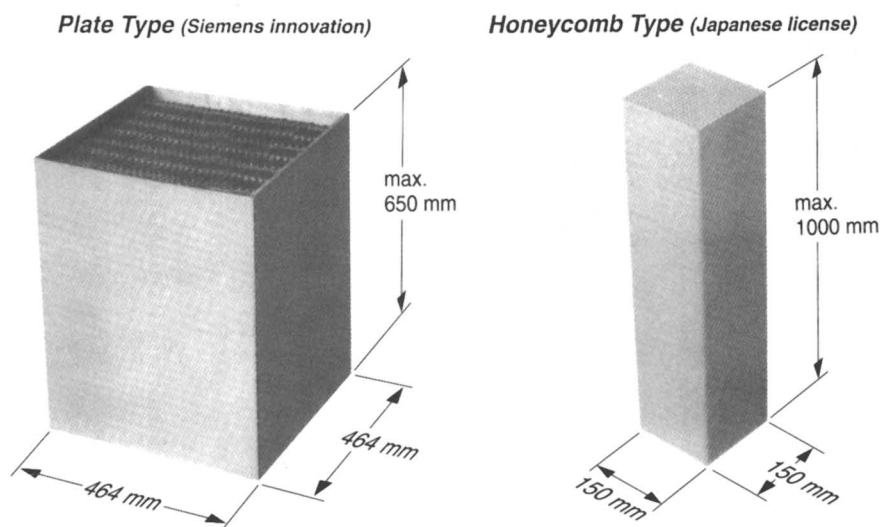


Figure 8: Basic types of SCR DeNO_x catalytic converters

tween the plates while the gap between the plates in lower dust applications ($5-15 \text{ g/m}^3 \approx 2-7 \text{ gr/scf}$) is reduced to 4 mm.

Another significant parameter for selection of catalytic converters is the SO_2 content of the flue gas. If an attempt is made to increase the activity of a catalytic converter in terms of the NO_x reaction, SO_2 oxidation increases simultaneously (see Figure 9). However, the sulfuric acid concentration produced by this reaction should be kept to a level which ensures that plant items downstream of the catalytic converter do not suffer any damage as a result. This means that it is possible to optimize the chemical composition with regard to the initial activity of the catalyst for every application.

However the initial activity of a catalyst is not the only critical factor, but also the aging or poisoning behavior in flue gas conditions. One well-known catalyst poison is arsenic. Arsenic concentration can be increased by a factor of 20, in slag tap furnaces with ash recirculation compared to boilers with dry ash extraction. As a result, titanium/tungsten catalysts in particular are deactivated extremely quickly, therefore a titanium/molybdenum catalyst ensures longer service life in a slag tap furnace despite its lower initial activity (8) (see Figure 10).

All in all, this situation was unsatisfactory and consequently Siemens has developed a new active phase (9) by thorough investigation of the poisoning mechanism. This new phase not only achieves but even exceeds the initial activity of Ti/W catalysts and in addition offers the poisoning resistance of Ti/Mo catalysts (10). Catalytic converters can therefore be fabricated with this new generation of active material, which will lead to optimal results, especially for coal firing.

Operating Results

Concerning the activity behavior in boilers with dry ash extraction almost, all catalysts behave as expected or even if much better. This means that the guaranteed service lives could be achieved or even significantly exceeded (see figure 11).

In slag tap furnaces, it can be seen that all catalysts containing molybdenum perform as expected, i.e. deactivation is not excessive (see Figure 12) and that the deactivation correlates to the As_2O_3 content of the flue gas.

In Figure 13 the blockage frequency of plate-type and honeycomb-type catalysts is compared. These catalysts have been operated downstream of a boiler with two DeNO_x reactors in high dust arrangement one of which containing a honeycomb-type catalyst and the other a plate-type catalyst. Both catalysts were therefore subjected to identical conditions. While a large number of channels are blocked in the honeycomb-type catalyst, only a few are blocked in the plate-type catalyst (see Figure 13).

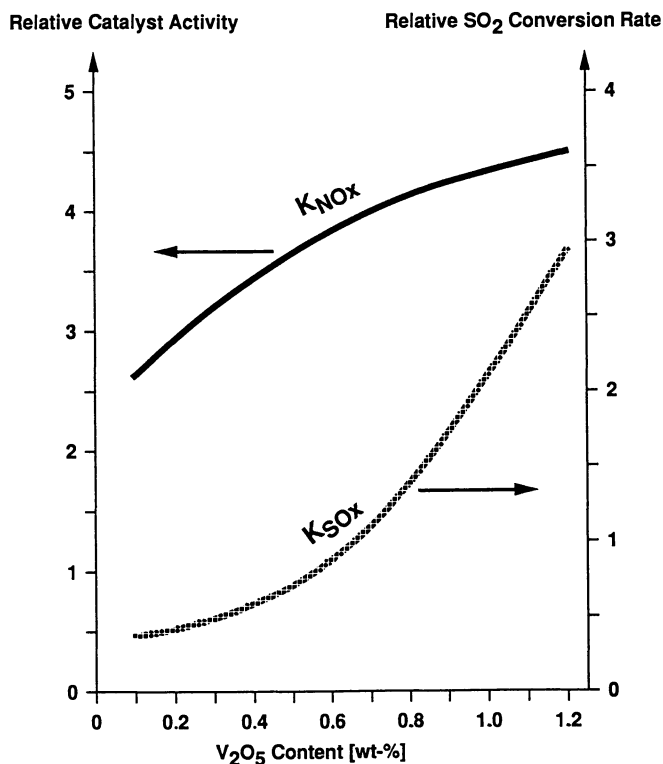


Figure 9: Catalyst activity and SO₂ conversion rate as a function of V₂O₅ content

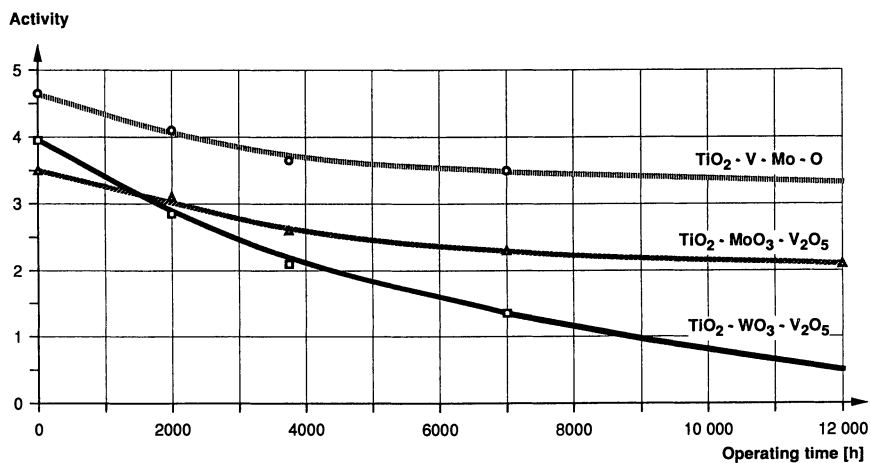


Figure 10: Typical activity profile of DeNO_x catalysts downstream boilers with high As₂O₃ content in the flue gas (eg: slag tap furnaces with 100% ash recirculation)

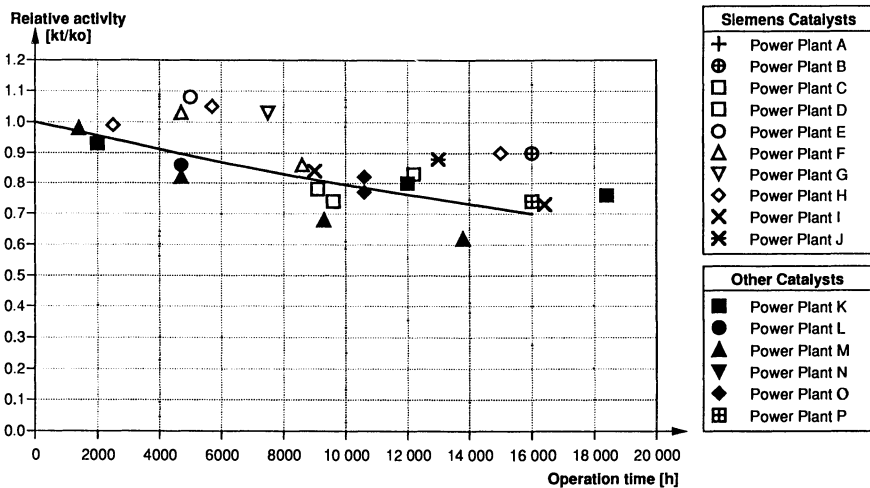


Figure 11: Activity profiles for selection of catalysts used in German power plants

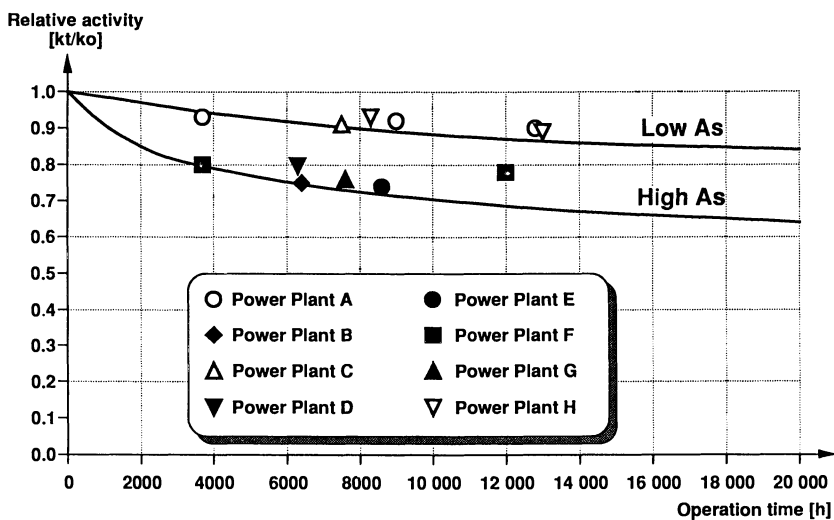


Figure 12: Activity profiles of poisoning resistant catalysts downstream of slag tap furnaces

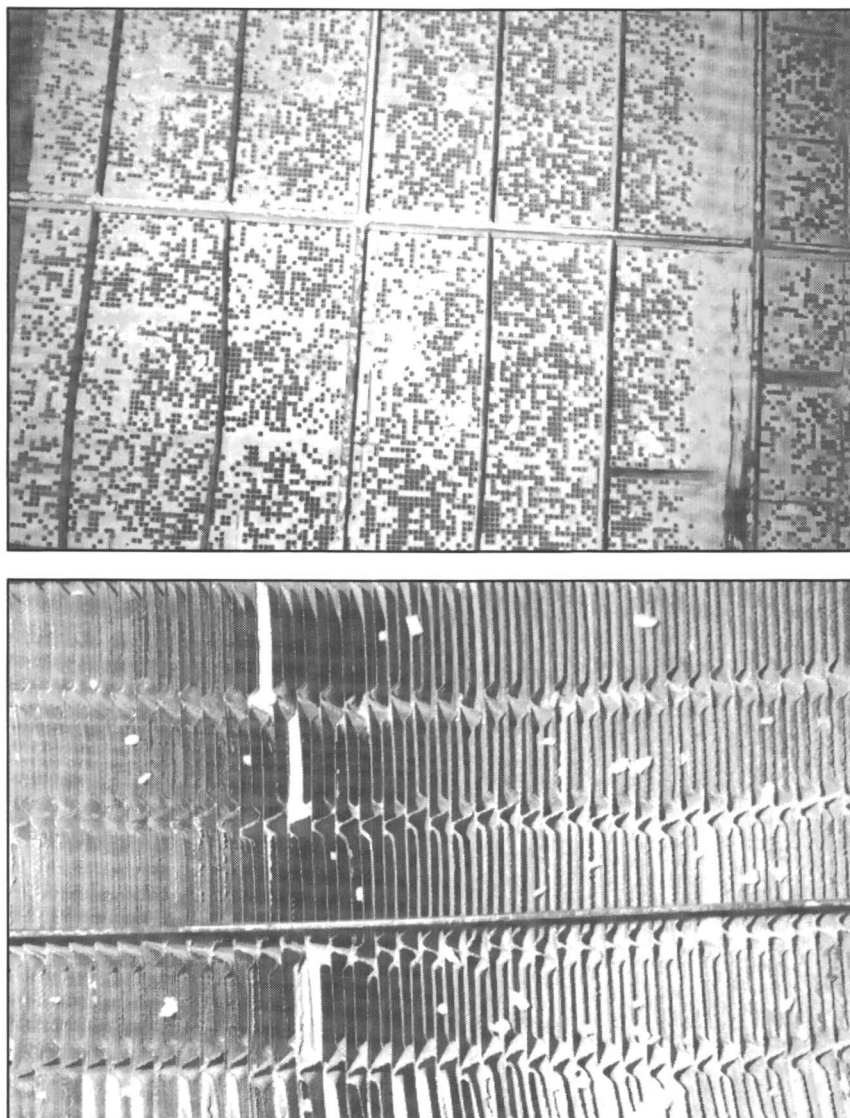


Figure 13: Comparison of blockage in a honeycomb and a plate-type catalytic converter after approx 10000 h of operation

Looking at the erosion pattern in Figure 14 it can be seen that the erosion stops in the plate-type after the metal mes has been exposed, while erosion continues through the full thickness of the all-ceramic honeycomb type (compare Figure 7). Both types of catalytic converters were exposed to comparable flue gas conditions.

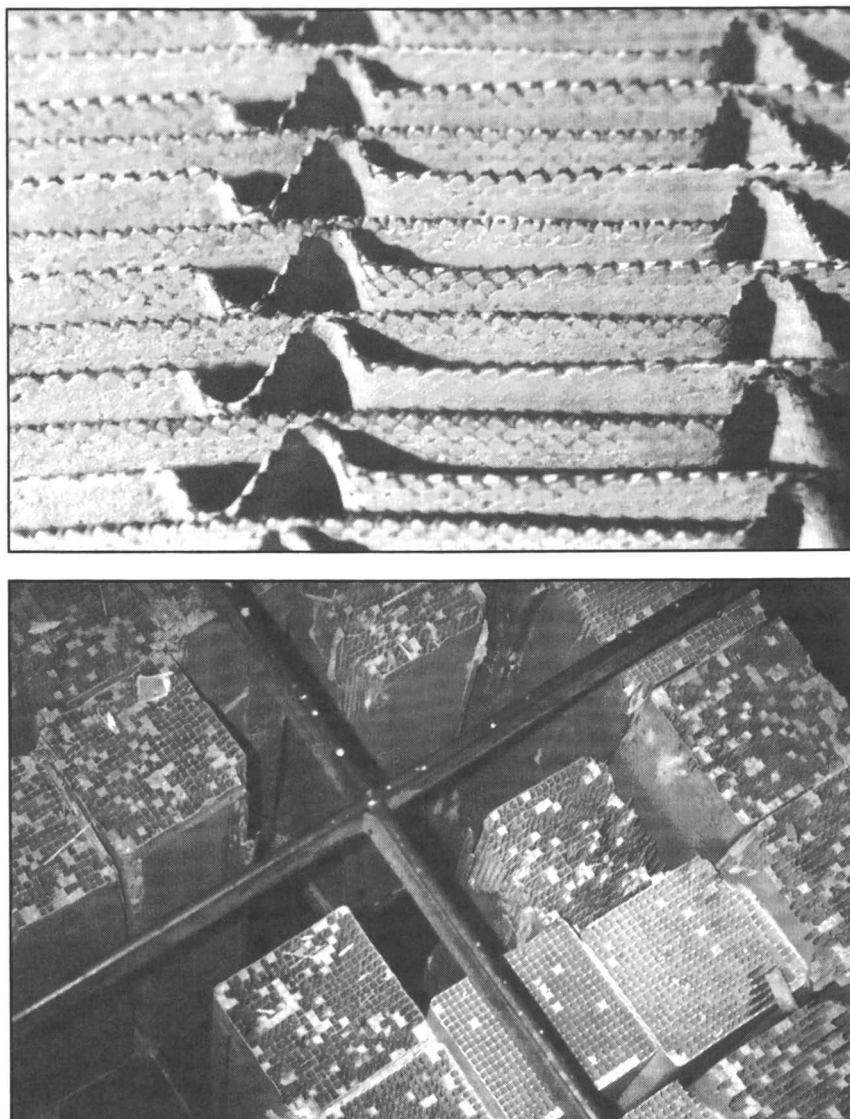


Figure 14: Erosion resistance of plate-type and honeycomb-type catalytic converters in high dust installations

New Applications

Applications of this catalytic converter system are not limited to stationary DeNO_x reactor designs or locations downstream of power plant boilers. In those applications where only low NO_x reduction is required, the catalytic converter can be integrated into the air preheater, especially when available space in the power plant is very limited (see Figure 15).

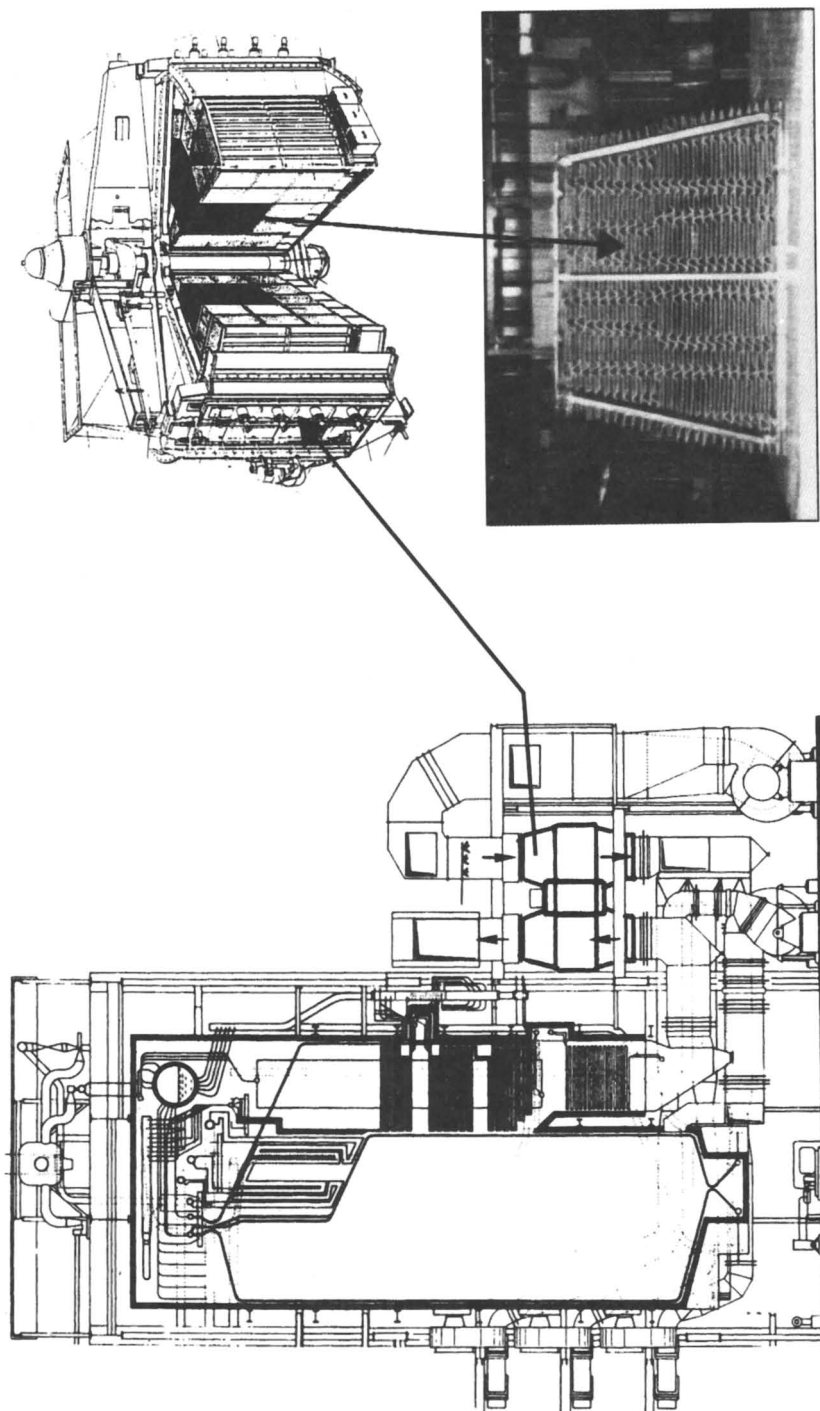


Figure 15: DeNO_x catalytic converter integrated in an air preheater

Furthermore, catalytic converters can be used for combined abatement of NO_x, dioxins and furans downstream of refuse incineration plants (see Figure 16). Although these abatements can be achieved by using common DeNO_x catalytic converters, investigations have been made in order Modified catalysts have been developed, which can have different chemical composition and/or pore structure. With these catalysts, the necessary catalyst volume can be significantly reduced. Dioxin and furan abatement efficiencies up to > 99.5% are possible (11).

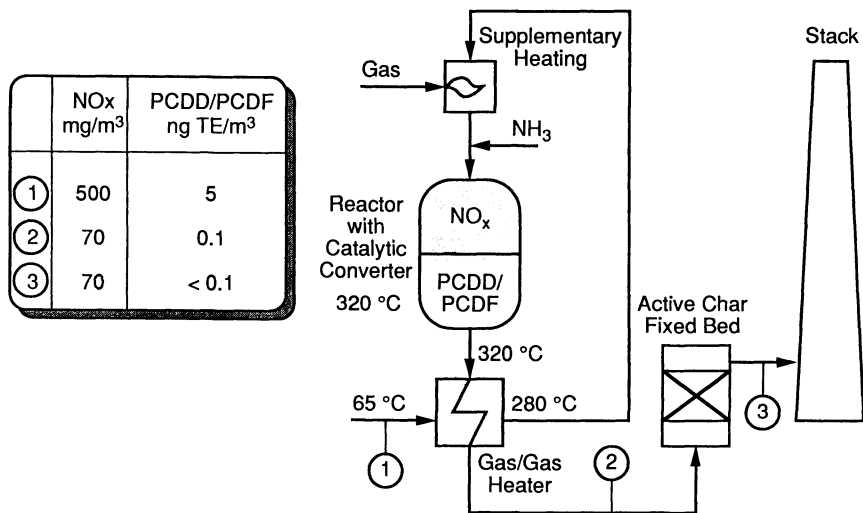


Figure 16: Combined NO_x and PCDD/PCDF reduction with SCR catalytic converters

Conclusions

An SCR DeNO_x reactor with a SIEMENS plate-type catalytic converter is a proven, low-fault system which achieves high NO_x abatement efficiencies (> 90%) and which has proven successful in particular in flue gases with a high dust content and high concentrations of problematic elements. This catalytic converter may also be integrated into the air preheater. Furthermore the catalyst can be used for a simultaneous NO_x and PCDD/PCDF reduction.

References

1. *Energiewirtschaftliche Tagesfragen* 1992, 3, 170.
2. Davids, P.; Lange, M., *Die Großfeuerungsanlagen-Verordnung, Technischer Kommentar*, VDI Verlag: Düsseldorf, 1984.

3. Krüger, H., *VGB Kraftwerkstechnik*, **1991**, 71, 371-395.
4. Jødal, M.; Nielsen, C.; Møller, H., *Kraftwerk und Umwelt*, **1991**, 97-100.
5. Beer J. K.; Balling L., *Modern Power Systems*, **1990**, 25-29.
6. Balling, L.; Gajewski, W.; Hein, D.; Kuschke, R.; Landgraf, N.; Ranly, H.; Reppisch, R.; Schmelz, H.; Sprehe, J.; Thomann, H.; Wilbert, E.-H. US Patent 4 812 296, **1986**; Hums, E.; Schmelz, H.; Hein, D. US Patent 4 849 392, **1987**.
7. Balling L.; Hein, D., *EPRI/EPA 1989 Joint Symposium on Stationary Combustion NO_x Control*, San Francisco, **1989**, Session 7a.
8. Balling L.; Spitznagel, G. W.; Sigling, S.; Schmelz, H.; Hums, E., *EPRI/EPA 1991 Joint Symposium on Stationary Combustion NO_x Control* Washington DC, **1991**, Session 4b.
9. Hums, E.; Spitznagel, G. W. US Patent 5 112 794, **1990**.
10. Hopfengärtner, G.; Borgmann, D.; Rademacher, I.; Wedler, G.; Hums, E.; Spitznagel, G. W., *J. Electron Spectrosc. Relat. Phenom.*, **1993**, 63, 91-117.
11. Hüttenhofer, K.; Balling, L.; Ramstetter, R., In *HdT-Fachbuchreihe SCR DeNO_x Katalysatoren*, Vulkan Verlag: Essen, **1992**, pp 182-187.

RECEIVED September 29, 1993

Chapter 15

Foreign Experience with Selective Catalytic Reduction NO_x Controls

Phillip A. Lowe¹ and William Ellison²

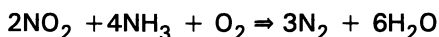
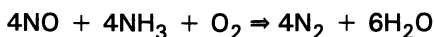
¹Intech Inc., 11316 Rouen Drive, Potomac, MD 20854-3126

²Ellison Consultants, 4966 Tall Oaks Drive, Monrovia, MD 21770-9316

A summary description of the technology, including applications upstream and downstream the flue gas particulate controls (termed high and low dust applications, respectively, in the literature) and applications downstream of the flue gas desulfurization controls (termed tail gas applications in the literature) is provided. The operating and maintenance experience from Germany and Japan is discussed in detail. Critical issues that need to be considered before the technology is applied to US, high sulfur coal service are highlighted.

Japanese Experience

In 1970 the Japanese initiated the use of selective catalytic reduction (SCR) technology for NO_x control on large electric utility boilers, including coal, oil, and gas service. The primary reactions governing the process are:



Depending upon the catalyst materials, the optimum reaction temperature is 300 - 400°C. Although this is termed a reduction catalyst, it is really a strongly oxidizing catalyst. In fact, the oxidation of other materials in the boiler flue gas, as will be discussed below, is one of the competing reactions that can lead to other operating problems. The efficiency of the NO_x reduction depends upon a number of factors such as the temperature of the flue gas, the NO_x concentration (especially for low NO_x conditions typical of gas firing), the amount of ammonia and its

distribution relative to the NO_x distribution within the flue gas, the amount of dust present in the flue gas, the SO₂ concentration in the flue gas, the amount and form of flue gas trace material concentrations, and to a lesser extent the amount of oxygen present. Engineers typically characterize the reaction as a function of the space velocity (the flue gas volumetric flow rate divided by the catalyst volume) or the linear velocity and the catalyst active area (the surface area exposed to the flue gas).

Initial coal-fired commercial service began in 1980(1). In general, the Japanese use dry bottom boilers (e.g., non slagging boilers) which fire high quality coal (less than 1% sulfur and 10% ash) and which operate in a base load mode. However, the Japanese have reported that they have operated at least one plant(2) with 2.5% sulfur coal and no performance degradation was experienced. The Japanese commercially developed two systems for placing the catalyst into the boiler-flue gas system, the high dust and the low dust configurations. Since many of their plants use high temperature electrostatic precipitators (ESP), a low dust design was developed which removed the flue gas particles before the gas entered the SCR housing. This is shown in Figure 1. If the ESP were a low temperature device, the SCR was placed immediately downstream of the boiler outlet and the configuration was termed the high dust design because the catalyst had to operate under the full particulate loading conditions of the boiler flue gas. Although the Japanese identified a tail-end design, it was not developed until the Germans determined it was needed for applications at power plants which used a slagging or wet bottom boiler, and in which part or all of the particulates collected at the ESP are re-introduced into the boiler to slag them for disposal. In the tail end system, the SCR is placed downstream of the flue gas desulfurization (FGD) equipment.

There are advantages and disadvantages of each of the basic configurations. If physical space exists immediately downstream of the boiler, the high dust design is often preferred because of its estimated lower costs. Catalyst volumes of 21.2 to 42.4 ft³/MWe have been reported in conversations with Germans, however, the U.S. EPA(3) has reported the volumes are 60-120 ft³/MWe. The larger volumes are for high dust applications, the smaller volumes are for tail end applications. After examining 624 U.S. boiler retrofit applications, the EPA(4) concluded that space requirements greatly favored the application of tail end SCR systems. In the high dust design, potential impurities within the flue gas make the catalyst design more important, and in fact during the initial Japanese and German high dust applications many operating problems were experienced (SCR system vendors now state that they understand the causes of those earlier problems and have corrected them in their present offerings). The low dust and tail end designs eliminate most of the particulate loading problems, but there still have been fouling problems with the air preheater (or a gas-gas reheater) in some low dust applications. If the ESP is a low temperature device, it also requires some flue gas reheating, which is a penalty on the total plant thermal efficiency. The tail end configuration treats

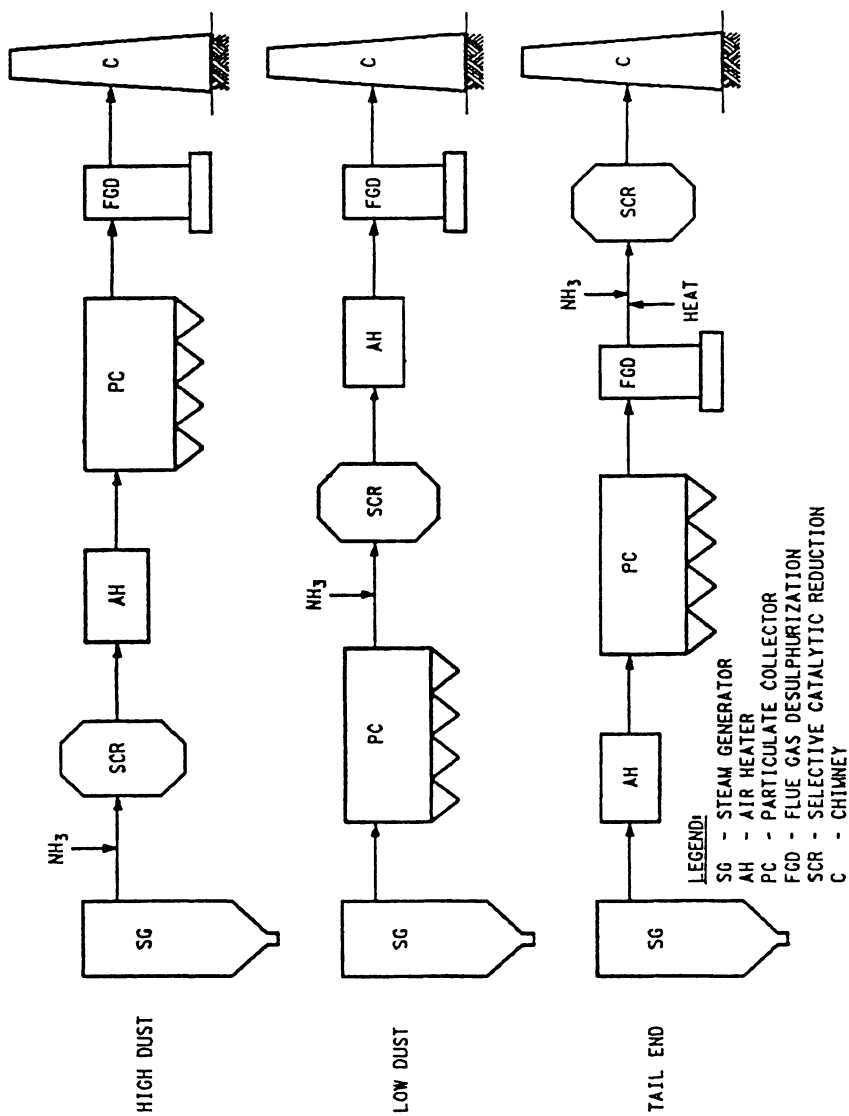


Figure 1. SCR Location Configurations

a very clean flue gas, but it has the highest flue gas reheating requirement. Its reheat requirements can decrease the plant operating efficiency by 1-3%, which is a significant economic penalty for a power plant.

Even after the extensive Japanese development and pilot plant operations, there were some initial problems, principally with the formation of deposits on the catalysts and down stream equipment and the physical erosion of some catalysts. Studies showed that ammonium bisulfates were forming, and they were depositing on the equipment or mixing with ash particles and the mixture was depositing on the equipment. Considerable Japanese additional product development was undertaken jointly by the utilities and the catalyst developers. The trade offs between the various operating parameters resulted in catalysts that had a wide operating range but also had considerable performance variability over the range. The trade off is illustrated in Figure 2 which shows the NO_x performance and the oxidation of sulfur dioxide to trioxide as a function of the flue gas temperature.

Most coal applications (especially high fuel sulfur applications) need to have the oxidation potential below 1% if ammonia salt (sulfite and bisulfate) problems are to be eliminated. The Japanese utility-supplier development teams eventually developed a long life, reliable SCR system for reducing NO_x emissions. Their approach included (5,6): changing the catalyst materials to control the reaction; using a dummy initial section or providing flue gas velocity controls to resist erosion of actual catalyst material; having the SCR provide a total of 80% or less NO_x control from the NO_x concentration that entered the SCR housing (however, recent designs have increased the NO_x removal to 90+ %); reformulating the catalyst designs to reduce its potential to oxidize sulfur dioxide to sulfur trioxide; reducing of the amount of ammonia injected by about 10-15 percent from the design specification (and thus lowering the attainable NO_x reduction); operating the SCR only during steady operations (it often is operated during slow transients); employing strict limitations on low temperature SCR operations; and operating with low sulfur fuels and low ash content coals. Because of continuing problems with instrumentation, control of the process has been based upon using calculated values of NO_x and ammonia, the measured values are principally used as a trim signal for the control setting (however, recent German designs have been able to use measured NO_x values as a control signal). The result has been the elimination of the severe fouling of the catalyst and down stream equipment and the erosion of the catalysts that was experienced during the initial commercial applications. Stable, long term, effective NO_x control is now being reported.

Although the Japanese design are for 80-85% NO_x removal, the plants usually operate at 70-75% removal. This reduction in NO_x removal efficiency was accepted in order to assure that the plant availability remains high, and it was also done in recognition that the instrumentation was not accurate enough to control the process at the very limit of its capability with a high level of confidence needed in the Japanese plant operational plans.

However, recent reports indicate that improved catalyst and system designs and operating controls allow for the operation of the NO_x removal at its full design rate.

In Japan, although the basic SCR system has remained relatively unchanged from the initial designs, the catalyst itself has been the subject of continuing improvement through research and development. During the decade of 1980 to 1989, the Japanese catalysts have become 15-20% more reactive in their NO_x conversion ability while reducing the pressure drop across the catalysts by 5-10% and the volume required to house the catalysts by up to 60%(7).

Flue gas flow straighteners to reduce flow maldistributions at the SCR reactor inlet, the use of flue gas velocity upper limits in the catalyst region, and the use of parallel flow catalyst geometries helped control erosion and plugging problems (plate type catalysts are now predominantly used for coal-fired service). The use of fuel additives normally used in boilers to keep the burners clean had to be suspended as another measure to control catalyst plugging by dust. In recent German work(8) with oil-fired boilers additives were developed to reduce the impact of high vanadium content oils on the formation of SO₃ during combustion. The additive has been successfully tested in pilot plant and operating plant studies, however the tests did not involve SCR units. Nevertheless, the German SCR suppliers are reporting this work as having demonstrated that they can use additives without harming the SCR system.

Extensive work has been performed on the modeling and design of the ammonia injection system in order to provide a well mixed, uniform distribution of ammonia into the SCR reactor. Multiple rows of catalyst sections are used in the SCR reactor (up to 7 separate rows have been employed, but 3 to 5 is normal(9)), and careful control of ammonia injection is used to help reduce ammonia slip (ammonia slip is the amount of ammonia that bypasses the SCR unreacted). Ammonia slip of 10-20 ppm was initially considered acceptable, but 2-5 ppm at the end of the catalyst life is now the current Japanese practice (in Germany the slip is typically less than 1 ppm). The limiting of the amount of excess ammonia also reduces the duty on the catalyst and the potential to produce bisulfates. The result has been a more rugged and longer life catalyst, but that solution has been a tradeoff since it has lowered by 10-20% the amount of NO_x reduction that can be achieved in actual operations.

Both metal and ceramic base materials are used for holding the active catalyst material in place. The metal is more resistant to breakage and generally leads to a lower gas pressure drop. The ceramic is lighter in weight. Both designs are suitable for many applications, estimated costs seem to be a major factor in the selection process. Heck et. al.(10) have argued that plate catalysts are preferred for high sulfur applications as they are easier to formulate for low SO₂ to SO₃ oxidation potential. Spitznagel et. al.(11) have reported that in Germany plate type designs are preferred for high dust applications or where a high fault tolerance would be desirable

(fault tolerance was defined as unplanned for conditions such as poor flue gas distribution, highly erosive fly ash in the flue gas, etc.).

The start-up and shut down of the plant and the SCR system can be an item of concern. The main SCR problem during these operational periods is the potential for damage to the catalyst by oil or oil mist and soot or moisture. The plant start-up is normally done with a light fuel oil until the exhaust gas temperature is proper for SCR operation. The Japanese (and the Germans) do not operate their SCR systems during the start-up and shut down periods. For each operating system there is a minimum flue gas temperature, below which operation with ammonia injection favors bisulfate formation with its potential deposition problems. Fires in the SCR catalyst due to ignition of uncombusted start-up heavy oils that had deposited on the catalyst surface have occurred in Japan(7). This suggests that in the U.S. for those plants that have a high unburned carbon carryover, control of carbon deposition in the SCR housing will be a special design consideration.

An important maintenance activity is the actions taken to control or remove soot and ammonium bisulfate deposits(6). Different utilities use different but related approaches. For example, at the coal-fired Shimonoseki Station, on-line soot blowing of the air preheater is done three times per day for two hours at a time (in Germany, normal soot blowing is once per shift, even if there is no SCR installed). Blowing is done from the hot and the cold side of the unit. Two tons of steam per hour are used. At other plants, water washing is used, using up to 2,500 tons of wash water per wash for a 375 MW boiler system. This introduces ammonia and other minerals into the waste water system, which requires additional environmental processing before the water can be released off site. It is noted that washing does not replace soot blowing requirements, and it can not be performed while the SCR is hot. It is, however, an effective way to remove bisulfate deposits from the SCR housing. It is not expected to be used more than once or twice a year.

Of special interest for U.S. considerations(12) is the special example of the Takehara Station Unit #1, a 250 MW coal-fired boiler. It burns a 2.3-2.5% sulfur coal. Because of the sulfur, the sulfur dioxide loading in the flue gas is 1,800 ppm. To control the formation of sulfur trioxide, and subsequently ammonia bisulfate production, a catalyst that only converts 0.1-0.2% of the dioxide to trioxide was developed. This performance occurs if the ammonia slip is limited to less than 0.2% of the injected ammonia. At such conditions, the maximum NO_x control is less than 70%. At NO_x control above 85%, the dioxide conversion increases to about 1%. In addition to bisulfate concerns, it was found that the coal ash deposits CaSi on the catalyst surface, which acts to decrease the catalyst activity. In low dust operating configurations, that causes a 10% catalyst deactivation after about 20,000 hours of operation. In a high dust operation, the catalyst deactivation would be about 40% during the same time period.

German Experience

1983 legislation in West Germany (Federal Republic of Germany) imposed stringent regulations to drastically reduce NO_x emissions from large boilers(13). The German utilities conducted over 70 pilot plant demonstration tests to prepare for the transfer of the Japanese SCR technology to German operating conditions. The Germans used both slagging and non slagging boilers (wet and dry bottom) and only low temperature ESPs. Their coals included more ash and sulfur than that typically used in Japan. During the pilot plant tests, it was found that the practice of recycling part of the ESP fly ash to the boiler for slagging and disposal increased the arsenic content in the flue gas (arsenic was a trace element in the coal ash). The resulting concentration was enough to poison the SCR catalyst, so the tail end or cold side SCR configuration was selected to mitigate this. With the SCR placed after the FGD, it was felt that the SCR would only have to treat a very clean flue gas. The retrofitting of NO_x removal systems on existing West German boilers larger than 110 MWe was completed by 1990, resulting in an average 70% reduction in utility plant NO_x emissions.

Design and operation by West German electric utilities for installation of SCR has included the following general considerations(14,15):

High Dust SCR Configurations. Prior Japanese SCR experience for coal is not broadly applicable.

- German plants burn a wide variety of low-rank domestic coals as well as coal cleaning waste (middlings) i.e. ballast coal with a high content of inerts and impurities; Japanese power stations typically burn high-quality imported coals.
- Slagging-type boilers are common in Germany, but not in Japan.
- At least 90% NO_x removal is required at some German plants while Japan utilities typically had to accomplish no greater than 80%

The SCR reactor housing is arranged to receive standardized catalyst modules, e.g. 2 m x 1 m, that can accommodate either honeycomb or plate catalysts. See Figure 3 for plate and honeycomb reactor comparisons. Plate types of catalyst have a higher resistance to deposition and erosion from the flue gas particulates, the honeycomb is self-supporting and allows for greater catalyst exposure and thus less catalyst volume(11) and is preferred in tail end or low dust designs. This design approach provided for a maximum competition among all suppliers of replacement catalyst, which ultimately had the impact of a 50% reduction in the costs of catalysts (while in Japan standard modules were not specified and thus each supplier tailored its design to unique physical dimensions. As a result, while in Germany the catalyst costs decreased, in Japan they were steady or rose slightly(9).

Detailed flow model testing is routinely used to help ensure adequate flue gas flow distribution in the SCR reactors. For a few power stations, a by-pass around the SCR reactors was used at boiler start-up and shut down

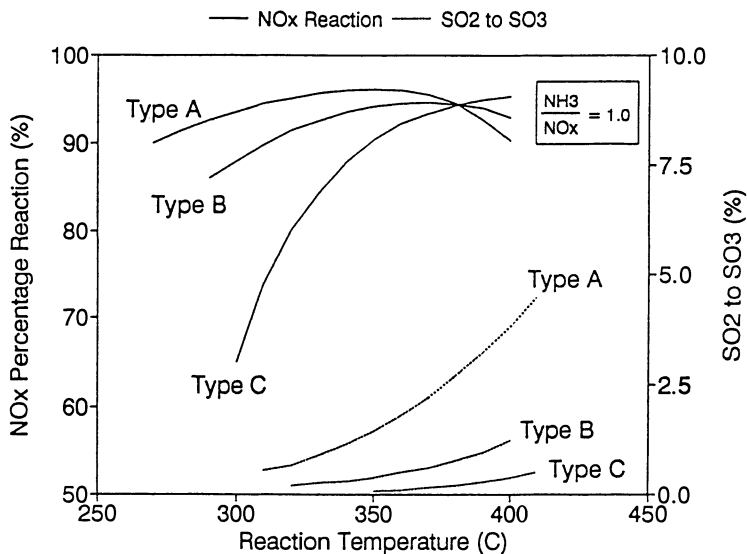
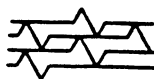
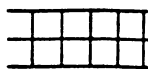


Figure 2. Typical SCR Catalyst NO_x Reduction and Oxidation Performance



Honeycomb

Plate

Figure 3. Configurations for Parallel Flow SCR Reactors

to avoid the hazard of fuel residue deposits on the catalyst. The need for a by-pass depends upon the boiler type, coal burned, number of shut downs per years, etc. and in many cases it has not been required.

Anhydrous liquid ammonia supply, typically shipped only by rail or sea, is invariably used (except when aqua ammonia is mandated, as for plants in populated areas). In some instances, government regulations call for double-wall designs for ammonia pipes and tanks as well as the use of underground tank placement while incorporating a means of preventing entry of ammonia leakage into the underlying soil. Such strict design requirements have resulted in doubling and tripling of the cost of the ammonia storage and supply systems. In high dust installations, almost 90% of the ammonia slip is absorbed on fly ash particles. It takes very little ammonia to make ash unsalable. The odor threshold is reached when ammonia content reaches 80 mg/kg of ash - equivalent to 3 ppm ammonia slip measured at the air-heater inlet when firing ballast coal, or 1.5 ppm when firing high-quality, low-ash coal.

To preserve catalyst life in high dust SCR installations in wet bottom boiler service, it has been necessary in some stations but not all to modify plant operation so as to recycle to the furnace only a portion of the fly ash catch usually so remelted. New German arsenic resistant SCR catalysts have removed this restriction on fly ash recirculation(16). Additionally, lime or limestone may be added to the coal to limit the poisoning effect of arsenic by bonding it as calcium arsenate.

In earlier designs to maintain temperature during part load and cyclic boiler operation, an economizer by-pass was provided, either on the flue gas or feedwater side. This expensive addition and complication is not required for the tail end SCR configuration. As noted above, new high dust SCR designs coupled with soot blowing have allowed the German designers to eliminate the need for an economizer by-pass.

Catalyst designs with a pitch of 7.0 to 7.5 mm have proved themselves in high-dust application. While this is true for both the plate and the honeycomb systems, the plate type appears to be less susceptible to fouling as well as to abrasion by fly ash(11).

In spite of the extensive pilot plant testing, initially some operational problems were encountered. The most significant have been the poisoning of the catalyst with alkali materials or arsenic from the trace amounts present in the coal ash and the impacts due to oxidation of SO_2 to SO_3 . Most poisoning problems occur if the total alkali content in the coal ash is greater than 10% by weight(21), but problems have occurred when the weight concentration is as low as 4%. Normally, the main alkali problems have been associated with arsenic and potassium. However, most of the operational problems were not catalyst related, they were typical scale-up problems such as flow distributions or temperature conditions. In all cases, the Germans have reported that they now understand the basis for any problem that occurred, and that there have not been repeat problems in their later plants.

There have been instances of significant corrosion as well as visible sulfuric acid mist discharge from the stack. Weiler and Ellison(15) report a tendency of the SO₃ to foul the air preheater by sulfuric acid caking and condensation. These conditions are aggravated by low ash content coal. Even with gross SO₂ emissions of only 1,500 to 2,000 mg/Nm³, (540 to 720 ppmv), precautions are necessary to minimize the rate of SO₃ formation in the catalyst reactor. With SO₃ concentrations of over 30 mg/Nm³ and fly ash loadings of only 10,000 mg/Nm³, preheater plate surfaces must be enameled and washed periodically (air preheater redesigns have eliminated the need for washing). With low-grade coal, acid condensation problems on downstream equipment has occurred, air preheater fouling has not been encountered, and high fly ash loading (60,000 mg/Nm³) is believed to adsorb and thereby counteract a significant portion of the SO₃ formed. The potential for the release of acid aerosols from the stack is a significant problem since wet FGD systems are designed for SO₂ absorption and typically cannot completely reduce sulfuric acid aerosol emissions. To correct this, sootblowing schedules have been modified to keep the boilers cleaner and flue-gas temperatures have been lowered to between 350° and 365°C (660° and 960°F) to reduce SO₃ concentrations at the air-heater inlet from 80 mg/m³ (22 ppm) to 20 mg/m³ (6 ppm).

The SCR system can also impact the wet limestone FGD system(17) by oxidizing manganese in the limestone. This results in a dark solid that makes the FGD catch (gypsum) unsalable in Germany. Also, there is a concern that the high dust SCR may oxidize mercury, which makes it soluble. The mercury then would contaminate the FGD waste water system. In any case, ammonia contamination of the FGD waste water has occurred, but only when the ammonia slip was allowed to be above 5 ppm. These SCR/FGD interactions could, in the U.S., increase the requirements for water treatment environmental controls; in Germany all wet FGD plants are equipped with waste water treatment plants.

Although the designs were based upon extensive catalyst testing, in some plants(18,19) the original estimated lifetime and the control of ammonia slip could not be simultaneously achieved. Also, the asymptotic decrease in catalyst activity experienced in pilot plants became a linear decrease in activity in operating plants (this may not be a real phenomenon but only a reflection of the uncertainties in the catalyst activity measurements). However, the catalyst life usually met the supplier's guarantees.

Tail End or Cold Side Configurations. Rotary regenerative heat exchangers principally are used to raise the flue gas temperature to the SCR operating condition. Additional heat exchangers are need to assure proper temperature regulation. The SCR reactors do not require catalyst cleaning. The penalty in power plant efficiency can be as great as 1-3%. Also, with the use of rotary regenerative heat exchangers the internal raw gas leakage has been disadvantageous (4-5% leakage), particularly at part load. The smaller the plant, the greater has been the leakage.

Tail end systems entail high operating expenses because of the intermediate flue-gas heating required and the added fan power requirements to send the treated flue gas to the stack. Honeycomb catalysts using a pitch of 3.6 to 4.2 mm that have been almost exclusively applied for tail end applications have proven themselves in this service without the need for soot blowing.

In specific German power plant applications utilizing Ljungstroem heat exchangers both for FGD reheat and for boosting SCR inlet temperature, unique catalyst fouling has occurred. In some German tail end installations, after only a few thousand operating hours, an extremely high fall off in catalyst activity was observed, particularly in the first layers of the plate type modules(20). This decline in catalyst effectiveness was attributed to the formation of a coating of silicon compounds on the catalyst surfaces, generally caused by the presence of silicon fluoride (SiF_4). Sulfuric acid, which condenses onto the FGD flue gas reheater plates, traps SiF_4 and HF. These compounds combine and later split at the clean gas side into highly corrosive hydrogen fluoride and SiF_4 . Solution to the problem proved to be the injection of lime hydrate downstream of the ESP. This compound reacts with acid gases to form calcium sulfate, calcium fluoride, and other calcium halide compounds. These solids are removed either in the FGD unit or by sootblowing after they deposit on the plates in the flue gas reheater.

In the case of a low dust SCR system installation serving a wet bottom boiler, catalyst fouling was a special problem. After a service time of 10,000 hours, ammonia slip rose to more than 10 ppm in order to maintain an 86% design NO_x removal efficiency. Deposition of silicon-based material was determined to be the sole reason for this catalyst surface poisoning, and the condition has since been resolved.

Application of SCR Technology to US High Sulfur Coal Service

It is clear that there is not a single best SCR design configuration. Each has advantages and disadvantages, and ultimately site-specific conditions will dictate the final selection. Table I shows the results of prior commercial decisions.

The Japanese decision were made mostly in the 1970s and early 1980s and were applied to both new plants and to retrofits to existing plants. The primary basis for selecting the high dust or low dust configuration appears to have been based on an analysis of the problems that might occur due to particulate material impacting the catalyst and also on the availability of a high temperature ESP.

In West Germany, the decisions were made in the early to mid 1980s and were applied predominantly as retrofits to existing plants. The decisions to select the tail end configuration appears to have been made on the basis of concern for catalyst poisoning in the slagging boiler plants where the ESP fly ash was recirculated (in whole or in part) back to the boiler to be slagged

for disposal or because space limitations precluded the use of high dust designs. However, this are a significant number of high dust SCR systems on German slag tap boilers. As noted above, that increased the concentration of alkali materials (e.g., arsenic, etc.), which were found to deactivate the catalyst. Otherwise, the tail end configuration was considered to be too expensive due to its flue gas reheat requirements.

TABLE I. SCR Distribution in Utility Coal-Fired Power Plants
SCR Percent of Installed Boiler Capacity

SCR Configuration	West Germany(16)	Japan(7)
High Dust	63	66
Low Dust	1	34
Tail End	36	-

Perhaps the single most important conclusion is that in spite of extensive development in both Japan and Germany, design and design scale-up problems have occurred when the pilot plant designs were scaled to commercial size (however, in all cases the plant operators and SCR suppliers have been able to overcome any operational problems and to continue to provide significant NO_x control with the SCR systems). Coal sulfur levels are often higher in the U.S. compared to Japanese and German experience. These concerns have used to justify the need for a U.S. pilot plant program, but the information also suggests that it will be difficult to anticipate all of the U.S. commercial operating plant conditions in the pilot plant operations. The U.S. has such a program underway, but unfortunately the system designers who successfully developed designs in Germany and Japan are not always included in the teams developing the U.S. pilot plants. Pilot plant operational problems have been reported:

- Significant catalyst deactivation either due to surface contamination or poisoning.
- Greater than expected ash loading and plugging on the catalyst.
- Silica deposition on the catalyst in a tail end configuration, suggesting an unanticipated fly ash interaction at this location.
- SO₃ formation in the tail end applications, leading to bisulfate deposits in the reheat heat exchangers.

The adverse effects of SO₂ to SO₃ conversion by high dust SCR systems in Germany have been most pronounced at power stations firing high grade (low ash content) coal that experience frequent boiler load swings and weekend shutdowns. This problem is also associated with operating boilers under fouled steam tube conditions, which increase the boiler outlet temperatures by up to 30°C. This type of operating condition is anticipated in U.S. plants. The higher flue gas temperature will increase the SCR SO₂ to SO₃ conversion rate, leading to a significantly increased potential for

bisulfate formation. This could be particularly troublesome in high sulfur coal operations.

In some German high dust SCR applications firing high-ash coal cleaning waste (middlings) with a total solid particulate loading as high as 60,000 mg/Nm³ (26 grain/DSCF), honeycomb type catalysts have had to be replaced by plate type catalysts to gain higher abrasion resistance and for reduced susceptibility to fouling by gas-borne fly ash. This condition may be important for many U.S. applications.

Conclusions

The U.S. applications at plants that experience large load swings or daily shut down and start-up will be challenging. These operational conditions have not been examined in great detail in Japan. There has been more detailed consideration for such daily operational requirements in Germany, many of their plants experience similar operating patterns. In addition, the regulators in those countries have allowed a time period during start-up or shut down when the NO_x control is not required. This is done to assure that the catalyst is not deactivated by bisulfates which could form at low temperature operational conditions that occur at start-up and shut down. However, U.S. regulators have historically required control during all transient conditions. This remains an unproven SCR operating condition that needs special attention for U.S. applications.

Most problems probably can be avoided if the U.S. SCR system suppliers rely upon commercial Japanese and German plant experiences when the operating conditions (e.g., coal quality, operating transients, etc.) are similar to the expected U.S. conditions. When conditions change from the existing experience base, it will be even more important for the U.S. suppliers to have detailed access to the Japanese and German suppliers. Also, pilot plant studies can be used to help reduce the level of uncertainty for a specific U.S. application, but it is important to re-emphasize that the pilot plant test results are not always directly transferable to full-scale plants.

Literature Cited

1. Sloss, L.L.; "NO_x Emissions From Coal Combustion", IEACR/36, March 1991.
2. Behrens, E.S.; "KHI Operating Experience of SCR on Coal Fired Utility Boilers and High Sulfur Industrial Fuel", Proceedings of the 1991 EPRI/EPA Joint Symposium on Stationary Combustion NO_x Control, Washington DC, March 1991.
3. EPA; "Evaluation and Costing of NO_x Controls for Existing Utility Boilers in the NESCAUM Region", EPA 453/R-02-010, December 1992.

4. EPA; "Retrofit Costs for SO₂ and NO_x Control Options at 200 Coal-Fired Plants", EPA 600/S7-90/021, March 1991.
5. Lowe, P.A.; "Selective Catalytic Technology", Burns & Roe Service Corp. report to the U.S. Department of Energy, December 1989.
6. Lowe, P.A.; Ellison, W.; "Understanding the German and Japanese Coal-Fired SCR Experience", Proceedings of the 1991 EPRI/EPA Joint Symposium on Stationary Combustion NO_x Control, Washington DC, March 1991.
7. Hjalmeresson, A-K; "NO_x Control Technologies for Coal Combustion", IEACR/24, June 1990.
8. Huettenhofer, K.; Spitznagel, G.W.; Sigling, R.; Rummenhohl, V.; "Effects on Catalytic Activity and SO₂/SO₃ Conversion of DeNO_x Catalytic Convertors Downstream of Oil-Fired Power Plants: Causes and Remedial Measures", to be published American Chemical Society.
9. Ando, J.; "Recent Developments in NO_x Abatement Technology in Japan", Bulletin of the Faculty of Science and Engineering, Chuo University, Vol. 32, 1989.
10. Heck, R.M.; Chen, J.M.; Speronello, B.K.; "Commercial Operating Experiences with High Temperature SCR NO_x Catalysts", 86th Annual Meeting Air and Waste Management Association, Denver, CO, June 1993.
11. Spitznagel, G.W.; Huttenhofer, K.; Beer, J.K.; "NO_x Abatement by SCR Catalysts", Proceedings of the American Chemical Society meeting April 1993, to be published.
12. Behrens, E.S.; Ikeda, S.; Yamashita, T.; Mittelbach, G.; Yanai, M.; "SCR Operating Experience on Coal-Fired Boilers and Recent Progress", Proceedings of the 1991 EPRI/EPA Joint Symposium on Stationary Combustion NO_x Control, Washington DC, March 1991.
13. Ellison, W.; "Assessment of SO₂ and NO_x Emission Control Technology in Europe", EPA-600/2-88-013, February, 1988
14. Rummenhohl, V.; Weiler, H.; Ellison, W.; "Experience Sheds Light on SCR O&M Issues", *Power*, September 1992.
15. Weiler, W.; Ellison, W.; "Progress in European FGD and SCR Applications". The 1990 SO₂ Control Symposium, New Orleans, LA, May 1990.

16. STEAG AG listing of German SCR Installations, 1992.
17. Gutberlet, H.; Dieckmann, H.J.; Schallert, B.; "Effects of SCR-DENOX Plants on the Downstream Parts of the Power Plant", *VGB Kraftwerkstechnik* (in German), 71 (6), June 1991.
18. Kitto, J.B.; LaRue, A.D.; Kulig, J.S.; "Coal-Fired NO_x Emission Control Technologies", Proceedings 6th Annual Pittsburgh Coal Conference, September 1989.
19. Lehmann, B.; "Experience Gained From the Flue Gas Purification Units for SO₂ and NO_x in the Power Stations of Neckarwerke Elektrizitätsvergnungs AG", United Nations Economic Commission for Europe, 5th Seminar on Emission Control Technology, Nuremberg, June 1991.
20. Ellison, W.; Weiler, H.; "Stack Gas Cleaning Optimization via German Retrofit Wet FGD Operating Experience", The 1991 SO₂ Control Symposium, Washington, D.C., December 1991.
21. Hjalmarsson, A-K; "Interactions in Emissions Control For Coal-Fired Plants", IEACR/47, March 1992.

RECEIVED September 30, 1993

Chapter 16

Low-Temperature Selective Catalytic Reduction NO_x Control

Phillip A. Lowe

Intech Inc., 11316 Rouen Drive, Potomac, MD 20854-3126

The early German applications of SCR NO_x control technology to slagging coal-fired boilers were based upon Japanese technology. Unanticipated problems such as catalyst poisoning by arsenic led the Germans to commercially develop a different SCR configuration, called the tail end or cold side application. Initial tail end applications used the Japanese/German SCR technology developed for 300-400 °C operation for an SCR application where the flue gas was at 90-150 °C. This resulted in a considerable economic penalty to reheat the flue gas to the SCR operating temperature. This paper discusses operational experience and new catalyst formulations that suggest that the tail end configuration may now be more economic than other SCR configurations, especially for U.S. coal-fired retrofit service.

Low Temperature SCR Experience

A companion paper(1) describes the development of SCR technology in Japan and Germany. Essentially, three configurations have been developed for locating the SCR reactor in the flue gas: the high dust design where it is located before the particulate control and is subjected to all of the contaminants in the flue gas but where the flue gas is in the catalyst's operating range; the low dust design where a high temperature particulate control is installed and the SCR can be located downstream of that device; and the tail end design where the SCR reactor is located downstream of the sulfur control process where the resulting clean flue gas temperature is below 150 °C. The configurations are shown in Figure 1.

The Germans operated over 70 pilot plants to test Japanese SCR designs under German coal-fired utility boiler operating conditions. From these tests and a few of the early operating systems on several wet bottom

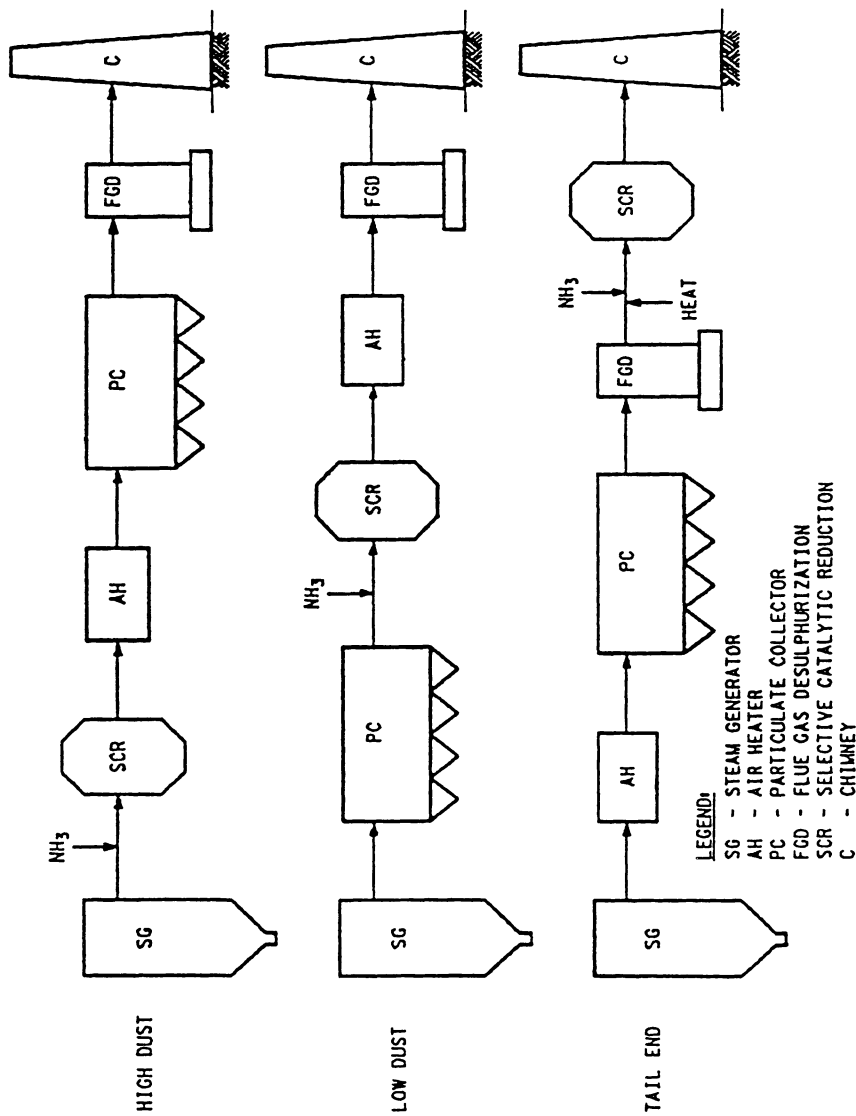


Figure 1. SCR Location Configurations

(e.g., slagging boilers) boilers, an unexpected premature deactivation of the catalyst was observed. It subsequently was found that the practice of recycling the fly ash catch from the particulate control back to the boiler to slag it also recycled the trace impurities of the coal ash. Alkali materials and especially arsenic were concentrated in the flue gas by this process, and their resulting concentrations poisoned the SCR catalysts. One solution to this problem was to place the SCR catalyst reactor downstream of all of the flue gas treatment processes (the particulate and the acid gas controls). At this location, the SCR treated a relatively clean flue gas. However, the flue gas had to be reheated from its final temperature back to the SCR operating temperature. This resulted in a 1-4% penalty in the overall thermal efficiency of the power plant, a very significant cost. In addition, the initial cost estimates assumed that the tail end catalysts would have the same operating life as those that operated in the contaminated high dust flue gas configuration, and in fact the early applications used the same SCR catalyst formulations rather than reformulating the catalyst to take advantage of the very clean operating environment of the tail end configuration. For a number of site specific reasons, the initial tail end SCR systems cost nearly three times the initial capital than did the initial high dust systems. These economic conditions (the failure to optimize the tail end SCR to its operating conditions, the flue gas reheat penalty, and the high capital costs for the initial tail end applications) resulted in a conventional wisdom that the high dust configuration is more economic and is the preferred SCR configuration. As is often the case with conventional wisdom, it does not keep up with new developments and thus may not generally be applicable to many new situations.

There have been a number of specific problems with the high dust configuration. It is recognized that in each case where a problem has been identified the designers and plant operators have made adjustments to allow the continued operations of the plant. Thus, many of these problems have been "solved", although if the same conditions do not exist at the next plant the solution may not be applicable or at least optimized. Thus, it is instructive to consider these issues and how they impact high dust configuration applications. These include:

1. The high dust system may significantly restrict the operating range of the boiler since the flue gas must be delivered at above 300 °C or else catalyst poisoning by bisulfates can occur in addition to the failure of the catalyst to provide the required level of NO_x reduction. To address this, boiler economizer bypass ducts have been installed, especially if the plant is to cycle to low power levels. When this is done, the plant thermal efficiency deteriorates significantly at low power conditions, a fact usually not addressed in cost comparisons between the high dust and tail end designs. Of course, if a low sulfur fuel is used or if boiler cycling is not required, this concern may not be relevant.

2. The high dust system requires the installation of soot blowers and the use of a dummy initial catalyst section. The soot blowers are required to control the dust buildup on the catalysts, which can block the flow distribution and reduce the overall NO_x reduction while increasing the ammonia bypass. The dummy catalyst layer is a sacrificial element which the initial dust particles impact and erode rather than impacting and eroding the catalyst itself. In the U.S., the catalyst is composed of metals that are considered as being toxic, thus any erosion of the catalyst may lead to serious air toxic emission problems. However, it is noted that new catalyst formulations are more resistant to erosion and if the fly ash is soft enough they may eliminate the need for sacrificial material. However, when sacrificial material and soot blowing are required, the resulting larger more complicated reactor system increases its capital and installation costs (soot blowing has been reported to increase the capital costs by about five percent).
3. In a high dust system the most highly reactive catalysts can not be used because such catalysts also convert SO₂ to SO₃. Sulfur trioxide can form sulfuric acid which attacks the flue gas ducting and downstream equipment, it also forms ammonium bisulfate, a sticky material that plugs and fouls downstream equipment. The use of less reactive catalysts results in the need for larger SCR reactors with their inherent impact on capital costs and places very stringent control requirements on the ammonia injection system (ammonia bypass of the SCR reactor must be less than 5 ppm and often less than 1-3 ppm). Restricting ammonia flow means that the upper limit of NO_x control is effectively less than 90% and probably less than 80-85%. A net result of these conditions has been that the catalysts have an operating life of about 2-4 years (some plants have operated for 5 years before additional catalyst material was required). It is noted that more reactive catalysts that still limit the conversion of SO₂ to SO₃ has been an area of active research. Thus, new catalyst formulations may reduce the impact of this concern.
4. In Japan over time, the operational control of the startup period at one plant became lax (not an unusual condition in a power plant). As a result, unburned fuel left the boiler and become imbedded in the dust on the SCR reactor. Subsequently, the SCR reactor oxidized the fuel and the resulting fire caused considerable damage. Although this problem is not an inherent problem with high dust SCR designs, it does demonstrate the coupling between the boiler and the high dust configuration SCR reactor, which can cause restrictions on the boiler operation.
5. Usually in retrofit conditions, there is very limited space available near the boiler for locating the high dust SCR reactor. When the SCR is to be connected to the duct work, the plant outage is long and may take over several months to complete. If the boiler walls must be penetrated in order to install bypass ducting, the costs and time delays can be significant. Plant shutdown increases costs as replacement

power must be purchased during the plant shutdown period. Most economic comparisons between high dust and tail end configurations ignore this important cost element. Although new construction sequencing concepts can reduce the down time required, high dust systems are inherently more difficult and time consuming to install in retrofit than are tail end configurations.

6. The use of slagging boilers that increased the concentration of arsenic in the flue gas lead to catalyst poisoning. One of the initial solutions was to introduce the tail end configuration or to modify the boiler operation to eliminate the recycling of fly ash to the boiler (now some new catalyst formulations are more resistant to arsenic poisoning and can be used in high dust, slagging boiler applications). In addition, some slagging boilers have been found³ to produce SiF₄, which under some part load conditions can deposit silicon on the catalyst of a high dust system. The silicon acts as a poison. This illustrates that all of the potential deposition/poison conditions may not be recognized before plant operations occur. While the same concern can be stated for tail end configurations, their inherently cleaner operating environment lowers the potential for such an unanticipated problem to occur.

There are a number of specific advantages, and some problems, associated with the tail end configuration:

1. As noted above, the flue gas must be reheated to the SCR operating temperature, which can cause up to a 4% reduction in the plant efficiency. As a result, several catalyst vendors and plant operators are developing low temperature SCR catalysts. With the newer catalyst formulations becoming available, it appears that the penalty can be limited to a 1% or less decrease in the plant thermal efficiency.
2. In a tail end system, the SCR is decoupled from the boiler and thus all part load operations can be performed as needed. Also, very importantly, boiler upsets and changes in the trace impurities of the fuel do not apply a direct impact on the SCR catalyst. Thus, the tail end design is inherently more flexible in terms of being able to successfully accommodate future (and presently unanticipated) changes in the power cycle or fuel. Since the system may have to be applied for over 40 years, this provides a significant increase in the plant owner's ability to accommodate changes that though presently unanticipated will nevertheless occur.
3. Tail end SCR designs can take advantage of the relatively clean flue gas (small trace element concentrations, low SO₂ concentrations) to use a highly reactive catalyst. This decreases the catalyst volume; at present the volume is typically one half of that required for a high dust design(13). Also, the catalyst life in clean flue gases has been demonstrated to be 10-15 years. These conditions significantly decrease the initial capital costs of the system as well as the ongoing operating costs.

4. Ammonia bypass can be set by environmental considerations and not to control the formulation of bisulfates (however, if a recuperative heat exchanger is used the ammonia slip and overall NO_x removal efficiency of the SCR system is lowered). However, a larger allowable ammonia discharge means that the catalyst can be operated with confidence over the full operating life at 90+% NO_x removal efficiencies.
5. Aside from the very first few installations, the net impact of all of these considerations has been that the tail end SCR costs, in practice, have been the same or lower than similar sized high dust systems.

Perhaps the best indication of the desirability of a given SCR design is the choice of the market place. Krueger(2) has identified the installed capacity (MW thermal) and the number of individual SCR units used at German and non German VGB affiliates. The details of the non German affiliates were not provided, but Table I shows the results for the German utilities. It shows that the initial applications selected the high dust configuration. But more of the newer plants have used the tail end configuration.

New Operating Information and SCR Designs

Some German plants(3) reheat the flue gas using a rotary heat reheater that introduces a small amount of hot untreated flue gas into the flue gas downstream of the desulfurization unit but upstream of the SCR unit. The introduced impurities have led to contamination of the SCR catalysts. The solution has been to improve the thermal efficiency of non contact reheaters or to use natural gas or some other clean fuel to reheat the flue gas prior to its being treated by the SCR system. However, the loss of catalyst activity in tail end applications has been much less than that experience by high dust systems(4), and the loss of catalyst activity in many of the high dust systems has been less than originally expected(5). Plants in Japan with SCR reactors treating flue gas with a cleanliness similar to that found in tail end plants have experienced 11-15 year catalyst lives(6).

The high dust SCR system has been found to affect the flue gas desulfurization (FGD) process at some plants(7). Sulfuric acid formed by the SCR catalysts has oxidized manganese in the FGD process, making the FGD sulfate product unacceptable to the building industry. Mercury oxidized by the SCR catalysts becomes soluble and ends up in the FGD waste water, complicating its treatment process. Tail end configurations do not have these complications. One interesting approach to controlling the sulfuric acid formation in high dust systems is to burn coals that have alkali ash or else a small amount of lime is added to the coal. The theory is that the lime or alkali neutralizes the acid as it is formed.

One of the early promising low temperature SCR designs was developed by Stadtwerke Duesseldorf(8,9,10). In this process, a two reactor system based upon using activated lignite coke or activated coke was

Table I. German SCR Utility Applications²

Year	High Dust SCR Capacity, MW _t	Application Number	Tail End SCR Capacity, MW _t	Application Number
1985	1468	3	-	-
1986	2100	3	-	-
1987	3352	5	2142	6
1988	11580	14	3398	5
1989	11421	19	16230	25
1990	8691	12	9764	33
1991	1916	3	241	5
1992	-	-	900	2
1993	1637	2	-	-

designed and installed at the 1000 MW Lausward electric power plant, the 200 MW Garath district heating plant, and the 200 MW Flingern refuse-to-energy plant. The utility Stadtwerke Duesseldorf has installed the system at 11 plants that treat over 5 million m^3 of flue gas(11).

In the Duesseldorf two reactor process, the first reactor bed is downstream of the FGD unit. It acts as an SO_2 polisher in that it removes the final SO_2 contamination from the flue gas. It also removes fine dust, metals such as mercury, other acid gases such as HCl, and for the incinerators it removes dioxins and furans. Since the metals and other toxic materials are removed in the first 100-200 mm of the bed, the bed is segmented to collect the trace materials in the leading section and the sulfur loaded carbon in the second section. This aids in subsequent disposal or recovery treatment of the spent activated carbon. Ammonia is added downstream of the first activated carbon reactor and the second reactor acts as a SCR catalyst removing the NO_x . These reactors operate at 90-120 $^\circ\text{C}$, thus they eliminate the need for flue gas reheating and the 1-4% thermal penalty associated with that process. Stadtwerke Duesseldorf has found that the operating costs of the activated carbon total process system is about one half of that of a similar metallic SCR catalyst system, both operating in a tail gas system. The operating costs are similar to those of a high dust system, but because of the ability to construct the tail gas system while the plant was operating (and thus avoiding a long down time to install the SCR system), the activated carbon system's capital costs are less than those estimated for a high dust system(8).

In this design, as the first reactor becomes loaded with sulfur or trace elements such as mercury, it is discharged and the spent bed material is sent to the boiler where it is blended with the fuel. Thus, the particulate and FGD systems are the sole points for removal of toxic and acid materials, and their design can be optimized for such service. Fresh activated carbon is added to the first reactor from the SCR reactor, and fresh activated carbon is added to the system at the SCR reactor. This system reduces the NO_x from 1,800 to 200 mg/m^3 (about 900 to 100 ppm), under special operating conditions 150 mg/m^3 was achieved(9).

However, the utility needs to achieve 100 mg/m^3 NO_x discharges (which are achievable by the metallic SCR catalysts), so they are examining other catalysts to replace the activated carbon NO_x control portions of the system. They are examining zeolite and titanium oxides which will operate at 100-120 $^\circ\text{C}$ (zeolite) or 170-250 $^\circ\text{C}$ (titanium oxides). These catalysts will require some flue gas reheating. Zeolite can be considered as a potential catalyst because of the clean nature of the flue gas. In a high dust environment, earlier German pilot plant tests showed that the zeolite became plugged and then failed prematurely. Although it is more expensive to operate the catalysts at the high end of their temperature range due to the need to reheat the flue gas, the zeolite and titanium catalysts are more efficient at reducing the NO_x at high temperatures. In tests(9) at 170 $^\circ\text{C}$, NO_x reductions of 95% have been observed; at 140-150 $^\circ\text{C}$, zeolite and

titanium dioxide produced 75% and 80% NO_x reductions, respectively. If the stoichiometric balance of ammonia to NO_x is increased above 1, some N₂O production is formed(12) with the zeolite catalysts. Keeping the ammonia to NO_x ratio at 0.9 eliminates this problem(9).

Other manufacturers are reported to be developing catalysts(11) that operate at 100-150 °C. The Shell International Chemie(13,14) has been developing a titanium/vanadium catalyst that will operate at 120-350 °C for 90% NO_x conversion. The greater the inlet NO_x concentration, the greater the NO_x percent reduction achieved. It has been applied commercially at chemical plants in Europe and at a refinery in Los Angeles. It requires a low dust and SO₂ environment, making it potentially suitable for the tail gas SCR configuration for coal- or waste-fired plants.

U.S. Application Considerations and Conclusions

A key issue for U.S. coal-fired SCR applications is that the U.S. coals contain as much as 2-6 times the amount of sulfur as compared to coals burned in Japan and Germany. The resulting additional SO₃ in the flue gas is a serious concern, since the addition of ammonia and the effects of the catalyst itself both lead to the production of ammonia bisulfate. The bisulfate is a serious problem since it plugs and fouls downstream equipment and it can severely shorten the catalyst life. Sulfate aerosols often are not adequately controlled by wet FGD scrubbing, and may be discharged from the plant stack.

German operating experience with fuels with higher sulfur levels has shown that the SCR system can produce sulfuric acid which results in acid attack of downstream equipment and the emission of sulfuric acid aerosols, even if a wet FGD system is used. Solutions to this type of problem have included lowering the boiler flue gas outlet temperature, adding lime to the flue gas, changing soot blowing and cleaning schedules, and limiting the boiler operating range. Since U.S. coals may have even greater sulfur contents, this could be an area of specific concern for SCR applications to U.S. coal-fired service conditions. A key lesson learned is that just monitoring the SCR effectiveness by catalyst activity measurements is insufficient to control sulfur-related problems(5).

Although specialized high dust SCR catalysts can be developed and demonstrated for U.S. operating conditions, it would be simpler and there would be a greater assurance that the design used at one plant could be transferred to another plant if tail gas SCR systems were developed. However, it is recognized that with proper engineering and development, either the high dust or the tail gas system should be a suitable NO_x control for U.S. conditions.

Literature Cited

1. Lowe, P.; Ellison, W.; "Foreign Experience With Selective Catalytic Reduction NO_x Controls", American Chemical Society Meeting, Denver, March-April 1993, to be published in the meeting proceedings.

2. Krueger, H.; "Status of NO_x Reduction in Power Plants of VGB Members", *VGB Kraftwerkstechnik*, 4, 1991.
3. Ellison, W.; Weiler, H.; "Stack Gas Cleaning Optimization Via German Retrofit Wet FGD Operating Experience", EPRI/EPA Joint Symposium on SO₂ Control", Washington, D.C., March 1991.
4. Hjalmeresson, A-K; "NO_x Control Technologies for Coal Combustion", IEACR/24, June 1990.
5. Rummenhohl, V.; Weiler, H.; Ellison, W.; "Experience Sheds Light on SCR O&M Issues", *Power*, September 1992.
6. Lowe, P.; Ellison, W.; "Understanding the German and Japanese Coal-Fired SCR Experience", Proceedings EPRI/EPA Joint Symposium on Stationary Combustion NO_x Control, Washington, D.C., March 1991.
7. Gutberlet, H.; Dieckmann, H.J.; Schallert, B.; "Auswirkungen von SCR-DENOX-Anlagen auf nachgeschaltete Kraftwerkskomponenten (Effects of SCR DENOX Plants on Downstream Plant Components)", *VGB Kraftwerkstechnik*, 71 (6), June 1991.
8. Kassebohm, B.; "The Semi-Dry Flue Gas Desulphurisation System in Duesseldorf", The Institute of Energy, London, September 1990.
9. Kassebohm, B.; Wolfering, G.; "Catalytic Flue Gas Denitrification at Low Temperature i.e. Without Reheating", *VGB Kraftwerkstechnik*, 4, 1991.
10. *Power International*, "Activated-Coke Filters Pioneered for Refuse-, Coal-Fired Plants", September 1991.
11. Kassebohm, B.; Wawrzik, U.; "The Three Stage Flue Gas Cleaning System of Duesseldorf", Materials and Energy From Refuse, 4, Oostende, Belgium, March 1992.
12. Hjalmeresson, A-K; "Interactions in Emissions Control For Coal-Fired Plants", IEACR/47, March 1992.
13. EPA, "Evaluation and Costing of NO_x Controls for Existing Utility Boilers in the NESCAUM Region", EPA 453/R-92-010, December 1992.

RECEIVED September 30, 1993

Chapter 17

Family of Versatile Catalyst Technologies for NO_x Removal in Power Plant Applications

R. M. Heck, J. M. Chen, B. K. Speronello, and L. Morris

Engelhard Corporation, 101 Wood Avenue, South Iselin, NJ 08830-0770

Limits on NO_x emissions from power plant installations often result in the use of catalytic emission control systems. The optimum type and size of the abatement system depends on a variety of performance requirements that are unique to each installation. The main design variable that affects the selection of the NO_x selective catalytic reduction catalyst is operating temperature. A family of versatile catalyst technologies has been developed by Engelhard to control NO_x over a wide range of temperature and exhaust gas composition. The technical differences between the catalyst technologies are discussed. Commercial installations are reviewed.

Oxides of nitrogen formed during combustion are caused either by the thermal fixation of atmospheric nitrogen (thermal NO_x) or by conversion of chemically bound nitrogen in the fuel. (1) Selective catalytic reduction (SCR) is recognized as the most effective commercial technology to control NO_x emissions from chemical plants and stationary power sources. The operating environment and process constraints for SCR systems vary greatly from one installation to another. These constraints, which include pressure drop limits, duct dimensions, exhaust gas particulate content, ammonia limits in the exhaust (i.e. NH₃ slip), SO₂ oxidation limits, temperature and NO_x concentration, all impact catalyst and system design.

For optimal performance under these varied constraints, catalysts of different physical and catalytic properties are required. Tailoring for these constraints, Engelhard has developed composite honeycomb SCR catalyst formulations which provide a high degree of flexibility to meet specific system configuration and performance needs. The composite catalyst is manufactured by bonding a layer of catalytic ingredients onto strong, thin walled ceramic honeycomb supports. This design results in both substantially reduced catalyst volume, and several unique selectivity characteristics(1).

0097-6156/94/0552-0215\$08.00/0

© 1994 American Chemical Society

This paper reviews some of the more critical factors that affect emissions control systems and describes how the specific requirements of such systems are better satisfied with a family of catalyst formulations and gives a summary of commercial installations.

Composite Catalyst Features

The three classes of reactions that can be catalyzed by a commercial SCR catalyst are given in Table I. They include the NO_x SCR reaction itself, plus ammonia oxidation and SO_2 oxidation to SO_3 . The SCR reaction between NO_x and NH_3 to form N_2 and water is the preferred reaction which removes NO_x from the exhaust stream. Ammonia oxidation consumes NH_3 in competition with the SCR NO_x reaction, and is undesirable because it lowers NO_x removal efficiency and increases NH_3 consumption. These competing reactions are shown schematically as a function of operating temperature in Figure 1. SO_2 oxidation is undesirable because the resultant SO_3 can react with excess NH_3 in the exhaust stream to form ammonium bisulfate that can plug and corrode downstream equipment. Combining these effects, the SCR NO_x catalyst is required to possess high SCR activity together with low activities for both ammonia and SO_2 oxidation. These properties depend on both catalyst chemical composition and catalyst structure.

Detailed kinetic analyses have revealed that with honeycomb catalysts, the SCR NO_x reaction rate is limited by a combination of gas phase mass transfer to the honeycomb surface and pore diffusion into the catalyst layer.(2,3) Under these conditions, all NO_x conversion occurs in an extremely thin layer of the catalyst surface. In contrast, the rates of the SO_2 and NH_3 oxidation reactions are mostly controlled by kinetic rates over the catalyst active sites and by the total weight of catalytic material in the reactor. Under these conditions, SO_2 and NH_3 penetrate deeply into the catalyst layer.

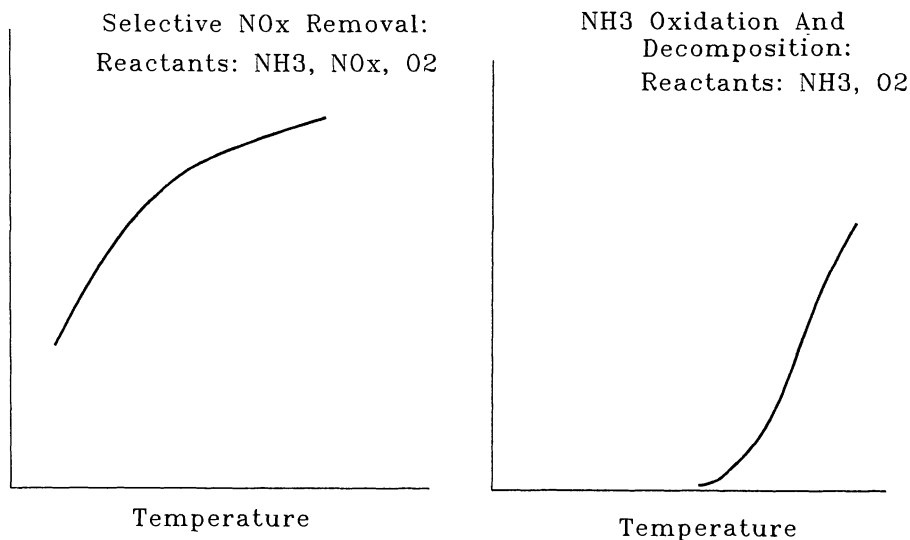
Since only a thin layer of catalyst is needed to achieve maximum NO_x conversion, and since extra catalyst below the necessary surface layer contributes to the undesirable oxidation reactions, the composite catalyst structure (with its thin catalytic layer) has inherently better selectivity compared to either extruded or plate designs (where the catalyst wall comprises a relatively massive layer of catalytic material).(1)

Selective Catalytic Reduction of NO_x

Selective catalytic reduction (SCR) of NO_x with ammonia was first discovered and patented by Dr. Gunther Cohn at Engelhard.(4) This initial work was targeted at nitric acid tail-gas exhausts, and used precious metal catalysts. It was not until the mid-1970's, however, that SCR entered widespread commercial use in Japan using base metal catalysts. The key performance criteria for SCR are analogous to complete oxidation systems: NO_x conversion, pressure drop, catalyst/system life, cost, and minimum SO_2 oxidation to SO_3 (for systems firing liquid fuels). Temperature is the single most important variable in NO_x SCR. No SCR catalyst can operate economically over the whole temperature range possible for power plant applications. As a result, three general classes of catalysts have evolved into commercial use:

Table I. Important Chemical Reactions Over NO_x SCR Catalyst

	Preferred Activity Level
NO_x SCR	
$4\text{NH}_3 + 4\text{NO} + \text{O}_2 \longrightarrow 4\text{N}_2 + 6\text{H}_2\text{O}$	High
$4\text{NH}_3 + 2\text{NO}_2 + \text{O}_2 \longrightarrow 3\text{N}_2 + 6\text{H}_2\text{O}$	High
SO₂ Oxidation	
$2\text{SO}_2 + \text{O}_2 \longrightarrow 2\text{SO}_3$	Low
NH₃ Oxidation	
$4\text{NH}_3 + 5\text{O}_2 \longrightarrow 4\text{NO} + 6\text{H}_2\text{O}$	Low
$4\text{NH}_3 + 3\text{O}_2 \longrightarrow 2\text{N}_2 + 6\text{H}_2\text{O}$	Low

Figure 1. Competing Reactions in SCR NO_x.

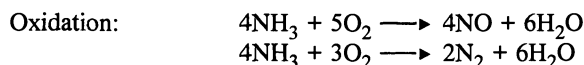
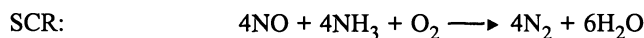
precious metals for operation at temperatures between 177 and 290°C, base metals for operation at temperatures between 260 and 450°C, and zeolites for operation at higher temperatures. The important catalyst characteristics for each operating temperature range are discussed below.

Low Temperature Operation

Low temperature, precious metal SCR catalysts have been installed on a small number of power plant turbines firing natural gas. Sensitivity to poisons makes precious metal SCR catalyst unsuitable for most co-generation applications, since variations in exhaust sulfur levels of as little as 0.4 ppm can shift the catalyst temperature window completely out of a system's operating temperature range.⁽⁵⁾ In addition, operation on liquid fuels is further complicated by the potential for deposition of ammonium-sulfate salts within the pores of the catalyst. However, once these limitations are realized and the proper design models developed, low temperature SCR systems provide the SCR system designer with an additional degree of design freedom.

Because the NO_x concentration in a combustion turbine exhaust is generally very low, the characteristic of low temperature SCR systems to manufacture nitrous oxide (N_2O) is not usually an issue. In other types of systems operating with higher concentrations of NO_x and ammonia, a low temperature SCR system will generate proportionally more nitrous oxide. Since nitrous oxide has been linked to both the destruction of stratospheric ozone and contribution to the greenhouse effect, there are reasonable odds that its emission will be controlled in the future.

The operating temperature range for low temperature SCR catalysts is determined by the balance between the SCR and ammonia oxidation reaction listed below and shown schematically in Figure 1.:



At low temperatures the SCR reaction dominates and NO_x conversion increases with increasing temperature. But as temperature increases, the oxidation reactions become relatively more important. Eventually as temperature increases further, the destruction of ammonia and generation of NO_x via the oxidation reactions causes overall NO_x conversion to reach a plateau and finally decrease with increasing temperature. The general form of this curve is shown in Figure 2. For low temperature SCR catalysts, the peak in NO_x conversion (>90%) typically occurs in a 40°C window between 177 and 316°C.

Medium Temperature Operation

The most popular SCR catalyst formulations are those comprising V_2O_5 supported on $\text{TiO}_2(\text{V}/\text{Ti})$. Ingredients such as tungsten and molybdenum may be added to diminish SO_2 oxidation activity and improve operation above 425°C but the basic formulation remains generally the same. These catalysts operate best in a temperature range

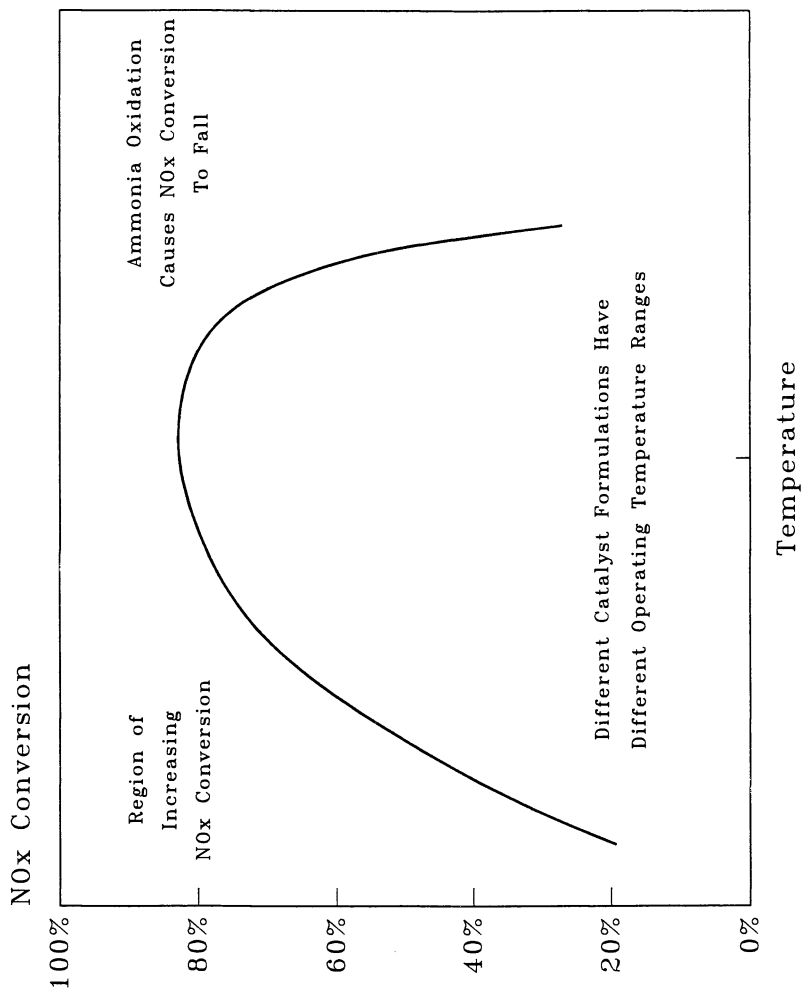


Figure 2. General Form of NO_x Reduction versus Temperature.

between 288 and 450°C. They are generally active and durable catalysts that have functioned well in power plant systems since the mid-1980's.

Medium temperature V/Ti catalysts have curves of NO_x conversion vs. temperature that are similar to low temperature catalysts (see Figures 1 and 2). NO_x conversion rises with increasing temperature to a plateau and then falls as ammonia oxidation begins to dominate the SCR reaction. However, for these medium temperature catalysts, the peak conversion occurs over a broad temperature range and the response is usually more gradual than with low temperature catalysts.

Medium temperature V/Ti SCR catalysts have one clear weakness compared to both low temperature precious metal and high temperature zeolite based catalysts; V/Ti catalysts are irreversibly deactivated by extended exposure to temperatures above 450°C. This is caused by the transformation of the high surface area anatase form of titania to the lower surface area rutile form. In contrast, typical precious metal SCR catalyst formulations may be heated to temperatures well above 538°C without excessive deactivation, and high temperature catalysts will operate at temperatures as high as 510 to 593°C depending on the formulation.

High Temperature Operation

The suitability of zeolite catalysts for SCR above 450°C has been known since the 1970's.(6) They have received limited acceptance for power plant applications, however, at least in part because their upper operating temperature limit (approximately 510°C) was lower than the exhaust temperature of the most popular turbine designs. Since the heat recovery boiler had to be split to accommodate either V/Ti or zeolite catalysts, most systems used the more active medium temperature V/Ti formulations. Recently Engelhard commercialized NOxCat ZNX zeolite SCR catalyst with the capability to operate at temperatures as high as about 593°C.(2) When NO_x is present this catalyst does not oxidize ammonia, so its NO_x conversion continually increases with increasing temperature. This catalyst is designed to operate in the direct exhaust of combustion turbines; either ahead of the heat recovery boiler or in simple cycle systems without heat recovery boilers.

Overall SCR Operation

Figure 3 summarizes the operating temperature ranges for the different SCR catalyst formulations. For temperatures between 177 and 219°C NOxCat LT-1 catalyst provides optimum NO_x removal. NOxCat LT-2 catalyst will provide the best performance for systems that operate between 249 and 321°C. For medium temperatures in the range of 300 to 425°C, NOxCat VNX V/Ti catalyst yields the optimum NO_x removal efficiency. Finally, for temperatures between about 400 and 593°C NOxCat ZNX catalyst maximizes NO_x conversion. This family of catalyst as designated in Table II, provides coverage over essentially the full temperature range possible for power plant applications.

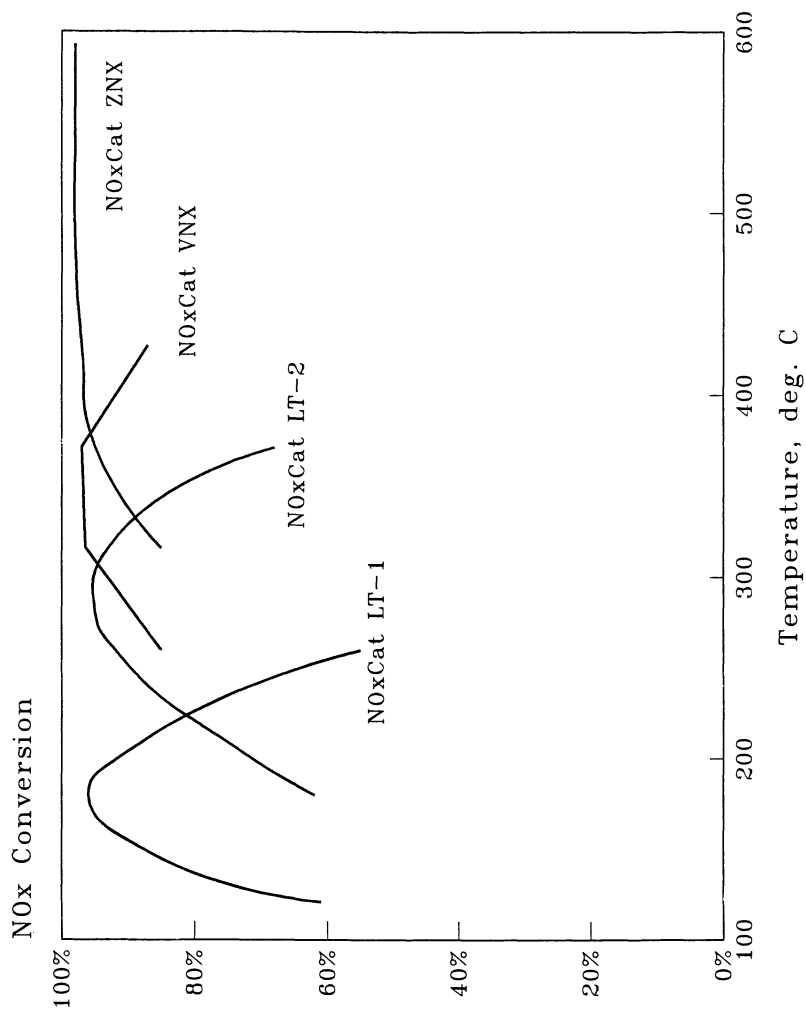


Figure 3. Operating Temperature Window of Different SCR Catalyst Formulations.

Table II. Effective Operating Temperature Ranges for Commercial NO_x Catalysts

Product	Temperature Range, °C
NO _x Cat LT-1	177 - 219
NO _x Cat LT-2	249 - 321
NO _x Cat VNX	300 - 425
NO _x Cat ZNX	400 - 593

Table III. Engelhard's SCR Catalyst Experience

Application	Catalyst	Flow (lb/sec)	Fuel	Start-up
Gas Turbine				
(1) BBC (50MW)	VNX	650	NG	11/90
(2) Westinghouse 251	VNX	422	NG	10/92
(1) Kawasaki 1	ZNX	23	NG	2/91
(1) Allison 3.5	VNX	38	NG	9/91
(1) Rolls Royce 25 MW	VNX	259	NG	8/92
(1) GE Frame 7	VNX	669	NG	1Q/93
(1) LM-2500	VNX	157	NG	5/93
(1) LM-6000	VNX	283	NG	4Q/93
Reciprocating Engine				
(1) 800 Hp	VNX	8	NG	1993
(1) 2000 Hp	VNX	97	NG	1985
(2) 4000 Hp	VNX	23	NG/DG	1986
(3) 1500 Hp	ZNX	9	NG	5/91
Industrial Heater/Boiler				
(1) Refinery Heater	VNX	84	NG	10/90
(1) Refinery Heater	ZNX/VNX	46	NG	10/90
(1) Boiler	VNX	26	NG	10/90
(1) Annealing Furnace	VNX	29	NG	1991
(5) Refinery Heater	VNX	16-31	NG	3/91
(1) Refinery Heater	VNX	39	NG	6/91
Chemical Plant				
(1) Process Off-Gas	ZNX	4	CP	8/90
(1) Nitric Acid Plant	VNX	99	NG	3/91
Field Tests				
(8) Gas Turbines	VNX/ZNX		NG	1987
(1) Coal Boiler · LD	VNX		Coal	1985
(1) Coal Boiler · LD	VNX/ZNX		Coal	1987
(1) Coal Boiler · HDW	VNX/ZNX		Coal	1989
(1) Coal Boiler · HDD	VNX/ZNX		Coal	1989

Commercial Experience

A number of SCR NO_x systems containing the vanadium/titania (VNX) and zeolite (ZNX) catalysts are now installed in commercial installation for gas turbines, reciprocating engines, industrial heaters and boilers and chemical plants. These installations are summarized in Table III. Note that the commercial installations include gas turbines, reciprocating engines, industrial heaters/boilers and chemical plants. A number of installations have been in operation for over five years. All of the commercial installations are meeting performance for NO_x conversion, NH₃ slip and pressure drop. Also a number of field tests have been successfully conducted on coal fired boilers.

Conclusion

Operating requirements for NO_x control varies substantially with each application. The dominant factor for design of an SCR NO_x system is the operating temperature. A number of catalyst formulations are needed to meet the requirements of the wide range of exhaust temperatures. Engelhard has developed a family of catalysts for selective catalytic reduction of NO_x designated NOxCat SCR. These different catalyst have been optimized to function best in each different power plant environment thus covering the complete range of operating temperatures.

Acknowledgement

The information included in this paper was generated in collaboration with several Engelhard colleagues, including Dr. John Byrne, Joseph Hansell and Marvin Tiller.

Literature Cited

1. Durilla, M.; Chen, J.M.; Speronello, B.K.; Heck, R.M. Presented at IGCI Meeting, Baltimore, MD, March, 1990.
2. Byrne, J.W.; Chen, J.M.; Speronello, B.K. *Catalysis Today*, **1992**, *13*, 33-42 (1992).
3. Chen, J.M.; Speronello, B.K.; Byrne, J.W.; Heck, R.M. Presented at AIChE National Meeting, San Diego, CA, August, 1990.
4. Cohn, J.G.; Steele, D.R. and Andersen, H.C. U.S. Patent 2 975 025, 1961.
5. Pereira, C.J.; Plumlee, K.W. and Evans, M. *2nd International Symposium on Turbomachinery, Combined-Cycle Technologies and Cogeneration*; IGTI, 1988; Vol. 3, pp. 131-136.
6. Pence, D.T.; Thomas, T.R. U.S. Patent 4 220 632, 1980.

RECEIVED September 30, 1993

Chapter 18

NO_x Control by Catalytic Combustion of Natural Gas

S. K. Agarwal¹, B. W.-L. Jang¹, R. Oukaci², A. Riley², and G. Marcelin²

¹Research Triangle Institute, P.O. Box 12194, Research Triangle Park, NC 27709

²Department of Chemical and Petroleum Engineering, University of Pittsburgh, Pittsburgh, PA 15261

The formation and destruction of NO_x in the catalytic combustion of methane have been studied using a series of La_{1-x}Sr_xCoO₃ catalysts. The emissions of NO_x are less than 3 ppm under lean combustion conditions at temperatures as high as 1000 °C. The NO_x concentration increases as the temperature is increased above that needed for complete methane conversion. CO concentration is negligible at this temperature. The characterization of catalysts by temperature-programmed desorption (TPD) and temperature-programmed reduction (TPR) shows changes in their oxidation-reduction properties due to Sr substitution which in turn affects the performance for methane combustion and NO_x reduction.

Natural gas is an important fuel for industrial combustion systems. Environmental regulations have led to greater emphasis on developing combustion techniques that reduce pollutant emission levels from conventional combustors. Catalytic combustion offers an alternative energy conversion process with many potential advantages over conventional combustors. Because the catalytic combustion process can be stabilized under lean fuel conditions, it can operate at a much lower temperature than conventional combustors, resulting in reduced emissions of NO_x and other undesirable products of combustion. As an example, regulations of various types are currently forcing NO_x emissions to near 25 ppm in most of the United States in stationary gas turbines. Regulations in Southern California and parts of the Northeast require NO_x levels less than 10 ppm, which can currently be met only by postcombustion gas treatment, such as selective catalytic reduction. Regulatory initiatives in Southern California and elsewhere may further restrict NO_x emissions.

Despite intense efforts to study the catalytic combustion (1-7), NO_x reduction (8-12), and NO_x decomposition (13-16), very little has been reported on the fundamental surface chemistry leading to the formation and destruction of NO_x

0097-6156/94/0552-0224\$08.00/0
© 1994 American Chemical Society

under real catalytic combustion conditions. This work reports the use of $\text{La}_{1-x}\text{Sr}_x\text{CoO}_3$ perovskite-type catalysts for methane combustion and NO_x control with the objective of examining the effect of catalytic surface reactions on the NO_x formation and destruction during catalytic combustion. Perovskite catalysts, especially those containing cobalt, have been shown to be relatively stable and active at the elevated temperatures of advanced combustion systems (6,7). These catalysts have also been reported to be active for NO_x destruction (15,16).

Experimental

Catalyst Preparation. A series of $\text{La}_{1-x}\text{Sr}_x\text{CoO}_3$ catalysts with varying Sr content ($x = 0.0, 0.1, 0.25, 0.5, \text{ and } 1.0$) was prepared by precipitation technique. Appropriate amounts of nitrate salts of La, Co, and Sr were dissolved in distilled water. The solution was heated to 70 °C and stirred on a heating plate. The corresponding hydroxides were precipitated by adding tetramethyl ammonium hydroxide to the solution. The slurry was filtered and the solid was washed with distilled water. The wet cake was dried overnight at 120 °C and calcined at 900 °C for 10 hours. Small amounts of the catalysts were further calcined at 1100 °C for 6 hours to examine the catalyst stability at higher temperature.

Reaction System. A fixed-bed laboratory-scale reactor system was used in this study. Figure 1 shows the schematic of this reaction system. The reactor consists of a 7-mm-I.D. and 40-cm long quartz tube. The reactor was heated in a single zone tube furnace and the temperature was controlled to ± 1 °C by a temperature controller. The catalyst bed, supported on quartz wool, corresponded to the middle of the heated zone of the furnace.

The gas flow rates were controlled by electronic mass flow controllers (MFCs). A portion of the mixed feed stream was continuously vented through a four-port valve. This valve arrangement allowed for the analysis of either the feed or the effluent without disrupting the gas flow to the reactor. A needle valve was used before the reactor to build the pressure to 10 psig, as required for proper operation of the feed MFC.

Effluent gases were analyzed for CH_4 , O_2 , CO , CO_2 , N_2 , NO , N_2O , and NO_2 using an HP 5890 gas chromatograph (GC) and a chemiluminescent NO_x analyzer. An 80486 personal computer with HP Chemstation software was used to control the GC.

Temperature-Programmed Reduction. Temperature-programmed reduction (TPR) experiments were carried out using an AMI-1 temperature-programmed desorption (TPD) system (Altamira Instruments) equipped with a thermal conductivity detector (TCD). The sample temperature was measured with a K-type thermocouple placed very close to the catalyst bed in order to ensure accurate temperature measurement. The TCD signal and the sample temperature were automatically recorded using a software package provided by Altamira Instruments.

Prior to TPR, all catalysts were pretreated in a flow of Ar (30 cc/min) at 200 °C for about 1 hour and then cooled to 50 °C, in an inert atmosphere. The TPR was carried out using a 5 percent H_2/Ar gas mixture. About 50 to 100 mg of catalyst

sample were used in each case. The temperature of the sample was linearly ramped from 50 to 900 °C at a rate of 5 °C/min. The H₂ consumption due to reduction was monitored using the TCD.

Temperature-Programmed Oxygen Evolution. Temperature-programmed oxygen evolution (TPOE) was carried out using a thermal analysis (TA) 2950 system with a thermogravimetric analyzer (TGA) module. The weight loss for all the catalysts was obtained by heating the sample in N₂ (flow rate = 30 cc/min) from 50 to 1000 °C using a linear ramp rate of 5 °C/min and holding at 1000 °C for 100 minutes. Approximately 8 to 18 mg of the sample was used in all cases.

Results and Discussion

Catalytic Methane Combustion. The methane combustion activities of the various strontium substituted La_{1-x}Sr_xCoO₃ perovskites are compared in Figure 2. Addition of small amounts of Sr (x = 0.1) resulted in a significant increase in the catalyst activity for methane combustion. The activity of catalysts with x = 0.25 and x = 0.5 was similar and between the activities of Sr-0 and Sr-0.1. However, the activity of Sr-1 was very low. Note that all catalysts, except Sr-1, exhibited a perovskite phase. The exceptionally low activity of Sr-1 for methane combustion can be explained by its nonperovskite type structure. Similar optima in methane combustion activity over La_{1-x}Sr_xCoO₃ were observed by Seiyama (6) and Arai et al. (4).

It is interesting to compare the catalytic combustion over these perovskites with noncatalytic combustion (gas phase). The results for gas-phase combustion are also shown in Figure 2. The activity of gas-phase reaction was significantly lower than for all the perovskites, but higher than the reaction over Sr-1 at 875 °C. In other words, it appears that the Sr-1 catalyst serves as a sink to the gas-phase generated radicals. It is well known that catalytic combustion at high temperature includes both heterogeneous and homogeneous reactions, and that the contribution of those reactions to the combustion is a function of reaction conditions and catalytic properties. Previous reports (3,17,18) showed that the catalytic surface tends to inhibit gas-phase ignition of the fuel mixture. Most of the time the inhibition effect is over-shadowed by the high activity of heterogeneous reaction. However, the inhibition effect of the Sr-1 catalyst on the homogeneous reaction can be clearly seen in the comparison in Figure 2.

The effect of temperature on methane conversion and on CO and NO_x emissions during catalytic and noncatalytic combustion is summarized in Figure 3. The methane combustion activity of Sr-0.5 catalyst calcined at 1100 °C is lower compared to the same catalyst calcined at 900 °C. This is likely related to the lower surface area of the higher temperature calcined catalyst (0.45 m²/g) compared to the lower temperature calcined catalyst (3.8 m²/g).

Differences in the oxidation activity of the various catalysts were clearly seen in the CO emissions. In general, the CO concentration in the effluent stream increased at reaction temperatures above 700 °C, passed through a maximum, and then decreased with temperature. Maxima in CO concentration over the catalysts were observed at 875 °C. It was, however, lower (850 °C) in the gas phase. Also, the maximum in CO concentration was higher in the absence of catalyst. As expected,

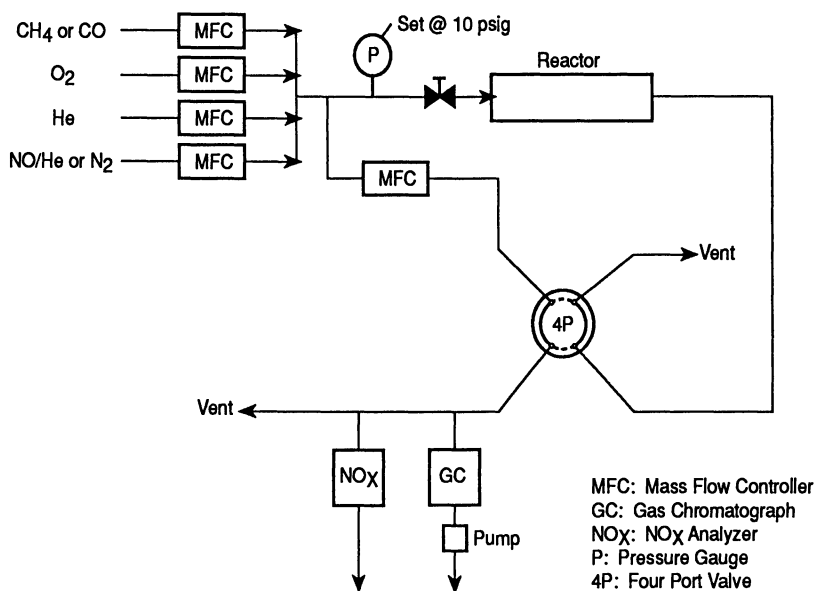
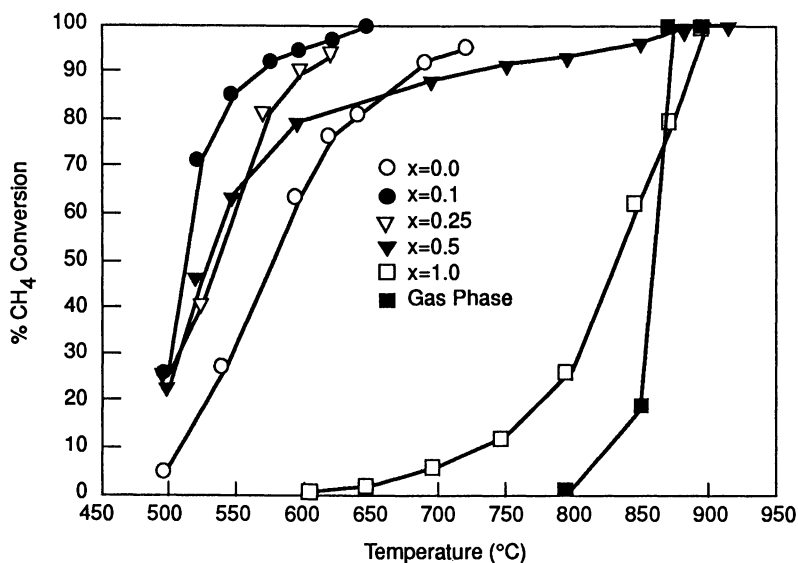


Figure 1. Schematic of reactor system.

Figure 2. Gas phase combustion and catalytic combustion over $\text{La}_{1-x}\text{Sr}_x\text{CoO}_3$ catalysts. 3.8% CH_4 in air; 70,000 cc/hr/g space velocity.

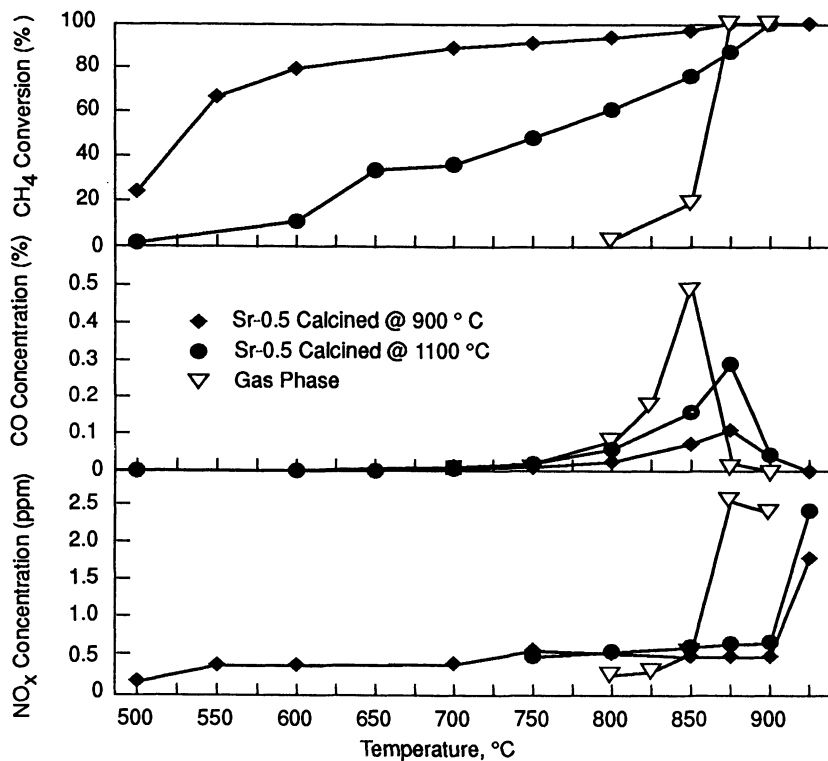


Figure 3. Methane conversion, NO_x formation and CO emission as a function of temperature over perovskite catalysts and gas phase reaction. 3.8% CH₄ in air; 70,000 cc/hr/g space velocity.

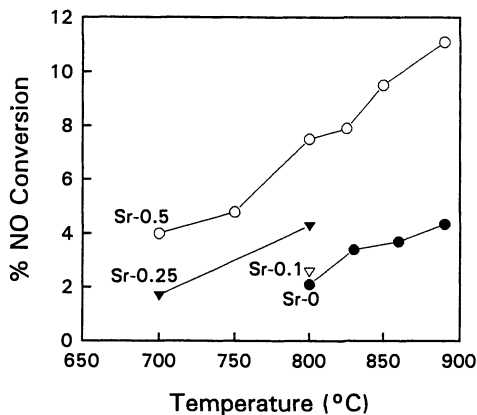


Figure 4. NO decomposition over La_{1-x}Sr_xCoO₃ catalysts. 4,950 ppm NO in helium; 1,600 cc/hr/g space velocity.

at 875 °C, the CO concentration over the low temperature calcined catalyst was lower than over the high temperature calcined catalyst. Note that the temperature at which the CO concentration became negligible corresponded with the complete conversion of methane in all cases.

The NO_x concentration in the effluent stream was very low (less than 1 ppm) up to about 850 °C. Above this temperature, a jump in the NO_x concentration to about 2.0 to 2.5 ppm was observed. Interestingly, this temperature (T_c) corresponded to the temperature at which the methane combustion was complete and CO concentration was zero.

The low NO_x concentration at temperatures below T_c would at first suggest that the reduction of NO_x with CH₄ and/or CO can be the pathway for NO_x destruction. As a result, the decomposition of NO and the reduction of NO with CH₄ and CO were examined under catalytic combustion conditions. Because of microscopic reversibility, any catalyst that promotes NO decomposition will also promote NO formation, with no net reduction in NO_x emissions. Catalysts that are active for NO_x decomposition should also be active for NO_x reduction since NO_x decomposition is believed to be the first step in the reduction reaction (17,18).

The NO decomposition activity of various La_{1-x}Sr_xCoO₃ catalysts is compared in Figure 4. The perovskite catalysts can decompose NO into N₂ and O₂ at high temperature; however, the kinetics are very slow as is evident from the very low space velocity, 1,600 cc/hr/g, used for NO decomposition compared to 70,000 cc/hr/g used for methane combustion. In general, the addition of Sr to La_{1-x}Sr_xCoO₃ increased the activity for NO decomposition. The effect of gas-phase oxygen on the NO decomposition activity was also examined. The addition of oxygen inhibited the NO decomposition activity suggesting that NO decomposition may have a limited role in NO_x control during catalytic combustion.

The reduction of NO with CO and methane was examined over Sr-0.5 catalyst at 50,000 cc/hr/g space velocity and the results are summarized in Figure 5. Clearly, CO is a much stronger reducing agent for NO reduction than CH₄. While the conversion of NO reached 80% (maximum possible because of NO/CO stoichiometry used in the experiment) with CO at temperatures as low as 500 °C, the conversion of NO with methane was significant only above 650 °C. Note that these experiments were conducted in the absence of any gas-phase oxygen.

To simulate the real catalytic combustion conditions, the effect of gas-phase oxygen on NO reduction was examined. In the cases of both CO and CH₄ as reducing agents, the addition of a small amount of gas-phase oxygen completely inhibited the reduction of NO. Similar results have been observed by Iwamoto and Hamada (19). These results suggest that NO decomposition and NO reduction with CO and CH₄ may be of limited significance in controlling NO_x emissions during catalytic combustion. The low NO_x concentrations observed during lean catalytic combustion may probably be due to the lower reaction temperature.

The addition of Sr to LaCoO₃ resulted in considerable differences in the activity for methane combustion and NO decomposition reactions. While an optimum in the methane combustion activity was observed with the Sr content in the La_{1-x}Sr_xCoO₃ catalyst, the NO decomposition activity increased monotonically with the Sr content. To correlate the changes in the catalytic properties with the physico-chemical properties, the catalysts were characterized by TPR and TPOE.

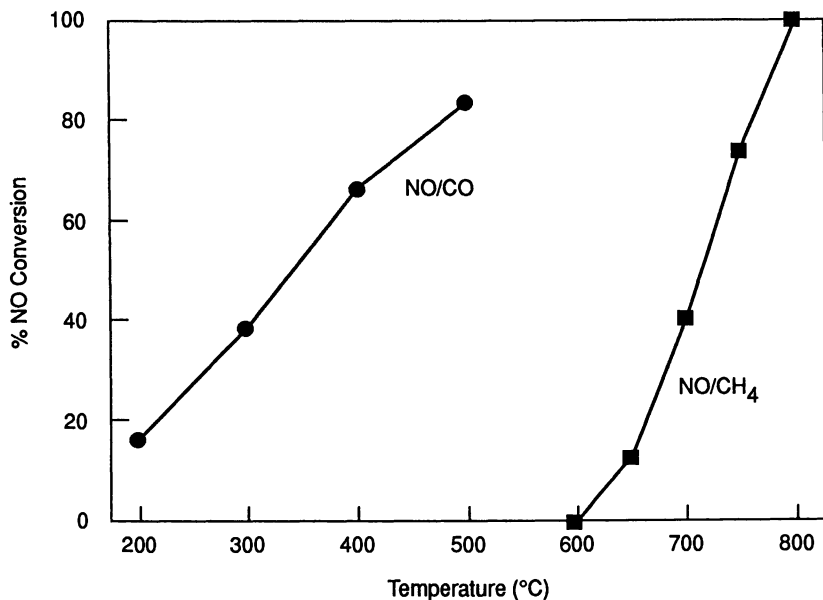


Figure 5. NO reduction by CO and methane as a function of temperature over Sr-0.5 catalyst. 50,000 cc/hr/g space velocity. NO/CO reaction: 5,000 ppm NO and 4,000 ppm CO; NO/CH₄ reaction: 4,200 ppm NO and 4,000 ppm CO. The diluent was helium.

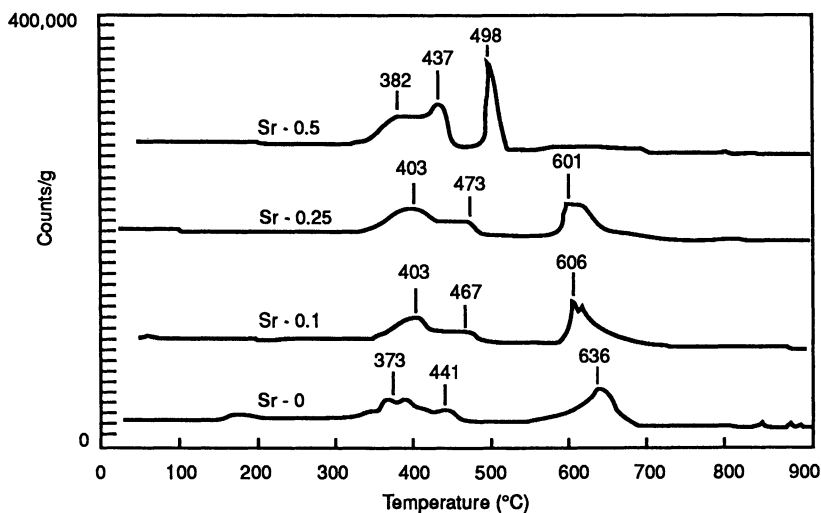


Figure 6. TPR profiles for La_{1-x}Sr_xCoO₃ catalysts.

The TPR profiles for the catalysts are shown in Figure 6. In all cases three distinct signals were observed: a low temperature peak (LTP) at 370 to 410 °C; an intermediate temperature peak (ITP) at 435 to 465 °C; and a high temperature peak (HTP) at 500 to 640 °C.

The LTP and ITP are typical of what is observed in supported Co catalysts and can be considered to be the easily reducible cobalt. The HTP most likely corresponds to reduction of the bulk phase. Integration of the signals gives the relative reducibility of the various perovskites. The relative areas of these signals are summarized in Table I. While the HTP area remained almost unchanged, the LTP and the ITP areas increased with the Sr content. The total reducibility of the catalyst increased with increasing Sr content. Since the ease of reduction may be associated with the lability of oxygen in the catalyst, it seems that the oxygen lability can be varied by varying the Sr content in the perovskite.

Table I. Degree of Reduction for Various Perovskite Catalysts

Run No.	Catalyst	LTP+ITP (area/g)	HTP (area/g)	Total Amount of Co Reduced (%)
1	Sr-0	19.4	21.9	65.5
2	Sr-0.1	21.3	19.3	71.9
3	Sr-0.25	27.8	21.0	79.6
4	Sr-0.5	34.0	18.5	83.0

The TPOE experiments for all catalysts exhibited similar weight loss profiles, i.e., virtually no weight loss until a very distinct loss at 725 to 810 °C. The weight loss in this region can be attributed to the oxygen evolution. The amount of oxygen evolved from the catalysts was calculated from their weight loss and is summarized in Table II. It can be seen that although the temperature of oxygen evolution did not change significantly with a change in Sr content, the amount of oxygen evolved

Table II. Amount of "O" Evolved From Various Perovskites

Catalyst	Weight Loss (%)	Amount of "O" ^a Evolved (μmol/g)	Total "O" in Catalyst (μmol/g)	Temperature ^b (°C)
Sr-O	0.8840	107.8	12,200	786
Sr-0.1	1.0600	132.5	12,500	789
Sr-0.25	1.3738	177.2	12,900	795
Sr-0.5	2.0018	272.2	13,600	798

^a The experimental error is ± 10%.

^b Temperature of oxygen evolved obtained from the differential of weight loss curve. It refers to the temperature at which the rate of oxygen evolution is maximum.

increases linearly with an increase in Sr content. The amount of oxygen evolved corresponded to ca 0.9% of the total oxygen atoms in the Sr-O catalyst. This number increased to ca 2% for Sr-0.5. This again suggests increasing lattice oxygen with an increase in Sr content. These results suggest that the increase in methane conversion and NO decomposition activity with Sr addition may be related to the oxygen lability in the catalyst.

Conclusion

The addition of Sr to LaCoO₃ causes considerable changes in the oxidation-reduction properties of these materials. The methane conversion exhibits an optimum with the Sr content in the catalyst, showing a maximum at x=0.1. The NO_x emissions are very low under lean catalytic combustion conditions, with the concentration being below 3 ppm at temperatures up to 1000 °C. The NO_x reduction reactions with CO and methane have limited significance in controlling the NO_x emission during catalytic combustion. The low NO_x emission during lean catalytic combustion is probably due to the low temperature.

Acknowledgments

The financial support provided by Gas Research Institute under contract #5092-260-2333 is gratefully acknowledged.

Literature Cited

1. Prasad, R.; Kennedy, L.A.; Rukenstein, E.R. *Catal. Rev.-Sci. Eng.* **1984**, *26*(1), 1-58.
2. Trimm, D.L. *Appl. Catal.* **1983**, *7*, 249-282.
3. Pfefferle, L.D.; Pfefferle, W.C. *Catal. Rev.-Sci. Eng.* **1987**, *29*(2&3), 219-267.
4. Arai, H.; Machida, M. *Appl. Catal.* **1991**, *10*, 81-94.
5. Pfefferle, L.D. GRI Final Report, GRI-92/0117, 1991.
6. Seiyama, T. *Catal. Rev.-Sci. Eng.* **1992**, *34*(4), 281.
7. Quinlan, M.A.; Wise, H.; McCarty, J.G. GRI Final Report, GRI-89/0141, 1989.
8. Mouaddib, N.; Feumi-Janton, C.; Garbowski, E.; Primet, M. *Appl. Catal.* **1992**, *A87*, 129-144.
9. Scharpf, E.W.; Benziger, J.B. *J. Catal.* **1992**, *136*, 342-360.
10. Cho, B.K. *J. Catal.* **1992**, *138*, 255-266.
11. Viswanathan, B. *Catal. Rev.-Sci. Eng.* **1992**, *34*(4), 337-354.
12. Nakamura, T.; Misono M.; Yoneda, Y. *Chemistry Letters* **1991**, 1589-1592.
13. Mizuno, N.; Tanaka, M.; Misono, M. *J. Chem. Soc. Faraday Trans.* **1992**, *88*(1), 91-95.
14. Li, Y.; Hall, W.K. *J. Catal.* **1991**, *129*, 202-215.
15. Bartley, J.J.; Burch, R.; Chappell, R.J. *Appl. Catal.* **1988**, *43*, 91-104.
16. Teraoka, Y.; Fukuda, H.; Kaguwa, S. *Chemistry Letters* **1990**, p.1-4.
17. Schefer, R.M. *Combust. and Flame.* **1992**, *45*, 171-190.
18. Barnett, H.C.; Hibbard, R.R. NACA Report 1300, **1959**, p.106.
19. Iwamoto, M., and Hamada, H. *Catal. Today* **1991**, *10*(57).
20. Heker, W.L.; and Bell, A.T. *J. Catal.* **1983**, *84*,200.
21. Lorimer, P.; and Bell, A.T. *J. Catal.* **1979**, *59*,223.

RECEIVED September 30, 1993

Chapter 19

Contemporaneous Removal of SO₂ and NO from Flue Gas Using a Regenerable Copper-on-Alumina Sorbent-Catalyst

G. Centi¹, N. Passarini², S. Perathoner¹, and A. Riva¹

¹Dipartimento di Chimica Industriale e dei Materiali, Via le Risorgimento 4, 40136 Bologna, Italy

²Divisione Servizi Ausiliari, Enichem ANIC, Piazza le Boldini 2, San Donato Milanese, Italy

The kinetics and reaction mechanism of SO₂ oxidation-sorption (DeSO_x) and simultaneous reduction of NO by NH₃/O₂ (DeNO_x) on copper oxide on alumina are presented with reference to the development of this system for the application to a dry technology for the removal of SO₂ and NO from flue gas based on a regenerable sorbent-catalyst. The DeSO_x reaction kinetics and differences for fresh and for stabilized samples and the influence of pellet diameter and support porosity characteristics on the efficiency of SO₂ capture are reported. Aspects of the nature of the active copper sites and differences between fresh and stabilized samples, regenerability of sulphated samples and behavior of copper-on-alumina in the conversion of NO to N₂ by NH₃/O₂ during the simultaneous capture of SO₂ are also discussed.

The worldwide trend toward lower levels of pollutant emissions from power generating plants has spurred significant interest in the development of new less costly technologies capable of reducing emissions of SO₂ (*DeSO_x*) and NO_x (*DeNO_x*). State-of-the-art power plants employ individual unit operations for SO₂ and NO_x control. Wet or dry flue gas desulphurization (FGD) systems can achieve 70 to 90% SO₂ removal, depending on process design, fuel characteristics and emission regulations, and selective catalytic reduction (SCR) systems are also achieving more than 80% NO reduction. A process design integrating SO₂ and NO_x removal in a single unit operation offers the potential for reducing the cost of environmental control; such a design, however, should adhere to the following requirements:

- minimum waste production or the formation of valuable by-products
- minimization of energy use, especially in the cooling or reheating of flue gas, i.e. the technology must operate at the same temperature as that of the flue gas after the first economizer (around 350°C)

0097-6156/94/0552-0233\$08.00/0
© 1994 American Chemical Society

- considerable flexibility of application to different situations and the possibility of an efficient retrofit to existing power generation plants
- high efficiency of SO₂ and NO abatement
- low overall cost.

The combined removal of SO₂ and NO using a dry process based on a regenerable copper-on-alumina sorbent-catalyst potentially fulfills these requirements and economic evaluations show a distinct advantage over possible competitive technologies (1). Various research groups have studied this technology (2 and references therein). In this work we shall discuss, in particular, the results obtained in a research program carried out within the framework of the E.E.C. BRITE-EURAM program.

Process Layout

The basic layout of the process is shown in Figure 1 together with the main chemical reactions involved. The copper-on-alumina catalyzes the oxidation of SO₂ to SO₃ which immediately reacts with the sorbent-catalyst to form surface metal-sulphate species. At the same time, copper ions catalyze the conversion of NO to N₂ in the presence of O₂ and added ammonia. The contemporaneous formation of sulphate species due to SO₂ capture has relatively little influence on the rate of this reaction in contrast to V-TiO₂ based monolith-type catalysts used in commercial SCR DeNO_x technologies (3). When the sorption capacity of the catalytic material is exhausted, the solid is transferred to a regeneration unit where a reducing agent (H₂-containing mixtures, CH₄) is added; a stream containing a high concentration (30% or more) of SO₂ is produced which can be sent to a conventional process for the generation of concentrated H₂SO₄ or possibly of S. The regenerated sorbent-catalyst is then transferred again to the reaction unit following previous reoxidation of the reduced copper.

The process is thus basically carried out in two main sections: the reaction unit for the oxidation-sorption of SO₂ and reduction of NO by NH₃/O₂ which operates at temperatures of around 350°C and the regeneration unit operating at about 500°C. The first reactor can be configured in different ways and the choice of the type of reactor (fluid-bed, gas-solid trickle bed and radial mobile-bed) (4) differentiates the various research projects on this topic. However, two important parameters associated with the type of reactor (a low pressure drop across the reactor and a low rate of sorbent-catalyst degradation by attrition) can be minimized by using a radial-type mobile-bed reactor. We shall refer in the following sections to the development of the catalyst-sorbent for this type of reactor configuration.

The Copper-on-Alumina System

The copper-on-alumina catalytic system has some advantages over other possible catalytic systems for this combined reaction of SO₂ and NO removal (2,4-11):

- less demanding reaction conditions for the regeneration than those required for many other metal sulphates in combination with a sufficiently high rate of SO₂ capture

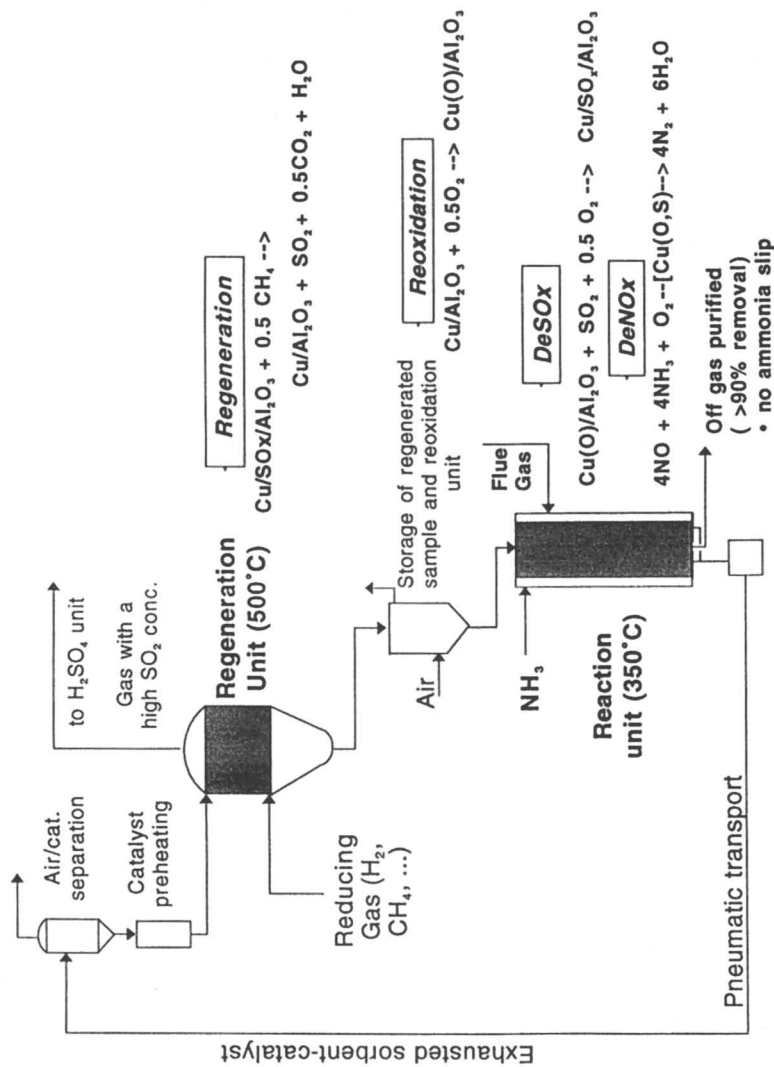


Fig. 1 Schematic process layout for the simultaneous removal of SO₂ and NO from flue gas using a regenerable copper-on-alumina sorbent-catalyst and the main chemical reactions involved in the various steps.

Table I. Textural properties of alumina pellets used as the support for copper oxide in the preparation of the sorbent-catalyst for the tests of simultaneous DeSO_x-DeNO_x

Sample	Pellet diameter range, mm	Surface Area, m ² /g	Mean diameter of pore, Å	Total pore volume, cm ³ /g
A	2.7-3.8	111	230	0.78
B	1.7-2.7	160	263	1.07
C	1.7-2.7	168	300	1.20

- good DeNO_x reaction rate in the presence of high SO₂ concentrations and little influence of the parallel process of sulphate formation
- high DeSO_x and DeNO_x activity at reaction temperatures compatible with those of the flue gas (around 350°C)
- good stability over extended operations (high number of reaction- regeneration cycles) in terms of both reactivity and mechanical properties
- relatively low costs of preparation.

Using this sorbent-catalyst it is therefore possible to design a process with efficiencies in SO₂ and NO removal above 90% with interesting overall economics. We shall discuss here some of the main catalytic, kinetic and mechanistic aspects of this system in particular for the DeSO_x reaction in order to evidence aspects of its reactivity and characteristics useful for the further development of this sorbent-catalyst system and of this technology for flue-gas cleanup.

Experimental

Copper-on-alumina samples were prepared by incipient wet impregnation using an aqueous Cu-acetate solution and pure γ -Al₂O₃ spherical pellets. Table I summarizes the main textural characteristics of the three types of alumina supports used. The amount of copper in the final catalyst was 4.5% wt as CuO. After impregnation and drying, the pellets were calcined at 500°C to decompose the acetate anions. The mean copper content in the final catalyst was checked by atomic adsorption spectroscopy. The homogeneous distribution of copper within the pellet diameter was verified by scanning electron microscopy (SEM). Reported in Figure 2a is a SEM micrograph of a copper-on-alumina sample prepared on type A alumina pellets (see Table I), whereas Figure 2b shows the corresponding Cu distribution maps obtained with x-ray CuK _{α} microprobe which evidences the homogeneous dispersion of copper within the pellet.

Catalytic and sorption tests were made in a quartz flow microreactor usually containing an amount of sample in the 1-5 g range in the form of powder (around 0.1 mm mean diameter) or pellets. The reactor inlet and outlet compositions were monitored continuously using an on-line mass quadrupole apparatus connected to a computer for

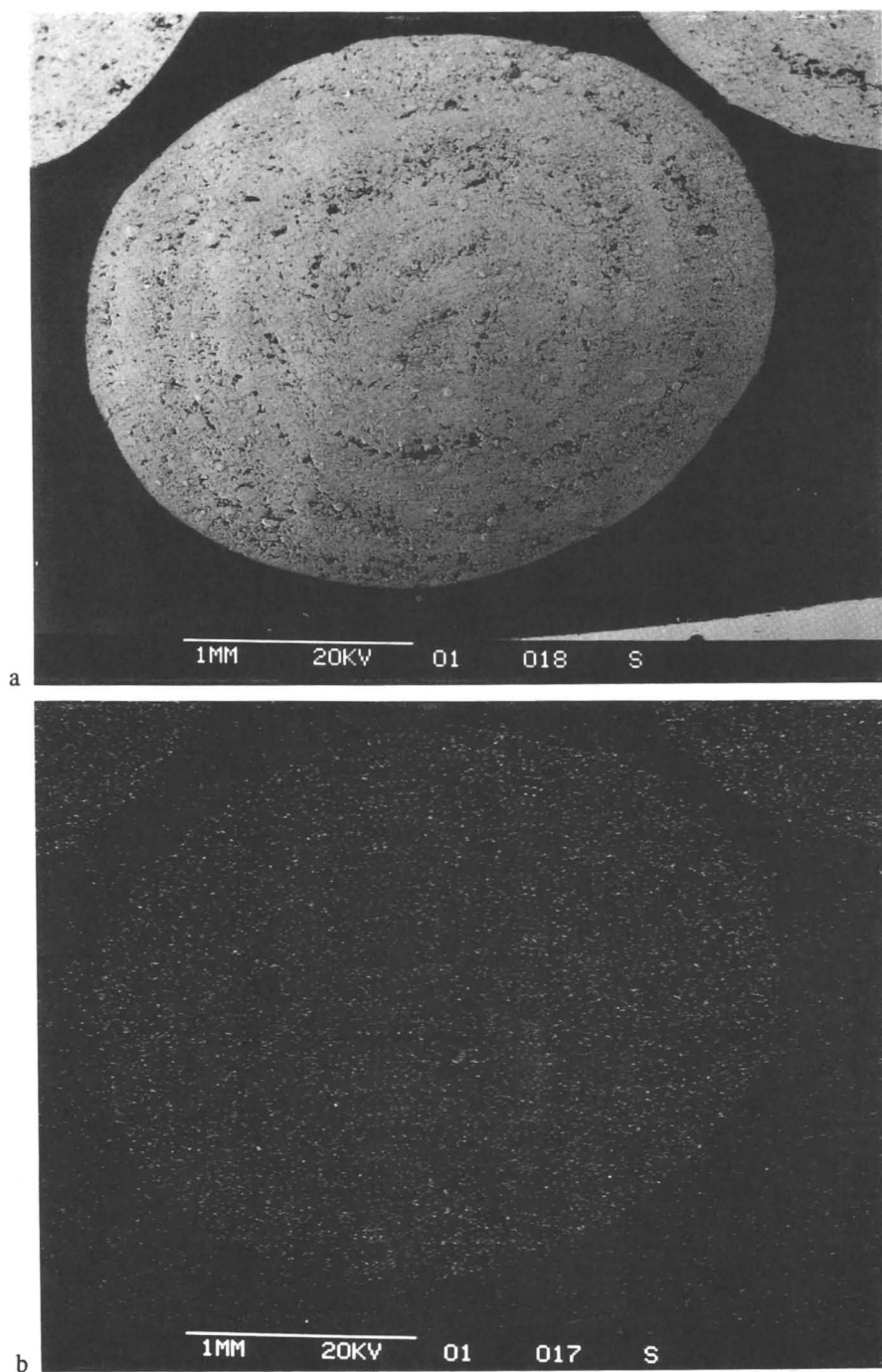


Fig. 2 (a) Scanning electron micrograph of a copper-on-alumina sample (on type A alumina, see Table I) and (b) corresponding distribution map of copper within the pellet as determined by Cu K α microprobe.

the elaboration of the data and control of mass balances. The total flow rate was usually 12 L/h; synthetic gas mixtures with the compositions reported in the figure legends were used in these tests. SO₂ sorption tests with a constant SO₂ concentration were made, on the contrary, by monitoring the weight change in a thermobalance flow apparatus. Further details on the apparatus for these tests and on the preparation procedure of the samples have been previously reported (2,4,11). Kinetic parameters were calculated using a non-linear regression analysis procedure (11).

Kinetic data for the study of the DeSO_x reaction were obtained in a microbalance flow apparatus using the sample grounded in particles with a mean diameter of 0.1 mm, because this apparatus allows to determine a direct relationship between rate of SO₂ capture and degree of sample sulphation. However, in order to check the absence of significant mass transfer limitations in the microbalance system, kinetic data obtained in this apparatus were used to fit the results obtained in a continuous flow fixed bed reactor by using an appropriate reactor model. The correct description of the latter results allows to exclude the presence of significant interphase mass transfer limitations in the type of microbalance apparatus used for the kinetic studies. More details on this apparatus were previously reported (11).

Results and Discussion

Behavior during the Simultaneous Removal of SO₂ and NO. Figure 3 shows a typical result obtained at 350°C over copper-on-alumina in the reduction of NO by NH₃/O₂ during the simultaneous oxidation-sorption of SO₂. The data were obtained in a fixed-bed microreactor using a synthetic gas composition in order to show more clearly and discuss the reaction kinetics and mechanism. It should be mentioned, however, that results in good agreement with those of Figure 3 were obtained using real flue gas deriving from a high-sulfur content gasoil and about hundred times higher amounts of the sorbent-catalyst. The catalytic behavior refers to the activity of a stabilized sample after several cycles of reaction-regeneration. In fact, an initial change in the catalytic and sorption reactivity was observed during about the first 3-5 cycles of reaction-regeneration and then the behavior remains approximately constant for extended operations (2). We shall refer hereinafter to a stabilized sample after this initial change in reactivity in comparison to that of a fresh initial sample. Some aspects of the nature of this transformation will be discussed in the following sections.

At 350°C a nearly complete conversion of NO is observed with a selectivity to N₂ of about 94-97% due to the formation of small amounts of N₂O (around 20-40 ppm) (Fig.3). No ammonia slip was detected even in the presence of excess ammonia with respect to the stoichiometric NH₃ to NO ratio of 1.0, because any excess ammonia remains adsorbed on the catalyst. In the first minutes from the starting of the feeding of the reacting mixture the conversion of NO is less than 100%, but rapidly reaches values of around 100%. This is related to an initial competition between adsorption of ammonia to form ammonium bisulphate and reaction of NH₃ with NO to form N₂ (6). In fact, it was previously shown (6) that the activity in the NO conversion with NH₃/O₂ in the absence of SO₂ of

copper-on-alumina samples is nearly independent of the presence on it of sulphate species. However, when sulphate species are present on the catalyst, a greater induction time is observed due to the competition between ammonia reaction with NO and with sulphate species. In addition, the mechanism of NO conversion over these catalysts probably involves the intermediate formation of nitrate-like species on the catalyst surface (7,8). Part of the initial change in the catalytic DeNO_x reactivity of stabilized copper-on-alumina is also related to the progressive accumulation of nitrate-like species on the catalyst surface and their role in the DeNO_x reaction mechanism (7,8). When the reaction temperature is lowered to about 300°C, the first mechanism of competitive formation of ammonium bisulphate becomes more relevant with a marked decrease in the initial conversion of NO and slower rate of reaching nearly complete conversion.

The removal of SO₂, due to its oxidation and sorption in the form of surface metal-sulphate complexes, is initially complete. After approximately one hour, the SO₂ starts to be detected in the reactor outlet stream and the percentage of SO₂ removal progressively decreases. The breakthrough time (defined as the time when the SO₂ outlet concentration becomes higher than 5% of the inlet value) and the rate of SO₂ removal decay obviously depend on the amount of sorbent-catalyst and its copper content as well as on the SO₂ molar flow rate. However, as we shall discuss later, the dispersion of copper in the particle grains, the porosity of the alumina support and the particle diameter are also additional very important factors.

Aspects of the Mechanism of SO₂ Capture. The mechanism of oxidation-sorption of SO₂ in the form of a regenerable surface metal-sulphate species over copper-on-alumina has been previously discussed in detail on the basis of reactivity measurements (2), infrared studies (2,9) and chemical analysis data (10), but it is worthwhile to review briefly the key aspects useful for the discussion in the following sections and to add some further evidence which can better clarify some aspects. Sorption tests both in a flow reactor and in a thermogravimetric apparatus clearly show that the initial rate of SO₂ uptake is high and tends to decrease proportionally to the amount of sulphate species on the catalyst. For the higher times in contact with the flow, the SO₂ to Cu molar ratio can be higher than the stoichiometric value for the complete transformation of CuO to CuSO₄, depending mainly on the reaction temperature (2,4,8). At a temperature above about 320°C, limiting values of SO₂ to Cu ratio in the 1.5-2.0 range can be obtained. This is clear evidence that the alumina support actively participates in the mechanism of SO₂ capture. Accordingly, the SO₂ to Cu ratio was found to depend considerably on the type of metal-oxide support (4). Sorption tests furthermore suggest that copper catalyzes the oxidation of SO₂ to SO₃, but SO₃ does not desorb in the gas phase and immediately reacts to form surface metal sulphates. The infrared characterization of SO₂ interaction with the copper-on-alumina (2,9) confirms that different metal sulphates form at different reaction rates. The various surface sulphate species observed were assigned to bidentate species linked to copper, aluminium or copper-aluminium ions. The latter species probably form at the interface of copper-oxide surface islands embedded in the alumina matrix. The

formation of bulk- type $\text{Al}_2(\text{SO}_4)_3$ or CuSO_4 species, on the contrary, is of minor importance, explaining why this catalyst does not rapidly lose its reactivity and mechanical strength properties in consecutive reaction-regeneration cycles notwithstanding the severe chemical transformations involved in the reaction and regeneration steps.

These metal sulphates are also characterized by different reducibilities and, in fact, in the first reaction cycle only about half of the amount of sulphate species on the catalyst can be eliminated in the regeneration step. This is shown in Figure 4 which reports the weight change observed during the regeneration step (using 2% H_2 at 420°C) in consecutive cycles of sulphation (at 250°C with 0.8% SO_2) and regeneration. Weight changes lower than 0 as equivalent SO_2 to Cu ratio are related to the reduction of copper oxide to metallic copper. In the first cycle only a part of the sulphate species formed can be regenerated, whereas after approximately 4 cycles all the sulphate species formed can be regenerated in the consecutive step. Figure 4 also clearly shows that the rate of regeneration of the sample after the first sulphation steps is lower than the rate for stabilized samples due to a change in the nature of the surface copper species. It is interesting to note that for the lower times-on-stream a clear autocatalytic effect on the rate of reduction can be observed especially in the first cycle (Fig. 4). This is related to the formation of limited amounts of CuS species in the reduction of CuSO_4 by H_2 . It is reasonable to assume that CuS catalyzes the reduction through an hydrogen spillover mechanism (5). The further reduction of CuS to metallic copper forms H_2S which, in fact, is detected in small amounts in the reduction by H_2 (5,8). The use instead of CH_4 as the reducing agent gives rise to only SO_2 in the regeneration step (5).

The DeSOx reaction mechanism can thus be summarized as follows: copper ions catalyze the oxidation of SO_2 to SO_3 in the presence of gaseous oxygen forming a probably S-bonded chemisorbed SO_3 species that further reacts with a nearby copper site or migrates to Al sites forming a bidentate sulphate species characterized by low symmetry and partially coordinating water molecules. For the higher sulphate coverages the latter mechanism probably becomes the one which controls the overall reactivity, but its relative contribution to the overall sorption rate decreases in stabilized samples as compared to fresh copper-on-alumina.

Kinetics of the DeSOx Reaction. In the contemporaneous removal of SO_2 and NO on copper-on-alumina two different types of kinetic processes are present, the first one involves the oxidation-sorption of SO_2 with a progressive decrease in the reaction rate as a function of the degree of sulphation (we shall refer hereinafter to SO_2/Cu molar ratio or briefly as S/Cu to indicate the degree of sulphation) and the second one a catalytic process of NO reduction, the rate of reaction of which is nearly independent of S/Cu. In order to limit the rate of solid transport between the reaction and regeneration units (Fig. 1) that considerably affects the life-time of the sorbent-catalyst and overall economics, an efficient use of the sorption capacity of the copper-on-alumina is necessary, i.e. a S/Cu ratio around 1.0 or above in the exhausted sample before regeneration must be achieved.

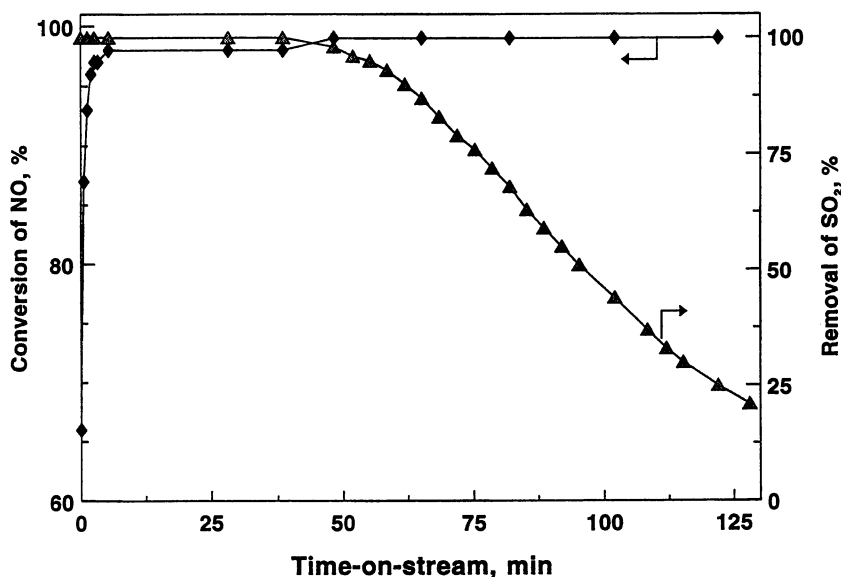


Fig. 3 Removal of SO₂ and NO at 350°C on stabilized copper-on-alumina in simultaneous DeSO_x-DeNO_x experiments. Exp. conditions: 800 ppm NO, 824 ppm NH₃, 3% O₂, 1990 ppm SO₂, 1 g catalyst, flow rate 12 L/h.

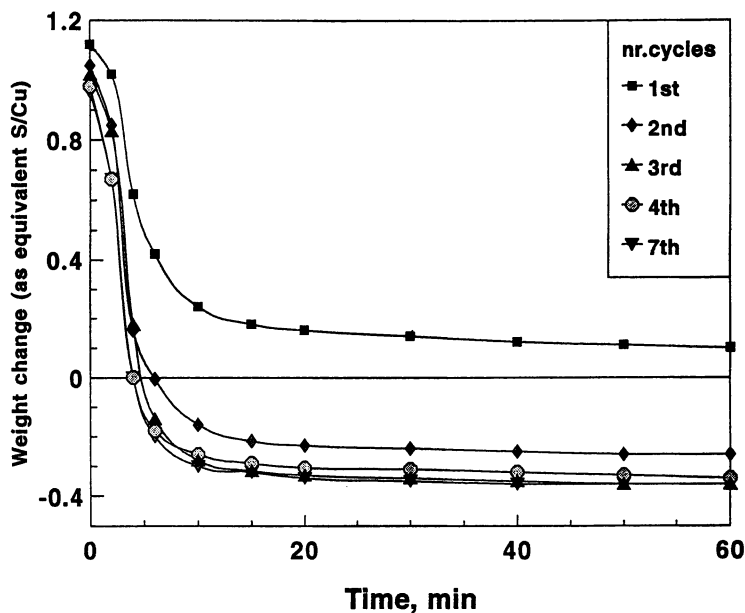


Fig. 4 Weight change (as equivalent S/Cu) per gram of copper-on-alumina as a function of time-on-stream in contact with a flow of 2% H₂ in helium at 420°C for the sample after different cycles of sulphation-regeneration.

Due to the progressive decrease in the rate of SO₂ capture as a function of S/Cu, in order to have a 90% or higher removal of SO₂, the gas- solid contact time in the radial-type mobile-bed reactor used in this project (see above and Fig. 1) is determined by the DeSOx deactivation kinetics, i.e. the gas-solid contact time required for the complete conversion of NO is significantly lower. We shall therefore discuss here only some aspects of the DeSOx reaction kinetics.

Fresh Sorbent-Catalyst. A complete analysis of the DeSOx reaction kinetics on a fresh copper-on-alumina sample has been previously reported (11), but we shall briefly add here some further data or comments on some previous results in order to highlight the key aspects useful for the following discussion.

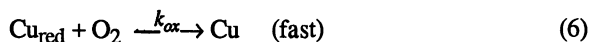
As indicated in the section on the DeSOx reaction mechanism, the sulphation process of copper-on-alumina involves the formation of surface bidentate sulphate species linked to copper or to alumina sites either on not-covered alumina particles or at the alumina-copper oxide interface region. In fact, even for loadings with copper oxide corresponding to the theoretical, complete coverage of alumina with a bidimensional copper oxide film (approximately 5% wt as CuO for an alumina of around 100 m²/g), patches of uncovered alumina are present. For higher copper loadings, the segregation of CuO microcrystallites is observed which negatively affects the life-time resistance of the sorbent- catalyst in several cycles of reaction-regeneration and conditions of solid transport.

Infrared analysis of the sulphation process (2,9) suggests that SO₂ is catalytically oxidized on copper sites to form S-bonded SO₃ which can then react with a second copper site or migrate on the surface to Al sites. From the kinetic point of view, this reaction mechanism can be modelled assuming two parallel reactions of formation of the two sulphate species involving different type of sites and first or second reaction orders. Alternatively, two consecutive reactions or a more complex kinetic reaction network can be considered that better simulates the reaction mechanism suggested by IR data (11). The fitting of the experimental values of S/Cu as a function of the time in contact with a large excess flow containing a constant concentration of SO₂ and of the reaction temperature in the 250-350°C range indicates that only two models are in good agreement with the experimental data. The first is based on two parallel reactions:



where Cu and Al indicate the concentration of free active sites of copper and alumina, S' a chemisorbed SO₂ molecule and CS and AS are surface sulphate species linked to copper or alumina, respectively. The second reaction network is based on a sequence of reactions in agreement with the experimental evidence and can be formally written as follows:





where eq. (3) corresponds to the oxidation of chemisorbed SO₂ (S') by free Cu sites forming chemisorbed SO₃ (S*) which can then interact with a second neighboring copper site forming a surface copper-sulphate (CS) or alternatively can migrate to Al sites to form a surface aluminum-sulphate (AS) leaving a reduced copper site rapidly regenerated by O₂. This second kinetic mechanism fits the results better [2.6% mean error as compared to 4.3% mean error for the mechanism according to eq.s (1) and (2)] (11) and especially provides a better description of the results in the intermediate range of reaction temperatures. This is shown in Figure 5 which compares the fit of the experimental values at different reaction temperatures (symbols) obtained according to model 1 [eq.s (1) and (2)] and model 2 [eq.s (3)-(6)]. Experimental data for this comparison were obtained in a microbalance apparatus. One should observe that at 350°C both models describe the experimental results well and that reaction temperatures lower than about 350°C were not convenient due to the presence of the competitive reactions on the conversion of NO discussed above. On the other hand, the kinetic reaction model based on eq.s (1) and (2) can be integrated analytically in the simple form:

$$\frac{S}{\text{Cu}} = \frac{(k_1 \cdot S') \cdot \text{Cu}_0 \cdot t}{1 + (k_1 \cdot S') \cdot \text{Cu}_0 \cdot t} + \frac{\text{Al}_0}{\text{Cu}_0} \cdot (1 - e^{-(k_2 \cdot S') \cdot t}) \quad (7)$$

where Cu₀ and Al₀ are the initial concentrations of Cu and Al (mol/g) at zero time-on-stream (t=0), respectively, and S' the concentration of chemisorbed SO₂. The analytical form of eq. (7) combined with the good fit at 350°C suggests that this reaction model may be more conveniently used for practical purposes. Table II reports the best values of the kinetic parameters at 350°C obtained according to model 1.

Figure 6 shows the dependence of the initial rate of sulphation at 350°C on the concentration of SO₂ in the reacting mixture. The initial rate (value extrapolated at zero degree of sulphation of copper-on-alumina from the dependence of S/Cu from time-on-stream and SO₂ concentration obtained in a microbalance apparatus) does not depend linearly on the SO₂ concentration. The dependence indicates a phenomenon of saturation of the active sites for the chemisorption of SO₂ according to a Langmuir-Hinshelwood kinetic model. However, it can be observed that in the range up to about 3000 ppm of SO₂, which is that more interesting for the application of the technology, the approximation of first order dependence (shown in Fig. 6 with a dashed line) can be considered sufficiently accurate:

$$S' = K_{\text{SO}_2} [\text{SO}_2] \quad (\text{mol/L}) \quad (8)$$

where $K_{\text{SO}_2} = 6.37 \cdot 10^{-2}$. The concentration of oxygen instead does not affect the overall rate when in excess to SO₂.

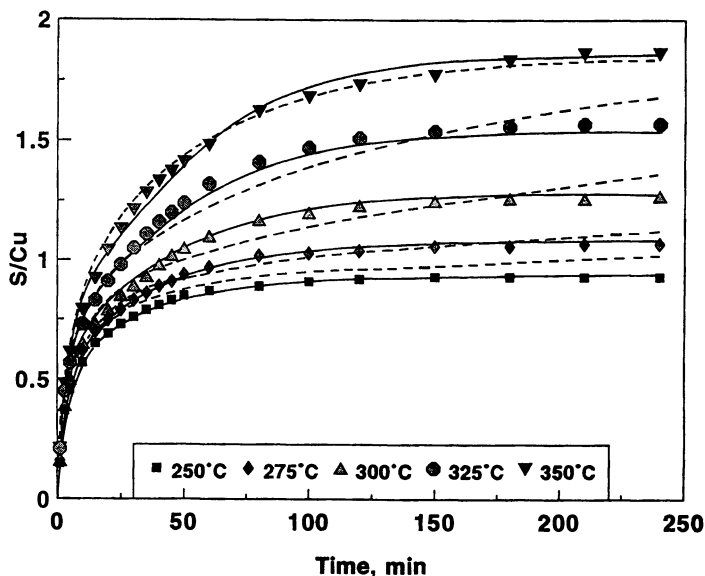


Fig. 5 Change in the S/Cu ratio as a function of time-on-stream and reaction temperature in a fresh copper-on-alumina. *Symbols*: experimental data. *Dashed line*: values calculated for model 1 [eq.s (1)-(2)]. *Solid line*: values calculated for model 2 [Eq.s (3)-(6)]. Exp. conditions: SO₂ and O₂ concentration (constant as a function of time on stream), 0.8% and 5.4% v/v, respectively.

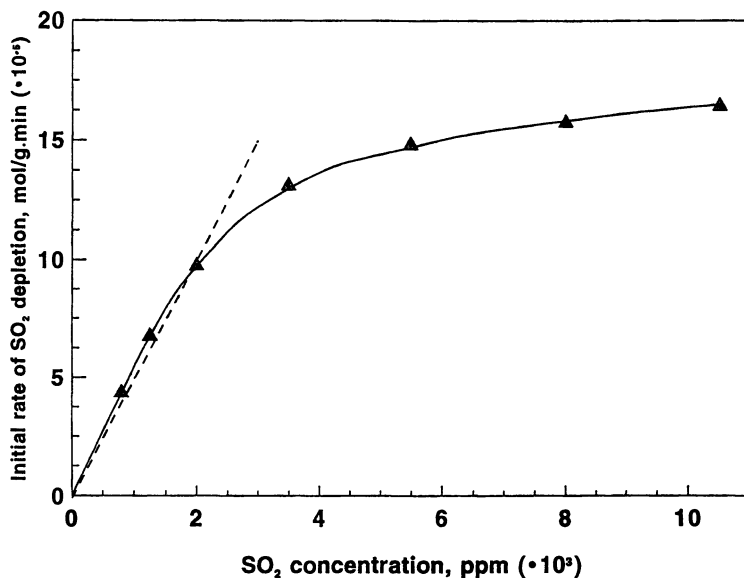


Fig. 6 Dependence of the initial rate (at zero degree of sulphation) of SO₂ capture at 350°C on the SO₂ concentration.

Table II. Best values of kinetic parameters at 350°C according to model 1 [eq.s (7)] determined for both fresh and stabilized copper-on-alumina samples (copper content $5.86 \cdot 10^{-4}$ mol/g)

<i>Sample</i>	k_1 L·g·mol ⁻² ·min ⁻¹	k_2 L·mol ⁻¹ ·min ⁻¹	Al_o/Cu_o
fresh	1.992E7	8.513E2	0.863
stabilized	4.367E7	1.322E3	0.587

It should also be pointed out that Figure 5 clearly shows that the sulphation process is a slower process than the regeneration (compare the time-on-stream dependence of the S/Cu ratio in Figs 5 and 4). Furthermore, temperatures higher than about 350°C in the reaction are not worthwhile, because above this temperature the parallel reaction of NH₃ oxidation becomes predominant with a reduction in the efficiency of NO removal. On the contrary, in the regeneration unit, higher reaction temperatures and rates are preferable in order to form a highly concentrated stream of SO₂. However, above about 500°C the stability and life-time of the sorbent-catalyst decrease considerably.

Stabilized Sorbent-Catalyst. After the first 3-4 cycles of reaction-regeneration, the sorbent-catalyst reactivity towards SO₂ oxidation-sorption or regeneration reaches a stationary condition, as discussed above. This stationary condition is characterized by the presence of a fraction of sulphate species linked to Al sites not-reduced during the regeneration step, but also by a different reactivity of copper sites towards both SO₂ oxidation-sorption and regeneration. This is probably related to a change in the nature and distribution of copper species (9). Initially, copper ions are present as patches of a surface spinel-type CuAl₂O₄ species embedded in the alumina matrix, but during regeneration very small particles of metallic copper form which, in the absence of sulphate species, tend to reform the surface copper spinel by oxidation (12). The presence of sulphate species on alumina (not eliminated during the first regeneration step), however, probably inhibits the transformation and thus very small highly reactive particles of CuO form, the sintering of which is inhibited by the residual sulphates. The copper particles remain therefore in a highly dispersed state.

The kinetic analysis of the rate of SO₂ capture as a function of the degree of surface sulphation confirms this tentative mechanism. Reported in Table II are best kinetic parameters found at 350°C for fresh and stabilized copper-on- alumina, according to eq. (7) based on two parallel reactions. Comparison of the kinetic parameters shows that as compared with the fresh catalyst, the stabilized catalyst has fewer surface sites of alumina available for the sulphation reaction (Al_o) and higher values of the kinetic constants of

reaction, according to the mechanism of surface transformation from the fresh to stabilized sample discussed above.

Role of Pellet Size and Porosity of the Support. The development of the copper-on-alumina for industrial application requires the use of support pellets with mechanical strength, texture and size characteristics suitable to minimize the pressure drop across the mobile-bed reactor and the formation of fines during the pneumatic transport between the various sections of the process (Fig. 1). Therefore the development of a system suitable for the desired final application demands a series of constraints on the characteristics of the sorbent-catalyst in terms of pellet diameter and form, porosity and surface area, and methodology of preparation which, on the other hand, considerably affect the overall rate of SO₂ capture and thus the reactor design.

The influence of the pellet diameter on the S/Cu vs. time-on-stream curves at a constant SO₂ concentration is shown in Figure 7. Results show that both alumina characteristics and pellet diameter considerably affect the rate of SO₂ capture. On the other hand, even for larger pellets the copper distribution may be assumed rather homogeneous as shown in Fig. 2. Therefore, the influence of pellet diameter on the rate of SO₂ capture may be mainly attributed to intraparticle diffusional limitations on SO₂. The analysis of the curve shape for the pellets with the larger diameter in comparison to that of the same sample in the form of powder suggests that the efficiency of sorbent-catalyst utilization passes through a maximum due to the initial presence of an intraparticle gradient of SO₂ concentration which progressively moves toward the inner core of the pellet for the progressive exhaustion of outer shells and at the same time a change in the rate constant of reaction due to the decrease in the amount of free Al and Cu sites. While it is evident that the classical "shrinking core" or "shell progressive" model is unable to describe correctly the reaction of sulphation of copper-on- alumina, models such as the "grain-micrograin" model of Sohn and Szekely (13) or other possible models of reacting porous solids (14) do not give presently an accurate description of the experimental results. Further studies are thus necessary to model the sulphation reaction in large copper-on-alumina pellets. The porosity and textural characteristics of the alumina pellets also have a considerable effect on the results as shown in Figure 7 which compares S/Cu vs. time-on-stream curves for alumina pellets with the same external diameter (2.7 mm), but the different textural properties summarized in Table I. As the mean diameter of the pores increases, the relative influence of diffusional limitations on SO₂ decreases sensibly. The presence of the intraparticle diffusional limitations discussed above has a considerable effect on the behavior in the reactor and especially the breakthrough time. This is shown in Figure 8 which compares the results in a fixed bed reactor for two commercial alumina samples (A and B of Table I) characterized by different textural properties and different particle size distributions. It can be seen that the proper design of the characteristics of the alumina support can have a considerable effect on the efficiency of utilization of copper-on-alumina in SO₂ oxidation-sorption and thus on the overall process economics which are highly dependent on this factor.

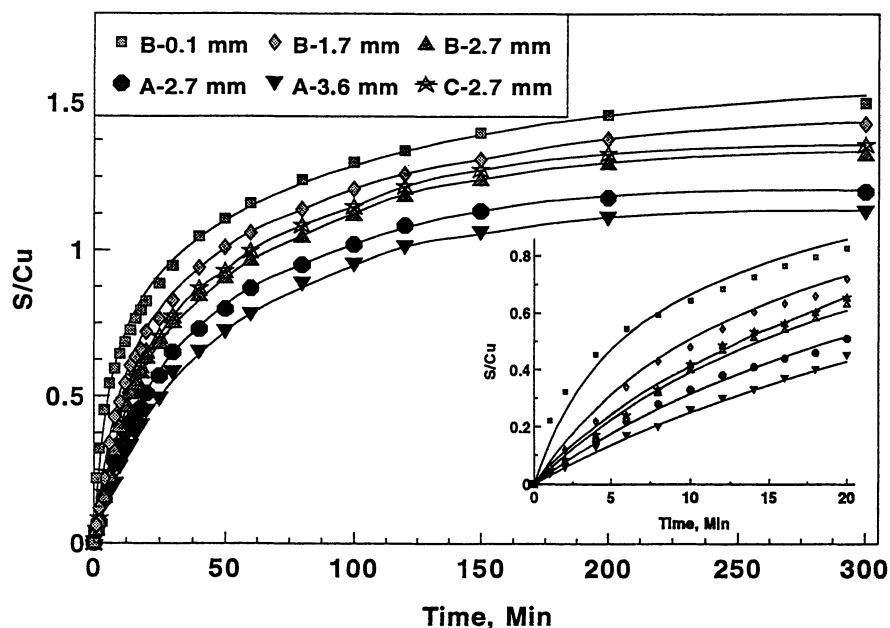


Fig. 7 Influence of pellet diameter and textural characteristics of the alumina support on the change in the S/Cu ratio at 350°C as a function of the time-on-stream. Shown in the inset on an expanded scale is the dependence for the shorter contact times. In the legend the letter indicates the type of alumina according to Table I and the following number the diameter of the pellet used. Exp. conditions: SO₂ and O₂ concentrations (constant as a function of time-on-stream), 0.26% and 2.4% v/v, respectively.

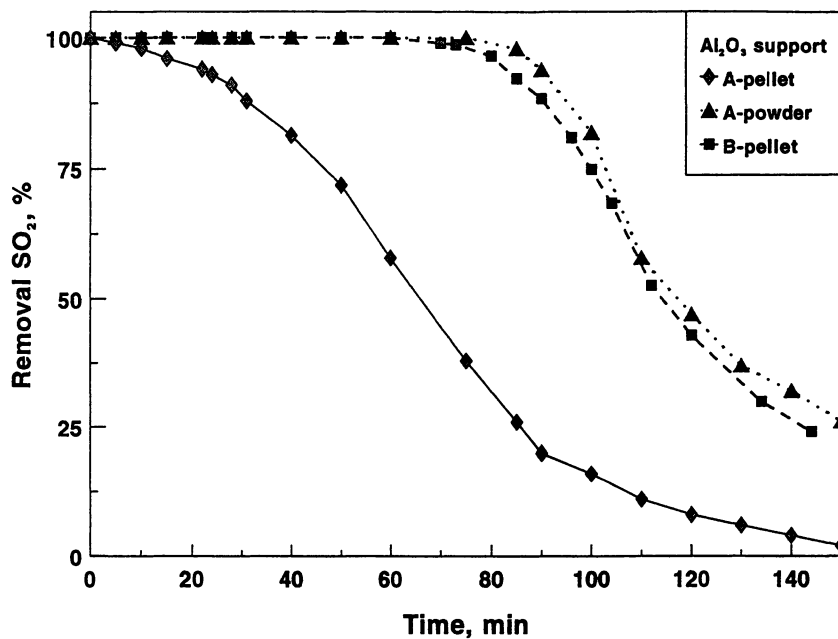


Fig. 8 Breakthrough curves of SO₂ sorption at 350°C using stabilized copper-on-alumina samples (4.5% wt. copper as CuO) and types A and B alumina (see Table I for characteristics and range of particle size for these samples). Exp. conditions: 3 g of sorbent-catalyst, 12 LK/h of total flow, 2035 ppm SO₂, 3% O₂.

Conclusions

The contemporaneous removal of SO₂ and NO from flue gas using a dry process based on a regenerable copper-on-alumina sorbent-catalyst makes it possible to obtain efficiencies of 90% or more in the removal of these pollutants at reaction temperatures of around 350C. The copper-on-alumina can be easily regenerated by a reduction treatment and shows stable activity in several cycles of reaction-regeneration. The slower process of the overall technology is related to the DeSO_x reaction kinetics and the decay of the rate of SO₂ capture as a function of the degree of sulphation. Proper design of support characteristics can minimize the presence of diffusional limitations on this rate and therefore maximize the efficiency in the use of the sorption capacity, reducing the rate of solid recirculation which has a negative influence on the life-time of the sorbent-catalyst.

Acknowledgment

This work was sponsored by the European Community BRITE-EURAM program (Contract BREU-CT 91-0547)

Literature Cited

1. Rubin, E.S.; Salmento, J.S.; Frey, H.C. *Integrated Environmental Control*, EPRI: Palo Alto CA, 1989.
2. Centi, G.; Passarini, N.; Perathoner, S.; Riva, A. *Ind. Eng. Chem. Research*, **1992**, *31*, 1947.
3. Bosh, H.; Janssen, F.J. *Catal. Today*, **1988**, *2*, 369.
4. Centi, G.; Riva, A.; Passarini, N.; Brambilla, G.; Hodnett, B.K.; Delmon, B.; Ruwet, M. *Chem. Eng. Sci.*, **1990**, *45*, 2679.
5. Kartheuser, B.; Hodnett, B.K.; Riva, A.; Centi, G.; Matralis, H.; Ruwet, M.; Grange, P.; Passarini, N. *Ind. Eng. Chem. Research*, **1991**, *30*, 2105.
6. Centi, G.; Passarini, N.; Perathoner, S.; Riva, A.; Stella, G. *Ind. Eng. Chem. Research*, **1992**, *31*, 1963.
7. Centi, G.; Passarini, N.; Perathoner, S.; Stella, L. *Proc. 13th Iberoamerican Simposio de Catalisis*, Segovia (Spain) July 1991, Vol. 1, p 355.
8. Centi, G.; Perathoner, S.; Kartheuser, B.; Hodnett, B.K. *Catal. Today*, **1993**, *17*, 103.
9. Waquif, M.; Saur, O.; Lavalley, J.C.; Perathoner, S.; Centi, G. *J. Phys. Chem.*, **1991**, *95*, 4051.
10. Centi, G.; Perathoner, S.; Kartheuser, B.; Rohan, D.; Hodnett, B.K. *Appl. Catal. B: Environmental*, **1992**, *1*, 129.
11. Centi, G.; Passarini, N.; Perathoner, S.; Riva, A. *Ind. Eng. Chem. Research*, **1992**, *31*, 1956.
12. Pepe, F.; Angeletti, C.; De Rossi, S.; Lo Jacono, M., *J. Catal.*, **1985**, *91*, 69.
13. Sohn, H.; Szekeley, J. *Chem. Eng. Science*, **1972**, *27*, 763.
14. Sahimi, M.; Gavalas, G.R.; Tsotsi, T.T., *Chem. Eng. Science*, **1990**, *45*, 1443.

RECEIVED September 30, 1993

Chapter 20

Pt-ZrO₂ Catalysts for the Oxidation of NO and SO₂ Effects of Sulfate

E. Xue, K. Seshan, P. D. L. Mercera, J. G. van Ommen, and
J. R. H. Ross¹

Faculty of Chemical Technology, University of Twente, P.O. Box 217,
7500 AE Enschede, Netherlands

Pt/ZrO₂-SO₄²⁻ catalysts showed higher activities for the oxidation of NO and SO₂ and higher selectivity for NO oxidation than the un-sulphated Pt/ZrO₂ catalyst. The presence of sulphate in the catalysts had significant influence on the desorption characteristics of NO and NO₂. An increase in the surface acidity and interaction between the surface sulphate groups with the oxygen in Pt oxides were probably the reasons for the improved behaviour of the sulphate-treated catalyst. It was found that a Pt/ZrO₂ catalyst after ageing in NO+SO₂+O₂ gas mixture exhibited a higher catalytic selectivity for NO oxidation than did the fresh sample; the presence of sulphate on this aged catalyst was observed by FT-IR and TPR experiments.

In order to meet legislative requirements for the emission of diesel engine exhaust, especially that of soot (particulates) and NO_x, a catalytic post-treatment of the exhaust is necessary. One of the catalytic approaches is using nitrogen dioxide, which could be obtained by catalytically oxidizing nitric oxide present in the oxygen rich diesel exhaust, to oxidize soot to less harmful CO₂ (1). Catalysts based on noble metals such as Pt have been found to be good for the oxidation of NO to NO₂ (1,2). However, the SO₂ present in the exhaust would be also oxidized over Pt catalysts to SO₃, the sulphates would then be formed and adsorbed on the soot, resulting in an increase of the apparent weight of the soot emitted (2,3). Development of the catalysts which would selectively oxidize NO to NO₂ without oxidising SO₂ to SO₃ is, therefore, of essential importance.

The surface acidity is known to be one of the important factors which can modify the performance of catalyst in many catalytic reactions. It is also known that the presence of sulphate on a ZrO₂ or Pt/ZrO₂ catalyst can modify remarkably the surface

¹Current address: Department of Industrial Chemistry and Life Science, University of Limerick, Plassey Park, Limerick, Ireland

acidity and as a consequence change the behaviour of the catalyst in catalytic reactions (4,5). It is therefore very interesting to see how a sulphate modification would influence a Pt/ZrO₂ catalyst for the oxidation of NO and SO₂. This is studied in this work by examining the performance of a Pt/ZrO₂ catalyst in the reactions, before and after the sulphate modification.

In many cases the presence of SO₂ in exhaust gases has a negative effect on the performance of catalysts. This is normally attributed as a poison effect of SO₂ and/or the formation of sulphate on the catalyst. For example, surface sulphate has been observed on γ -Al₂O₃ when contacted with a gas mixture containing SO₂ and O₂ (6,7). It is interesting to see whether there would be sulphate formation on the Pt/ZrO₂ catalyst, and if so, how the performance of the catalyst would be affected. This is also examined in the present work.

Experimental

Catalyst Preparation. The details of the catalysts used in this study are given in Table 1. Monoclinic ZrO₂ (RC-100, Daiichi Kigenso Kagaco Kogyo Inc., Japan) was used as support in this study. The ZrO₂ powder was first calcined at 500 °C in air for 15 hours and then pressed into pellets, crushed and sieved into grains of size ranging from 0.3 to 0.6 mm. This material is termed below as ZrO₂-0.

Pt(NH₃)₄Cl₂ (Johnson Matthey Chemicals, U.K.) was used as precursor in preparing the platinum containing catalysts. A standard material, designated Pt/ZrO₂, was made by dry impregnation of ZrO₂-0 with precursor containing 1 wt % of Pt, drying at 100 °C and calcination at 500 °C for 2 h. Pt/ZrO₂-1NS was prepared as follows: 5 g of ZrO₂-0 was first contacted with 1.1 cm³ of 1N H₂SO₄, dried at 100 °C for 2 h, and then impregnated with Pt(NH₃)₄Cl₂; the resultant material was dried once more at 100 °C for 2 h and the catalyst was finally calcined at 500 °C in air for 2 h. Pt/ZrO₂-5NS was prepared by the same procedure as that for Pt/ZrO₂-1NS, but 5N H₂SO₄ was used instead of 1N H₂SO₄ during the sulphation of ZrO₂-0; Pt/ZrO₂-5NS therefore has a higher sulphate content than does Pt/ZrO₂-1NS.

Table 1 The catalysts prepared

Catalyst	Total area / m ² g ⁻¹	SO ₄ ⁼ load / wt %	Pt load / wt %	Pt dispersion / %
ZrO ₂ -0	46	0	-	-
Pt/ZrO ₂	41	0	1	38
Pt/ZrO ₂ -1NS	43	1	1	< 5
Pt/ZrO ₂ -5NS	37	5	1	< 5

Activity Measurements. The activity experiments were carried out in a fixed bed reactor system. The gas composition and flow were controlled by means of mass flow controllers. A Nitrogen Oxidise Analyzer (Model 8840, Monitor Labs Inc. USA) was used to measure the concentration of NO and NO₂, continuously. The concentration of SO₂ was monitored on line by a Defor SO₂ Analyzer (Maihak GmbH, Germany). The experimental parameters such as reaction temperature, inlet gas concentration and flow

were all controlled by a computer programme and monitored by a Apple IIe computer connected to the system. The conversions of both NO and SO₂ over were determined by measuring the concentration changes between inlet and outlet of the reactor. Table 2 shows the experimental parameters used in this study. These corresponded to those in a typical diesel exhaust (8-12). The catalyst load in the reactor for the activity measurement was 1.00 g, and the reaction gas mixtures were NO+O₂, SO₂+O₂ or NO+SO₂+O₂.

Table 2 The experimental conditions

Temperature	/°C	200 ~ 400
Pressure	/atm.	1
Catalyst load in reactor	/mg	1000
Gas volume flow	/cm ³ min ⁻¹	400
Inlet gas composition		
NO	/ppm	500
SO ₂	/ppm	50
O ₂	/vol. %	10
N ₂	-	balance

Temperature Programmed Desorption (TPD). Temperature programmed desorption experiments were conducted in the same set-up as that used for the activity measurements. The pre-treating gas was led over the catalyst bed till the maximum reaction temperatures (400 °C). The catalyst was then cooled to room temperature in the same gas stream. The gas flow was changed to N₂ and catalyst bed was purged in N₂ for about one hour. After the signals for NO, NO₂ and/or SO₂ from the analyzers had dropped to zero, TPD was started in N₂ (400 cm³ min⁻¹) with a heating rate of 10 °C min⁻¹. The concentrations of the desorbed NO, NO₂ and/or SO₂ were recorded as a function of temperature.

Results

Catalytic Activities and Selectivity. A series of activity experiments were carried out to see the effect of sulphate treatment on the performance of the catalysts listed in Table 1. The results of the experiments are shown in Figures 1 to 4.

Figures 1 and 2 show the NO conversions over the catalysts, in the absence and presence of SO₂, respectively, as function of reaction temperature. The thermodynamic equilibrium conversions for NO oxidation under the conditions used are plotted as dotted lines. It can be seen that the sulphate-modified catalysts, Pt/ZrO₂-1NS and Pt/ZrO₂-5NS, both show higher NO conversions than does the non-modified Pt/ZrO₂ catalyst, either in the presence or in the absence of SO₂. It should be noted that there are two points at 400 °C which are even higher than the equilibrium conversions, one for Pt/ZrO₂-1NS in Figure 1 and the other for Pt/ZrO₂-5NS in Figure 2. Although the exact reason for the larger conversion is not yet clear, one possibility which can be considered is that the NO was partly decomposed over the catalyst at this temperature. Comparing Figure 1 with Figure 2, it is clear that the difference in the performance between Pt/ZrO₂

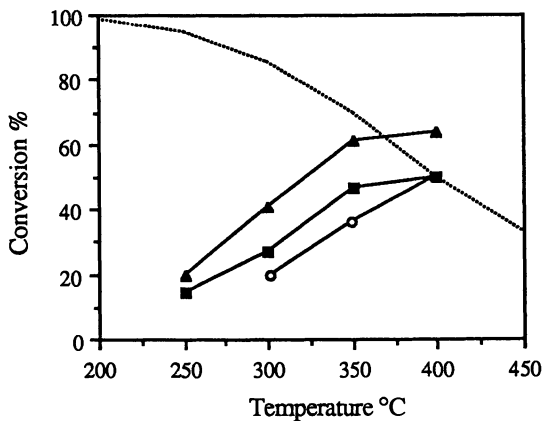


Figure 1 NO conversions in the absence of SO₂ (NO=500 ppm, O₂=10 %), over (○) Pt/ZrO₂; (▲) Pt/ZrO₂-1NS; (■) Pt/ZrO₂-5NS; (---) equilibrium conversion of NO.

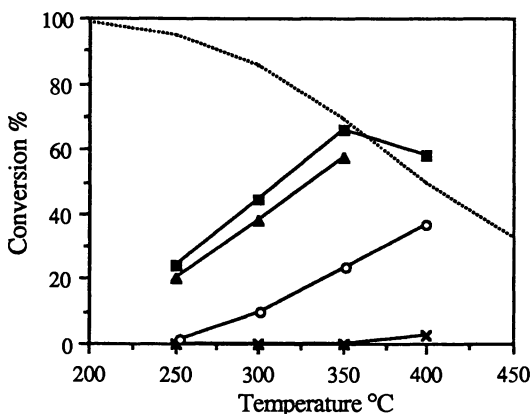


Figure 2 NO conversions in the presence of SO₂ (NO=500ppm, SO₂=50 ppm, O₂=10 %), over (×) ZrO₂-0; (○) Pt/ZrO₂; (▲) Pt/ZrO₂-1NS; (■) Pt/ZrO₂-5NS; (---) equilibrium conversion of NO.

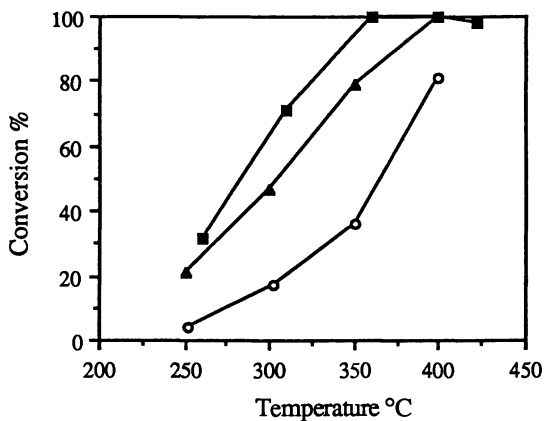


Figure 3 SO₂ conversions in the absence of NO (SO₂=50ppm, O₂=10 %), over (○) Pt/ZrO₂; (▲) Pt/ZrO₂-1NS; (■) Pt/ZrO₂-5NS.

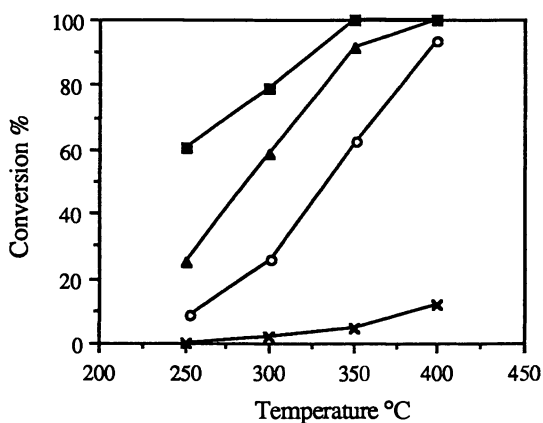


Figure 4 SO₂ conversions in the presence of NO (NO=500 ppm, SO₂=50 ppm, O₂=10 %), over (×) ZrO₂-0; (○) Pt/ZrO₂; (▲) Pt/ZrO₂-1NS; (■) Pt/ZrO₂-5NS.

and the sulphate-modified catalysts, Pt/ZrO₂-1NS and Pt/ZrO₂-5NS, was more pronounced when SO₂ was present than when SO₂ was absent. This is very significant because SO₂ is present under real conditions. It was observed earlier (2) that the presence of SO₂ suppressed the conversion of NO over a Pt/SiO₂ (EuroPt-1) catalyst. The same trend was observed over Pt/ZrO₂ (open circles in Figures 1 and 2) but the influence was almost negligible in the case of Pt/ZrO₂-1NS (closed triangles in Figures 1 and 2) however, the trend was reversed for Pt/ZrO₂-5NS (closed squares in Figures 1 and 2); i.e. when SO₂ was present, the conversions of NO went up with this catalyst.

The conversions of SO₂ versus temperatures, both in the absence and presence of NO over the various catalysts, are shown in Figures 3 and 4. A higher activity for the oxidation of SO₂ was observed over the sulphate-modified catalysts, Pt/ZrO₂-1NS and Pt/ZrO₂-5NS, than that over Pt/ZrO₂, both in the presence and absence of NO. A promotional effect of NO on the oxidation of SO₂ was observed over all three catalysts (see Figures 3 and 4), although this effect was less pronounced compared to that over the Pt/SiO₂ (EuroPt-1) catalyst (2). The ZrO₂-0 support showed negligible conversions of NO and SO₂ (points x in Figures 2 and 4) compared to those over the Pt-containing catalysts.

The selectivity factor, S_R, defined as the ratio of the number of moles of NO converted to that of SO₂ converted, is plotted against the reaction temperatures for various catalysts in Figure 5. The results show clearly that the sulphate-modified catalysts give much higher selectivity than the unmodified catalysts, especially at lower temperatures. (It should be noted that the NO conversions at temperatures higher than 350 °C are limited by the equilibrium, NO + 1/2 O₂ ↔ NO₂, and that the SO₂ conversions reach almost 100 %; a comparison of the selectivity factors has therefore little significance at higher temperatures). It can be seen from Figure 5 that Pt/ZrO₂-1NS gave a better selectivity for NO oxidation than did Pt/ZrO₂-5NS. However, it was observed that the best selectivity was obtained for the Pt/ZrO₂ catalyst aged in the reaction gas mixture (open diamond in Figure 5).

Ageing Tests. Figure 6 shows the conversions of NO and SO₂ over Pt/ZrO₂ and Pt/ZrO₂-5NS as a function of ageing time at the constant temperature of 300 °C. Before the ageing tests, both catalysts had been used for the activity test in the NO+SO₂+O₂ gas mixture in temperature range of 200 °C to 400 °C for about 4 hours and then cooled to room temperature; the catalyst was then heated to 300 °C and the ageing test was started. Experimental values start at t = 4 h; this corresponds to the moment when the gas mixture NO+SO₂+O₂ was switched from the bypass to the reactor.

It can be seen that the NO conversion over the Pt/ZrO₂ catalyst decreased slightly while that of SO₂ decreased relatively rapidly with time, especially in the first few hours. That the data of NO and SO₂ conversions at the starting point are different from those in Figure 2 is due to the fact that catalyst had previously been used for the activity test (i.e., it had been 'aged' in the reaction gas for 4 hours), the trends of the changes in the conversions of NO and SO₂ are more interesting here. The selectivity of the Pt/ZrO₂ catalyst after ageing for 14 hours increased remarkably (see also in Figure 5). Over the Pt/ZrO₂-5NS catalyst, however, the conversions of NO and SO₂ both remained constant with time.

TPD. The TPD results for the different catalysts after different pre-treatments are given in Figures 7 to 9, which show the concentrations of NO, NO₂ and SO₂ as a function of

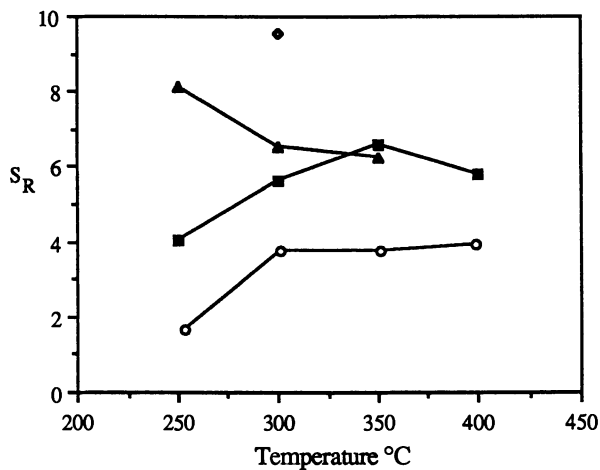


Figure 5 The selectivity of the catalysts for the oxidation of NO over that of SO₂. (○) Pt/ZrO₂; (▲) Pt/ZrO₂-1NS; (■) Pt/ZrO₂-5NS; (◇) Pt/ZrO₂ aged in the reaction mixture.

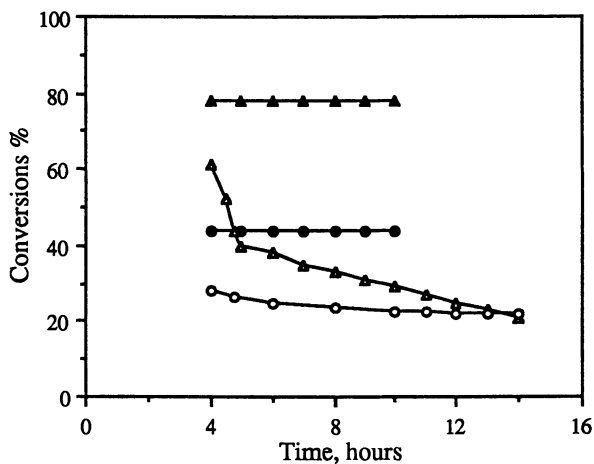


Figure 6 Conversions of NO and SO₂ upon ageing (at 300 °C) for Pt/ZrO₂ and Pt/ZrO₂-5NS. Inlet gas: NO=500 ppm, SO₂=50 ppm, O₂=10%. (○) NO conversion, Pt/ZrO₂; (△) SO₂ conversion, Pt/ZrO₂; (●) NO conversion, Pt/ZrO₂-5NS; (▲) SO₂ conversion, Pt/ZrO₂-5NS.

temperature. The details of catalyst load and the pre-treating gases used are given in the figures. Figure 7 shows the NO and NO₂ desorption curves for Pt/ZrO₂ after the catalyst was pre-treated with 500 ppm of NO. It can be seen that the desorption of NO (solid line) occurs over a broad temperature range, with a series of three maxima: peak I has a maximum at a temperature around 100 °C, peak II is centered at around 200 °C and peak III is at about 390 °C. Peak II appears to be the predominant form of desorption of NO from Pt/ZrO₂. A small amount of NO₂ was desorbed from Pt/ZrO₂ at high temperatures (dotted line), the peak being centered at about 370 °C.

The TPD results of Pt/ZrO₂-5NS after pre-treatment with 500 ppm of NO are shown in Figure 8. The NO desorption (solid line) appears to be less broad than that over Pt/ZrO₂. The desorption curve seems to be composed mainly of a desorption peak centered at about 90 °C and a small peak centered at about 200 °C; these seem to correspond respectively to the peaks I and II in Figure 7. The NO₂ desorption occurs only at low temperature (dotted line), the peak is relatively large and this is thus very different from that for Pt/ZrO₂.

The results of TPD of SO₂ from the different catalysts after pre-treatment with an SO₂+O₂ mixture are plotted in Figure 9. All the catalysts showed similar behaviour for the desorption of SO₂. Desorption started at around 300 °C over all the catalysts and continued up to about 450 °C, the increase being fastest with Pt/ZrO₂-5NS and slowest with Pt/ZrO₂.

TPR. TPR experiments were carried out using both fresh and used Pt/ZrO₂, Pt/ZrO₂-1NS and Pt/ZrO₂-5NS catalysts. The results are shown in Figures 10 to 12, in which H₂ uptake is shown as a function of temperature for each catalyst, fresh and used.

The TPR trace of the fresh Pt/ZrO₂ catalyst shows one reduction peak at around 190 °C but the TPR trace of the used Pt/ZrO₂ shows two peaks (Figure 10). The low temperature peak is similar to that of the fresh catalyst; the second H₂ uptake peak appears at a higher temperature, the peak maximum being at about 440 °C.

Figure 11 shows the TPR patterns of the fresh and used Pt/ZrO₂-1NS samples. There are two peaks visible in the TPR trace of the fresh catalyst: one appears with a maximum at around 200 °C and the other at about 480 °C. The TPR trace of the used catalyst shows at least two peaks, one centered at about 200 ~ 250 °C and the other at about 450 °C. The peak for the used sample of Pt/ZrO₂-1NS at the higher temperature appears to be relatively very large.

The results for TPR of Pt/ZrO₂-5NS are shown in Figure 12. The TPR curves of both fresh and used catalysts show a great similarity and almost overlap each other. The reduction peaks occur only at higher temperature with a peak maximum around 440 °C. There is little evidence of a peak at lower temperatures.

FT-IR Spectra. In order to try to identify the presence of sulphate on the catalyst surface, FT-IR spectra of the catalysts were recorded after different treatments, and the results are summarized in Figure 13. In general, the assignment of the bands which appear in the spectra is as follows. The band at wavenumber around 3400 cm⁻¹ is related to surface hydroxyl group while the bands at around 1630 cm⁻¹, 1400 cm⁻¹ and 740 cm⁻¹ correspond to the (monoclinic) zirconia. The bands appearing at around 1230 cm⁻¹, 1140 cm⁻¹ and 1040 cm⁻¹ are typical of surface sulphates on zirconia (5,13).

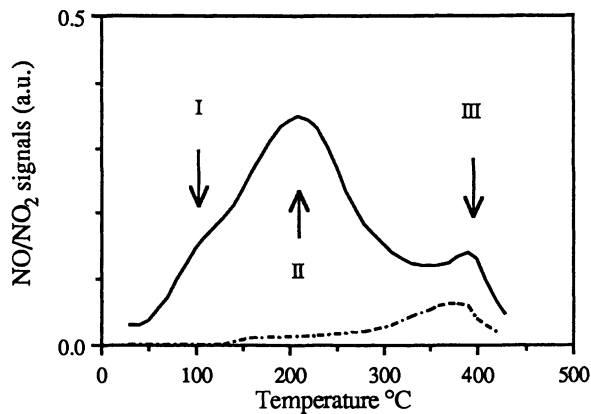


Figure 7 TPD of NO and NO₂ for Pt/ZrO₂ (400 mg), pretreatment of the catalyst: NO = 500 ppm. (—) NO signal; (---) NO₂ signal.

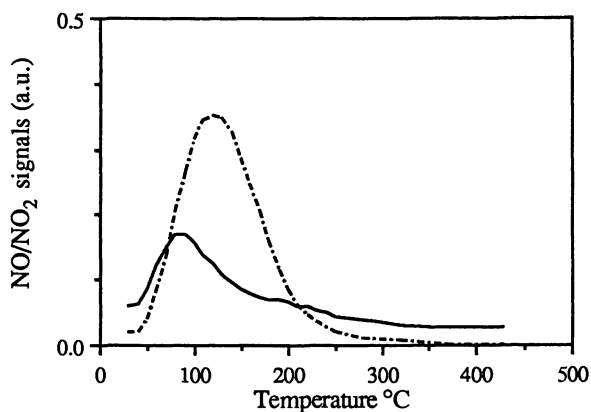


Figure 8 TPD of NO and NO₂ for Pt/ZrO₂-5NS (400 mg), pretreatment of the catalyst: NO = 500 ppm. (—) NO signal; (---) NO₂ signal.

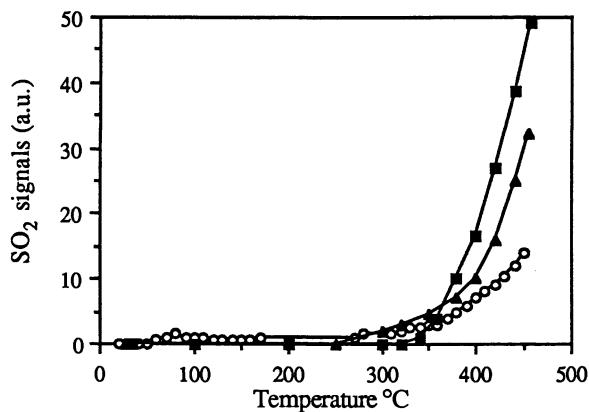


Figure 9 TPD of SO₂ for the different catalysts, pretreatment of the catalysts: SO₂ = 500 ppm, O₂ = 10 %. (○) Pt/ZrO₂, 1g; (▲) Pt/ZrO₂-1NS, 1g; (■) Pt/ZrO₂-5NS, 1g.

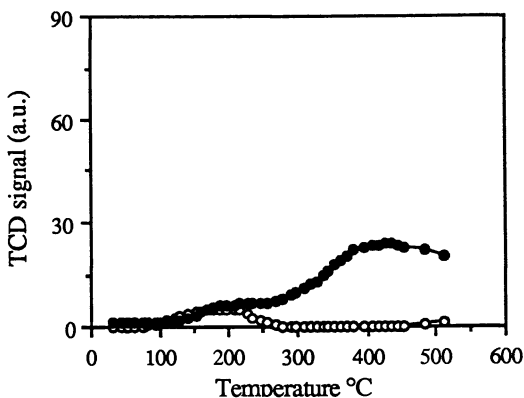


Figure 10 TPR traces of the fresh and used Pt/ZrO₂ catalysts. (○) fresh sample, 100 mg; (●) used sample, 100 mg.

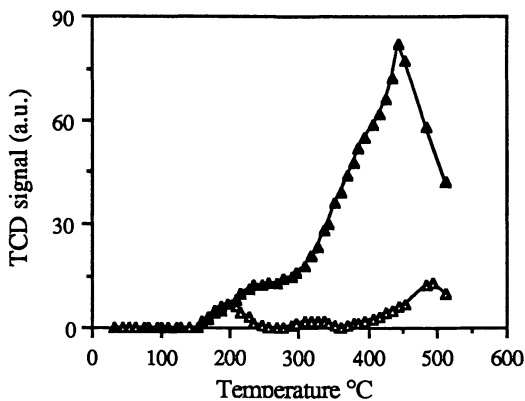


Figure 11 TPR traces of the fresh and used Pt/ZrO₂-1NS catalysts. (Δ) fresh sample, 100 mg; (\blacktriangle) used sample, 100 mg.

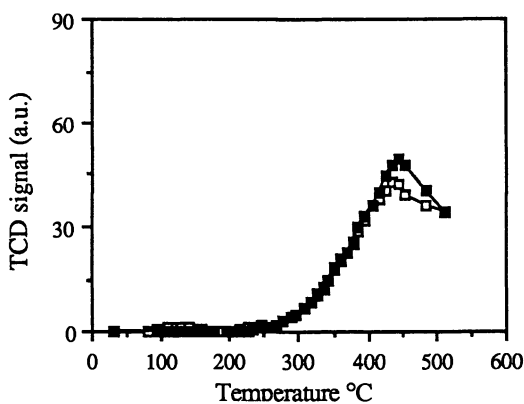


Figure 12 TPR traces of the fresh and used Pt/ZrO₂-5NS catalysts. (\square) fresh sample, 100 mg; (\blacksquare) used sample, 100 mg.

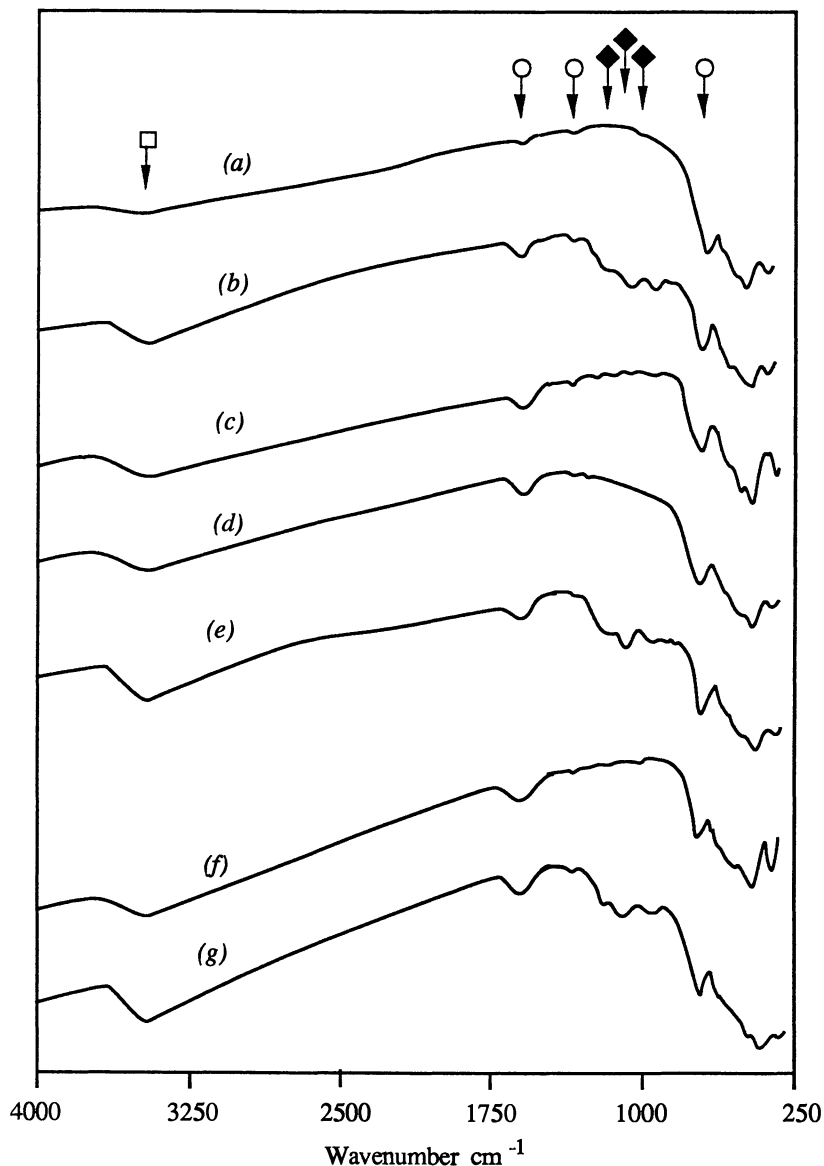


Figure 13 FT-IR spectra of the catalysts after different treatments. (a) fresh Pt/ZrO₂; (b) used Pt/ZrO₂; (c) fresh Pt/ZrO₂-1NS; (d) fresh Pt/ZrO₂-1NS after TPR; (e) fresh Pt/ZrO₂-5NS; (f) fresh Pt/ZrO₂-5NS after TPR; (g) used Pt/ZrO₂-5NS. (□) OH- group; (○) ZrO₂; (◆) surface sulphate group.

As can be seen from the spectra, the fresh Pt/ZrO₂ (Figure 13, spectrum *a*) shows no surface sulphate; both fresh Pt/ZrO₂-1NS (spectrum *c*) and Pt/ZrO₂-5NS (spectrum *e*) show the presence of sulphate on the catalyst surface, there being relatively more on Pt/ZrO₂-5NS. Of the used catalysts, both the non-sulphate-treated Pt/ZrO₂ (spectrum *b*) and Pt/ZrO₂-5NS (spectrum *g*) show similar spectra with strong sulphate bands; after H₂ reduction (in the TPR system), the sulphate bands of the used sample of Pt/ZrO₂-1NS (spectrum *d*) were diminished compared with those in the fresh Pt/ZrO₂-1NS (spectrum *c*), while the intensity of the surface sulphate bands of Pt/ZrO₂-5NS after reduction (spectrum *f*) were smaller than those of the fresh sample of Pt/ZrO₂-5NS without H₂ reduction (spectrum *e*).

Discussion

The Effect of Sulphate on the Adsorption/Desorption Characteristics of the Catalysts. It is well established that the major effect of sulphate treatment of ZrO₂ is a change in the surface acidity due to the formation of a superacid ZrO₂-SO₄⁼ (4). The introduction of Pt onto ZrO₂-SO₄⁼ is reported to increase the surface acidity even further; a Pt/ZrO₂-SO₄⁼ catalyst has much stronger surface acidity than a non-sulphated Pt/ZrO₂ catalyst (14). The difference in the surface acidity is expected to influence the adsorption /desorption features of the catalyst and therefore to affect the performance of catalyst.

The gas molecules used in this work, NO, NO₂, SO₂ and SO₃, are all acidic. The adsorption of these acidic molecules is therefore likely to become less extensive and/or weaker on the Pt/ZrO₂-SO₄⁼ catalyst, a material which has been treated with sulphate and which is therefore more acidic, in comparison to the non-sulphate-modified Pt/ZrO₂. The results of TPD of NO, NO₂ and SO₂ measurements, as shown in Figures 7 to 9, are in agreement with this, showing decreases in the adsorption strength of these molecules on Pt/ZrO₂-5NS. The desorption of NO shifts to lower temperatures with Pt/ZrO₂-5NS in comparison to that on Pt/ZrO₂ (Figures 7 and 8); the desorption of NO₂ from Pt/ZrO₂-5NS occurs also only at the lower temperature (Figures 7 and 8). The desorption of SO₂ also shows the same trend (Figure 9).

The maximum reaction activity requires the optimum strength of the adsorption of reactant molecules on the catalyst surface. The weakening of adsorption strength of the reactant molecules can therefore lead to two different effects on the activity, depending on the original strength of adsorption. If the original adsorption of the reactants was too strong, the weakening of the adsorption would result in a promotional effect on the activity because the reactant molecules gain more mobility on the catalyst surface; in contrast, if the original adsorption was already fairly weak, further weakening of the adsorption strength of the reactants would reduce the catalytic activity since the reaction molecules would desorb before the surface reaction takes place. The former situation seems to apply in our case since the adsorption of NO and/or NO₂ as well as of SO₂ seems to be rather strong on the non-sulphate Pt/ZrO₂ (Figures 7 to 9) in comparison to the sulphate-modified Pt/ZrO₂-5NS; thus, an enhancement of the activity for the oxidation of NO and that of SO₂ over the sulphate modified catalysts, Pt/ZrO₂-1NS and Pt/ZrO₂-5NS, is expected.

The mechanism of the adsorption/desorption of NO₂ and SO₂ on a Pt catalyst is likely to be quite complicated, not only because of the different adsorption states present (see the multi-peak features of the TPD spectra, Figures 7 to 9) but also because of the

possible existence of an interaction between NO_x and SO₂, as was shown in the earlier work for the Pt/SiO₂ catalyst (2). The reaction mechanism on the Pt/ZrO₂-SO₄⁼ catalyst may also be modified due to the presence of the surface sulphate groups. For example, the NO oxidation reaction is probably changed from having a mechanism of the Langmuir-Hinshelwood type on Pt/ZrO₂ to having an Eley-Rideal type on Pt/ZrO₂-SO₄⁼. Figure 14 shows these two types of the reaction scheme. As shown in Figure 7 that there is a fair amount of NO adsorbed on the surface of Pt/ZrO₂ catalyst at the reaction temperatures (250 ~ 400 °C), the reaction may take place predominantly between the adsorbed NO and oxygen; however, in the case of Pt/ZrO₂-SO₄⁼ catalyst the adsorption of NO in the same temperature range is much less (see Figure 8) that the oxidation of NO may preferably occur between the gas NO molecules and the surface oxygen. Further studies are required to elucidate the exact nature and mechanism of the surface reactions.

The Effect of Sulphate on the Surface Pt. The TPR trace of the freshly calcined Pt/ZrO₂ catalyst showed a H₂ uptake peak with maximum at around 190 °C (Figure 10); this peak is believed to correspond to the reduction of the surface Pt oxides since a TPR experiment with the ZrO₂ support alone did not show any H₂ uptake peak in this temperature range. The TPR measurement for the fresh sample of Pt/ZrO₂-1NS, however, showed two H₂ consumption peaks (Figure 11). The peak at lower temperature can be considered to be caused by the reduction of the surface Pt as this peak appeared in the same temperature range as that of the fresh Pt/ZrO₂ catalyst. The peak at higher temperature, which was also observed with either the used Pt/ZrO₂ or the used Pt/ZrO₂-1NS catalysts, is probably related to the reduction of the surface sulphate groups (these surface sulphate groups will be discussed later in the following section). In case of the fresh Pt/ZrO₂-5NS catalyst, the TPR measurement showed that the H₂ uptake occurred mainly at high temperature and the peak at the low temperature range seemed to be absent (Figure 12). These results indicated that the surface Pt became less reducible by H₂ when the sample had been pre-sulphated, for example, with 5N H₂SO₄; this probably means that the reduction of surface Pt of the catalysts is affected by the presence of surface sulphate.

Hosoi et al (15) have also observed that the hydrogen adsorption ability of Pt/ZrO₂-SO₄⁼ was much lower than that of Pt/ZrO₂ catalyst, but gave no reason for the phenomenon. One possibility is that Pt could be trapped in a cage of surface sulphate groups or 'buried' under a layer of sulphate during the calcination. This may explain the lower accessibility of the Pt to H₂ in the TPR experiments and the lower Pt dispersion values (see Table 1); it cannot, however, explain the observed increase in the catalytic activity of the sulphate-modified catalysts. Formation of Pt sulphate may be ruled out since it is not stable at the calcination temperature we used, for instance Pt(SO₄)₂·4H₂O will be decomposed at 150 °C (16). Another possibility would be that surface sulphate bonded to the zirconia support may interact with the surface Pt through oxygen in Pt oxides; the former modifies the surface acidity of the catalyst and the latter makes the Pt oxides less reducible but probably helps the reduction of the surface sulphate. This may explain the observed higher catalytic activity, lower reducibility of surface Pt and lower measured Pt dispersion values when surface sulphate is present. From the present study it is difficult to visualize the exact picture, however, the assumption of surface sulphate sitting on the ZrO₂ and interacting with the surface Pt oxides seems more favourable from the point of view of the experimental observations.

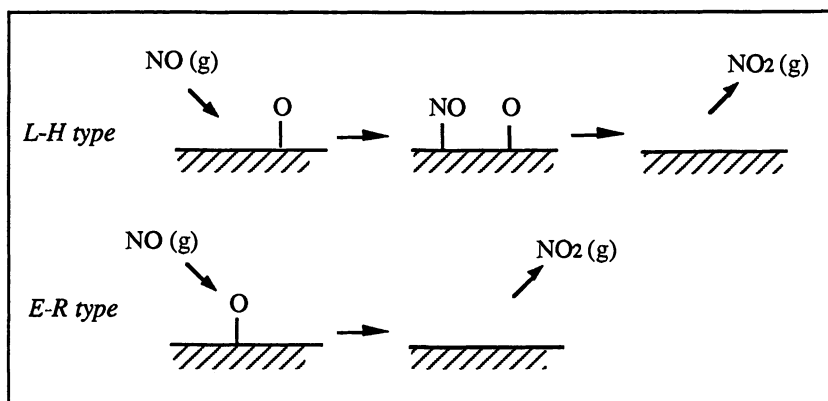


Figure 14 Two possible schemes of the NO oxidation reaction on the catalyst: Langmuir-Hinshelwood (L-H) type and Eley-Rideal (E-R) type.

The Reduction of Surface Sulphate. The results of the FT-IR measurements (Figure 13) show clearly the presence of the surface sulphate groups in the fresh Pt/ZrO₂-1NS (spectrum *c*) and fresh Pt/ZrO₂-5NS (spectrum *e*), both being sulphate-modified catalysts, though the intensities of sulphate bands are relatively different. Figure 13 also shows that the fresh Pt/ZrO₂-1NS after the TPR experiment (spectrum *d*) gave a similar spectrum to that of fresh Pt/ZrO₂ catalyst (spectrum *a*) and that the sulphate bands in the spectrum (*f*) of the fresh Pt/ZrO₂-5NS catalyst after TPR were substantially weaker than those of the fresh sample of Pt/ZrO₂-5NS (spectrum *e*).

The reduction of the surface sulphate by H₂ treatment can also be seen from the TPR results. Comparing the TPR patterns of the fresh Pt/ZrO₂-1NS and Pt/ZrO₂-5NS catalysts (Figures 11 and 12) to that of the fresh (un-sulphated) Pt/ZrO₂ catalyst (Figure 10), there was an extra H₂ uptake peak shown up at higher temperature for the sulphated catalysts; since the difference between these catalysts was mainly that the former catalysts were pre-sulphated thus hold sulphate on their surface but not the latter one, the appearance of this extra peak may be attributed to the reduction of the surface sulphate by H₂. The relative difference in the intensity of the high temperature reduction peaks in TPR patterns between the fresh sample of Pt/ZrO₂-1NS and Pt/ZrO₂-5NS (Figures 11 and 12) may therefore be due to the relatively different amounts of surface sulphate present on the catalysts. After the TPR experiment part of the surface sulphate in the samples had been removed, the sulphate bands in the spectra measured with these samples were thus weakened. From these observations it may be concluded that the surface sulphate can be removed (at least partly) by a H₂ treatment.

The Sulphation of Pt/ZrO₂ by Ageing in an NO+SO₂+O₂ Mixture. The changes in the activity of the Pt/ZrO₂ catalyst upon ageing (Figure 6) indicate that the catalyst surface changes markedly in the reaction environment. FT-IR results (Figure 13) show that the used Pt/ZrO₂ sample gave a similar spectrum to that of the fresh Pt/ZrO₂-5NS sample (comparing spectrum *b* to spectrum *g*); this implies that surface sulphates were probably formed on the Pt/ZrO₂ catalyst after use. The results of TPR measurements with the Pt/ZrO₂ samples (see Figure 10) show also that sulphates were present on the used sample, as can be seen from the appearance of the extra H₂ uptake peak at high temperature in the TPR curve (closed circles).

These results indicate that sulphates are formed on the surface of Pt/ZrO₂ after use in a reaction gas mixture containing NO+SO₂+O₂. The formation of the sulphate on the catalyst may be responsible for the change of its performance. It is possible that under the reaction conditions, the SO₂ was converted into SO₃ over the catalyst, this SO₃ could then combine with the surface OH⁻ group to give surface SO₄⁼ species which may react further with the ZrO₂ support to form ZrO₂-SO₄⁼; as a consequence, the surface Pt was modified. This is perhaps the reason for the catalytic selectivity being improved gradually with time. In case of the pre-sulphated catalysts, the sulphation may have been occurred during calcination of the catalysts; therefore there would be no ageing effect to be expected.

In the discussion of the results for the Pt/SiO₂ catalyst (2) we showed that some sort of complex surface species (N_x-S_y-O_z) may be formed on the catalyst surface when both NO and SO₂ are present in the feed gas. The presence of this surface species has a negative impact on the performance of the catalyst in two ways: one is that it causes a

decrease in the overall conversions of NO but an increase in that of SO₂; the other is that it leads to a partial deactivation of the catalyst. The results of the present study on Pt/ZrO₂ catalyst, however, show a very different picture: the presence of NO+SO₂+O₂ in the feed gas can be of benefit to the performance of a Pt/ZrO₂ catalyst for both the oxidation of NO and of SO₂ due to the formation of surface sulphate species, probably on the zirconia.

Catalyst Acidity. It is known that the surface acidity of Pt/ZrO₂-SO₄⁼ is quite different from that of Pt/ZrO₂. A Pt/ZrO₂ catalyst has mainly Lewis acid sites on the surface and a Pt/ZrO₂-SO₄⁼ has both Brønsted and Lewis acid sites (14). The Lewis acidity of Pt/ZrO₂-SO₄⁼ is stronger than that of Pt/ZrO₂; the Lewis acidity of Pt/ZrO₂-SO₄⁼ is easily converted to Brønsted acidity by the presence of H₂O (5). It is probable that the stronger Lewis acidity favours the desorption of adsorbed product molecules from the catalyst surface and therefore promote the oxidation reaction; the presence of Brønsted acidity does not favour the reaction but may be helpful in the formation of SO₄⁼ on the surface; this will be especially so in the case when SO₂+O₂ is passed over the catalyst and when SO₄⁼ formation gives rise to more Lewis acid sites.

The Effect of Sulphate Treatment on the Surface Area of the Catalysts. It is reported that a sulphate-modified zirconia shows a higher surface area than does the non-sulphate zirconia; for example, a ZrO₂ sample prepared from ZrOCl₂ has a surface area of 100 m² g⁻¹ while a sulphate ZrO₂ sample gives 187 m² g⁻¹, both after calcination at 500 °C (5,17,18). The increase in surface area as a result of the sulphate treatment has been explained by Arata (5) as being due to cracking of the oxide into fine particles and also to delayed crystallization of the zirconia. The sulphate-modified catalysts prepared in this work, Pt/ZrO₂-1NS and Pt/ZrO₂-5NS, however showed no increase in the surface area compared to that of Pt/ZrO₂ (see Table 1). This may be due to the fact that the zirconia we used had already been calcined at 500 °C; it had already crystallized before the sulphate treatment. It can be concluded that the change in surface area of the support is unlikely to be the reason for the change in the catalytic activity and selectivity.

The Properties of the Aged Pt/ZrO₂ Catalysts. We have discussed that the catalytic behaviour of a Pt/ZrO₂ catalyst changes upon ageing, the aged catalyst showed the presence of residual sulphate on the surface which is considered to be responsible for the change of the performance. It should be noted that the type of Pt/ZrO₂-SO₄⁼ catalyst formed by ageing Pt/ZrO₂ in the reaction gas mixture was not exactly the same as those prepared by pre-treating the ZrO₂ support followed by impregnation with Pt salt, this can be seen by comparing the results of Figure 6 with those of Figures 2 and 4 that the aged Pt/ZrO₂ catalyst exhibited a much higher selectivity for the oxidation of NO over that of SO₂ than the Pt/ZrO₂-1NS and Pt/ZrO₂-5NS catalysts, although the activity for the oxidation of NO was slightly lowered. The TPR pattern of the used (aged) Pt/ZrO₂ sample was also different from those of freshly made Pt/ZrO₂-1NS and Pt/ZrO₂-5NS catalysts (Figures 10 to 12). From the FT-IR spectra of Figure 13, it can also be seen that the bands at around 1240 cm⁻¹ are different for the used Pt/ZrO₂ (spectrum *b*) and the fresh Pt/ZrO₂-5NS (spectrum *e*) catalysts.

Conclusions

The following conclusions can be reached in this study. Pt/ZrO₂-SO₄⁼ catalysts, prepared by pre-treating ZrO₂ with sulphuric acid, have much higher activity for the oxidation of NO and of SO₂ than does the non-sulphated Pt/ZrO₂; the selectivity for the NO oxidation is also improved by the sulphate modification. The modification of the surface acidity seems to be the major cause of the change of the catalytic behaviour.

When a Pt/ZrO₂ catalyst is aged in a gas mixture containing NO+SO₂+O₂ it shows a higher catalytic selectivity for the oxidation of NO over that of SO₂. The formation of surface sulphates on the aged Pt/ZrO₂ catalyst was observed with the FT-IR and TPR experiments. The interaction between the ZrO₂-SO₄⁼ and Pt sites on the catalyst was probably responsible for the modification effect of the surface sulphates. The sulphate groups in the catalysts, either introduced by pre-treating support ZrO₂ with H₂SO₄ or formed during ageing of the catalysts, can be at least partly removed by a H₂ treatment.

References

- 1 Cooper, B.; Thoss, J. E. *SAE Technical Paper Series*, 890404 (1989).
- 2 Xue, E; Seshan, K.; Ommen, J. G. van; Ross, J. R. H. *Appl. Catal. B: Environmental* **1993**, *2*, 183.
- 3 Wong, V. W.; Yu, M. L.; Mogaka, Z. N.; Shahed, S. M. *Soc. Automot. Eng.* **1984**, *P-140*, 97.
- 4 Tanabe, K.; Misono, M.; Ono, Y.; Hattori, H. *New Solid Acids and Bases, Their Catalytic Properties*, Kodansha: Tokyo, 1989; p 199.
- 5 Arata, K. *Adv. Catal.* **1990**, *37*, 165.
- 6 Chang, C. J. *Catal.* **1978**, *53*, 374.
- 7 Waqif, M.; Saur, O.; Lavalley, J. C.; Perathoner, S.; Centi, G. *J. Phys. Chem.* **1991**, *95*, 4051.
- 8 Lox, E. S.; Engler, B. H.; Koberstein, E., In *Catalysis and Automotive Pollution Control II*, Crucq, A. Ed.; Elsevier: Amsterdam, 1991; p 291.
- 9 Hare, C. T.; Bradow, R. L. *SAE Technical Paper Series* 790490, (1979).
- 10 Hare, C. T.; Baines, T. M. *SAE Technical Paper Series* 790424, (1979).
- 11 *Dieselmotoren a, 5th Ed*, serie motorvoertuigtechniek 3; Stichting V.A.M.: Voorschoten (The Netherlands), 1987; p 48.
- 12 Ministry of Health and Environmental Protection (ed) *Handbook of Emission factors, Part I Non industrial Sources*; Government Publishing Office: The Hague, 1980; p 63.
- 13 Nakamoto, K.; Fujita, J.; Tanaka, S.; Kobayashi, M. *J. Am. Chem. Soc.* **1957**, *79*, 7904.
- 14 Ebitani, K.; Konishi, J.; Horie, A.; Hattori, H.; Tanabe, K. In *Acid-Base Catalysis*, Tanabe, K.; Hattori, H.; Yamaguchi T.; Tanaka, T., Eds.; Kadanasha: Tokyo, 1988; p 491.
- 15 Hosoi, T.; Kitada, S.; Shimisu, T.; Imai, T.; Nojima, S. *Shokubai.* **1990**, *32*, 117.
- 16 Weast R. C.; Astle, W. J. (eds.) *CRC Handbook of Chemistry and Physics, 63rd Ed.*; CRC Press Inc.: Florida, 1982; p B-129.
- 17 Matsushashi, H.; Hino M.; Arata, K. *Chem. Lett.* **1988**, p 1027.
- 18 Arata K.; Hino, M. *Appl. Catal.* **1990**, *59*, 197.

RECEIVED September 30, 1993

Chapter 21

Future Fuels: An Overview

John N. Armor

Air Products & Chemicals, Inc., 7201 Hamilton Boulevard,
Allentown, PA 18195

The title of this section of the book is different from the narrower title of "Reformulated Gasoline" used for the Symposium. Reformulated gasoline is just one aspect of the impact of catalysis upon the need for new or improved fuels. A major reformulation of gasoline is now required in the USA by the Clean Air Act Amendment of 1990. Reformulated fuels include oxygenates as a major source of clean-burning, high octane liquid fuel. Oxygenates added to gasoline burn more efficiently and provide lower CO and ozone levels. Methyl *tert*-butyl ether [MTBE] is readily produced by the reaction of methanol with isobutylene over solid acid catalysts. MTBE is currently one of the largest and fastest growing chemicals in the USA. In addition to reformulating gasoline, alternative fuels are being considered, such as methanol, other alcohols, natural gas, and propane because they may be cheaper, more readily available, or offer cleaner emissions upon combustion. Also, new solid acid superacid catalysts are needed for low temperature, selective isomerization of normal to branched alkanes in order to increase the octane number of gasoline. Opportunities abound in catalysis to enhance productivity, reduce production costs, increase product selectivity, simplify process steps, and reduce energy consumption (1).

With regard to methanol as a fuel, a lot of research is focused on higher conversion routes to methanol from syngas [CO/H₂], slurry phase routes which efficiently remove heat, and lower temperature catalysts. However, momentum is building for producing methanol directly from methane, instead of converting methane to CO/H₂ and then to methanol. It certainly would be more attractive to reduce this two step route to one exothermic reaction which might also be able to cogenerate energy. It would also be attractive to convert methane to other high quality motor fuels. In addition, the direct oxidation of hydrocarbons to alcohols with molecular oxygen would be particularly attractive by avoiding current multiple step processes. This needs to be done with greater selectivity, yield, and catalyst life to the resulting oxygenate. With the growth of MTBE, there is a large demand for isobutylene as a feedstock. Improved catalytic technology to convert C₄ hydrocarbons directly to

isobutylene by dehydrogenation or oxidative dehydrogenation would be particularly attractive.

Olefin alkylation in refineries is traditionally carried out using sulfuric acid or hydrofluoric acid. Concerns over their corrosiveness as well as potential safety and environmental hazards associated with these acids is raising interest in alternative catalytic materials. Such issues (1) have already forced one refinery to spend \$100 million to replace or modify its HF usage.

Improved technology is also required to maximize the production of motor fuels from heavier petroleum based distillates and residues. Superior catalysts are necessary to remove sulfur to permit higher selectivity and milder process conditions in hydrodesulfurization and hydrodenitrification processes. In addition, future trends to process heavier petroleum feedstocks will increase the demand for hydrogen in refineries (2). Processes which co-produce hydrogen will be particularly attractive in future refinery schemes. Beyond the need for more hydrogen within the refineries, hydrogen is often regarded as the fuel of the future, especially because it is clean burning. Process technologies are needed which produce hydrogen without using fossil fuels.

A half-day session on catalysts related to the Reformulation of Gasoline was assembled by R. Wormsbecher of W. R. Grace and chaired by T. Roberie also of W. R. Grace. Dr. Roberie provided the following summary of the session: "The focus of the papers in this session was mainly on catalysts, catalytic technologies and strategies to be used by the petrochemical and refining industries and catalysts' suppliers for meeting the requirements for gasoline reformulation as imposed by the 1990 Clean Air Act Amendments. The keynote speaker, Ugo Bozzano of UOP, began with an excellent overview of both the use and short comings of EPA's complex model for predicting the effect of individual gasoline properties on automobile emissions. The remainder of the session, in general, dealt with two of the most pressing issues facing the petrochemical industry today - iso-olefin production for oxygenates and sulfur reduction in gasoline. According to presentations from W. R. Grace and Engelhard, the need for iso-olefins could be met through the use of novel FCC catalysts which have significantly reduced hydrogen transfer activity which lowers the conversion rate of iso-olefins to isoparaffins. Lyondell Petrochemical also described a method for increased iso-olefin production using a unique skeletal isomerization process designed for butene and pentene isomerization. Sulfur reduction in gasoline was viewed as being a key but complicated issue for refineries facing reformulation. For high sulfur feeds, the potential for lowering sulfur in gasoline from the FCC unit to acceptable limits via catalysts cracking was shown to be feasible. Mechanistic studies using model compounds have shown that FCC catalysts, currently under development, can affect the cracking of sulfur compounds, particularly thiophene derivatives, through both hydrogen transfer and zeolite pore restriction mechanisms."

Manuscripts of two of these presentations were accepted for publication in this book. A paper by J. Barin Wise and D. Powers of Lyondell Petrochemical Co. describes a new process with high yield and selectivity for the isomerization of normal olefins to iso-olefins for the production of blendable ethers in the production of reformulated gasoline. Another paper by scientists at W. R. Grace & Co. explores the possibility of catalytically reducing the sulfur content of gasoline produced in an FCC

unit. Obviously, these two manuscripts and the brief reports in this overview describe only a small part of the active research being done in future fuels via catalysis. Perhaps at the next international symposium on this topic more authors will be able to report additional progress in the area of Future Fuels. From the introductory comments provided in this overview, there are certainly lots of opportunities.

References

1. Armor, J. N. *Appl. Catal. B*, **1992**, *1*, 221-256.
2. Simonsen, K. A.; O'Keefe, L. F.; Fong, W. F. *Oil Gas J. Mar.* 22,1993, pp. 45-58.

RECEIVED November 8, 1993

Chapter 22

Highly Selective Olefin Skeletal Isomerization Process

J. Barin Wise and Don Powers

Lyondell Petrochemical Company, 8280 Sheldon Road, P.O. Box 777,
Channelview, TX 77530-0777

The 1990 Clean Air Act has increased the demand for blendable ethers while at the same time reducing vapor pressure limits. The California Air Resources Board (CARB) has recently required further olefin reduction as well. Iso-olefins are required for the production of several of these ethers. One attractive route for production of additional ethers is the isomerization of normal olefins to iso-olefins using new high selectivity catalysts. In the case of C₅ olefins, the isomerization and subsequent etherification of these components provides additional oxygenates while reducing vapor pressure and olefin content. Previous development work has illustrated the difficulty in achieving high selectivities with reasonable cycle lengths. The new Lyondell Process meets these objectives while maintaining relatively low capital costs.

Recent implementation of the 1990 United States Clean Air Act has created an increased demand for oxygenates for use in gasoline blending. MTBE, currently the primary oxygenate used in gasoline blending, is produced using isobutylene as a primary component. Isobutylene is also required for production of ETBE.

In addition, future regulations restricting the level of olefins in gasoline are expected since olefins have been shown to promote the formation of ozone in the atmosphere (1). Figure 1 shows a distribution of olefins in gasoline based on carbon number.

Olefins enter the atmosphere primarily through the evaporation of gasoline. The olefin evaporation rate increases as the carbon number decreases. Figure 2 shows the average vapor pressure of olefins versus carbon number.

The relative potential for the formation of ozone by various olefins can be represented by the product of the reactivity, vapor pressure and distribution in gasoline. Figure 3 shows the relative potential of olefin formation by carbon number.

0097-6156/94/0552-0273\$08.00/0

© 1994 American Chemical Society

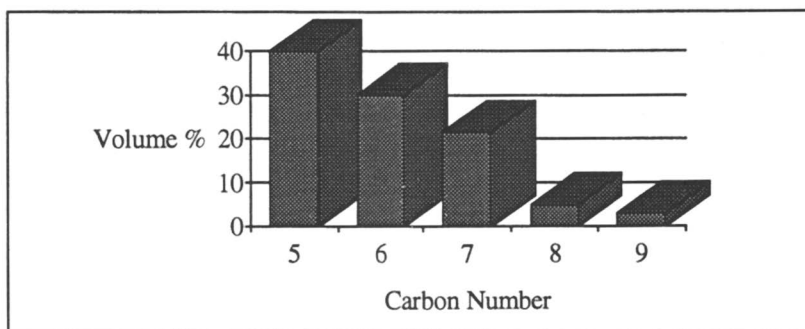


Figure 1: Distribution of Gasoline Olefins (Reproduced with permission from reference 1. Copyright 1993 K. Rock)

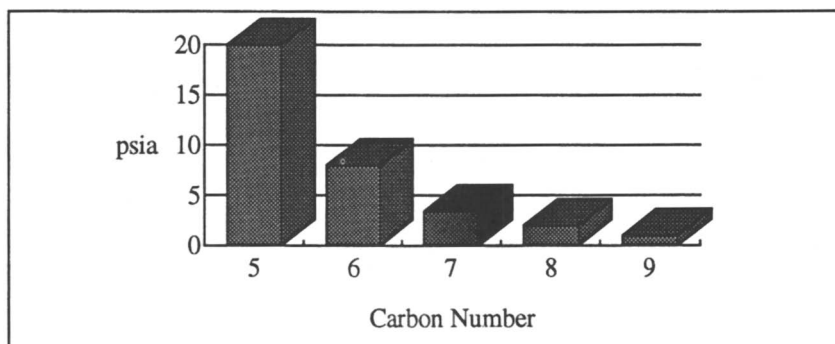


Figure 2: Vapor Pressure of Gasoline Olefins (Reproduced with permission from reference 1. Copyright 1993 K. Rock)

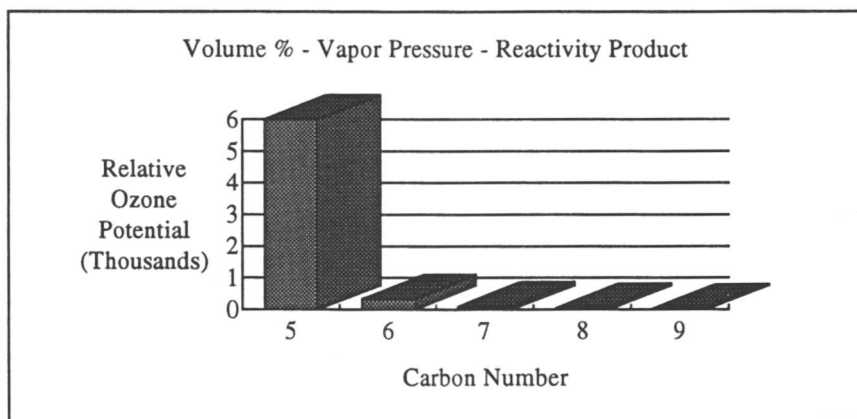


Figure 3: Relative Ozone Potential of Gasoline Olefins (Reproduced with permission from reference 1. Copyright 1993 K. Rock)

In order to meet the increased demand for oxygenates while reducing olefin content and vapor pressure in gasoline, the petrochemical and refining industries will not only require additional quantities of iso-olefins such as isobutylene and isoamylene to form ethers such as MTBE, ETBE and TAME but will also require an alternate disposition for current olefins in gasoline. Lyondell Licensing, Inc. a wholly owned subsidiary of Lyondell Petrochemical Company, is working to increase the supply of iso-olefins while reducing the level of olefins in gasoline with a unique Olefin Skeletal Isomerization Process (2).

Background

Three years ago, Lyondell Petrochemical Company identified a need for technology to convert normal butylenes, produced during operation of its steam cracker, to isobutylene for the production of MTBE.

At the time, no technology was commercially available for the isomerization of normal butenes to isobutylene. The only proven technology available was to isomerize n-butane to i-butane followed by a dehydrogenation step to produce isobutylene. Capital requirements for these technologies are high with significant licensing fees. A review of literature and patent information suggested that difficulties with rapid catalyst deactivation and substantial by-product formation made most options commercially unattractive (3-6).

Lyondell concluded that in order for this process to be commercially feasible, a low cost fixed bed catalytic process was required. Such a system was expected to require less capital investment and be easier to operate than a moving bed system. In addition, the injection of halogen or acid was to be avoided due to safety, environmental and metallurgical concerns. In order to meet these criteria, Lyondell set out to develop a process which would exhibit long cycle times between regenerations while providing near equilibrium yields of isobutylene with high selectivity.

Isobutylene and isoamylene yields are limited to equilibrium concentrations in the product stream. For C₄ olefin isomerization, 42 wt.% isobutylene (based on butenes in the feed) represents the equilibrium concentration at optimal reactor temperature, pressure and space velocity. Equilibrium yields of isoamylenes, which consist of 2-methyl-2-butene and 2-methyl-1-butene, at reaction temperature, pressure and space velocity total 73 wt.% based on pentenes in the feed.

Once a successful catalytic process was developed for butene isomerization, pentene isomerization would be even easier since the activation energy for skeletal isomerization of C₅'s is lower than that of C₄'s.

Catalyst Screening and Commercial Testing

A small Bench Scale Reactor was used to screen catalysts and evaluate process conditions. The size of this unit was ideally suited for testing catalyst preparations produced at the laboratory scale. This reactor operates 24 hours per day on a 7-day per week schedule. These studies led to early initial success and many subsequent improvements in catalyst performance. Figure 4 shows this unit, which occupies three hoods within the laboratory. This unit continues to operate to evaluate catalyst improvements.



Figure 4: Bench Scale Reactor (under vent hoods)

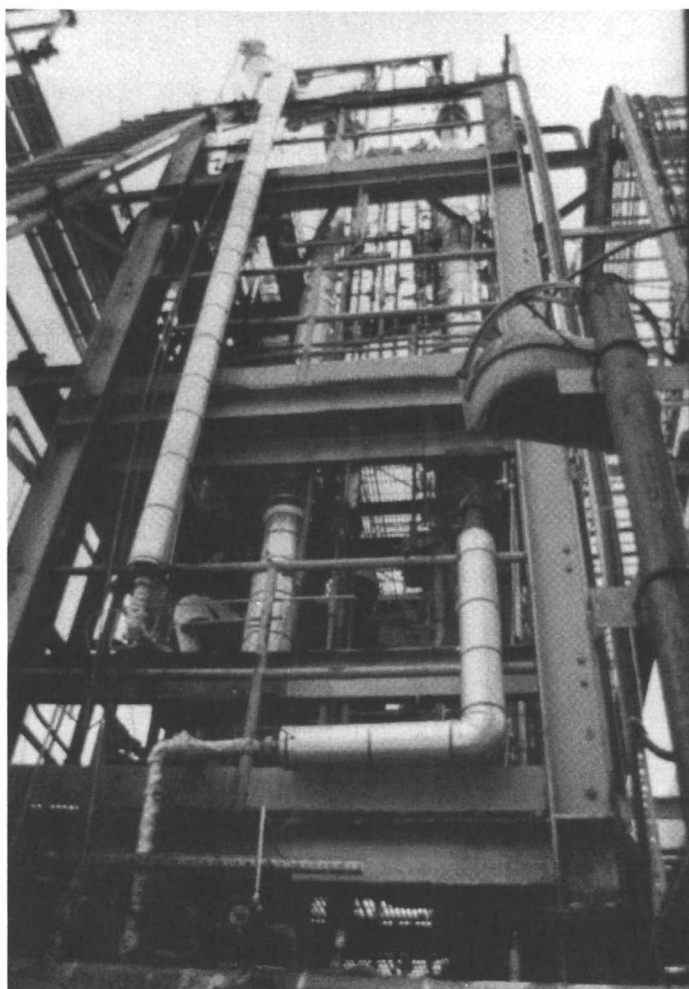


Figure 5: Process Development Unit

After initial success with the bench scale reactor, Lyondell began work in a larger existing pilot plant called the "Process Development Unit" (Figure 5).

Catalyst samples for this unit were prepared at a larger semi-works scale in order to obtain information on scale up of the catalyst manufacturing process. This unit was then used to test the effect of multiple catalyst regenerations on catalyst performance. The larger unit also provided an opportunity for intermediate scale up before going on to larger scale commercial equipment.

In order to fully demonstrate the operability of this process, a commercial demonstration was performed using existing equipment at the Channelview plant. The process was operated for a three month period using raffinate II feed at an average rate of 3,000 BPSD. During this time, commercial MTBE product was produced using an existing MTBE unit. At the conclusion of this three month test, the demonstration unit was converted back into its original service due to product inventory requirements. Figure 6 shows a photograph of the commercial reactors used for this demonstration. When available, this unit will be used to test further improved catalyst formulations.

The catalyst that was used to test n-butene isomerization to isobutylene was also used to isomerize n-pentenes to isoamylene at the laboratory scale. The initial results from this testing were extremely positive.

Results and Discussion

The goal of the catalyst development program was to develop a catalyst that would convert normal olefins to iso-olefins at near thermodynamic equilibrium concentrations with minimal by-product formation. The operating conditions are low pressure, typically just above atmospheric, with temperatures between 720 and 810 °F.

The catalyst of choice is a zeolite containing extrudate exhibiting long cycle lengths between regenerations. This catalyst converts n-olefins to iso-olefins at yields slightly below equilibrium with high selectivity to the iso-olefin being produced. The catalyst does not require the addition of halogens, acids or steam to maintain activity. Conversion and selectivity reflect the feed (FD) and effluent (EFF) concentrations of butene-1 (B1), cis and trans Butene-2 (B2) and isobutylene (IB1). Conversion is defined as follows:

$$\text{Conversion, wt. \%} = \frac{(\text{wt. \% B1} + \text{wt. \% B2})\text{FD} - (\text{wt. \% B1} + \text{wt. \% B2})\text{EFF}}{(\text{wt. \% B1} + \text{wt. \% B2})\text{FD}} \times 100$$

selectivity is calculated as:

$$\text{Selectivity, wt. \%} = \frac{(\text{wt. \% IB1})\text{EFF} - (\text{wt. \% IB1})\text{FD}}{(\text{wt. \% B1} + \text{wt. \% B2})\text{FD} - (\text{wt. \% B1} + \text{wt. \% B2})\text{EFF}} \times 100$$

and yield is calculated as:

$$\text{Yield, wt. \%} = \frac{(\text{wt. \% IB1})\text{EFF} - (\text{wt. \% IB1})\text{FD}}{(\text{wt. \% B1} + \text{wt. \% B2})\text{FD}} \times 100$$



Figure 6: Commercial Demonstration Unit

Figure 7 graphically illustrates the improvement in catalyst performance achieved as a result of our catalyst development program. This figure shows the isobutylene yield versus run time characteristic of this process. The time scale represents a single catalyst cycle. Isobutylene yields have been normalized for butene content in the feed. Commercial raffinate-II feed with 72% butene content was used to feed the reactor. A component breakdown of commercial raffinate-II is presented in Table I.

Table I. Raffinate-II Composition

Isobutane	4.86 wt.%
Isobutylene	1.69 wt.%
1-Butene	41.87 wt.%
n-Butane	23.31 wt.%
t-2-Butene	17.20 wt.%
c-2-Butene	10.95 wt.%
C ₅ +	0.12 wt.%

Catalyst improvements in the development program have focused on reducing the catalyst coking rate to improve cycle time while maintaining conversion and selectivity. The improvement illustrated in Figure 7 is a result of modifications made in the catalyst preparation process.

Figure 8 shows the high selectivity to isobutylene that is typically achieved using our catalyst. With each catalyst improvement, the data clearly shows a significant increase in run time at equilibrium isobutylene yield.

Another way to represent this data is to look at the average yield and selectivity over a given catalyst cycle time. Figure 9 shows the average conversion, selectivity and yield for this catalyst over a 290 hour (12 day) cycle. Over this cycle time, the average conversion of normal butenes is 44% with a selectivity to isobutylene of greater than 90%.

Figure 10 shows the same information to an average cycle time of 480 hours (20 days). In this case, the average selectivity to isobutylene increases to 92 wt.%. The increase in average selectivity partially compensates for the decrease in conversion exhibited by the longer cycle. The resulting yield of isobutylene decreases by only 2.7 wt.%. The primary by-products formed are gasoline boiling range material and small amounts of propylene.

Through experimentation, we have also seen evidence of saturates conversion in butene isomerization early on in the cycle. This conversion of saturates is demonstrated in figure 11.

Figure number 12 shows the results from a recent laboratory scale test of our improved second generation catalyst using TAME raffinate as the feedstock. Feedstock characteristics for TAME unit raffinate feeding an isomerization unit are shown in Table II. The average conversion, average selectivity and yield of isoamylene are shown for a cycle time of 206 hours. The selectivity to isoamylene starts out at greater than 90 wt% and approaches 100 wt.% as the cycle progresses. This increase in average selectivity partially compensates for the decrease in

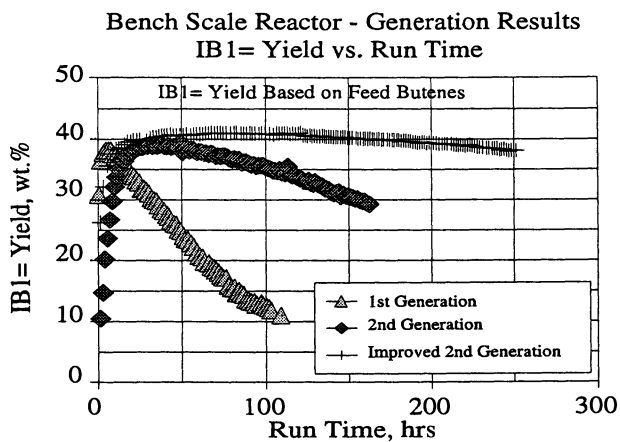


Figure 7: Isobutylene Yield vs. Run Time

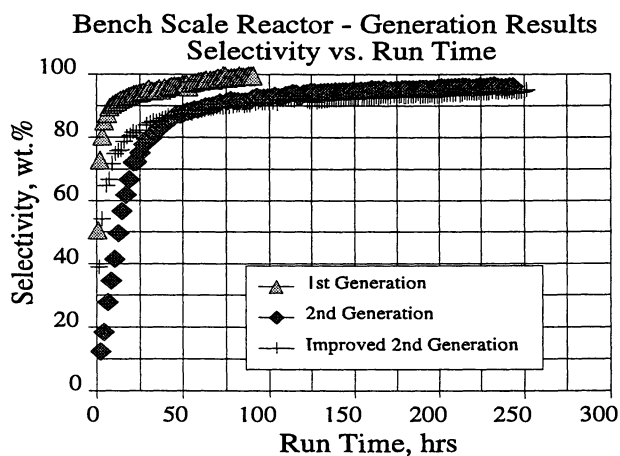


Figure 8: Selectivity vs. Run Time

Improved Second Generation
 290 Hour Cycle Time
 44 wt. % Conversion
 90 wt. % Selectivity

Lights	<0.1 wt. %
Propylene	0.5 wt. %
Isobutylene	39.6 wt. %
C ₅ ⁺	4.0 wt. %

Yield based on Butenes in Feed

Figure 9: Butene Isomerization Results

Improved Second Generation
 480 Hour Cycle Time
 40 wt. % Conversion
 92 wt. % Selectivity

Lights	<0.1 wt. %
Propylene	0.3 wt. %
Isobutylene	36.9 wt. %
C ₅ ⁺	2.8 wt. %

Yield based on Butenes in Feed

Figure 10: Butene Isomerization Results to 480 Hours

Saturates Conversion - BSR

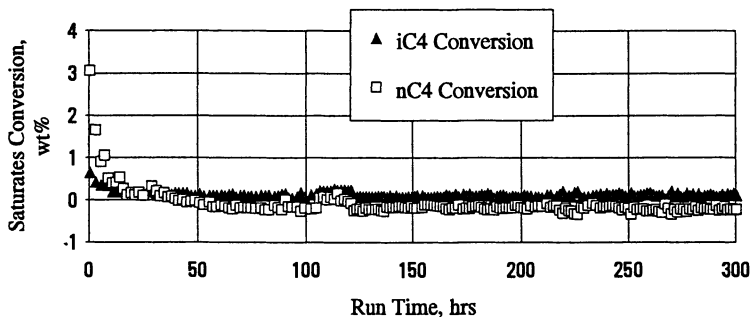


Figure 11: Saturates Conversion

Improved Second Generation

206 Hour Cycle Time

65 wt.% Conversion

95 wt.% Selectivity

Lights	0.0 wt. %
Isobutylene	0.4 wt. %
Isoamylenes	60.8 wt. %
C ₆ ⁺	1.0 wt. %

Yield based on Pentenes in Feed

Figure 12: Pentene Isomerization Results

Improved Second Generation

336 Hour Cycle Time

62 wt.% Conversion

98 wt.% Selectivity

Lights	0.0 wt. %
Isobutylene	0.2 wt. %
Isoamylenes	61.0 wt. %
C ₆ ⁺	0.8 wt. %

Yield based on Pentenes in Feed

Figure 13: Pentene Isomerization Results to 336 Hours

conversion exhibited by the longer cycle. The primary by-products formed are gasoline boiling range material and small amounts of C₄ and C₃ olefins.

Table II. TAME Raffinate Composition

Propylene	1.93 wt. %
Propane	0.49 wt. %
Isobutane	0.59 wt. %
t-2-Butene	0.65 wt. %
c-2-Butene	1.32 wt. %
n-butane	0.96 wt. %
3-methyl-1-butene	1.16 wt. %
Isopentane	57.77 wt. %
1-Pentene	2.72 wt. %
n-pentane	7.75 wt. %
t-2-Pentene	16.63 wt. %
c-2-Pentene	6.20 wt. %
2-methyl-2-butene	0.47 wt. %

Figure number 13 shows the same information to a cycle time of 336 hours. In this case, the average selectivity to isoamylenes increases to 98 wt.%. Average conversion to this cycle time showed a marginal decrease to 62 wt.% indicating that yield continues at equilibrium with the effluent pentenes.

Process

The butene and pentene isomerization processes are characterized by low capital cost and simple design. Figure 14 shows a process flow diagram for the Butene Isomerization process.

In this flow scheme, cold feed to the Isomerization Unit is vaporized and heated in a set of feed/effluent exchangers prior to final heating to reaction temperature in the fired heater. This heat integration greatly improves overall energy efficiency.

The reactor effluent, after cooling in the feed/effluent exchangers, is then compressed to a pressure at which butylenes can be condensed using cooling water. This compressor discharge is then fed to a distillation column for removal of heavies prior to being sent to an MTBE unit.

Either an electric motor or steam turbine can be used to drive the compressor for this application. If refrigeration is available, then the compression requirement can be reduced or eliminated.

Figure 15 depicts a process flow scheme for a Pentene Isomerization Process. The higher boiling point for pentenes eliminates the need for compression. As a result, the C₅ olefins exiting the reactor can easily be condensed with cooling water. The light ends are removed by distillation and the column bottoms are sent to a TAME unit. The option of using a column to remove light ends may not be necessary if the small amount of light ends can be tolerated in the TAME unit

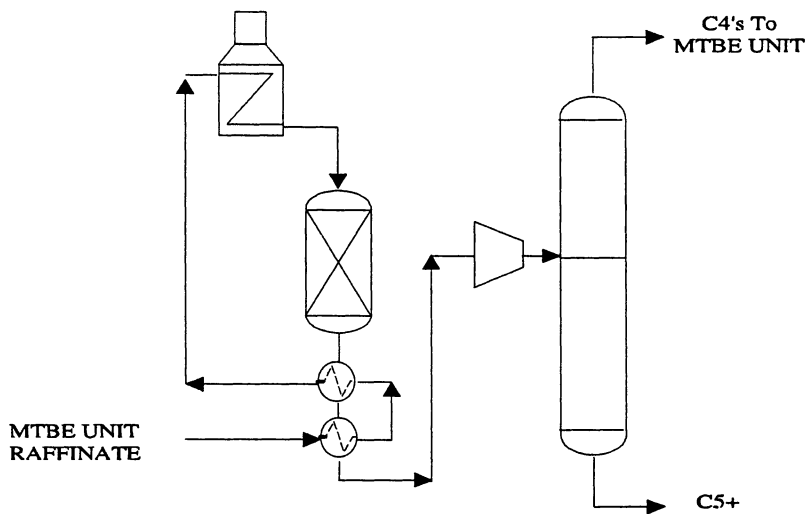


Figure 14: Process Flow Diagram for Butene Isomerization

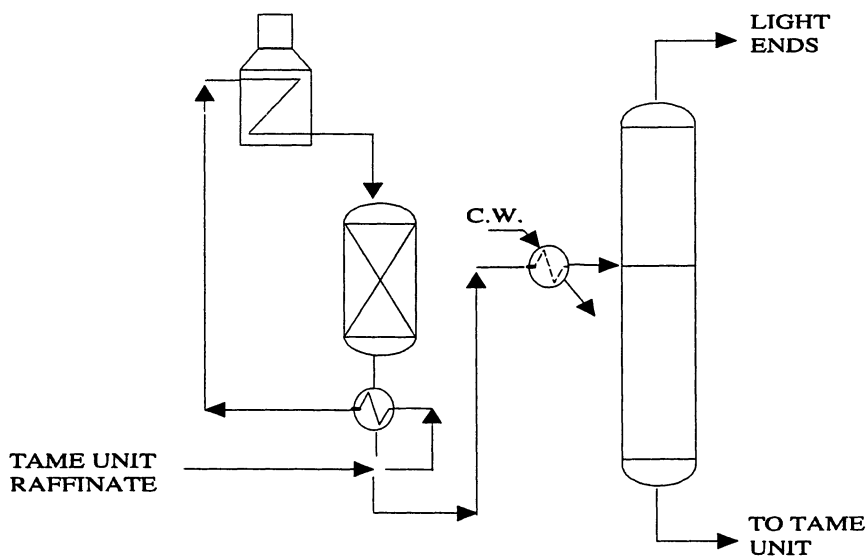


Figure 15: Process Flow Diagram for Pentene Isomerization

raffinate. For those who choose to install a DME tower in the TAME unit, the light ends will be removed along with the oxygenates.

At the end of each operating cycle, the reactor is taken off-line and the catalyst is regenerated. Regeneration is accomplished by flowing a preheated mixture of air and nitrogen over the catalyst. Regeneration is either once-through or flue gas can be recycled to conserve nitrogen.

Conclusion

The Lyondell catalyst system has been tested commercially and offers long cycle lengths, high yield and high selectivity. The Lyondell Olefin Isomerization Process is simple in design and operation and is the low cost process option for the production of iso-olefins to meet the growing demand for oxygenates such as MTBE, ETBE and TAME.

As a reflection of Lyondell's commitment to Licensing of this process, Lyondell Licensing, Inc. has joined forces with CDTECH, a partnership between ABB Lummus Crest Inc. and Chemical Research & Licensing Co., to further develop and commercialize the Lyondell Olefin Isomerization Process.

Literature Cited

1. Rock, K.L.; deCardenes, T.; Fornoff, L. C₅ Olefins: A New Refinery Challenge; 1993 NPRA Annual Meeting, San Antonio.
2. Powers, D.H.; Murray, B.D.; Winquist, B.H.C.; Callender, E.M.; Varner, J.H. U.S. Patent pending.
3. Giovanni, M.; Fattore, V.; Notari, B.; Process For Isomerizing Alkenes; U.S. Patent 4,038,337, 1977.
4. McGrath, B.P.; Crowthorne; Turner, L. U.S. Patent 3,345,428, 1967.
5. Szabo, J.; Perrotey, J.; Szabo, G.; Duchet, Jean-Claude; Cornet, D. *J. Mol. Cat.*, **1991**, *67*, 79-90.
6. Choudhary, V.R.; Doraiswamy, L.K. *J. Catal.*, **1971**, *23*, 54-60.

RECEIVED September 30, 1993

Chapter 23

Reaction Kinetics of Gasoline Sulfur Compounds

Catalytic Mechanisms for Sulfur Reduction

Robert H. Harding¹, Robert R. Gatte¹, Jacqueline A. Whitecavage¹, and Richard F. Wormsbecher²

¹Research Division and ²Grace-Davison Chemical Division, W.R. Grace & Company—Conn., 7379 Route 32, Columbia, MD 21044

One of the key elements of gasoline reformulation is the reduction of the gasoline-range sulfur compounds produced by fluid catalytic cracking (FCC). This paper probes the reaction kinetics of refractory gasoline-range thiophene derivatives (thiophene, tetrahydrothiophene, and alkylthiophenes) in an effort to determine the mechanisms of sulfur compound cracking in the FCC unit. The gasoline-range sulfur compounds were analyzed using gas chromatography with an atomic emission detector. Our results show that the FCC catalyst affects the cracking of sulfur compounds through hydrogen transfer mechanisms. An experimental FCC catalyst is shown to reduce gasoline sulfur content in the Davison Circulating Riser (DCRTM) pilot unit. Model compound tests show that the activity of the catalyst is due to both its catalytic and adsorptive properties.

Recent environmental legislation has had broad impact on the fuel industry. The 1990 Clean Air Act requires reformulated gasoline to have lower aromatics, lower sulfur content, and higher oxygen content than current gasoline. In this paper we focus on the gasoline sulfur content. Since gasoline sulfur content reversibly inhibits the activity of automobile catalytic converters, average gasoline sulfur content is expected to be dramatically lowered by the Clean Air Act. In addition, the California Air Resources Board has restricted average sulfur content to 40 ppm after 1996. Since regular grade gasoline averaged 384 ppm in 1990 (National Petroleum Refiners Association survey), sulfur reduction will be a high priority for refiners in the coming decade.

There are several methods currently available to reduce gasoline sulfur content. The most effective single variable is the choice of gas oil. The use of low sulfur gas oil feedstocks can reduce gasoline-range sulfur dramatically.

0097-6156/94/0552-0286\$08.00/0
© 1994 American Chemical Society

However, the gas oil pool is evolving towards more refractory, high-sulfur feedstocks. Increased hydrotreating and hydrodesulfurization are other options for large refineries. However, currently 50% of the refineries lack sufficient hydrotreating capacity to achieve desulfurization(1). In addition, severe hydrotreating significantly alters the gasoline composition, typically leading to lower octane numbers. Since fluid catalytic cracking (FCC) naphtha contributes between 75 and 90% of the sulfur in the gasoline pool(2), methods which affect FCC gasoline sulfur content directly would also be desirable.

In this paper we explore the possibility of catalytically reducing sulfur content of the gasoline produced in the FCC unit. In riser and fixed bed studies, approximately 4% of the gas oil sulfur compounds produce gasoline-range sulfur products. Our measurements with a GC Atomic Emission Detector show that gasoline-range sulfur compounds are primarily thiophene derivatives and benzothiophene (3). Therefore we have studied the reaction kinetics of thiophene, alkylthiophenes, and tetrahydrothiophene, and the effect of FCC catalyst properties on their reaction pathways. Our results show that the primary reaction products of thiophene in a realistic hydrocarbon environment are alkylthiophenes and tetrahydrothiophene which remain in the gasoline range. The tetrahydrothiophene cracks readily to form H₂S. The latter pathway is the primary catalytic route to the removal of sulfur compounds from the gasoline range. Alkylthiophenes react through isomerization and chain-cracking, and our measurements show that the rate of chain-cracking and dealkylation is not affected by the proximity of the S atom (e.g. 2-hexylthiophene and 3-hexylthiophene crack at the same rate).

The sulfur products of a standard USY-based catalyst and a new experimental catalyst termed GSRTM (Gasoline Sulfur Reduction) are compared. The results show that the GSR technology reduces the sulfur content of the final gasoline by 15% in riser tests. Our model compound results show that the GSR technology dramatically increases the cracking rate of tetrahydrothiophene. Sorption of sulfur compounds also plays a strong role in GSR activity.

Experimental

The hexadecane, thiophene, tetrahydrothiophene, and 2-ethylthiophene used in this experiment were all 99+ % purity gold label Aldrich products. The 3-n-hexylthiophene and the 2-n-hexylthiophene were 99% purity products from TCI America and Lancaster, respectively. Each of the sulfur compounds were mixed with hexadecane to a 5000 ppm sulfur level, determined by LECO sulfur analysis. Hexadecane conversion was determined by gas chromatography (Hewlett Packard 5890 equipped with a 19091S-001 50 m Fused Silica Capillary column). Complete separation of the peaks was achieved with the temperature program: 0 to 35 °C at 3 °C/min, 1.5 °C/min to 70 °C, 3.0 °C/min to 250 °C, hold at 250 °C for 5 minutes. Repeated chromatograph runs demonstrated a variation of less than .1 wt% in the final hexadecane concentrations.

For the model compound tests, each catalyst was pressed to 40/80 mesh size, placed in a quartz reaction tube, and preheated for 30 minutes at 500 °C under 10 cc/min nitrogen flow. The reaction tube was maintained at temperature

with a three zone furnace and actual catalyst temperature was measured with a type K thermocouple in the center of the catalyst bed. The model compound mixture was pumped into the reaction chamber with a syringe infusion pump (Harvard Apparatus #22) at the rate of .6 g/min. Nitrogen was co-fed with the hydrocarbons at the rate of 10 cc/min set by mass flow controller. The products of the cracking reactions were collected for three minutes. Thus, the product selectivities represent an average over a deactivating catalyst. Space velocity was varied by changing the amount of catalyst in the reactor tube. To maintain constant reactor heat capacity the catalyst was diluted with alundum (EM Science, calcined for 2 hrs. at 1300 °F) to a constant bed volume of 4 ml. Alundum alone shows less than 1 % conversion for these hydrocarbons.

Liquid products were collected in an ice bath and then analyzed on the gas chromatograph. The volume of the gas products was determined by water displacement. The gas products were analyzed by FID and TCD on a Varian Vista 6000 Gas Chromatograph equipped with a 50 m Chrompack Fused Silica column 7515. Only mass balances above 97% are reported in this study.

Kinetic measurements were performed on three catalysts: A USY zeolite-based catalyst with unit cell parameter 24.24 Å; A REY zeolite-based catalyst with 4.73 wt% rare earth content and unit cell parameter 24.49 Å; and a USY zeolite /GSR catalyst that is a modification of the USY catalyst with GSR technology. All three catalysts have the same active matrix with surface area of 24 m²/g. In order to simulate the steam-deactivation that occurs in the commercial unit, prior to cracking experiments each catalyst was steam-deactivated for 4 hours at 1500 °F (95% steam, 5% air).

The riser cracking results were obtained with the Davison Circulating Riser (DCRTM) reaction unit, a 5 kg scale model riser unit described in ref. 4. This pilot-scale testing unit is a moving fluidized bed that continuously circulates FCC catalysts from the riser reaction zone to a regenerator where the coke is removed from the catalyst in an oxidizing steam environment. The DCR study was performed with a low sulfur gas oil characterized in Table I.

The Gas Chromatography Atomic Emission Detector (GCAED) permits very accurate determination of the ppm concentrations of sulfur species. The technique is described in detail in ref. 5.

Results and Discussion

To evaluate the cracking kinetics of gasoline-range sulfur compounds, we examined the cracking of thiophene, tetrahydrothiophene, 2-n-hexylthiophene, and 3-n-hexylthiophene as mixtures with hexadecane at the 5000 ppm S level. The sulfur compounds were tested with hexadecane in an effort to maintain a reasonable hydrocarbon environment during the thiophene derivative cracking. Earlier results (2) showed that to a first approximation, the conversion level of the co-reacting hexadecane (which ranged from approximately 5-80% conversion level in these studies) had no effect on the overall rate of sulfur compound cracking.

The catalytic cracking products of thiophene in hexadecane over a rare earth Y catalyst (REY) are shown in Figure 1. The primary products are ethylthiophene, methylthiophene and tetrahydrothiophene. A small quantity of

H₂S was also measured. These results show that the primary reaction pathway for thiophene under industrial FCC conditions is alkylation with the co-reacting feed and hydrocarbon product species. A second major pathway is hydrogen transfer to produce the saturated tetrahydrothiophene ring. All of the reaction products remained in the gasoline range except for the hydrogen sulfide. Our later experiments with tetrahydrothiophene show that the hydrogen sulfide measured in this experiment is probably derived from the secondary cracking of tetrahydrothiophene.

Table I. Feedstock Properties

API @60 F	27.8
Aniline Pt. F	182
Sulfur wt%	0.47
Total Nitrogen wt%	0.07
Conradson Carbon wt%	0.16
Ni ppm	0.14
V ppm	0.10
Fe ppm	0.4
Simulated Distillation:	
Vol%	Temp°F
ibp	338
10	486
20	549
40	640
60	762
80	840
90	916
fbp	1065

To determine the cracking rates of the sulfur compounds relative to hexadecane we use a technique described in ref. 6 for determining the cracking kinetics of model compound mixtures in FCC. Determining the initial rates of reaction is a challenging problem in fluid catalytic cracking due to the complex convolution of catalyst deactivation, competitive adsorption between products and reactants, and volume expansion. To avoid these problems, we crack a binary mixture of two model compounds and determine their relative reaction rates with the following technique.

The cracking of the mixture can be represented by two coupled nonlinear equations

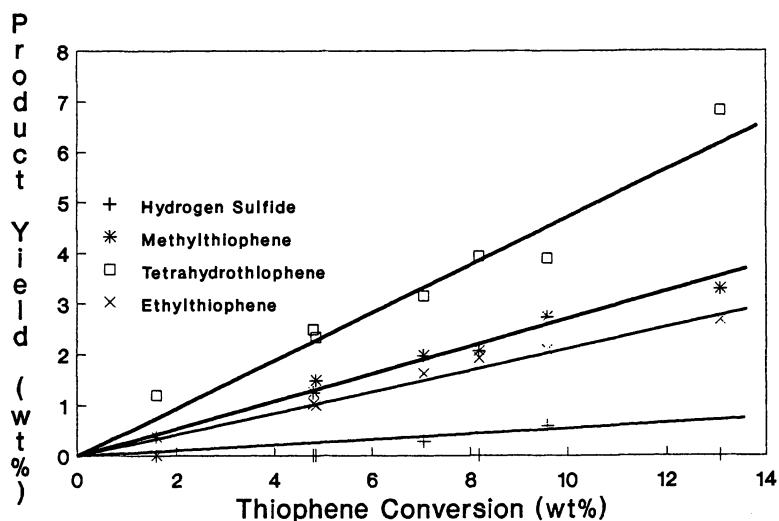


Figure 1: Sulfur product yields of thiophene over the REY catalyst. The thiophene was tested as a 5000 ppm S mixture with n-hexadecane to maintain a realistic hydrocarbon environment.

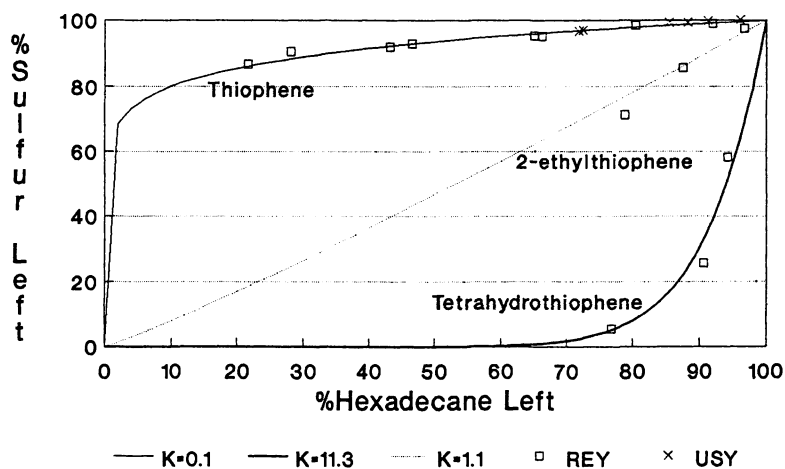


Figure 2: Relative utilization curves of thiophene, 2-ethylthiophene, and tetrahydrothiophene over REY (\square) and USY (\times). The axes represent the percent of each reactant that remains after cracking. Sulfur compounds were tested as a 5000 ppm S mixture with n-hexadecane.

$$-\frac{dC_H}{dt} = \frac{K_H \sum_j k_{Hj} C_H [1+G\tau]^{-N}/[VE]}{1+[K_H C_H + K_S C_S + \sum_j [C_{H0}-C_H] K_{Hj} n_{Hj} + \sum_j [C_{S0}-C_S] K_{Sj} n_{Sj}]/[VE]}, \quad (1)$$

$$-\frac{dC_S}{dt} = \frac{K_S \sum_j k_{Sj} C_S [1+G\tau]^{-N}/[VE]}{1+[K_H C_H + K_S C_S + \sum_j [C_{H0}-C_H] K_{Hj} n_{Hj} + \sum_j [C_{S0}-C_S] K_{Sj} n_{Sj}]/[VE]}, \quad (2)$$

where subscripts H and S represent hexadecane and the sulfur compound respectively, C is the concentration, K is the Langmuir-Hinshelwood-Hougen-Watson (LHHW) adsorption constant, k_j is the first order reaction rate constant through the j th reaction pathway, G and N are the decay parameters for time-on-stream τ , C_0 is the initial concentration in the reaction mixture, K_j is the adsorption constant of the products through reaction pathway j , n_j is the stoichiometry of reaction pathway j , and [VE] represents the volume expansion of the mixture.

We reduce eqs. 1 and 2 by examining dC_H/dC_S and find that

$$\left(\frac{C_H}{C_{H0}} \right) = \left(\frac{C_S}{C_{S0}} \right)^{\frac{K'_H}{K'_S}}. \quad (3)$$

By examining the relative conversions of hexadecane and the sulfur compound in this manner we use equation (3) to determine a ratio of effective first order rate constants K' that is independent of the decay rate, most competitive sorption terms, and the volume expansion of the mixture. In Figure 2 we plot C_H vs. C_S for thiophene, 2-ethylthiophene, and tetrahydrothiophene for the REY catalyst. To examine the effect of hydrogen transfer, we also include USY for the thiophene mixture. We find that thiophene has 1/10th the overall reaction rate of hexadecane under these conditions. No difference is observed between the two faujasite types, which indicates that the increased hydrogen transfer kinetics of the REY does not alter the relative cracking rates of the thiophene and the hexadecane. The hydrogen transfer steps affect only secondary reactions in this model compound mixture. The reaction rates of tetrahydrothiophene and 2-ethylthiophene were similarly determined to be 11.3 and 1.1 times as fast as hexadecane, respectively.

Application of this multi-component cracking technique is more complex in the case of 2-hexylthiophene cracking, since a primary reaction is isomerization to 3-hexylthiophene. The reaction pathways are drawn schematically in Figure 3. A correction to eq. 3 is necessary to compensate for the re-isomerization of the 3-hexylthiophene to 2-hexylthiophene (with rate K_{XI}). We have cracked both 2-hexylthiophene and 3-hexylthiophene in mixtures with hexadecane in an effort to unravel this effect and to determine whether the proximity of the S atom affects the cracking rates of the alkyl chain. Results are shown in Figure 4. We find that the rate of disappearance of both species are identical ($K_x = K_y \approx 3.9$ times the cracking rate of hexadecane). This rate does not include isomerization. The

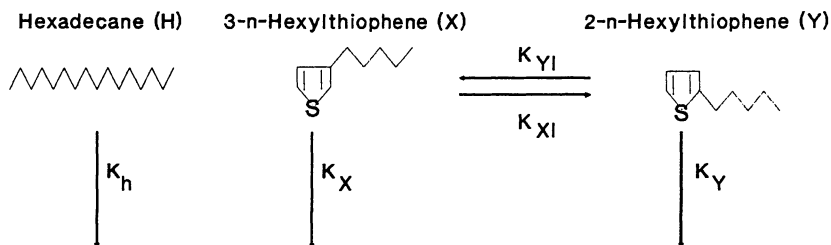


Figure 3: Reaction schematic for hexylthiophene cracking. By examining the change of both hexylthiophene isomers with respect to the change in hexadecane concentration, we are able to determine the ratio of K_X and K_H .

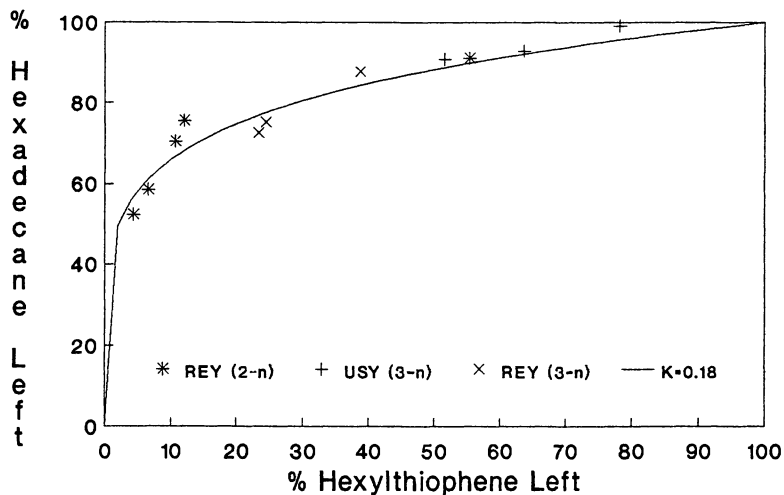


Figure 4: Relative utilization curves of hexylthiophene and hexadecane. The axes represent the percent of each reactant that remains after cracking. 3-n-hexylthiophene was tested with both REY (x) and USY (+). 2-n-hexylthiophene was tested with REY (*).

overall disappearance rate of hexylthiophene cracking ($K_X + K_{XI}$ or $K_Y + K_{YI}$ in the schematic) is 5.5. Since both species fall on the same line, the cracking rate of alkyl chains is insensitive to the proximity of the S atom. Again we find that the hydrogen transfer rate of the catalyst does not affect the rate of hexylthiophene utilization: USY and REY produce the same overall cracking rates.

Developing Sulfur Technology. Based on this kinetic information, Grace Davison has been developing a new proprietary technology for sulfur reduction in the fluid catalytic cracking unit referred to as GSR (Gasoline Sulfur Reduction). Figure 5 shows a comparison of the gasoline-range sulfur compounds produced by the standard USY catalyst and USY/GSR in the DCR riser unit. These results are described in more detail in ref 4. The plot shows a 60 ppm reduction in sulfur concentration for a full range gasoline, which is approximately a 15% decrease. The GSR technology represents the first FCC catalyst system that provides a significant reduction of gasoline sulfur.

Table II. Reduction of Gasoline-range Sulfur Compounds with GSR Technology
DCR Riser Data, Interpolated to 66% Conversion

Sulfur Product (ppm)	USY	USY/GSR	Approximate %change
Mercaptans	2.7	0.0	-100%
Thiophene	27.5	23.8	-13%
Methylthiophenes	67.1	59.6	-11%
Tetrahydrothiophene	10.3	6.1	-40%
C ₂ -thiophenes	87.8	73.3	-16%
C ₃ -thiophenes	60.5	54.3	-10%
C ₄ -thiophenes	63.3	53.5	-16%
Benzothiophene	127.2	119.9	-6%
% Feed Sulfur			
Hydrogen Sulfide	35.2	41.4	+17%
Sulfur in Gasoline	3.8	3.0	-21%
Sulfur in LCO/HCO	57.5	54.1	-6%

Table II compares the sulfur concentrations derived from these two catalysts. We find that most of the sulfur compounds are removed in proportion to their concentration, which suggests a strong adsorptive component to the removal. However, mercaptans and tetrahydrothiophene are removed at a significantly higher rate by the GSR technology. We examined the relative utilization rates of tetrahydrothiophene and hexadecane for USY and USY/GSR. The results are shown in Figure 6. Comparing these results with Figure 2, we find that unlike thiophenic compounds, tetrahydrothiophene cracks at a much slower rate for USY than for REY (2.5 vs 11.4 times the rate of hexadecane cracking, respectively). The GSR technology dramatically increases the cracking/removal

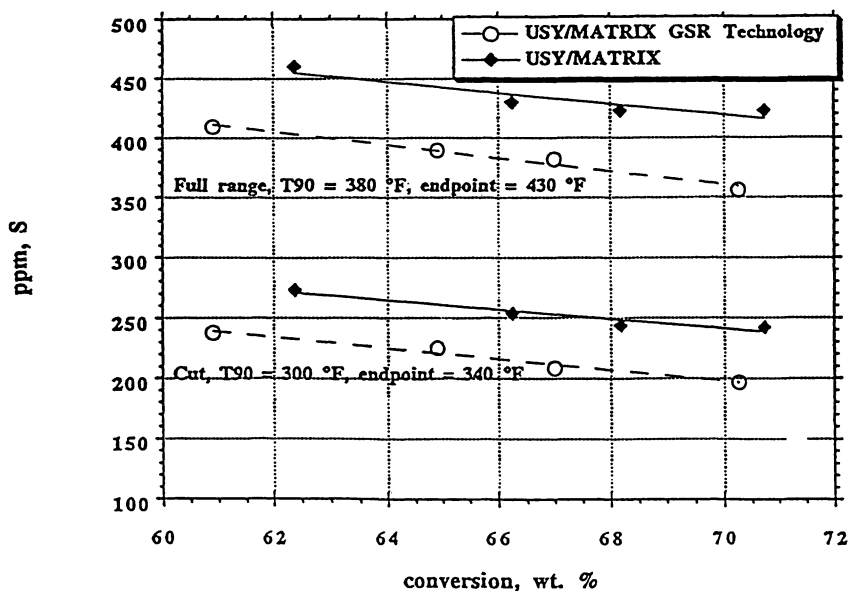


Figure 5: A comparison of the sulfur concentration in the gasoline produced in the Davison Circulating Riser (DCR) by USY (\blacktriangle) and USY/GSR (\circ). Results are shown for both the full range gasoline ($T_{90}=380^{\circ}\text{F}$) and a cut gasoline ($T_{90}=300^{\circ}\text{F}$). (Reproduced with permission from ref. 4.)

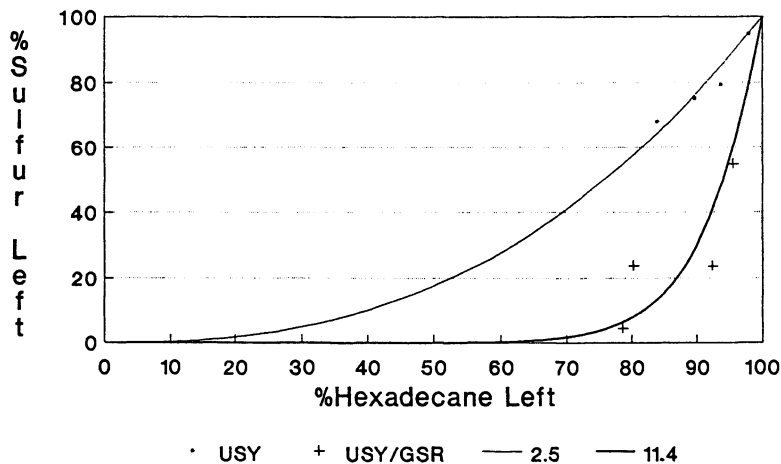


Figure 6: Relative utilization curves of tetrahydrothiophene and hexadecane with USY ($*$) and USY/GSR ($+$) catalysts.

rate of tetrahydrothiophene from USY, returning it to the cracking rate of the high hydrogen transfer catalyst REY. Increases in hydrogen sulfide production confirm that this removal is catalytic in nature.

Conclusion

This study focussed on the cracking activity of sulfur compounds in the gasoline-range. Since GCAED results show that gasoline-range sulfur compounds are primarily thiophene derivatives, we used binary mixture experiments to determine the cracking rates of thiophene, tetrahydrothiophene, 2-ethylthiophene, and the hexylthiophenes with respect to hexadecane. The results show that the gasoline-range sulfur compounds have significant cracking rates under FCC conditions, but that the primary reaction pathway is alkylation of the thiophene ring. Hydrogen transfer to tetrahydrothiophene and subsequent ring opening to form H₂S is the primary mechanism to remove sulfur from the gasoline. Our results show that the position of the alkyl chain with respect to the sulfur atom does not dramatically influence the cracking rate.

Our results also show that the reaction rates of sulfur compounds in gasoline span approximately two orders of magnitude. We find that tetrahydrothiophene reacts very rapidly over zeolite catalysts. We speculate that the small amount of tetrahydrothiophene observed in FCC gasoline is primarily derived from the cyclization of gas oil mercaptans and disulfides, rather than from hydrogen transfer of gasoline-range thiophene derivatives. Hexadecane and its cracking products provide a hydrogen-rich environment relative to a gas oil. Therefore we expect that hydrogen transfer to thiophenes may be slower in an actual FCC feed than in our model compound experiments.

A new catalyst technology referred to as GSR removes sulfur compounds from gasoline through both adsorption and catalytic routes. The GSR technology primarily enhances the cracking of tetrahydrothiophene to H₂S. The developing GSR technology may give the refiner a low-capital alternative to feed hydrotreating or hydrodesulfurization in order to meet the requirements of the Clean Air Act. It should be particularly useful for reducing the sulfur level in the FCC naphtha to desired levels.

Acknowledgements

The authors thank Ted Peders and Jeff Delmartin for their careful catalyst testing and Tom Albro and Jack Stuff for their methods development work on the GCAED. We also thank W. R. Grace & Co. - Conn. for permitting this publication.

Literature Cited

1. Thrash, L. H. *Oil Gas J.* **1991**, Mar. 18, p. 89.
2. *NPRA Gasoline Survey Section A, Revised Sulfur Data*, March 1991.

3. Gatte, R. R.; Harding, R. H.; Albro, T. G.; Wormsbecher, R. F. *Fuel Chemistry Symposia, ACS National Meeting*, San Francisco, CA, April 1992.
4. Wormsbecher, R. F.; Weatherbee, G. D.; Kim, G.; Dougan, T. J. *Paper AM-93-55; NPRA Annual Meeting*, San Antonio, TX, March 1993.
5. Albro, T.G.; Dreifuss, P. A.; Wormsbecher, R. F.; *J. High Resol. Chromatog.*, in press.
6. Harding, R. H.;Gatte, R. R.; Pereira, C. J. *J. Cat.*,**1993**,*140*,41-52.

RECEIVED September 30, 1993

Chapter 24

Volatile Organic Compounds: An Overview

John N. Armor

Air Products & Chemicals, Inc., 7201 Hamilton Boulevard,
Allentown, PA 18195

Like automotive catalysts, the area of heterogeneous catalysts for the control of volatile organic compounds [VOC] is an established technology and business. There are several detailed reviews on this topic (1,2) which include opportunities for using catalysts to resolve tougher emission control problems (3,4). The Clean Air Act of 1990 calls for a 90% reduction in the emissions of 189 toxic chemicals (70% of these are VOCs) over the next 8 years. Catalytic VOC destruction at certain concentrations permits oxidation at lower temperatures which saves fuel costs and avoids other emissions problems. Typical catalysts include metal oxides and Pt or Pd supported alumina on a metal mesh, a ceramic honeycomb, or on beads. Key operational parameters are temperature, space velocity, contaminant level and composition, and poisons or inhibitors. In the field, impurities and poisons, especially sulfur and chlorohydrocarbon compounds, can limit optimal performance. Recently developed catalysts are designed to extend the useful life of oxidation catalysts by improving their tolerances to these poisons. Because of the low contaminant levels (~1000 ppm) and the large volumes of gas to be heated, it is necessary to use very active catalysts operating at low temperatures. There are a number of new catalysts being developed as well as several others already commercially available.

Catalytic combustion is a way to control VOCs and includes methane combustion and CO oxidation (5). [Thermal combustion is also another popular alternative.] Beyond traditional combustion, areas where catalysts are used to eliminate VOC emissions include: can, paper and fabric coating chemicals; manufacture of organic chemicals (e.g., acrylonitrile, formaldehyde, cumene, caprolactam, maleic anhydride, etc.); plywood manufacture; tire production; asphalt blowing; odor control from fish meal processing; odor control from offset printing; evaporants from waste water plants; volatiles from urine; oxidation of formaldehyde emissions; removal of gasoline vapors; and contaminated air within a submarine.

One common technique for catalytic incineration employs an afterburner with a catalyst to promote the oxidation of VOCs to CO₂ and H₂O. Generally the waste gas is pre-heated to ~300°C using natural gas or oil fuel burners. A mixing chamber

downstream from the preheater distributes the combustion products from the burner into the waste gas. Following the mixing chamber is a catalyst bed usually consisting of finely divided Pt/Al₂O₃ on a ceramic or metal structure. A heat exchanger follows to transfer heat from the hot exhaust gas to the cooler, inlet waste gas (4).

Jerry Spivey and Sanjay Agarwal of the Research Triangle Institute led the sessions on VOCs. They summarized the papers within these sessions as follows: A total of 16 papers were presented in this full day session on VOC Control. Increased environmental awareness, coupled with governmental regulations, has resulted in control requirements for VOC emissions from various sources. In addition to conventional catalytic oxidation, other technologies, including photocatalytic oxidation, are being developed as an alternative. The advantage of photocatalytic oxidation is the very low temperature required for this process. Dave Ollis (North Carolina State University) discussed the prospects and promises of this technology for VOC control. Ali T. Raissi (Florida Solar Energy Center) showed a specific application of photocatalysis: destruction of nitroglycerin vapors. A Gervasini (Universita di Milano) discussed the use of only ozone to lower the reaction temperature for VOC oxidation. The catalytic oxidation of a wide variety of VOCs, including hydrocarbons, chlorocarbons, chlorofluorocarbons, and nitrogen-containing compounds was presented. These types of compounds present a challenge since they poison many traditional deep oxidation catalysts. Steve Homeyer (Allied Signal) discussed a new family of commercial catalysts for the destruction of nitrogen-containing compounds. A. R. Amundsen (Engelhard) also discussed the development of a commercial catalyst for chlorocarbon destruction. Martin Abraham (University of Tulsa) also discussed the oxidation of amines using Pd and other catalysts. Gary Masonick (Prototech) showed how to regenerate oxidation catalysts. Several interesting applications of VOC control were discussed in this session. Linda Parker (New Zealand Institute for Industrial Research) presented an interesting application of removing ethylene and CO from fruit cold storage containers. Of the various catalysts investigated for this application, a Pt-zeolite was found to be the most active with complete conversion of ethylene below 100°C. CO₂ lasers represent another application of oxidation catalysis where there is a need to continuously convert CO to CO₂. Kenneth Brown (Old Dominion University) discussed the noble-metal/reducible-oxide catalysts developed by NASA for this application. Joe Rossin (Geo Centers) discussed the transient response of oxidation catalysts for military applications, where very high conversion and minimal deactivation are essential. Variations of catalytic oxidation system are being developed to improve the overall system performance. Yuri Matros (Washington University) described the reverse flow process for VOC oxidation. This process offers low energy requirements, making it cost effective for gases with fairly low VOC concentrations. In addition to metal oxides, other materials such as zeolites are also being examined for VOC oxidation. S. Karmakar and S. Chatterjee (University of Akron) described the metal exchanged/impregnated zeolite catalysts for the oxidation of chlorocarbons and CFCs. Russell Drago (University of Florida) and Mark Vandersall (Rohm and Haas) showed the applicability of Amborsorb® carbon-based catalysts for chlorocarbon and hydrocarbon oxidation. Eric Lundquest (Rohm and Haas) presented work on related catalysts for the esterification of industrial chemicals, reducing waste and VOC emissions.

Many of the presentations within this day long session are described further within this section of the book. Topical areas reflecting future research needs in VOCs include: increased catalyst life; reduced operating costs via catalyst improvements [temperature, activity, resistance to poisons, etc.]; and extended catalyst performance. The latter refers to making these catalysts operate under more extreme conditions, such as the catalytic oxidation of trace impurities in aqueous media or the ability of a catalyst to remove a wider spectrum of volatile organic components.

References

1. Spivey, J.J. *Ind. Eng. Chem. Res.* **1987**, *26*, 2165-2180.
2. Drohan, D. *Pollution Engn.* September 15, 1992, pp. 30-33.
3. Chiang, P-C; Chang, P; You, J-H. *J. Hazardous Matls.* **1992**, *31*, 19-28.
4. Armor, J. N. *Appl. Catal. B*, **1992**, *1*, 221-256.
5. Pferfferle, L.D.; Pferfferle, W.C. *Catal. Rev. Sci. Eng.*, **1987**, *29*, 219-267.

RECEIVED November 8, 1993

Chapter 25

Catalysts for Low-Temperature Oxidation of Ethene

Linda M. Parker and John E. Patterson

The New Zealand Institute for Industrial Research and Development
(Industrial Research Limited), P.O. Box 31–310, Lower Hutt, New
Zealand

The focus of this work was to develop a catalyst for complete oxidation of volatile organic contaminants at temperatures less than 100°C, one application being the removal of ethene from fruit storage areas. A wide range of catalysts were surveyed using a mini-reactor coupled to a mass spectrometer and a total hydrocarbon detector. For 300 ppm ethene, 0.6% O₂ in N₂ with a volume space velocity of 60000 h⁻¹, all the oxide materials tested reacted at >300°C. Pt asbestos and Pd alumina gave 50% conversion at 145°C, but for Pt and Pd on zeolites this was ~100°C. HZSM-5 also behaved as an oxidation catalyst with 100% conversion of ethene at 200°C. Reactivity of PtCsNaY(T) remained constant after conversion of 5 g ethene/ g catalyst.

This work describes the initial development of a low temperature oxidation catalyst for the removal of ethene from fruit storage areas. Ethene is a gaseous plant hormone that causes fruit ripening, and removal to less than 0.03 ppm is important to preserve fruit in an unripened state. The catalysts must also function with reduced oxygen concentrations and in the presence of water. For example, in kiwifruit cool stores the atmosphere is controlled at 2% oxygen and 5% carbon dioxide with 100% humidity at 0°C.

For catalytic oxidation of volatile organic contaminants (VOCs), large volumes of air must be heated to the reaction temperature of the catalyst. To improve efficiency heat exchangers can be used to heat the incoming air to the catalyst reaction temperature. Commercial units are available for ethene removal from fruit coolstores which use this method with a supported platinum catalyst held at ~270°C (1). The contaminant could also be removed by sorption at room temperature followed by desorption and catalytic oxidation of the concentrate (2) at a higher temperature. A third alternative is to develop a catalyst which reacts at as low a temperature as possible. Development of a low temperature oxidation catalyst would

0097-6156/94/0552-0301\$08.00/0
© 1994 American Chemical Society

enable a simpler and less expensive reactor system that could be used in transportation containers and shop storage areas.

Other applications are envisaged for low temperature oxidation catalysts, such as improvement of quality of air inside buildings by removal of organics, such as formaldehyde, released by synthetic materials. The "ultimate" goal is a catalyst which will completely oxidize all VOCs in a gas stream at its inlet temperature (3). For this highly active, non specific catalysts are required. The temperature at which oxidation occurs depends upon both the reactant and the catalyst, with most reactions occurring above 200°C, well above the "ultimate" goal (3). Only a few heterogenous oxidation reactions have been reported to occur below 50°C (eg 3,4,5).

Both metal oxides and supported noble metals are useful oxidation catalysts. Metal oxides in which the metal can assume more than one valence state, are p-type semi-conductors, and produce a surface on which oxygen will readily chemisorb. Oxides of V, Cr, Mn, Fe, Co, Ni and Cu are typical examples. Metal oxides have a lower activity than noble metal catalysts but they have greater resistance to some poisons, especially halogens, As, Pb and P. The noble metals remain in their reduced, metallic state under most conditions and provide surface sites for dissociative adsorption of oxygen. Only Pt and Pd are used in practical systems because of their stability and cost. Reaction occurs either between adsorbed oxygen and a gas phase reactant, or with both oxygen and the reactant sorbed on the surface.

In most noble metal oxidation catalysts the metal is deposited on a high surface area support such as alumina (6,7,8,9), silica (5) and zirconia (10). Zeolites are also suitable supports, but have not been widely used for practical oxidation catalysts. Their main applications are in synthesis reactions such as the conversion of alkanes to aromatics (11,12,13). The use of zeolites as substrates for oxidation catalysts would give the following advantages over simpler substrates:

1. There are a wide range of zeolite structures available with variable aluminium concentrations, enabling zeolites with specific properties to be selected as catalyst supports.
2. They have high internal surface areas and can preferentially sorb reactants.
3. They enable much greater control over metal particle size distribution than do other supports (14,15) because the restricted dimensions in zeolites isolate engaged metal particles from each other and stabilise small metal clusters. Addition of cations such as Ca^{2+} , Mg^{2+} , Cu^{2+} , Ni^{2+} , Cr^{3+} and Mn^{2+} alter the mechanism of noble metal particle formation during catalyst preparation by blocking the small cages of the zeolite (16) or impeding the migration and coalescence of primary particles. This also assists in retaining a greater dispersion of noble metal in the product (17).
4. Additional cations (including H^+) can be incorporated to alter catalyst reactivity. For example, the presence of protons (Bronsted acid sites) gives additional reactions characteristic of zeolite acid sites (18). For palladium zeolites it is suggested that complexes of the type $[\text{Pd}_n\text{H}_2]^{2+}$ are formed which greatly increases the rate of some reactions (19,20).

Oxidation catalysts for ethene have been developed for partial oxidation to ethene oxide. These are silver sponge (21) or silver on a support such as $\gamma\text{Al}_2\text{O}_3$ (22), and they are typically operated at $>230^\circ\text{C}$. A zeolite impregnated with silver (30% $\text{Ag}^\circ\text{Ca}^{2+}\text{A}$) was reported to give an ethene conversion and yield of ethene oxide comparable to other catalysts (23). Complete oxidation of ethene was reported over vanadium oxide catalysts between 440 to 500°C (24) but no other references to low temperature, complete oxidation of ethene have been found. In this work a wide range of possible catalysts for ethene oxidation have been surveyed. A mini-reactor coupled to a mass spectrometer and a total hydrocarbon detector enabled the oxidation temperature of ethene for each catalyst to be determined. The most promising catalysts appeared to be noble metal supported on zeolites. These were then tested under constant reaction conditions. The effects of reduced oxygen concentration and increased humidity were determined to obtain an indication of catalyst reactivity in fruit coolstore atmospheres.

Experimental

Preparation of Catalyst Samples.

Zeolites Used. HZSM-5 (prep #816) was synthesised as described in a patent application (25) and contained 1.48 wt % Al. Silicalite (prep 3, 7/4/86) was synthesised as described by Parker et al. (26) with 0.14 wt % Al. Zeolite Y (Linde Y, SK40, lot no. 9680801014) (8.5 wt % Al) and zeolite 5A (Linde batch #1457220) were obtained from Union Carbide, USA. Zeolite Y (lot #ST1192) was obtained as pellets containing 25 parts alumina to 100 parts zeolite from Tosoh, Japan and contained 15.8 wt% Al (including the binder).

Nomenclature of Ion Exchanged Zeolite samples. The sample names are given with the metal then the cations preceding the zeolite name. For example, "PtCaNaY(L)" represents a sample for which Ca^{2+} then Pt^{2+} were exchanged into Na^+Y zeolite. The Pt^{2+} was then reduced to the metal before catalysis. The "L" designates a sample of Linde Y and a "T" designates a sample of zeolite Y from Tosoh.

Ion Exchange of Zeolites. The zeolites were first exchanged in a 0.5 M of the appropriate salt solution, then filtered and washed. This was followed by exchanging two times in saturated solutions of either $\text{Pt}(\text{NH}_3)_4\text{Cl}_2$ or $\text{Pd}(\text{NH}_3)_4\text{Cl}_2$ solutions containing excess ammonia. The zeolite Y samples were heated on a steam bath to increase the degree of exchange. The samples were filtered, washed and dried.

Analysis of Zeolites. Analysis for Pt was carried out by digestion in hot aqua regia followed by AA spectroscopy. The other cations were analysed by HF/ HClO_4 digestion followed by AA or AE spectroscopy.

Other Catalysts. *Al/Ni Hydrotalcite*: was prepared by heating 0.01 mole $\text{Al}(\text{NO}_3)_3 \cdot 9\text{H}_2\text{O}$, 0.02 mole $\text{Ni}(\text{NO}_3)_2 \cdot 6\text{H}_2\text{O}$, 0.05 mole NaOH and 0.15 mole Na_2CO_3 in 35 ml H_2O at 80°C in a sealed container for 2 days.

Mixed iron oxide: was prepared by heating 0.01 mole $\text{Al}(\text{SO}_4)_3 \cdot 18\text{H}_2\text{O}$, 0.02 mole $\text{FeSO}_4 \cdot 7\text{H}_2\text{O}$ and 0.1 mole NaOH in 35 ml H_2O at 80°C in a sealed container for 2 days. The crystalline product was identified by Xray Diffraction as Fe_2O_3 and Fe_3O_4 .

Cerium oxide: was a laboratory grade reagent.

Unsupported P-V-O salt: A mixture of phosphorus and vanadium salts were prepared following the method of Centi et al.(27). The solution was evaporated then calcined at 400°C .

P-V-O on zeolite Y: This was prepared following the method of Centi et al.(27). This was filtered without washing and dried at 50°C for 1 h in air.

Platinum and Palladium on Iron Sand Ceramics: Porous iron sand ceramic (28) was ground then: A. 0.01 g $\text{Pd}(\text{NH}_3)_4\text{Cl}_2$ dissolved in 1 ml water was added to 0.20 g ground ceramic, mixed then dried overnight under vacuum. B. ~ 0.2 g of bright platinum (Matthey PBV158) was mixed with 0.23 g ground ceramic.

Pt asbestos: contained 5% Pt and was supplied by Hopkin and Williams.

Pd on activated alumina: contained 10% Pd and was supplied by Fluka AG Buchs SG.

Pd on charcoal: contained 10% Pd on activated charcoal and was supplied by Menu AG Darmstadt.

Silver sand: was prepared in this laboratory with silver deposited on silica sand using a method for preparation of mirrors by silver deposition.

Catalyst pretreatment. The metal ion exchanged zeolites were pretreated before testing to obtain the reduced metal. The sample was reduced by heating from room temperature at $10^\circ\text{C}/\text{min}$. to 300°C in a 1% H_2/Ar gas stream and holding for 1 hour. The sample of liquid bright Pt on iron sand was reduced by gently heating over a flame.

Catalyst testing Method. The mini-reactor system for catalyst testing is shown in figure 1. The catalyst (~ 10 mg) was held in a glass tube by silica wool to give a bed 1.3 mm diameter and ~ 7 mm deep placed in a temperature controlled furnace. The sample tubes could be readily interchanged and the packed sample retained for further study. For initial experiments the gas flow rate was controlled at 10 ml/min by a needle valve. In later experiments, the gas flow rate was more precisely controlled by a fixed capillary leak at ~ 1 ml/min. The reacted gas was analyzed by a Dycor MA100M mass spectrometer and/or a total hydrocarbon detector (29) which was very sensitive for traces of ethene. Sample temperature, output from the total hydrocarbon detector and mass spectra were recorded against time using speciality software (30). Experiments were carried out by heating the sample to 300°C then cooling at $12^\circ\text{C}/\text{min}$, to reduce effects of sorbed ethene. For catalysts that reacted at less than 100°C ethene was also sorbed during cooling, obscuring the minimum reaction temperature. To determine reaction temperatures, stepping experiments were carried out in which the catalyst was held at constant temperature until a steady state was reached.

Results and Discussion

Tables I, II and III show the results of the catalyst survey under three different sets of conditions. The results from the cooling experiments can be used to rank the catalysts in order of activity. Lowering the mass flow rate of ethene reduces the observed reaction temperatures, with the lowest temperatures observed for 140 ppm ethene at 6000 h⁻¹ (Table III). This results in physisorption of ethene on the zeolites partially obscuring most reaction temperatures in the cooling experiments. Therefore stepping experiments were also carried out. Although differences in measured temperatures were observed, both the cooling and stepping (steady state) experiments ranked the catalysts in the same order of activity. The only exceptions were the copper exchanged zeolites which sorbed ethene very strongly.

Cerium oxide was the only oxide that reacted with ethene below 300°C (Table I). Figure 2 shows the results obtained with a sample of ground iron sand ceramic where no reaction was observed. This is effectively a "blank run" and shows that no measurable reaction occurs on the reactor surfaces under the experimental conditions.

The silver catalysts tested showed low reactivity, with silver on silica sand reacting above 300°C. Silver deposited on zeolite 5A (AgCaA) strongly sorbed ethene giving a low T_{10%} of ~60°C. However, the carbon dioxide ion signal showed that the oxidation reaction started at ~150°C but was not complete by 300°C.

For Pt on asbestos (figure 3), reaction of ethene is clearly shown by a drop in ethene and oxygen concentrations and the total hydrocarbon detector signal. A corresponding increase in carbon dioxide concentration occurred, with no other products observed. Increasing the oxygen concentration in the gas stream decreased the reaction temperature, with T_{50%} dropping from 145°C to 105°C (compare Table I and Table II).

The Pd on charcoal catalyst was not effective above 200°C because the charcoal oxidised before oxidation of ethene occurred. Pd on alumina (figure 4) was slightly more reactive than Pt on asbestos, but decreased in activity with increasing oxygen content (T_{50%} rose from 155 to 165°C and T_{100%} rose from 156 to 190°C). The carbon dioxide signal increased slowly with temperature after the ethene and THD signals declined, suggesting that partial oxidation products may have also formed.

Some Pt and Pd zeolite samples showed greater reactivity than Pt on asbestos and Pd on alumina. Distinct differences were also observed between zeolites loaded with Pt and those with Pd. For example, for Pd on zeolite Y, addition of Ca²⁺ cations increased the ethene reaction temperature but for Pt on zeolite Y the reverse occurred. For PdCaNaY(L) increasing oxygen and decreasing ethene concentrations in the gas stream also increased the reaction temperature, similar to the effect observed for Pd on alumina (see figures 5A and B). For PtCaNaY increasing the oxygen concentration greatly decreased the reaction temperature in a similar manner to Pt asbestos (see figures 6A and B). These differences imply different ethene reaction mechanisms for Pt and Pd catalysts, with perhaps only partial oxidation occurring over Pd catalysts. Therefore the Pt catalysts were investigated in more detail as catalysts for complete oxidation are required.

A series of catalysts were prepared with different cations in a similar manner and tested under the same conditions. The ethene oxidation results, ranked in order

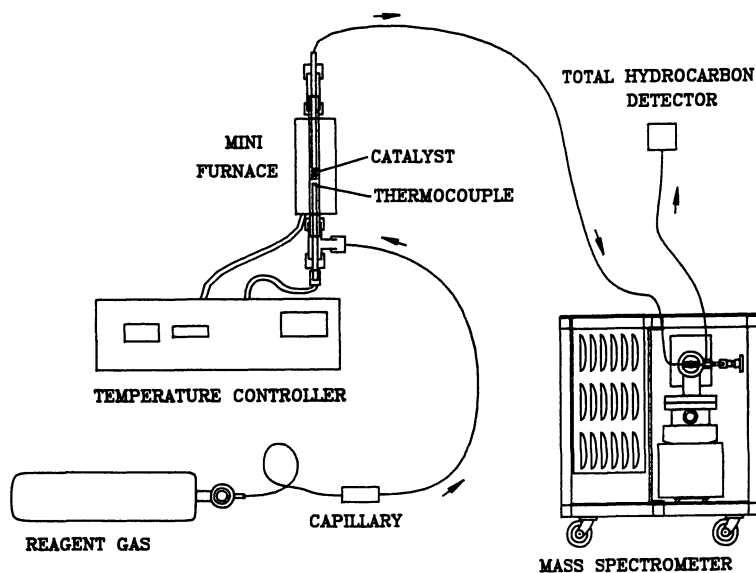


Figure 1. A schematic diagram of the mini-reactor system used for catalyst testing.

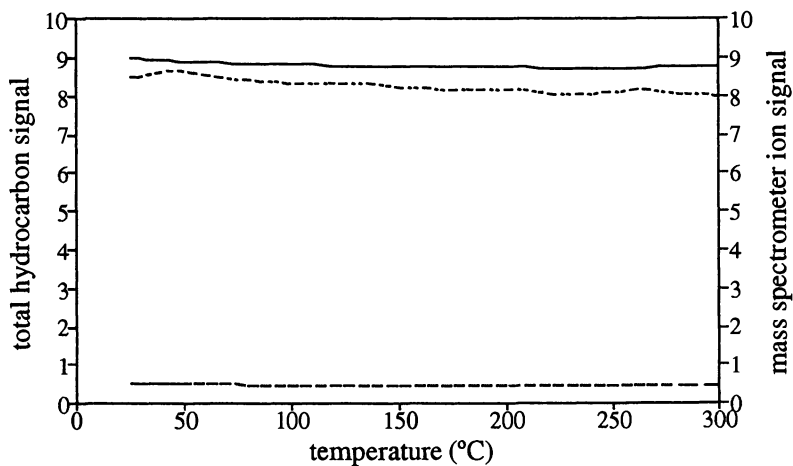


Figure 2. Results for 300 ppm ethene and 0.6% oxygen in nitrogen over iron sand ceramic at 60000 h^{-1} . The total hydrocarbon detector signal (—) and the mass spectrometer ion signals of ethene (-----) and carbon dioxide (.....) are shown versus the iron sand ceramic temperature.

Table I: Summary of catalyst tests for 300 ppm ethene and 0.6% O₂ in N₂ at a volume space velocity of 60000 h⁻¹. The catalysts were cooled at 12°C/min from 300°C.

Catalyst	T _{10%} (THD)	T _{50%} (THD)	T _{100%} (THD)	T _{100%} (CO ₂)
Al/Ni hydrotalcite	>300	>300	>300	>300
iron sand ceramic	>300	>300	>300	>300
liquid bright Pt on iron sand ceramic	>300	>300	>300	>300
Pd on iron sand ceramic	>300	>300	>300	>300
Mixed iron oxides	>300	>300	>300	>300
unsupported P/V salt	>300	>300	>300	>300
P-V-O on Y	>300	>300	>300	>300
silver sand treated with HCl	>300	>300	>300	>300
cerium oxide	~300	>300	>300	>300
AgCaA	~60	280	>300	>300
Pd on charcoal	>200	>200	>200	>200
CuNaY(L)	30?	45?, 150	>300	>300
PdCuHZSM-5	140	180	225	>300
HZSM-5	166	176	200	-
PtNH ₄ NaY(L)	27?	150	214	235
Pd on alumina	120	146	156	200
Pt on asbestos	92	145	174	200
PdCaNaY(L)	83	136	230	230
PdHZSM-5	62	106	254	235
PdNaY(L)	36	103	176	>300
CuZSM-5	29	47	161	>300
PdCaZSM-5	28?	105	158	216
PtCaNaY(L)	40	100	160	215

T_{10%}, T_{50%} and T_{100%} are the temperatures, in °C, at which the given percentage of ethene has reacted, as measured by the total hydrocarbon detector (THD).

T_{100%} (CO₂) is the temperature above which the CO₂ evolution is constant.

Table II: Summary of catalyst tests with 130 ppm ethene in air at a volume space velocity of 60000 h⁻¹. The catalysts were cooled at 12°C/min from 300°C

Catalyst	T _{10%} (THD)	T _{50%} (THD)	T _{100%} (THD)	T _{100%} (CO ₂)
PdCaNaY(L)	174	235	310	>300
Pt silicalite	138	169	220	~200
PdCuHZSM5	126	165	209	>300
Pd on alumina	124	165	190	>300
PtHNaY(L)	30	150	190	180
PtCsNaY(T)	85	113	150	150
Pt on asbestos	76	105	131	188
PtCaNaY(L)	51	66	92	~100
PtCuNaY(L)	46	58	77	115

T_{10%}, T_{50%} and T_{100%} are the temperatures, in °C, at which the given percentage of ethene has reacted, as measured by the total hydrocarbon detector (THD).

T_{100%} (CO₂) is the temperature above which the CO₂ evolution is constant.

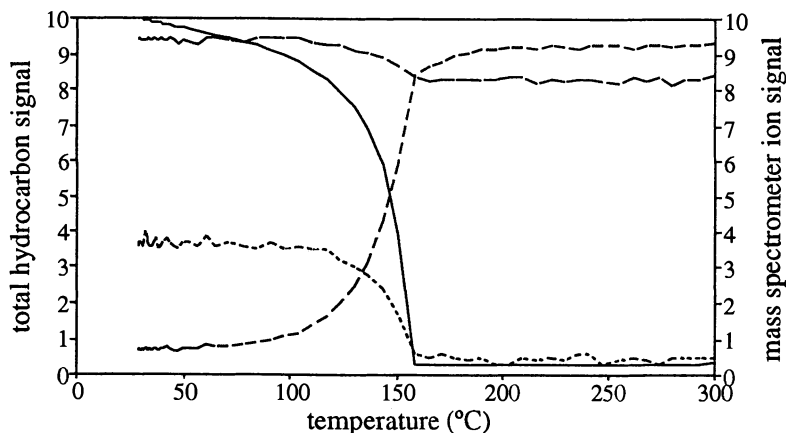


Figure 3. Results for 300 ppm ethene and 0.6% oxygen in nitrogen over Pt on asbestos at 60000 h⁻¹. The total hydrocarbon detector signal (—) and the mass spectrometer ion signals of ethene (-----), oxygen (.....) and carbon dioxide (-.-.-) are shown versus catalyst temperature.

Table III: Summary of catalyst tests with 140 ppm ethene in N₂ with 0.3% oxygen at a volume space velocity of 6000 h⁻¹

Catalyst	Pt wt%	Na wt%	other cation wt %	test type	T _{10%} (°C) (THD)	T _{50%} (°C) (THD)	T _{100%} (°C) (THD)
HZSM-5	0	-	0	step cool	>180 ~20	190 ~20	200 ~30
CuZSM-5	0	-	-	step cool	>70 90	- 100	150 120
PtHZSM-5 #2	0.25	0.06	0	step cool	130 46	135 89	140 150
Pt silicalite	0.08	0.07	0	step cool	95 30	105 85	130 100
PtBaNaY(L)	3.84	0.11	1.14 (Ba)	step cool	>100 55	105 70	110 90
PtHNaY(L)	2.80	1.41	0	step cool	90 20	105 28	110 33
PtCuZSM-5	1.76	0.08	0.05 (Cu)	step cool	>80 20	95 40	100 65
PtMgNaY(L)	2.93	1.32	0.45 (Mg)	step cool	- 22	83 30	100 60
PtCaNaY(L)	1.00	0.47	4.14 (Ca)	step cool	75 20	85 35	105 45
PtCsNaY(T)	3.17	1.11	0.01 (Cs)	step cool	- 20	60 22	70 27
PtHZSM-5 #1	0.71	0.10	0	step	-	-	60

cool: the catalyst was cooled from 300°C at 12°C/min

step: the catalyst was held at a constant temperature until a constant ethene concentration was obtained

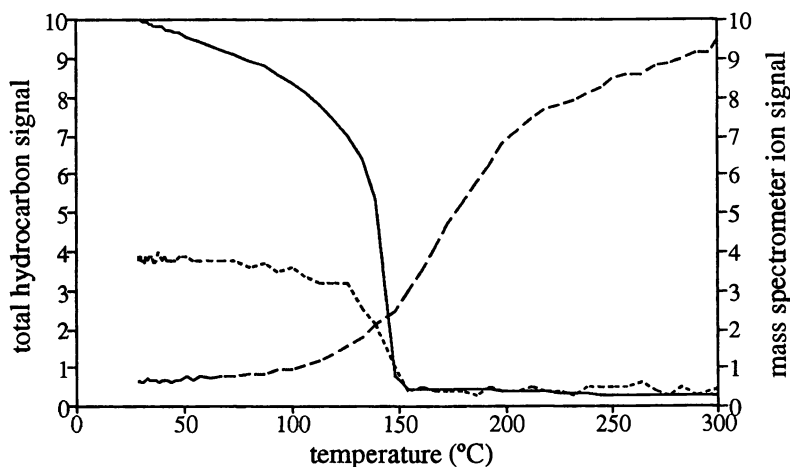


Figure 4. Results for 300 ppm ethene and 0.6% oxygen in nitrogen over **Pd on alumina** at 60000 h^{-1} . The total hydrocarbon detector signal (—) and the mass spectrometer ion signals of ethene (·····) and carbon dioxide (- - - -) are shown versus catalyst temperature.

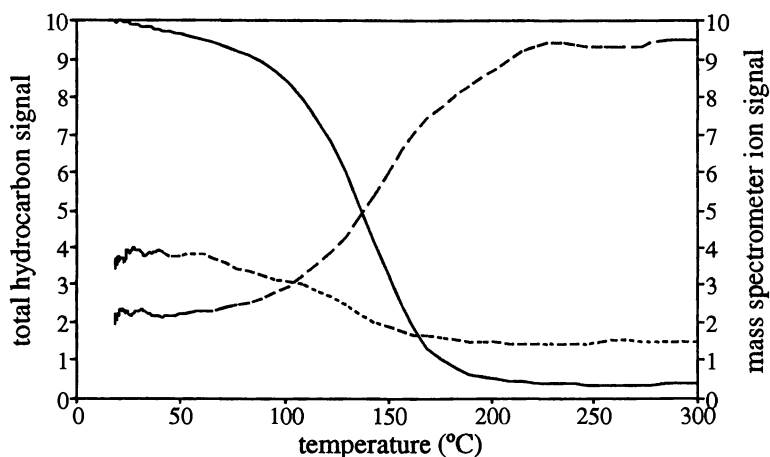


Figure 5A. Results for 300 ppm ethene and 0.6% oxygen in nitrogen over **PdCaNaY(L)** at 60000 h^{-1} . The total hydrocarbon detector signal (—) and the mass spectrometer ion signals of ethene (·····) and carbon dioxide (- - - -) are shown versus catalyst temperature.

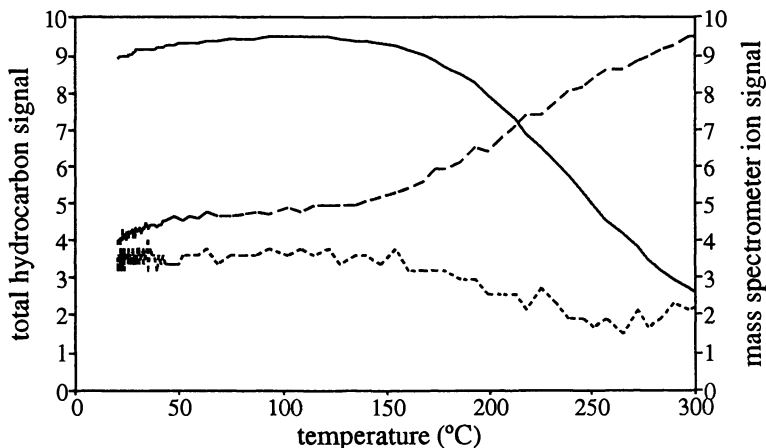


Figure 5B. Results for 130 ppm ethene in air at 60000 h⁻¹ over PdCaNaY(L) at 60000 h⁻¹. The total hydrocarbon detector signal (—) and the mass spectrometer ion signals of ethene (· · · · ·) and carbon dioxide (---) are shown versus catalyst temperature.

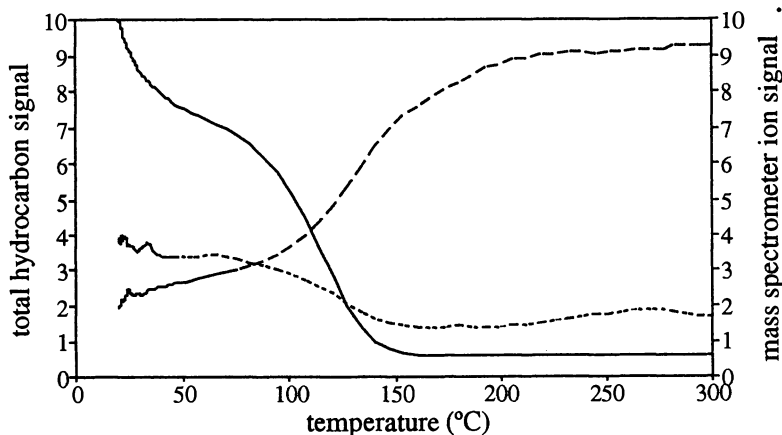


Figure 6A. Results for 300 ppm ethene and 0.6% oxygen in nitrogen over PtCaNaY(L) at 60000 h⁻¹. The total hydrocarbon detector signal (—) and the mass spectrometer ion signals of ethene (· · · · ·) and carbon dioxide (---) are shown versus catalyst temperature.

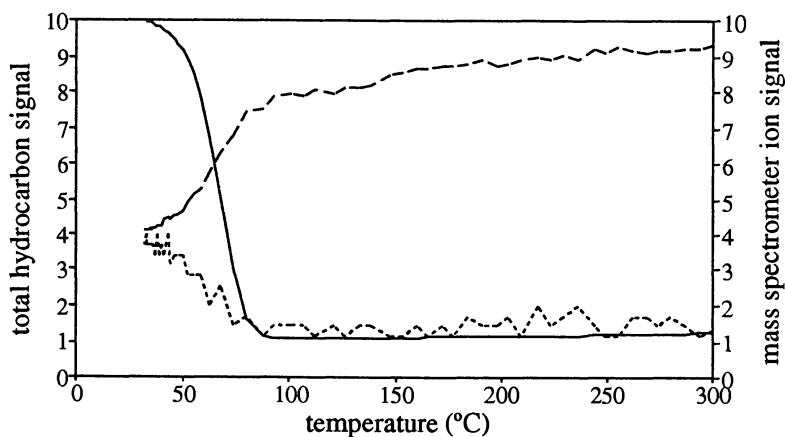


Figure 6B. Results for 30 ppm ethene in air at 60000 h^{-1} over PtCaNaY(L) at 60000 h^{-1} . The total hydrocarbon detector signal (——) and the mass spectrometer ion signals of ethene (-----) and carbon dioxide (.....) are shown versus catalyst temperature.

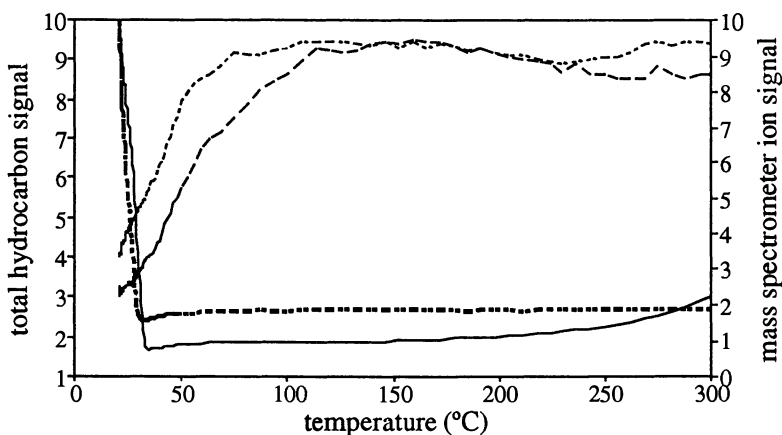


Figure 7. Shows the effect of adding water vapour to 140 ppm ethene and 0.3% oxygen in nitrogen reacting over PtCaNaY(L) at 6000 h^{-1} . The total hydrocarbon detector signal with out water vapour (-----) and with water vapour(——), and the mass spectrometer ion signal of carbon dioxide without water vapour (-----) and with water vapour(.....) are plotted versus catalyst temperature.

of increasing reactivity, are shown in Table III along with the Pt and cation concentrations. The Pt concentration varied with different cations for the same zeolite. This may be an effect of the additional cation. The Pt concentration is also greater for zeolites with higher aluminium concentration as they have a greater cation exchange capacity. The lowest Pt concentration is recorded for silicalite, a low aluminium form of ZSM-5.

The bulk Pt concentration was not the most important criteria for reactivity. For zeolite Y, there was no correlation of Pt concentration with reactivity. For ZSM-5, the best catalyst was produced with a Pt content of 0.71%. However, in the silicalite sample with only 0.08% Pt a high proportion of Pt must be held in reactive sites as it was more reactive than a ZSM-5 sample containing 0.25% Pt. HZSM-5 with zero Pt also functioned as an oxidation catalyst above 180°C. For this catalyst there was a very narrow temperature range between no reaction and complete reaction. At less than 180°C no reaction occurred but above 200°C complete reaction occurred. Evolved carbon dioxide increased as ethene decreased and no other products were observed.

Catalyst reactivity appears to be influenced by the zeolite structure with ZSM-5 producing more reactive catalysts at lower bulk Pt concentrations than zeolite Y.

For zeolite Y, the presence of an additional cation influences reactivity and perhaps dictates Pt uptake. However, there is no obvious correlation between cation charge or ionic radii of the additional cation and catalyst reactivity. More detailed catalyst characterisation is required to determine how the cations have effected the nature of the reactive Pt particles. The Cu²⁺ exchanged zeolites had a very high sorption capacity for ethene, resulting in low results for T_{10%} and T_{50%} in the experiments where the sample was cooled at 10°C/min. A temperature stepping experiment for CuZSM-5 showed that no reaction occurred at 70°C, but complete reaction occurred from 150°C. Addition of Pt to this catalyst increased reactivity with 100% reaction occurring from 100°C.

In fruit cool stores atmospheric conditions include low oxygen concentrations and ~100% humidity at 0°C. Tables I and III show that the catalysts function well at a low oxygen concentration with the reaction temperature depending upon the ethene mass flow rate. Water vapour has little effect on the reaction temperature as shown in figure 7, where no significant difference was observed when water vapour was added into the gas stream by a bubbler at 20°C.

Catalyst lifetimes for two catalysts were tested. PtHZSM-5 was held at 60°C in a flow of 130 ppm ethene in air at 10 ml/min for 3½ days. Constant reactivity was observed over that period. For PtCsNaY(T), a gas stream of 1% ethene in air was passed over the catalyst held at 100°C. After 66 h, 100% conversion was still occurring. The catalyst had converted 5 g ethene/ g catalyst with no loss of activity.

Conclusions

We have produced a range of ethene oxidation catalysts that are effective below 100°C in the low oxygen and high humidity conditions typically found in cool store atmospheres. These catalysts are the zeolites ZSM-5 and Y, with Pt incorporated. Additional cations have a marked effect on the activity of zeolite Y with PtCsNaY and PtCaNaY being the best catalysts. However, no correlation with cation charge

or ionic radii was noted. More detailed study of the catalysts is required to understand these effects and to prepare improved catalysts.

We have also shown that HZSM-5, without Pt, functions as an oxidation catalyst for ethene. Copper exchange of both ZSM-5 and zeolite Y results in a zeolite that has a very high sorption capacity for ethene. CuHZSM-5 reacted with ethene at temperatures $\sim 50^\circ\text{C}$ lower than HZSM-5.

Literature Cited

1. Catalytic ethene scrubbers are produced by ISOLCELL ITALIA SPA.39055 Laives (BZ) - Zona Industriale - Via Meucci, 7
2. Note in *App. Catal.* **1991**, 73, N4.
3. Spivey J.J.; *Ind. Eng. Chem. Res.*, **1987**, 26, 2165.
4. McCabe R.W.; Mitchell P.J. *Appl. Catal.* **1986**, 27, 83.
5. Gonzalez R.D.; Nagai M. *Appl. Catal.*, **1985**, 18, 57.
6. Skoglundh M.; Lowendahl L.O.; Ottersted J.-E. *App. Catal.* **1991**, 77, 9.
7. Oh S.H.; Mitchell P.J.; Siewert R.M. *J. Catal.* **1991**, 132, 287.
8. Loof P.; Kasemo B.; Andersson S.; and Frestad A. *J. Catal.* **1991**, 130, 181.
9. Jackson S.D.; Willis J.; McLellan G.D.; Webb G.; Keegan M.B.T.; Moyes R.B.; Simpson S.; Wells P.B.; Whyman R. *J. Catal.* **1993**, 139, 191.
10. Hubbard C.P.; Otto K.; Gandhi H.S.; Ng K.Y.S. *J. Catal.* **1993**, 139, 268.
11. Mielczarski E.; Bong Hong S.; Davis R.J.; Davis M.E. *J. Catal.* **1992**, 134, 359.
12. McVicker G.B.; Kao J.L.; Ziemiak J.J.; Gates W.E.; Robbins J.L.; Treacy M.M.J.; Rice S.B.; Vanderspurt T.H.; Cross V.R.; Ghosh A. K. *J. Catal.* **1993**, 139, 48.
13. Shipiro E.S.; Joyner R.W.; Khabib M.M.; Pudney P.D. *J. Catal.* **1991**, 127, 366.
14. Jaeger N.I.; Jourdan A.; Schulz-Ekloff G.; Kleine A.; Ryder P.L. In *Innovation in Zeolite Materials Science*; Grobet P.J. et al. Editors, Elsevier, The Netherlands, **1988**, p191.
15. Jaeger N.I.; Jourdan A.L.; Schulz-Ekloff G. *J. Chem. Soc. Faraday Trans.* **1991**, 87, 1251.
16. Feeley J.S.; Sachtler W.H.M. *Catal. Lett.* **1991**, 9, 377.
17. Homeyer S.T.; Sachtler W.M.H. In *Zeolites: Facts, Figures, Future*, Jacobs P.A.; van Santen R.A. Editors, Elsevier, The Netherlands, **1989**, p975.
18. Chow M.; Park S.H.; Sachtler W.M.H. *Appl. Catal.*, **1985**, 19, 349.
19. Sachtler W.H.M.; Calcanti F.A.P.; Zhang Z. *Catal. Lett.*, **1991**, 9, 261.
20. Homeyer S.T.; Karpinski Z.; Sachtler W.M.H., *J. Catal.*, **1990**, 123, 60.
21. Yong Y.S.; Cant N.W., *J. Catal.*, **1990**, 122, 22.
22. Johnson D.L.; Verykios X.E. *J. Catal.*, **1983**, 79, 156.
23. Minachev and Isakov, In *Zeolite Chemistry and Catalysis*, J.A. Rabo Ed.; ACS Monograph 171, **1976**, p585.
24. Mori K.; Miyamoto; Murakami Y. *J. Phys. Chem.* **1984**, 88, 2741.
25. European Patent Application 0028516.
26. Parker L.M.; Bibby D.M.; Meinhold R.H. *Zeolites*, **1985**, 5, 384.
27. Centi G.C.; Tvaruzkova Z.; Trifiro F.; Jiru P.; Kubelkova L. *Appl. Catal.*, **1984**, 13, 69.

28. MacKenzie K.J.D.; Brown I.W.M.; Ranchod P.; Meinhold R.H.; *J. Materials Science*, **1991**, *26*, 769.
29. Figaro Engineering INC., 1-5-3 Senbanishi Inc, Mino, Ooka 562, Japan.
30. Patterson J.E., *Programs for the Dycor Portable Mass Spectrometer*, DSIR Chemistry Internal Report: Petone, New Zealand, **1991**.

RECEIVED September 30, 1993

Chapter 26

Transient Response of a Monolithic Oxidation Catalyst

Effects of Process Conditions

Alec A. Klinghoffer and Joseph A. Rossin¹

Geo-Centers, Inc., 10903 Indian Head Highway, Fort
Washington, MD 20744

The transient response of a monolithic oxidation catalyst has been investigated by exposing the catalyst to high concentration pulses of chloroacetonitrile. For the purposes of this text, transient response is defined as the rate at which the catalyst temperature (and hence activity) increases with time following a step change in concentration. Experiments were conducted employing air inlet temperatures of 365, 500 and 435°C, challenge concentrations of 5,000 and 10,000 ppm (v/v) and a residence time of 0.25 seconds. Both the feed and effluent concentration of chloroacetonitrile, and the catalyst temperature were monitored simultaneously in real-time. Results indicate that increasing the challenge concentration from 5,000 to 10,000 ppm (v/v) greatly increases the transient response of the catalyst. Also, for air inlet temperatures of 435°C, the rapid increase in the catalyst temperature results in a greater than 99.9% removal of the challenge dose.

Present air purification systems designed for removal of chemical warfare (CW) agents from air streams are based solely on activated, impregnated carbon, namely ASC whetlerite. While these filters function well against a wide range of chemical agents, they possess several shortcomings. First, the present day carbon filter has a limited capacity for agents which are removed by chemical reaction and those which are weakly adsorbed. Second, prolonged environmental exposure has been shown to reduce the capacity of these filters for agents which are removed by chemical reaction (1). The result of these shortcomings is to impose change-out and disposal requirements which may present logistical burdens to the user. Alternative filtration processes, such as catalytic oxidation, are currently under investigation in an effort to develop technologies which may alleviate the above mentioned burdens.

¹Corresponding author

The nature of a chemical attack coupled with the high toxicity of agent molecules makes the separation of CW agents from streams of air a complex process. During a chemical attack, high concentrations (in excess of 1%) of nonpersistent gases (such as cyanogen chloride, hydrogen cyanide and phosgene) can be achieved within seconds of bomb burst, and can be maintained for a few minutes prior to decay (2). Due to the high toxicity associated with many CW agents, an air purification system will be required to remove in excess of 99.9% of the dose of agent challenged to the filter during the attack. When confronted with a rapid change in concentration, such as the scenario described above, a catalytic filter would be expected to behave as follows. Initially, the catalyst bed would be at a temperature consistent with that of the inlet air. At the on-set of the chemical attack, the temperature of the catalyst bed will begin to rise, ultimately approaching its adiabatic value which, depending on the agent, may be several hundred degrees above the temperature of the inlet air. As the catalyst temperature approaches its adiabatic value, the performance of the catalyst is expected to increase significantly; i.e. the effluent concentration is expected to rapidly decrease. However, the rate at which the catalyst temperature increases may be such that a significant dose of agent may pass through the catalyst bed unreacted prior to the catalyst achieving its adiabatic temperature.

Studies involving the transient response of oxidation catalysts which have been reported in the open literature have focused on automotive applications. Young and Finlayson (3-5) developed a mathematical model to study the transient response of a monolithic catalyst for scenarios encountered by automobiles. Their results indicated that under certain conditions, the adiabatic catalyst temperature could be achieved in less than one minute from cold start (cold catalyst exposed to hot exhaust gas). Similar numerical results have been reported by Oh and Cavendish (6) and Heck et al. (7). For chemical defense applications, if the catalyst temperature rises rapidly relative to the duration of the chemical attack, then the dose of agent which elutes from the catalyst bed during the transient phase may be minimal. Should this be the case, the system can take advantage of the heat generated by the chemical reaction, and thereby reduce the energy cost. On the other hand, if the increase in catalyst temperature is slow relative to the duration of the chemical attack, then the performance of the catalyst will be representative of that achieved during isothermal operation. Should this be the case, a relatively high air inlet temperature, and corresponding high energy cost, may be required to achieve the desired reduction level.

A study is currently underway aimed at evaluating catalytic oxidation as a means of providing breathable air for military collective protection applications (e.g. airframes, shelters and vehicles). The initial phase of this effort involves investigating the performance of commercially available catalysts against model compounds, i.e. compounds which are structurally similar to specific CW agents but less toxic. In the present study, chloroacetonitrile ($\text{ClCH}_2\text{C}\equiv\text{N}$) has been chosen as a model compound for cyanogen chloride ($\text{ClC}\equiv\text{N}$). These two compounds are similar, with the exception that the chlorine atom associated with cyanogen chloride has been replaced by a $-\text{CH}_2\text{Cl}$ group to make chloroacetonitrile. Results obtained with model compounds will be compared to those obtained with CW agents at a later date. Through the use of model compounds, the amount of agent testing required during full scale testing can be

greatly minimized, thereby reducing test costs and minimizing risks to the operators. Results of a kinetic rate study conducted over a 1% Pt/Al₂O₃ catalyst (8) indicated that the oxidation of chloroacetonitrile is nonlinear in reactant concentration and strongly inhibited by the adsorption of hydrochloric acid, a reaction product. A monolithic oxidation catalyst was selected for this investigation. These materials are currently employed by the automotive industry to control exhaust emissions, although other applications do exist (9,10). Desirable properties of this catalyst include high reactivity, low thermal mass, and excellent thermal stability. The objective of the present study is to evaluate the effects of challenge concentration and air inlet temperature on the transient response of a monolithic oxidation catalyst following exposure to a step change in chloroacetonitrile concentration. In order to meet this objective, techniques were developed to deliver a pulse concentration to the catalyst bed, and to monitor the feed and effluent concentrations of chloroacetonitrile in real time.

Experimental Methods

Materials. Reagent grade chloroacetonitrile was purchased from Aldrich Chemical Company. The catalyst employed in this study was purchased as a commercial automotive catalytic converter from Walker Muffler, Inc. The monolith had square channels and possessed a cell density of 62 channels/cm². The chemical composition of the washcoat was determined using energy dispersive X-ray spectroscopy (EDS) employing a Tracor Northern 5700 EDS/WDS automation system interfaced with a JEOL 35CF scanning electron microscope. Analyses were performed at six discrete locations within an individual channel. Results of the analyses were averaged together and provided the following composition (by weight): 12% cerium, 0.2% rhodium, 1.6% palladium, 0.7% platinum, 85% aluminum oxide. Since the washcoat thickness was approximately 0.05mm, it was felt that the contribution of the cordierite substrate did not interfere with the analyses.

Catalyst Preparation. Catalyst samples were prepared by first separating the catalytic converter housing from the catalyst. Once separated, catalyst samples were cut from the monolith block using a 3.5 cm diameter diamond tipped core saw. The resulting catalyst core was approximately 3.1 cm in diameter and 5.4 cm long, yielding a volume of approximately 40 cm³. Extreme care was taken to cut the catalyst core perpendicular to the ends of the monolith block. The outer surface of the catalyst core was coated with a thin layer of alundum cement. A thin layer of glass wool was then wrapped around the catalyst core, which was then loaded into a 3.2 cm i.d. Pyrex reactor. Preparing and loading the catalyst in this manner served to improve the seal between the catalyst core and reactor wall and thus minimized by-passing of the feed stream. Once loaded, six 0.08 cm diameter fine wire thermocouples were placed at discrete locations within separate channels of the monolith. Five of the thermocouples occupied channels located near the center of the monolith. These thermocouples were placed at distances of 0.5, 1.0, 3.1, 4.0 and 5.0 cm from the entrance of the catalyst, respectively. A sixth thermocouple was located within a channel half way between the centerline and the reactor wall at 1.7 cm from the entrance of the monolith. The number of channels obstructed by the thermocouples (six) was small relative to the

number of channels which remained open (over 470). Therefore, the effects of the thermocouple location on the residence time will be minimal.

Equipment. A schematic representation of the fixed bed reactor system is illustrated in Figure 1. Dry, oil-free air from a PSA air dryer was metered to the reactor using either a 0-5 or 0-20 NL/min mass flow controller. NL (normal liter) is defined as one liter of dry air at 0°C and one atmosphere pressure. The water saturator was by-passed so that the experiments could be conducted in dry air. This is because the presence of water in the feed stream can effect the performance of the mass spectrometer used to analyze the reactor effluent. Previous studies have indicated that the presence of water in the feed stream has no effect on the rate at which the reactant chloroacetonitrile is oxidized (8). Chloroacetonitrile was delivered to the air stream as a saturated vapor from a sparger system. A separate stream of PSA dried air was metered to the sparger system using a 0-0.5 NL/min mass flow controller. The sparger system consisted of a series of three 250 ml polytetrafluoroethylene jars. All jars were filled to approximately 75% capacity with liquid chloroacetonitrile. The sparger system was completely submerged in a temperature controlled, circulating water bath. A back pressure regulator was located down stream of the sparger system and was used to maintain a constant pressure of 11 psig over the liquid chloroacetonitrile contained within each sparger. The concentration of chloroacetonitrile in the stream exiting the sparger system was controlled by adjusting the temperature of the water bath. The concentrated chloroacetonitrile stream exiting the sparger system was delivered to a three-way stream selector valve. This valve served to vent the stream to a fume hood, or deliver the stream to the main air stream.

The reactor consisted of a 3.2 cm i.d. Pyrex tube approximately 100 cm long. The top 60 cm of the reactor (preheat zone) were filled with 4 mm glass beads. The glass beads provided further mixing of the feed gas as well as surface area for heating the incoming feed stream to reaction temperature. The catalyst core was located approximately 7 cm below the preheat zone. The reactor assembly was housed in an 8.9 cm diameter aluminum block. The aluminum block was electrically heated, and the temperature of the catalyst was controlled by controlling the temperature of the aluminum block. Two 50 liter scrubbing vessels, filled with water, were located following the reactor. These vessels served to remove acid gas reaction products from the effluent stream, thus preventing corrosion of the back pressure regulator, located downstream of the vessels. The back pressure regulator was used to maintain a constant pressure of 4.5 psig on the system. All feed and effluent lines were constructed of 316 stainless steel tubing and were electrically heated to approximately 90°C.

A small portion of the feed stream, diverted at a point just before the preheat zone, was delivered to a Hewlett-Packard 5890 gas chromatograph equipped with a flame ionization detector (FID) for analysis. The concentration of chloroacetonitrile in the feed stream was determined in real-time by delivering the sample stream (flow rate equals 200 Nml/min) directly to the FID, without the use of a column. The concentration-time profile of the feed was obtained from the height of the peak recorded on a Hewlett-Packard 3396A integrator. Catalyst temperatures from each of the six thermocouples were monitored in real-time using an Omega OM500 multi-

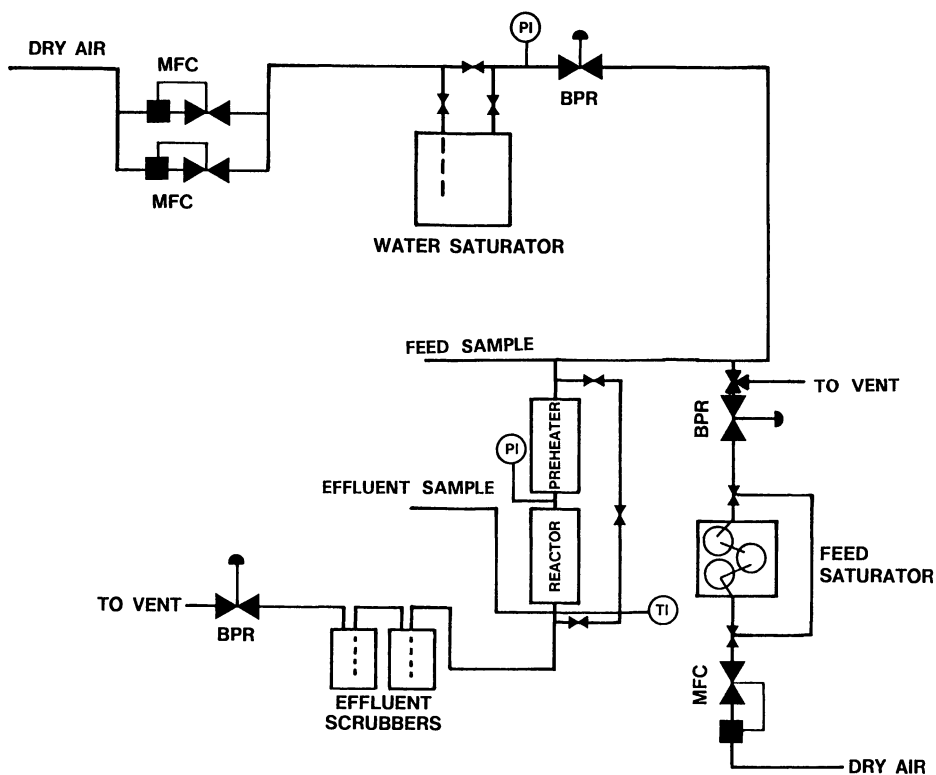


Figure 1: Schematic Representation of Catalytic Reactor System.

channel data logger. This unit reported all temperatures simultaneously at 5 second intervals. Immediately following the reactor, a portion of the effluent stream was delivered to the Hewlett-Packard 5971A mass spectrometer for analysis. Quantitative effluent concentrations of chloroacetonitrile were determined by continuously monitoring the parent ion of chloroacetonitrile ($MW = 75$).

Procedure. Pulse challenge data were recorded employing air inlet (inlet to the catalyst) temperatures of 365, 400 and 435°C at a reaction pressure of 4.5 psig and a residence time (calculated at 0°C, one atmosphere) of 0.25 seconds for feed concentrations of 5,000 and 10,000 ppm. In all cases, the duration of the pulse was three minutes. Runs were initiated by first allowing the catalyst to reach the desired operating temperature in air flowing. A pulse challenge of chloroacetonitrile was delivered to the system as follows. First, air was allowed to flow through the sparger system at the desired flow rate for at least 30 minutes prior to the initiation of the challenge to allow for equilibration. During this time, dry air was flowing through the reactor, and the concentrated chloroacetonitrile stream was vented to a fume hood. Following the equilibration period, the run was initiated by diverting the concentrated chloroacetonitrile stream to the dry air stream. The run was terminated following three minutes by returning the concentrated chloroacetonitrile stream to vent. During the challenge, the chloroacetonitrile feed and effluent concentrations, as well as the catalyst temperatures, were monitored continuously.

Results and Discussion

Transient Response to a Step Change in Concentration. During the pulse testing, no attempts were made to identify reaction products. However, effluent analyses were performed while operating the catalyst under steady-state conditions. Reaction products consisted of CO_2 , HCl and NO_x (no attempts were made to identify water). No products of partial oxidation were observed. Figure 2 illustrates the feed and effluent concentration of chloroacetonitrile as a function of time during a three minute pulse challenge. Results reported in Figure 2 correspond to a challenge concentration of 10,000 ppm, an air inlet temperature of 400°C, and a residence time of 0.25 seconds. In reporting all concentration data, dead time, i.e. the time required for the feed and effluent streams to travel to their respective analytical devices, has been taken into account. The observance of low concentrations of chloroacetonitrile in the effluent prior to time zero has been attributed to axial diffusion of the pulse and/or errors associated with the estimation of dead time. Figure 3 reports the corresponding axial catalyst temperature profiles prior to and at discrete times during the challenge. Temperature measurements are reported for thermocouples located near the center most channels of the monolith. The size of the thermocouple was such that the channel was severely obstructed. Therefore, the temperature measurements reported are assumed to be representative of the solid catalyst rather than the fluid stream. Although attempts were made to operate the reactor adiabatically, radial temperature gradients were observed.

Results presented in Figure 2 show that the feed concentration profile very nearly represents that of a pulse. The feed rises rapidly to the desired concentration, which is

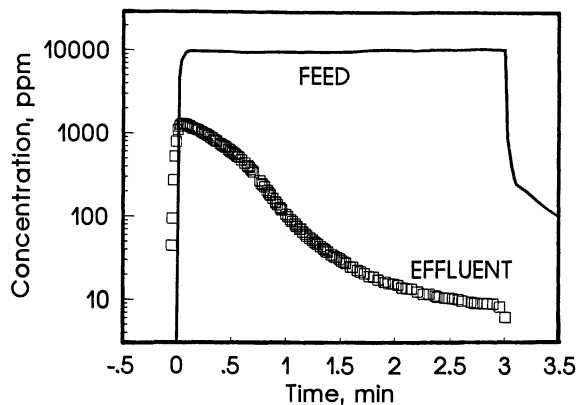


Figure 2: Feed and Effluent Concentrations of Chloroacetonitrile as a Function of Time During a 10,000 ppm Pulse Challenge. Air inlet temperature = 400°C, residence time = 0.25 s.

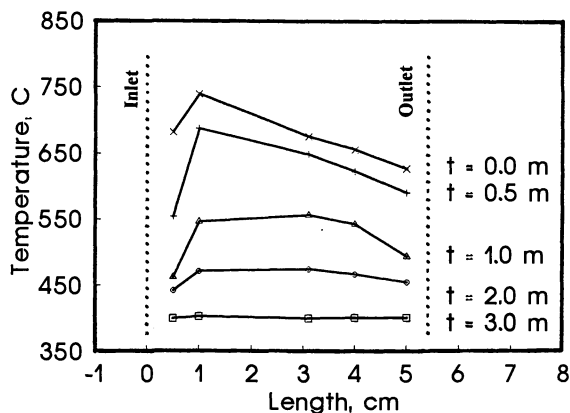


Figure 3: Axial Catalyst Temperature Profiles at Discrete Times During a 10,000 ppm Chloroacetonitrile Pulse Challenge. Air inlet temperature = 400°C, residence time = 0.25s.

maintained for three minutes, then decreases rapidly upon termination. Figure 2 shows that the effluent concentration of chloroacetonitrile decreases significantly over the duration of the challenge, from 1,300 to 9 ppm. The decrease in concentration is due to a rapid increase in the catalyst temperature throughout the duration of the challenge, as shown in Figure 3. Oxidation reactions are highly exothermic. For the oxidation of chloroacetonitrile, the heat of reaction is estimated to be 1,050 kJ/mol. Based on the heat of reaction, an adiabatic temperature rise on the order of 350°C would be expected for the 10,000 ppm challenge. Heat transfer and mass transfer/chemical reaction within a monolith is a complex process and has been discussed previously (3-7,9,11-13). Prior to the introduction of the challenge, the entire catalyst is at a temperature consistent with that of the inlet air (400°C). Upon introduction of the challenge, the catalyst temperature begins to rise as a result of the heat generated by the chemical reaction accumulating within the catalyst. At 0.5 minutes, the temperature of the catalyst has increased somewhat uniformly following the first centimeter, indicating that the reaction is distributed over the entire length of catalyst (as opposed to a large fractional conversion occurring near the entrance). If a large fraction of reactant were consumed within a region near the entrance to the catalyst, then the reaction occurring over the remainder of the catalyst would be minimal, as would the corresponding heat generation. Should this be the case, the increase in temperature near the end of the catalyst would be much less than that observed near the entrance, and the conversion would be significantly higher than the 87 to 95% levels observed over this period of time. At one minute, the catalyst temperature has increased significantly over the first centimeter; however, at 3.1 cm, the catalyst temperature begins to decrease in the axial direction. This result indicates that a large fraction of the reactant (90% or more) is being consumed upstream of the 3.1 cm thermocouple, and results in the presence of a "hot spot", i.e. a location within the catalyst bed where the temperature is at a maximum. The continued increase in the catalyst temperature with time past the 3.1 cm mark is a result of heat transfer from the fluid stream. At two minutes into the challenge, the temperature of the catalyst at the "hot spot," located one cm into the catalyst, has risen substantially, nearly 300°C above the air inlet temperature. This temperature increase corresponds to 80% of the adiabatic temperature rise, and provides direct evidence that a large fraction of the reactant is being consumed over the first centimeter of the catalyst. By oxidizing the majority of the reactant near the front of the catalyst, the remainder of the catalyst can be used to achieve very high levels of concentration reduction, 99.85% in this instance. Just prior to termination of the challenge, the temperature of the "hot spot" has risen approximately 350°C above the air inlet temperature, and corresponds well with the expected adiabatic temperature rise. It should be noted that during the final minute of the challenge, the effluent concentration has not decreased significantly, from 15 to 9 ppm, even though the temperature of the catalyst has increased over the entire length. At these high temperatures, it is likely that the reaction has become severely limited by external mass transfer resistances. As a result, increases in the catalyst temperature will not significantly effect the effluent concentration (conversion).

Effects of Challenge Concentration on Transient Response. Decreasing the challenge concentration results in decreasing the heat value associated with the feed stream, thereby reducing the potential to raise the catalyst temperature. Figure 4 compares the effluent concentration of chloroacetonitrile as a function of time for challenge concentrations of 5,000 and 10,000 ppm. Data presented in this figure were recorded employing an air inlet temperature of 400°C, a residence time of 0.25 seconds, and a pulse duration of 3 minutes. The challenge concentration profiles have been omitted from this figure due to crowding. Figure 5 reports the temperature of the "hot spot" as a function of time during the 5,000 and 10,000 ppm challenges. Since the location of the "hot spot" changed with time, the temperatures reported in Figure 5 correspond to the location within the catalyst which achieved the greatest temperature upon termination of the challenge. Decreasing the challenge concentration resulted in decreasing the concentration of chloroacetonitrile first observed in the effluent stream from about 1,300 ppm to about 200 ppm. These values correspond to conversions of 87 and 96%, respectively. The increase in conversion with decreasing challenge concentration was to be expected based on the results of Klinghoffer and Rossin (8), who have shown the oxidation of chloroacetonitrile to be nonlinear in concentration. The effluent concentration decreased throughout the duration of the challenge for both feed concentrations, however, the effluent concentration decreased at both a faster rate and to a greater degree for the 10,000 ppm challenge. For example, following one minute, the effluent concentration has decreased slightly more than one order of magnitude for the 10,000 ppm challenge, while for the 5,000 ppm challenge, the effluent concentration has decreased by only a factor of four. Further, just prior to termination, the effluent concentration has decreased two orders of magnitude for the 10,000 ppm challenge, while for the 5,000 ppm challenge, the effluent concentration has decreased by a factor of 40. As shown in Figure 5, the increased rate at which the effluent concentration decreased for the 10,000 ppm challenge can be attributed to the temperature of the "hot spot" increasing at a greater rate and to a greater extent. This behavior is to be expected, since, by virtue of its greater concentration, the 10,000 ppm challenge has the potential to generate more heat.

Figure 6 reports axial catalyst temperature profiles recorded two minutes into the challenge. Results presented in this figure show that decreasing the challenge concentration has resulted in locating the "hot spot" further into the catalyst. For the 5,000 ppm challenge, the catalyst temperature recorded one cm into the monolith has increased only 50°C above the air inlet temperature, while for the 10,000 ppm challenge, the temperature at this location has increased nearly 300°C. These temperature rises correspond to 25 and 80%, respectively, of the adiabatic value and indicate that a much greater conversion has occurred over the first centimeter of the monolith when employing the 10,000 ppm challenge. Based on the location of the "hot spot", one would expect a greater fractional conversion for the 10,000 ppm challenge, since a significantly greater conversion is achieved over the first centimeter of the monolith. However, this is not the case, as essentially the same conversion is achieved upon termination of the challenge for both runs. The reason for this behavior has been attributed to the presence of radial temperature gradients, which were more significant (as a result of the greater temperatures) for the 10,000 ppm challenge.

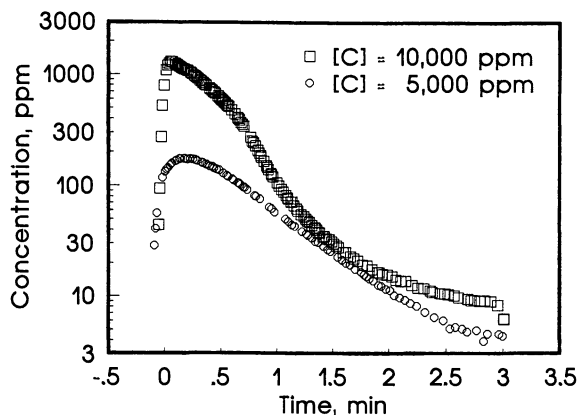


Figure 4: Effluent Concentration of Chloroacetonitrile as a Function of Time for 5,000 and 10,000 ppm Pulse Challenges. Air inlet temperature = 400°C, residence time = 0.25 s.

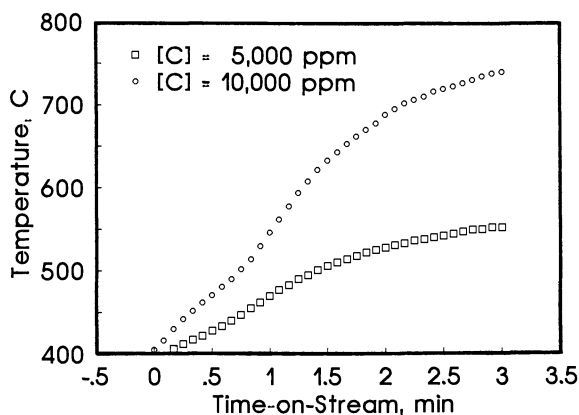


Figure 5: Temperature of the Catalyst "Hot Spot" as a Function of Time for 5,000 and 10,000 ppm Chloroacetonitrile Challenges. Air inlet temperature = 400°C, residence time = 0.25 s.

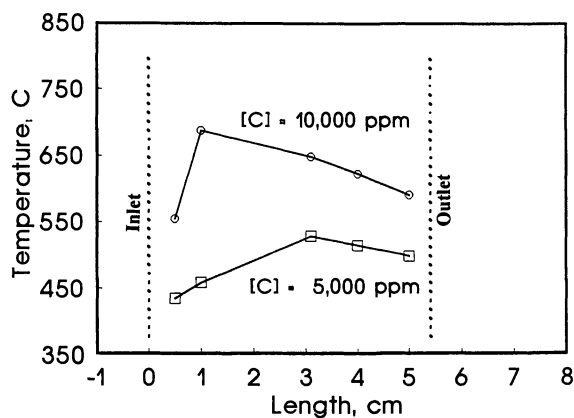


Figure 6: Axial Catalyst Temperature Profiles Recorded Two Minutes Into the Run for 5,000 and 10,000 ppm Chloroacetonitrile Challenges. Air inlet temperature = 400°C, residence time = 0.25 s.

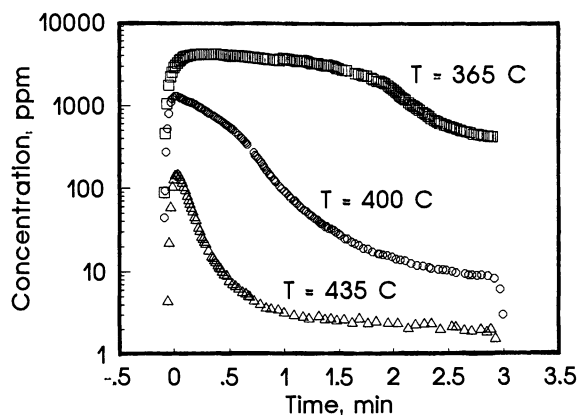


Figure 7: Effluent Concentrations of Chloroacetonitrile as a Function of Time During a Pulse Challenge for Air Inlet Temperatures of 365, 400 and 435°C. Challenge concentration = 10,000 ppm, residence time = 0.25 s.

Effects of Air Inlet Temperature on Transient Response. Increasing the air inlet temperature will result in increasing the rate of chemical reaction. Figure 7 shows the effluent concentration of chloroacetonitrile as a function of time for air inlet temperatures of 365, 400 and 435°C. All data reported in this figure employ a challenge concentration of 10,000 ppm, a residence time of 0.25 seconds, and a pulse duration of three minutes. Figure 8 reports the temperature of the "hot spot" as a function of time for the three air inlet temperatures reported. Since the location of the "hot spot" changed with time, the temperatures reported in Figure 8 correspond to the location within the catalyst which achieved the greatest temperature upon termination of the challenge. Note from the results presented in Figures 7 and 8 that increasing the air inlet temperature resulted in increasing the rate at which the effluent concentration decreased, as well as increasing the rate at which the temperature of the "hot spot" increased. For the run conducted with an air inlet temperature of 435°C, the effluent concentration decreased rapidly over the first minute of the challenge. This behavior corresponds well with an equally rapid increase in the temperature of the "hot spot," to 335°C above the air inlet temperature, recorded over the same time period. For the run conducted with an air inlet temperature of 365°C, the effluent concentration does not begin to decrease at an appreciable rate until approximately two minutes into the challenge. Correspondingly, the temperature of the "hot spot" begins to increase at an appreciable rate at this time. It should be noted that in the case of the run which employed an air inlet temperature of 435°C, the temperature rise of the catalyst (390°C) exceeded the adiabatic value (350°C). This result has been observed by others in both experimental (13) and modeling (5,7) studies, and is a result of the rate of mass transfer/chemical reaction being greater than the heat transfer rate.

It is interesting to note that although the runs conducted with air inlet temperatures of 365 and 400°C achieved similar "hot spot" temperatures, the effluent concentrations achieved just prior to termination of the challenges are significantly different; 400 versus 9 ppm, respectively. Based on the "hot spot" temperatures, one would expect the effluent concentrations to be similar. The data presented in Figure 9 provide an explanation for these observations. Figure 9 reports the axial catalyst temperature profile recorded two minutes into the challenge for each of the three air inlet temperatures. Results presented in this figure show that increasing the air inlet temperature placed the "hot spot" closer to the inlet. For example, two minutes into the challenge, the hot spot shifts from 4.0 cm to 1.0 cm and 0.5 cm as the air inlet temperature is increased from 365 to 400 to 435°C, respectively. The shifting of the "hot spot" towards the entrance of the monolith is consistent with the numerical results reported by Heck et al. (7). By locating the "hot spot" closer to the inlet, the remainder of the catalyst may be used to achieve high concentration reductions. For the run conducted at 365°C, the "hot spot" is located so far into the catalyst that an insufficient volume remains to achieve the high concentration reductions. Therefore, although the runs conducted with air inlet temperatures of 365 and 400°C achieved similar "hot spot" temperatures, the difference in the effluent concentrations achieved upon termination of the challenge can be attributed to the location of the "hot spot."

For applications such as chemical defense where one must focus on the dose of reactant which elutes through the catalyst prior to the achievement of steady-state

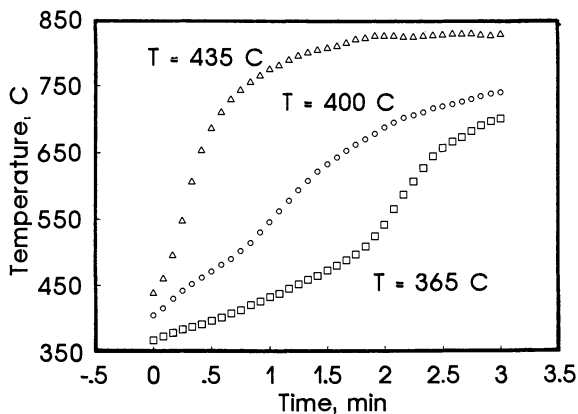


Figure 8: Temperature of Catalyst "Hot Spot" as a Function of Time During a Pulse Challenge for Air Inlet Temperatures of 365, 400 and 435°C. Challenge concentration = 10,000 ppm, residence time = 0.25 s.

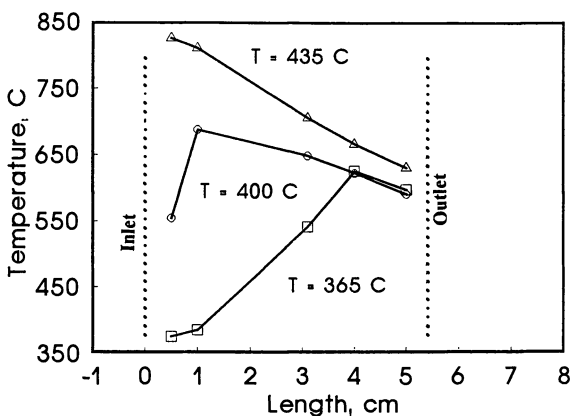


Figure 9: Axial Catalyst Temperature Profiles Recorded Two Minutes Into the Run for Air Inlet Temperatures of 365, 400 and 435°C. Challenge concentration = 10,000 ppm, residence time = 0.25 s.

(adiabatic) conditions, the transient response of the catalyst becomes an important design consideration. The results shown in Figures 7 through 9 indicate that changes in the air inlet temperature effect not only the initial conversion, but also the rate at which the catalyst temperature increases (thus the rate at which the effluent concentration decreases) and the location of the "hot spot." The location of the "hot spot" is very important. Should, as in the case of the run conducted with an air inlet temperature of 365°C, the "hot spot" be located well into the catalyst, a high conversion cannot be achieved at any time during the challenge. Also important in minimizing the dose which elutes through the catalyst during the transient period are the initial conversion and rate at which the catalyst temperature increases. Results presented in Figure 7 show that for an air inlet temperature of 400°C, the catalyst functions quite efficiently, achieving low effluent concentrations, once sufficient catalyst temperatures have been achieved. However, because of the magnitude of the initial effluent concentration (1,300 ppm) and the rate at which the catalyst temperature increases, only a 97.6% reduction of the challenge dose is achieved. Further increasing the air inlet temperature to 435°C reduces the initial effluent concentration (140 ppm) and increases the rate at which the catalyst temperature increases sufficiently to allow for a 99.91% reduction of the challenge dose.

Conclusions

Both the challenge concentration and air inlet temperature can have a significant effect on the transient response of the catalyst. Decreasing the challenge concentration results in decreasing the initial effluent concentration of chloroacetonitrile, and decreasing the rate that the catalyst temperature increases. Decreasing the challenge concentration also affects the location of the "hot spot," placing it further into the catalyst as the challenge concentration is decreased. Increasing the air inlet temperature results in locating the "hot spot" closer to the catalyst entrance, decreasing the initial effluent concentration, and increasing the rate at which the catalyst temperature increases.

Acknowledgments

The authors are grateful to the U.S Army for financial support under contract DAAA15-91-C-075.

Literature Cited

- 1 Rossin, J.; Petersen, E.; Tevault, D.; Lamontagne, R.; Isaacson L. *Carbon* **1991** *29*, 197.
- 2 Latimer, W.M. *Military Problems with Aerosols and Nonpersistent Gases*; National Defense Research Committee Report, Div. 10: Washington, DC. 1946; Chapt. 16.
- 3 Young, L.C.; Finlayson, B.A. *Chem.-React. Eng. II; Adv. Chem. Ser.*; American Chemical Society: Washington, DC., 1974, Vol. 133; pp 629-643.
- 4 Young, L.C.; Finlayson, B.A. *AIChE J.* **1976**, *23*, 331.
- 5 Young, L.C.; Finlayson, B.A. *AIChE J.* **1976**, *23*, 343.

- 6 Oh, S. H.; Cavendish, J.C. *Ind. Eng. Chem. Prod. Res. Dev.* **1982**, *21*, 29.
- 7 Heck, R.H.; Wei, J.; Katzer, J.R. *AIChE J.* **1976**, *22*, 477.
- 8 Klinghoffer, A.A.; Rossin, J.A. *Ind. Eng. Chem. Res.* **1992**, *31*, 481.
- 9 Irandoust, S.; Andersson, B. *Catal. Rev.-Sci. Eng.* **1988**, *30*, 341.
- 10 Schmidt, T. In *Catalysis and Automotive Pollution Control II*; Crucq, A. Ed.; Elsevier: Amsterdam, The Netherlands, 1991, pp 55-74.
- 11 Heck, R.H.; Wei, J.; Katzer, J.R. *Chem.-React. Eng. II; Adv. Chem. Ser.*; American Chemical Society: Washington, DC., 1974, Vol. 133; pp 34-45.
- 12 Votruba, J.; Sinkule, J.; Hlavacek, V.; Skrivanek, J. *Chem. Eng. Sci.* **1975**, *30*, 201.
- 13 Hegedus, L., *AIChE J.* **1975**, *21*, 849.

RECEIVED September 30, 1993

Chapter 27

Low-Temperature Deep Oxidation of Aliphatic and Aromatic Hydrocarbons

Mark T. Vandersall¹, Stephen G. Maroldo¹, William H. Brendley, Jr.¹,
Krzysztof Jurczyk², and Russell S. Drago²

¹Research Laboratories, Rohm and Haas Company, Spring
House, PA 19477

²Department of Chemistry, University of Florida, Gainesville, FL 32611

A new series of low temperature oxidation catalysts have been developed that comprise first-row transition metal oxides dispersed on a new class of synthetic carbonaceous supports, the Ambersorb adsorbents. Data are reported here demonstrating high conversion using these catalysts for the deep oxidation of aliphatic and aromatic compounds to CO₂ and H₂O. The process temperatures required are only 175-250 °C, which is a substantial reduction over conventional oxidation systems. As such, these catalysts should offer cost advantages over the use of adsorption on activated carbon or thermal or catalytic oxidation for environmental control and remediation.

Public awareness of the harmful effects of volatile organic chemical (VOC) emissions and non-volatile organic compounds has led to increasingly stringent environmental regulations. The citizens of the world are demanding clean air, clean water, and pollution free land to safeguard our biosphere not only for the present but also for centuries to come. These concerns have been heard by the chemical industry in general, which is pursuing the goal of cleaner, safer, and more efficient plants. The control of VOC emissions and difficult to dispose of by-products is of key importance. While the primary objective is the elimination of processes producing hazardous waste, the management and control of harmful by-products are of immediate concern.

This paper will present the important roles played by the synergistic association of new, novel carbonaceous adsorbents with catalytic technology in protecting the environment by the deep oxidation of aliphatic and aromatic hydrocarbon pollutants.

At present, two technologies are utilized for the control of semi-volatile and volatile organic compound emissions. Both have inherent drawbacks.

1. Granular Activated Carbon (GAC) - GAC is used as a control technology to adsorb VOCs from air and water streams.(1) GAC is, however, dependent on operating conditions to be effective. For the adsorption of organic chemicals from air, for example, relative humidity can adversely affect the adsorption capacity of the carbon for these organics, with the decrease becoming very significant as the relative humidity of the VOC stream is increased above approximately 50%. In addition, GAC is generally rebedded after breakthrough requiring transportation of the hazardous chemical contained on the GAC to incinerators located at specific sites. These large volumes of GAC are transported as hazardous wastes for regeneration or disposal, thereby increasing costs and generating concerns over safety issues.
2. Thermal Oxidation - Thermal oxidation of VOC's is used primarily with air-stripping as a means of destruction of hazardous wastes.(2) This method of operation is associated with high energy requirements and operating costs because of the high temperatures required for incineration.

In cooperation with the University of Florida, we have developed a new series of low temperature catalysts that comprise transition metal oxides dispersed on a new class of synthetic carbonaceous adsorbents (Ambersorb adsorbents; Ambersorb is a registered trademark of Rohm and Haas Company).(3) These patented adsorbents, sometimes called carbon molecular sieves (CMS), offer a variety of pore size distributions with high internal surface area and high diffusivity of organic molecules to active metal oxide sites.(4,5) In addition, these adsorbents function as robust catalysis supports.

Previous work has shown that Ambersorb adsorbent-supported transition metal oxides are effective catalysts for the deep oxidation of halogenated hydrocarbons at low temperatures.(3) The studies described in this paper further demonstrate extremely high conversions for the deep oxidation of aliphatic and aromatic hydrocarbons to CO₂ and H₂O. The catalytic process temperatures are low, typically in the range of 170-250 °C which is a substantial reduction over conventional thermal oxidation systems.(2) Preliminary results with butane, hexane, and toluene are presented.

Experimental

The carbon supports used in this study were synthetic carbonaceous adsorbents from Rohm and Haas Company (Ambersorb 563 and 572 adsorbents).(4,5) The Ambersorb adsorbents are made by the patented pyrolysis of sulfonated styrene-divinylbenzene copolymers. The process produces adsorbents with tailorable and reproducible surface area and pore volume distribution. The adsorbents are spherical particles with diameters

between 300 and 850 μm . Prior to use, the carbons were dried at 120 $^{\circ}\text{C}$ under vacuum for at least 18 hours.

Catalysts were prepared by impregnation to incipient wetness.⁽⁶⁾ Metal nitrate salts were purchased from Fisher Scientific Company and Aldrich Chemical Company, Inc. In a typical preparation, an appropriate amount of the nitrate salt of the desired transition metal (*e.g.*, $\text{Co}(\text{NO}_3)_2 \cdot 6\text{H}_2\text{O}$) was dissolved into a solution of 10% methanol in water. The amount of solution used was that required to fill all of the pores of the adsorbent. This metal salt-containing solution was then added dropwise to the adsorbent, while stirring, over the course of about 15 minutes. At the end of the addition, the adsorbent was damp in appearance but no liquid phase was present. This imbibed sample was allowed to stand for approximately four hours and then was placed into a 110 $^{\circ}\text{C}$ vacuum oven to dry overnight. Following the drying, the metal-loaded adsorbent was placed into a 3.75 cm diameter quartz pyrolysis tube and heated, under a nitrogen atmosphere, to 360 $^{\circ}\text{C}$ for two hours. Thermogravimetric analysis with mass spectral analysis of the off gases indicated that these temperatures were sufficient to volatilize the nitrate groups, leaving the metal oxide on the carbon surface.

Catalysts were tested in a pyrex glass reactor with an internal diameter of 10 mm and with a coarse glass frit as a bed support. A type J thermocouple was taped to the outside of the glass at a position approximately 1 cm above the frit, and the entire reactor was wrapped with fiberglass tape and flexible heating tape. The temperature was controlled with a Controls and Automation, Ltd. Model 9000 PID controller using the thermocouple as the sensor. Temperature regulation was quite good, generally within 1 $^{\circ}\text{C}$ of the setpoint.

The feed gases used in these tests were either delivered from a cylinder or, for the case of hexane and toluene, from passing air through an impinger tube filled with the organic liquid. In some experiments, water was also present in the feed stream. This was generated by passing the air through a Milligan jar filled with water and then on to the impinger tube. Flow rate was controlled by needle valves or by use of a Porter Instrument Co. Model VCD-1000 flow controller. Actual flow rates were measured with a Humonics Inc. Optiflow 520 digital soap-film flowmeter.

Product gases were analyzed by gas chromatography using two different techniques. One technique involved sampling the gas through a septum with a gas syringe and then injecting this sample into a Varian Model 3700 gas chromatograph (GC). In the other method, on-line analysis was achieved by sampling the product gas stream with a 6-port rotary valve and a 1 cm^3 sample loop mounted on a Hewlett-Packard Model 5880A GC. For the latter case, a 1 m \times 1/8" stainless steel 1% SP-1000 on 60/80 Carbowack B column was used. Flame ionization detectors were used on both GC systems. Conversions were calculated as the difference of the inlet and outlet concentrations, expressed as a percentage of the inlet concentration.

Results and Discussion

Surface areas and pore volume distributions of the carbon supports were determined by nitrogen porosimetry using a Micromeritics ASAP-2400 porosimeter. Typical values for these materials are shown in Table I. For comparison purposes, data are also shown for a standard vapor-phase granular activated carbon (Calgon Carbon Corp. Type BPL, 12x30 mesh). The pore volumes listed were calculated by the porosimeter using the BJH method. This method uses the Halsey equation for the adsorbed layer thickness and the Kelvin equation for the capillary condensed vapor and is widely-used to characterize meso and macroporous solids.(7) The pore size classification used corresponds with IUPAC-recommended definitions.(8) The BJH pore volume distributions for both undoped Ambersorb 572 adsorbent and 5% (by weight) CoO on Ambersorb 572 adsorbent are shown in Figure 1. The nitrogen porosimetry data indicate that there is roughly a 15% loss in surface area and the t-plot micropore volume of the support due to incorporation of the metal oxide.

Table I. Typical properties of the carbon supports

Property	Ambersorb 563 adsorbent	Ambersorb 572 adsorbent	Calgon Type BPL 12x30
BET surface area (m ² /g)	550	1100	1100
Micropore volume (cm ³ /g)	0.23	0.41	0.47
Mesopore volume (cm ³ /g)	0.14	0.19	0.07
Macropore volume (cm ³ /g)	0.23	0.24	0.03
Bulk density (g/cm ³)	0.53	0.49	0.48

To determine the hydrophobicity of the carbonaceous supports used in this study, water vapor adsorption isotherms were measured by exposing predried, weighed samples of the adsorbents to atmospheres of controlled humidity for two weeks. Previous experience had shown that this two-week period was sufficient for each sample to reach equilibrium with the headspace water vapor concentration. The relative humidity for each sample was established by using standard sulfuric acid solutions for which the humidity as a function of solution composition is well known.(9) The specific uptake of water was computed for each adsorbent at each relative humidity, and these data are shown graphically in Figure 2. In general, the Ambersorb adsorbents are more hydrophobic than typical GACs (compare with Calgon Type BPL carbon) and, in particular, Ambersorb 563 adsorbent is substantially more hydrophobic, having only about 25% of the water uptake of Calgon Type BPL carbon.

Conversion of hexane was measured using a flowrate of 3 cm³/min hexane in air. For these experiments, a catalyst weight of 1.0 g was utilized,

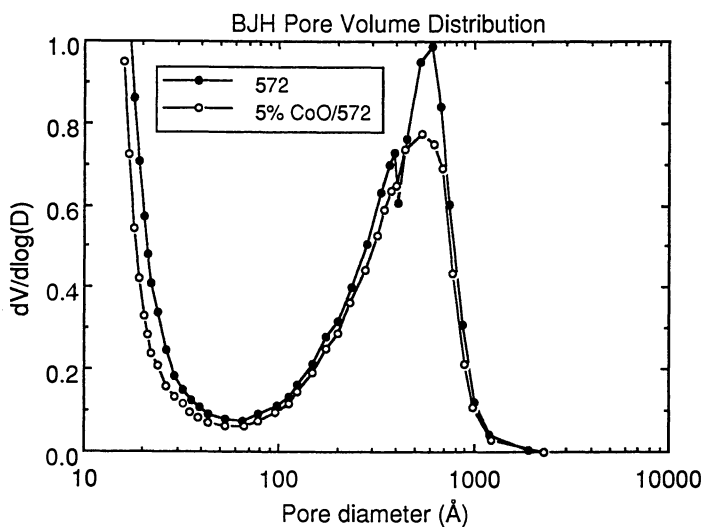


Figure 1. BJH pore volume distribution for Ambersorb 572 adsorbent and for 5% CoO on Ambersorb 572 adsorbent.

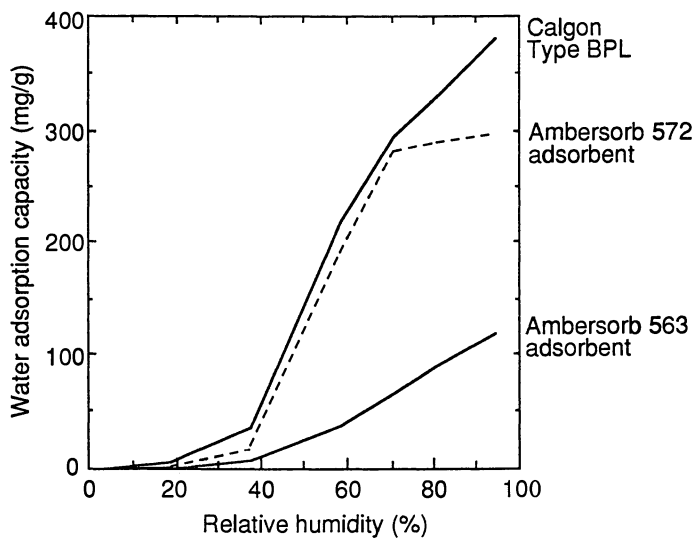


Figure 2. Water vapor adsorption isotherms for the carbonaceous supports.

corresponding to an approximate space velocity (SV) of 150 h^{-1} . Catalyst composition and reaction conditions, along with the initial hydrocarbon conversion, are shown in Table II. In general, conversion fell with time, with deactivation taking place more quickly at lower temperatures. For the runs at $250 \text{ }^\circ\text{C}$, the decrease in conversion was only a few percent at 100 hours time on stream, whereas for the runs at $175 \text{ }^\circ\text{C}$, conversion fell to the 50% level in the same time period. The deactivation curve for one of the catalysts tested is shown in Figure 3. The catalysts could, however, be reactivated by switching the feed stream to air (no hydrocarbons) and increasing the temperature to $250 \text{ }^\circ\text{C}$ for 15 hours, whereupon the conversion returned to 99.8%.

Table II. Conversion using hexane feed stream

Hexane (ppmv)	Dopant level (%)	Dopant	Support	Temperature ($^\circ\text{C}$)	Initial conversion (%)
2000	5	MnO	572	250	99.9
1000	5	MnO	572	200	99.8
1000	5	MnO	563	250	99.7
1000	5	MnO	563	175	99.9
2000	5	CoO	572	250	99.9
1000	5	CoO	572	200	99.8
1500	5	ZnO	572	175	99.9
1000	10	ZnO	563	175	99.9

This pattern of deactivation is suggestive of a "coking" mechanism whereby, at lower temperatures, deposition of carbon or other partially oxidized organics at the active sites or in the transport pores leads eventually to loss of activity. Heating the catalyst to higher temperatures with an air feed can evidently oxidize and burnoff these coke products and recover the activity. The apparent induction period shown in Figure 3 suggests that buildup of a substantial amount of carbonaceous deposits may be necessary before any reduction in reaction rate is observed. Additional work is necessary, however, to further understand the details of the deactivation mechanism.

Butane conversion was measured in a similar fashion using a flowrate of $3 \text{ cm}^3/\text{min}$ butane in air and 1.0 g of catalyst ($\text{SV } 150 \text{ h}^{-1}$). Catalyst composition and reaction conditions, along with the initial hydrocarbon conversion, are shown in Table III. The catalysts tended to deactivate more quickly with the butane feed than they did with hexane. Activity at $175 \text{ }^\circ\text{C}$ is also apparently lower as shown by the initial conversion of 51% for 5% MnO on Amborsorb 572 adsorbent.

Toluene conversion was also measured in a similar fashion using a flowrate of $3 \text{ cm}^3/\text{min}$ toluene in air but with a charge of 2.0 g of catalyst ($\text{SV } 75 \text{ h}^{-1}$). Catalyst composition and reaction conditions, along with the initial hydrocarbon conversion, are shown in Table IV. For these runs, virtually no

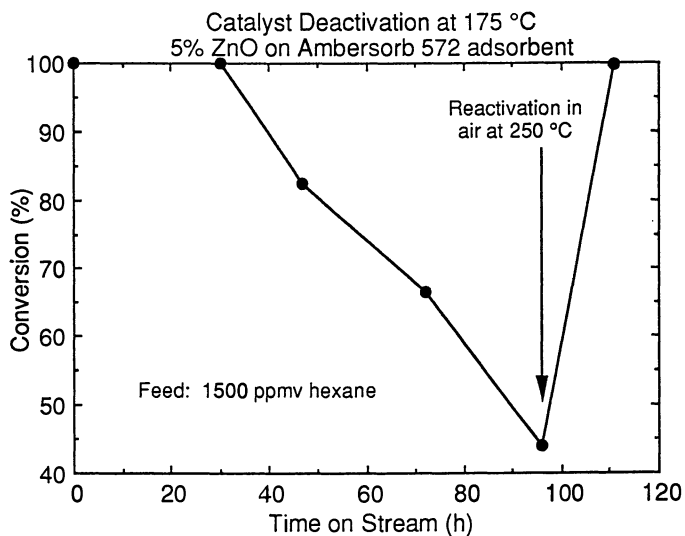


Figure 3. Deactivation of 5% ZnO on Ambersorb 572 adsorbent at 175 °C with a feed stream of 1500 ppmv hexane.

deactivation of the catalyst was seen during 105 hours of time on stream. Speciation of the product gases indicated that the major product gas was CO₂.

Table III. Conversion using butane feed stream

Butane (ppmv)	Dopant level (%)	Dopant	Support	Temperature (°C)	Initial conversion (%)
30000	5	MnO	572	250	99.8
2000	5	MnO	572	175	50.8
5000	5	CoO	572	250	99.8

Table IV. Conversion using toluene feed stream

Toluene (ppmv)	Dopant level (%)	Dopant	Support	Temperature (°C)	Initial conversion (%)
600	5	CoO	572	210	99.0
1300	5	CoO	563	250	99.9

Additional tests were run at a much higher concentration of toluene vapor using water as a co-feed (22000 ppmv of each species) and with a flowrate of 50 cm³/min and 1.0 g of catalyst (SV 2500 h⁻¹). For these runs, three catalysts with varying levels of CoO were used. The conversions are shown in Table V where it is clear that, despite the short contact time, the high concentration, and the low temperature, good conversion is achieved. These data suggest that, under these conditions, metal loading levels as low as 1% by weight are quite effective. The surface areas, pore volumes, and toluene conversions of these catalysts decreased as the metal loading level was increased. These changes may be due to either poor dispersion of the metal oxide (aggregation in the micropores) or to a decrease in the toluene diffusivity because of transport pore constriction. Additional work is planned to characterize the CoO dispersion and to measure the effective diffusivity of toluene in these catalysts which should be helpful in understanding the observed changes.

Table V. Conversion using toluene feed stream at short contact times

Toluene (ppmv)	Dopant level (%)	Dopant	Support	Temperature (°C)	Initial conversion (%)
22000	1	CoO	572	175	95.5
22000	2	CoO	572	175	80.6
22000	10	CoO	572	175	77.5

Conclusion

These preliminary results clearly show that first-row transition metals, when dispersed on Amborsorb adsorbent supports, are effective catalysts for the deep oxidation of aliphatic and aromatic compounds at relatively low temperatures. Although the flowrates used in this work are generally lower than those typical for commercial thermal or catalytic oxidation systems, it should be possible to optimize the catalyst composition to reduce the required contact time while ensuring near 100% hydrocarbon destruction efficiency. Because these catalysts are effective at low operating temperatures, the energy requirements for a catalytic oxidation unit using these materials are expected to be significantly lower than for conventional oxidation systems. As a result, the operating costs of such a system should be lower and therefore yield significant savings over the lifetime of an environmental remediation project.

As catalyst supports, the Amborsorb adsorbents appear to offer a unique combination of advantages. The high surface area of these adsorbents, in conjunction with significant meso- and macroporosity, should allow the synthesis of highly dispersed catalysts with high diffusivity. Consequently, as shown above, excellent activity can be obtained at relatively low process temperatures. In addition, the hydrophobic nature of the supports should be beneficial in processes where high water vapor concentrations are present, either by offering reduced sensitivity to water inhibition of active sites, or by enhanced hydrothermal stability under process conditions where silica or alumina supports would be unsuitable.

Literature Cited

1. Graham, J.; Ramaratnam, M. *Chemical Engineering*, February 1993, 6-12.
2. Agarwal, S.K.; Spivey, J.J. *Appl. Catal. A: General*, 1992, 81, 239-55.
3. Petrosius, S.C.; Drago, R.S. *J. Chem. Soc. Chem. Commun.*, 1992, 4, 344-5.
4. Neely, J.W.; Isacoff, E.G. *Carbonaceous Adsorbents for the Treatment of Ground and Surface Waters*; Marcel Dekker: New York, NY, 1982.
5. Maroldo, S.G.; Betz, W.R.; Borenstein, N. U.S. Patent 4 839 331, 1989.
6. Satterfield, C.N. *Heterogeneous Catalysis in Practice*; McGraw-Hill: New York, 1980; p 82.
7. Barrett, E.P.; Joyner, L.G.; Halenda, P.P. *J. Am. Chem. Soc.*, 1951, 73, 373-380.
8. Sing, K.S.W.; Everett, D.H.; Haul, R.A.W.; Moscou, L.; Pierotti, R.A.; Rouqu  rol, J.; Siemieniewska, T. *Pure & Appl. Chem.*, 1985, 57, 603-19.
9. Weast, R.C. (ed.) *Handbook of Chemistry and Physics, 51st Ed.*; Chemical Rubber Co.: Cleveland, OH, 1970; p E-40.

RECEIVED November 1, 1993

Chapter 28

Deep Oxidation of Chlorinated Hydrocarbons

Russell S. Drago¹, S. C. Petrosius¹, G. C. Grunewald¹, and
William H. Brendley, Jr.²

¹Department of Chemistry, University of Florida, Gainesville, FL 32611

²Rohm and Haas Company, Spring House, PA 19477

Catalysts comprising metal oxides dispersed in Ambersorb[®] carbonaceous adsorbents are shown to be effective in the decomposition of halogenated hydrocarbons by air at and below 250° C. A wide range of chlorinated hydrocarbons are converted selectively to CO₂, CO and HCl. Surprisingly the Ambersorb adsorbent supports exhibited significant activity in the absence of metal oxide species. Trends in reactivity with catalyst variation suggest that the carbonaceous adsorbent pore content and acidity are determining factors in the catalytic activity. Kinetic studies of methylene chloride decomposition over undoped Ambersorb adsorbent show a first order dependence on CH₂Cl₂ concentration and an activation energy of 11.0 kcal/mol. Further examination of the catalytic decomposition process suggests that a source of hydrogen, either as a component of the chlorinated hydrocarbon or as an added reagent, is necessary to regenerate the catalyst. Water not only served this function but also was found not to saturate the active site for adsorption.

Halogenated hydrocarbons have enjoyed widespread acceptance as solvents in the chemical industry because of their relative inertness in chemical processes and their ability to dissolve many organic compounds. However, the toxicity and carcinogenic properties of halogenated organics have raised industry awareness of the need for proper disposal of these hazardous materials (1). Indeed, public awareness has led to more stringent emission regulations by the federal, state, and local government agencies.

Presently, air stripping and incineration are the preferred method of disposal but temperatures exceeding 1000 K are required to obtain complete decomposition (2,3). Highly toxic materials such as dioxin are often formed as byproducts. With low concentration of contaminant in the gas phase, the process becomes exceedingly inefficient as the entire volume of gas must be heated to the combustion temperature. Incinerator fuel costs alone may reach 40% of the total operating costs (4). Consequently, development of

0097-6156/94/0552-0340\$08.00/0

© 1994 American Chemical Society

In Environmental Catalysis; Armor, J.;

ACS Symposium Series; American Chemical Society: Washington, DC, 1994.

low-temperature processes for halogenated waste disposal can offer significant improvement over present methods.

Spivey (5) presents an exhaustive review (to 1987) of low-temperature oxidative decomposition catalysts for application in environmental remediation. The majority of the catalysts can be put into two categories: transition metal oxides (either unsupported or adsorbed onto an inorganic oxide support) and supported noble metals. The noble metal catalysts (Pd, Pt, Rh, Ru) are poor choices for oxidation of halogenated hydrocarbons because of their high expense and their propensity to poisoning by the Cl₂ and HCl produced in the reaction (6,7). A number of patents have been issued for destruction of halogenated hydrocarbons with metal oxide catalysts (8) but optimum temperatures for these systems are usually >300° C and the halogenated hydrocarbon concentration typically is limited to less than 10,000 ppm.

This study investigates Ambersorb carbonaceous adsorbents as catalyst for the catalytic combustion of halogenated hydrocarbons at low temperatures (<250° C). Analyses of the factors influencing reactivity, such as temperature, atmosphere and pore structure of the adsorbent provide insight into the reaction mechanism.

Experimental

The Ambersorb carbonaceous adsorbents utilized in this study and their relevant structural properties are listed in Table I. These adsorbents are prepared by the patented pyrolysis of sulfonated styrene-divinylbenzene resins and have very reproducible surface areas and pore volumes (9).

Table I. Structural Parameters of Ambersorb Adsorbents

Adsorbent	Surface Area Volume (m ² /g)	Micropore Volume (ml/g)	Mesopore Volume (ml/g)	Macropore Volume (ml/g)
Ambersorb 563	600	0.22	0.16	0.24
Ambersorb 572	1200	0.49	0.26	0.24

Chlorinated reactants were purchased from Aldrich Chemical Company as were the metal salts. All gases (air, hydrogen, helium, argon, and nitrogen) were supplied by Liquid Air Company.

Reaction products were analyzed on a Varian 3700 gas chromatograph equipped with a 3m x 1/8" stainless steel Poropak Q (100/120 mesh) column and a thermal conductivity detector. Light gases (CO₂, CO, N₂, O₂, H₂O) were analyzed on a 15' x 1/8" Carboxen 1000 (60/80 mesh) column on the same detector. GCMS was accomplished on a Varian 3400 GC associated with a Finnegan 700 ion-trap mass spectrometer. Porosimetry data were performed on a Micromeritics 2300 porosimeter.

The reactor for all runs was a packed-bed, 10 mm diameter glass flow reactor. A coarse glass frit supports the catalyst. The reactor tube is heated either with a commercially available Thermolyne Briskheat flexible electric heat tape or a resistance oven consisting of nichrome wire wrapped around a 4" pyrex tube with quartz wool packing material for even heating. The

heating element is controlled by a digital temperature controller model CN-2041 (Omega Engineering) equipped with a J-type thermocouple and once equilibrated provided temperature control to $\pm 2^\circ\text{C}$.

A 2.0 g sample of catalyst (48 mm bed height) is used in the experiments and the sample is covered with a 15 cm length of glass beads for mixing and heating the reactants prior to catalyst contact. A model FL-320 rotameter (Omega Engineering) is used to obtain flow control of gas feeds from 0.2 ml/min up to 50 ml/min. A soap bubble meter in the post-catalyst zone is used to determine overall flow rates of the gases. The halogenated reactants are delivered with an air stream either by passing the gas through a reservoir or by pumping a liquid feed to the top of the heated zone with a custom-built motorized syringe pump. The vapor pressure of the hydrocarbon and the temperature of the reservoir determines the substrate concentration in the air stream for the reservoir delivery method; the rate of the constant delivery volume sets the concentration for the syringe method. The typical hydrocarbon concentration is 60,000 ppm for optimum decomposition efficiency at 1.0 ml/min air flow. The liquid volume feed rate for the halogenated reactants are 0.01-0.05 ml/hr for the reservoir method and 0.05-0.10 ml/hr for the syringe pump method.

Gas samples taken before and after the catalyst bed are compared to determine conversions. A halogen mass balance is performed by collecting the HX produced in an aqueous NaOH bubbler placed at the reactor outlet and back-titrating to quantify the HX produced. The mass of the catalyst is checked after reaction to determine if loss of carbonaceous support occurs; for all experiments at 250°C there is no weight loss of the catalyst, even after 150 hours of reaction.

All catalysts are prepared by a pore-filling method (to incipient wetness) whereby only enough solvent is used to fill the void space of the adsorbent; this procedure ensures intimate contact of the dopant solution with the interior support surface (meso and micro-pores). The soluble precursor species CrO_3 , TiCl_4 , KMnO_4 , $\text{Ce}(\text{NO}_3)_3$, SbCl_5 , NH_4VO_3 , H_2SO_4 , $\text{Co}(\text{NO}_3)_2$ and FeCl_3 are utilized in the catalyst preparations. The solvent is water in all cases except for TiCl_4 where CH_2Cl_2 is used. Once impregnated, the catalysts are converted to the hydrated oxide or oxychloro forms in a number of different ways. Titanium tetrachloride is hydrolyzed in moist air whereas iron and antimony chlorides are treated with base to obtain the oxides. In all other cases, heating of the impregnated support to the reaction temperature of 250°C under air leads to oxide formation. The catalysts are all 14% metal oxide by mass unless otherwise noted.

Results and Discussion

Catalytic Combustion Reactivity Studies. Methylene chloride was selected as our initial study of the catalytic combustion of halogenated hydrocarbons because of its high vapor pressure and the hydrogen balance:



The reaction obviously is more complicated than shown in Equation (1) because carbon monoxide is observed occasionally in the exit stream. Regardless of the final carbon product (CO or CO_2) the chloride-hydrogen balance is the same. The activities of the metal oxide/Amborsorb carbonaceous adsorbent catalysts for the above reaction at 250°C are presented in Table II. Unexpectedly, the control experiments with undoped

Ambersorb adsorbents led to substantial oxidation of CH_2Cl_2 . This is consistent with detailed studies of oxidative dehydrogenation reactions over oxide catalysts which report (10-13) that oxygen-containing carbon species in the coke formed from hydrocarbon reacting at acidic sites plays an important role in the redox chemistry (14).

Table II illustrates the catalytic activity of Ambersorb adsorbent supports with CrO_3 , $\text{KMnO}_4/\text{Ce}(\text{NO}_3)_3$ and TiO_2 . These metal oxide catalysts give conversions higher than 90% and in the case of the chromium catalysts, the conversion is essentially 100%. These results demonstrate the ability of the metal oxide/porous Ambersorb adsorbent catalysts to completely destroy chlorinated hydrocarbons from a contaminated air stream. Alumina-supported Cr_2O_3 is reported to be effective in the catalytic decomposition of methylene chloride (4) and chloroform (15) at temperatures ranging from 350°C to 550°C . However, a rapid drop in activity of this catalyst occurred by loss of the metal as volatile CrO_2Cl_2 . No volatilization of the metal species occurs with the Ambersorb resin catalysts even after 150 hours of continuous reaction.

One will observe that iron and antimony oxide supported on Ambersorb adsorbents give conversions which were lower than that of the support itself. The preparation of both of these catalysts involves treatment of the chloride precursor with sodium hydroxide to obtain the hydrated oxide. It is conjectured that this would neutralize any acidic sites on the carbonaceous resin and suggests that the catalytic combustion reaction is influenced by the resin acidity as reported in the decomposition of 1,2-dichloroethane over $\text{TiO}_2/\text{SiO}_2$ (16). To investigate the importance of acidic sites, a five gram sample of Ambersorb 563 adsorbent was washed with 8.3×10^{-2} moles of aqueous ammonia. A measurable drop in activity approximating 10-15% is observed with this system. Addition of 8.8×10^{-3} moles of sodium hydroxide to 5 grams of Ambersorb 563 resin produces an even larger drop in activity of ~30 to 40%. It is our conclusion that adsorbent acidity influences the catalytic activity of the undoped catalyst support in the deep oxidation reaction.

Pore Structure. Pore structure of the carbonaceous adsorbent is a determining factor in adsorption efficiency (9) and, therefore, has a significant impact on the catalytic efficiency of the low-temperature decomposition process. We believe that the pore size distribution with Ambersorb adsorbents allows for facile diffusion of reactant molecules to active sites in the pore interior and to the metal oxide for catalytic destruction and for rapid diffusion of products out of the porous carbonaceous adsorbent. The availability of macropores ($>500 \text{ \AA}$), mesopores (500-20 \AA) and micropores ($< 20 \text{ \AA}$) is significant.

Reactivity Studies. In addition to methylene chloride, a number of other halogenated hydrocarbons were employed in the catalytic combustion reaction and the results are presented in Table III. The Ambersorb 563/ CrO_3 catalyst is used and flow rates and reactant feed rates are varied to illustrate that optimization of these variables can lead to effective oxidation. An aromatic reactant, 1,2,4-trichlorobenzene, was utilized as a model for polychlorinated biphenyls (PCBs) and it is observed that the reactivity is comparable to that seen for methylene chloride under similar conditions. Complete decomposition of trichlorobenzene is expected with catalyst

Table II. Activity of Various Ambersorb Adsorbent Catalysts in the Catalytic Combustion of Methylene Chloride^a

Catalyst	Conversion (%) ^b
Ambersorb 563	69 (+3)
Ambersorb 563/CrO ₃	99.9 (±0.1)
Ambersorb 563 (NaOH)	32 (+4)
Ambersorb 563 (NH ₄ OH wash)	52 (+4)
Ambersorb 563, CrO ₃ ^d	48 (+3)
Ambersorb 572	78 (+3)
Ambersorb 572/CrO ₃	99.9 (±0.1)
Ambersorb 572/KMnO ₄ /Ce(NO ₃) ₃	95 (+1)
Ambersorb 572/TiO ₂	93 (+1)
Ambersorb 572/H ₂ SO ₄	83 (+3)
Ambersorb 572/V ₂ O ₅	82 (+3)
Ambersorb 572/Cobalt Oxide	75 (+4)
Ambersorb 572/Iron Oxide	65 (+4)
Ambersorb 572/Sb ₂ O ₅ ^c	52 (+3)

a 250° C, 1 ml/min air flow, 2.0 g catalyst, [CH₂Cl₂]=60,000 ppm, 72 hour reaction time.

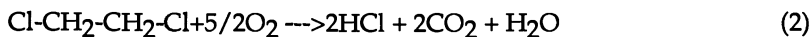
b Conversions based on GC analysis and HCl product quantification.

c Metal chloride-doped carbon support treated with base to obtain hydrated metal oxide species.

d A layer of Ambersorb 563 over a layer of CrO₃, separated by a plug of glass wool.

concentration optimization and longer residence times. The compound 1,1,2,2-tetrachloroethane is hydrogen deficient, but can be decomposed if an external hydrogen source is provided. Water can perform this function. Better conversions are anticipated with optimization of the amount of water added. Methylene bromide serves to illustrate that brominated organics can be oxidized effectively.

Experiments with 1,2-dichloroethane (DCE) demonstrate the influence of water on catalytic reactivity (Table III). For the DCE reaction, the molecule contains sufficient hydrogen for the complete oxidation to HCl with the remainder forming water according to the following equation:



Reactivity of DCE under standard reaction conditions with Ambersorb 572/TiO₂ is impressive with >99% conversion. Upon addition of water to the reaction at a feed rate about 10 times that of DCE, the activity is still high at 94% conversion. With the undoped Ambersorb support, the conversion with water and without water is identical at 97% (±2). These results are in stark contrast to literature reports for the reaction catalyzed by zeolites (17) where a decrease of between 10 and 60% were observed with water addition. LZ-Y52 zeolite in our system showed significant water sensitivity. These observations indicate that Ambersorb catalyst systems do not exhibit competitive adsorption of water which is a major factor known to occur with aluminosilicates.

Table III. Reactivity of Ambersorb Catalysts with Halogenated Hydrocarbons ^a

Reactant	Catalyst	Air Flow ^b ml/min	Reactant Feed ^c ml/min	H ₂ O Feed ^d ml/hr	Conversion %	Reaction Time ^e hr
Methylene Chloride	563/CrO ₃	1.0	0.05	0	>99	
Methylene Chloride	563/CrO ₃	5.0	0.05	0	32	
1,2,4-Trichlorobenzene	563/CrO ₃	6.0	0.06	0	19	
Tetrachloroethylene	563/CrO ₃	1.0	0.05	0.01	16	
1,1,2,2-Tetrachloroethane	563/CrO ₃	1.0	0.05	0.01	63	
Methylene Bromide	563/CrO ₃	1.0	0.005	0	93	
1,2-Dichloroethane	572	1.0	0.05	0	97	
1,2-Dichloroethane	572	1.0	0.05	0.12	97	
1,2-Dichloroethane	572/TiO ₂	1.0	0.05	0	>99	
1,2-Dichloroethane	572/TiO ₂	1.0	0.05	0.12	94	
1,2-Dichloroethane	LZ-Y52	1.0	0.05	0	23	
1,2-Dichloroethane	LZ-Y52	1.0	0.05	0.12	4	
Carbon Tetrachloride	563	1.0	0.014	0	73	5
Carbon Tetrachloride	563	1.0	0.014	0	47	48
Carbon Tetrachloride	563	1.0	0.014	0	5	120
Carbon Tetrachloride	563	1.0	0.014	0.06	15	140
Carbon Tetrachloride	563	1.0	0.014	0.60	47	170

^a Conditions: 250° C, 2.0 g catalyst, 72 hrs reaction (unless mentioned).

^b Air flow is dictated by reaction stoichiometry and reactant feed rate.

^c Reactant feed rate is dependent on volatility and method of delivery.

^d Water is used either as a source of protons or to demonstrate adsorption competition.

^e Time refers to CCl₄ reaction which is presented as a function of time as well as water feed rate. For all other reactions a steady state conversion is listed, which is not a function of the reaction time.

Carbon tetrachloride is a model compound for the general category of fully chlorinated, non-olefinic hydrocarbons. Table III identifies the results of the catalytic destruction of carbon tetrachloride using undoped Amborsorb 563 adsorbent. The conversion after five hours is 73% compared to a conversion of 68% for methylene chloride under identical conditions. Energies for C-Cl bonds in chlorinated methane derivatives are typically on the order of 20-25 kcal/mol lower than the corresponding C-H bond energies, indicating thermodynamic favorability of C-Cl bond cleavage over C-H bond cleavage. This coupled with a 2:1 ratio of C-Cl bonds in CCl_4 versus CH_2Cl_2 accounts for the increased reactivity. The decline of activity after 120 hours demonstrates that a reactant is being depleted; in this case it is most likely the hydrogen necessary to form the HCl product. Addition of water at 0.06 ml/hr increases conversion from 5% to 15%. At 0.60 ml/hr the conversion rises to 47%, indicative of water providing the hydrogen needed for conversion to HCl and CO_2 . The reaction is in effect a hydrolysis reaction. The excess water required over the stoichiometric amounts illustrates that water is not used efficiently in this reaction.

It is desirable to attain lower temperatures for the deep oxidation reaction in order to apply the technology to existing adsorbent regeneration methods which operate at 140 to 170°C in steam regeneration (9). Amborsorb adsorbents, utilized in groundwater remediation and wastewater purification, may be in-situ regenerated with steam to remove adsorbed organic contaminants and attain initial pore volume capacity. Catalytic oxidation at these lower temperatures would not only remove these organic contaminants but also simultaneously destroy the organic compound. The catalytic oxidation of CH_2Cl_2 was performed at lower temperatures in the presence of water vapor and these results are presented in Figure 1. Undoped Amborsorb 563 carbonaceous adsorbent is the catalyst and water is introduced by saturating the air stream in a water bubbler before contacting the reactor. With a water-saturated air flow, a fairly smooth decline in activity is observed down to 150° C where 15% conversion is observed.

Activation Energy. An Arrhenius plot for the temperature range of 250 to 375°C is shown in Figure 2 for a flow rate of 3 ml/min. The activation energy (E_a) derived from a least squares treatment on this plot is 11.0 kcal/mol ($A=177.5\text{s}^{-1}$), which is comparable to that observed for the same reaction over cerium and chromium oxides supported on zeolites (17). The low value of the activation energy compared to even the weaker C-Cl bond dissociation energy (73 kcal mol⁻¹ in CCl_4) indicates substantial interaction of species formed in the transition state with the catalyst.

Catalyst Characterization. Porous carbon catalysts have been found to possess high metal dispersion and this effect has been observed by scanning electron microscopy (SEM) (18). Scanning electron micrographs of Amborsorb 563 are presented in Figure 3 (6000 and 30,000 magnification). At 6000 magnification, there is a large fault in the sample which provides a view of the interior pore structure arising from the copolymer precursor. The micrograph at 30,000x illustrates the detail for a pore of macroporous dimensions with mesopores observed as small cracks in the surrounding surface. Micropores, created during the pyrolysis of the copolymer, are too small to see but are cited to be the defining character which accounts for the molecular sieving action observed for many carbon materials (19-21).

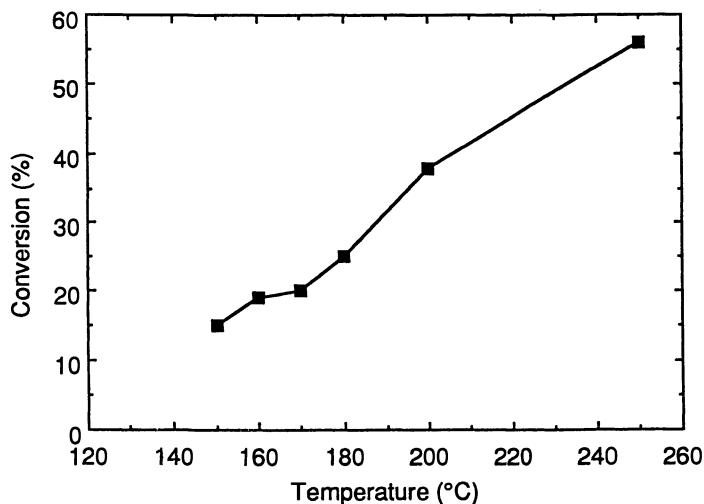


Figure 1. Activity of Ambersorb 563 adsorbent in the Deep Oxidation of Methylene Chloride as a Function of Temperature in the Presence of Water (ca. 0.01 ml/hr).

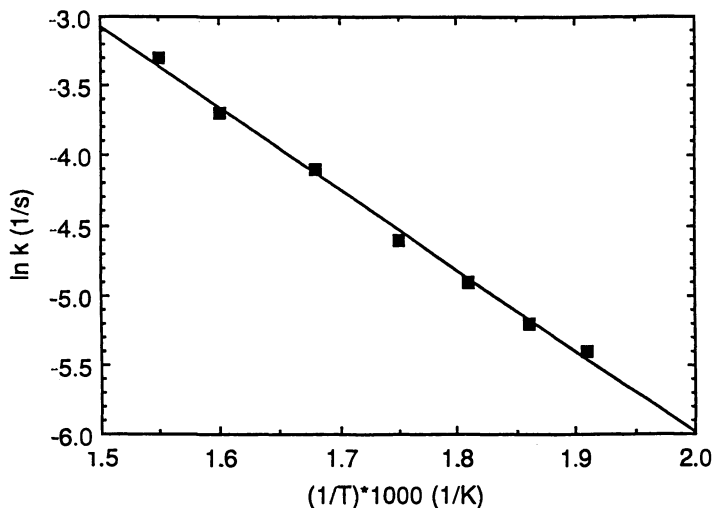


Figure 2. Arrhenius Plot (First Order, $\ln k$ vs. Temperature⁻¹) for the Deep Oxidation of Methylene Chloride at 3/ ml/min. Air Flow and 2.0 g Catalyst Sample. Linear Regression Gives a Best-Fit Line of $\ln k = (-5.543 \times 10^3)(1/T) + 5.179$. These Values Give $E_a = 11.0$ kcal/mol and Arrhenius Constant = 177.5 s⁻¹.

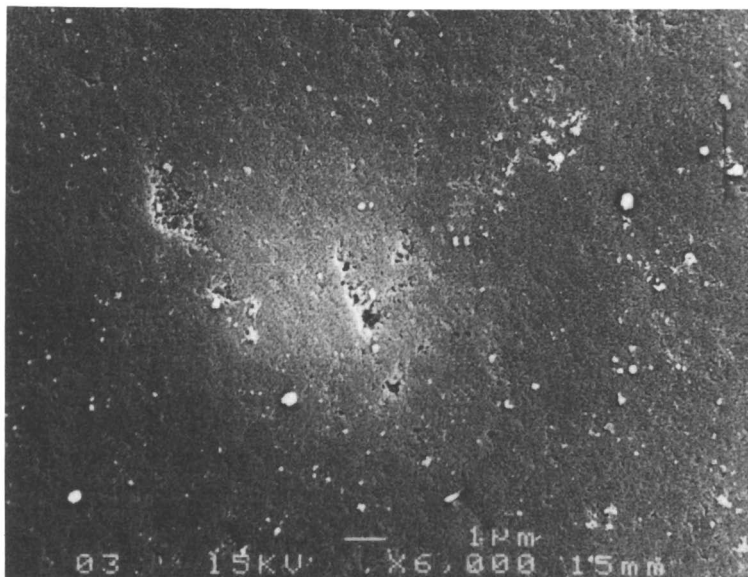


Figure 3(a). Scanning Electron Micrograph of Ambersorb 563 adsorbent, 6000X Magnification.

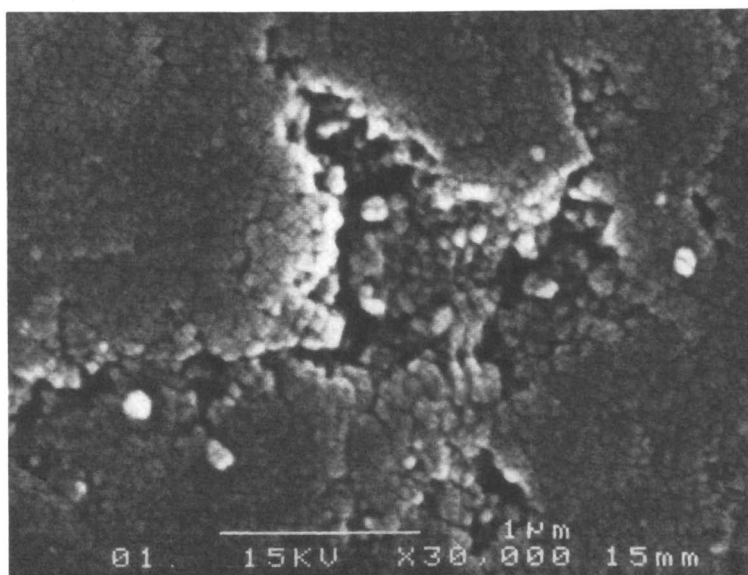


Figure 3(b). Scanning Electron Micrograph of Ambersorb 563 adsorbent, 30,000X Magnification.

The micrographs in Figure 4 are of $\text{CrO}_3/563$ catalyst at 6000 and 30,000 magnification, respectively, and reveal some qualitative information about catalyst structure. This sample has been heated to 250°C and used in a catalytic reaction for an extended period of time. One might expect that CrO_3 , which has a melting point of 195°C , would melt and recrystallize upon cooling into aggregates, or large crystallites, unless it was highly dispersed and anchored to the surface. The absence of large crystallites observed in Figure 4 is strong evidence that dispersion and adhesion to internal surface sites has occurred. The synergistic activity of $563/\text{CrO}_3$ catalyst presented in Table II is also indicative of this high level of dispersion and attachment of metal oxide to the carbonaceous surface.

Table IV presents porosimetry data compiled on Ambersorb 572 adsorbent and Ambersorb 572/metal oxide catalysts. These data illustrate clearly a trend toward decreasing surface area and micropore volume, with little change in mesopore volume. The macropore volume numbers suggest a decrease with metal loading level but it is generally considered that nitrogen porosity is not very reliable for macropore volume determinations.

Table IV. Porosimetry Data on Metal-doped Ambersorb Catalysts

	Ambersorb 572/CoO doped		
	1% CoO/572	2% CoO/572	10% CoO/572
BET Surface Area (m^2/g)	1204	1088	903
t-plot micropore volume (cc/g)	0.457	0.406	0.336
Pore Volume Distribution (cc/g)			
micropores:	0.495	0.443	0.368
mesopores:	0.220	0.221	0.195
macropores:	0.237	0.215	0.162

Additional studies of Scanning Electron Microscopy (SEM) with Energy Dispersive Spectrometry (EDS) and Transmission Electron Microscopy (TEM) were used on metal-doped Ambersorb resins to determine the gross distribution of the metal and the morphology of the metal deposited within the pores. SEM-EDS on Ambersorb 572 impregnated with ZnO or CuO gave interesting data as revealed in Table V.

The count data indicate the two samples are different in their distribution of metal oxide. Ambersorb 572/ ZnO counts are reasonably constant across the interior of the Ambersorb adsorbent bead, suggesting that the metal oxide concentration is invariant to position whereas the Ambersorb 572/ CuO shows a greater concentration of metal oxide near the bead surface. The morphology of the metal oxide within the pores of the Ambersorb resin was investigated using TEM techniques. This technique confirms metal oxide present in the meso- and micropores with the metal oxide finely dispersed and not clogging the pores. These data suggest that the metal oxide may reside in the meso and micropores or only in the macro-meso pores depending on size and the diffusivity of the metal oxide in the solvent used for pore penetration. In any case there is a high level of dispersion for the metal oxide on the support.

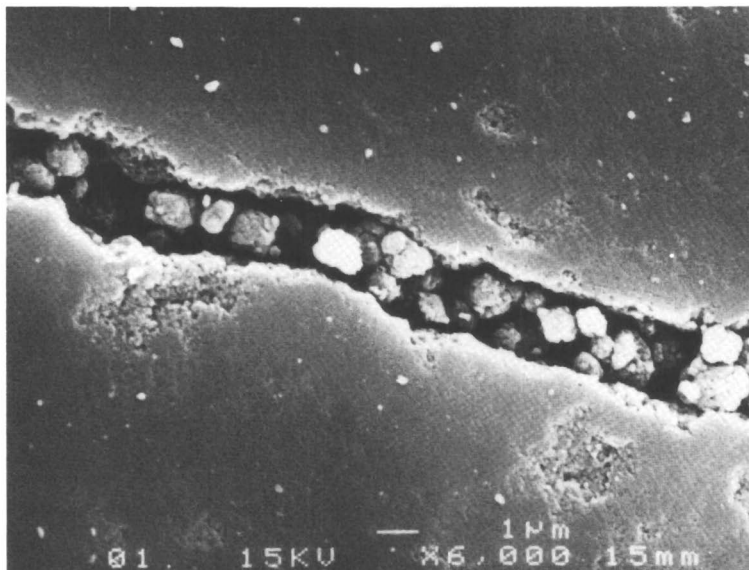


Figure 4(a). Scanning Electron Micrograph of $\text{CrO}_3/563$, 6000X Magnification.

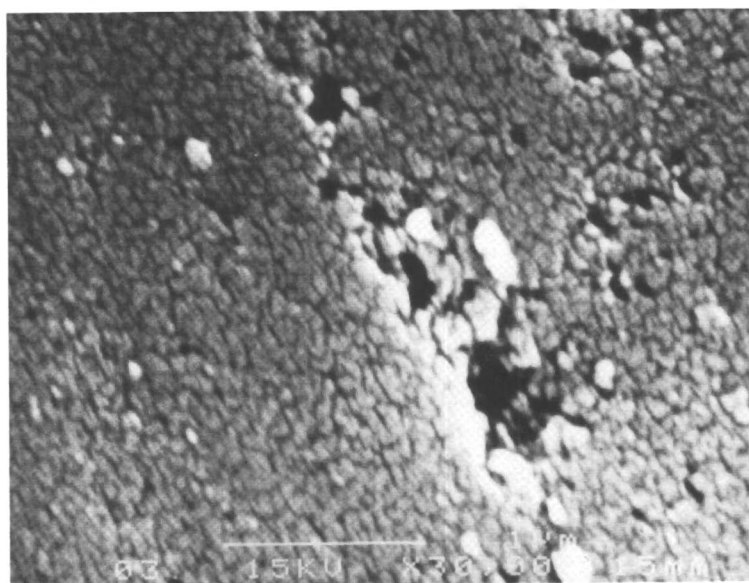


Figure 4(b). Scanning Electron Micrograph of $\text{CrO}_3/563$, 30,000X Magnification.

Table V. SEM-EDS Count Data for Ambersorb/Metal Oxide

Ambersorb 572/ZnO	Ambersorb 572/CuO
5263	3412
5565	2551
5484	2436
5518	2452
4573	3213

Conclusions

A number of metal oxides supported on Ambersorb carbonaceous adsorbents have shown ability to decompose halogenated organic compounds to CO₂, CO and HX at low temperatures. Surprisingly and unexpectedly, Ambersorb adsorbents demonstrate catalytic activity without metal oxides. These adsorbents demonstrate catalytic activity because of acidic sites within the pore distribution. Fast kinetics are due to the presence of macro-meso- and micropores present in the adsorbents. The metal oxide doped Ambersorb adsorbents revealed the metal is present in the macro-meso- and micropore region in some cases and only in the macro and meso in other cases. In addition, there is a significant dispersion of the metal as viewed by SEM and TEM.

The presence of hydrogen, either as part of the reactant molecule (as in CH₂Cl₂) or as part of an additive such as water, was determined to be important for efficient decomposition of the organic to carbon oxides and HX. Excess water in the reaction stream do not inhibit the reaction in any way and even promoted the reaction at lower temperature.

Ambersorb adsorbents and metal-oxide doped Ambersorb resins show potential for environmental catalysis destruction of halogenated hydrocarbons in both liquid and vapor phase remediation applications.

Acknowledgments

We thank the Rohm and Haas Company for their financial support of this project as well as Dr. Robert Antrim of Rohm and Haas Company Analytical Group for SEM and TEM measurements. Mr. Richard Crockett of the Major Analytical Center at the University of Florida also is acknowledged for performing microscopy measurements.

Literature Cited

1. Norstrom, R.J.; Simon, M.; Muir, D.C.G.; Schweinsburg, R.E. *Environ. Sci. Tech.* **1988**, *22*, 1063.
2. Josephson, J. *Environ. Sci. Tech.* **1984**, *18*, 222A.
3. Huang, S.L.; Pfefferle, L.D. *Environ. Sci. Tech.* **1989**, *23*, 1085.
4. Manning, M.P. *Hazard. Waste* **1984**, *1*, 41.
5. Spivey, J.J. *Ind. Eng. Chem. Res.* **1987**, *26*, 2165.

6. Mendyka, B.; Rutkowski, J.D. *Environ. Prot. Eng.* **1984**, *10*, 5.
7. Tichenor, B.A.; Pallazolo, M.A. AIChE Annual Meeting, November 10-15, 1985, No. 486.
8. Dockner, T.; Sauerwald, M.; Krug, H.; Irgang, M. U.S. Patent 4 943 671, 1990.
9. Neely, J.W.; Isacoff, E.G. *Carbonaceous Adsorbents for the Treatment of Ground and Surface Waters*; Marcel Dekker, Inc.: New York, NY 1982; 68
10. Alkhazov, T.G.; Lisovskii, A.E. *Kinet. Katal.* **1976**, *17*, 434.
11. Fiedorow, R.; Przystajko, W.; Sopa, M.; Dalla Lana, I.G. *J. Catal.* **1981**, *68*, 33.
12. Menon, P.G. *J. Mol. Catal.* **1990**, *59*, 207.
13. Alkhazov, T.G.; Lisovskii, A.E.; Gulakhmedova, T.K. *React. Kinet. Catal. Lett.* **1979**, *12*, 189.
14. Cadus, L.E.; Gorriz, O.F.; Rivarda, J.B. *Ind. Eng. Chem. Res.* **1990**, *29*, 1143.
15. Weldon, J.; Senkan, S.M. *Combust. Sci. Technol.* **1986**, *47*, 229.
16. Imamura, S.; Tarumoto, H.; Ishida, S. *Ind. Eng. Chem. Res.* **1989**, *28*, 1449.
17. Chatterjee, S.; Greene, H.L. *J. Catal.* **1991**, *130*, 76.
18. Allen, G.C.; Curtis, M.T.; Hooper, A.J.; Tucker, P.M. *J. Chem. Soc. Dalton Trans.* **1973**, 1675.
19. Lamond, T.G.; Metcalfe, J.E.; Walker, P.L., Jr. *Carbon* **1965**, *3*, 59.
20. Eguchi, Y. *Sekign Gokkai Shi* **1970**, *13(2)*, 105.
21. Koresh, J.E.; Soffer, A. *J. Chem. Soc. Farad. Trans. I.* **1981**, *77*, 3005.

RECEIVED September 30, 1993

Chapter 29

Low-Temperature Catalytic Combustion of Volatile Organic Compounds Using Ozone

Antonella Gervasini, Claudia L. Bianchi, and Vittorio Ragaini

Dipartimento di Chimica Fisica ed Electrochimica, Università di Milano,
Via Golgi 19, I-20133 Milan, Italy

A coupled technique utilizing a combustion catalyst and ozone as oxidant was used to perform the complete combustion of several volatile organic compounds (VOC), such as halogenated and non-halogenated aliphatic and aromatic molecules. The decrease of the catalytic combustion temperature when using ozone as oxidant instead of oxygen, led to a remarkable reduction of energy consumption. VOCs were fed at low concentration (≤ 2000 ppm in air) as pure compounds as well as in mixtures. On the selected catalyst, barium promoted copper-chromite oxide supported on alumina (Ba-CuO-Cr₂O₃/Al₂O₃), a comparative study of the combustion of several compounds with and without ozone was performed. The formation of hazardous products of incomplete combustion (PIC) was verified. Surface characterization by XPS analysis of the catalyst in fresh form and after use was performed in order to find out structure-activity relationships.

Volatile organic compounds (VOCs) have long been regarded as source of air pollution due to their harmful effects on human health and on environment. A variety of industrial processes, for instance, for the manufacture of organic chemicals, polymers, and herbicides, as well as processes involving printing, painting, and cleaning and degreasing of metals, vent many different VOC and halogenated VOC wastes (1).

According to their commercial value and vented amount, VOCs can be treated in order to either recover or eliminate them. In the former case, adsorption on charcoal and condensation methods are used (1). As concerns the elimination, the preferred technologies are the thermal and the catalytic combustion (2,3). In the combustion of VOCs, the desired reaction is the complete oxidation to harmless compounds as CO₂ and H₂O. HCl and, in some cases, Cl₂ are also present among the products when chlorinated VOCs are destroyed (4).

In the absence of dusts and catalyst poisons, the use of the catalytic combustion is preferred to the thermal one from economic considerations (1). In fact, a remarkable reduction of energy consumption is effective, due to the

lower operating temperatures with respect to those of thermal combustion systems. The catalytic incinerators can be energetically self-sufficient or they require a moderate amount of auxiliary fuels.

When low VOC concentrations have to be treated (i.e., from 1000 to 2000 ppm), the heat of combustion could be too low to auto-sustain the reaction.

Temperatures ranging from 300 to 350°C have to be reached to make active the at-present usual catalysts. The auto-sustained state is particularly difficult to be achieved when compounds with low heat of combustion, as halogenated VOCs, are destroyed.

The increase of temperature following the adiabatic combustion of a given VOC can be calculated as a function of its concentration in air by means of the relevant heat of combustion. The trends of such increases of temperature for the VOCs employed in this work are reported in Figure 1. The combustion heat data are collected in Table I. Figure 1 shows that the catalyst should be active at temperatures around 100°C to allow a self-sustained reaction with non-chlorinated VOCs at concentration of 5 g/Nm³ and with chlorinated VOCs at concentration as high as 15 g/Nm³ or more. With the aim of performing the VOC combustion at such low temperatures, low temperature oxidation catalysts (LTC) (5) and/or new technologies are under study.

Several types of catalytic systems have been successfully used to eliminate VOCs, the most interesting ones belong to two categories: transition metal oxides, such as Cr, Cu, Fe, Mn, and supported noble metal catalysts (Pd and Pt) (5-7). The noble metal catalysts are the most active ones, however they are severely inhibited in their performance by the halogen atoms, as recently suggested in literature (4,8).

A catalytic technology in which ozone is used as oxidant to perform the complete combustion of various classes of VOCs has never been reported in literature, as far as the authors know. Ozone is a powerful oxidizing agent, exceeded in its oxidation potential only by fluorine (9). The strong electrophilic nature of ozone imparts to it the ability to react with a wide variety of organic and organometallic functional groups (10). Most of the ozone reactions are based on the cleavage of carbon-carbon double bond and on reaction with nucleophilic compounds. The coupled technique, in which a catalyst and ozone are utilized, has been studied in order to realize low temperature VOC combustions.

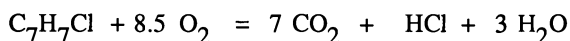
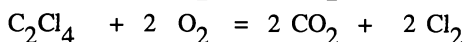
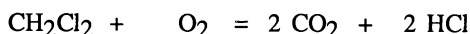
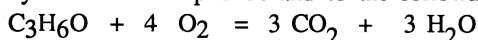
In this study, comparisons among catalytic combustions carried out with and without ozone are reported.

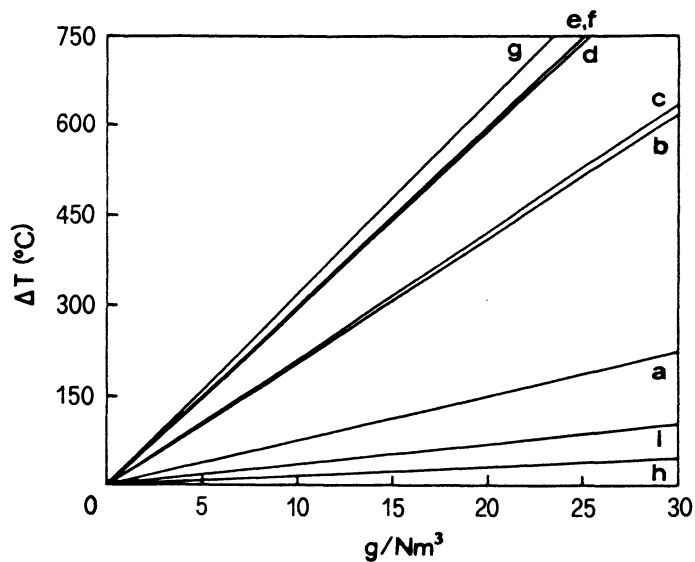
Experimental

Materials and Catalysts. The VOCs used in this work were all commercial products of guaranteed degree of purity (> 99.0 %). The various aliphatic, aromatic, and halogenated VOCs are listed in Table I.

As a toxicity index, the *Threshold Limit Value* (TLV) formerly known as *Maximum Allowable Concentration* (MAC) was chosen (11).

The standard enthalpy of combustion ($\Delta_c H^\circ$) of each compound, was calculated according to the stoichiometry of complete combustion to CO₂ and H₂O for hydrocarbon compounds and to the following reactions for the other organics:





a, dichloromethane
 b, p-chlorotoluene
 c, acetone
 d, benzene
 e, toluene
 f, styrene
 g, cyclohexane
 h, carbontetrachloride
 i, tetrachloroethylene

Figure 1. Calculated adiabatic ΔT following the complete combustion of the used VOCs (see reactions in Experimental) as a function of their concentration in air.

Table I. General Properties of the Studied VOCs

Name	Formula	Mol. Weight	TLV ^a		$\Delta_c H^{\circ}$ ^b	
			ppm	mg/m ³	kcal/mol	kcal/g
Benzene	C ₆ H ₆	78.11	10	30	-759.2	-9.72
Cyclohexane	C ₆ H ₁₂	84.16	300	1050	-885.2	-10.5
Toluene	C ₇ H ₈	92.13	100	375	-903.7	-9.81
Styrene	C ₈ H ₈	104.14	50	215	-1022.7	-9.82
Acetone	C ₃ H ₆ O	58.08	750	1800	-404.1	-6.96
Carbon-tetrachloride	CCl ₄	153.84	5	32	-71.3	-0.46
Dichloromethane	CH ₂ Cl ₂	84.94	100	350	-115.3	-1.35
Tetrachloroethylene	C ₂ Cl ₄	165.85	50	340	-186.3	-1.12
p-Chlorotoluene	C ₇ H ₇ Cl	126.58	50	260	-858.2	-6.78

^a TLV = Threshold Limit Values for VOCs are expressed in parts per million (ppm) which stands for parts of gases or vapors per million parts of air as well as in milligrams per cubic meter (mg/m³).

^b $\Delta_c H^{\circ}$ = Average values of the standard combustion enthalpy in the temperature range from 300 to 1000°C.

Table II. Physico-Chemical Characteristics of the Catalysts

Catalyst ^a	Code	Metal content (M - %)	Surface area (m ² /g)	P.A.B.D. ^b (g/cm ³)
Pd/Al ₂ O ₃	PDL	Pd - 0.5	200	0.4
Pd/Al ₂ O ₃	PDH	Pd - 1.0	200	0.4
Pt/Al ₂ O ₃	PTL	Pt - 0.5	200	0.4
Pt/Al ₂ O ₃	PTH	Pt - 1.0	200	0.4
Ba-CuO-Cr ₂ O ₃ /Al ₂ O ₃ ^c	BCC	Ba - 5.4 Cu - 23.2 Cr - 21.9	110 ^d - 77 ^e	1.0
Fe ₂ O ₃ /Al ₂ O ₃	FEO	Fe - 17.3	140	0.7

^a All the catalysts are in extrudate physical form.

^b P.A.B.D. = Packed Apparent Bulk Density.

^c Commercial code: Cu-1230 E.

^d Surface area of the non thermal treated catalyst and after thermal treatment of the catalyst at 450°C.

^e Surface area of the catalyst after thermal treatment at 700 and 900°C.

The $\Delta_c H^\circ$ values, averaged in the temperature range from 300 to 1000°C, are reported in columns 6 and 7 of Table I.

All the catalysts were kindly supplied from Engelhard Industries Italy. They are listed in Table II together with their physico-chemical characteristics. Three different types of catalyst formulations were tested: supported noble metal catalysts at low metal content, Pd and Pt at 0.5 %, (PDL and PTL) and at high metal content, Pd and Pt at 1 %, (PDH and PTH), supported mixed copper-chromite oxide, (BCC), and supported iron oxide (FEO). The support was alumina for all of the catalysts. All the catalysts were used as received. The BCC sample was also utilized after calcination in air at 450, 700, and 900°C.

Physico-Chemical Analysis. X-ray photoelectron spectra (XPS) were collected in an M-Probe apparatus (Surface Science Instruments). The source provided monochromatic Al K α radiation (1486.60 eV). The energy scale was calibrated with reference to the 4f_{7/2} level of a freshly evaporated gold sample (84.00 eV), the 2p_{3/2} level of copper (932.47 \pm 0.10 eV), and the 3s level of copper (122.39 \pm 0.15 eV). A spot size of 200 x 750 μ m and a pass energy of 25 eV were used for the single region acquisition spectra; the resolution was 0.74 eV. An electron gun was used working with a value of 3 eV. The 1s level of hydrocarbon contaminant carbon (284.60 eV) was used as internal reference. The spectra were carried out on powder samples pressed on an insulating adhesive tape. The pressure in the analysis chamber averaged 5 x 10⁻⁹ mbar. The spectra were collected at several points in repeated samples in order to check the reproducibility (\pm 0.20 eV). The XPS peaks were deconvoluted using a peak-fitting routine. The lines used in the fitting of a peak envelope are defined according to their centered position, half-width, shape (Gaussian or Lorentzian distribution), and intensity. The best fit of the experimental curve by a tentative combination of bands were searched.

BET surface area was measured by Sorptomatic 1900 series (Carlo Erba Instruments) by nitrogen adsorption at liquid nitrogen temperature.

Laboratory Plant and Experimental Procedure. The laboratory plant had a total capacity of 50 NI/h. It schematically consisted of a dosing pump for VOC injection, a thermostated mixing chamber, an ozonizer, and an electrically heated tubular quartz reactor (Ragaini, V.; Bianchi, C.L.; Forcella, G.; Zanzottera, G.; Gervasini, A. *Proc. Int. School for Innovative Technologies for Cleaning the Environment*, 1993, in press.).

For each run 2 cm³ of catalyst in extrudate physical form was introduced in the reactor (700 mm long, with 200 mm isothermal zone, 15 mm i.d.). The reactor temperature, controlled by a programmer, was allowed to change at constant rate from ambient up to 600°C. The reaction was carried out at a space velocity of 20,000 h⁻¹ [(N cm³ air/h)/cm³ catalyst] (space velocity of 5,000 h⁻¹ was utilized in special runs) under a continuous stream of the reactant gas in air at atmospheric pressure. Dosed amounts of VOCs, as pure compounds as well as in mixtures, were mixed with air in the thermostated mixing chamber before being introduced in the reaction line. The VOC concentrations ranged from 250 to 2000 ppm (v/v).

The ozonizer (HRS Engineering, Italy) was set just before the catalytic reactor. Ozone was generated from air by electric discharge (i.e., corona effect). Typical runs was performed at fixed frequency (1000 Hz) and peak

voltage 15-20 kV. The ozone concentration at the inlet and at the outlet of the reactor was not quantitatively analyzed. However, from the characteristics of the ozonizer it is possible to know the amount of ozone generated. The ozone concentration ranged from 1 to 2 % (w/w) in air. Regarding the ozone concentration at the outlet of the reactor, it is well known that ozone thermally decomposes to oxygen; its half-life is dependent on temperature and on oxygen concentration (9). Taking into account the contact time of the reacting gases (0.2 s) and the reactor temperature (from 50 to 500°C) during the reaction, it is certain that ozone was quite absent at the outlet of the reactor.

The air stream outcoming from the reactor was analyzed by an on-line gas-chromatograph (Perkin Elmer, Sigma-115) equipped with a FID detector. The column, 1 m long, was packed with 1.75 % bentone 34 on 100/120 Supelcoport. For each run, a plot of the residue concentration of VOC vs. temperature was constructed.

Two traps, a cold trap for the collection of condensable products of incomplete combustion (PIC) and a silver sponge trap for trapping the hydrochloric acid vapors, were placed between the catalytic reactor and the gas-chromatograph.

Results and Discussion

Reactivity in the Combustion With and Without Ozone. The activity of the various catalysts was compared for the combustion of styrene and toluene. The reactions were performed under a continuous stream of reagents in air, varying the temperature from 100 up to 600°C.

Figure 2 shows the concentration profiles of styrene as a function of reaction temperature for the noble metal supported catalysts (PDL, PDH, PTL, and PTH) and for the mixed oxide catalyst (BCC). In the Figure, the points represent the lowest VOC concentration achieved at each temperature. All the catalysts displayed activity starting from 100°C. As expected, the noble metal catalysts showed the greater activity. However, the BCC catalyst could satisfactorily compare with the other ones. The TLV of styrene (50 ppm) was reached in the temperature range from 180 to 240°C according to the following catalyst activity order: PTH > PDH > PDL > PTL > BCC.

The analogous concentration profiles obtained for the combustion of toluene on BCC and FEO are reported in Figure 3. In this case, the catalysts did not show activity at temperatures lower than 250°C. Temperatures of 400 and 450°C were required to abate the toluene concentration below its TLV (100 ppm) with BCC and FEO, respectively. Higher temperatures were required to remove toluene with respect to styrene, being styrene more reactive because of its ethylenic double bond.

Among the studied catalysts, BCC was chosen to carry out the study of the effect of ozone in the catalytic destruction of chlorinated and non-chlorinated VOCs. This catalyst was more active than the other base metal oxide catalyst considered, FEO. On the other hand, the activity of BCC was not so far from the ones displayed by the noble metals, that were employed as high activity reference catalysts. Noble metals, even if more active, were not suitable for combustion reactions involving halogenated compounds, as they are severely deactivated by halogen atoms (4,8).

Copper-chromite catalysts are used in a variety of chemical processes, including hydrogenations, hydrogenolysis, hydrations, dehydrogenations, as well as oxidations (12,13). BCC is a typical copper-chromite catalyst containing a copper oxide and copper chromite spinel phase. A barium compound is added in the

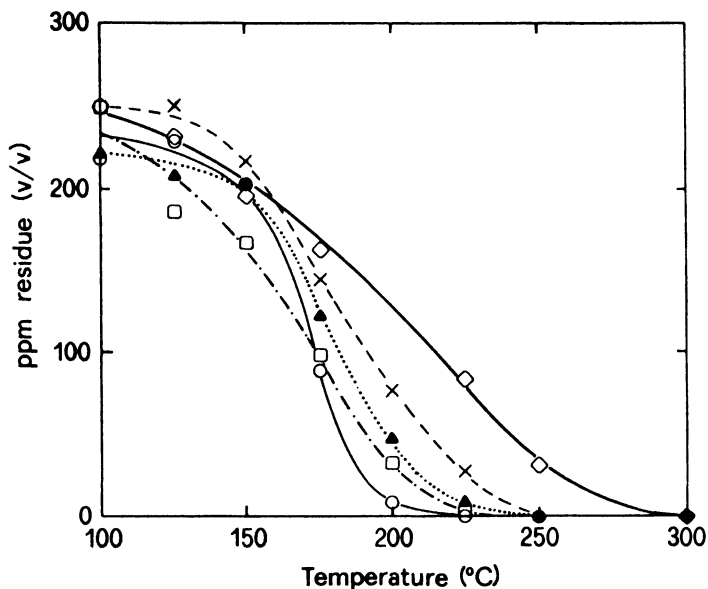


Figure 2. Concentration profiles of styrene during catalytic combustion without ozone on PDL (···▲···), PDH (··□··), PTL (·-X-), PTH (—○—), and BCC (—◇—) catalysts, as a function of temperature. Feed concentration, 250 ppm.

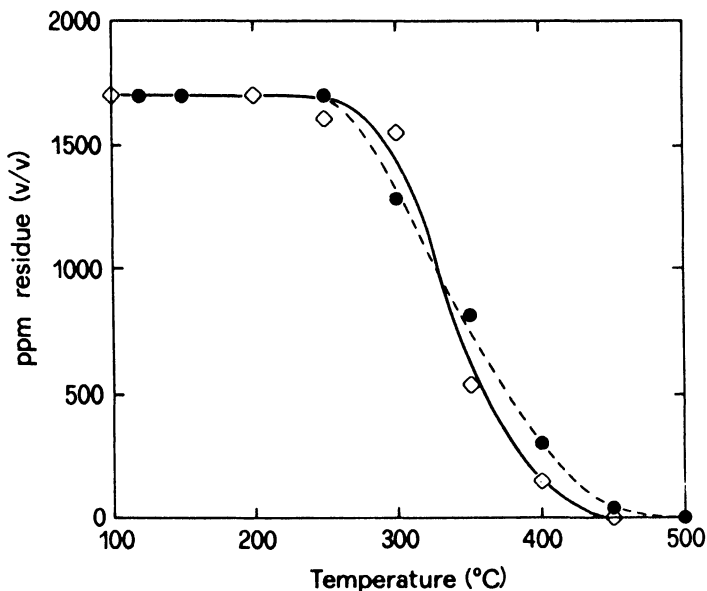


Figure 3. Concentration profiles of toluene during catalytic combustion without ozone on BCC (—◇—) and FEO (---●---) catalysts, as a function of temperature. Feed concentration, 1700 ppm.

formulation as a stabilizer. The catalyst activity is very sensitive to thermal treatment procedures in the various gas atmospheres, being that the surface Cu and Cr species are easily subjected to transformations of their oxidation states.

BCC was employed for the catalytic combustions in the as-received form and after calcination treatments in air at 450, 700 and 900°C. Table III reports the results of the combustion, performed both with and without ozone, of three VOCs of different chemical nature: an oxygenate (acetone), a hydrocarbon (toluene), and a halogenated (dichloromethane) compound. The thermal treatment of the catalyst caused a loss of activity in every case, particularly detectable when oxygen was utilized as oxidant. The most remarkable activity loss was observed after calcination of BCC at 700°C. Minor decreasing of the activity was observed after treating the catalyst at temperatures higher than 700°C. The behavior can be connected to changes in Cu and Cr oxidation states on the catalyst surface following the thermal treatment, as it will be described and discussed later.

Table III shows that the complete abatement of acetone was obtained at 250°C on as-received BCC, and at 300°C or more on air calcined BCC. For toluene, such a complete abatement occurred at temperatures around 300°C on both as-received and 450°C-calcined catalyst, whilst it was achieved at 400°C on the catalyst calcined at 700°C. On the contrary, the combustion of toluene was far from total at reaction temperatures up to 400°C when the calcination treatment was performed at 900°C. Dichloromethane, for which higher abatement temperatures were in any case necessary, was fully removed at temperature as high as 500°C. In this case, the catalyst thermal treatment at high temperatures (> 700°C) affected its activity to a lesser extent. It can be noticed on the basis of the data of Table III that the use of ozone always permitted to achieve higher VOC abatements.

To test the influence of ozone when used as oxidant, a series of combustion runs of a wider number of pure and mixed VOCs were performed. As-received BCC was employed, being more active than the calcined catalyst. Comparisons between the catalytic combustions with/without ozone on BCC catalyst, performed on a series of non-halogenated (14) and halogenated VOCs (Ragaini, V.; Bianchi, C.L.; Forcella, G.; Zanzottera, G.; Gervasini, A. *Proc. Int. School for Innovative Technologies for Cleaning the Environment*, 1993, in press.), were previously reported. In these studies, the effect of the electric discharge in air to generate ozone, as a function of the used peak voltage, on the decomposition of various VOCs was also discussed.

In Figure 4, the temperatures required to achieve 50 % destruction of three hydrocarbons, one oxygenate and four chlorinated organics with or without ozone are compared. The abatement of aromatic and chlorinated compounds was strongly affected by ozone, whilst acetone was poorly affected. Styrene, dichloromethane and p-chlorotoluene were found to be particularly sensitive to the presence of ozone. In fact, even at temperatures lower than 50°C, they were 50 % abated. Not only the nature of VOC but their concentration too is an important parameter in order to obtain better abatements when using ozone instead of oxygen. As discussed in Ref. 14 the use of ozone as oxidant was particularly powerful at low VOC concentration (i.e., < 1000 ppm). Decreasing the VOC concentration, the [VOC]/[O₃] ratio increases, leading to an increase of attack points of O₃ on VOC molecule.

Table III. Catalytic Activity of BCC Catalyst in the Combustion of Three VOCs With and Without Ozone as a Function of Catalyst Treatment

H. T. T. ^a of Catalyst	none	450°C	700°C	900°C				
Reaction temperature (°C)	% Conversion (v/v)							
	without ozone		with ozone		without ozone		with ozone	
<i>Acetone</i> (feed 1300 ppm)								
60	0	20.7	0	0	0	0	0	0
100	0	22.5	0	15.0	0	0	0	0
200	65.5	66.2	33.4	61.0	13.1	37.5	18.5	31.6
250	100	100	82.4	93.5	74.0	85.5	71.4	83.6
300	100	100	100	100	100	100	98.6	99.0
400	100	100	100	100	100	100	100	100
<i>Toluene</i> (feed = 570 ppm)								
120	0	46.0	-	-	0	28.2	0	29.6
140	0	65.4	5.3	55.0	-	-	0	38.3
200	64.6	84.2	14.0	64.9	0	30.9	9.3	70.0
260	89.6	95.6	82.1	88.4	23.0	52.4	33.9	77.2
300	96.5	100	97.4	99.3	60.2	80.3	53.3	89.6
400	100	100	100	100	96.4	99.1	84.8	98.7
<i>Dichloromethane</i> (feed = 500 ppm)								
100	0	42.8	0	25.0	0	25.8	0	25.0
200	7.8	57.4	13.8	35.2	0	29.8	3.2	37.2
300	55.2	87.4	60.2	66.0	19.2	36.8	16.6	41.8
400	96.2	98.0	94.8	97.0	58.6	78.6	69.6	83.8
450	100	99.4	99.0	99.4	82.4	89.8	91.2	95.4
500	100	100	100	100	95.0	97.0	95.2	98.0

^a H.T.T. = High Temperature Treatment.

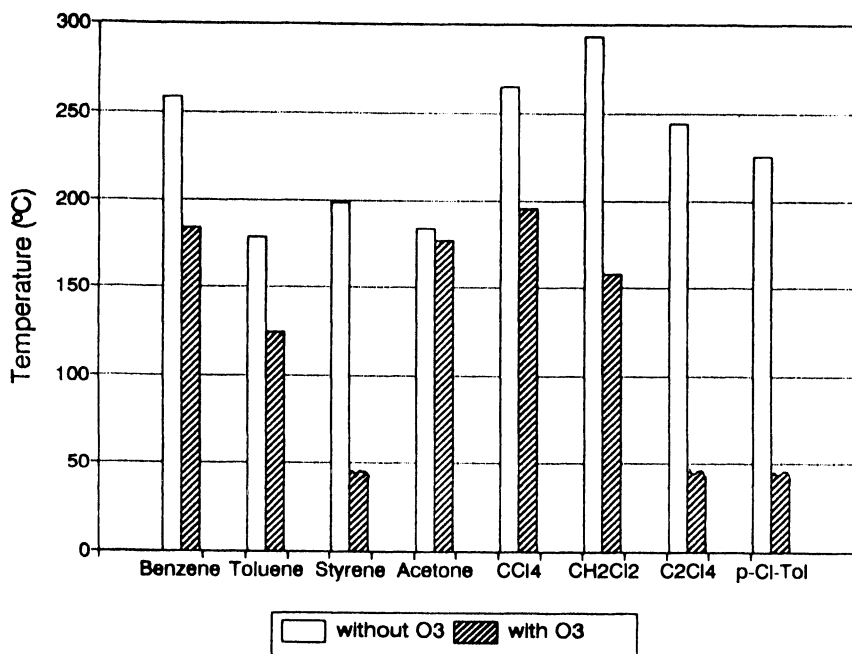


Figure 4. Comparison of the temperatures required to achieve 50 % abatement by catalytic combustion with and without ozone on a series of pure VOCs on BCC catalyst in as-received state. Feed concentrations: benzene, 1000; toluene, 1000; styrene, 250; acetone, 1100; carbontetrachloride, 1000; dichloromethane, 500; tetrachloroethylene, 1000; p-chlorotoluene, 250 ppm.

The catalytic combustion profiles of a ternary mixture of toluene, acetone, and dichloromethane in relative amounts 1:2:1, respectively, for a total feed of 2370 ppm of the organic mixture are compared in Figure 5 with the profiles of the relevant pure compounds fed separately in the same amount as in mixture.

In the runs without ozone (Figure 5 a), the three organics lay roughly on a unique curve. Only the chlorinated compound was abated with little more difficulty. This one was destroyed at lower temperatures when fed in mixture than when it was fed as pure compound. On the contrary, pure toluene and acetone were better abated than in mixture.

A different behavior was observed in the catalytic combustions performed with ozone (Figure 5 b). In the mixture, toluene was preferentially destroyed with respect to acetone and dichloromethane. Both toluene and acetone were more easily abated when fed as pure compounds than as VOC mixture. In the combustion with ozone, dichloromethane was abated at lower temperatures when it was as pure compound, because the other organics, in particular toluene, successfully competed in the reaction with ozone.

Pure toluene was found to be easier abated, with or without ozone, than in mixture also with other organic compounds, for instance, hydrocarbons as benzene, styrene, and cyclohexane.

During the combustion of chlorinated organics the formation of hydrochloric acid and chlorine could be effective. A silver sponge trap was placed after the reactor to block these products. After the reaction the silver sponge was weighted; appreciable gain of mass was not detected in any case.

XPS Characterization. Considerable dispute exists with regard to the identity of the active species in copper chromite catalysts. Depending upon the type of application, different active species have been claimed (15). This suggested that we performed a detailed XPS analysis on BCC catalyst.

BCC catalyst was initially characterized in the as-received state followed by characterization after calcination treatments in air at 450, 700, and 900°C.

The Cu(2p_{3/2}) spectra of BCC catalyst are shown in Figure 6. In the as-received state, two distinct Cu species were detected by deconvoluting the experimental curve. At higher binding energies (B.E.), a Cu(II) species was detected. It can be assigned to either CuO or Cu(OH)₂ on the basis of its energy value, 934.5 eV (15,16). A second Cu species at lower B.E. (932.4) was assigned to Cu(I) species. After calcinations at 450 and 700°C, a broad and lower-B.E. peak was observed in the B.E. region of the Cu(II) species, indicating the presence of unstable copper species. Upon calcination at 900°C, the sole presence of a Cu(I) species was revealed. This is in agreement with what is known about the trend of copper to reduce itself to lower oxidation states during high temperature treatments.

Cr(2p_{1/2}, 2p_{3/2}) XP spectra of BCC catalyst are reported in Figure 7 as a function of catalyst heat treatment. Cr(III) was the dominant species present on BCC catalyst in the as-received state as well as after the calcination treatments, (B.E. = 576.5). The presence of Cr(VI) species was detected at higher B.E., 579.3 eV, on the as-received BCC catalyst and after the calcinations at 450 and 700°C. After calcination at 900°C, the Cr(VI) species disappeared. Clearly, Ba stabilized the Cr(VI) state under conditions where it would normally decompose. In fact the thermal decomposition of CrO₃ into Cr₂O₃ is known to occur with only gentle heating.

The deep modifications that were observed when comparing the activity of BCC in the as-received form and after thermal treatment at 450°C with the

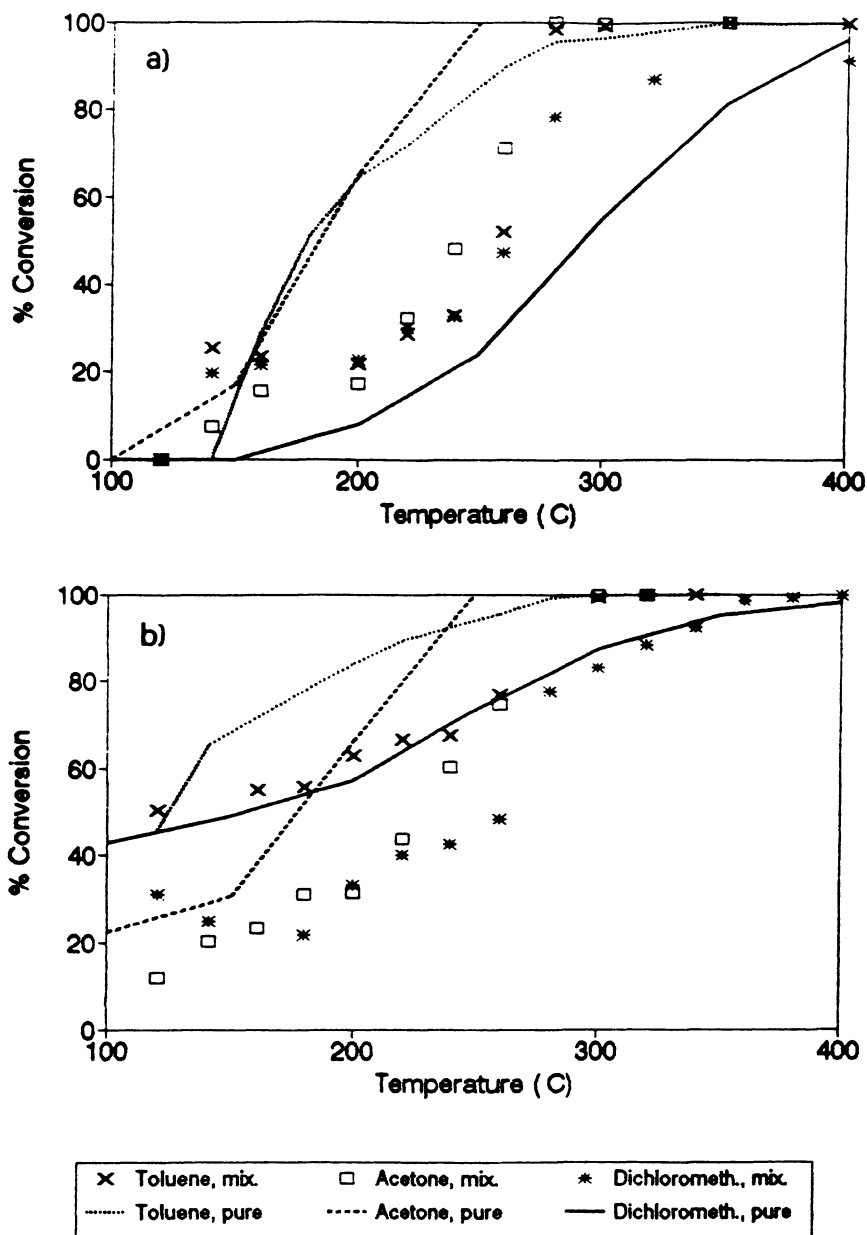


Figure 5. Comparison of toluene, acetone, and dichloromethane catalytic combustion on BCC catalyst, in as-received form, as pure compounds and as ternary mixture (Feed concentrations: toluene, 570; acetone, 1300; dichloromethane, 500 ppm), without ozone (a) and with ozone (b).

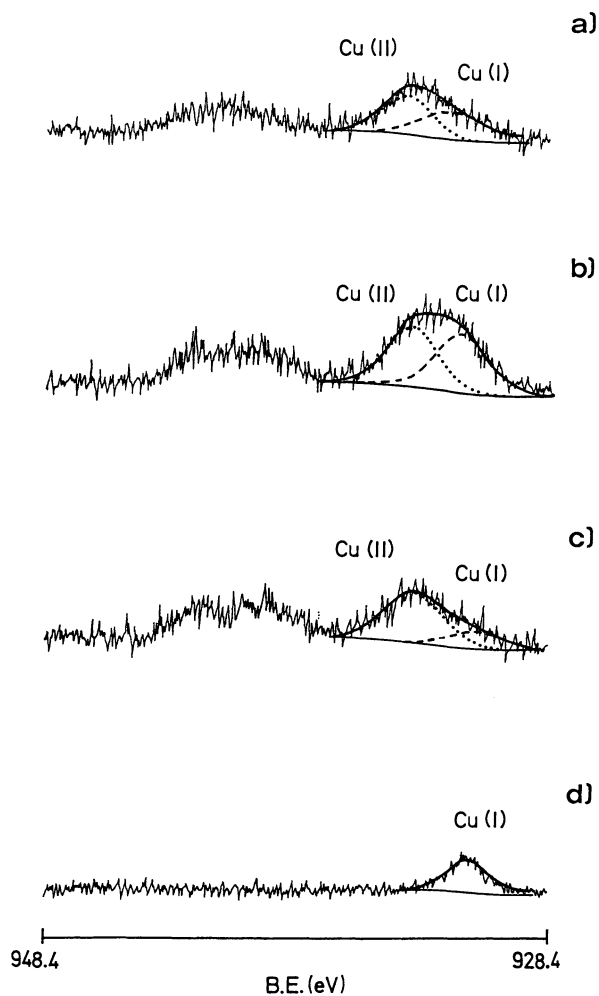


Figure 6. Cu($2p_{1/2}$, $2p_{3/2}$) spectra for BCC catalyst in the as-received state (a), after calcination at 450°C (b), 700°C (c), and 900°C (d).

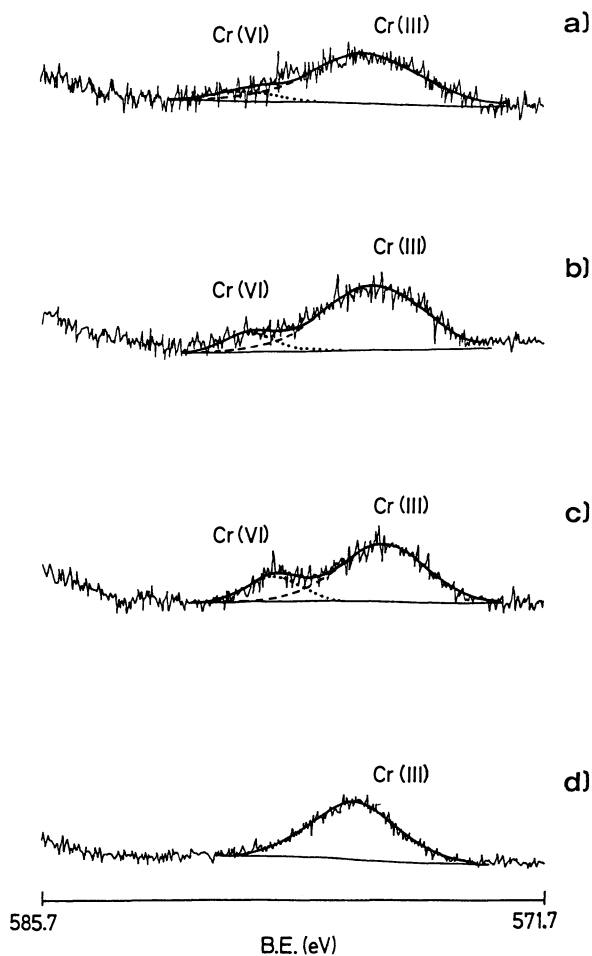


Figure 7. Cr(2p_{1/2}, 2p_{3/2}) spectra for BCC catalyst in the as-received state (a); after calcination at 450°C (b), 700°C (c), and 900°C (d).

activity of BCC treated at higher temperatures (700 and 900°C) apart from the type of VOC (Table III) can be connected to the changes of the Cu surface species rather than to changes of Cr species, as detected by XPS analysis. A definite amount of Cu(I) and Cu(II) species seems to be an important requirement to obtain a high activity combustion catalyst. Regarding the Cr species, important modifications on the catalyst surface could not be detected following the thermal treatments up to 700°C. The disappearance of Cr(VI) and Cu(II) species on BCC calcined at 900°C did not cause a further decrease of the catalytic activity in every case.

XP spectra of the used BCC catalyst, after toluene combustion with ozone, in the as-received form and after thermal treatment at 900°C, were collected too. The peak area ratios of Cr(III) to Cr(VI), and of Cu(I) to Cu(II) species, permitted a comparison between the fresh and used catalyst. The Cr(III)/Cr(VI) ratio in as-received BCC decreased from 12 to 7 going from the fresh to the used catalyst, whilst the Cu(I)/Cu(II) ratio decreased from 4 to 0.6. An analogous increase of Cr(VI) and Cu(II) species was observed for the used 900°C-calcined catalyst. In this case, the Cr(III)/Cr(VI) and the Cu(I)/Cu(II) ratio were 4 and 0.2, respectively.

The observed surface oxidation of catalyst after use can be ascribed to the oxidant ozone power. This behavior can indicate that the oxidant action of ozone occurs not only in the gaseous phase but also on catalyst. Ozone decomposition probably gives rise to the formation of active oxygen radicals on the catalyst surface.

Micropollutant Analysis. It is well known that the catalytic combustion of halogenated organics minimizes the possibility of production of hazardous products of incomplete combustion (PIC), such as polychlorodibenzodioxines (PCDDs) and polychlorodibenzofurans (PCDFs), with respect to thermal processes (2). However, the formation of Cl₂ instead of HCl, when not sufficient hydrogen is present in the feed, as organic matter and/or water vapor, can increase the possibility of formation of such pollutants (17).

Two possibilities can be invoked to explain the formation of PCDFs and PCDDs (18): i) the formation of chemically similar precursor substances, such as chlorinated phenols, during the combustion process, ii) *de novo* synthesis from chemically different precursor compounds and sources of chlorine during the combustion.

The formation of PCDD and PCDF compounds could be effective in particular when mixtures of halogenated and aromatic VOCs are destroyed. Moreover, the presence of ozone, used as oxidant, that is more able than oxygen to form cyclic ozonide structures (9,10), could favor the formation of PCDDs and PCDFs.

To investigate this possibility, PCDDs and PCDFs were searched among the products of the catalytic combustion of a benzene and tetrachloroethylene mixture performed with ozone. The reaction was carried out at 350°C by feeding 1000 ppm of a 1:1 molar mixture (10 NI/h) at space velocity of 5000 h⁻¹. The gas outstreaming the reactor was condensed in a cold trap during 134 h. As concerns the PCDD compounds, only pentachlorodibenzodioxine and heptachlorodibenzodioxine were found at a concentration of 0.445 and 0.230 ng/Nm³, respectively. Tetrachlorodibenzodioxine, the most toxic dioxine (relative toxicity 1 according to the German Office of Health), and hexachlorodibenzodioxine (relative toxicity 0.001), were absent. Regarding the PCDF compounds, pentachlorodibenzofuran, hexachlorodibenzofuran, heptachlorodibenzofuran, and octachlorodibenzofuran were found at a concentration of 0.592, 0.466, 0.308, and 0.538 ng/Nm³, respectively. Tetrachlorodibenzofuran was absent.

The results show a reassuring situation. The most toxic dioxines and furans (i.e., the tetrachlorodibenzodioxine and tetrachlorodibenzofuran) were not found among the products of combustion. The sum of all the dioxine and furan compounds is 2.58 ng/Nm³. This value is about three order of magnitude less than the limits for the emission of such pollutants in air. Moreover, the very low amount of PCDD and PCDF compounds produced during the combustion can suggest that a low amount of free chlorine is released during the combustion. HCl or HClO, from chlorine and water reaction, could be the main chlorinated products formed.

Conclusions

The innovative technique employed in this work, in which the catalytic removal of VOCs is assisted by ozone, appears really efficient to remove pure as well as mixed VOCs at low temperature. The decrease of reaction temperature leads to a remarkable reduction of energy consumption. In fact, by a comparison between the energy needed to generate ozone (i.e., 5-10 Wh/m³ air) and the energy saved by using ozone, in terms of decreasing of reaction temperatures, it results that an amount of 10-15 Wh/m³ of energy was saved, depending on the type of VOC oxidized.

The technique is particularly useful for the treatment of medium-low VOC concentrations in air. It is noteworthy the efficiency of this coupled technique also for the removal of halogenated organics without the formation of toxic micropollutants.

Acknowledgments

Acknowledgment is due to the Istituto Mario Negri of Milano (Italy) and particularly to Dr. E. Benfenati and Dr. R. Fanelli who performed the analyses of furans and dioxines.

The authors are grateful to Engelhard Industries Italy for supplying the catalysts.

Literature Cited

1. Barresi, A.; Mazzarino, I.; Ruggeri, B. *La Chimica e l'Industria* **1989**, *71*, 64.
2. Barresi, A. *Acqua Aria* **1991**, *7*, 649.
3. Spivey, J.J. In *Catalysis*; Bond, G.C.; Webb, G., Eds.; Royal Society of Chemistry, Cambridge, 1989; Vol. 8, pp 157-203.
4. Lester, G.R. *82nd Air & Waste Management Association Ann. Mtg.*, 1989.
5. Noordally, E.; Richmond, J.R.; Tahir, S.F. *First Eur. Work. Mtg. Environmental Industrial Catalysis*, 1992, p 175.
6. Mazzarino, I.; Barresi, A. *First Eur. Work. Mtg. Environmental Industrial Catalysis*, 1992, p 149.
7. Hermia, J.; Vigneron, S. *First Eur. Work. Mtg. Environmental Industrial Catalysis*, 1992, p 161.
8. Hung, S.L.; Pfefferle, L.D. *Environ. Sci. Technol.* **1989**, *23*, 1085.
9. Kirk-Othmer *Encyclopedia of Chemical Technology*, 3rd ed.; Wiley: New York, 1980; Vol. 16, p 683.
10. Razumovskii, S.D.; Zaikov, G.E. *Ozone and Its Reactions With Organic Compounds*, Studies in Organic Chemistry 15; Elsevier: Amsterdam, 1984.
11. Sax, N.I. *Dangerous Properties of Industrial Materials*; Van Nostrand Reinhold: New York, 1983, 6th ed.
12. Grimblot, J.; Gengembre, L.; D'Huysser, A. *J. Electron. Spectrosc. and Relat. Phenom.* **1990**, *52*, 485.

13. Engelhard Corporation, *Raising Performance Standards in Base Metal Catalysts*, 1991.
14. Ragaini, V.; Bianchi, C.L.; Forcella, G.; Gervasini, A. In *Trends in Ecological Physical Chemistry*; Bonati, L.; Cosentino, U.; Lasagni, M.; Moro, G.; Pitea, D.; Schiraldi, A., Eds.; Elsevier: Amsterdam, 1993; p 275.
15. Schreifels, J.A.; Rodero, A.; Swartz, W.E., Jr. *Applied Spectrosc.* **1979**, *33*, 380.
16. Bianchi, C.L.; Cattania, M.G.; Ragaini, V. *Surf. Science Technol.* **1992**, *19*, 533.
17. Gullett, B.K.; Bruce, K.R.; O'Beach, L. *Waste Management and Research* **1990**, *8*, 203.
18. Jay, K.; Stieglitz, L. *Chemosphere* **1991**, *11*, 987.

RECEIVED September 30, 1993

Chapter 30

Other Opportunities for Catalysts in Environmental Problems: An Overview

John N. Armor

Air Products & Chemicals, Inc., 7201 Hamilton Boulevard,
Allentown, PA 18195

The actual number of applications of catalysis to solve environmental problems is quite large (1). A number of topics were only touched upon in this symposium, and those manuscripts are grouped together within this section of the book. Topics which were not discussed at all within this Symposium included: catalysts for the preparation of HFCs as replacements for CFCs, removal of ozone emissions; removal of nitrous oxide; destruction of toxic gases such as nerve gas; alternative catalytic technology to displace the use of chlorine-based intermediates in chemical synthesis and processing; and waste minimization.

With the implementation of the Clean Air Act Amendments of 1990, there are intense efforts by companies that produce or consume chemicals to reduce the amount of chemical waste they generate. Where even small amounts of multiple by-products are produced, at a multi-million pound per year scale, these by-products can become sizable in volume (see Table I). Disposal costs or imposed reduction of waste by local regulations will force suppliers and users to minimize the generation of waste. Alternatively, one can try to avoid undesirable by-products by developing new process routes or finding ways to convert these "wastes" into marketable products. For example a process which uses formaldehyde, a known carcinogen, is now much less desirable than one which uses alternative C₁ feedstocks (e.g., methanol, CO/H₂, etc.).

There are a number of processes for removing SO_x from exhaust streams. The problem is there is still no universally acceptable solution. Figure 1 shows the atmospheric sulfur cycle showing the number of ways sulfur enters the atmosphere (3). In the atmosphere SO_x contributes to atmospheric pollution and smog. It is a major contributor to acid rainfall. Current commercial approaches to remove SO_x from stack gas exhausts produce large quantities of sulfur by-products which need to be sold or buried. Large amounts of elemental sulfur are produced by petroleum refineries in the process of desulfurization of petroleum feedstocks. In the United States, the preference for burial of waste has come under increasing economic pressure as the availability of

0097-6156/94/0552-0372\$08.00/0
© 1994 American Chemical Society

In Environmental Catalysis; Armor, J.;
ACS Symposium Series; American Chemical Society: Washington, DC, 1994.

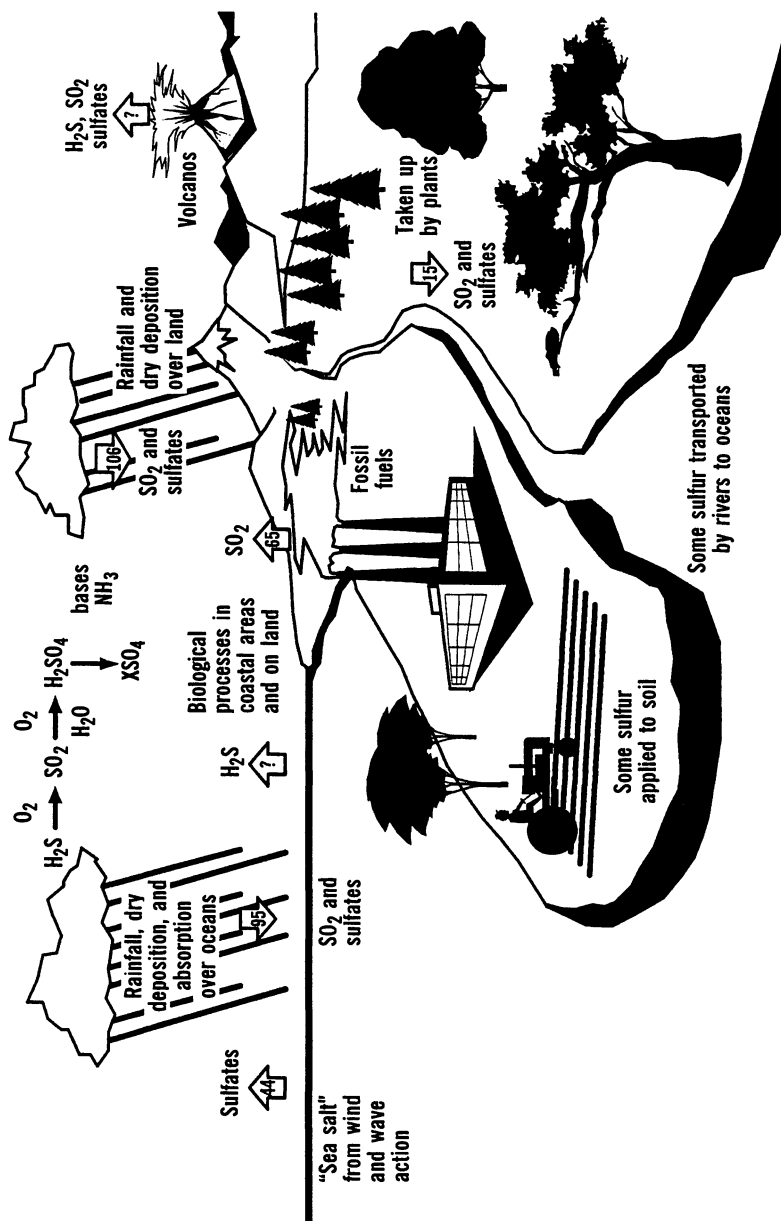


Figure 1. The atmospheric sulfur cycle. (Reproduced with permission from reference 3. Copyright 1991 Lewis Publishers, a subsidiary of CRC Press)

Table I. Production of by-products

Product	Kg of By-product per Kg of products	Product (tons)
Oil Refinery	~0.1	$10^6 - 10^8$
Bulk Chemicals	<1 - 5	$10^4 - 10^6$
Pharmaceuticals	25 - 100	$10 - 10^3$
Fine Chemicals	5 - 50	$10^2 - 10^4$

(Reprinted with permission from reference 2. Copyright 1992 Society of Chemical Industry.)

acceptable disposal sites diminishes and as society becomes less tolerant of "throw away" disposal approaches. We need to produce a more valuable, marketable sulfur by-product or develop more efficient technologies for treating the sulfur waste.

Among the manuscripts within this book are two papers that focus on specific approaches to removal of sulfur oxides and the intermediates involved. They represent only a sampling of a great deal of work on this topic; yet there is a need for much more because the problem has no clear solution. In addition there are two other papers dealing with niche opportunities for catalysis. Robert Farrauto of Engelhard summarized these papers as follows: "*Catalytic Bromine Recovery From HBr Waste* by P. F. Schubert, R. D. Beatty, and S. Mahajan: A new catalyst and process for the oxidation of HBr to Br₂, and its subsequent recovery was described. The unidentified catalyst functions below 300°C, and the process utilizes multitubular heat exchangers to control the large reaction exotherms. The process has been satisfactorily demonstrated in a pilot plant reactor for over 600 hours. Commercialization is planned. *Application of Supported Gold Catalysts in Environmental Problems* by S. Tsubota, A. Udea, H. Sakurai, T. Kobayashi and M. Haruta: This investigation reported on the use of gold supported on Fe₂O₃ containing supports for low temperature oxidation of CO and select hydrocarbons. Other gold containing catalysts were found active for NO reduction with CO (using Co₃O₄ as a support) and the hydrogenation of CO₂ (using ZnO and TiO₂ as supports).

References

1. Armor, J. N. *Appl. Catal. B*, **1992**, *1*, 221-256.
2. Sheldon, R. A. *Chem. Ind.*, December 7, 1992, pp. 903-906.
3. Environmental Chemistry; Manahan, S. E., Ed.; 5th Ed., Lewis Publishers, Boca Raton, FL, 1991, p. 271.

RECEIVED November 16, 1993

Chapter 31

Reduction of SO₂ to Elemental S over Ceria Catalysts

Wei Liu and Maria Flytzani-Stephanopoulos

Department of Chemical Engineering, Massachusetts Institute of Technology, Cambridge, MA 02139

Bulk cerium oxide, pure or doped with other rare earth oxides is a good catalyst for the reduction of SO₂ with CO to elemental sulfur at temperatures above 500 °C. The production of COS is negligible over these catalysts when a feed gas of stoichiometric composition([CO]/[SO₂]=2) is used. The effect of dopant oxides on the catalytic activity of ceria is correlated with the change of oxygen ionic conductivity and vacancy energetics that the dopants impart into the ceria lattice. The highest activity is observed with a CeO₂ catalyst doped with 1 at % La₂O₃. Effects of water vapor on the catalyst activity and selectivity are discussed.

Desulfurization of combustion exhaust gases is presently a costly process often involving complex flow sheets and "throw-away" sorbents. Directly reducing sulfur dioxide to elemental sulfur over a catalyst is attractive, because it produces a salable product without any solid waste to dispose of. Several processes have been proposed and developed over the last twenty years. The Allied Chemical catalytic SO₂ reduction with natural gas was applied to SO₂-rich(>5%) smelter off-gases(1). Direct flue gas reduction by synthesis gas over an undisclosed catalyst is under development by the Parsons Company(2). However, both processes require an expensive Claus plant to complete the elemental sulfur recovery.

Other processes under development are two-stage, dry regenerative flue gas cleanup processes, whereby dilute-SO₂ streams are scrubbed in a metal oxide sorber and then, in the regenerator the spent sorbent is regenerated for re-use with concomitant emission of a concentrated SO₂ stream

suitable for sulfur recovery. The regenerator-off gas has only a fraction of the flue gas volume, and contains no oxygen. Recovery of sulfur from this type gas in a single-stage catalytic converter, avoiding the multistage Claus plant, would decrease the cost and accelerate the commercialization of the dry regenerative flue gas cleanup process.

The direct reduction of SO_2 by CO to elemental sulfur is thermodynamically favorable but it proceeds very slowly in the absence of a catalyst. A secondary undesirable reaction can occur between CO and elemental sulfur forming COS, which may also reduce SO_2 to elemental sulfur through reaction 3. COS is more toxic than SO_2 and its production should be minimized in a sulfur recovery process.



Although reaction 1 has considerable background, no substantial commercial experience exists and only some laboratory studies have been reported. Ryason and Harkins(3) tested Cu, Pd, Ag, Co or Ni supported on alumina as catalysts for the simultaneous reduction of SO_2 and NO by CO. The SO_2 reduction by CO on $\text{Fe}/\text{Al}_2\text{O}_3$ and $\text{Cu}/\text{Al}_2\text{O}_3$ catalysts was extensively studied by Khalafalla, et al(4,5) and Short, et al (6,7), respectively. Bazes et al(8) investigated the perovskites LaCoO_3 and CuCo_2O_4 , and the oxide mixture $\text{CeO}_2\text{-Co}_3\text{O}_4$ as catalysts for the same reaction. The production of COS usually proceeds to a substantial extent on these catalysts. Happel et al(9,10) lowered the COS formation rate by using the perovskite LaTiO_3 . More recently, Hilbert and Campbell(11,12) found that $\text{La}_{1-x}\text{Sr}_x\text{CoO}_3$ is an active catalyst for SO_2 reduction by CO. The highest selectivity toward elemental sulfur was obtained on a catalyst with $x=0.3$.

In addition to the formation of COS during the SO_2 reduction by CO, the presence of water in the feed gas has a major effect on both the catalytic activity and selectivity. The water may poison the catalyst and participate in the reactions, for example, the water-gas shift reaction. It was reported(5,7) that water significantly poisoned the $\text{Cu}/\text{Al}_2\text{O}_3$ and $\text{Fe}/\text{Al}_2\text{O}_3$ catalysts, and also lowered the reaction selectivity toward elemental sulfur. The water vapor effects on the other catalysts previously studied, however, have not been reported.

The redox reaction mechanism has been proposed for the SO_2 reduction by CO(10, 12). According to this mechanism, the reductant removes oxygen from the catalyst surface while the oxidant gives up its oxygen to the catalyst, so that the catalyst surface is constantly reduced/oxidized during the course of the reaction. Bulk cerium oxide

has been identified as an active catalyst for the SO₂ reduction in our previous work(13). It is well known that CeO₂ has high oxygen vacancy and mobility, and these properties can be further enhanced by doping other metal ions into its fluorite-type crystal lattice. The present studies attempt to test if the catalytic activity of CeO₂ can be improved by incorporating dopant ions into its lattice, and to explore other CeO₂-containing catalysts.

Experimental

Apparatus and Procedure. All catalysts were tested in a laboratory-scale, packed bed flow reactor, which consists of a 1.0 cm I.D. x 50 cm long quartz tube with a porous quartz frit placed at the middle for supporting the catalyst. The reactor tube is heated by a Lindberg furnace. The reaction temperature is monitored by a quartz tube sheathed K-type thermocouple placed at the top of the packed bed and controlled by a Wizard temperature controller. The reacting gases, all certified calibration gas mixtures balanced by helium(Matheson), are measured with rotameters and mixed prior to the reactor inlet. The resulting gas mixture flows downward through the packed bed. Water vapor is introduced with helium bubbling through a heated water bath. The pressure drop of gas flowing through the assembly is small. Thus, experiments were carried out under nearly atmospheric pressure. A cold trap attached at the outlet of the reactor is used to collect the elemental sulfur from the product stream. The product gas stream, free of sulfur and particulates, is analyzed by a HP5880A Gas Chromatograph(GC) with a Thermal Conductivity Detector(TCD). Helium is used as the GC carrier and reference gas, each at 30 cc/min. The detector and oven temperatures are set at 200 °C and 60 °C, respectively. A 1/4" O.D. x 6' long packed column of Chromosil 310(from SUPELCO) provides good separation of CO, CO₂, COS, H₂S, CS₂, and SO₂ under these conditions. The TCD shows linear response to all the compounds mentioned above and a detection limit of less than 100 ppm by volume.

The fresh and used catalysts were typically activated by heating for one hour in 10% CO/He at 600 °C. After activation, the reacting gases were introduced and the reaction temperature was raised to about 650 °C. When a steady-state reaction was reached, the temperature was lowered in steps of about 50 °C until the reaction was quenched. In catalysts evaluation test, the inlet gases of 1 vol % SO₂ and 2 vol % CO were used, while the total flow rate was kept at 200 sccm. The packed height of catalyst bed was around 7 mm and the contact time was 0.01 to 0.05 g.s/cc(STP). The elemental sulfur yield, i.e., the fraction of inlet SO₂ converted into elemental sulfur, was derived from the material balance of carbon and sulfur, and occasionally checked by titration of the sulfur collected in the cold trap.

Catalyst Preparation. All bulk catalysts were prepared by the well-known amorphous citrate method(14) from nitrate precursors(from Aldrich). This method provides well dispersed mixed oxides or mixed oxide compounds. The catalyst prepared in this way has large fraction of macropores(>1 mm in diameter) which facilitates pore diffusion. The preparation procedure is outlined as follows: metal nitrates and citric acid of molar ratio one are dissolved in de-ionized water, separately; the citric acid solution is added into the nitrate solution dropwise under constant magnetic stirring; the resulting mixed solution is concentrated into a viscous fluid in a rotary evaporator(70 - 80 °C); the viscous fluid is then transferred on a dish in a vacuum oven where a solid foam is formed during overnight drying(70-80 °C, 15 KPa); the solid foam is calcined at 600 °C in a muffle furnace under flowing air for 2-3 hours; the resulting solid is crushed and sieved; Particles between 20 to 35 mesh(420-840 μm) are typically used in the tests. The supported catalysts were prepared by the conventional wet impregnation method. The slurry of the support and metal nitrate solution was degassed in vacuum so that the nitrate solution fully filled the pores of the support during impregnation. The impregnated catalyst was dried for 10 hours at 100 °C and then calcined for 3 hours at 600 °C. The catalysts tested in this study are shown in Table I.

The catalysts were characterized by X-ray powder diffraction (XRD) for crystalline phase identification and BET -N₂ desorption for surface area measurement. Well crystallized CeO₂ phase was identified by XRD. The XRD analysis and surface area measurement were performed on a Rigaku 300 X-ray Diffractometer and FlowSorb II 2300 Micromeritics, respectively.

Results and Discussion

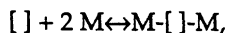
CeO₂ Catalyst. Figure 1 shows the experimental results of SO₂ reduction by CO on the bulk CeO₂ catalyst prepared in this work(Table I). When a feed gas of lower CO content than the stoichiometric was used, any SO₂ reacted was converted into elemental sulfur. When the CO content exceeded the stoichiometric amount, 100% SO₂ conversion was achieved at lower reaction temperature, but COS became a major product. For example, when the CO to SO₂ ratio was 3, the SO₂ conversion was 100 % with 36 - 62 % yield of elemental sulfur over the temperature range of 530 to 700 °C and corresponding 64 - 38 % of COS yield. The elemental sulfur yield increased with the reaction temperature.

In the following discussion and figures, only the elemental sulfur yield will be presented. Because a feed gas of nearly stoichiometric composition was used and the COS formation was always negligible in these studies, the elemental sulfur yield corresponds with the SO₂ conversion.

Doped CeO₂ Catalysts. It is well known that the oxygen vacancy and mobility of CeO₂ can be enhanced by introducing di- or tri-valent metal

ions into its lattice. Y₂O₃ dopant was studied by Wang, et al(15). Some of their results are listed in Table II. Both the oxygen ionic conductivity and activation enthalpy varied with the Y₂O₃ dopant concentration. 1% Y₂O₃ dopant generated the highest oxygen conductivity and the lowest activation enthalpy. Y₂O₃-doped cerium oxide catalysts (Table I) were prepared and tested in this work. Figure 2 shows the effect of the Y₂O₃ dopant on the catalyst activity. The 1% Y₂O₃ doped ceria catalyst (CeO₂(Y)) showed higher activity than either the pure CeO₂ or a 10% Y₂O₃-doped ceria (CeO₂(10Y)). Thus, more than 95% elemental sulfur yield was obtained over the CeO₂(Y) at 600 °C, that is, at 50 °C lower temperature than for the other two catalysts.

When two tri-valent metal ions are introduced in the CeO₂ crystal structure, one oxygen vacancy is created,



where [] and M denote the oxygen vacancy and trivalent dopant cation, respectively. The dopant ion and created oxygen vacancy form energetically associated pairs as denoted by M-[]-M. Different dopants will bring about different crystal structure change and interaction of vacancy-ion pair, thus resulting in different oxygen mobility. Table III lists some experimental results from the studies by Gerhardt-Anderson and Nowick(16), together with the calculated association enthalpy by Butler, et al(17). The 1% Sc₂O₃ dopant in CeO₂ generated the strongest vacancy-ion association and had the lowest oxygen conductivity among trivalent ion-doped ceria. The CeO₂(La) had comparable oxygen conductivity to CeO₂(Y) at low temperature, but had a little lower association enthalpy than the CeO₂(Y). The experimental results of SO₂ reduction by CO on the bulk cerium oxide catalyst doped with these elements are compared in Figure 3 on the same total surface area basis. More than 95% sulfur yield was obtained at 600 °C for all three catalysts. When the reaction temperature was lowered, the sulfur yields on the CeO₂(Sc) and CeO₂(La) catalysts fell off steeply at about 600 °C and 560 °C, respectively, while the sulfur yield on the CeO₂(Y) catalyst decreased gradually from 600 °C. The CeO₂(La) catalyst showed the highest activity.

Shown in Figure 4 is the light-off behavior of the reaction of SO₂ with CO over different catalysts. For this study, we started with the fresh catalyst without any pretreatment by a reducing agent and raised the reaction temperature from 500 to 700 °C in a 50 °C-step, holding at each temperature for half an hour. The reaction was lighted off at the same temperature (around 650 °C) over all the La₂O₃-doped ceria catalysts, independent of dopant content and the amount of catalyst used. But, the reaction did not light-off on the CeO₂(Sc) catalyst even at temperatures as high as 690 °C. After one-hour heating under reacting atmosphere at 690

Table I. Catalysts Tested in This Study

No.	Catalyst	Composition ^a	Surface Area (m ² /g)	
			fresh ^b	used ^c
1.	CeO ₂	CeO ₂	34.0	29.0
2.	CeO ₂ (Y)	1 at % Y ₂ O ₃	27/23 ^d	9.5/20 ^d
3.	CeO ₂ (10Y)	10 at % Y ₂ O ₃	19.8 ^d	19.3 ^d
4.	CeO ₂ (Sc)	1 at % Sc ₂ O ₃	47/30 ^d	30/27 ^d
5.	CeO ₂ (La)	1 at % La ₂ O ₃	34.0	19.5
6.	CeO ₂ (6La)	6 at % La ₂ O ₃	32.6	22.8
7.	CeO ₂ (20La)	20 at % La ₂ O ₃	37.5	19.4
8.	CeO ₂ (35La)	35 at % La ₂ O ₃	28.8	17.2
9.	CeO ₂ (5Mg+La)	1 at % La ₂ O ₃ + 5 at % MgO	30.2	22.4
10.				
11.	Cu/CeO ₂ (La)	1.4 wt % Cu	31.4	25.0
12.	Co/CeO ₂ (La)	3.4 wt % Co	30.0	23.0
	Mn/CeO ₂ (La)	1.4 wt % Mn	31.0	24.5

^a "at %" denotes the corresponding metal atomic percentage.

^b Measured before use.

^c Measured after about 6-hour reaction time on-stream.

^d Fresh catalysts were further calcined for 15 hours at 750 °C after 3-hour calcination at 600 °C.

Table II. Variation of Oxygen Conductivity and Activation Enthalpy With Composition of CeO₂:Y₂O₃ (data from Wang et al. (15))

mole % Y ₂ O ₃	Hσ(eV) ^a		σ (ohm-cm) ⁻¹
	at 180 °C	at 180 °C	at 580 °C
0.0%	0.92	3 x 10 ⁻⁸	2 x 10 ⁻⁴
1%	0.79	1.8x 10 ⁻⁶	8 x 10 ⁻³
10%	1.15	1.5x10 ⁻⁷	4.5x10 ⁻³

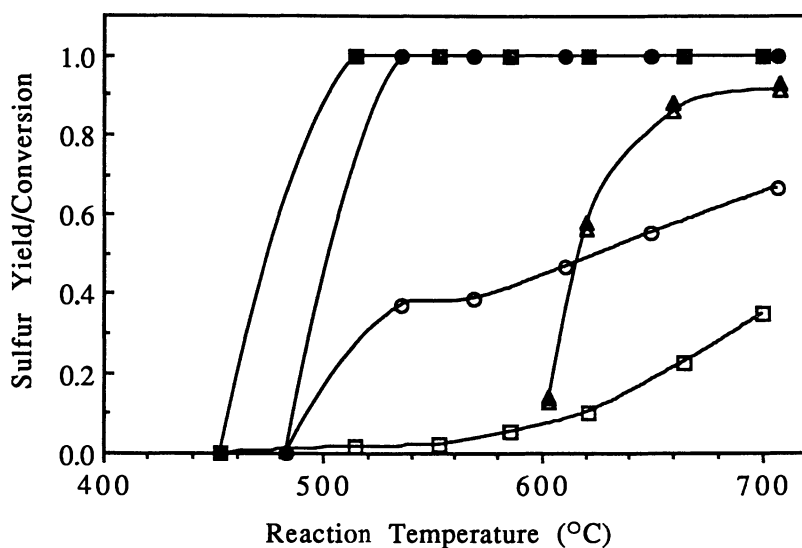
^aH_σ related to σ by Tσ ∝ exp(-Hσ/RT)

Table III. Association Enthalpy h_A and Conductivity for Solid Solutions of Different Dopants in CeO₂
(data from Gerhart-Anderson and Nowick(16))

Dopant	Ionic radius (Å)	$h_A(\text{ev})^a$		$\sigma(\text{ohm-cm})^{-1}$ 1% D ₂ O ₃ at 400 °C
		1% D ₂ O ₃	6%D ₂ O ₃	
La ³⁺	1.18	0.14/0.26 ^b	0.18	3.27x10 ⁻⁴
Gd ³⁺	1.06	0.12/0.17 ^b	0.16	5.3x10 ⁻⁴
Y ³⁺	1.01	0.21/0.38 ^b	0.26	3.27x10 ⁻⁴
Sc ³⁺	0.87	0.67/0.62 ^b	-	4.43x10 ⁻⁷
Mg ²⁺	0.89	1.23 ^b	-	-
Ca ²⁺	1.12	1.12 ^b	-	-

^a h_A related to σ by $T\sigma \propto \exp(-(h_A + h_m)/RT)$

^bdata calculated by Butler et al.(17).



[CO]/SO ₂]	4	3	1.8
Elemental Sulfur Yield	■	●	▲
SO ₂ Conversion	□	○	△

1% inlet SO₂, 0.017 s.g/cc (STP)

Figure 1. Elemental Sulfur Yield and SO₂ Conversion on Bulk CeO₂ Catalyst.

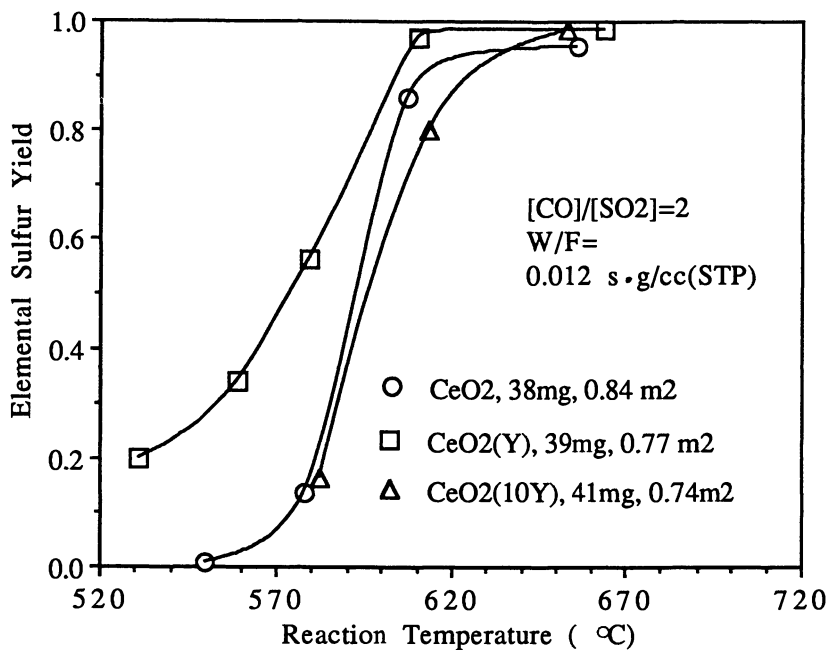


Figure 2. Effect of Y_2O_3 Dopant Content in Ceria on Catalyst Activity.

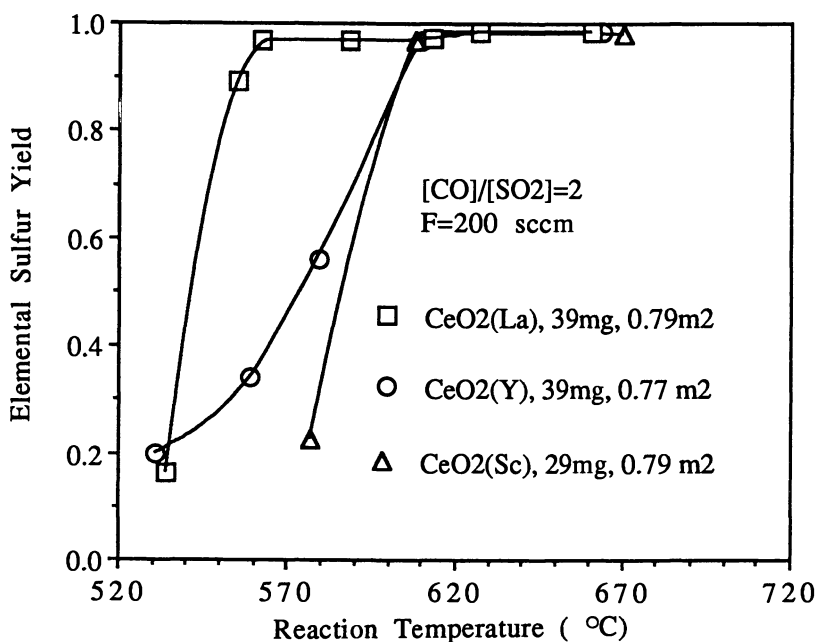


Figure 3. Effect of Different Dopants in Ceria on Catalyst Activity.

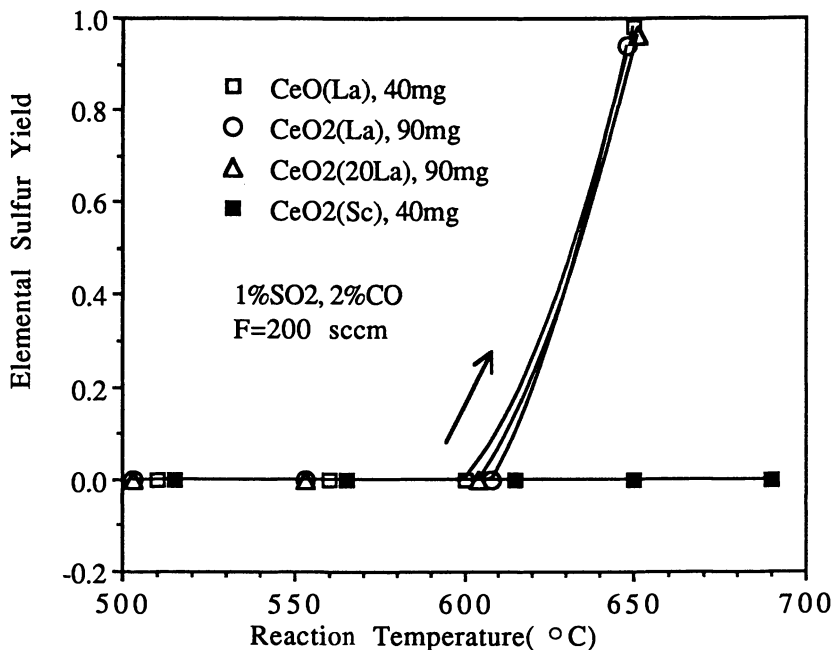


Figure 4. Light-off Behavior over Doped Ceria Catalysts in the Absence of Activation.

°C, the CeO₂(Sc) catalyst still appeared pale yellow (as a fresh ceria), while an activated (reduced) catalyst has a dark blue color. This experiment indicated that the La₂O₃-doped catalyst can be used without activation by a reductant gas, but, higher reaction temperature is needed to initiate the reaction.

The effect of La₂O₃ dopant concentration on the fall-off behavior is shown in Figure 5. Increasing the dopant concentration from 1% to 35 at% did not change the catalyst performance. On the other hand, incorporation of 5 at% MgO into the 1% La₂O₃-doped ceria greatly decreased the catalytic activity. The fall-off temperature over CeO₂(5Mg+La) catalyst is about 50 °C higher than that on the CeO₂(La). XRD analysis revealed the existence of only the ceria crystal phase in these oxide compounds. The vacancy association energy in MgO-doped ceria is 1.23 eV, much higher than that in the La₂O₃-doped ceria, 0.26 eV, as shown in Table III. This strong association stabilized the oxygen vacancy and thus capped outside oxygen on the CeO₂(5Mg+La) catalyst surface. Higher temperature would be needed to remove the more strongly bonded surface capped oxygen to maintain the reduction/oxidation cycle. This issue will be further addressed later. The CeO₂(La) catalyst was used in further studies because of its superior performance.

CeO₂(La) Catalyst. Figure 6 shows the effect of contact time on the elemental sulfur yield over the CeO₂(La) catalyst. The contact time did not change the product selectivity. More than 95% sulfur yield was always achieved under complete SO₂ conversion. The elemental sulfur yield curve fell off at a lower temperature when a longer contact time was used. However, above a value of 0.02 g-s/cc(STP) contact time, the fall-off temperature stays at about 500 °C. This is the temperature associated with the reduction of surface capping oxygen of ceria according to Yao and Yao's studies(18). Therefore, when the reaction temperature is below 500 °C, CO cannot reduce the catalyst surface to provide the active sites for SO₂ reduction. The catalyst showed good stability as indicated by Figure 7. No deactivation was observed during a 11-hour steady-state run at 532 °C. As stated before, only a small amount of COS was formed with the dry feed gas of nearly stoichiometric composition.

For the same contact time, 0.02 g-s/cc(STP), the fall-off temperature over the CeO₂(La) catalyst shown in Figure 5 is about 50 °C higher than that in Figure 6. The feed gas used in the studies shown in Figure 5 was contaminated by a small amount of water vapor(400 ppm). This indicated that the catalyst may be poisoned by water vapor.

Water Vapor Effects. The introduction of water vapor in the reacting atmosphere may affect the catalytic activity by adsorption on the catalyst

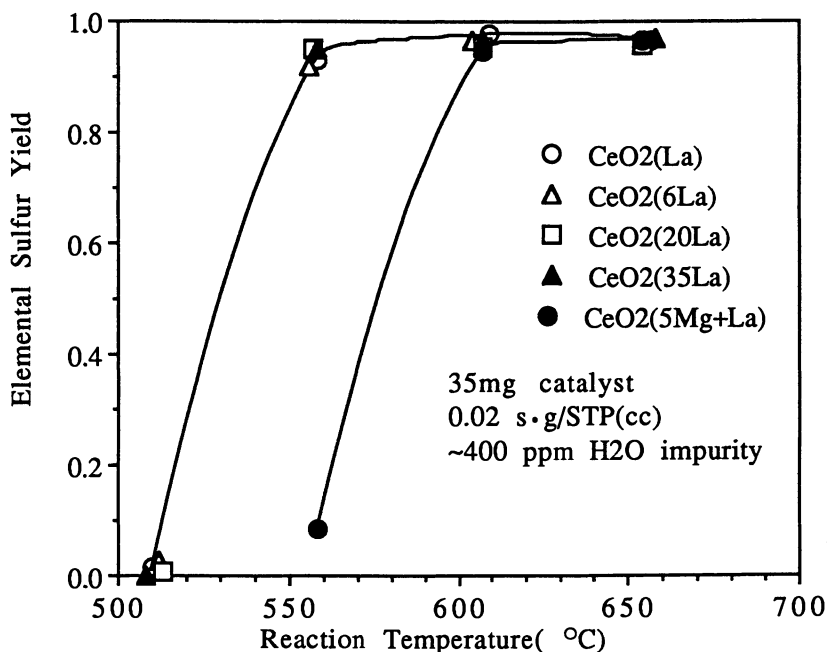


Figure 5. Effects of La₂O₃ Dopant Content and MgO Dopant in Ceria on Catalyst Activity.

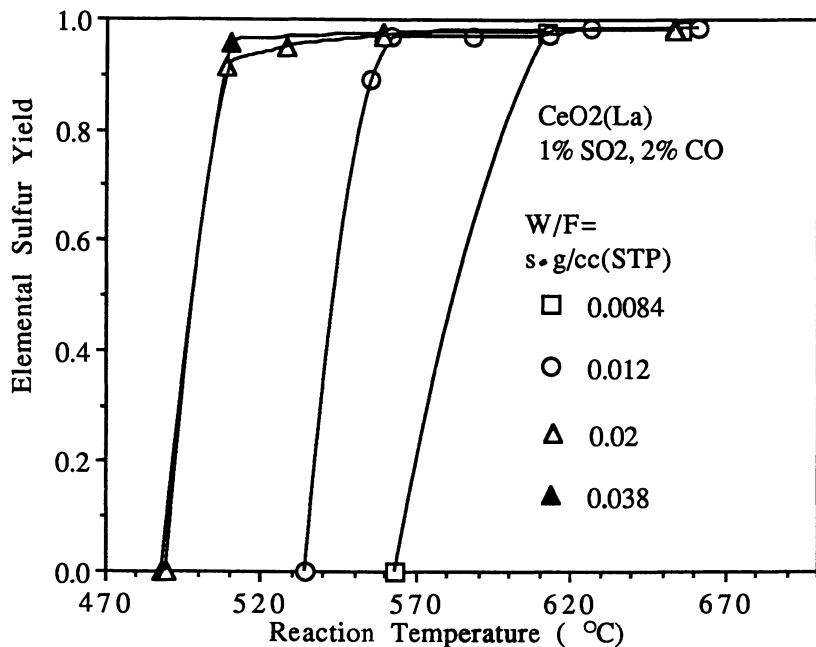


Figure 6. Effect of Contact Time(g·s/cc(STP)) on the Activity of the CeO₂(La) Catalyst.

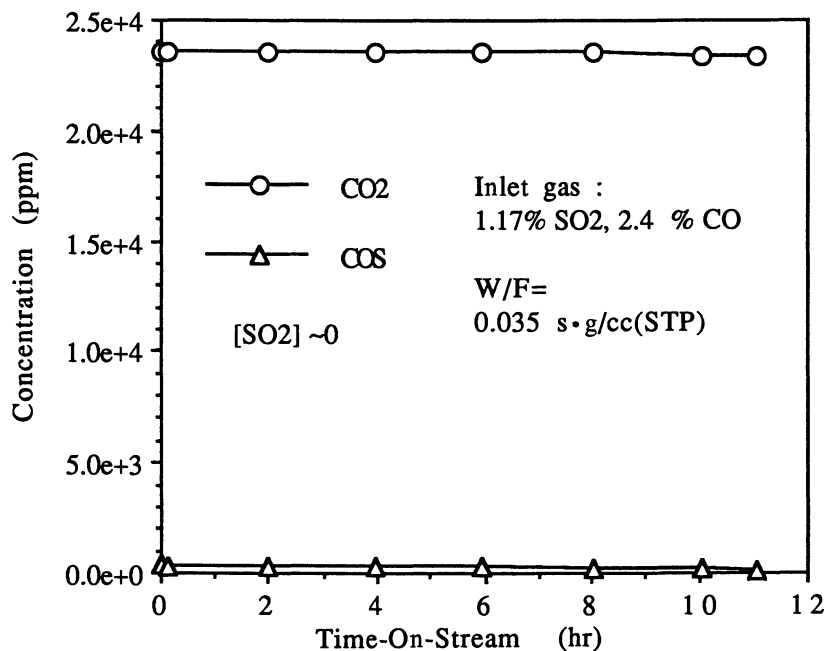


Figure 7. Long-Term Activity of CeO₂(La) Catalyst at T=532 °C.

surface, and change the product distribution through the following reactions:



The [S] in reaction 6 indicates any kind of sulfur source, such as metal sulfide and adsorbed surface sulfur. The reactions 4-7 listed above are thermodynamically feasible under present conditions. Separate experiments carried out in our laboratory demonstrated that the CeO₂(La) is an active catalyst for the COS hydrolysis (reaction 4), the water-gas shift (WGS) reaction (reaction 5), and the Claus reaction. 99% of COS was hydrolyzed to H₂S over the tested temperature range from 250 to 650 °C.

The effects of water vapor on the SO₂ reduction by CO are illustrated in Figure 8. Upon the addition of 3% H₂O, three small peaks of CO₂, H₂S, and SO₂, appeared simultaneously. The CO₂ peak may result from the reaction of H₂O with adsorbed CO on the catalyst surface, and the H₂S and SO₂ peaks may be produced by the reverse Claus reaction of adsorbed surface sulfur and H₂O. In the presence of 3% H₂O, sulfur compounds in the product stream consisted of H₂S, SO₂ and elemental sulfur, while COS was negligible. The ratio of H₂S to SO₂ was approximately stoichiometric, because in the feed gas the stoichiometric ratio of [CO]/[SO₂]=2 was used. When the reaction temperature was lowered from 660 to 617 °C, no apparent product distribution change was seen. When the temperature was lowered to 580 °C, the H₂S decreased a little while the SO₂ increased a little. The catalyst quickly deactivated when the temperature was further lowered to 540 °C, while no deactivation was observed for the dry feed gas at this temperature (see Figure 6). Li et al (19,20) in their studies of CO adsorption on ceria found that surface OH groups inhibit CO adsorption and that CO adsorption depends on the degree of surface dehydroxylation. Apparently, then, in the present study the water vapor lowered the catalyst activity for SO₂ and CO reaction by taking up the active surface sites for CO chemisorption. The overall effect of water vapor is displayed as partial poisoning of the catalyst and promotion of H₂S formation.

The variation of product gas distribution with the [CO]/[SO₂] ratio is shown in Figure 9. The H₂S formation increased with the [CO]/[SO₂] ratio; conversely, the SO₂ concentration decreased with the [CO]/[SO₂]. The maximum elemental sulfur yield was obtained around the stoichiometric

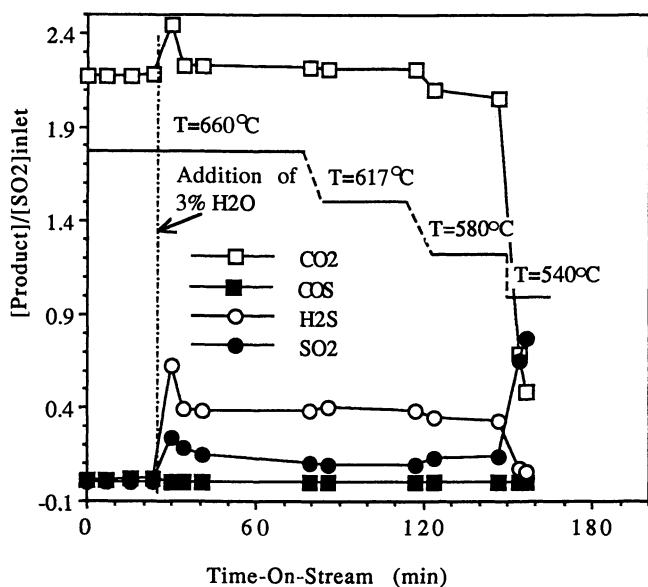


Figure 8. Product Distribution with Temperature on CeO₂(La) Catalyst in the Presence of Water Vapor (1.07% SO₂, 2.2% CO, 3% H₂O; 0.043 g/s/cc(STP)).

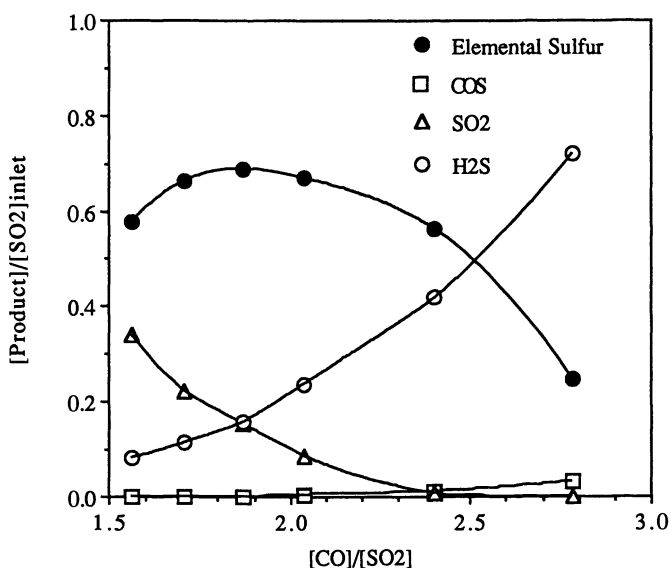


Figure 9. Product Distribution with the [CO]/[SO₂] Ratio on CeO₂(La) Catalyst in the Presence of Water Vapor at 610 °C (1 % SO₂, 1.5 % H₂O; 0.043 g/s/cc(STP)).

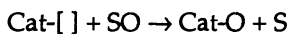
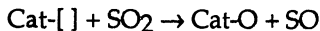
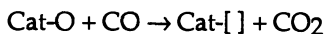
[CO]/[SO₂] ratio. In the region of [CO]/[SO₂] > 2, H₂S may be produced by hydrolysis of COS and the reaction of the adsorbed sulfur on the catalyst surface with hydrogen from the WGS reaction. In the region of [CO]/[SO₂] < 2, COS formation is negligible and thus, the H₂S may come mainly from the reaction of surface sulfur with hydrogen. Because more reductant gas was consumed to produce H₂S than elemental sulfur, there was not enough reductant left for the reduction of SO₂ so that some of the inlet SO₂ was not reduced. This became more obvious when less CO was used in the feed gas. Although the reverse Claus reaction 7 is thermodynamically feasible at high temperature, this reaction would give a simultaneous production of H₂S and SO₂. This is not the case as shown in Figure 9. Further testing showed that at a given temperature the H₂S formation increased with the water vapor content. In a practical application, since the H₂S and SO₂ in the product stream are in stoichiometric amount when the [CO]/[SO₂] is around 2, a downstream Claus reactor may be directly used to convert the H₂S and SO₂ into elemental sulfur. Alternatively, for a dry regenerative flue gas desulfurization process, the product gas from the sulfur recovery unit can be recycled to the sorber after condensation and collection of sulfur.

Impregnated CeO₂(La) catalyst. In another series of tests, transition metal-impregnated CeO₂(La) catalysts were investigated. The catalyst compositions are shown in Table I and test results are plotted in Figure 10. Similar to the previous results with the bulk catalysts, more than 95% elemental sulfur yield could be obtained at high temperature, but the elemental sulfur yield fell off steeply as the temperature was decreased. The Cu/CeO₂(La) catalyst showed the highest activity and the Mn/CeO₂(La) was the least active. The Co/CeO₂(La) catalyst lost its activity completely at 625 °C upon addition of 2.5% H₂O, while the sulfur yield on the Cu/CeO₂(La) was lowered from 97% to 65% due to the formation of H₂S. This value is a little higher than the 55% elemental sulfur yield obtained on the CeO₂(La) catalyst. The fall-off temperature for the Cu/CeO₂(La) catalyst was about 480 °C. Although the Cu supported on the CeO₂(La) did not significantly improve the activity and selectivity of the CeO₂(La) catalyst in the present study, it did have different performance from the g-Al₂O₃-supported Cu catalyst reported in earlier literature(6,7). More COS was formed on the Cu/Al₂O₃ catalyst than that on the Cu/CeO₂(La), indicating a strong metal-support interaction for the latter system.

Mechanistic Considerations. Two reaction mechanisms have been proposed for the reduction of SO₂ by CO, namely the redox mechanism(10,12) and the COS intermediate mechanism(21-23). According to the latter, CO first forms a COS intermediate with the

sulfided catalyst, and then COS reduces SO₂ to elemental sulfur. The evidence used to argue in favor of this mechanism is (i) XRD-detected metal sulfide in the used catalyst, and (ii) COS formation upon passing CO gas through the catalyst bed. In the present study, only the ceria(CeO₂) crystal phase was found in the fresh and used ceria catalyst by XRD analysis. In another test, when the steady-state reaction over the CeO₂(La) catalyst was reached at 650 °C, the feed gas was switched to He, and after a ten-minute flush, CO was allowed to scavenge the catalyst surface for half an hour. No COS was detected in the exit gas stream. The same results were obtained at 600 °C and 550 °C. Furthermore, a significant amount of CO₂ was released during the regeneration of a spent ceria catalyst with CO, while no COS was observed. These results argue against the COS intermediate mechanism for SO₂ reduction by CO over ceria catalysts. However, our tests have shown that CeO₂(La) is also a good catalyst for the reduction of SO₂ by COS, with more than 96% SO₂ converted to elemental sulfur over the temperature range from 390 to 650 °C.

We postulate that the SO₂ reduction by CO on ceria proceeds via the redox mechanism(10,12):



We found that the catalyst had to be pre-reduced to initiate the reduction/oxidation cycle at low temperature. This is evidenced by the catalyst color change. The fresh CeO₂ was pale yellow and had no activity. The activated catalyst appeared dark blue, which is the characteristic color of partially reduced CeO₂. The reaction proceeds easily on the catalyst pretreated by a reducing agent, such as CO. In contrast, the reaction is difficult to start in the reacting atmosphere due to the presence of both a reductant(CO) and an oxidant(SO₂), and may need high temperature (Figure 4). As one oxygen vacancy is created by the release of one CO₂ molecule, the SO₂ donates its oxygen to that vacancy to form a SO group. The SO is mobile on the surface until it finds another vacancy to donate its oxygen or a vacancy may migrate to a neighboring site to accept its oxygen. High oxygen mobility in the catalyst will facilitate the oxygen transfer from one site to another on the surface or from the bulk to the surface. However, the oxygen vacancy can be taken up by other molecules existing in the reacting gas phase, such as H₂O and O₂. The more strongly these impurity oxygen atoms attach to the vacancy, the more severe a poisoning effect they will bring about. The creation of oxygen vacancies on the surface is, then, a key step.

Incorporation of dopant ions into ceria lattice enhances the oxygen vacancy concentration and mobility. But, the vacancies created by the dopant on a fresh catalyst surface are always capped by the oxygen atoms from ambient oxygen or water. Therefore, the capping oxygen has to be removed to activate the catalyst. The oxygen vacancy and the dopant ion are associated pairs by a certain energy. The stronger this association, the lower the vacancy energy state is and the more strongly the vacancy is capped by an outside oxygen. In other words, strong association increases the difficulty of removing the capping oxygen. The $\text{CeO}_2(\text{La})$ material of lower association energy than the $\text{CeO}_2(\text{Y})$, showed higher activity, although these two catalysts have same oxygen ionic conductivity (Table III and Figure 3). The $\text{CeO}_2(\text{Sc})$ has the highest vacancy-ion association energy among tri-valent ion-doped ceria so that the reaction cannot proceed (Figure 4) without removing the strongly capped surface oxygen in a highly reducing atmosphere. As discussed earlier, the vacancy association energy in the MgO doped ceria is 1.23 eV (Table III), even greater than that of the $\text{CeO}_2(\text{Sc})$, 0.67 eV. Apparently, the addition of 5 at% MgO into the $\text{CeO}_2(\text{La})$ greatly stabilized the oxygen vacancy and decreased the catalytic activity (Figure 5). Table III indicates that the association energy increases with dopant content. Therefore, increasing the dopant concentration does not necessarily enhance the catalytic activity. This is evidenced by the data shown in Figure 5, where increasing La_2O_3 dopant from 1 to 35 at % had no effect on the catalyst performance. For a catalyst, surface adsorption/desorption processes are always important in addition to these oxygen vacancy and mobility properties. Because MgO is a more basic oxide than La_2O_3 and La_2O_3 is more basic than CeO_2 , the present results indicate that the acid/base properties of the catalyst play little role in the reduction of SO_2 by CO.

Conclusions

Cerium oxide is an active catalyst for SO_2 reduction by CO and its activity can be enhanced by doping La_2O_3 into its lattice. More than 95% elemental sulfur recovery can be achieved on CeO_2 -based catalysts at reaction temperatures about 500 °C or higher when the feed gas has the stoichiometric composition. The reaction of SO_2 with CO on the catalyst appears to proceed according to the redox mechanism. The results of our work demonstrate a correlation of the catalytic activity with the oxygen vacancy mobility and energetics in a doped ceria catalyst. Water vapor partially poisons the ceria catalysts and promotes the production of H_2S . The elemental sulfur yield is lowered in the presence of water. Additional work with transition metal modified cerium oxide catalysts is underway to address these issues.

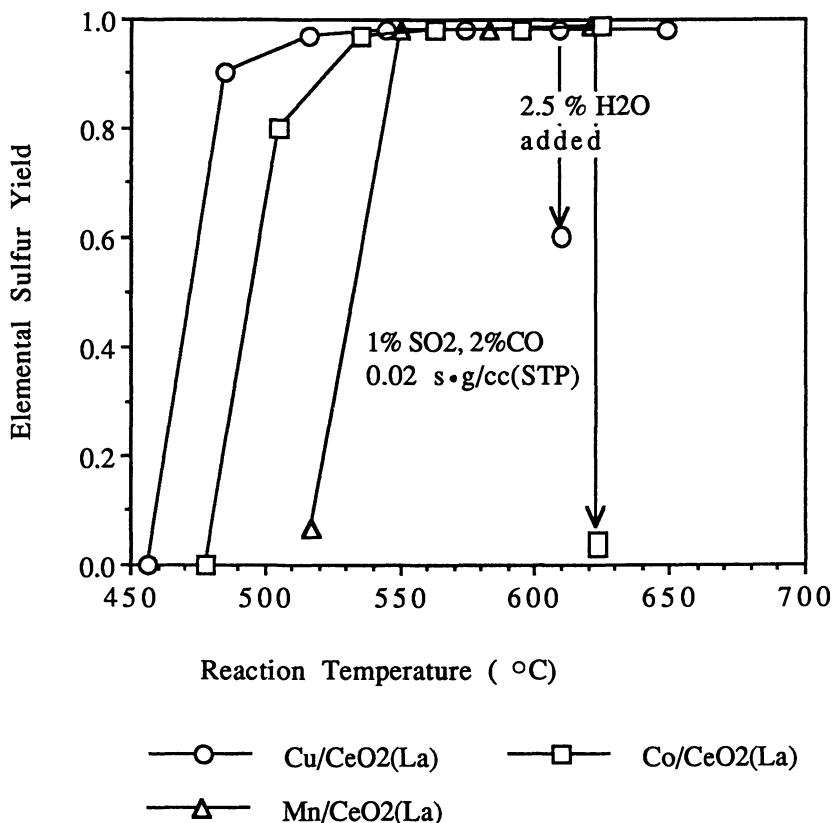


Figure 10. Activity of Metal-Impregnated CeO₂(La) Catalysts in the Presence and Absence of Water Vapor.

Acknowledgements

This work was financially supported by the U.S. Department of Energy under the University Coal Research Program, Grant No. DE-FG-92PC92534.

Literature Cited

1. Hunter, W.D., Jr. *Power*, **1963**, *63*, 117-119.
2. Kwong, K.V.; Merzner, R.E., III; Hong, C.C. In 1991 SO₂ Control Symposium: Washington, DC, 1991 December 3-6, Vol.2, Session 5B-Paper 8.
3. Ryason, P.R.; Harkins, J. J. *Air Pollut. Contr. Ass.* **1967**, *17*, 796-799.
4. Khalafalla, S.E.; Foerster, E.F.; Haas, L.A. *Ind. Eng. Chem., Prod. Res. Develop.* **1971**, *10*, 133-137.

5. Khalafalla, S.E.; Haas, L.A. In *Sulfur Removal and Recovery Industrial Processes*; Pfeiffer, J.B., Ed.; Advances in Chemistry Series No. 139; American Chemical Society: Washington, DC, 1975, pp60-64.
6. Querido, R.; Short, W.L. *Ind. Eng. Chem., Process Des. Develop.* **1973**, *12*, 10-18.
7. Okay, V.C.; Short, W.L. *Ind. Eng. Chem., Process Des. Develop.* **1973**, *12*, 291-294.
8. Bazes, J.G.I.; Careto, L.S.; Noble, K. *Ind. Eng. Chem., Prod. Res. Develop.* **1975**, *14*, 264-268.
9. Happel, J.; Hnatow, M.A.; Bajars, L.; Kundrath, M. *Ind. Eng. Chem., Prod. Res. Dev.* **1975**, *14*, 154-158.
10. Happel, J.; Leon, A.L.; Hnatow, M.A.; Bajars, L. *Ind. Eng. Chem., Prod. Res. Dev.* **1977**, *16*, 150-154.
11. Hibbert, D.B.; Campbell, R.H. *Appl. Catal.* **1988**, *41*, 273-287.
12. Hibbert, D.B.; Campbell, R.H. *Appl. Catal.* **1988**, *41*, 289-299.
13. Flytzani-Stephanopoulos, M.; Hu, Z. U.S. Patent 5 242 673, 1993.
14. Courty, P.; Marcilly, C. In *Preparation of Catalysts III*; Poncelet, G.; Grange, P.; Jacobs, P.A.; Ed.; Elsevier Science Publishers: Amsterdam, The Netherlands, 1983, pp485-519.
15. Wang, D.Y.; Park, D.S.; Griffith, J.; Nowick, A.S. *Solid State Ionics* **1981**, *2*, 95-105.
16. Gerhardt-Anderson, R.; Nowick, A.S. *Solid State Ionics* **1981**, *5*, 547-550.
17. Butler, V.; Catlow, C.R.A.; Fender, B.E.F.; Harding, J.H. *Solid State Ionics* **1983**, *8*, 109-113.
18. Yao, H.C.; Yao, Y.F.Y. *J. Catal.* **1984**, *86*, 254-265.
19. Li, C.; Sakata, Y.; Arai, T.; Domen, K.; Maruya, K.; Onishi, T. *J. Chem. Soc., Faraday Trans. 1*, **1989**, *85*, 929-943.
20. Li, C.; Sakata, Y.; Arai, T.; Domen, K.; Maruya, K.; Onishi, T. *J. Chem. Soc., Faraday Trans. 1*, **1989**, *85*, 1451-1461.
21. Haas, L.A.; Khalafalla, S.E. *J. Catal.* **1973**, *29*, 264-269.
22. Haas, L.A.; Khalafalla, S.E. *J. Catal.* **1973**, *30*, 451-459.
23. Baglio, J.A. *Ind. Eng. Chem. Prod. Res. Dev.* **1982**, *21*, 38-41.

RECEIVED September 30, 1993

Chapter 32

Hydrolysis of COS on Titania Catalysts Mechanism and Influence of Oxygen

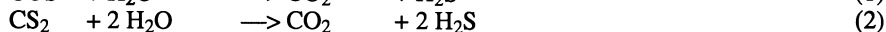
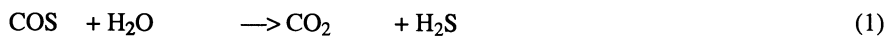
H. M. Huisman, P. van der Berg, R. Mos, A. J. van Dillen, and
J. W. Geus

Department of Inorganic Chemistry, Utrecht University, Sorbonnelaan
16, P.O. Box 80083, 3508 TB, Utrecht, Netherlands

The hydrolysis of COS on titania was studied by infra-red spectroscopy. The results are compared with the hydrolysis on alumina. At low temperatures, the mechanism on titania shows close resemblance to the hydrolysis on alumina. The influence of oxygen was investigated by means of infra-red experiments and catalytic activity measurements. On the titania surface, sulfate formation was observed. The sulfate formation increases the surface acidity and thus decreases the rate of hydrolysis. Fast recovery of the original activity was observed after reduction of the sulfated surface by H₂S at relatively low temperatures. This smooth regeneration is the cause of the much better oxygen resistivity of titania as compared to that of alumina catalysts, and not the fact that surface sulfates do not form.

The Claus process is used to convert H₂S into elemental sulfur. The first stage of this process comprises the high-temperature combustion reaction of H₂S with O₂ to sulfur with a yield of 70%, leaving SO₂ and H₂S in a 1 to 2 mole ratio. The second, catalytic stage, involving two or three reactors, is used to convert the remaining SO₂ and H₂S into sulfur. Problems arise when COS or CS₂ are present. Reaction with residual hydrocarbons within the burner results in the formation of COS and CS₂. These compounds do not easily react over the Claus catalyst. Consequently, SO₂ is emitted due to the combustion of COS and CS₂ with oxygen within the incinerator (1-4).

The most favored route for COS and CS₂ conversion is that of hydrolysis to H₂S (reactions 1 and 2).



The same catalyst as is used for the reaction between H₂S and SO₂ in the catalytic Claus converters (reaction 3) can catalyze the hydrolysis reactions (2).



γ -Alumina is the catalyst most often used for the Claus reaction. Since also the hydrolysis of COS and CS₂ is accelerated by γ -alumina, research has been carried out aiming to understand the hydrolysis of COS on alumina (1,5-7).

The use of γ -alumina, however, brings about severe problems. When oxygen is present in the feed, which can be due to insufficient mixing of the gases in the re-heaters of the Claus plant, sulfation of the surface of alumina causes deactivation of the catalyst. Although the deactivated catalyst can be reactivated in a flow of H₂S at elevated temperatures, H₂S is emitted as SO₂ during the regeneration.

Fiedorow (11) obtained evidence that COS is adsorbed on the basic sites of the alumina surface, probably on basic hydroxyl groups. IR-spectroscopic investigations have revealed that the adsorbed COS reacts to hydrogen thiocarbonate, which decomposes subsequently into H₂S and CO₂ (5,7). Most recently Lavalley et al have discussed the poisoning effect of oxygen on the reactivity of γ -alumina catalysts (7). The authors claim the increased acidity of the catalyst due to sulfate formation causes the poisoning effect of oxygen (7,12).

Several authors reported on results obtained with titania as a catalyst in this reaction. It has appeared that titania is much more resistant against sulfation; deactivation caused by oxygen thus does not occur (8-10).

The aim of our study is to elucidate the better resistance of titania catalysts to oxygen. We first of all investigated the mechanism of COS hydrolysis on a titania catalyst. Therefore an in-situ infra-red study was performed to confirm the thiocarbonate mechanism on alumina and to establish whether the same mechanism is operative on titania. By the use of in-situ experiments we can get information on the essential steps in the hydrolysis reaction.

The titania surface shows a close resemblance to the γ -alumina surface; on both surfaces acidic and basic hydroxyl groups are present. The γ -alumina surface is described by Knözinger (13). Woning and van Santen studied the titania surface. The differences with regard to the acid and base properties between two types of titania surfaces, anatase and rutiel, are minor. Anatase contains slightly more basic hydroxyl-groups (14). The similar properties of titania and alumina surfaces suggest that the hydrolysis of COS proceeds according to the same mechanism on the two oxides. Recent results of Lavalley et al. indicate a similar mechanism of COS adsorption on TiO₂ as on Al₂O₃. Infra-red results show adsorption of COS in the form of hydrogen thiocarbonates and involvement of the hydroxyl-groups of titania in the adsorption of COS (15).

Futhermore an important question to be answered is whether the deactivating influence of oxygen on titania catalysts, analogously to what has been found with γ -alumina (7,12), can be attributed to an increased surface acidity caused by the formation of sulfate. Although sulfate formation on titania is thermodynamically less favored than that on γ -alumina, Saur et al observed sulfate on titania surfaces (16). Busca et al. measured a higher surface acidity, when titanium sulfates were used in the preparation of the catalyst (17). Lavalley et al. reported a irreversible deactivation of titania in COS hydrolysis, after impregnating the catalyst with (NH₄)₂SO₄ (17). It is therefore not likely that the higher resistance of titania to oxygen poisoning is due to the inability of the titania surface to react to sulfates, which was suggested by Pearson (2).

To investigate the formation of sulfate on titania, we used infra-red spectroscopy. The influence of the formation of sulfate on the activity of titania in the hydrolysis is investigated and discussed. Furthermore, the stability of sulfated titania surfaces is studied by temperature-programmed reaction with H₂S.

Experimental

The experiments were performed on either a titania catalyst from Degussa (P25, 50 m²/gram, 85% anatase and 15% rutiel) or an alumina catalyst from Engelhard (Al 4172 P, 230 m²/gram).

The diffuse reflectance infra-red experiments (DRIFT) were carried out using an environmental cell (Spectra Tech). The infra-red apparatus was a Perkin Elmer 1620. The temperature of the powdered sample was measured with a thermocouple within the sample itself, spectra could be measured at temperatures between 300 and 1200 K. About 20 ml per minute of gas of 1 bar pressure at 298 K was passed through the cell. The following gasses were used: N₂ (99.999% purity), O₂ (99.999%), COS (97%, also containing air, H₂S, and CO₂), H₂S (99.7%), and SO₂ (99.7%), all supplied by Hoek Loos. 1.5% water could be admitted to the gas flow by means of saturation of the N₂-flow at 298 K.

The activity measurements and the TPR measurements were performed in an automated microflow apparatus, the gases were sampled every 15 seconds beyond the reactor with an on-line quadrupole mass spectrometer (Balzers, QME 420, operating temperature 398 K). Reactivities were measured using 1% COS, 18% H₂O, and balance argon at 1 bar (200 ml/minute flow rate, 0.2 gram catalyst, GHSV 12000 hour⁻¹). The TPR experiments were carried out using 2% H₂S in balance argon, the temperature ramp was 10 K per minute.

Results and Discussion

DRIFT experiments with Alumina. After keeping the alumina catalyst for 15 minutes at 475 K in a N₂ flow, the catalyst was cooled down to 325 K and N₂ with 30% COS (water-free) was admitted to the sample. After this pretreatment still a large amount of adsorbed water and all the surface hydroxyl-groups were present, as was apparent from the infra-red spectrum. Figure 1 shows the difference spectra of the catalyst before and during exposure to COS. The spectra recorded at 325, 375, 425 and 475 K are represented. Infra-red absorption caused by physisorbed COS was not detected due to the absorption of gas-phase COS, the absorption caused by adsorbed COS was reported at 2000 cm⁻¹ (1). The absorptions at 1330 and 1570 cm⁻¹ are due to the formation of hydrogen thiocarbonates, as was mentioned by Lavalley (7). At 1230, 1440, and 1650 cm⁻¹ absorption due to hydrogen carbonates is detected. The absorption at 1650 cm⁻¹ is at the same position as the absorption due the water, but absorption caused by water is subtracted by using difference spectra. Upon heating the catalyst from 325 K to 425 K the absorption bands caused by hydrogen thiocarbonate increase and the absorption bands caused by water (at 1650 and 3350 cm⁻¹) and caused by hydrogen carbonate decrease. Since the spectra have been corrected for adsorbed water using difference spectra, desorption of water leads to a negative peak in the spectrum shown in figure 1 at 1650 cm⁻¹. Measuring the infra-red spectra at 475 K, shows the absorptions due to hydrogen thiocarbonate have decreased and they are absent at 525 K. At 475 K and higher temperatures CS₂ is observed in the gas phase (1530 cm⁻¹), due to the disproportionation reaction of COS to CO₂ and CS₂. This reaction only proceeds if no water is present.

The stability of the adsorbed species is of interest, since the hydrogen thiocarbonate is supposed to be an intermediate species in the hydrolysis reaction. The absorption spectra as a function of the period of time after removal of the COS from the gas phase is shown in figure 2. During this experiment the temperature was 325 K. After removal of COS from the gas phase, N₂ was admitted to the cell.

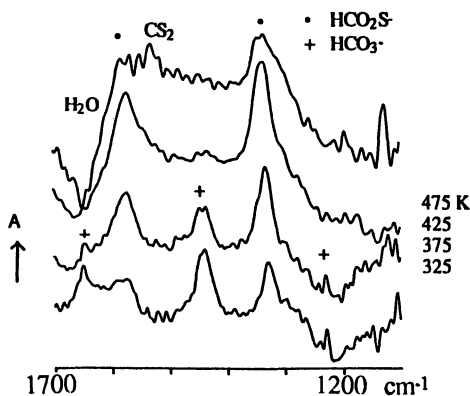


Figure 1: difference DRIFT spectra of COS adsorption on alumina. Spectra are recorded at 325, 375, 425, and 475 K. Difference spectra are obtained by subtracting the spectrum of unexposed alumina at the same temperature. Spectra are shifted to prevent overlap.

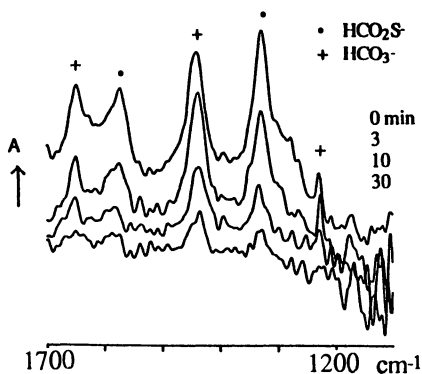


Figure 2: difference DRIFT spectra recorded 0, 3, 10, and 30 minutes after exposure of alumina to COS. Spectra are recorded at 325 K. Spectra are shifted to prevent overlap.

The spectra (recorded at 325 K) show a continuous decrease of the hydrogen thiocarbonate bands after 3, 10, and 30 minutes, indicating that adsorbed hydrogen thiocarbonate is not stable and may be an intermediate in the reaction. Also to be noted is the initial increase (after 3 minutes), and subsequent decrease of the hydrogen carbonate band. This maximum exhibit by the hydrogen carbonate may be attributed to the reaction of hydrogen thiocarbonate with water on the surface to hydrogen carbonate. More likely is, however, that the formation of hydrogen carbonate is caused by the increase in the amount of CO_2 in the gas phase originating from the dissociation of hydrogen thiocarbonate. At higher temperatures (375, 425 K) similar results are obtained, i.e., even a faster decline of the hydrogen thiocarbonate absorptions is observed.

Experiments with 1.5% water present in the gas flow, together with 30% COS, do not lead to absorption bands caused by sulfur containing species in the temperature range studied.

Another experiment was performed to investigate the interaction of H_2S with the alumina catalyst. Admission of H_2S to the sample did not affect the absorption spectra (an absorption at 2550 cm^{-1} caused by the S-H stretch might have been expected (19,20)).

Titania. To study the interaction of COS with titania we followed the same procedures as with the above experiment with alumina. After keeping the catalyst at 475 K and cooling down in N_2 to 325 K, 30% COS in N_2 was admitted to the catalyst. The resulting spectra are shown in figure 3. Just as described previously for alumina, hydrogen thiocarbonate and hydrogen carbonate have been formed and the amount of water on the surface has decreased.

Nevertheless important differences can be observed. The absorption bands caused by hydrogen thiocarbonate are peaking at 1160 and 1590 cm^{-1} , and the bands caused by hydrogen carbonate are at 1270 and 1470 cm^{-1} . The markedly differing frequencies of the hydrogen thiocarbonate absorptions reveal a somewhat different configuration of this species on titania. Our results are in contrast with the results of Lavalley et al. (15). They found adsorptions due to thiocarbonates at 1577 and 1330 cm^{-1} , similar to hydrogen thiocarbonates on alumina. This discrepancy might be caused by the strongly different amount of COS admitted to the catalyst. Lavalley et al admitted $350\text{ }\mu\text{mol.g}^{-1}$ COS, while we used a continuous stream of 30% COS in N_2 . This results in a differing amount of COS adsorbed and might also affects the amount of hydroxyls remaining unreacted. Therefore differing adsorption might be expected.

More important than the difference in structure of the hydrogen thiocarbonate, is the influence of the temperature on the steady state concentration of the adsorbed species. On the alumina catalyst, the thiocarbonate species are apparent at temperatures up to 475 K, whereas on the titania catalyst the bands caused by hydrogen thiocarbonate already have disappeared at 375 K. The disappearance of the hydrogen thiocarbonate species is accompanied by the appearance of an absorption band at 2550 cm^{-1} (this part the spectra is not shown in the figures). This absorption has to be attributed to the formation of an SH species (19,20).

The rate of disappearance of the species adsorbed on titania is also measured, in a similar experiment as previously described with alumina. The spectra of the adsorbed species shown in figure 4 are recorded at 323 K. After the removal of COS from the gas flow, the bands caused by hydrogen thiocarbonate disappear within about 90 minutes, at about the same rate as with alumina. The hydrogen carbonate absorptions seem to remain unaffected.

The live-time of the hydrogen thiocarbonate species is dropped steeply when after the removal of COS, 1.5% H_2O is added to the gas flow. Instead of the relatively slow

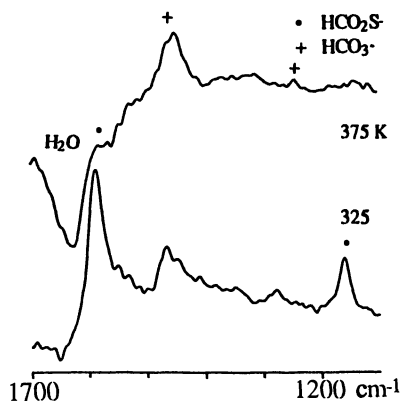


Figure 3: difference DRIFT spectra of COS adsorption on titania. Spectra are recorded at 325, and 375 K. Difference spectra are obtained by subtracting the spectrum of unexposed titania at the same temperature. Spectra are shifted to prevent overlap.

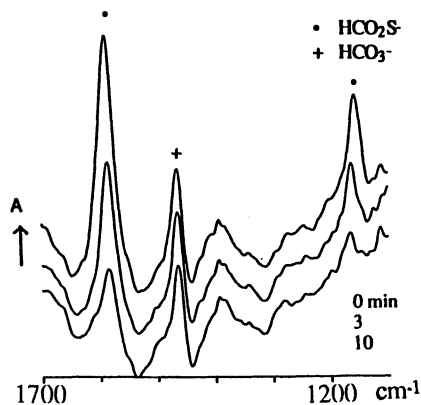


Figure 4: difference DRIFT spectra recorded 0, 3, and 10 minutes after exposure of titania to COS. Spectra are recorded at 325 K. Spectra are shifted to prevent overlap.

decrease of the amount of hydrogen thiocarbonate observed when no water is present, the hydrogen thiocarbonate absorptions disappear within three minutes with 1.5% H₂O.

The behavior of the infra-red absorption bands caused by hydrogen thiocarbonate when the nitrogen flow contains both 30% COS and 1.5% water reflects the behavior during the hydrolysis reaction. The spectra, recorded at 325, 375 and 425 K, are plotted in figure 5.

At 323 K no bands due to S-H or hydrogen thiocarbonate are apparent. Only a slight increase in the amount of adsorbed H₂O is measured. Without water in the gas flow hydrogen thiocarbonate is present at 325 K, see figure 3. Reaction between water and COS does not take place at this temperature as can be concluded from the non-formation of CO₂ in the infra-red apparatus (no CO₂ or carbonate is observed in the infra-red spectra). Also in the activity measurements no CO₂ is measured at this low temperatures. Therefore, we must conclude that at 323 K water is able to block adsorption sites for COS.

At 375 K, the formation of hydrogen thiocarbonates is observed when both 30% COS and 1.5% water is admitted to the sample. Apparently, water cannot block sites at this higher temperature. Consequently, a steady-state concentration of hydrogen thiocarbonate is present on the surface, due to reaction of water and COS. We showed previously (figure 3) that without water no hydrogen thiocarbonate is present at 375 K. It is evident that without water in the gas flow no detectable amounts of hydrogen thiocarbonate are stable on the surface. This is caused by the reaction of COS with the hydroxyl-groups initially present on the surface to CO₂ and H₂S. Without water in the gas flow the hydroxyl-groups and water molecules on the surface are rapidly exhausted and in the steady-state no adsorbed thiocarbonate is present.

In the spectrum recorded at 425 K, only a decrease in the adsorption due to water, and an increase in the adsorption due to hydrogen carbonates is measured (figure 5). Hydrogen thiocarbonates are not present in high concentrations; the adsorptions at 1590 and 1160 cm⁻¹ are absent or almost absent. Since the COS hydrolysis reaction is running fast at these temperatures (see further on) we conclude that the decomposition of hydrogen thiocarbonates is fast, and that therefore the steady state concentration of hydrogen thiocarbonates is low.

The absorption bands caused by the formation of SH species by exposure of the catalyst to COS at 375 K, can also be measured when 30% H₂S is added to the gas flow. SH absorptions can be measured at temperatures between 323 and 375 K; beyond 375 K no detectable amount of S-H is present anymore. On Al₂O₃ no S-H absorptions could be detected.

The adsorption of H₂S is impeded by addition of 1.5% H₂O to the gas flow. Water apparently can block adsorption sites for H₂S, or water can react fast with S-H species on the surface to form H₂S_(gas).

Site-blocking agents. The infra-red experiments indicate that the mechanism of COS hydrolysis involving a hydrogen thiocarbonate intermediate, as described in literature for alumina, is also operative with the hydrolysis on titania. The fact that analogous mechanisms proceed on alumina and titania can also be demonstrated by adding a small amount of pyridine to the gas flow during an activity measurement. Pyridine is able to block acid sites on the catalyst surface, and can also create basic sites. Addition of pyridine to the gas flow during an activity measurement on alumina results in an increase in conversion of COS. Fiedorow thus concluded that basic sites are involved in the reaction mechanism (11). Just as reported for alumina, we observe a steep (reversible) increase in activity on admission of pyridine to the gas flow during an activity measurement with a titania catalyst. Admission of some formic acid, on the other hand, decreases the activity of the titania catalyst. The effects of pyridine and

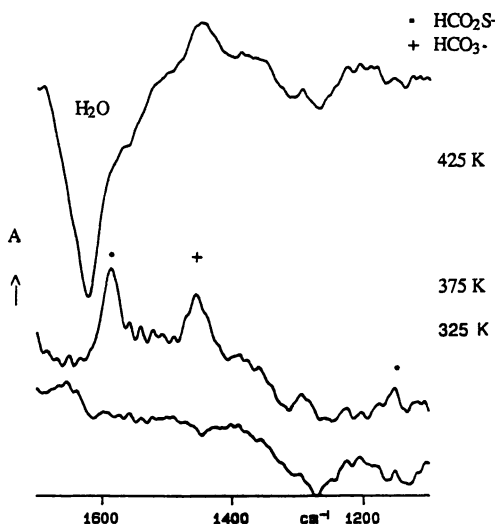


Figure 5: difference DRIFT spectra of COS adsorption on titania. Spectra are recorded at 325, 375 and 425 K. Difference spectra are obtained by subtracting the spectrum of unexposed titania at 325 K. Spectra are shifted to prevent overlap.

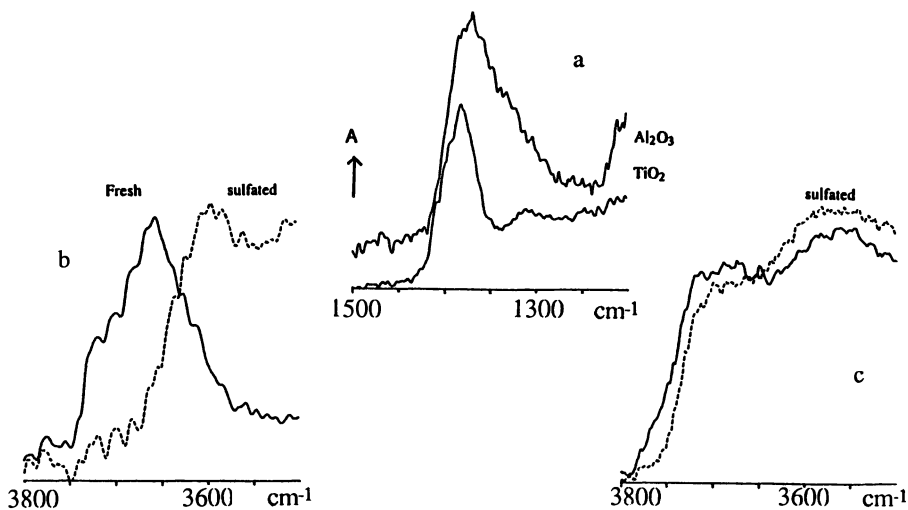


Figure 6a: DRIFT spectra of sulfate formation on titania and alumina. Spectra recorded at 675 K. Spectra are recorded after exposure of the samples to SO_2/O_2 . Spectra are shifted to prevent overlap. (not difference spectra.)

Figure 6b: DRIFT spectra of hydroxyl-groups of titania at 675 K before and after exposure to SO_2/O_2 .

Figure 6c: DRIFT spectra of hydroxyl-groups of alumina at 675 K before and after exposure to SO_2/O_2 .

formic acid demonstrate the need for basic sites on the titania catalyst, just as was demonstrated earlier for the alumina catalyst. The experiments with site-blocking agents firmly support the conclusions from the results of the infra-red experiments.

Formation of sulfates. A simplified sulfation procedure is used to examine the influence of oxygen on the hydrolysis activity. Instead of using a H_2S , SO_2 , O_2 flow, to simulate operating conditions within a Claus reactor, we used a SO_2 , O_2 flow in order to prevent the formation of elemental sulfur. Most sulfation experiments have been performed at 675 K to accelerate the sulfation process. The higher temperature is chosen because sulfation of alumina surfaces is reported to be slower without H_2S in the gas flow (21,22). Experiments performed at 475 K confirm the experimental results obtained at 675 K, but the formation of sulfate is much slower at 475 K.

In order to investigate the formation of sulfates on Al_2O_3 and TiO_2 , a gas flow containing 20% O_2 and 20% SO_2 in N_2 is passed over the catalyst kept at 675 K during 45 minutes. After removal of the O_2 and SO_2 , the infra-red spectra of both alumina and titania show absorption bands due to sulfate formation (for alumina at 1360 cm^{-1} , for titania at 1370 cm^{-1}). The spectra are presented in figure 6a. The relative amount of sulfate present can not be abstracted from the intensity of the infra-red adsorptions; the surface area of the samples are different. Furthermore, the use of the diffuse-reflectance technique also provides problems in estimation of amount of sulfates present.

In a flow of pure nitrogen the absorption bands remain, which indicate that the formation of sulfates is irreversible at 675 K. The sulfate bands agree with those measured by Lavalley (7) and Chang (18).

The formation of sulfate is accompanied by a shift of the OH stretch vibration to lower wavenumbers. The shift to lower wavenumbers is most conclusively measured on titania; the OH stretch vibration shifts from $3740\text{--}3600$ to $3600\text{--}3540\text{ cm}^{-1}$. The shift is caused by the formation of more acidic OH, probably via the formation of hydrogen sulfite (7). The shift in the OH stretch vibration of alumina is only to be seen in a small decrease in absorption of the most basic hydroxyl-groups; the hydroxyl-groups with the highest wavenumber. The shift of the OH stretch for alumina and titania is shown in figure 6b and 6c, respectively.

Reviewing the results of the infra-red experiments it may be concluded that the results do not justify titania being expected to be more oxygen resistant than alumina. The hydrogen thiocarbonate mechanism as described in the literature is not only valid with alumina but also with titania. Furthermore, the sulfate formation with titania is about as severe as with alumina, and is, even more pronouncedly as with alumina, responsible for a decrease in the concentration of basic hydroxyl groups.

Activity test of a sulfated titania catalyst. The rate of hydrolysis of COS as a function of temperature has been measured before and after a treatment of the titania catalyst with 10% O_2 , 1% SO_2 , and 6% H_2O in argon at 675 K for 60 minutes. The activity was measured as function of temperature between 350 and 650 K. The temperature ramp was 10 K per minute. The activity curve of the fresh catalyst was identical going up and down in temperature. After sulfation the initial activity, measured going up in temperature, was very low. The results are shown in figure 7.

The treatment with SO_2 and O_2 almost completely destroys the initial activity of the catalyst. At rising temperatures, however, the activity starts to recover at about 620 K, probably caused by the presence of H_2S , that results from the hydrolysis of COS. On cooling down, the recovery of the activity is evident; the activity of the catalyst is exactly the same as before sulfation. An alumina catalyst does not exhibit this fast recovery of the reactivity.

The regeneration of the catalyst has been studied using TPR experiments with

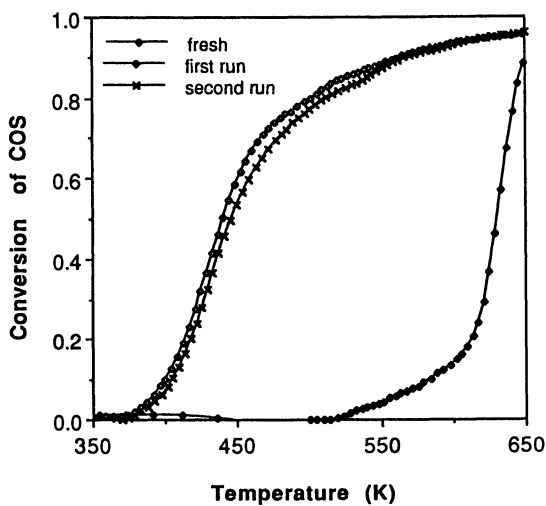


Figure 7: Conversion of COS as function of temperature with the titania catalyst before and after treatment of the catalyst with SO_2/O_2 .

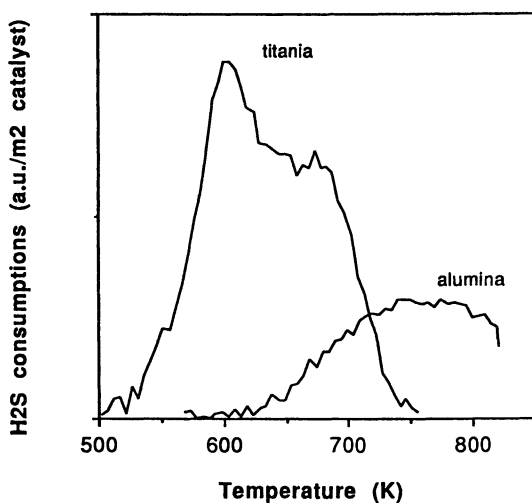


Figure 8: Temperature programmed reaction of a sulfated titania and alumina catalyst.

sulfated catalyst. H_2S was used as a reducing agent of the sulfates, since H_2S is always present in the Claus gas stream.

TPR of sulfates with H_2S . To sulfate the surface of the catalysts an alumina and a titania catalyst are treated with a gas flow containing 10% O_2 , 1% SO_2 , and 6% H_2O in argon for 60 minutes at 675 K. After cooling the catalysts to 375 K, the gas flow is replaced by a flow containing 1% H_2S and 6% H_2O in argon. The temperature of the catalyst is subsequently raised with 10 K per minute. The results of these TPR measurements are shown in figure 8. During the H_2S consumption elemental sulfur, SO_2 , and H_2O are formed. Before, during, and after the experiment, the catalyst was white. It is therefore concluded that no reduction of Ti^{4+} to Ti^{3+} proceeds during the experiment. A sulfated titania surface is reduced at appreciably lower temperatures than a sulfated alumina surface. It is interesting to note that the H_2S consumption per m^2 of the titania catalyst is higher, while the sulfation period was about the same with both catalysts. The reduction of titania and alumina sulfates with H_2 was described by Saur et al. (16). According to these authors the reduction of a sulfated titania surface proceeds at about 725 K, and of a sulfated alumina surface at even higher temperatures. The reduction of the surface sulfates of titania and alumina with H_2S is obviously proceeding more easily than with H_2 .

Usual Claus operating temperatures are between 523 and 623 K. After incidentally poisoning of the catalyst caused by oxygen spillage, the presence of H_2S in the feed can regenerate a titania catalyst. The Claus reactor is being operated at temperatures at which a sulfated titania catalyst is easily regenerated. Sulfated alumina surfaces, on the other hand, are much more difficult to regenerate, as is observed in technical plants.

Conclusions

The infra-red data presented show the formation of hydrogen thiocarbonates when COS is admitted to both alumina and titania surfaces. The hydrogen thiocarbonates present on titania show infra-red adsorption bands different from those observed on alumina (alumina 1330 and 1570 cm^{-1} , titania 1160 and 1590 cm^{-1}). Not clear is how the different adsorptions have to be interpreted. The temperature range in which the thiocarbonates are present on alumina and titania shows interesting differences. On alumina surfaces hydrogen thiocarbonates are present up to 523 K, whereas on titania surfaces infra-red absorption bands due to hydrogen thiocarbonate have disappeared already above 375 K. The infra-red experiments with water indicate a reaction between water and hydrogen thiocarbonate, but also site blocking by water of sites that adsorb H_2S and COS. It cannot be decided whether the dissociation of hydrogen thiocarbonates proceeds via hydrogen carbonates, or the hydrogen carbonates results for adsorption of CO_2 from the gas phase. Lavalley et al. proposed a reaction scheme in which the hydrogen thiocarbonate was attacked by water resulting in H_2S , CO_2 and a hydroxyl-group (15).

Experiments with site-blocking agents prove that the catalytic hydrolysis of COS requires basic sites; exposure to formic acid reduces and to pyridine increases the activity of titania.

Titania is the better oxygen-resistant catalyst under normal Claus operating conditions, in spite of the severe initial deactivation of titania after sulfation. The experiments carried out to elucidate the better resistance to oxygen of titania catalysts have shown the higher resistance to be due to the much better reducibility of the sulfates of titania with H_2S as compared to the sulfates of alumina. The better reducibility explains the difference in oxygen sensitivity well. During normal Claus operating

conditions, some H₂S is always present. The H₂S is able to keep the titania surface free from sulfate. Under these conditions the alumina surface is irreversibly sulfated and is thus deactivated.

Acknowledgement. The research described in this paper was financially supported by the Shell International Research Company B.V., Den Haag.

References

1. Chuang, T.T., Dalla Lana, I.G., Lui, C.L., *J. Chem. Soc., Faraday Trans. 1*, **1972**, *69*, 3, 643-651.
2. Pearson, M.J., *Hydrocarbon Proc.*, **1981**, *60*, 131-134.
3. Dupin, T., Voirin, R., *Hydrocarbon Proc.*, **1982**, *61*, 189-191.
4. Maglio, A., Schubert, P.F., *Oil & Gas J.*, **1988**, *86*, 85-90.
5. Deason, D.L., Eur Pat Appl., EP 195534 A1, **1986**.
6. Akimoto, M., Dalla Lana, I.G., *J. Catal.*, **1980**, *62*, 84-93.
7. Lavallay, J.C., Aboulayt, K., Lion, M., Bachelier, J., Hebrard, J.L., Luck, F., Symposium on NO_x and SO₂ Control in Stationary Sources, American Chemical Society, Atlanta Meeting, April 14-19, **1991**, 51-58.
8. Dupin, T., Voirin, R., *Hydrocarbon Proc.*, **1982**, *61*, 189-191.
9. Coward, R.S., Skarat, W.M., *Oil & Gas J.*, **1985**, Apr 8, 86-94.
10. Nougayrede, J. et al., *Oil & Gas J.*, **1987**, *85*, 65-68.
11. Fiedorow, R., Leaute, R., Dalla Lana, I.G., *J. Catal.*, **1984**, *85*, 339-348.
12. Przystajko, W., Fiedorow, R., Dalla Lana, I.G., *Appl. Catal.*, **1985**, *15*, 265-275.
13. Knözinger, H., Ratnasamy, P., *Catal. Rev.*, **1987**, *17*, 31-70.
14. Woning, J., Van Santen, R.A., *Chem. Phys. Lett.*, **1983**, *101*, 541-547.
15. Bachelier, J., Aboutlayt, A., Lavallay, J.C., Legendre, O., Luck., *Catal. Today*. **1993**, *17*, 55-62.
16. Saur, O., Bensitel, M., Mohammed Saad, A.B., Lavallay, J.C., Tripp, C.P., Morrow, B.A., *J. Catal.*, **1986**, *99*, 104-110.
17. Busca, G., Saussey, H., Lavallay, J.C., Lorenzelli, V., *Appl. Catal.*, **1985**, *14*, 245.
18. Chang, C.C., *J. Catal.*, **1978**, *35*, 374-385.
19. Deo, A.V., Dalla Lana, I.G., Habgood, H.W., *J. Catal.*, **1971**, *21*, 270-281.
20. Data, A., Cavell, R.G., Tower, R.W., George, Z.M., *J. Phys., Chem.*, **1985**, *89*, 443-449.
21. Quet, C., Tellier, J., Voirin, R., *Stud. Surf. Sci., Catal., (Catal. Deact.)*, Elsevier Scientific Publishing Company, Amsterdam, **1980**, *6*, 323-329.
22. Saussey, H., Vallet, A., Lavallay, J.C., *Mater. Chem. Phys.*, **1983**, *9*, 457-466.

RECEIVED September 30, 1993

Chapter 33

Catalytic Bromine Recovery from HBr Waste

Paul F. Schubert, Richard D. Beatty, and Suresh Mahajan

Catalytica, Inc., 430 Ferguson Drive, Mountain View, CA 94043

A high activity HBr oxidation catalyst maintained greater than 98% bromine recovery from a commercial waste 48% HBr stream during approximately 600 hours on stream in a 5,000-kg/yr pilot plant. Heat management, critical for control of the highly exothermic HBr oxidation, was accomplished using aqueous instead of anhydrous HBr and a tube and shell reactor design. At HBr solution feed rates of 1.2 kg/h and an inlet temperature of 275 °C, the maximum temperature rise measured was 12 °C, demonstrating effective heat management. The novel catalyst has superior activity and stability compared to earlier copper oxide- and cerium oxide-based catalysts. The new catalyst is also resistant to deactivation by propionic acid and HCl contaminants.

Bromination of organic compounds is widely used for the manufacture of flame retardants, pharmaceuticals, and bromobutyl rubber. These bromination reactions often produce HBr as a reaction byproduct, since bromination of aromatic and alkyl compounds typically results in incorporation of only one of the two bromine atoms in the bromine molecule. In some processes, the volume of waste HBr produced can be a major fraction of the total product mass. This is particularly true in flame retardant manufacture, where high levels of bromine substitution are frequently required to achieve the desired flame retarding properties for the product (*1*). For example, in the synthesis of decabromodiphenyl oxide (equation 1) the waste HBr represents almost 46 wt % of the total reaction products.



The level of bromination of common flame retardants, and the fraction of reactants that forms waste HBr is given in Table I.

Table I. Waste HBr Formed in Synthesis of Common Flame Retardants

Flame Retardant	Wt% Br in Molecule	Fraction of HBr in Total Products
Hexabromobenzene	88.8	0.473
Decabromobiphenyl	84.7	0.462
Decabromodiphenylether	83.3	0.458
Pentabromotoluene	82.1	0.454
Pentabromophenol	78.2	0.453
Tribromophenol	72.5	0.423
Tetrabromobisphenol A	58.8	0.373

Although there is some use for the HBr in manufacture of heavy drilling fluids (e.g., CaBr₂, ZnBr₂), alkyl bromides (e.g., methyl bromide), and other organic bromides(2), the desirability of recycling the waste HBr to bromine has long been recognized (3). This is currently practiced primarily by the Kubierschky process(4), which uses chlorine as the oxidant. In this process, anhydrous HBr is first converted to NaBr by absorption using an aqueous NaOH scrubber (equation 2). The NaBr produced is then contacted with chlorine gas to produce bromine (equation 3).



Chlorination gives high yields of bromine, but produces a sodium chloride waste stream which requires disposal. The total amount of NaCl solution generated is approximately 2 kg (0.7 kg NaCl and 1.3 kg H₂O) per kg of bromine recovered (Table II).

Table II. Bromine Recovery Methods

Process	Oxidant	Waste	Recovery	kg Waste/ kg Br ₂
Kubierschky *	Cl ₂	NaCl + H ₂ O	> 99	2.04
Peroxide **	H ₂ O ₂	H ₂ O	60–85	0.44
Catalytica	O ₂	H ₂ O	> 99	0.11

*Based on 48% HBr

**Based on 50% H₂O₂

Hydrogen peroxide as the oxidant for conversion of HBr to bromine (5–8) does not have the environmental penalty of waste salt disposal (equation 4) and is used commercially on a limited scale.



However, the bromine recovery efficiency is only 65–80 wt %. Efficiency can be increased through the addition of NaBrO₃(9), but this increases costs and also produces a salt byproduct requiring disposal.

Catalytic oxidation of HBr using oxygen offers the potential for high recovery efficiency without the production of salt byproducts that require disposal (equation 5).



Attempts to develop a catalyst and process for reaction extend over 50 years (3) and used a wide range of catalytic promoters and supports (Table III). These catalysts and processes were never commercialized. The catalysts and process developed at UOP in the late 1960s appear to be the most advanced, providing the greatest catalyst activity and stability(13–15). The earliest catalysts in the patent examples used magnesia or alumina as the catalyst support (13). However, as these catalysts are not stable under the reactor conditions, they were replaced with zirconia-supported catalysts in subsequent patent examples (14,15). The most active catalyst developed was 3% copper oxide on zirconia. The zirconia was stable under the reaction conditions, but the catalyst experienced severe deactivation due to copper migration at the temperatures required to achieve high HBr conversion (300 °C). Cerium oxide on zirconia was not susceptible to migration but had insufficient activity to achieve high conversions in reasonable bed sizes.

Table III. HBr Oxidation Catalysts

Promoter(s)	Promoter Form(s)	Support(s)	Process Temp (°C)	Reference
Cu, Co, Mn, Th, Ce, Ni	Chloride	Pumice, brick tile, ceramic	325–425	(3)
Ce, none	Oxide	Pumice, quartz	700–1000	(10–11)
Ru	Chloride	Pumice, SiO ₂ , Al ₂ O ₃	325–400	(12)
Cu, Ce	Oxide	MgO-ZrO ₂ , Al ₂ O ₃ , TiO ₂ , ZrO ₂	350–450	(13, 14)
Ce, Mn, Cr, Fe, Ni, Co, Cu	Oxide	ZrO ₂	225–600	(15)
Cu-Ce-K	Chloride, Bromide	Al ₂ O ₃	300–400	(16)
Pt, Pd	–	Al ₂ O ₃ , SiO ₂ , molecular sieves	175–700	(17)
V	Oxide	Al ₂ O ₃	400–500	(18)

We believe that inadequate heat management is one of the key technical reasons these catalysts and processes were never commercialized. The HBr oxidation reaction is highly exothermic, with ΔH_{rxn} equal to -33.3 kcal/g-mol at 600 K. Since most HBr-generating brominations produce anhydrous HBr, this was typically fed directly over the catalyst with oxygen as an oxidant. This system gives an adiabatic temperature rise of nearly 2000 °C. This temperature increase is beyond the limits of conventional heat management techniques, and materials of construction for the reactor capable of

withstanding such temperatures are not available. Furthermore, the extremely high local temperatures within the catalyst particles would cause volatilization of most proposed catalytic promoters. The potential problem of promoter volatility and migration is well established in the literature (13, 14, 17). Substituting air for oxygen can decrease the adiabatic temperature rise to about 1000 °C, but this decrease is not sufficient to overcome these problems.

The addition of water to the system by using 48% aqueous HBr instead of anhydrous HBr can reduce the adiabatic temperature rise to about 320 °C for oxygen and about 280 °C for air oxidation. These temperature rises are low enough to be effectively controlled using standard tube and shell heat exchanger-type reactors to manage the heat release. This type of reactor allows semi-isothermal operation, minimizing the temperature both at the surface of the catalyst particles, thereby reducing the potential for promoter migration, and at the tube wall. Materials of construction are available which can withstand the corrosive HBr, Br₂, H₂O, O₂ process stream at normal operating temperatures (250–350 °C).

Once the heat release from the process is effectively controlled, catalyst design can be meaningfully addressed. A commercially viable HBr oxidation catalyst requires high activity, to minimize the catalyst bed volume, and excellent stability, to minimize catalyst changeout. In addition, the catalyst should be resistant to deactivation by the contaminants present in typical waste HBr streams. Common contaminants include organics and brominated organics from the upstream bromination process, chlorides (which are frequently present in low concentrations with bromides), and inorganic bromides (corrosion products or bromination catalysts) and other soluble salts. Most inorganic materials can be removed in the feed vaporizer so that they do not come in contact with the catalyst. However, volatile organics and HCl would contact the catalyst, and their effect on catalyst stability presents important catalyst performance issues.

In addition to requiring excellent catalyst performance, a commercially viable process requires a reasonable level of flexibility to respond to the constantly changing operating environment of a chemical plant. Key issues are the ability to handle variable flows and concentrations.

A novel catalyst, Brocat™ catalyst, has been developed which is superior in activity and stability to the prior art catalysts. It is also resistant to deactivation by the types of contaminants described above. The performance of this catalyst and the flexibility of the process designed to utilize this catalyst are presented in this paper.

Experimental

Catalyst Preparation. CuO₂/ZrO₂ Catalyst. A sample containing nominally 3% CuO in ZrO₂ catalyst was prepared following the method of Louvar and de Rosset (14). A solution was prepared by dissolving 126.1 g of zirconyl chloride (ZrOCl₂·8H₂O) in 140 ml of deionized water. A second solution was prepared by dissolving 4.6 g of copper nitrate (Cu(NO₃)₂·2.5H₂O) in 7 ml of distilled water. The two solutions were mixed together. A 121.2 gm aliquot of 50% NaOH solution was diluted to 500 ml. The copper and zirconia containing solution was slowly added to the caustic solution, giving a light blue color. The solids were separated by centrifugation and washed four times with a 0.3 wt % NaOH solution. The solids were dried at 130 °C for 14 hours. The resulting powder was pressed to give a granular material.

CeO₂/ZrO₂ Catalyst. A sample containing nominally 9% CeO₂ in ZrO₂ was prepared following the method of Louvar and de Rosset (14). A solution was prepared by dissolving 180 g of zirconyl chloride (ZrOCl₂·8H₂O) in 200 ml of deionized water. A second solution was prepared by dissolving 24.9 g of cerium sulfate (97% CeSO₄) in 200 ml of 0.5 N sulfuric acid. The two solutions were rapidly mixed together. A white precipitate formed immediately. The solution with precipitate was allowed to stand overnight to allow complete precipitation. The slurry was centrifuged, and the supernatant was decanted and discarded. A 0.35% ammonium nitrate solution was added to the centrifuge tube, and the liquid was discarded again after centrifuging. The solids were removed from the centrifuge tube and washed twice with 600 ml aliquots of 0.35% ammonium nitrate solution. The solids were dried at 120 °C for 20 hours, producing a white solid. The solid was crushed and sieved to produce a 20-by-30 mesh fraction. This fraction was placed in a furnace at room temperature. The temperature was increased at 50 °C/min and then held at 600 °C for 2 hours.

Brocat Catalyst. The Brocat catalyst was prepared by impregnation of a proprietary 3.1-mm diameter cylindrical catalyst support with an aqueous solution containing the catalyst precursors using incipient wetness techniques. The material was dried and calcined. For experiments using the laboratory scale testing unit, the material was ground to give a 20-by-30 mesh fraction. For pilot unit use, unground material was used.

Laboratory-Scale Testing. Test Unit. The laboratory-scale test unit is shown schematically in Figure 1. The reactor is an 8-mm-i.d. quartz tube located in a tube furnace. The quartz tube is packed with 1 ml of 20-by-30 mesh catalyst particles. The catalyst bed is positioned in the tube using quartz wool above and below the bed, with quartz chips filling the remainder of the reactor. The furnace temperature is controlled by a thermocouple inserted into the reactor tube. The position of the thermocouple varied depending on the objectives of the experiment. For most experiments, the thermocouple was placed about 3 mm above the catalyst bed. This allowed operation at constant feed temperature into the reactor. Typical operating temperatures were in the 250–400 °C range.

The oxygen and nitrogen fed to the reactor were controlled using Brooks 5850E Series mass flow controllers. The oxygen flow rate was maintained at 6.0 ml/min. Aqueous HBr was delivered to the vaporizer using Harvard Apparatus 22 syringe pumps at a delivery rate of 6.0 cc/hour. The vaporizer consists of a 5-mm o.d. quartz tube located in a tube furnace operated at the reactor inlet temperature. The vaporizer effluent then enters the reactor. The effluent of the reactor passed through traps containing aqueous 4 molar KI to collect HBr and Br₂. The remaining gas stream passed through a sodium hydroxide trap before release to the vent.

Catalyst Activity Tests. The activity of the catalysts was studied using the laboratory testing unit. The catalyst was loaded into the reactor, and the system was allowed to heat up to the desired bed temperature in a flow of nitrogen. When the desired temperature was reached, the gas flow was switched to oxygen, and delivery of the HBr solution was started. The process was allowed to stabilize for about an hour before the samples were used to evaluate catalyst performance. Samples were collected in 20–30 minute intervals and analyzed for HBr and bromine. Typical test duration was 2–3 hours.

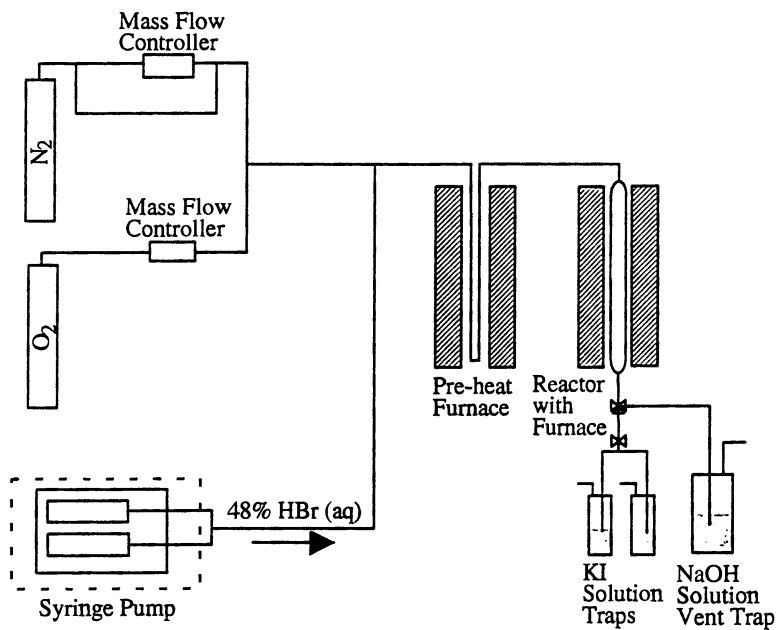


Figure 1. Laboratory bromine test unit.

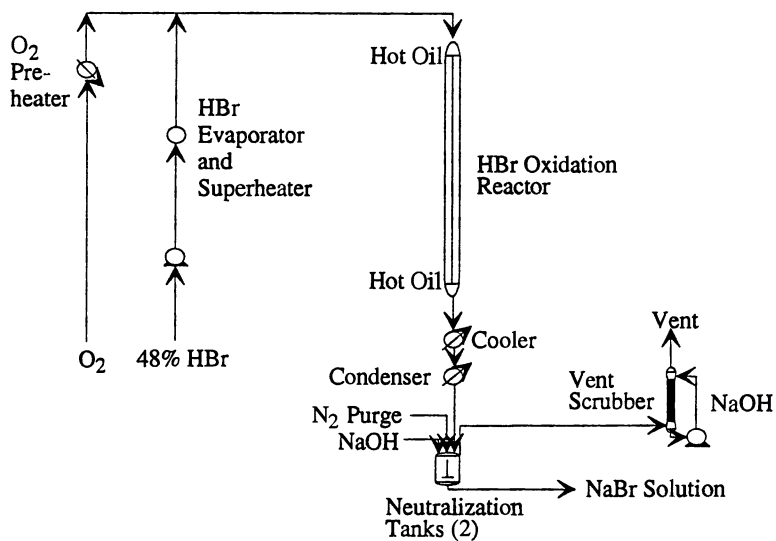
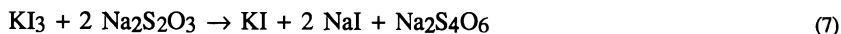


Figure 2. Pilot unit design.

HBr Feed Streams. Reagent grade HBr was used in all comparative studies among the Brocat, CeO₂, and CuO catalysts. Studies using model contaminants were conducted using HBr streams that had been prepared by addition of 0.7 wt % propionic acid or 1 wt % HCl gravimetrically.

Analytical. The amount of bromine oxidation can be determined by analyzing the effluent of the reactor. Bromine produced in the reactor reacts with iodide in the KI trap according to equation 6. The I₃⁻ produced can be titrated with sodium thiosulfate (equation 7), and the amount of bromine formed calculated. These titrations were done colorimetrically. Once the sodium thiosulfate titration is complete, the unreacted HBr present in the system can be titrated using NaOH solution (equation 8). The NaOH titration was done potentiometrically using a Metrohm 686 Titroprocessor.



Collection of organics in the effluent was done by cooling the KI trap with ice, followed by a second trap using a dry ice/acetone bath to ensure that no organics were lost. Organic products were not observed in the second trap. Analysis of the organics was done using a gas chromatograph and GC/mass spectrometer. Analysis of the catalyst was done using ICP.

Pilot Unit Testing. Pilot Unit Design. The pilot unit was designed to simulate performance of a multitubular reactor by construction and operation of a single full-scale tube. The resulting unit has an annual bromine recovery capacity of approximately 5,000 kg/yr. A schematic of the pilot unit design is shown in Figure 2. The aqueous 48% HBr feed is pumped to a vaporizer and superheater where it is heated to the reactor temperature. It is then mixed with preheated oxygen or air before it enters the reactor. The HBr feed rate is monitored gravimetrically. The HBr reservoir has a capacity of about 20 liters, and is replaced as needed during operation. The gas flow rates are controlled using Brooks mass flow controllers.

The reactor consists of two sections of 2.54-cm i.d. by 2-m long jacketed pipes with a 0.2 m long U-tube section of pipe filled with unpromoted catalyst support between the two halves. The temperature of the reactor is controlled by flowing hot oil through the jacket of the reactor. The temperature profile of the reactor can be monitored using twelve thermocouples positioned approximately every 0.34 m throughout the bed, except for the portion between the sixth and seventh thermocouples. This section includes the U-tube, and the spacing between the thermocouples is 0.67 m. The composition in the reactor can be monitored using six sample ports positioned approximately every 0.7 m. The reactor effluent is cooled and condensed, and then neutralized with NaOH to minimize storage of bromine on-site.

The aqueous HBr used for the pilot unit study was a commercial waste HBr stream from an aromatic bromination reaction. It was passed through a carbon absorption bed prior to use in the pilot unit. It had the following analysis:

HBr	47.69 wt %
Density	1.50 g/ml
Free bromine	57 ppm
Organic contaminants	< 100 ppm methoxytoluene
Inorganic chloride	0.02 wt %
Sulfate	6.7 ppm
Sodium	1.2 ppm

A sample of 35 wt % HBr used to study the effects of reduced acid concentration on unit performance was prepared by diluting this standard pilot unit feed with distilled water.

The catalyst charged to the reactor consisted of 2.303 kg of 1/8-in. diameter catalyst extrudates. The reactor tube was vibrated during the loading procedure to help the catalyst pack efficiently. In addition, a 56.4-cm layer of unpromoted support was placed at the inlet of the reactor bed to allow monitoring of the temperature of the reactor feed before the catalyst. The pressure drop across the reactor was typically between 150 and 200 torr.

During start-up, the system was brought to temperature under nitrogen flow. When the reactor reached 200 °C, distilled water was pumped through the system. After the desired inlet temperature was reached, the oxygen and 48% HBr were substituted for nitrogen and water respectively. The standard operating conditions for the pilot unit reactor are as follows:

Feed rates	1.22 kg/hr of 47.69 wt % HBr
Inlet pressure	972.5 torr
Residence time	1.5–2 seconds
Reactor inlet temperature	274–275 °C

Catalyst activity and stability were monitored by analyzing product gas samples from the reactor sample ports. The conversion samples are collected by trapping in 4 molar KI solution and analyzed as previously described.

Results and Discussion

HBr Oxidation Catalyst Evaluation. The performance of the Brocat catalyst and the two optimum catalysts prepared based on the UOP patents are shown in Figure 3 for reagent grade 48% HBr feeds. The CeO₂-on-zirconia catalyst was essentially inactive below 300 °C and required temperatures at or above 350 °C to achieve significant reaction rates. At 350 °C, the CeO₂ started with very low activity and increased gradually to the activity shown over about 2 hours. After 2 hours, the activity of this catalyst showed a very slight decrease over the next 20 hours. Visual and chemical analysis of this catalyst showed no significant cerium migration. The activity of the CuO-on-zirconia catalyst was intermediate between the CeO₂-on-zirconia catalyst and the Brocat catalyst. This catalyst achieved high activity within 20 minutes of delivery of the first HBr. However, examination of the catalyst after completion of each test showed approximately 75% loss of copper from the top of the bed after 20 hours on

stream at 350 °C. Copper deposits on the quartz chips downstream of the catalyst bed were observed. This is consistent with previous literature reports, and this rapid deactivation of this catalyst makes it commercially unacceptable. The Brocat catalyst showed excellent catalytic activity over the entire temperature range. This catalyst reached high activity within the first 20 minutes of operation. The catalyst typically decreased about 10% in activity over the next 20 hours and maintained constant activity thereafter. Analysis of the Brocat catalyst in these tests showed no evidence of promoter migration even after 100 hours on stream.

Contaminant Studies. Water soluble contaminants such as propionic acid or HCl may be expected to be contained in waste HBr streams at concentrations near 1%, while most insoluble contaminants should be present only at ppm levels. The effects of 0.7 wt % propionic acid in the aqueous HBr feed were studied as a function of temperature using a model feed (Figure 4). At 292 °C, the activity of the catalyst declined rapidly, with the catalyst becoming nearly inactive within 5 hours. Analysis of the spent catalyst showed a grey carbon residue on the catalyst. By increasing the reactor temperature to 320 °C, constant activity could be maintained, and no residue was observed. Analysis of the effluent from the 320 °C test showed no hydrocarbon products in the aqueous or bromine phases. This indicates that operating conditions capable of combusting certain organic contaminants in the waste HBr stream can be selected.

Addition of 1% HCl to the 48% HBr feed caused an activity decline at 300 °C greater than that observed for the Brocat catalyst reaching typical steady state (Figure 5). This decline in activity could be eliminated by increasing the operating temperature to 320 °C. Elemental chlorine is not observed as a product of this reaction. Catalytic oxidation of the HCl to chlorine at significant rates requires temperatures in excess of 400 °C. If oxidation did occur, the chlorine produced would rapidly react with HBr present in the reactor to convert it to bromine (equation 9).



Pilot Unit Studies. The pilot unit was designed to evaluate catalyst activity and stability and the effects of variations in process parameters on bromine recovery. The reactor is a single tube with the same dimensions as an individual tube from a full-scale multitubular reactor that would be used for a commercial bromine recovery unit. This allows excellent simulation of the performance of any tube in such a reactor and makes scale-up to such a reactor straightforward. The catalyst charge in the pilot unit was operated intermittently for 30 hours to debug the operation and determine optimum operating conditions for a long-term catalyst life test. The catalyst life test consisted of 563 hours of operation (Figure 6). During the catalyst life test, the reactor maintained HBr conversion in excess of 98% over the entire operation with the brief exception of the unit upset described below. A total of approximately 340 kg of bromine was produced during the life test. The only major upset experienced during operation was at about 200 hours on stream in the unit, when a leak developed in the oxygen feed system. This is apparent in Figure 6. Once the system was repaired, the operation was returned to steady state.

The pilot unit conversion profile as a function of reactor length for operation

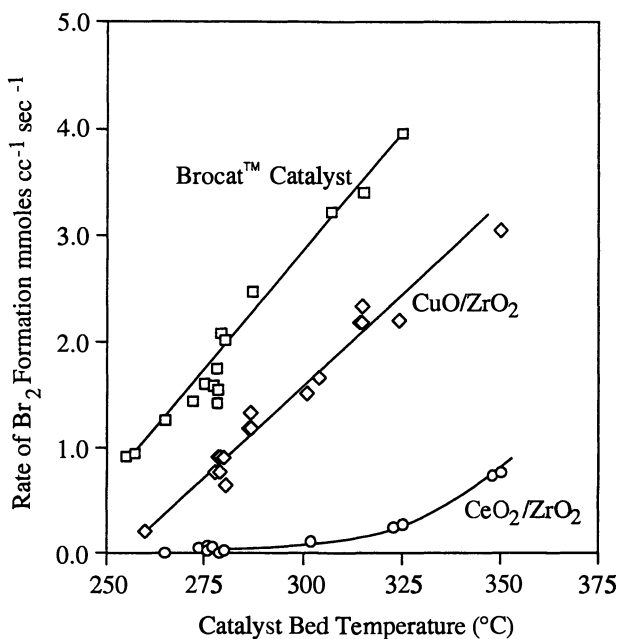


Figure 3. HBr oxidation catalyst performance in laboratory-scale test unit.

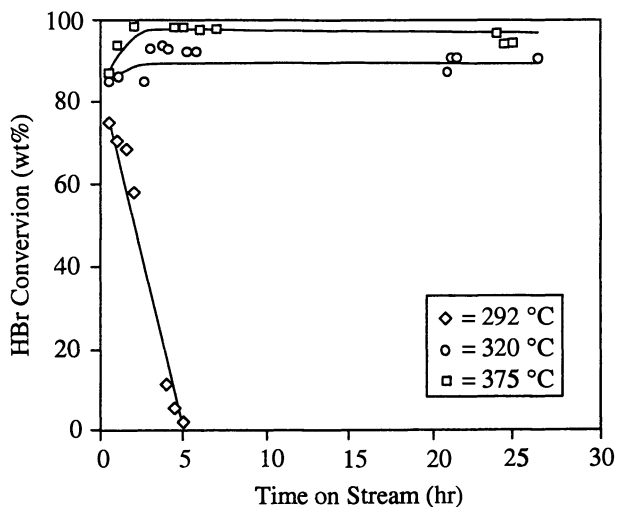


Figure 4. Effect of temperature on Brocat catalyst performance with 0.7 wt% propionic acid-contaminated feed in laboratory-scale test.

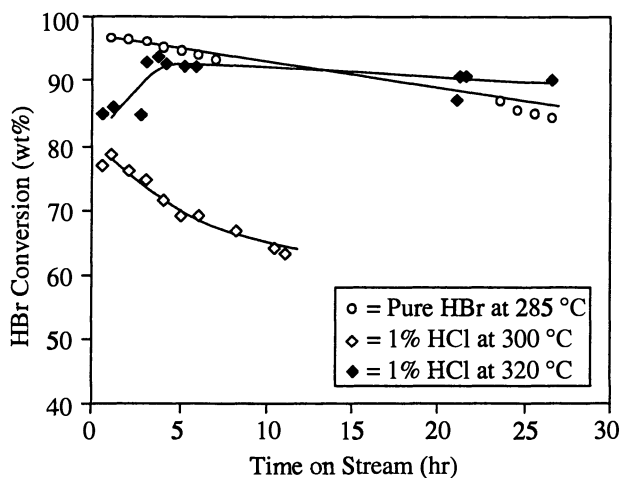


Figure 5. Effect of temperature on Brocat catalyst performance in laboratory-scale test unit.

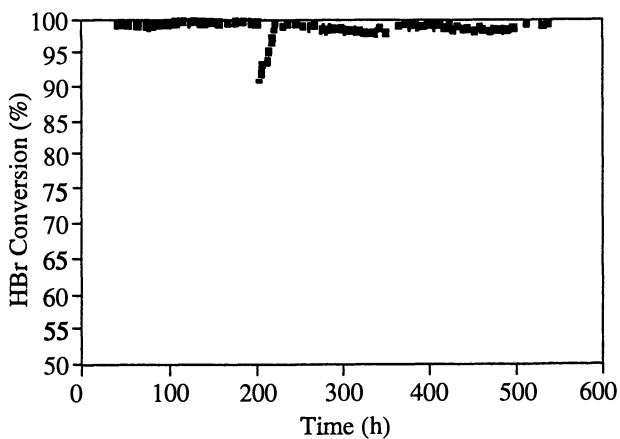


Figure 6. Brocat pilot unit catalyst life test under standard operating conditions.

at standard conditions is shown in Figure 7. The data show that the HBr conversion reached 95% in the first meter of the catalyst bed. The remaining 2.5 meters were required to achieve 99% conversion. The temperature profile of the bed confirmed that most of the reaction is taking place near the top of the catalyst bed. A maximum temperature rise of about 12 °C was observed at the first thermocouple (5.9 cm below the top of the catalyst bed), and the temperature decreased to the inlet temperature within 1 meter of the reactor inlet. The conversion at the point where the maximum temperature was observed should be about 42.5% based on the conversion profile. If the reactor were an adiabatic reactor, this would correspond to an adiabatic temperature rise of 135 °C. This 123 °C difference between the calculated adiabatic temperature rise and the measured reactor temperature verifies the effectiveness of the tube and shell reactor design in achieving heat management for the catalytic system.

The reactor temperature profile was stable during the 563 hours on stream under standard operating conditions. However, over the first 150 hours of operation, a slight decrease in conversion was observed from the first three sample ports, although greater than 98% conversion was maintained at the reactor outlet. After that period, the conversion remained essentially constant for all of the sample ports. This suggests that some thermal sintering of the catalyst occurred, and once a steady state condition was achieved, the activity remained constant. If promoter migration or catalyst poisoning were occurring, a shift in the position of the exotherm and a broadening of the temperature profile would be expected.

Process Condition Variability Studies. A series of studies was conducted to determine the effects of various parameters on performance. These studies are summarized in Table IV.

Table IV. Pilot Unit Parametric Studies

HBr Concentration (wt%)	Oxidant	HBr Feed Rate (kg/h)	HBr Conversion (wt%)	Bromine Production (kg/l-h)	Maximum Exotherm (°C)
48	Oxygen	1.2	99	0.33	13
48	Air	1.2	98	0.33	9
35	Oxygen	1.1	98.5	0.30	8
48	Oxygen	1.6	96.5	0.42	8
48	Oxygen	0.9	99.7	0.23	15

Flow Rate Effects. The effects of flow rate on catalytic performance are important to determine both the potential maximum throughput for the reactor and the potential effects of variable flow rates through different tubes of a commercial multitubular reactor. As expected, changing the feed rates to the reactor affects both the HBr conversion and the maximum exotherm and the width of the temperature peak. A 30% increase in feed rate dropped the conversion from 99% to 94.5% and decreased the exotherm maximum to only 9 °C. Increasing the inlet temperature by 1.5 °C had little effect on residence time, but increased the conversion to 96.4%. Conversion in excess of 99% should be possible by further temperature increases, but this was not attempted. Decreasing the flow rate of the aqueous HBr and oxygen by about 30%

increased the conversion to 99.7% and the exotherm maximum to 15 °C. The width of the spike observed in the temperature profile was significantly decreased.

These results indicate that high conversion is readily achieved over a broad range of flow rates. In many processes utilizing a multitubular reactor, precise balancing of the flow rates is required both to achieve high overall conversion and to minimize undesirable side reactions which reduce selectivity. Since catalytic HBr oxidation is 100% selective, and high HBr conversion could be achieved over a wide range of flow rates, precise balancing of flow rates in all of the tubes of a multitubular reactor is not critical to achieving high bromine yields. Furthermore, upstream process excursions producing high flow rates should have a limited impact on HBr conversion.

HBr Concentration. Obtaining a 48% HBr solution using aqueous scrubbing of a gaseous waste HBr stream from a bromination reactor is relatively simple. However, lower concentrations are possible depending on the operation of such a unit and the rate of HBr evolution from the bromination process. The effect of decreased HBr concentration was studied using a 35% HBr solution prepared by diluting the standard pilot unit feed with distilled water. The HBr and oxygen flow rates were adjusted so that the residence time in the reactor was the same as the standard operating conditions. At a 275 °C inlet temperature, 96% conversion was obtained at the reactor exit, and an exotherm of only 6 °C was observed. Increasing the reactor inlet temperature to 278 °C increased conversion to 97.5%, and further increasing the temperature to 281 °C brought the conversion to 98.5–99.1%. Therefore, high HBr conversion can be achieved with more dilute HBr solutions. However, this may not be economically advantageous, since the increased volume of water processed would increase the energy required for feed vaporization per pound of bromine recovered. Furthermore, it would increase the size of the downstream bromine–water separation equipment required, increasing both capital and operating costs.

Air as the Oxidant. Pure oxygen is the oxidant of choice for the catalytic oxidation process because it minimizes the amount of noncondensable gases downstream of the reactor. This minimizes the amount of bromine which must be removed before venting and the energy required to remove it. However, the ready availability of atmospheric air makes it a viable alternative for commercial operation. Air was tested in the reactor using the standard HBr feed rate and reactor inlet temperature. The presence of the nitrogen diluent reduced the residence time in the reactor by about 12% and the conversion at the reactor exit to 97.8%. Increasing the reactor inlet temperature to 278.2 °C increased conversion to 99.0%. These results show that high HBr conversion can be achieved while substituting air for oxygen.

Conclusions

Effective heat management can be achieved for the catalytic HBr oxidation process using a combination of aqueous instead of anhydrous HBr and a tube and shell heat exchanger reactor design. This gave a maximum measured temperature rise in the reactor of about 12 °C, which is much lower than the 2000 °C adiabatic temperature rise predicted for the anhydrous HBr and oxygen system. This reduced temperature increase allows construction of the reactor from conventional alloys and aids in minimizing catalyst promoter migration, both of which presented problems in earlier attempts to develop this process.

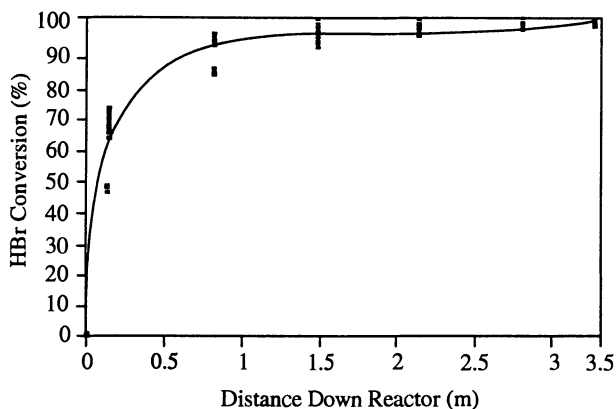


Figure 7. HBr conversion as a function of distance down the reactor in the pilot unit at standard operating conditions.

With resolution of the heat management issue, it was possible to develop a catalyst which provides high activity and stability. The new Brocat catalyst showed at least twice the activity of the unstable CuO/ZrO_2 catalyst, and 10 to 20 times higher activity than the more stable $\text{CeO}_2/\text{ZrO}_2$ catalysts. The Brocat catalyst also showed resistance to deactivation due to contaminants in the HBr feed. The combustion of propionic acid observed over the Brocat catalyst is particularly advantageous because it provides a method for removal of undesirable organics and potentially brominated organics from recycle streams. Removal of these materials is not possible by chlorine or hydrogen peroxide recycle methods, thus their applicability is limited.

The high, stable activity demonstrated during the 563-hour catalyst life test demonstrates the viability of the catalyst for service in a commercial system. The lack of any shift in position of the temperature maximum and the essentially constant conversion achieved throughout the life test suggests indefinite catalyst life. We believe, given the catalyst's excellent performance, that catalyst deactivation and the need to replace it will be determined more by unit upset than by more gradual catalyst aging effects.

The excellent catalyst performance and the flexibility of the system in maintaining high bromine recovery efficiency under widely varying flow conditions indicate that a commercial multitubular reactor should readily achieve high bromine yields. The 100% selective bromination reaction and the high conversion observed at 30% excess flow indicate that the precise balancing of flows through the tubes of a multitubular Brocat unit is not as critical as that for many catalytic processes that use these types of reactors.

Overall, this work demonstrates that the Brocat catalyst using a 48% aqueous HBr feed stream and a multitubular reactor concept is a viable process for recovering bromine from waste HBr. This system achieves much higher bromine yields than the hydrogen peroxide-based bromine recovery process without generating a waste salt stream requiring disposal.

Acknowledgements

The authors would like to acknowledge the efforts of Phat Lu, Mark Muroaka, and Thomas Rostrup-Nielsen in the preparation and testing of the catalyst at the laboratory and pilot stages and Shannon Downey and George Voss for development of the analytical methods. We would further like to acknowledge the support and advice of David Schubert, Robert Garten, and Eric Evitt.

References

1. Cullis, C. F. In *Bromine Compounds: Chemistry and Applications*; Price, D.; Iddon, B.; Wakefield, B. J., Eds.; Elsevier: New York, NY, 1988, pp 301–331.
2. Schubert, P. F.; Mahajan, S.; Beatty, R. D.; Rostrup-Nielsen, T.; Schubert, D. W.; Lu, P. T. *CHEMTECH*, **1993**, 23, 37.
3. Hooker, G. W. U.S. Patent 2 163 877, 1939.
4. Yaron, F. In *Bromine and Its Compounds*; Jolles, Z. E., Ed.; Academic Press: New York, NY, 1966, pp 3–40.
5. John, D. H. O. In *Bromine and Its Compounds*; Jolles, Z. E., Ed.; Academic Press: New York, NY, 1966; p 100.
6. Reeve, K. M.; Dear, K. M. In *Advances in Organobromine Chemistry*; Desmurs, J.-R.; Bernard, G., Eds.; Elsevier: New York, NY, 1991; Vol. 1, pp 127-134.
7. Reeve, K. M.; Jeff, M. *Proceedings, Chemicals and the Environment Symp.*, 1992, pp 59-63.
8. Calloue, G.; Isard, A. U.S. Patent 4 029 732, 1977.
9. Jenker, H.; Strang, R. German Patent DE 27 13 345 C2, 1982.
10. Mugdan, M. British Patent 585 728, 1947.
11. Mugdan, M. U.S. Patent 2 536 457, 1951.
12. Heemskerk, J.; Stuiiver, J. C. Netherlands Patent Appl. 6 404 460, 1964.
13. Lester, G. R. U.S. Patent 3 310 380, 1967.
14. Louvar, C. J.; de Rosset, A. J. U.S. Patent 3 346 340, 1967.
15. Lester, G. R. U.S. Patent 3 353 916, 1967.
16. Massonne, J.; Meyer, B. U.S. Patent 3 379 506, 1968.
17. Hay, R. G.; Walsh, W. L. U.S. Patent 3 437 445, 1969.
18. Eisenhauer, G.; Strang, R.; Amm, A. Eur. Pat. Appl. 0 179 163 A1, 1984.

RECEIVED September 30, 1993

Chapter 34

Application of Supported Gold Catalysts in Environmental Problems

Susumu Tsubota, Atsushi Ueda, Hiroaki Sakurai, Tetsuhiko Kobayashi,
and Masatake Haruta

Government Industrial Research Institute of Osaka, Midorigaoka
1-8-31, Ikeda 563, Japan

Small gold particles deposited on metal oxides exhibit extraordinarily high catalytic activities at low temperatures. For example, Au/ α -Fe₂O₃ can catalyze the oxidation of CO at a temperature as low as -70°C. The reaction is not retarded but accelerated by moisture contained in reaction gases. These unique properties of supported gold catalysts show a potential of their applications in a variety of environmental problems. The catalytic nature of supported gold depends on the kind of metal oxides supports. The suitable supports which we have found are NiFe₂O₄ for NO_x reduction by CO and for the oxidation-decomposition of trimethylamine, Co₃O₄ for the complete oxidation of CH₄ and C₃H₈, Al₂O₃ for NO_x reduction by C₃H₆ in the presence of O₂ and H₂O, and ZnO for CO₂ hydrogenation to methanol.

Gold has long been regarded as catalytically far less active than platinum group metals(1). However, our work(2, 3) and recent publications by other groups (4-8) have clearly shown that gold is extraordinarily active for low-temperature oxidation of CO when it is highly dispersed and deposited on reducible metal oxides, hydroxides of alkaline earth metals, or amorphous ZrO₂. Some of our gold catalysts are already commercialized for room-temperature air purification(9) and for selective CO gas sensors(10). In addition, it has been found that by selecting suitable metal oxides as supports, gold becomes active for many other reactions including the complete oxidation of hydrocarbons, reduction of NO, and hydrogenation of CO and CO₂(11-15). This paper presents several examples of supported gold catalysts which are applicable to environmental problems.

Experimental

In the experiments performed to investigate the effect of metal oxide supports for the oxidation of CO and H₂, all the samples had an atomic ratio of Au/Me=1/19(where Me is metal of oxide support) and were all prepared by coprecipitation (2) except for Au/SiO₂. The atomic ratio was found to give the highest activities for the reactions.

0097-6156/94/0552-0420\$08.00/0
© 1994 American Chemical Society

The coprecipitate was washed and then dried under vacuum overnight and finally calcined in air at 400°C for 5h. These coprecipitated catalysts are denoted as c, Au/Me=X/Y.

Gold supported on SiO₂ and supported gold catalysts with smaller gold loadings were prepared by deposition-precipitation followed by washing, drying, and calcination in air at 400°C for 4h (3). These samples are denoted as d.p., Au=Xwt%.

Standard catalytic activity measurements were carried out in a fixed bed reactor using 200mg of catalysts of 70 to 120 mesh size. A standard gas containing 1 vol% H₂ or CO in air was dried in a silica gel and P₂O₅ column and passed through the catalyst bed at a rate of 67 ml/min (SV=20,000h⁻¹·ml/g-cat.). The reaction gases used in the activity measurements for other reactions were; CH₄(0.25vol%), C₃H₈(0.1vol%), C₃H₆(0.1vol%), or (CH₃)₃N(0.05vol%) balanced with air, 0.1vol% NO and 0.1vol% CO balanced with He, 0.1vol%NO, 0.05vol%C₃H₆, 5vol%O₂, 1.8vol%H₂O, and a 50 atm. mixture of CO₂ and H₂ with a molar ratio of 1/3. The conversions of reactants were determined by analyzing effluent gases by gas chromatography.

The particle size of gold was determined by high-resolution TEM(Hitachi H-9000) photography. TPD measurements were carried out by using an apparatus equipped with a TCD detector after treating the samples in an O₂ or He stream at 400°C for 10h and then cooling down to 0°C. For TPD of surface CO species, after CO injection, the desorbed species were identified by a quadrupole mass analyzer (ANELVA AQA-100 MPX). FT-IR measurements were conducted at room temperature by using Nicolet 20SXC after pretreating the samples in a He stream at 200°C for 30 min.

Results and Discussion

Characterization of supported gold catalysts. The cross sectional view in high magnification TEM photographs shows that gold particles are not spherical but hemispherical in shape with diameters below 5nm and are deposited on metal oxide with their flat plane attached to the metal oxide(11). This structure provides stability of small gold particles against coalescence during many catalytic reactions. Table 1 shows the preparation methods, specific surface areas, mean particle diameters of gold, temperatures for 50% conversion of H₂ and CO in their oxidation.

Catalytic nature in CO and H₂ oxidation. It is very interesting that supported gold differs completely from unsupported gold in catalysis(2). Unsupported gold metal particles are poorly active for the oxidation of CO at temperatures below 300°C, however, they can catalyze the oxidation of H₂ at much lower temperatures. This feature is commonly observed with other noble metal catalysts like palladium supported on Al₂O₃.

Table 1 Preparation methods, specific surface areas, mean particle diameters of gold and temperature for 50% conversion of H₂ and CO of gold catalysts

Catalysts	Preparation method	Diameter of gold particle [nm]	T _{1/2} [CO]	T _{1/2} [H ₂]	BET surface area [m ² /g]
			[°C]	[°C]	
Au/α-Fe ₂ O ₃	c, 5/95	4	ca. -70	27	40
Au/Co ₃ O ₄	c, 5/95	6	ca. -70	50	57
Au/TiO ₂	d.p., 3.3wt%	3.5	-35	28	40

On the other hand, supported gold catalysts are extraordinarily active for CO oxidation. The reaction can take place even at -70°C , whereas hydrogen oxidation requires temperatures above room temperature. This result appears to be a reflection of the catalytic properties of support metal oxides, which are usually more active for CO oxidation than H_2 oxidation.

The most highly active gold catalysts for low-temperature CO oxidation were obtained with TiO_2 , Fe_2O_3 , Co_3O_4 , NiO , $\text{Be}(\text{OH})_2$, $\text{Mg}(\text{OH})_2$ as supports. Figure 1 shows that, over gold supported on TiO_2 , $\alpha\text{-Fe}_2\text{O}_3$ and Co_3O_4 , turnover frequencies (TOFs) based on surface gold atoms are almost independent of the kind of metal oxide support, while they are significantly dependent on the particle diameter of gold.

Based on the experimental results obtained from FTIR, TPD and kinetic experiments, we have proposed a mechanism for CO oxidation on supported gold(16). Carbon monoxide is reversibly adsorbed on gold particles and partly migrates toward support oxides and there it reacts with adsorbed oxygen to form bidentate carbonate species. The decomposition of the carbonate intermediate appears to be rate-determining. If the active sites for oxygen adsorption might be created in the interfacial perimeter around the gold particles, the active sites of oxygen should increase proportionally to the inverse second power of the particle diameter.

Commercial gold catalysts are produced in which Au is deposited on $\alpha\text{-Fe}_2\text{O}_3$ which had been earlier coated on Al_2O_3 honeycombs or beads. These catalysts contain a reduced amount of gold, typically 0.4 wt% and applicable to practical uses in removing odor and CO from air at room temperature. Figure 2 shows that CO oxidation is enhanced when moisture is contained in reaction gas(9). This catalytic feature is also observed in other supported gold catalysts. This appears to be one of major advantages of supported gold catalysts for use in the environment. The reason for enhancement by moisture is now under investigation.

Catalytic combustion of hydrocarbons and trimethylamine. In reactions other than the oxidation of CO and H_2 , we have also observed noteworthy support effects. Figure 3 shows that catalytic activity, expressed by temperature for 50% conversion in the oxidation of CH_4 , C_3H_8 , and C_3H_6 , decreases in the order of $\text{Au}/\text{Co}_3\text{O}_4 > \text{Au}/\text{NiFe}_2\text{O}_4 > \text{Au}/\text{ZnFe}_2\text{O}_4 > \text{Au}/\alpha\text{-Fe}_2\text{O}_3$ (17). The metal oxides with higher oxidation activities can give more active supported gold catalysts. It should be noted that in the oxidation of unsaturated hydrocarbons such as C_3H_6 , Pt and Pd catalysts were more active than for any supported gold catalysts. However, in the oxidation of saturated hydrocarbons like CH_4 and C_3H_8 , some supported gold catalysts are more active than Pt catalyst supported on Al_2O_3 . The most highly active $\text{Au}/\text{Co}_3\text{O}_4$ catalyst is as active as, for example, a commercial $\text{Pd}/\text{Al}_2\text{O}_3$ catalyst. These results, although obtained with different metal loadings, therefore prove that gold should be included as one of catalytically active metals in the oxidation of saturated hydrocarbons.

Supported gold catalysts are more active in the oxidation-decomposition of $(\text{CH}_3)_3\text{N}$, one of typical odor compounds, than supported Pd and Pt catalysts. The activity order observed is, however, not a simple reflection of the oxidation activities of metal oxide supports. Ferric oxide and ferrites can give rise to more active gold catalysts than simple Co_3O_4 which is the most active base metal oxide(17), Figure 4 shows that supported gold catalysts are also advantageous over Pt group catalysts in that they yield N_2 more selectively than N_2O and NO.

NOx reduction. Ferric oxide, which has been reported to be the most active, can catalyze the CO + NO reaction at a temperature above 150°C (18)

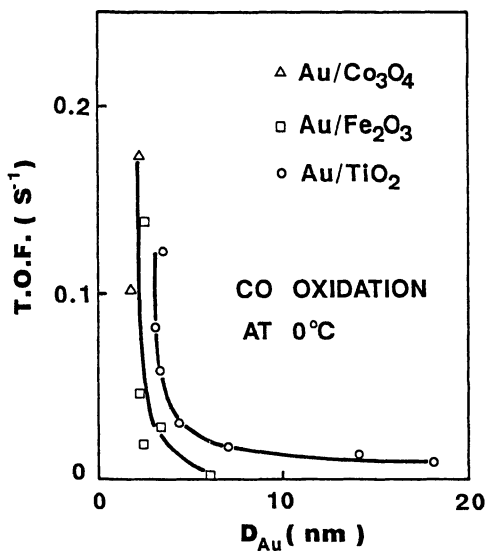
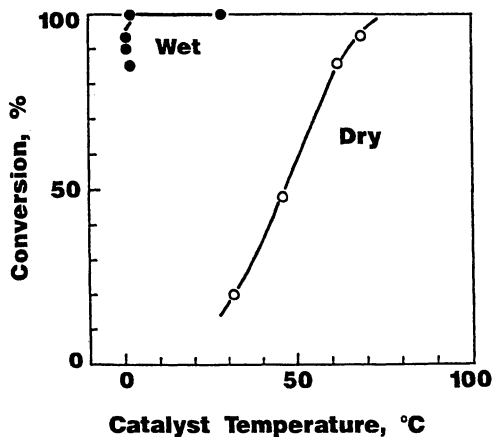
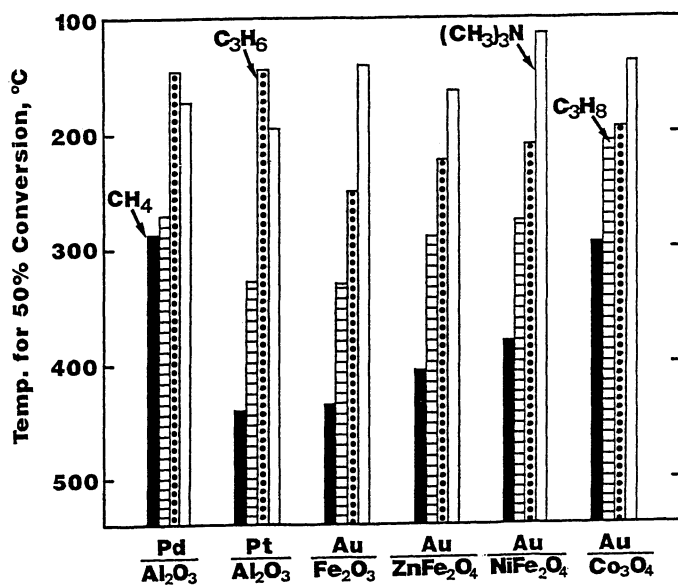


Figure 1 Turnover frequencies as a function of the mean particle diameters of gold in CO oxidation at 0°C.



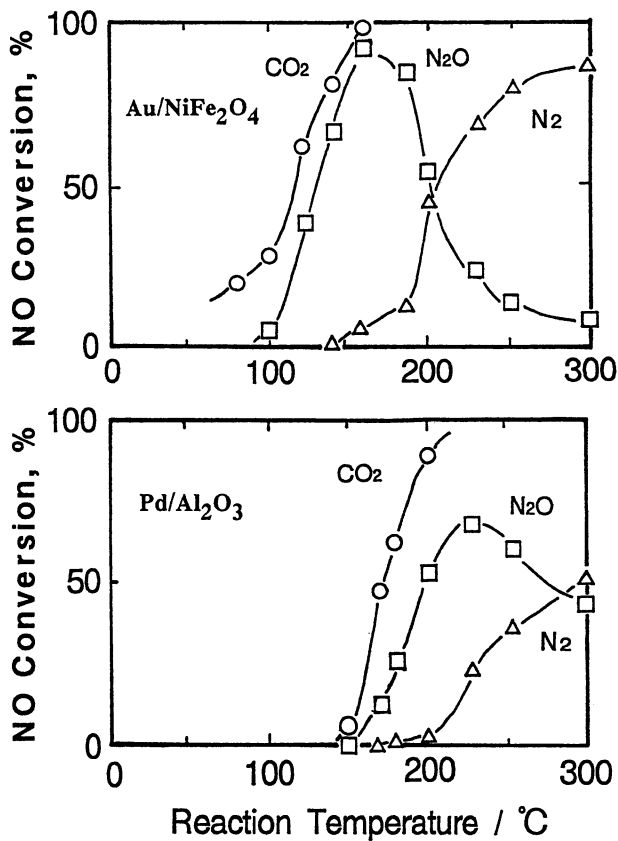
(\circ) dried at 0°C with SiO_2 gel column.
 (\bullet) bubbled into water at 0°C.
 Reaction gas: CO 1vol% in air; $SV=2 \times 10^4 h^{-1} ml/g\text{-cat.}$

Figure 2 Effect of moisture on CO conversion over Au/ α - Fe_2O_3 - Al_2O_3 Beads catalyst (Reproduced with permission from reference 9)



Pd and Pt catalysts; 1 wt%, Au catalysts; 5 at% (ca. 10 wt%)
 Reaction gases: CH₄ 0.25 vol% ; C₃H₈ 0.1 vol% ; C₃H₆, 0.1 vol% ;
 (CH₃)₃N 0.05 vol% in air; SV = 2 × 10⁴ h⁻¹ ml/g-cat.

Figure 3 Catalytic activities of supported gold catalysts for the oxidation of hydrocarbons



Pd catalyst; 1wt%, Au catalyst; 5at%
 Reaction gas: (CH₃)₃N 0.05vol% in He; SV= 2x10⁴ h⁻¹ ml/g-cat.

Figure 4 The concentration of reactants and products of the oxidation-decomposition of (CH₃)₃N as a function of temperature

Publication Date: February 23, 1994 | doi: 10.1021/bk-1994-0552.ch034

The deposition of gold on ferric oxide enhances the catalytic activity to lower the reaction temperature by about 50 °C. Figure 5 shows that when a ferric oxide support is replaced by ferrites of Co or Ni, the activity is so noticeably increased that CO + NO reaction can take place even at room temperature. At 70°C, complete reduction to N₂ abruptly prevails consuming CO almost quantitatively. This tendency was also observed in the oxidation-decomposition of (CH₃)₃N and appears to be a reflection of the activating ability of the metal oxides for the N-O and C-N bonds. As far as we have studied until now, Au/NiFe₂O₄ has been the most active catalyst both for the decomposition of (CH₃)₃N and for NO reduction with CO. Some supported gold catalysts have been found to be tolerant against moisture(19).

For commercial application, the effect of oxygen is very important. Table 2 shows some examples of our work on the selective reduction of NO by hydrocarbons in the presence of oxygen and moisture. Gold supported on Al₂O₃ can reduce 40% of NO to N₂ at 300°C even in the copresence of 5% O₂. It is also interesting that this activity is retained in the copresence of moisture. This is a unique property of gold catalysts compared to other de-NO_x catalysts proposed, such as Cu-ZSM5.

Table 2 The selective reduction of NO by hydrocarbons in the presence of O₂ and moisture

Catalysts /temperature (°C)	Conversion of NO to N ₂ (%)				
	200	250	300	350	400
Au/Al ₂ O ₃	7.2	20.1	39.7	30.2	15.4
Au/TiO ₂	5.5	8.1	11.6	25.5	18.9
Au/MgO	4.3	6.2	10.3	24.2	20.3

Au catalysts 1wt%, prepared by deposition precipitation.

Reaction gas; NO 0.1vol%, C₃H₆ 0.05vol%, O₂ 5vol%, H₂O 1.8vol% in He;

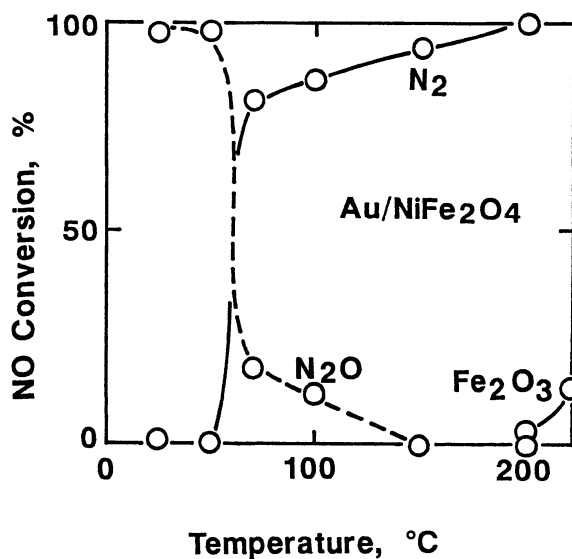
SV= 2x10⁴ h⁻¹ ml/g-cat.

CO₂ hydrogenation. Table 3 shows methanol yields in the hydrogenation of CO₂ over gold catalysts as a function of temperature. Although Cu was believed to be the only active metal species for the synthesis of methanol, gold has been found to be almost as active(20). A similar conclusion has also been reported for amorphous ZrO₂ support by Baiker et al. (15). Ferric oxide and ZnO appears to be the most desirable supports for methanol synthesis, however, because Fe₂O₃ is reduced to Fe₃O₄ during the reaction, ZnO can be regarded as the best support among simple metal oxides. It is interesting to note that ZnO is the most effective catalysts in the hydrogenation of CO₂ over both Cu and Au based catalysts.

Table 3 Methanol yields in the hydrogenation of CO₂ over supported gold catalysts

Catalysts /temperature (°C)	Methanol yield (%)					
	150	200	250	300	350	400
Au/ZnO (c, 1/19)	0	0	2.3	5.3	1.7	0.5
Au/Fe ₂ O ₃ (c, 1/19)	0.3	2.0	5.4	3.6	0.9	0.3
Au/TiO ₂ (d.p., 3.3wt%)	0.0	0.5	1.3	1.0	0.3	0.0
Cu/ZnO (c, 1/19)	0.0	1.8	4.4	5.0	1.8	0.6

Reaction gas, CO₂/H₂=1/3; 50at; SV=3,000h⁻¹ml/g-cat.



Au catalyst; 5at%

Reaction gas. NO 0.1vol% , CO 0.1vol% in He; SV= 2×10^4 h⁻¹ ml/g-cat.

Figure 5 The concentration of products of NO+CO reaction over Au/NiFe₂O₄ as a function of temperature

Conclusion

Gold supported on a variety of metal oxides exhibits unique catalytic properties and has a prosperous potential in environmental catalysis.

1. Low-temperature activities are often observed over supported gold catalysts. The activities are usually enhanced by moisture.
2. Catalytic properties can be tunable by selecting suitable metal oxide supports; TiO₂, Fe₂O₃, Co₃O₄, NiO, Be(OH)₂, Mg(OH)₂ for CO oxidation, Co₃O₄ for the catalytic combustion of hydrocarbons, NiFe₂O₄ for NO reduction by CO and oxidation-decomposition of trimethylamine, Al₂O₃ for NO reduction by C₃H₆ in the presence of O₂ and H₂O, and ZnO for CO₂ hydrogenation to produce methanol.

Literature Cited

- 1 Schwank, J. *Gold Bull.*, **1983**, *16*, 103.
- 2 Haruta, M.; Yamada, N.; Kobayashi, T.; Iijima, S., *J. Catal.* **1989**, *115*, 301.
- 3 Tsubota, S.; Haruta, M.; Kobayashi, T.; Ueda, A.; Nakahara, Y. In *Preparation of Catalysts V*; Poncelet, G.; Jacobs, P.A.; Grange, P.; Delmon, B., Eds.; Elsevier: Amsterdam, 1991; p.695.

- 4 Gardner, S. D.; Hoflund, G. B.; Upchurch, B. T.; Schryer, D. R.; Kielin, E. J.; Schryer, J. J. *Catal.* **1991**, *129*, 114.
- 5 Takamatsu, S.; Ishi-i, M.; Imagawa, M.; Kinbara, H.; Kikuta, T.; Fukushima, T. *Shokubai*(Catalyst, Cat. Soc. Jpn.), **1992**, *34*, 126.
- 6 Tanielyan, S. K.; Augustine, R. L. *Appl. Catal. A, General*, **1992**, *85*, 73.
- 7 Knell, A.; Barnickel, P.; Baiker, A.; Wokaun, A. J. *Catal.* **1992**, *137*, 306.
- 8 Lin, S. D.; Bollinger, M.; Vannie, M. A. *Catal. Lett.* **1992**, *17*, 245.
- 9 Haruta, M.; Takase, T.; Kobayashi, T.; Tsubota, S. *Cat. Sci. Techn.*; Yoshida, S.; Takezawa, N.; Ono T., Eds.; Kodansya Ltd.: Tokyo, 1991, Vol. 1; p.331.
- 10 Funazaki, N.; Asano, Y.; Yamashita, S.; Kobayashi, T.; Haruta, M. *Proc. 4th Intern. Meet. Chem. Sensors*, Tokyo, 1992, 606.
- 11 Haruta, M. *Now & Future*(publ. by Japan Ind. Techn. Assoc.), **1992**, *7*, 13.
- 12 Frost, J. C. *Nature* **1988**, *334*, 577.
- 13 Lin, S.; Vannice, M. A. *Catal. Lett.* **1991**, *10*, 47.
- 14 Shaw, E. A.; Walker, A. P.; Rayment, T.; Lambert, R. M. J. *Catal.*, **1992**, *134*, 747.
- 15 Baiker, A.; Kilo, M.; Maciejewski, M.; Menzi, S.; Wokaun, A. *Proc. 10th Intern. Congr. Catal.*, Budapest, 1992, 208.
- 16 Haruta, M.; Tsubota, S.; Kobayashi, T.; Ueda, A.; Sakurai, H.; Ando, M. *Shokubai* (Catalyst, Cat. Soc. Jpn.) **1991**, *33*, 440.
- 17 Haruta, M.; Ueda, A.; Tsubota, S.; Kobayashi, T.; Sakurai, H.; Ando, M. *Proc. 1st. Japan-EC Joint Workshop on the Frontiers of Catal. Sci. Techn.*, Tokyo, 1991, 173.
- 18 Shelef, M.; Otto, K. J. *Catal.* **1968**, *10*, 408.
- 19 Ueda, A.; Kobayashi, T.; Tsubota, S.; Sakurai, H.; Ando, M.; Haruta, M.; Nakahara, Y. *Proc. 1st. Japan-EC Joint Workshop on Frontiers of Catal. Sci. Techn.*, Tokyo, 1991, 272.
- 20 Sakurai, H.; Haruta, M.; Kobayashi, T.; Tsubota, S.; Ueda, A.; Ando, M. *Proc. 1st Meeting on CO2 Fixation*, Tokyo, 1991, 26.

RECEIVED September 30, 1993

Author Index

- Agarwal, S. K., 224
Alemany, Pere, 140
Armor, John N., 2,90,170,270,298,372
Bartholomew, C. H., 74
Beatty, Richard D., 405
Beer, J. K., 172
Berg, P. van der, 393
Bianchi, Claudia L., 353
Brendley, William H., Jr., 331,340
Centi, G., 22,233
Chen, J. M., 215
Chuang, Steven S. C., 157
Datye, Abhaya, 39
Davidson, J., 74
Debnath, Santanu, 157
Dillen, A. J. van, 393
Drago, Russell S., 331,340
Ellison, William, 190
Flytzani-Stephanopoulos, Maria, 7,375
Gandhi, H. S., 53
Gatte, Robert R., 286
Gervasini, Antonella, 353
Geus, J. W., 393
Gopalakrishnan, R., 74
Grunewald, G. C., 340
Haack, L. P., 66
Harding, Robert H., 286
Haruta, Masatake, 420
Heck, R. M., 215
Hecker, W. C., 74
Hirano, Hideki, 114
Hoffmann, Roald, 140
Huisman, H. M., 393
Hüttenhofer, K., 172
Jang, B. W.-L., 224
Jen, H. W., 53
Jurczyk, Krzysztof, 331
Kharas, Karl C. C., 39
Klinghoffer, Alec A., 316
Kobayashi, Tetsuhiko, 420
Liu, Wei, 375
Lowe, Phillip A., 190,205
Mahajan, Suresh, 405
Marcelin, G., 224
Maroldo, Stephen G., 331
Mercera, P. D. L., 250
Morris, L., 215
Mos, R., 393
Nieuwenhuys, Bernard E., 114
Nigro, C., 22
Ommen, J. G. van, 250
Oukaci, R., 224
Parker, Linda M., 301
Passarini, N., 233
Patterson, John E., 301
Perathoner, S., 22,233
Petrosius, S. C., 340
Powers, Don, 273
Ragaini, Vittorio, 353
Riley, A., 224
Riva, A., 233
Robota, Heinz J., 39
Ross, J. R. H., 250
Rossin, Joseph A., 316
Sakurai, Hiroaki, 420
Schubert, Paul F., 405
Seshan, K., 250
Shelef, M., 66
Siera, Jacobus, 114
Speronello, B. K., 215
Spitznagel, G. W., 172
Srinivas, Girish, 157
Stafford, P., 74
Stella, G., 22
Summers, J. C., 94
Tanaka, Ken-ichi, 114
Tsubota, Susumu, 420
Ueda, Atsushi, 420
Vandersall, Mark T., 331
Ward, Thomas R., 140
Whitecavage, Jacqueline A., 286
Williamson, W. B., 94
Wise, J. Barin, 273
Wormsbecher, Richard F., 286
Xue, E., 250
Zhang, Yanping, 7

Affiliation Index

- Air Products & Chemicals, Inc.,
2,90,170,270,298,372
AlliedSignal Environmental Catalysts, 94
AlliedSignal Research & Technology, 39
Brigham Young University, 74
Catalytica, Inc., 405
Cornell University, 140
Dipartimento di Chimica Industriale
e dei Materiali, 22,233
Ellison Consultants, 190
Engelhard Corporation, 215
Enichem ANIC, 233
Ford Motor Company, 53,66
Geo-Centers, Inc., 316
Government Industrial Research Institute
of Osaka, 420
Intech Inc., 190,205
Leiden University, 114
Lyondell Petrochemical Company, 273
Massachusetts Institute of Technology, 7,375
New Zealand Institute for Industrial Research
and Development, 301
Research Triangle Institute, 224
Rohm and Haas Company, 331,340
Siemens AG, 172
Università di Milano, 353
University of Akron, 157
University of Florida, 331,340
University of New Mexico, 39
University of Pittsburgh, 224
University of Tokyo, 114
University of Twente, 250
Utrecht University, 393
W.R. Grace and Company—Conn., 286

Subject Index

A

- Acidity of catalyst, sulfate effect, 266
Adhesion in three-way catalyst
ceramic support vs. Fermi level, 151,153
charge transfer, 150*t*,152*f*
experimental description, 141
Fermi level for N₂O₂ adsorption, 153,154*f*
Fermi level for NO adsorption, 151,153,154*f*
Fermi level variation, 151*t*,152
geometry, 141–146,148
interactions affecting adhesive
properties, 147,149–150
models, 146–148*f*
Adsorbents, synthetic carbonaceous, 332
Adsorption–desorption characteristics of
catalysts, sulfate effect, 262–264*f*
Air, role as oxidant in catalytic bromine
recovery from HBr waste, 417
Air–fuel ratio of exhaust, palladium
catalyst aging effect, 105–109*f*
Air inlet temperature, transient response
effect for monolithic oxidation
catalyst, 326*f*–329
γ-Al₂O₃, use as support for NO and
N₂O₂ adsorption on metal catalysts, 146
Aliphatic hydrocarbons, low-temperature
deep oxidation, 331–339
Alkaline earths, cocation effect in
catalytic decomposition of NO using
copper ion exchanged ZSM-5 zeolites,
8–20
Alternative fuels, examples, 270
Alumina
adhesion of Rh, Pd, and Pt, 140–154
diffuse reflectance IR experiments, 395–397
γ-Alumina, catalyst for Claus reaction and
COS hydrolysis, 394
Aromatic hydrocarbons, low-temperature
deep oxidation, 331–339
Atmospheric sulfur
cycle, 372,373*f*
removal, 372,374
Au–γ-Al₂O₃, role in NO reduction by
hydrocarbon in oxidizing atmosphere, 61
Automobile exhaust, NO_x removal methods,
53–54
Automotive emission control catalysts,
function, 90
Automotive three-way catalyst, advantages
for purification of automotive exhaust
gas, 114

Affiliation Index

- Air Products & Chemicals, Inc.,
2,90,170,270,298,372
AlliedSignal Environmental Catalysts, 94
AlliedSignal Research & Technology, 39
Brigham Young University, 74
Catalytica, Inc., 405
Cornell University, 140
Dipartimento di Chimica Industriale
e dei Materiali, 22,233
Ellison Consultants, 190
Engelhard Corporation, 215
Enichem ANIC, 233
Ford Motor Company, 53,66
Geo-Centers, Inc., 316
Government Industrial Research Institute
of Osaka, 420
Intech Inc., 190,205
Leiden University, 114
Lyondell Petrochemical Company, 273
Massachusetts Institute of Technology, 7,375
New Zealand Institute for Industrial Research
and Development, 301
Research Triangle Institute, 224
Rohm and Haas Company, 331,340
Siemens AG, 172
Università di Milano, 353
University of Akron, 157
University of Florida, 331,340
University of New Mexico, 39
University of Pittsburgh, 224
University of Tokyo, 114
University of Twente, 250
Utrecht University, 393
W.R. Grace and Company—Conn., 286

Subject Index

A

- Acidity of catalyst, sulfate effect, 266
Adhesion in three-way catalyst
ceramic support vs. Fermi level, 151,153
charge transfer, 150*t*,152*f*
experimental description, 141
Fermi level for N₂O₂ adsorption, 153,154*f*
Fermi level for NO adsorption, 151,153,154*f*
Fermi level variation, 151*t*,152
geometry, 141–146,148
interactions affecting adhesive
properties, 147,149–150
models, 146–148*f*
Adsorbents, synthetic carbonaceous, 332
Adsorption–desorption characteristics of
catalysts, sulfate effect, 262–264*f*
Air, role as oxidant in catalytic bromine
recovery from HBr waste, 417
Air–fuel ratio of exhaust, palladium
catalyst aging effect, 105–109*f*
Air inlet temperature, transient response
effect for monolithic oxidation
catalyst, 326*f*–329
γ-Al₂O₃, use as support for NO and
N₂O₂ adsorption on metal catalysts, 146
Aliphatic hydrocarbons, low-temperature
deep oxidation, 331–339
Alkaline earths, cocation effect in
catalytic decomposition of NO using
copper ion exchanged ZSM-5 zeolites,
8–20
Alternative fuels, examples, 270
Alumina
adhesion of Rh, Pd, and Pt, 140–154
diffuse reflectance IR experiments, 395–397
γ-Alumina, catalyst for Claus reaction and
COS hydrolysis, 394
Aromatic hydrocarbons, low-temperature
deep oxidation, 331–339
Atmospheric sulfur
cycle, 372,373*f*
removal, 372,374
Au–γ-Al₂O₃, role in NO reduction by
hydrocarbon in oxidizing atmosphere, 61
Automobile exhaust, NO_x removal methods,
53–54
Automotive emission control catalysts,
function, 90
Automotive three-way catalyst, advantages
for purification of automotive exhaust
gas, 114

B

- Barium-promoted copper chromite oxide, low-temperature combustion of volatile organic compounds using ozone, 354–368
- Brocat, use in bromine recovery from HBr waste, 408–418
- Bromination of organic compounds applications, 405
 - production of HBr, 405,406*t*
- Bromine recovery from HBr waste, catalytic, *See* Catalytic bromine recovery from HBr waste
- Butane conversion, low-temperature deep oxidation, 336,338*t*
- Butene, isomerization process, 275–285
- Byproducts, production, 372,374*t*

C

- C₃H₆ reduction of NO
 - Arrhenius plot for Cu–ZSM-5, 55,56*f*
 - C₃H₆ concentration effect over Cu–Al₂O₃, 58,59*f*
 - experimental procedure, 54–55
 - flow rate vs. activity over Cu–ZSM-5, 55,57*f*
 - initial reactant concentration rate, 55,58*t*
 - NO concentration effect over Cu–Al₂O₃, 58,60*f*
 - O₂ content effect over Cu–Al₂O₃, 58*t*,59*f*
 - O₂ content effect over Pd–ZSM-5, 58,62*f*
 - previous studies, 54
 - reactions, 61,63–64
 - temperature effect
 - Au–γ-Al₂O₃, 61,62*f*
 - Cu–Al₂O₃, 55,57*f*,58
 - Cu–ZSM-5, 55,56*f*
 - Pd–ZSM-5, 58,60*f*
- Carbon filter, limitations, 316
- Carbon molecular sieves, 332
- Carbonaceous adsorbents, synthetic, 332
- Catalysis, number of applications to solve environmental problems, 372
- Catalyst(s)
 - categories, 341
 - low-temperature oxidation of ethene, 301–313
 - monolithic oxidation, process condition effect of transient response, 316–329

Catalyst(s)—*Continued*

- role in fuel production, 270–271
- sulfate effect on adsorption–desorption characteristics, 262–264*f*
- sulfate treatment effect on surface area, 266
- Catalyst(s) for cleanup of NH₃, NO_x, and CO from nuclear waste processing facility
 - Cu–ZSM-5 effect on CO and NH₃ conversion, 76–78
 - Cu–ZSM-5 + Pt–Al₂O₃ effect on conversion, 84,85*t*,87*f*
 - experimental procedure, 75–76
 - NH₃–NO ratio effect on NH₃ and CO conversions, 78–81*f*
 - NO_x reduction by NH₃ on metal ion exchanged ZSM-5 vs. that of previous studies, 85–87
 - Pt–Al₂O₃ effect on CO conversion, 76,77*f*
 - Pt–Al₂O₃ effect on NH₃ conversion, 78,82–84
 - requirements, 74
- Catalyst performance
 - sulfate effect, 250–251
 - surface acidity effect, 250
- Catalyst technologies, NO_x removal in power plant applications, 215–223
- Catalytic bromine recovery from HBr waste air as oxidant, 417
 - analytical procedure, 411
 - catalyst activity test procedure, 409
 - catalyst preparation, 408–409
 - commercial requirements, 408
 - contaminant studies, 413–415*f*
 - flow rate effects, 416–417
 - HBr concentration effects, 417
 - HBr feed streams, 411
 - HBr oxidation catalyst(s), 407*t*,412–414*f*
 - heat management, 407–408
 - interest, 406
 - laboratory testing unit, 409,410*f*
 - methods, 406*t*,407
 - pilot unit design, 410*f*–412
 - process condition effects, 416*t*–417
- Catalytic combustion
 - control of volatile organic compounds, 298
 - elimination of volatile organic compounds, 353

- Catalytic combustion of natural gas for
NO_x control using La_{1-x}Sr_xCoO₃ catalysts
catalyst preparation, 225
catalytic methane combustion, 226–232
CO vs. methane effect on NO reduction,
229,230f
experimental description, 224–225
gas-phase combustion and catalytic
combustion, 226,227f
NO decomposition vs. catalyst, 228f,229
reaction systems, 225,227f
regulations for NO_x emissions, 224
strontium effect, 229–232
temperature-programmed oxygen evolution
procedure, 226
profiles for catalysts, 231t,232
temperature-programmed reduction
procedure, 225–226
profiles for catalysts, 229–231t
temperature vs. CO emission,
226,228f,229
temperature vs. methane conversion,
226,228f
temperature vs. NO_x formation,
226,228f,229
- Catalytic converters for diesel engine
exhaust control, need, 91
- Catalytic decomposition of nitric oxide
over promoted copper ion exchanged
ZSM-5 zeolites
activity–exchange level relationship, 7–8
advantage, 7
catalyst characterization, 9,11t
catalyst synthesis, 8–9,11t
contact time vs. catalyst activity,
17,19,20f
conversion measurement procedure, 9–10
experimental description, 8
kinetics, 15–18f
kinetics study procedure, 9–10
NO decomposition in O₂-containing gases
vs. catalyst, 13–16f
NO decomposition without O₂ vs.
catalyst, 10,12f–14f
previous studies, 8
rare earth metal cation modified
catalysts, 17,18f
temperature effect, 14f–16f
- Catalytic decomposition of NO, use for NO_x
removal, 4
- Catalytic emission control systems for
power plants
commercial experience, 222t,223
competing reactions, 216,217f
composite catalyst features, 216,217f,t
rate-limiting reactions, 216
reactions catalyzed, 216,217t
selective catalytic reduction of NO_x,
216,218
temperature-determined operation,
218–222t
- Catalytic filter for chemical warfare
agent removal, requirements, 317
- Catalytic reduction of NO, role of
hydrocarbon oxidation, 53–64
- Ce–Rh–SiO₂ catalyst, NO–CO reaction
effect, 157–166
- CeO₂ catalyst, SO₂ reduction to S, 378,381f
- CeO₂(La) catalyst, SO₂ reduction to S,
383,385f
- Ceria catalysts, SO₂ reduction to S,
375–391
- Cerium
promoter in three-way catalysts, 157–158
role in NO–CO reaction, 158–166
- Challenge concentration, transient
response effect for monolithic
oxidation catalyst, 324–326f
- Chemical warfare agents
catalytic filter, requirements, 317
removal from streams, complexity, 317
removal systems, 316
- Chemical waste, reduction efforts, 372
- Chlorinated hydrocarbons, deep oxidation,
340–351
- Claus process
γ-alumina as catalyst, 394
description and problems, 393
- Closed-loop control of automotive emissions,
palladium-only catalysts, 94–111
- CO, catalysts for cleanup from nuclear
waste processing facility, 74–87
- CO conversion
Cu–ZSM-5 effect, 76,77f
Cu–ZSM-5 + Pt–Al₂O₃ effect, 84,85t,87f
Pt–Al₂O₃ effect, 76,77f
- CO oxidation, role of supported gold
catalysts, 421–423f
- CO₂ hydrogenation, role of supported gold
catalysts, 426t

- Contemporaneous SO₂ and NO removal from flue gas using regenerable copper-on-alumina sorbent-catalyst advantages, 233,249
 behavior during simultaneous removal, 238–239,241f
 copper distribution map within alumina pellet, 236,237f
 copper-on-alumina system, 234,236
 design requirements, 233–234
 experimental procedure, 236,238
 kinetics of SO₂ oxidation-sorption, 240,242–246
 pellet size effect, 246,247f
 porosity of support effect, 246,247f
 process layout, 234,235f
 scanning electron micrograph of sample, 236,237f
 SO₂ capture mechanism, 239–241f
 SO₂ sorption, breakthrough time, 246,248f
 textural properties of alumina supports, 236t
- Conversion, definition, 277
- Copper chromite oxide, barium-promoted, low-temperature combustion of volatile organic compounds using ozone, 354–368
- Copper-exchanged zeolite activity on NO conversion
 activity, 28–30
 comparison to that of Cu-loaded oxides, 36–37
 copper effect, 35t
 copper species effect, 30–33f
 experimental procedure, 24
 NO concentration effect, 28–30
 O₂ effect, 32–36
 sample preparation, 23–24
 temperature effect, 32,34f
- Copper-exchanged ZSM-5 zeolite
 reasons for interest, 66
 X-ray photoelectron study, 67–72
- Copper ion exchanged zeolite molecular sieve, use for NO_x removal, 4
- Copper ion exchanged ZSM-5 zeolites, catalytic decomposition of NO, 7–20
- Copper-loaded oxide reactivity on NO conversion
 catalyst pretreatment effect, 24,26t
 comparison to that of Cu-exchanged zeolites, 36–37
- Copper-loaded oxide reactivity on NO conversion—*Continued*
 experimental procedure, 24
 NO reactivity 24–26t
 O₂ effect, 26–28,35–36
 O₂ vs. selectivity to N₂, 24–26
 sample preparation, 23
 temperature effect, 28,29f
- Copper-on-alumina sorbent-catalyst, contemporaneous SO₂ and NO removal from flue gas, 233–249
- COS conversion
 γ-alumina as catalyst, problems, 394
 hydrolysis to H₂S, 393
- COS hydrolysis on titania catalyst, *See* Hydrolysis of COS on titania catalysts
- CS₂ conversion, hydrolysis to H₂S, 393
- Cu-γ-Al₂O₃, role in NO reduction by hydrocarbon in oxidizing atmosphere, 55,57–60
- Cu-ZSM-5
 CO conversion effect, 76,77f
 NH₃ conversion effect, 76–78
 NO decomposition, 22–33
 NO reduction by hydrocarbon in oxidizing atmosphere, 55–57f
- Cu-ZSM-5 deactivation
 amorphous film formation in aged material, 45,47f–49f
 crystallinity of fresh catalyst, 45–47f
 CuO formation vs. aging, 42,43f
 experimental procedure, 39,40
 halo formation from amorphous material vs. aging, 42,44,46f
 intensity of reflections vs. aging severity, 44t,45,48
 micropore volume vs. deactivation severity, 42,43f,48
 performance of catalyst after treatment vs. temperature, 40–42
 performance of fresh catalyst, 40,41f
 role of sintering, 39
 sintering processes, 48,51
- Cu-ZSM-5 + Pt-Al₂O₃, CO and NH₃ conversion effect, 84,85t,87f
- CuO-Al₂O₃ and CuO-SiO₂, use for NO decomposition, 23
- Cupric sintering, role in Cu-ZSM-5 deactivation, 39–51

D

Deactivation of Cu-ZSM-5, *See* Cu-ZSM-5 deactivation

Deep oxidation of chlorinated hydrocarbons
activation energy, 346,347f
carbon support, structural parameters, 341t
catalyst characterization, 346,348–351
catalytic combustion reactivity, 342–344t
experimental procedure, 341–342
pore structure effect, 343
previous studies, 341
reactivity vs. hydrocarbon, 343–346
reactivity vs. hydrogen, 346,347f
reactivity vs. temperature, 346,347f

Desulfurization of combustion exhaust
gases, expense, 375

Diesel engine exhaust
catalytic posttreatment methods, 250
control using catalytic converters, 91
legislative requirements for emission, 250

Diffuse reflectance IR experiments
alumina, 395–397
titania, 397–400f

Doped CeO₂ catalyst, SO₂ reduction to S,
378–384

E

Emission control, mobile engine, 90–91

Emission standards, development in
Germany, 173,175f

Environmental legislation, impact on fuel
industry, 286

Environmental problems, application of
supported gold catalysts, 420–426

Ethene, requirements of low-temperature
oxidation catalyst for removal, 301

F

Flue gas, contemporaneous SO₂ and NO
removal using regenerable copper-on-
alumina sorbent-catalyst, 233–249

Foreign experience, SCR NO_x controls,
190–202

Formic acid, site-blocking agent for COS
hydrolysis, 399,401

Fuel industry, impact of environmental
legislation, 286

Future fuels, examples and production
methods, 270–271

G

Gasoline olefins, 273–275

Gasoline sulfur content
reaction kinetics for sulfur reduction,
286–295
reduction methods, 286–287
regulations, 296

Gasoline sulfur reduction
comparison to conventional technology,
293,294f
development, 293
reduction of gasoline-range sulfur
compounds, 293t–295

German experience with selective catalytic
reduction NO_x controls
high-dust configurations, 196–199
regulations, 196
tail end configurations, 199–200
transfer of technology to operating
conditions, 196

Germany, power plant capacity, 172,173t

Gold, catalytic activity, 420

Gold catalysts, supported, *See* Supported gold
catalyst application to environmental
problems

Granular activated carbon, use for control
of volatile organic compounds, 331–332

H

H₂ oxidation, role of supported gold
catalysts, 421–422

Halogenated hydrocarbons
advantages as solvents, 340
deep oxidation using catalysts, 341–351
disposal methods, 340–341

HBr

bromine recovery, 406–408
production from bromination of organic
compounds, 405,406t
recycling process, 406

Heterogeneous catalysts, control of volatile
organic compounds, 298–299

Hexane conversion, low-temperature deep
oxidation, 334,336t,337f

High-dust applications, SCR technology, 191–193

High-dust configuration

flue gas desulfurization effect, 210

German utility applications, 210,211*t*

location, 205,206*f*

problems, 207–209

High-sulfur coal service, U.S. application of SCR technology, 200–202

Highly selective olefin skeletal

isomerization process

advantages, 285

bench-scale reactor, 275–277

butene isomerization, 279,281*f*

catalyst performance, improvement, 279*t*,280*f*

catalyst screening, 275,277

commercial testing, 277,278*f*

development, 275

isobutylene yield vs. run time, 279,280*f*

operating conditions, 277

pentene isomerization, 279,282*f*,283*t*

process development unit, 276*f*,277

process flow diagram for butene and pentene isomerization, 283–285

saturates conversion in butene

isomerization, 279,281*f*

selectivity vs. run time, 279,280*f*

Hydrocarbon(s)

chlorinated, deep oxidation, 340–351

halogenated, *See* Halogenated

hydrocarbons

low-temperature deep oxidation, 331–339

NO_x removal, 4

Hydrocarbon combustion, role of supported

gold catalysts, 422,424*f*

Hydrocarbon oxidation, role in catalytic

reduction of NO, 53–64

Hydrofluoric acid, safety issue, 271

Hydrolysis of COS on titania catalysts

activity test of sulfated titania catalyst, 401–403

diffuse reflectance IR experiments

alumina, 395–397

titania, 397–400*f*

experimental procedure, 394–395

site-blocking agents, 399,401

sulfate formation, 400*f*,401

temperature-programmed reaction of sulfates with H₂S, 402*f*,403

I

Impregnated CeO₂(La) catalyst, SO₂ reduction to S, 388,391*f*

In situ infrared spectroscopy of NO–CO

reaction on Rh–SiO₂ and Ce–Rh–SiO₂

experimental procedure, 158

reaction on Ce–Rh–SiO₂, 160–162*f*

reaction on prereduced and preoxidized

Rh–SiO₂, 158–160

steady-state isotropic transient study,

160,163–166*f*

Isomerization process, highly selective

olefin skeletal isomerization, *See*

Highly selective olefin skeletal

isomerization process

J

Japanese experience with selective

catalytic reduction NO_x controls

ammonia injection system design, 194

base material design, 194–195

catalyst improvement, 194

commercial operation, 191

fuel additives, 194

NO_x reduction, significant factors, 190–191

product development trade-offs, 193,197*f*

reactions governing process, 190

removal efficiency, 193–194

SCR location configurations, 191,192*f*

soot and ammonium bisulfate deposit

control, 195

start-up and shut-down of plants, 195

system features, 193

Takehara Station Unit 1, 195

K

Kinetics of gasoline sulfur compounds for

sulfur reduction, *See* Reaction kinetics of

gasoline sulfur compounds for sulfur

reduction

L

La_{1-x}Sr_xCoO₃ catalysts, role in NO_x

control by catalytic combustion of

natural gas, 224–232

- Lead poisoning, palladium-only catalysts
for closed-loop control, 103,104f
- Lean-burn engines
emission control, 90
need for catalyst other
than three-way catalyst, 53
- Low-dust applications, SCR technology,
191–193
- Low-dust configuration, location, 205,206f
- Low-temperature catalytic combustion of
volatile organic compounds using ozone
applications, 368
catalysts, physicochemical characteristics,
356t,357
concentration vs. catalyst, 358,359f
concentration vs. temperature, 358,359f
experimental procedure, 354,357–358
laboratory plant, 357
micropollutant analysis 367–368
physicochemical analytical procedure, 357
pure catalyst vs. mixture, 363,364f
temperature vs. ozone concentration,
358,360–362f
temperature vs. volatile organic compound
concentration in air, 354,355f
volatile organic compounds, properties,
354,356t,357
X-ray photoelectron spectra vs. heat
treatment, 363,365–367
- Low-temperature deep oxidation of
aliphatic and aromatic hydrocarbons
advantages, 339
butane conversion, 336,338t
carbon supports, hydrophobicity, pore
volume, and properties, 334–335f
experimental procedure, 332–333
hexane conversion, 334,336t,337f
toluene conversion, 336,338t
- Low-temperature oxidation catalyst,
applications and examples, 301–302
- Low-temperature oxidation catalyst for
ethene removal
additional cation vs. reactivity, 313
bulk Pt concentration vs.
reactivity, 313
catalyst preparation and pretreatment
procedure, 304
catalyst testing method, 304,306f
experimental condition effect on
activity, 305,307–309t
- Low-temperature oxidation catalyst for
ethene removal—*Continued*
experimental description, 303
mini-reactor system for catalyst testing,
304,306f
nomenclature of ion-exchanged zeolite
samples, 303
palladium on alumina, 305,310f
PdCaNaY(L), 305,310–311f
platinum on asbestos, 305,308f
previous studies, 303
PtCaNaY(L), 305,311–313
reaction on reactor surfaces, 305,306f
requirements, 301
water vapor vs. reactivity, 312f,313
zeolites
analytical procedure, 303
ion-exchange procedure, 303
structure vs. reactivity, 313
- Low-temperature selective catalytic
reduction NO_x control
catalysts, 212–213
designs, 210,212–213
economic considerations for
configuration choice, 205,207
high-dust configurations, 207–209
operating information, 210
U.S. applications, 213
- M
- Metal–alumina surfaces, nitric oxide
reactions, 140–154
- Metal oxides
deep oxidation of chlorinated
hydrocarbons on synthetic
carbonaceous adsorbents, 340–351
oxidation catalysts, 302
- Methanol, production methods, 270
- Methyl *tert*-butyl ether, production, 270–271
- Mobile engine emission control
catalyst requirements, 90
catalytic converters for diesel engine
exhaust control, 91
lean-burn engine, 90
- Monolithic oxidation catalyst, process
condition effect of transient
response, 316–329
- Motor fuels, production methods, 271

N

Natural gas

catalytic combustion for NO_x control,
224–232

emission regulations, 224

industrial combustion systems, 224

NH₃, catalysts for cleanup from nuclear
waste processing facility, 74–87

NH₃ conversion

Cu–ZSM-5 effect, 76–78

Cu–ZSM-5 + Pt–Al₂O₃ effect, 84,85*t*,87*f*

Pt–Al₂O₃ effect, 78,82–84

NH₃–NO ratio, NH₃ and CO conversion
effect, 78–81*f*

Nitric oxide

catalytic decomposition over promoted
copper ion exchanged ZSM-5 zeolites,
7–20

standards for automotive industry, 140

Nitrosyl reduction, mechanism, 140

NO

chemical transformations, 2,3*f*

contemporaneous removal with SO₂ from
flue gas using regenerable copper-on-
alumina sorbent–catalyst, 233–249

production, 2

NO and N₂O₂ adsorption on bare and
supported metal catalysts

adhesion, 147,149–150

adhesion energies, 150*t*,151

ceramic support vs. Fermi level, 151,153

charge transfer, 150*t*,152*f*

Fermi level for N₂O₂ adsorption, 153,154*f*

Fermi level for NO adsorption, 151,153,154*f*

Fermi level variation, 151*t*,152

geometry, 141–146,148

models, 146–148*f*

NO–CO reaction, Rh–SiO₂ and Ce–Rh–SiO₂
catalyst effects on reaction, 157–166

NO conversion

O₂ effect on reaction mechanism, 35–36

O₂ effect on reactivity of Cu-based
zeolites and oxides, 22–37

NO decomposition, need for catalyst, 22

NO oxidation, sulfate effect on Pt–ZrO₂
catalysts, 250–266

NO reduction

hydrocarbon oxidation, 53–64

mechanism study, 66–67

NO reduction in three-way catalyst

adhesion, 147,149–150

adhesion energies, 150*t*,151

charge transfer, 150*t*,152*f*

dinitrosyl species as reaction

intermediates, 140–141

experimental description, 141

Fermi levels, 151*t*–154*f*

geometry, 141–146,148

models, 146–148*f*

NO reduction with hydrogen over Pt,

Rh, and Pt–Rh alloy surfaces

comparative studies, 129–135

experimental procedure, 115–116

mechanistic studies using Pt_{0.25}–Rh_{0.25}(100)

single-crystal surface as model
catalyst, 120–121

NO + H₂ and NO + NH₃ reactions

10-mbar range, 126–129

10⁻⁶–10⁻⁸-mbar range, 123–126

reactions, 114–115

silica-supported catalysts, 116–120

silica-supported catalysts vs.

single-crystal surfaces, 135–138

spectroscopic data, 121–123

NO₂, source of health and

environmental problems, 2

NO_x

catalysts for cleanup from nuclear
waste processing facility, 74–87

composition, 2

environmental removal, commercial

approaches, 2

selective catalytic reduction, 216,218

NO_x abatement, SCR catalysts, 172–188

NO_x control

catalytic combustion of natural gas,
224–232

foreign experience with selective
catalytic reduction, 190–202

low-temperature SCR, 205–213

NO_x emissions

causes, 215

power plants, control methods, 170–171

removal methods, 233

NO_x reduction, role of supported gold
catalysts, 422,426*t*,427

NO_x removal

automobile exhaust, methods, 53–54

catalytic decomposition of NO, 4

- NO_x removal—*Continued*
power plant applications, catalyst technologies, 215–223
reduction with hydrocarbons, 4
selective catalytic reduction, 2
- Noble metals, role in automotive emission control catalysts, 94,95f
- Nonvolatile organic compounds, regulation of emissions, 331
- Nuclear waste processing, NO_x and CO pollutants, 74
- O
- O_2 , role in Cu-based zeolite and oxide reactivity in NO conversion, 22–37
- O_2 emissions, removal methods, 233
- Olefin(s) in gasoline
future regulations, 273
ozone formation, 273,274f
reduction methods, 275
vapor pressure, 273,274f
- Olefin skeletal isomerization process,
highly selective, *See* Highly selective olefin skeletal isomerization process
- Organic compounds, volatile, *See* Volatile organic compounds
- Oxidation catalyst, monolithic, process condition effect of transient response, 316–329
- Oxidation of hydrocarbons, role in catalytic reduction of NO, 53–64
- Oxidation of NO and SO_2 , 250–266
- Oxygen, COS hydrolytic effect, 401–403
- Oxygenates
gasoline blending, demand, 273
reformulated fuels, 270
- Ozone, use as oxidant in low-temperature catalytic combustion of volatile organic compounds, 354–368
- P
- Palladium
adhesion to alumina, 140–154
automotive emission control catalysts, 94,95f
- Palladium-only catalysts for closed-loop control
amount of noble metal used, 110,111f
- Palladium-only catalysts for closed-loop control—*Continued*
comparison of 50% Pt–Rh reduction, 96,97t,99f
development, 96
durability at stoichiometry after severe engine aging, 94,95f
exhaust air:fuel ratio effect on aging, 105–109f
lead poisoning, 103,104f
manifold mounted converter advantages, 106,109f–111f
performance characteristics, 97–111
problems, 94,96
rich NO_x performance, 103
 SO_2 poisoning, 103,105t
thermal durability performance, 97–102
- PdCaNaY(L), catalyst for low-temperature oxidation of ethene, 305,310–311f
- Pd–ZSM-5, role in NO reduction by hydrocarbon in oxidizing atmosphere, 58,60f,62f
- Pentene, isomerization process, 275–285
- Perovskite catalysts, role in NO_x control by catalytic combustion of natural gas, 224–232
- Plate-type catalytic converters
activity profile with high As_2O_3 content, 182,183f
applications, 187–188f
arrangement, 178,179f
catalyst activity and SO_2 conversion rate vs. V_2O_5 content, 182,183f
development, 173,177
dust deposition vs. geometric and fluid dynamic parameters, 178,180f
erosion resistance, 178,180f
operating results, 182,185–186f
selection according to operating conditions, 177t
selection criteria, 178,182,183f
- Platinum
adhesion to alumina, 140–154
catalyst, NO reduction effect, 114–138
role in automotive emission control catalysts, 94,95f
surface, sulfate effect, 263
- Power plant(s), catalytic emission control systems, 215–223

- Power plant capacity of Germany
emission standards, development, 173,175*f*
emissions from typical hard coal fired
plant, 172,174*f*
NO_x removal measures, 173,175*f*
power sources, 172,173*f*
- Power plant emissions, control methods,
170–171
- Process condition effect on transient response
of monolithic oxidation catalyst
air inlet temperature, 326*f*–329
catalyst preparation 318–319
challenge concentration, 324–326*f*
equipment, 319–321
experimental procedure, 317–318,321
step change in concentration, 321–323
- Pt–Al₂O₃
CO conversion effect, 76,77*f*
NH₃ conversion effect, 78–84
- Pt–Rh alloy surfaces, NO reduction effect,
114–138
- Pt–ZrO₂, sulfation by aging, 265–266
- Pt–ZrO₂ catalysts
properties of aged catalysts, 266
sulfate effect on NO and SO₂ oxidation,
250–266
- PtCaNaY(L), catalyst for low-temperature
oxidation of ethene, 305,311–313
- Pyridine, site-blocking agent for COS
hydrolysis, 399,401
- R
- Reaction kinetics of gasoline sulfur
compounds for sulfur reduction
catalytic cracking products of
thiophene, 288–290*f*
cracking rate determination, 289,291
cracking reactions pathways, 291,292*f*
experimental procedure, 287–288
feedstock properties, 288,289*t*
hydrogen transfer rate effect, 290*f*–292*f*
sulfur compound cracking rates relative to
that of hexadecane, 290*f*–293
sulfur technology, developing, 293*t*–295
- Reactivity of Cu-based zeolites and oxides
in NO conversion, O₂ effect, 22–37
- Reduction of NO, catalytic, role of
hydrocarbon oxidation, 53–64
- Reduction with hydrocarbons, use for NO_x
removal, 4
- Reformulated gasoline, requirement of
Clean Air Act Amendment, 270
- Rh catalyst
NO reduction effect, 114–138
performance improvement, 157
- Rh–SiO₂ catalyst, NO–CO reaction effect,
157–166
- Rhodium
adhesion to alumina, 140–154
automotive emission control
catalysts, 94,95*f*,140
- Rich NO_x performance, palladium-only
catalysts for closed-loop control, 103
- S
- Selective catalytic reduction (SCR)
catalyst properties, 215
catalytic converters for NO_x control
activity profile(s)
catalysts, 182,184*f*
high As₂O₃ content, 182,183*f*
poisoning resistant catalysts, 182,184*f*
application(s), 187–188*f*
application to U.S. high-sulfur coal
service, 200,201*t*,203
arrangement, 178,179*f*
blockage frequency vs. converter type,
182,185*f*
catalyst activity and SO₂ conversion
rate vs. V₂O₅ content, 182,183*f*
description, 173,176*f*
development of plate-type
converters,173,177
dust deposition vs. geometric and fluid
dynamic parameters, 178,180*f*
erosion resistance, 178,180*f*,186*f*
German experience, 196–200
Japanese experience, 190–195,197
operating results, 182,184–186*f*
selection according to operating
conditions, 177*t*
selection criteria, 178,182,183*f*
types, 178,181*f*
description, 216,218
location configurations, 191–193

- Selective catalytic reduction (SCR)—
Continued
 operating environment and process constraints, 215
 NO_x removal, 2
- Selective catalytic reduction reactor,
 location configurations, 205,206f
- Selectivity, definition, 277
- Selectivity factor, definition, 255
- Semivolatile organic compounds, emission control methods, 331–332
- Sintering, cupric, role in Cu–ZSM-5 deactivation, 39–51
- SO₂, contemporaneous removal with NO from flue gas using regenerable copper-on-alumina sorbent–catalyst, 233–249
- SO₂ oxidation, sulfate effect on Pt–ZrO₂ catalysts, 250–266
- SO₂ poisoning, palladium-only catalysts for closed-loop control, 103,105t
- SO_x emissions from power plants, control methods, 170–171
- Stack gas emissions from power plants, catalytic control methods, 170–171
- Stadtwerke Duesseldorf, low-temperature SCR design, 210,212
- Strontium, role in NO_x control by catalytic combustion of natural gas, 224–232
- Sulfate(s)
 formation during COS hydrolysis, 400f,401
 temperature-programmed reaction with H₂S, 402f,403
- Sulfate effect on Pt–ZrO₂ catalysts for NO and SO₂ oxidation
 activity measurement procedure, 251,252t
 adsorption–desorption characteristics of catalysts, 262–264f
 aging tests, 255,256f
 catalyst acidity, 266
 catalyst preparation, 251t
 experimental description, 250–251
 Fourier-transform IR spectra, 257,261f,262
 NO conversion with and without SO₂, 252,253f,255
 properties of aged Pt–ZrO₂ catalysts, 266
 Pt–ZrO₂ sulfation by aging, 265–266
 reduction of surface sulfate, 265
 selectivity, 255,256f
- Sulfate effect on Pt–ZrO₂ catalysts for NO and SO₂ oxidation—*Continued*
 SO₂ conversion with and without NO, 252,254f,255
 surface Pt, 263
 temperature-programmed desorption procedure, 252
 temperature-programmed desorption vs. pretreatment, 255,257–259f
 temperature-programmed reduction vs. fresh and used samples, 257,259–260f
 treatment effect on catalyst surface area, 266
- Sulfate surface, reduction, 265
- Sulfated titania catalyst, activity test, 401–403
- Sulfur compounds, gasoline, *See* Gasoline sulfur content
- Sulfur dioxide reduction to elemental sulfur
 methods, 375–376
 redox reaction mechanism, 376–377
 water in feed gas effect, 376
- Sulfur dioxide reduction to elemental sulfur over ceria catalysts
 apparatus, 377
 association enthalpy and conductivity for solid solutions of dopants, 379,381t
 catalyst preparation, 378,380t
 CeO₂ catalyst, 378,381f
 CeO₂(La) catalyst, 384,385f
 dopant vs. activity, 379,382f
 doped CeO₂ catalysts, 378–384
 experimental procedure, 377
 impregnated CeO₂(La) catalyst, 388,391f
 light-off behavior, 379,382,384f
 mechanisms, 388–390
 water vapor effect, 384,386–388
 Y₃O₃ dopant content vs. activity, 379,380t,382f
- Sulfur reduction, catalytic mechanisms, and reaction kinetics, 286–295
- Sulfuric acid, safety issue, 271
- Supported gold catalyst application to environmental problems
 characterization of catalysts, 421t
 CO oxidation, 421–423f
 CO₂ hydrogenation, 426t
 experimental procedure, 420–421
 H₂ oxidation, 421–422
 hydrocarbon combustion, 422,424f
 NO_x reduction, 422,426t,427
 trimethylamine combustion, 422,425f

- Supported noble metals, use as oxidation catalysts, 302
- Surface acidity, catalyst performance effect, 250–251
- Surface platinum, sulfate effect, 263
- Surface sulfate, reduction, 265
- Synthetic carbonaceous adsorbent(s), 332
- Synthetic carbonaceous adsorbent supported metal oxides for deep oxidation of chlorinated hydrocarbons
activation energy, 346,347*f*
carbon support, structural parameters, 341*t*
catalyst characterization, 346,348–351
catalytic combustion reactivity, 342–344*t*
experimental procedure, 341–342
pore structure effect, 343
previous studies, 341
reactivity vs. hydrocarbon, 343–346
reactivity vs. hydrogen, 346,347*f*
reactivity vs. temperature, 346,347*f*
- Synthetic carbonaceous adsorbent supported transition metal oxides for low-temperature deep oxidation of aliphatic and aromatic hydrocarbons
advantages, 339
butane conversion, 336,338*t*
carbon supports
hydrophobicity, 334,335*f*
pore volume, 334*t*,335*f*
properties, 334*t*
experimental procedure, 332–333
hexane conversion, 334,336*t*,337*f*
toluene conversion, 336,338*t*
- T**
- Tail end configuration
advantages, 209–210
German utility applications, 210,211*t*
location 205,206*f*
problems, 209
- Tail gas applications, SCR technology, 191–193
- Temperature
NO_x selective catalytic reduction
catalyst effect, 215–223
role in catalytic decomposition of NO over promoted copper ion exchanged ZSM-5 zeolites, 8–20
- Thermal combustion, control of volatile organic compounds, 298
- Thermal durability performance, palladium-only catalysts for closed-loop control, 97–102
- Thermal oxidation, control of volatile organic compounds, 331–332
- Titania
catalyst for COS hydrolysis, 394–403
diffuse reflectance IR experiments, 397–400*f*
- Toluene conversion, low-temperature deep oxidation, 336,338*t*
- Transient response
oxidation catalysts, automotive applications, 317
process conditions for monolithic oxidation catalyst, 316–329
- Transition metal(s), cocation effect in catalytic decomposition of NO using copper ion exchanged ZSM-5 zeolites, 8–20
- Transition metal oxides, low-temperature deep oxidation of aliphatic and aromatic hydrocarbons using synthetic carbonaceous adsorbents, 331–339
- Trimethylamine combustion, role of supported gold catalysts, 422,425*f*
- Turnover frequency
CO₂ formation, definition, 163
definition, 15
- U**
- United States high-sulfur coal service, application of SCR technology, 200–202
- V**
- Volatile organic compounds
advantages of catalytic combustion for elimination, 353–354
control using heterogeneous catalysts, 298–299
elimination methods, 353
emission control methods, 331–332
future research needs, 300

Volatile organic compounds—*Continued*
low-temperature catalytic combustion,
354–368
recovery methods, 353
regulations, 298,331
source of pollution, 353

W

Water, SO₂ reduction to S effect, 376
Water vapor, SO₂ reduction to S,
384,386–388

X

X-ray photoelectron spectroscopy
Cu–ZSM-5 zeolite
analytical system, 67–68
Cu core level spectra vs. reactor
treatment, 68–71
Cu core level spectra vs. reductive
treatments, 71,72f

X-ray photoelectron spectroscopy—
Continued
Cu–ZSM-5 zeolite—*Continued*
experimental description, 67
previous studies, 67
treatments, 68,69t
zeolite studies, 67

Y

Yield, definition, 277

Z

Zeolite(s), advantages as supports for
oxidation catalysts, 302
Zeolite degradation, role in Cu–ZSM-5
deactivation, 39–51
ZSM-5 zeolites, copper ion exchanged,
catalytic decomposition of NO, 7–20

Production: Charlotte McNaughton
Indexing: Deborah H. Steiner
Acquisition: Rhonda Bitterli
Cover design: Bob Sargent

Printed and bound by Maple Press, York, PA